JAW MECHANICS OF THE PTEROSAUR SKULL CONSTRUCTION AND THE EVOLTUION OF TOOTHLESSNESS

Dissertation
zur Erlangung des Grades
Doktor der Naturwissenschaften
Dr. rer. nat.

am Fachbereich Chemie, Pharmazie und Geowissenschaften
der Johannes Gutenberg-Universität in Mainz

Michael Fastnacht
geb. am 09.05.1970 in Tuttlingen
Mainz 2005

Dekan:
1. Gutachter:
2. Gutachter:

Tag der mündlichen Prüfung:

Diss. Joh. Gutenberg-Univ. Mainz	**228 S.**	**520 Abb., 97 Tab., 142 Anl.**	**Mainz, Oktober 2005**

Erklärung

Ich versichere hiermit, die vorliegende Arbeit selbstständig und nur unter Verwendung der angegebenen Quellen und Hilfsmittel verfasst zu haben.

Michael Fastnacht
Mainz, Oktober 2005

Ergo ubi diluvio tellus lutulenta recenti
solibus aetheriis altoque recanduit aestu,
edidit innumeras species; partimque figuras
rettulit antiquas, partim nova monstra creavit.
illa quidem nollet, sed te quoque, maxime Python,
tum genuit, populisque novis, incognita serpens,
terror eras: tantum spatii de monte tenebas.

Da nun also die Erde, noch frisch überschlammt von der Sintflut,
glühte im brütenden Brand der himmlischen Sonne, da warf sie
zahllose Arten ans Licht; teils brachte sie wieder die alten
Formen, teils auch schuf sie zuvor nicht gesehene Wesen.
Zwar wollte sie es nicht, doch auch dich, du riesiger Python,
zeugte sie da, und du warst, unheimliche Schlange, der neuen
Völker Schrecken, so vieles Gevierte decktest am Berg du.

Ovid, Metamorphosen

„Habe Mut, Dich
Deines eigenen Verstandes
zu bedienen“

Immanuel Kant

„Isn‘t she gorgeous?“

Steve Irwin

ABSTRACT

The investigation of the biomechanics of organismic structures yields important information about the understanding of evolutionary processes. In the present study, pterosaur skull constructions were analysed using a combined approach of finite element analysis (FEA), static investigations as well as applying classical beam theory and lever mechanics. The study concentrates on the operating regime „bite“, where loads are distributed via the dentition or a keratinous rhamphotheca into the skull during jaw occlusion.

As a first step, pterosaur tooth constructions were analysed. The different morphologies of the tooth construction determine specific operational ranges, in which the teeth perform best (= greatest resistance against failure). The incomplete enamel-covering of the pterosaur tooth constructions thereby leads to a reduction of strain and stress and to a greater lateral elasticity than for a complete enamel cover. This permits the development of high and lateral compressed tooth constructions. Further stress-absorption occurs in the periodontal membrane, although its mechanical properties can not be clarified unambiguously.

A three-dimensionally preserved skull of *Anhanguera* was chosen as a case-study for the investigation of the skull constructions. CT-scans were made to get information about the internal architecture, supplemented by thin-sections of a rostrum of a second *Anhanguera* specimen. These showed that the rostrum can be approximated as a double-walled triangular tube with a large central vacuity and an average wall-thickness of the bony layers of about 1 mm. On base of the CT-scans, a stereolithography of the skull of *Anhanguera* was made on which the jaw adductor and abductor muscles were modelled, permitting to determine muscular forces. The values were used for the lever mechanics, cantilever and space frame analysis. These studies and the FEA show, that the jaw reaction forces are critical for the stability of the skull construction. The large jugal area ventral to the orbita and the inclined occipital region act as buttresses against these loads. In contrast to the orbitotemporal region which is subject to varying loading conditions, the pattern in the rostrum is less complex. Here, mainly bending in dorsal direction and torsion occur. The hollow rostrum leads to a reduction of weight of the skull and to a high bending and torsional resistance.

Similar to the Anhanguera skull construction, the skulls of those pterosaur taxa were analysed, from which enough skull material is know to permit a reliable reconstruction. Furthermore, FEA were made from five selected taxa. The comparison of the biomechanical behaviour of the different skull constructions results in major transformational processes: elongation of rostra, inclination of the occipital region, variation of tooth morphology, reduction of the dentition and replacement of teeth by a keratinous hook or rhamphotheca, fusion of naris and antorbital fenestra, and the development of bony and soft-tissue crests. These processes are discussed for their biomechanical effects during bite:

• During occlusion a longirostrine skull has a higher velocity and acceleration of the lower jaw than a brevirostrine skull. This is further amplified by an inclined occipital region due to the lengthening of the adductor muscles. A similar muscle-lengthening effect may be deduced from the presence of an orbitotemporal crest. Brevirostrine skull constructions show higher bite forces at the anterior end of the rostrum than longirostrine skulls.

• The presence of an anterior bony crest results in reduction of shear and comparison stress and a higher tendency for bending than twisting, decreasing the tendency of failure of the skull construction. A similar effect is present for a medial bony crest, which also stabilises the premaxillary-nasal member during occlusion. Soft-tissue crests are neglectable for the present operating regime.

• Fusion of naris and antorbital fenestra is the consequence of an elongated rostrum in which this area is less stressed than in a brevirostrine skull construction. Whereas in the latter the bars bordering the naris and antorbital fenestra stabilise the skull construction against failure, the separating maxillary-nasal bar between both fenestra gets less-stressed and more oblique the longer the rostrum is. This leads to a complete reduction of this bar and formation of the nasoantorbital fenestra.

• With the exception of the Gallodactylus skull construction, the reduction of the dentition follows the formation of an anterior keratinous hook on the rostrum. This hook and furthermore, the development of a keratinous rhamphotheca results in a reduction of especially torsional and shear loads and has a shock-absorbing effect. Subsidiary, the overall weight of the skull is reduced. The presence of the rhamphotheca permits the lateral narrowing of the skull construction.

Certain optional operational ranges for feeding are assigned to the different skull constructions and previous hypotheses (e.g. skimming) are verified. Using the principle of economisation, these processes help to establish irreversible transformations and to define possible evolutionary pathways. The resulting constructional levels and the structural variations within these levels are interpreted in light of a greater feeding efficiency and reduction of bony mass combined with an increased stability against the various loads. The biomechanical conclusive pathways are used for comparison and verification of recent hypothesis of the phylogenetic systematics of pterosaurs.

KURZFASSUNG

Die Untersuchung der Biomechanik organismischer Strukturen liefert Informationen für das Verständnis evolutionärer Prozesse. In der vorliegenden Studie wurde die Schädelkonstruktion von Flugsauriern durch eine kombinierte Analyse mittels Finiter Elemente Analyse (FEA), Statik, Hebelmechanik und Balkentheorie untersucht. Das operationelle Regime umfasst dabei den Biss bei der Nahrungsaufnahme, bei dem Kräfte über die Zähne oder einer keratinösen Schnabelscheide in den Schädel eingeleitet werden.

Im ersten Schritt wurden die Zahnkonstruktionen der Flugsaurier analysiert. Die unterschiedliche Morphologie bestimmt spezifische optionale operationelle Rahmen, in denen eine Zahnkonstruktion einen maximalen Widerstand gegen Versagen besitzt. Die unvollständige Schmelzbedeckung führt dabei zu einer Reduktion von Spannung und Deformation und einer erhöhten lateralen Elastizität gegenüber einer vollständig schmelzbedeckten Zahnkonstruktion. Dies erlaubt die Ausbildung langer und lateral komprimierter Zahnkonstruktionen. Die periodontale Membran bewirkt eine weitere Reduktion der Spannung, wenngleich ihre genauen mechanischen Eigenschaften nicht bestimmt werden können.

Als Fallstudie für die nachfolgenden Untersuchungen wurde ein dreidimensional erhaltener Schädel von *Anhanguera* analysiert. Um Informationen über Internstrukturen zu erhalten, wurde eine Computertomographie angefertigt und Anschliffe eines weiteren Rostrums von *Anhanguera* untersucht. Diese zeigen, dass das Rostrum als ein dreieckiger Tubus mit einer Doppelwandung und einem zentralen Hohlraum betrachtet werden kann, wobei die Dicke der einzelnen Knochenwände rund 1 mm beträgt. Mit Hilfe der CT-Daten wurde eine Stereolithographie des *Anhanguera*-Schädels erstellt, auf der mittels Knetmasse die Adduktoren- und Abduktorenmuskeln modelliert und die Muskelkräfte ermittelt wurden. Die resultierenden Werte gingen in die Analyse der Hebel- und Kragarmmechanik, sowie der Statik des Fachwerkmodells ein. Zusammen mit der FEA zeigte sich dabei, dass die Gelenkreaktionskräfte kritisch für die Stabilität der Schädelkonstruktion sind. Das großflächige Jugale ventral der Orbita und die schräg gestellte Okzipitalregion wirken hier als versteifende Elemente. Im Gegensatz zur Orbitotemporalregion, die wechselnden Spannungen unterliegt, besteht die Belastung des Rostrums im wesentlichen nur aus Biegung und Torsion. Der Hohlbau des Rostrums bewirkt dabei eine Verringerung des Gewichts und einen hohen Widerstand gegenüber Biegung und Torsions.

Auf der Basis der Fallstudie wurden die Schädelkonstruktionen derjenigen Flugsaurier untersucht, von denen eine verlässliche Schädelrekonstruktion möglich ist. Darüberhinaus wurde eine FEA von fünf ausgewählten Taxa angefertigt. Der Vergleich der Morphologie und des mechanischen Verhaltens der verschiedenen Schädelkonstruktionen liefert wesentliche Transformationsprozesse: Verlängerung des Rostrums, Kippung der Okzipitalregion, Variation der Zahnmorphologie, Reduktion der Bezahnung und Ersatz durch einen keratinöse Schnabelscheide oder Hornschnabel, Fusion der Naris mit dem Antorbitalfenster und die Entwicklung von knöchernen oder Weichteilkämmen. Diese werden bezüglich des Effekts für die Schädelmechanik bei der Okklusion diskutiert:

• Ein longirostriner Schädel zeigt eine höhere Geschwindigkeit und Beschleunigung des Kieferschlusses als ein brevirostriner Schädel. Dies wird durch eine Kippung der Okzipitalregion verstärkt, bedingt durch die Verlängerung der Adduktorenmuskeln. Ein ähnlicher Effekt lässt sich für einen Orbitotemporalkamm annehmen. Brevirostrine Schädel dagegen zeigen höhere Bisskräfte am anterioren Ende des Rostrums und eine niedrigere Geschwindigkeit und Beschleunigung des Kieferschlusses.

• Das Vorhandensein eines Rostralkamms bewirkt eine Reduktion der Scher- und Vergleichsspannung und eine Tendenz zur Biegung anstatt zur Torsion. Dies verringert die Wahrscheinlichkeit des Versagens der Struktur. Ein ähnlicher Effekt lässt sich für einen Medialkamm nachweisen, der darüberhinaus bei der Okklusion den Prämaxillar-Nasal-Stab dorsal des Antorbitalfensters stabilisiert. Für das untersuchte operationelle Regime sind Weichteilkämme bezüglich ihres mechanischen Effektes vernachlässigbar.

• Die Fusion von Naris und Antorbitalfenster ist das Resultat einer Verlängerung des Rostrums, bei der dieser Bereich weniger Spannung erfährt als in einem brevirostrinen Schädel. Im letzteren haben die Naris und Antobritalfenster begrenzenden Streben eine wichtige Stützfunktion. In einem longirostrinen Schädel hingegen unterliegt die Maxillar-Nasal-Strebe zwischen Naris und Antorbitalfenster nur geringen Spannungen und ist umso flacher schräg gestellt, je länger das Rostrum ist. Dies führt schließlich zur vollständigen Reduktion der Strebe.

• Mit Ausnahme der Gallodactylus-Schädelkonstruktion erfolgt die Reduktion der Bezahnung von anterior, in Zusammenhang mit der Ausbildung einer keratinösen Schnabelscheide am anterioren Rostrumsende. Diese, wie auch der Hornschnabel bewirken eine Reduktion besonders der Scher- und Torsionsspannungen. Daneben wird auch das Gewicht des Schädels reduziert. Das Vorhandensein des Hornschnabels ermöglicht eine laterale Verschmälerung der Schädelkonstruktion.

Den einzelnen Schädelkonstruktionen werden bestimmte optionale operationelle Bandbreiten der Nahrungsaufnahme zugeordnet und so bisherige Hypothesen zur Nahrungsaufnahme getestet. Mit Hilfe des Ökonomieprinzips lassen sich unumkehrbare Transformation bestimmen und evolutionäre Abläufe konstruieren. Die sich daraus ergebenden konstruktionellen Ebenen und Variation innerhalb dieser werden im Rahmen einer erhöhten Effizienz der Nahrungsaufnahme und Reduktion des Gewichtes bei gleichzeitig erhöhter Stabilität gegenüber Spannungen interpretiert. Das resultierende evolutionäre Ablaufdiagramm wird zum Vergleich und Verifikation aktueller Hypothesen der phylogenetischen Systematik von Flugsauriern benutzt.

CONTENTS

1. INTRODUCTION

1.1 Aim of the study

In 1784, Cosimo Alexandro Collini, the first curator of the Natural History Collection at the Naturalienkabinett in Mannheim published the description of an unknown, strange fossil vertebrate with unusually long arms from the Jurassic Solnhofen limestone. Although he noticed certain morphological affinities to bats and birds, he supposed that the animal represented a "sea creature". The affiliation of the specimen to reptiles and its identification as an extinct flying animal was yet to be determined by later scientists such as George Cuvier who named the specimen *Pterodactylus antiquus*. Since the 18th century, the knowledge of pterosaurs has been greatly expanded by further findings of pterosaur fossils. Especially the localities of Solnhofen/Eichstätt in Germany (see overview in Barthel et al. 1990, Wellnhofer 1983, 1991a), Chapada do Araripe in Brazil (Buisonjé 1980, Dalla Vecchia 1993, Campos & Kellner 1985, 1997, Fastnacht 2001, Frey & Martill 1994, 1998, Frey & Tischlinger 2000, Frey et al. 2003a, 2003b, Kellner 1984, 1989, 2001, Kellner & Campos 1988, 1994, 2002, Kellner & Tomida 2000, Leonardi & Borgomanero 1985, Martill & Frey 1998, Martill & Unwin 1989, Price 1971, Veldmeijer 2002, 2003, Wellnhofer 1985, 1987, 1991a, 199b, 1991c, Wellnhofer & Kellner 1991) and most recently Liaoning in China (Dalla Vecchia 2002, Dong 1982, Dong & Lü 2005, Ji & Ji 1988, 1997, 1998, Ji & Padian 1999, Lü 2002, 2003, Lü & Ji 2005, Unwin et al. 2000, Wang & Lü 2001, Wang & Zhou 2003, Wang et al. 1999, Zhou et al. 2003) have not only yielded a diverse pterosaur assemblage including complete skulls but additionally remains of the soft-tissue parts of the animals.

Besides the wing construction, the diverse skull morphology is the typical anatomical feature of pterosaurs (Fig.1.1). *Batrachognathus* and *Anurognathus* e.g. have brevirostrine, rounded skulls, whereas most other pterosaurs are characterised by a narrow longirostrine skull. In some taxa (e.g. *Pteranodon*, *Quetzalcoatlus*) the length of the rostrum exceeds the length of the orbitotemporal skull region multiple times.

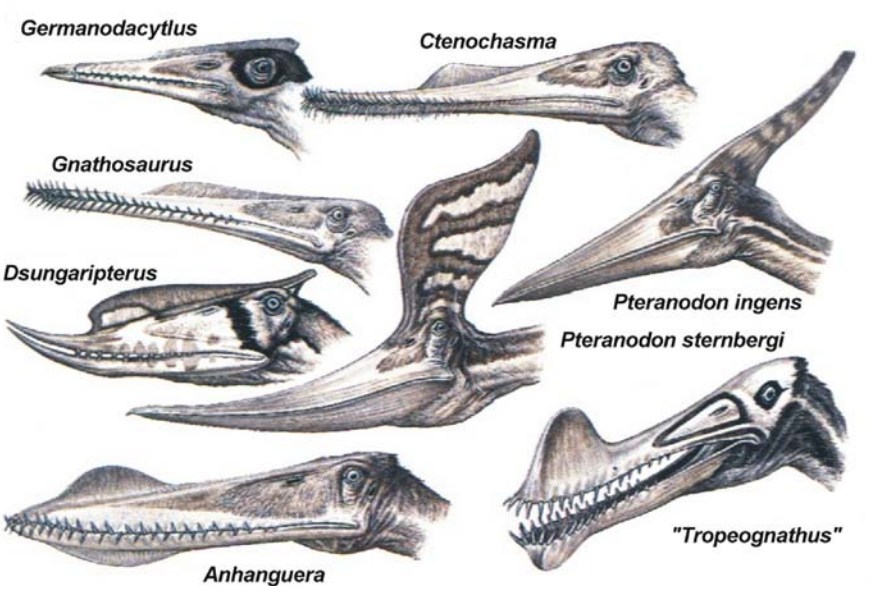

Fig. 1.1: Samples of different skull morphologies and dentition types in pterosaurs (Wellnhofer 1991a). The shown specimen of "*Tropeognathus*" was referred to *Criorhynchus* by Fastnacht (2001).

The dentition of the jaws is variable in pterosaurs (Fig.1.1). Whereas the Late Triassic taxa *Eudimorphodon* has multicuspid teeth, most pterosaurs possess slender, pointed teeth, which could be arranged as dense sets of teeth (e.g. *Ctenochasma*), interpreted as a straining apparatus (Wellnhofer 1991a) or e.g. in an expanded terminal rosette with enlarged teeth (e.g. *Coloborhynchus*), interpreted as a skimming device (Fastnacht 2001). The dentition can be reduced at the anterior (e.g. *Rhamphorhynchus*, *Dsungaripterus*) or at the posterior part of the rostrum (e.g. *Galloda-*

cytlus, *Pterodactylus*). Some taxa are even edentulous (e.g. *Pteranodon*, *Tapejara*, *Quetzalcoatlus*) and bear keratinous beaks (Wellnhofer 1991a) .

Most pterosaurs skulls have medial bony crests (Fig.1.1), which can be situated at various regions of the skull (Wellnhofer 1991a). The crests of *Coloborhynchus* or *Criorhynchus* are limited to the premaxillary portion of the rostrum (Fastnacht 2001, Owen 1874, Veldmeijer 2003, Wellnhofer 1987), whereas in *Anhanguera* the crests extends to the maxillary (Campos & Kellner 1985, Kellner & Tomida 2000, Wellnhofer 1985). A maxillofrontoparietal crest is developed in taxa like *Gnathosaurus* or *Germanodactylus* (Frey & Tischlinger 2000, 2003c) In *Tapejara*, *Tupuxuara* and *Dsungaripterus* the crests runs almost along the entire dorsal skull margin (Frey et al. 2003c, Kellner 1989, Kellner & Campos 1994, Wellnhofer & Kellner 1991, Young 1964). Crests on the parietal and occipital occur e.g. in *Pteranodon* or *Nyctosaurus* (Bennett 2001a, 2003, Eaton 1910, Williston 1891). Some taxa as *Coloborhynchus*, *Criorhynchus* and *Tapejara* also bear crests on the mandible (Fastnacht 2001, Veldmeijer 2003, Wellnhofer 1987, Wellnhofer & Kellner 1991). Besides these bony crests, soft-tissue crests are preserved in the lithographic limestones of Solnhofen/Eichstätt (Germany) and Crato Formation (Brazil) (Campos & Kellner 1997, Frey & Tischlinger 2000, Frey et al. 2003c, Tischlinger & Frey 2001). In certain taxa like *Tapejara* these crests are about five times higher than the entire skull length (Frey et al. 2003c). Only speculations based on so far untested hypotheses exist about the function of these crests. According to Wellnhofer (1991a) and Kellner & Campos (2002) the following potential functions are proposed:

- steering/navigation device
- aerodynamic stabiliser during flight
- hydrodynamic stabiliser during feeding in water
- mechanical stabiliser for the rostrum during bite
- signal function

Only few remarks about the jaw and feeding mechanics of pterosaurs exist in the literature. Eaton (1910), Bramwell & Whitfield (1974) and Wellnhofer (1980) compared the helical joints in pterodactyloids with the jaw joints in *Pelecanus*. In this recent bird group, the jaw abduction leads to the spreading of both rami of the mandible. The throat pouch thereby is enlarged and prey is trapped within. Eaton (1910) proposed the existence of a similar throat pouch in *Pteranodon*, although soft-tissue preservation is not present in this taxon. This view was contradicted by Bennett (2001b) who gave evidence for a close resemblance of the *Pteranodon* mandible to the mandibular rami of stringinid owls. Accordingly, a throat pouch would have been missing in *Pteranodon* and the helical jaw joint would have allowed to spread the mandibular rami only slightly in lateral direction. Brown (1943) and Kripp (1943) proposed a plunge-diving fishing mode for *Pteranodon*, a high impact-foraging mode which, as supposed by Bennett (2001b), is well within range of the fragility of the skeleton.

Another pterosaur with a helical jaw joint is *Ornithocheirus bunzeli* (Wellnhofer 1980). Wellnhofer (1980) reconstructed this taxon as well as *Rhamphorhynchus* as an analogue to the extant skimmer *Rhynchops* (Fig. 1.2), who snatches the food out of the water during low flight. Following Wellnhofer (1991a) the spear-like, anteriorly orientated teeth in *Rhamphorhynchus* would support this mode of feeding by acting similar to spears. Recently, Kellner & Campos (2002) published a description of the new genus *Thalassodromeus* for which they proposed a skimming life-habit, too.

Hence, a comprehensive discussion of the optional feeding ranges of the different pterosaur taxa based on the jaw mechanics is missing. Frey et al. (2003c) described possible pathways for the evolution of pterosaur rostra, but did not support their hypotheses with numerical analyses.

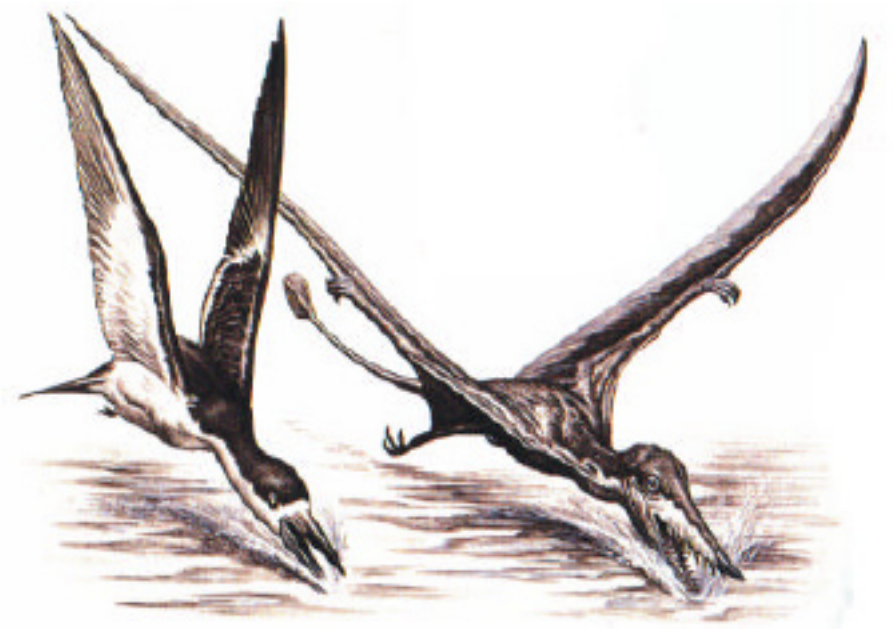

Fig. 1.2: Reconstruction of *Rhamphorhynchus* as analogue to the extant skimmer *Rhynchops* (Wellnhofer 1991b).

The aim of this dissertation is to clarify the feeding options of the various pterosaur skull constructions by analysing the constructional morphology of the pterosaur skulls. In doing so, the mechanical effects of the different crest-types during the bite are evaluated. The biomechanical analyses allow to determine possible transformations and irreversible structural changes between different constructional types following the concept established by Herkner (1999), Salisbury (2000) and Salisbury & Frey (2001), which will be described in the methodological chapter. Thereby, an evolutionary pathway with regard to the origin of toothlessness and crests is developed. Finally, the evolutionary pathway will be compared with recent analyses of the phylogenetic systematics of pterosaurs (Kellner 2003, Unwin 2003).

1.2. History of research of skull mechanics

The analytical approach to the jaw mechanics of vertebrates has its beginning in the early 1930ths when - especially in Germany - scientists began to analyse skulls by means of graphical statics and theoretical stress trajectories (Kripp 1932, 1933a, 1933b, 1933c, 1935a, 1935b, Marinelli 1938, Starck 1935, 1940). The investigations by Kripp already included a high degree of abstraction and comparison with the mechanical behaviour of objects designed by human beings. Kripp introduced the term “construction” in the context of his technical-mechanical approach to describe jaw mechanics (Kripp 1993a: 471). With only few exceptions (Tucker 1954, 1955) most research after WWII concentrated on a more “descriptive-functional” morphology of tetrapod skull mechanics neglecting the numerical-constructional approach of Kripp and others (e.g. Barghusen 1968, 1973, Beecher 1977, Bock 1964, 1966, Bramble 1978, Crompton & Hotton 1967, DeMar & Barghusen 1972, Dullemeijer 1956, 1959, Klaauw 1945, Moss & Young 1960, Olson 1961, Scapino 1965, Zusi 1959, 1962, 1967).

In 1978 Buckland-Wright published his outstanding paper about force transmission in the cat skull. He was the first outside the fields of human medicine and primatology to measure stress patterns during bite *in vivo*. His experiments triggered further research, mostly focusing on recent tetrapod jaw mechanics, e.g. on mammalian mastication, the biomechanical role of sutures to skull strength and cranial kinesis in lizards and birds (e.g. Barel et al. 1977, Bock 1999, Bout & Zweers 2001, Bramble & Wake 1985, Crompton 1995, Erickson et

al. 2003, Herrel et al. 2001, Herring 1994, Herring & Mucci 1991, Herring et al. 2001, Hylander 1979a, 1985, Jaslow 1990, Langenbach et al. 2002, Rafferty & Herring 1999, Rafferty et al. 2003, Ravosa et al. 2000, Schwenk 2000, Sun et al. 2004, Swartz 1991, Teng & Herring 1998, Thomason 1991, Weijs W.A. & Van Ruijven 1990, Weijs et al. 1987, Witmer & Rose 1991). Increasing knowledge about human jaw mechanics and better understanding of organic tissue biomechanics, helped to verify the mainly theoretical models based on the descriptive-functional approach. At the same time, the numerical-constructional approach to skull mechanics was "re-discovered" by applying lever mechanics, beam theory and other principles from the field of technical mechanics (Bock & Kummer 1986, Druzinsky & Greaves 1979, Gingerich 1971, 1979, Greaves, 1982, 1985a, 1985b, 1988a, 1988b, 1991a, 1991b, 1995, 2000, Hylander 1979b, Nobiling 1977, Preuschoft 1989, Preuschoft et al. 1985, Thomason & Russell 1986, Weishampel 1993). The universality of these principles permitted to use them not only on extant but likewise on extinct animals. This approach was enhanced, when finite element analysis (FEA) was applied to organismic constructions. Originally developed for engineering purposes, this numerical method was first introduced in orthopaedic medicine and used for designing implants serving specific biomechanical needs (Huiskes & Chao 1983). It soon became apparent, that FEA could also be used as a tool for analysing the biomechanical behaviour of organismic substances like bone, teeth, muscles and other types of connective tissues (for an overview of applications see Fastnacht et al. 2002). Whereas until today FEA has become one of the most important methods in human biomechanics, it was introduced only reluctantly to vertebrate morphology. The initial investigation using FEA to analyse the mechanical behaviour of the beak of the shoebill (Guillet et al. 1985) was more or less ignored by the scientific community. It was not until 1993, when Russell and Thomason, in a paper on the biomechanical consequences of the mammalian palate, again pointed to the potential of FEA in analysis of vertebrate structure. Two years later, Thomason et al. (1995) demonstrated that the mammalian palate increases torsional stiffness during bite by using FEA. At the same time, Rensberger (1995, 2000) applied FEA to the mechanics of mammalian teeth. He was able to show that the microstructure of mammalian enamel corresponds with stress concentrations within the enamel determined by FEA. Only few other workers (Marx 1994, Pfretzschner 1994) followed his approach to verify the mechanical behaviour of teeth. Especially in mammals the FE models had to be rather simplistic because of the complex arrangement of prisms in mammalian enamel. In reptiles, the biomechanical behaviour of teeth is only poorly understood (Sander 1999) and comparable analyses using FEA have not been carried out so far.

To date, only a small number of further research projects on tetrapod skull mechanics using FEA have been attempted outside the fields of human medicine and primatology. Daniel & McHenry (2000) modelled the skull of *Alligator mississippiensis* and analysed the force transmission during bite. The incorporation of muscle loading allowed to complement previous work, in which the skull was treated as a beam. The same approach was followed by Rayfield et al. (2001) to investigate the force transmission patterns in a geometrical accurate model of the skull of *Allosaurus.* With the reconstruction of the adductor muscle force, it was possible to demonstrate that the bite of *Allosaurus.* must have been relatively "weak" (Rayfield 2001: 1033). This is in contrast to the high cranial strength of the skull as determined by FEA, which would allow much higher forces before failure of the bones. Rayfield et al. (2001) explained this discrepancy by an "overbuilt" skull (i.e. high safety factor) and proposed high impact forces during biting. However, the putative inconsistency

may represent an artifact of the model (see section on "Methods" for this problem in FEA) or may be caused by other factors, which are not scientifically accessible (Reif 2003).

Her work was continued in 2004 and 2005, by investigating a model of the skull of *Tyrannosaurus rex*. However, this time this did not used a quantitative approach but compared the consequences of two alternatively skull models for the stress regimes (Rayfield 2004, 2005). Whereas the first model was akinetic, the second one included mobile joints similar to the one present in the skull of *Tyrannosaurus rex*. Rayfield (2004, 2005) was able to show that the mobile joints in the skull model had a shock-absorbing effect and she referred the robusticity of the nasal of *Tyrannosaurus rex* to a peak of compressive and shear stresses in this region.

In 2002 Jenkins et al. investigated the biomechanics of synapsid rostra based on FEA. The analyses were based on previous work on the biomechanics of carnivore and primate skulls and the influence of cranial sutures on force transmission. By comparison of the different force transmission patterns, the authors deduced the existence of specific trophic ecotypes within synapsids. In the same volume, Preuschoft & Witzel (2002) expanded their former work on FEA of skulls of humans and other primates to the biomechanical investigation of other mammals and reptiles. The approach used by the authors ('virtual synthesis') differs from others by not analysing accurate models but an unspecific homogeneous solid model on which the initial conditions (functional spaces for the eye openings, muscle forces, and the placement of the dental arcade, including assumed bite forces) are applied. Based on the resulting stress patterns, non-stressed areas can be identified and removed, leading to change of the shape of the model. The reduction of shape is repeated iteratively, producing a more exact form which corresponded well with the arrangement of bony material in the relating skulls. Hence, Preuschoft & Witzel (2002) concluded that the relative shape and length of the tooth row is determined solely by the stress patterns and not by the selective influence of lifestyle characteristics. Both authors also presented a virtual syntheses of a *Diplodocus* skull using FEA (Witzel & Preuschoft 2005).

All these analyses using FEA carried out so far, demonstrated that this tool has a high potential for testing biomechanical hypotheses and to extend previously simplistic approaches to a level which hitherto has not been possible. However, it still has to be evaluated whether FEA really is vital for the questions in concern or if a more simple or more abstract model will be more adequate, considering the need for relatively sophisticated and expensive hard- and software. Despite a possible strong resemblance of finite element models to the "real" objects, FEA is based on a idealisation and simplification and therefore on a reductionist model (Fastnacht et al. 2002). The results may look more accurate, but may not be more reliable than that of other methods. Furthermore it is the lack of basic data and inadequate boundary conditions, especially in fossil taxa, which may produce numerical correct results but which does not represent the natural conditions. Thus, a careful evaluation of these influences on the assumptions is vital for any FEA.

2. THEORETICAL FRAMEWORK

2.1 Definitions, concepts and paradigms of biomechanical research

Despite a long history of research on vertebrate mechanics, the terminology often lacks a common, unequivocally accepted definition. This is especially evident in the case of the terms "biomechanics", "functional morphology" and "constructional morphology". Therefore, these terms are briefly discussed here.

2.1.1 Biomechanics

The term "biomechanics" is generally applicable to the mechanical behaviour of a structure or partial structure. According to Zweers (1985) structure itself is defined as "any distinguishable extension in space, that can be measured in terms of distance, position, size and/or shape" (Zweers 1985: 255). Each structure possesses certain material (mechanical) properties, which will result in a specific response when loads are applied. This response, called biomechanical behaviour, is related to the entity studied. Compact bone for example will react viscoelastically when loads are applied until a certain point, after which it starts to yield until fracture occurs (Currey 2002). If the loads are applied over a long period of time with a small gradient, even creeping is possible (Bowman et al. 1994). This behaviour is characteristic for bone and differs from other structural materials. Additionally, a system or subsystem shows a biomechanical behaviour: a leg may behave under certain aspects similar to a spring (Alexander 2003, Biewener 2003) or a muscle can be compared to a pneu (Otto 1995, Herkner 1999).

The mechanical response of a material or a structure strongly depends on the character of the load applied. Bone resists tension and compression well, but is especially susceptible to failure caused by shear or torsional loads. This fact is accounted for by listing different material properties, e.g. bending strength, compressive strength etc. The architectural configuration of a material also influences its mechanical behaviour. Compact bone e.g. reacts different than cancellous bone. Even only microstructural differences between distinct taxa will lead to measurable differences of the mechanical properties of the same material. Finally, it is the choice of the methods, conditions and testing apparatus used who may result in different values for the same species. Dry bone e.g. behaves different than fresh, wet bone or different degrees of mineralisation e.g. in the equine radius will result in a different biomechanical behaviour (Currey 1999).

2.1.2 Functional morphology

While the term "biomechanics" can be used as a general term, "functional morphology" specifies a structure under a given function or the functional correlation between different individual elements of a structure (Nachtigall 1991, Dullemeijer 2001). From a methodological point of view, the functional investigation is focused only on the elements of an organism/structure relevant for the function of interest (e.g. the leg of a walking animal or the enamel microstructure of a tooth), neglecting non-functional aspects. The functional analysis itself is based on principles from physics, engineering and secondarily chemistry and cybernetics. Whereas a pure description of a given morphology can only be typological, the functional morphologists seeks to explain the structure as a specialisation to a certain function. Function can be either understood under an etiological or historical view as the task "for which it was designed by natural selection" acting in the past ("selected ef-

fects" after Neander 1991: 173) or under an ahistorical view as a contribution to the capacity of an organism regardless of its history (Amundson & Lauder 1993-94).

Considering the evolutionary history of organisms, there has been a long debate whether form follows function or vice versa (Padian 1995). Most contemporary evolutionary biologists would agree that form is constrained by function or, alternatively, that the analysis of form allows to predict its functions. This is only partially accepted here. Even in extant taxa, unexpected functions of a structure are common (Lauder 1995) as a structure usually does have several functions simultaneously and functions which may not be discernible. As Lauder (1995) demonstrated, the correlation between structure and function of the muscoskeletal system in living animals may be erroneous or even a circular argument. Predicting function in fossil taxa is even more problematic, albeit "phylogenetically appropriate" extant "model taxa" may exist (Rudwick 1964, Reif 2003). Especially for newly developed structures or structures without known counterparts in extant organisms, functional explanations may be limited to speculations.

In consequence, the expression "adaptation" has to be limited to a very narrow scope. Adaptation as defined by Simpson (1953) and Bock & Wahlert (1965) is the fact that an organism cannot exist without its specific habitat; this trivial definition may be misleading since reason and consequence can easily be mixed up (for a more broader definition see Mahner & Bunge 2000). Commonly, adaptation is used with the often teleological concept of an active adjustment to changing environmental conditions. This "active adaptation" is true in only very specific cases like e.g. the reaction of a sense organ to changed physical conditions, the increasing number of red blood cells to compensate a decreasing oxygen level or the modification of bone structure in the light of a changed mechanical environment (Wolf 1892). In an evolutionary context, adaptationism is hard to quantify and epiphenomena may be mixed up with causes (Gould 2002). The strict adaptionist concept implicates that organisms are optimally fitted to their surrounding (and only to this) environment (Bonik et al. 1977c), whereas organisms can alternatively be viewed as being "good enough to survive" in their environment (Reif et al. 1985). The latter view does not object trends of optimisation but admits different levels of optimisation and even the existence of apparent non-optimised animals (although after Reif (2003) all living organisms show a high degree of adaptation).

An idealised approach of a mono-functional optimisation is common in functional morphology. The optimisation is measured as a better performance, ignoring structural or historical constraints and further utilitarian functions. This "atomistic" approach is not practicable in explaining organismic structures or even the organism itself. In a "holistic" organismic context, optimisation never reaches an absolute maximum and only represent local maxima in the possible morphospace (Schmidt-Kittler 2003, pers. comm.). For all these reasons, the adaptionist program has been under heavy attack, although this often merely concerns issues of terminology (e.g. Gould & Lewontin 1979, Gould & Vrba 1982, Levinton 2001, Pigliucci & Kaplan 2000, Reif 2003).

Less problematic and ideologically tainted is the use of the term "specialisation". An organism may be specialised in a certain way, but this does not exclude other evolutionary traits or new environmental options as long as the specialisation is not unfavourable in a new environment. A specialisation may be subject to a functional change and may give rise to new structures or allow to inhabit new environments. Generalists often lack specialisations seen in more specialised organisms, although they are adapted too, since no living animal can survive with a low degree of adaptedness (Reif 2003).

Another term closely related to functional morphology is "biological role", which is often mixed up with function. It was introduced by Bock & Wahlert (1965) to specify the role of a structure in a specific environmental setting. In contrast to a specific function, the biological role of a structure includes all the actions or uses of the structure by the organism in the course of its life history (Bock & Wahlert 1965). The biological role can only be determined in the natural environment and not by artificial conditions e.g. in the laboratory (Bock & Wahlert 1965). Although more comprehensive than the pure mono-functional concept, the verification of the biological role in fossil taxa and organisms whose life history is not known, is not possible (Bock & Wahlert 1965).

2.1.3 Constructional morphology

Like functional morphology, the fundamentals of constructional morphology are based on nomological-deductive explanations (Bock 1991), namely from physics and mechanics. However, where functional morphology only investigates functions of specific structures, constructional morphology considers organisms as integrated entities (Weber 1958, Gould & Lewontin 1979, W.F. Gutmann 1987). In this context, an organism cannot be reduced to an assemblage of different detachable functional units but represents a coherent object, comprised of interdependent and force transmitting operating parts (Herkner 1999). These must be arranged in a pattern that permits the organism to operate, i.e. energy input and conversion must be possible (W.F. Gutmann 1989, 1992, M. Gutmann 1996). The German term "Kraftschluss" for the coherence at the level of structured organisms (M. Gutmann 1996) has to be avoided, since it is already preoccupied in mechanics where it defines a special type of connection, solely characterising force transmission by friction (Beitz & Grote 1997). Since constructional morphology uses mechanical terminology, such ambiguities must be avoided. Instead the term "traction" is proposed here as a proper description of coherence. If non-mechanical aspects are considered for coherence, the term "capacity" can still be applied as a measure of efficiency (Herkner 1999).

The process of interpreting the mechanical operation of a structure determined by its structural properties and the way it is assembled is referred to as "construction". Originally proposed as a German term ("Konstruktion"), there have been debates whether these terms really have a similar meaning in both languages. Whereas Bock (1991) suggested the use of the German term, others favoured the English translation (e.g. Reif 1982, Reif et al. 1985, K. Vogel 1989b, 1991). Recently, Salisbury (2001) postulated the incongruent use of this term in both languages. However, the pertinent references in both German and English language (Duden, Oxford Dictionary) disagree with this view. The English term is thus used in this work in accordance to other morphological literature.

To interpret aspects of form and optional operational ranges, organisms can be viewed as analogues to machines (Erlach 1994, Fastnacht et al. 2002, M. Gutmann 1996, W.F. Gutmann & Bonik 1981, W.F. Gutmann & Weingarten 1991, W.F. Gutmann & Edlinger 1994a, D.S. Peters & W.F. Gutmann 1973, Herkner 1999, Rudwick 1964, Salisbury & Frey 2000, Weingarten 1994). Machines need energy input to operate and have to be structured in respect to their mode of operation. The structure can only be specified as long as the machine is working, i.e. as long as the machine is coherent. As soon as the machine stops, it is no longer coherent, because there is no longer actively driven force transmission. Although the pieces are still connected and the structure is still existent in its position, energy conversion (work and performance) has stopped. The term "coherence" not only comprises active force transmission and the fact that all parts of the machine have to keep together,

but it additionally includes the non-mechanical aspect of energy conversion, which is necessary to allow the machine to work. The nature of the energy input is predetermined by the structure of the machine (Herkner 1999).

Like machines, organisms have to be coherent to work by energy conversion and force transmission. Like in machines energy input is needed to permit functioning . Because of this correspondence, certain aspects and principles of organismic operation can be reconstructed by coherence and on the level of a engineering model. Whereas the functional aim of machines is pre-defined and the design engineer has to develop the structure according to the machine`s future use, the structural relations in organisms must be re-constructed (Herkner 1999). It has to be emphasised that the machinery paradigm is not consistent with the view that organisms or parts of organisms are machines as proposed by Descartes (see Ablondi 1998) and other authors (e.g. Bock, 1989, Driesch 1935, Graber 1886a, 1886b). In constructional morphology machines are not models *of* organisms but models *for* organisms (W.F. Gutmann & Weingarten 1992, Weingarten 1994). This paradigm is further specified by stating that machines are used *as models* for models of organisms. They are referred to as organismic constructions or bionomic constructions, the latter incorporating regenerative aspects of ontogeny and reproduction (M. Gutmann & Herkner 1992). Like in machines, the bionomic construction determines its performance and the optional operational range and environment. Unlike the design process of engineers for machines, functions in bionomic constructions are not implicated per se, but originate as constructional options. This view contradicts considerations used in functional morphology where the number of parts of an organism is viewed as a proxy for the number of functions (McShea 2000).

A second difference between bionomic constructions and man-made machines is the fact, that the latter lack vitalistic attributes like automobility, autodestructivity and autonomy. For this reason, hypotheses about organisms which remain on the level of machine models are reductionist and may not be empirical attestable (Nida-Rümelin 1994). Especially in the publications of the "Senckenberg Arbeitsgruppe für Phylogenie" (SAP) this reductionism is common (Nachtigall 1991, Rieß et al. 1989). The concept of reductionism in science has been the topic of hot debates (Penzlin 1994). Besides an inevitable epistemological reductionism, "holistic" theories can only be erected by combining "sub"-theories from various scientific approaches including independent models of and for different aspects of the topic at issue (Mahner & Bunge 2000). Consequently, the machinery paradigm is not holistic, but only represents one possible approach. Predictions from a model level without reference to real but only schematised organisms are *per se* without scientific, explanatory content (Rieß et al. 1989). By abandoning the dogmatic view of explanatory ultimateness, constructional morphology can have evidential value for analysing organisms and their phylogeny as will be demonstrated here. Furthermore, constructional morphology is one of the essential fundamentals for the analysis of fossil ecosystems (Boy 1998, 2003).

2.2 Vertebrates as bionomic constructions

Mechanical coherence of vertebrates (and all other organisms) starts on the molecular level. The actine-myosine reaction, enzymatic catalysis, the energy transfer by ATP or neuronal activity are examples for coherence at the level of physiological processes (Bonik 1977, Edlinger 1992, Fastnacht et al. 2002, W.F. Gutmann & Edlinger 1994b, S. Vogel 2001). However, the molecular aspects especially on a morphogenetic level are poorly understood (Fastnacht et al. 2002).

On cellular level, biochemical reactions take place in an operationally enclosed hydraulic compound. The individual cell can be regarded as a mantle-infill-construction with a mantle of low bending resistance and a filling, which only can transmit compressive forces (Herkner1999). This model is different from the term "pneu" proposed by Otto (1995), which lacks the differentiation between purpose-aimed and "natural" mantle-infill-constructions. Originally this model is based on fillings by air (for further details see Herkner 1999).

Besides the machine model, the hydraulic approach was used extensively not only by several members of the SAP but also others scientists to explain operational aspects of soft-part organisms (Alexander 1968, Bonik 1976, 1977, Bonik et al. 1976a, 1976b, 1976c, 1977a, 1977b, Chapman 1974, Clark & Cowey 1958, Gudo M. & Ammar M. 2001, W.F. Gutmann 1972, 1973, 1989, 1994, 1996a, 1996b, W.F. Gutmann & Bonik 1981, W.F. Gutmann & Edlinger 1994b, W.F. Gutmann & Weingarten 1988, Harris & Crofton 1957, Herkner, 1999, Kier 1982, 1985, Kier & Smith 1985, Koehl et al. 2000, Kull 1994, Wainwright 1970, Wainwright et al. 1976). Models for vertebrates can be constituted by applying hydraulic principles to explain the maintenance of body form and especially muscular activities (Gutmann 1973, Frey et al. 1993b, Herkner 1989, 1999, Salisbury & Frey 2001). Similar to the machine model, the hydraulic approach is useful only to interpret certain aspects of the morphology and operation of organisms (Gläser 1995, Herkner 1999), rather than presenting a holistic approach.

By the combination of the machinery models with hydraulic principles, the interpretational scope of the model for the organism will be expanded (Mahner & Bunge 2000). Organism can be interpreted as structured, coherent entities who actively transmit forces by energy consumption. The structures can be viewed as subunits of a mantle-fill-construction based on the hydraulic model or as mantle-fill-constructions of their own which need energy to operate (Herkner 1999).

In vertebrates (and analogous in other organisms), the organs and the different tissue types including bones can be interpreted as such subunits. They are integrated, interdependent elements in the operating entity of the organism (or, more exactly, the model for the organism). The coherence is ensured mainly by connective tissue containing tensile fibres. Important tissues of this type are the areolar (in the omentum), elastic (e.g. ligaments or elastic cartilage), firm (e.g. in the Dura Mater), and collagenous connective tissues (non-elastic, as string or plate-like binders e.g. in tendons or aponeuroses) and the reticular fibres (consisting of tensile and bending resistant fibres arranged in a meshwork) (Fastnacht et al. 2002). These tissues determine the form of hydraulic elements such as organs, adipose tissue and air or liquid (e.g. blood, lymph, urine, adipose tissue) filled cavities. In most cases, the form of the hydraulic subunits is not spherical like in an ideal model, but influenced by interactions between different elements. The hydraulically stabilised meshwork of connective tissue is referred to as bracing system (Frey et al. 1993, Herkner 1999). It ensures maintenance of the body form and active force transmission by muscular activity.

The hydraulic system of organisms is controlled by muscles which permit enlargement and contraction of a cavity filled by a fluid (Chapman1974). The tongues of mammals and reptiles, the penis of mammals and the trunk of elephants are examples for such muscular hydrostats (Kier 1992, Kier & Smith 1985). Even muscles can be viewed as hydraulic elements (Herkner 1999, Kier 1992, Kier & Smith 1985, S. Vogel 2001, 2003), consisting of contractile muscle cells anchored in the connective tissue network. The tensile forces produced by shortening of the muscle fibres along their axis can be transmitted via intermitting tensile phases such as tendons or ligaments by surpassing the periosteum directly into the bone. During the contractional phase, the

internal pressure of the muscle increases because of the incompressibility of hydraulic bodies. Bulging of the muscle takes place, causing compressive forces on adjacent e.g. bony surfaces (Teng & Herring 1998). Since muscles are unable to re-extend on their own after contraction, an antagonistic device must maintain coherence. This may be achieved by other groups of muscles, which will be placed under tension, elastic recoiling substances or by using non-muscular hydraulics or flow-induced pressure (S. Vogel 2001).

The insertion of muscles on stiff elements like bones in the vertebrate body adjusts and controls the mobility of these elements, which are constrained by the degree of freedom of their articulations. The whole arrangement can be viewed as a lever-system with non-compressive, non-tensile beams of relatively high bending strength (bone or cartilage) and tensile members which work antagonistically as controlling devices. Under the aspect of coherence, bone can be regarded as a mineralised phase of the connective tissue network (Fastnacht et al. 2002). Bony elements as well as dentine, enamel, cartilage and keratin are components of relatively high stiffness compared to soft-tissue. In the case of bone, these stiffening structures can be developed superficially (e.g. osteoderms, carapace and plastron) or internally as struts. Struts guarantee the shape constancy of a hydraulic construction. Keratin is only found superficially because of its epidermal origin and cartilage only as an internal stiffening structure (S. Vogel 2003). In contrast to cartilage, bone can not be viewed as an hydraulic stiffened structure as proposed by some authors (Kafka 1983, Otto 1995), because the viscous interaction of the marrow with the trabecular structure is negligible except for extremely high applied load rates (Arramon & Cowin 1997).

The mineralisation of bone is guided by the connective tissue and only induced non-pathologically in places where it is not in conflict with the operation of the organism i.e. force transmission within the organism (Carter et al. 1998). Hence, it is the mechanical regime which influences during histogenesis which kind of tissue is induced (Kummer 1961, Gooch & Tennant 1997, Pauwels 1980), constrained by developmental processes like the proliferation of progenitor cells. The molecular processes during this mechanotransduction are still poorly understood (Burger 2001, Cowin & Moss 2001, Gooch & Tennant 1997, Martin et al. 1998) .

The influence of the acting forces can be directly deduced by the change of the internal architecture of bones (Wolff 1892). This principle found its way into biological and medical teaching books as Wolff's law, but more correctly has to be called Wolff's theorem, because it does not represent a law in an ontological sense (Mahner & Bunge 2000). The theorem proves that in cancellous bone trabeculae are arranged according to the stress trajectories caused by external forces. A change in direction or magnitude of the forces would cause a rearrangement (remodelling) of the trabeculae, making bone a highly dynamic system reflecting the external loading regimes by its internal architecture. This process of adaptive bone remodelling has been investigated intensively in recent years, especially in human medicine, although its exact mechanisms are still poorly understood (e.g. Bagge 2000, Bertram & Swartz 1991, Boyde 2003, Brown 2001, Burger 2001, Cowin 2001, Cowin & Moss 2001, Currey 1984, 2002, Doblaré & García 2002, Fung 1990, Godship & Cunningham 2001, Gooch & Tennant 1997, Hazelwood et al. 2001, Lee et al. 2002, Martin et al. 1998, Morgan et al. 2003, Pauwels 1980, Prendergast & van der Meulen 2001, Ramtani S. & Zidi M. 2001, Turner 1992, Vincent 1982, Wainwright et al. 1976, Xinghua et al. 2002). The investigation showed that bone can be viewed only rather idealistically as an optimised structure; bone adaptation should rather be modelled as an optimisation process in progress. After Bertram & Swartz (1991) the paradigm of Wolff's trajectorial theory may have been too easily accepted and came across as a "conceptional blinder", so that other potentially important factors were

never taken into account. As Cowin (1997, 2001) demonstrated, Wolff's theorem is not based on real bones, but on a model of a bone using a false premise. These objections may explain why in some cases Wolff's theorem fails to explain certain phenomena which are observed on real bones (Meers 2002).

The corollary of Wolff's theorem, the determination of the mechanical behaviour of cancellous bone (i.e. the structure composed by multiple trabeculae) by the arrangement and mechanical properties of the trabeculae has been verified by *in vivo* measurements (Goodship & Cunningham 2001, Teng & Herring 1998). However, the trabecular structure including its anisotropy of architecture and material properties is hard to quantify (Odgaard 1997).

For constructional purposes, modelling bony elements can only be simplified, at least for practical reasons. This is also true for muscles and the different meshworks of connective tissue, which possess complex and distinct material properties. Although the investigation of such isolated tissue types *per se* is of little impact to understand the operation of an organism, it is essential to develop representative models for this purpose, because organisms are composed of interfacing elements of different material properties. The coherence must be destroyed to quantify the material properties, because *in vitro*-measurements are complex and technically limited. Coherence will be regained in the form of the model for the specimen and its operational simulation (Fastnacht et al. 2002).

2.3 Evolutionary pathways of bionomic constructions

Like organisms, bionomic constructions are be subject to ontogenetic and evolutionary developments. Ontogenetic changes are caused by structural decomposition in terms of abrasion, material fatigue and corrosion (Herkner 1999). These processes must be compensated by re-formation and structural replacement. The construction has to incorporate external material, because not all decomposition products can be used again (Herkner 1999). These are non-identical aspects in a construction which tends to remain structurally identical (M. Gutmann & Herkner 1992). Growth is caused by incremental material accretion during structural regeneration until its constructional growth limit. The non-identical reproduction processes will then lead to the collapse of the construction. The construction only maintains its entity through the reproduction of new autonomous, reproductive and coherent constructions. Again, this operation possesses identical and non-identical aspects. At this, structural changes are inevitable by retaining certain constructional invariants (Herkner 1999). An evolutionary process results only, if this change is irreversible e.g. by the loss of structures and the construction still retains its coherence and its bionomic properties (W.F. Gutmann & Weingarten 1988). Hence, in the context of constructional morphology, evolution can be defined as the gradual, irreversible transition between two types of bionomic constructions. The possible transformational changes are limited by various constraints (Alexander 1985, Bürger 1986, Dullemeijer 1991, Gould 1989, 2002, Maynard Smith et al.1985, D.S. Peters 1985a, Reif 1975, Reif et al.1985, Seilacher 1970, K. Vogel 1989a, 1989b). The historical-phylogenetic constraints describe the very basic principle that a new construction is liable to the constructional preconditions given by its ancestral construction. Without this, transformation series would not be detectable because all changes could be reversible or new structures could appear randomly. The occurrence of multiple evolutionary pathways as described by Bock (1959) can by explained by this type of constraints.

A second group of constraints are the functional/adaptive constraints (ecological/adaptive constraints in Seilacher 1970), which include internal as well as external aspects. The internal aspects are characterised

by coherence and active force transmission, without which the construction is not operational. The external aspects are more complicated, since they comprise the interaction between the organism and its environment which is often interpreted as a process "producing optimised solutions". The latter view is an idealisation since for only very few exceptions, organisms can not be viewed as being "optimally designed" but rather being "good enough" to survive (Reif et al. 1985). Because of coexistence of other constraints, only local optima are possible. Hence, the use of optimally "adapted" models is rather limited and may be misleading in interpreting organismic structure (see chapter 2.1.2).

Morphogenetic constraints are ahistoric. They are based on the limits of evolutionary change given by the laws of physics, chemistry and as included by Reif et al. (1985), cybernetics and geometry (architectural constraint in Seilacher 1970). This concerns the materials used in constructions with specific chemical and material properties as well as size limitations and effects (e.g. maximum cell sizes, adhesion, viscosity and inertia).

In the past decades, the importance of constraints has been questioned by so called "adaptationists" and "anti-adaptationists". Whereas the latter, initiated by the famous spandrels-article by Gould & Lewontin (1979), argued for a strong influence of constraints on evolution, the antagonists favoured the role of natural selection to explain evolutionary patterns. But as demonstrated by Lauder (1981), Lewens (2002), Reif (2002) and Sansom (2003), both views can be integrated into a framework of historical causal explanations by offering complementary arguments. The task of constructional morphology is to propose evolutionary processes and to reconstruct possible evolutionary pathways based on the determination of constraints. During evolution, these constraints define the optional organismic scope by naming possible operational variations and predicting *ad hoc* variations, which have no influence on the model of a specific mechanism. The resulting evolutionary pathway based on these transformation models are *per se* ahistoric. It is the impact of selection as an historical factor which affects whether and how often certain constructional levels were realised by "real" organisms. Hence, the evolutionary pathways of organismic constructions provide the polarity criterion for any phylogenetic reconstruction (D.S. Peters & W.F. Gutmann 1971). On a very low systematic level e.g. between species, the detection of these pathways may not be always possible, especially in case of exclusively fossil groups. K. Vogel (1989b) points out the difficulties to determine biomechanically based differential diagnosis and efficiency gradients in brachiopods. Here only propaedeutic methods like comparative morphology are applicable or the assessment of probabilities has to be used instead (Bonik et al. 1977, D.S. Peters 1972).

3. METHODS

3.1 Reconstructional method

3.1.1 Theoretical background

The aim of an evolutionary pathway diagram is to reconstruct the structural transformation steps leading from a starting construction to an end construction. For this purpose, organisms have to be interpreted by a constructional analysis using constructional principles determined by models. Constitution of a model inevitably involves simplification by disregarding "irrelevant" aspects. These aspects have to be specified and reasons for their omission have to be given. As Bonik et al. (1977c) pointed out, it can never be ruled out that alternative theories with the "irrelevant" aspects can be proposed. It is not possible to include the evolution of the complete organism with all it subunits and processes, only the evolution of partial aspects can be investigated (Bonik et al. 1977c). The constructional analysis of a 'partial model' has to consider how this aspect contributes to the overall bionomic and coherent construction.

To distinguish linguistically between constructional level and "real" organism, the genus-name is not put in italic and used with the term "construction" when constructions are concerned (e.g. the Anhanguera skull construction, based on the pterosaur genus *Anhanguera*).

Furthermore, for a better readability special anatomical features will be addressed to by their anatomical names also on the constructional level, although more precisely they should be specified only by their mechanical means (e.g. bars, struts etc.).

All recent or fossil organisms may serve as an end construction after interpretation as a bionomic construction (W.F. Gutmann & Bonik 1981). A theoretical end construction is possible, but only if it can serve as starting construction for a transformation to a recent or fossil bionomic construction. Starting constructions can be either hypothetical or recent or fossil bionomic constructions. They establish the morphological base (historical-phylogenetic constraints) for the evolutionary pathway and specify the basal operational range of the structures of interest.

The transformational steps between starting and end constructions are characterised by the irreversibility of structural changes and are canalised by functional/adaptive and morphogenetic constraints. All transformation levels must retain their bionomic coherence and must be operable (= not fail). The transformations are characterised by structural changes without any hiatus between successive constructions. These alterations can cause an adjustment of the operational ranges of the antecedent construction and lead to an increase in overall efficiency and the reproductive efficiency of the construction (*Ökonomieprinzip* after D.S. Peters & W.F. Gutmann 1971). This increase in efficiency can consist in a better utilisation of already used energy sources or by making so far non-accessible sources available ('economisation' in Bonik et al. 1977c). A second possibility is to keep the energy amount constant but to improve the internal conversion (D.S. Peters 1985b, 'optimisation' in Bonik et al. 1977c). These principles do not necessarily imply simplification of structures. An increased complexity is "advantageous", if the overall efficiency is increased and the construction retains its bionomic coherence (Bonik et al. 1977c). An increase of efficiency of certain performances by structural changes may simultaneously lead to a decrease in other performances, making it important to consider the consequences for the bionomical coherence of the construction and for the overall reproductive efficiency. Certain performances may even decrease in efficiency, e.g. the reduction of limbs or organs, if the overall efficiency is not reduced

by this process (Herkner 1999). Under these aspects, selection can be understood as an evaluation of the energy expense of a bionomic construction (Herkner 1999).

The evolutionary pathways as anagenetic systematics are not similar to a phylogenetic tree or a cladogram, although they too may show branching points leading to different end constructions (D.S. Peters 1972). The pathways do not imply genealogical affinities between the branches since, from a methodological point of view, it can only be determined which premises have to exist for a certain pathway and not how often these pathways were realised during the course of evolution. The reconstruction of evolutionary pathways may lead to transformations to merely hypothetical constructions (Herkner 1999). This is not reasonable, since it is the aim to designate recent or fossil organisms to the reconstructed evolutionary pathway and not to explain what may have come to existence. Pathways referring only to hypothetical constructions are without any scientific explanational value (Rieß et al. 1989).

3.1.2 Reconstructing a biomechanical transformation model for the evolution of skull biomechanics of pterosaurs in the operating regime "bite"

The anatomy of pterosaurs skulls is interpreted as an organismic construction in the operating regime of biting. Since pterosaurs became extinct at the end of the Cretaceous, the boundary conditions of the operating regime could only be set up by comparison with extant vertebrates. The transmission of forces by the teeth into the jaws and the influence of the special pterosaurian enamel pattern then could be simulated and analysed. To establish the basic biomechanical characteristics of the pterosaur skull construction, a model of a three-dimensionally preserved, fully prepared skull of Anhanguera was studied in detail by thin-sectioning, CT scanning, 3D modelling, space frame analysis, lever mechanics and finite element analysis (FEM). This included the reconstruction of muscular structures involved in the operation regime. These analyses were used to develop representative models for other pterosaur skulls, which were previously studied by the author or based on data from the literature. Determining the operational options based on the respective biomechanical behaviour, allowed to categorise the skulls. This was done by verifying invariable structural characteristics and features, which most likely represent structural variations because they result in similar operational consequences.

Between the different categories possible transformations and their operational consequences then were tested. This included irreversible (e.g. replacement of teeth by a keratinous rhamphotheca) as well as economical transformations (e.g. increased torsional, shearing and bending resistance). In all cases, anatomical coherence had to be maintained during the transformation. Only those transformations were considered to be irreversible, which resulted in an operational change by mechanical restriction, so that a reversal was not possible under the aspects of anatomical coherence/continual operation.

These steps lead to an interdependent meshwork of constructions including the constitution of intermediary hypothetical skull constructions to which no fossil skulls could be assigned to. By the designation of end constructions, the whole meshwork could be assembled into an evolutionary pathway diagram. Consequently, a hypothetical starting construction could be determined, as an expression for the beginning of the evolutionary continuum (Herkner 1999).

3.1.3 Comparison with phylogenetic analyses

The evolutionary pathway diagram was plotted against the cladograms proposed by Kellner (2003) and Unwin (2003), both representing the most actual and comprehensive analyses of the phylogenetic systematics of pterosaurs. The different species from the cladograms were assigned to the different constructional levels and the transformational pathways were integrated into the cladogram to see, if and how often the pathways were detectable in the cladogram. The differences were discussed in the light of the character analysis given by the authors and own observations at the skulls.

3.2 Topological-reconstructional methods

3.2.1 3D reconstructions of pterosaur skulls and rostra

To reconstruct the morphology and dimensions of the skulls, pterosaur skulls in the following collections were studied (institutional abbreviations in brackets):

American Museum of Natural History, New York, U.S.A. (AMNH)

- Bayerische Staatssammlung für Paläontologie und historische Geologie, München, Germany (BSP)
- British Museum of Natural History Museum, London, United Kingdom (BMNH)
- Forschungsinstitut und Naturmuseum Senckenberg, Frankfurt am Main, Germany (SMF)
- Institut für Geologie und Paläontologe, Eberhard Karls-Universität Tübingen, Germany (IGPT)
- Jura Museum, Eichstätt, Germany (SOS)
- Museo Civico di Scienze Naturali "E. Caffi", Bergamo, Italy (MCSNB)
- National Natuurhistorisch Museum, Leiden, The Netherlands (RGM)
- Goldfuß-Museum, Rheinische Friedrich-Wilhelms-Universität Bonn, Germany (GPIB)
- Staatliches Museum für Naturkunde, Karlsruhe, Germany (SMNK)
- Staatliches Museum für Naturkunde, Stuttgart, Germany (SMNS)
- Texas Memorial Museum, The University of Texas at Austin, Texas, U.S.A. (TMM)
- The Museum, Texas Tech University, Lubbock, Texas, U.S.A. (CM)

The data from species which were not housed in these collections were taken from the literature. In cases where no three dimensional skulls were present, the morphology was reconstructed by either taking and scaling the measurements from other specimens of the same species, published reconstructions or from closely related or generalised skull profiles. Tab. 3.1 lists the details for the species studied herein and the methods applied for three-dimensional reconstruction.

3.2.2 Sectioning

To get an impression of the internal architecture of pterosaur rostra, a partial, three dimensionally preserved rostrum was sectioned in the transverse plane. For this purpose, the rostrum was moulded in epoxy resin and cut into 14 slices, the anterior nine measuring 9 mm in thickness, the posterior 15 mm in thickness. The anterior and posterior surfaces of each section were digitised as tif-files using a scanner. The files were then imported into the graphic software package CorelDRAW™ (Corel Corporation) and the bony substance was traced by black lines.

Pterosaur taxon	Basis for reconstruction	Remarks
Angustinaripterus	Xinlu et al. (1983), Wellnhofer (1991a)	Ventral view generalised rhamphorhynchoid after Wellnhofer (1978)
Anhanguera	AMNH 22444 AMNH 22555 AMNH 25555 BSP 1982 I 90 BSP 1990 I 44 SMNK 2859 PAL	
Anurognathus	Döderlein (1923), Wellnhofer (1975b, 1978, 199a)	Ventral view generalised rhamphorhynchoid after Wellnhofer (1978)
Austriadactylus	SMNS 56342	Ventral view generalised rhamphorhynchoid after Wellnhofer (1978)
Batrachognathus	Rjabinin (1948), Wellnhofer (1978, 1991a)	Ventral view generalised rhamphorhynchoid after Wellnhofer (1978)
Cacibupteryx	Gasparini et al. (2004)	anterior end of skull interpolated
Campylognathoides	Wellnhofer (1974, 1978)	
Cearadactylus	Leonardi & Borgomanero (1985)	Ventral view generalised ornithocheirid after Wellnhofer (1987)
Coloborhynchus	RGM 401 880 SMNK 2302 PAL	
Criorhynchus	BSP 1987 I 46	
Ctenochasma	BSP 1920 I 57 BSP 1935 I 24 SMNS 81803 SOS 2197	
Dimorphodon	BMNH R 1034	Ventral view generalised rhamphorhynchoid after Wellnhofer (1978)
Dorygnathus	SMNS 50164 SMNS 52999 SMNS 55886	
Dsungaripterus	BSP 1980 I 44 (cast) SMNK without number (cast)	
Eudimorphodon	MCSNB 2888	Ventral view generalised rhamphorhynchoid after Wellnhofer (1978)
Gallodactylus	IGPT without number	Ventral view generalised pterodactyloid after Wellnhofer (1991a)
Germanodactylus	BSP 1892 IV 1 BSP AS I 745 SOS 21	Ventral view generalised pterodactyloid after Wellnhofer (1991a)
Gnathosaurus	BSP AS VII 369 SOS 1951. 84	after Wellnhofer (1978) Ventral view generalised pterodactyloid after Wellnhofer (1991a)
Huanhepterus	Dong (1982)	Ventral view generalised pterodactyloid after Wellnhofer (1991a)
Istiodactylus	BMNH R 3877	
Jeholopterus	Wang et al. (2002)	Ventral view generalised rhamphorhynchoid after Wellnhofer (1978)
Ludodactylus	SMNK PAL 3828	Ventral view generalised ornithocheirid after Wellnhofer (1987)
Nyctosaurus	Miller (1972), Wellnhofer (1978)	
Parapsicephalus	BMNH R 1613 (cast)	anterior end of skull interpolated
Peteinosaurus	Wellnhofer (1991a)	Ventral view generalised rhamphorhynchoid after Wellnhofer (1978)
Phobetopter	Wellnhofer (1991a)	Dorsal view generalised dsungaripterid after BSP 1980 I 44 (cast)
Plataleorhynchus	Howse & Milner (1995)	posterior end of skull and ventral view modelled after *Ctenochasma*
Preondactylus	Wild (1983b), Dalla Vecchia (1998)	Ventral view generalised rhamphorhynchoid after Wellnhofer (1978)

Tab. 3.1: Reconstructional detail for studied specimens. See chapter 3.2.1 for institutional abbreviations.

Pterosaur taxon	Basis for reconstruction	Remarks
Pteranodon	AMNH 149 BMNH R 4078 BMNH R 4006	Dorsal view after Wellnhofer (1978) and Bennett (2001a)
Pterodactylus antiquus	BSP AS I 739	Ventral view after *Pterodactylus kochi*
Pterodactylus elegans	SMNS 5802 SOS 4007 (*Pt. longicollum*)	Ventral view after *Pterodactylus kochi* *Pt. longicollum* similar skull to *Pt. elegans*
Pterodactylus kochi	BMNH R 3949 BSP I 1937 18a BSP AS IXI 3 BSP 1969 I 82 BSP AS V 29 BSP 1883 XVI 1 BSP 1878 VI 1 SOS 45-1 SOS 4592 SOS 4008	
Pterodactylus micronyx	BSP 1911 I 31 BSP 1936 I 50 SOS 4006	Ventral view after *Pterodactylus kochi*
Pterodaustro	BMNH without number (cast)	Dorsal view generalised pterodactyloid after Wellnhofer (1991a)
Quetzalcoatlus	TMM 41961-1 TMM 41954-62 TMM 42161-1 TMM 42422-30	modified after reconstruction by Kellner & Langston (1996) and 3D model by Langston (2001, pers. comm.)
Rhamphorhynchus	BMNH R 2786 BMNH R 37002 BSP 1867 II 2 BSP 1927 I 36 BSP 1929 I 69 BSP AS I 772 CM 11434 SMNS 52338 SOS 2810 SOS 4009 SOS 4599	
Santanadactylus	BSP 1982 I 89 SMF without number	Missing parts generalised ornithocheirid after Wellnhofer (1987)
Scaphognathus	GPIB 1304 SMNS 52295	Ventral view generalised rhamphorhynchoid after Wellnhofer (1978)
Sinopterus	Wang & Zhou (2003)	Dorsal view generalised pterodactyloid after Wellnhofer (1991a) and after skull models of *Tapejara*
Sordes	BMNH R 10044 (cast)	Ventral view generalised rhamphorhynchoid after Wellnhofer (1978)
Tapejara	AMNH 24440 SMNK PAL 2343 SMNK PAL 2839	Dorsal view generalised pterodactyloid after Wellnhofer (1991a) and after skull models of *Tapejara*
Thalassodromeus	Kellner & Campos (2002)	Dorsal view generalised pterodactyloid after Wellnhofer (1991a) and after skull models of *Tupuxuara*
Tupuxuara	Kellner & Campos (1989)	Dorsal view generalised pterodactyloid after Wellnhofer (1991a) and after skull models of *Tupuxuara*
Zhejiangopterus	Cai & Wei (1994)	Dorsal view generalised pterodactyloid after Wellnhofer (1991a) and *Quetzalocoatlus* reconstruction

Tab. 3.1 continued.

3.2.3 CT scanning and visualisation

Because the internal architecture of more complete skulls could not be obtained by sectioning, CT scanning was chosen as a non-invasive method. CT scans were made at the Klinik für Neuroradiologie at the Klinik der Johannes Gutenberg-Universität Mainz using a Siemens Somatom S CT scanner. Tomographic images were taken every 1 to 1.5 mm, relying on the anterior-posterior length and the quality of the specimen (see Appendix C).

The following pterosaur specimens were investigated by CT scanning:

- anterior portion of rostra and lower jaw of *Coloborhynchus robustus*, SMNK 2302 PAL
- upper jaw of *Coloborhynchus spielbergi*, RGM 401 880
- lower jaw of *Anhanguera sp.*, SMNK 1281 PAL
- upper jaw of *Anhanguera sp.*, SMNK 3895 PAL

The DICOM-images produced by the CT scanner were analysed using the software MiniViewer ConVis (ConVis Medizinische Datenverarbeitung GmbH & Co. KG).

Further data were yielded by CT scans made by the High Resolution X-Ray CT facility at the Department of Geological Sciences, University of Texas at Austin, USA. The scans are freely accessible at the Digital Morphology Library webpage (http://www.digimorph.org). The following scans are available:

- posterior part of skull of *Anhanguera santanae* (AMNH 25555)
- skull of *Rhamphorhynchus muensteri* (CM 11434)

3.2.4 3D Computer methods

The three dimensional model of the *Anhanguera* skull was created by import and batch processing of the DICOM images (from CT scanning) into the visualisation software package Amira™ 2.2 (Indeed - Visual Concepts GmbH). This software allowed a direct import of the model as a .stl-File (stereolithographic file) into different FEM solvers as well as the creation of a stereolithographic model of the skull. The model was analysed using the FE software ANSYS™ (SAS IP, Inc.). This work was done by Dipl.-Ing. N. Hess (Institut für CAE-Anwendungen of the Fachhochschule für Technik und Gestaltung, Mannheim).

Three dimensional models of the skulls of *Pterodactylus*, *Dimorphodon*, *Coloborhynchus*, *Santanadactylus* and *Pteranodon* were created for the import into the FE solver software, using Pro/Engineer™ (Parametric Technology) at the Institut für CAE-Anwendungen of the Fachhochschule für Technik und Gestaltung, Mannheim. The models were created on base of reconstructive drawings of the skulls, gained by direct observation on the fossil skulls. The models were then import into ANSYS™. Due to schedule limitations no further skulls could be investigated, because the work was done in the course of a student research project at the Institut für CAE-Anwendungen of the Fachhochschule für Technik und Gestaltung, Mannheim (G. Schlese & Y. Hamidon).

Whereas the model of the Rhamphorhynchus tooth was done directly and analysed in ABAQUS™ (ABAQUS, Inc) by N.Hess, the model of the teeth and partial jaw was created in Pro/Engineer™ and imported in ANSYS™. The latter work was part of a student research project at the Institut für CAE-Anwendungen of the Fachhochschule für Technik und Gestaltung, Mannheim (Berg 2002).

The space frame analysis of the model for the skull of *Anhanguera sp.*, SMNK 3895 PAL, was created using XRST™ 6.31 of the D.I.E. XEMiliy™ 2000 (A&T Wölfer Software). The bars were modelled as hollow, square bar wood (NH,GKIII(S7),LfH) from the material library of the software.

3.2.5 Reconstruction of jaw musculature

The reconstruction of the jaw muscles is based on a 200% scaled up stereolithographic model of the partial skull of *Anhanguera sp.*, SMNK 3895 PAL, made at the Fachhochschule für Technik und Gestaltung, Mannheim. The attachment areas of the muscles were identified by the occurrence of rugosities, crests, ridges or depressions on the original skull of *Anhanguera sp.*, SMNK 3895 PAL. The muscles were modelled with plasticine and attached to the model. Because of the overall weak muscular impressions, only the major muscles (Musculus adductor mandibulae, M. pseudotemporalis, M. pterygoideus anterior and posterior, M. depressor mandibulae) were reconstructed. They were assigned using comparative anatomy with crocodiles as the closest extant relatives of pterosaurs.

For the determination of the force vectors, the muscles were considered to be non-pennate. In this case, the physiological cross-section is identical with the cross-sectional area of the plasticine "muscle", which was measured with a calliper, scaled down to the original size of the skull and then calculated. Following the rule of thumb that 100 mm^2 of a muscular cross-section produces a maximum of 60 N (Tittel 1994), the maximum force was estimated for each muscle. The second method, proposed by Sinclair & Alexander (1987), for reconstructing the muscle forces is based on the mass of the muscle. The mass was calculated with a density of 1000 kg/m^3 and the resulting forces were calculated after the equations given by Sinclair & Alexander (1987). As these results are more inaccurate than the ones from the first method, they were only used for control.

The direction of the force vectors was depicted as arrows in lateral, dorsal, posterior and ventral illustrations of the skull including the designation of the areas of muscular attachments. Time-dependent changes in muscular force production were not accounted for.

The pattern reconstructed for *Anhanguera* was used for as a model for all other skulls investigated in this study, based on the fact that the architecture of the orbitotemporal region is rather conservative in pterosaurs. The areas of attachment and the direction of the force vectors were adjusted depending on the respective, partially reconstructed skull anatomy. For the FEA the amount of the muscular force vectors were considered to be identical independent of which species was investigated. This is due to high error range which makes a quantitative approach using absolute values rather speculative.

3.3 Numerical methods

3.3.1 Basic biomechanics

When forces (F) are applied to an area (A) of a structure, **stress** (σ) will result, defined as

$$\sigma = F / A. \quad (1)$$

If the value of σ is positive, the stress is called **compressive stress** (σ_c), if negative **tensile stress** (σ_t). Forces applied oblique to an area induce **normal stress** (σ_n) perpendicular to the area and **tangential stress** (σ_{xy}) in the plane of the area. If the forces are applied solely parallel to the area, only **shear stresses** will occur (τ). The stress a material can take before it fails, is called **strength**.

Stressing a structure will lead to a change in length of the structure. The ratio of change in length to the original length of the structure is called **strain** (ϵ). The relationship between stress and strain can be ascertained experimentally and plotted in a stress-strain-diagram (Fig. 3.2).

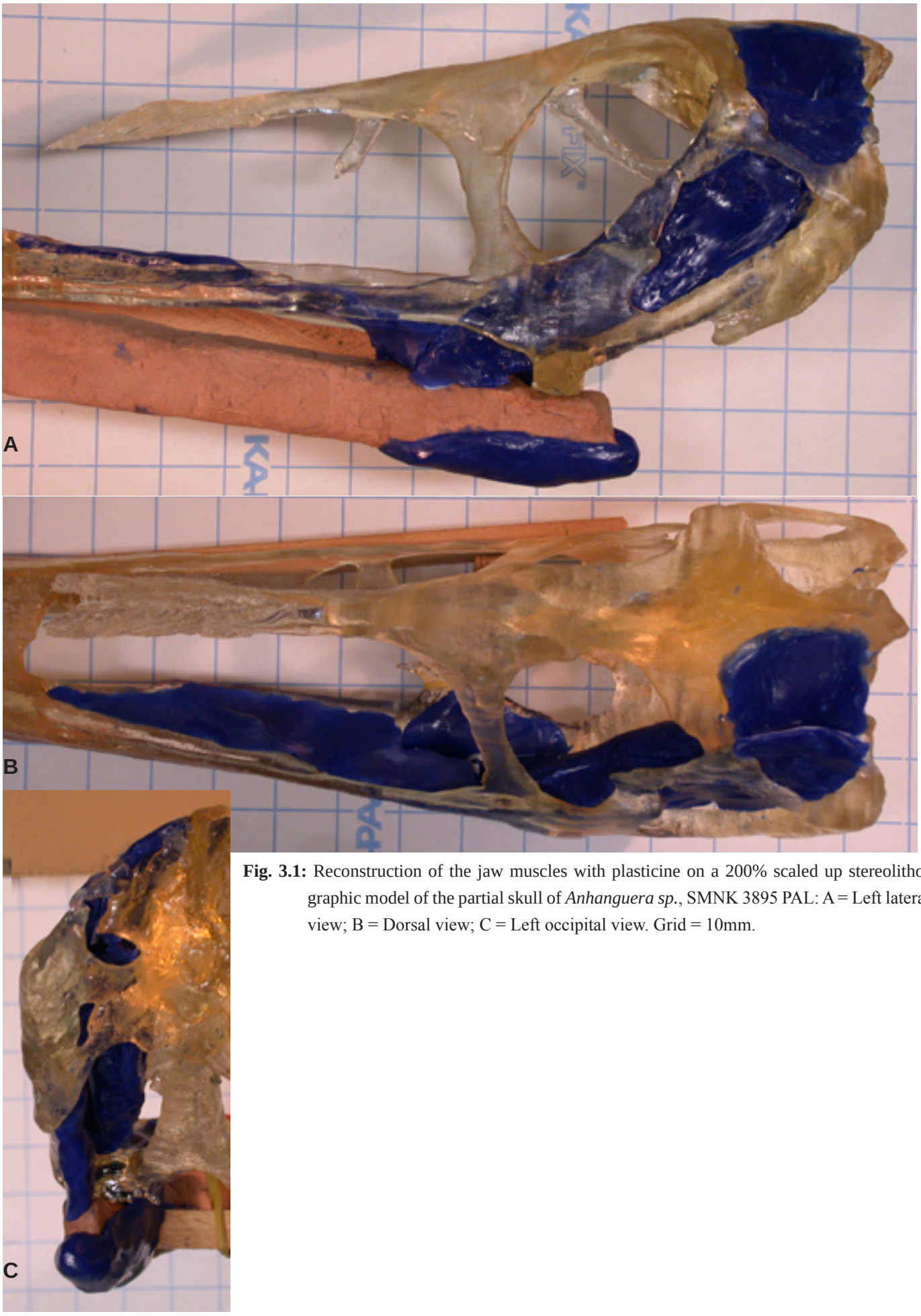

Fig. 3.1: Reconstruction of the jaw muscles with plasticine on a 200% scaled up stereolithographic model of the partial skull of *Anhanguera sp.*, SMNK 3895 PAL: A = Left lateral view; B = Dorsal view; C = Left occipital view. Grid = 10mm.

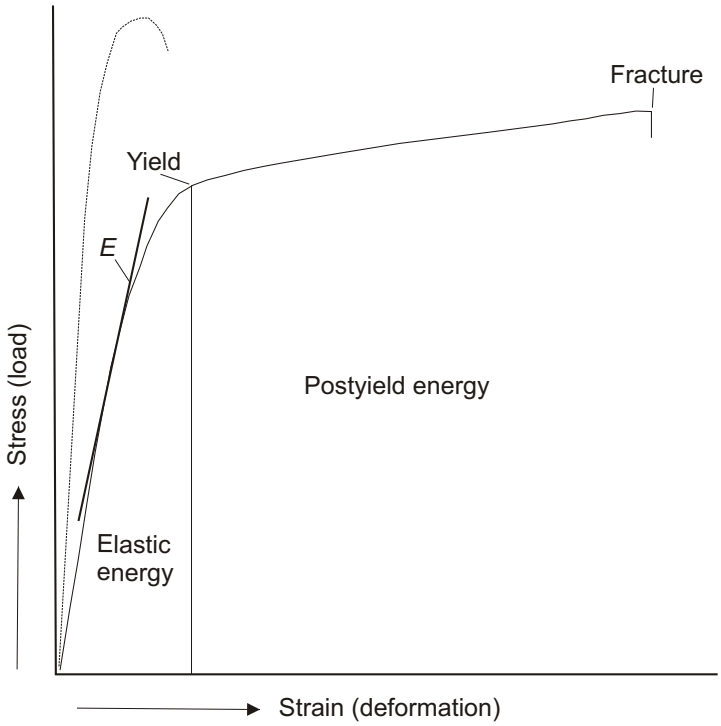

Fig. 3.2: Stress-strain curve of a bone loaded in tension. For tensile specimens, the curve is identical with the load-deformation curve. The material will behave elastically until the yield point, after which deformation is irreversible. The Young's modulus of elasticity is the angle between the tangent of the elastic part of the curve to the abscissa. Dotted line shows stress-strain-relationship of the same material in impact loading. After Currey (2002)

In the linear region of the curve, this ratio is called the modulus of elasticity (E) or alternatively the **Young's modulus** (of elasticity), defined as

$$E = \sigma / \epsilon. \quad (2)$$

Geometrically it corresponds to the tangent of the angle made by the curve to the abscissa. The steeper the initial part of the curve is, the stiffer the material is and the greater is E.

As the force F is directly proportional to strain ϵ, it is followed:

$$F = E \times \epsilon. \quad (3)$$

This equation is called **Hooke's Law.**

Accordingly in case of shear stress, the **shear modulus** (G) can be expressed by the ratio of shear stress (τ) to shear strain (γ). Both moduli, G and E are related to each other via the **Poisson ratio** (υ) with

$$E = 2G\,(1 + \upsilon). \quad (4)$$

The Poisson ratio is defined as the ratio of transverse strain to longitudinal strain.

G, E and υ are called **material properties**. Their values are specific for certain materials and are accessible by mechanical indentation tests or by non-invasive methods like numerical modelling, optical methods and others. The values of material properties used in this work are listed in Tab. 3.2.

Material	E (GPa)	υ	Ultimate Tensile Strength (MPa)	Ultimate Compressive Strength (MPa)
Bone	14.7	0.3	135	143
Enamel	84.1	0.33	10.3	297
Dentine	14.2	0.31	105.5	384

Tab. 3.2: Material properties of bone, enamel and dentine (after http://http://www.lib.umich.edu/dentlib/Dental_tables/intro.html, University of Michigan-NIDR Materials Science Research Center)

In most materials, the elastic and other material behaviours will vary according to the direction of loading. This means that the material is **anisotropic.** Another complication for predicting the mechanical behaviour will result when considering effects of specimen geometry or ontogenetically induced changes of mineralisation. To describe the elastic behaviour completely, a profound knowledge of the elastic constants is needed, measuring up to twenty-one independent elastic properties. The comprehensive description of the elastic behaviour has been proven to be very difficult with present-day techniques (Currey 2002). Even considering a material as **orthotropic** with three perpendicular planes of mirror symmetry will result in the need of nine measurements (three Young's moduli, three shear moduli and three independent Poisson ratios). An alternative would be to consider the material as **isotropic**, having similar material properties in all directions. For the investigation of bone, Cowin & Hart (1990) proved a significant error by modelling bone as isotropic in absolute values of the results. In contrast to view, Kabel et al. (1999) demonstrated that the concept of an effective isotropic tissue modulus is well usable for practical purposes and within confident limits of the results (5-15 % error range). Using isotropic material properties will inevitably lead to a simplified model, but the computational time for numerical analyses is drastically reduced at the same time. It has also to be considered, that the values of individual material properties have relatively broad limits of variation, depending on the methods and specimens from which they were obtained. Hence, exact results in a strict sense[1] analysing organismic materials cannot yet be achieved for biological and palaeontological purposes. Only in human medicine, the results are approaching more and more confident values, by using CRAY-supercomputers.

3.3.2 Loading cases, moments and stiffness of structures

The most basal loading cases are **compressive load**, **tensile load** and **shear** (Fig. 3.3B-D), for which each material has characteristic strength values (Tab. 3.2). A more complex loading pattern is **torsion**, caused by torque (= twisting moment). It results from of a force couple which acts in opposite directions, perpendicular

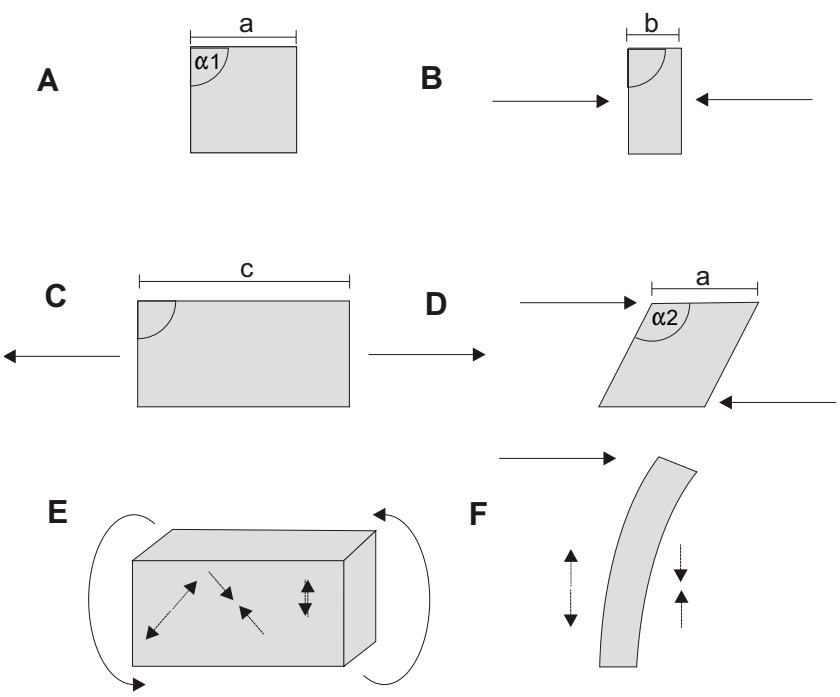

Fig. 3.3: Basic Stress regimes: A) Unstressed body with length a and angle α; B) Compressive forces acting on body: a decreases to b, α is constant; C) Tensile forces acting on body: a increases to c, α is constant; D) Shear forces acting on body: a is constant, α increases; E) Torque with tensile, compressive and shear stress (from left to right) in the body; F) Bending of body with tensile stress on concave and compressive stress on convex side.

1 Of course, the results are numerically exact in such a way that the mechanical behaviour a lower leg e.g. made of wood can be calculated exactly if all boundary conditions and material properties are known. However, this does not reflect the natural situation, in which a lower leg - with the exception of some extant pirates - is made of the much more complex material "bone".

to the axis of the structure (Fig. 3.3E). As a consequence, tensile, compressive and shear stress will occur in the body, twisting it.

Torsional stiffness and strength can be described in terms of the **polar moment of inertia** (*J*). It is a measure of distribution of material in the cross-section of a structure (Fig 3.4). For a solid cross-section the mathematical expression is as follows:

$$J = \pi\ (d^4/32) \quad (5)$$

with d = diameter of structure, for a hollow circle

$$J = \pi/32\ (d_o^{\,4} - d_i^{\,4}) \quad (6)$$

with d_o = outer diameter and d_i = inner diameter. More complex cross-sections can be described by derived equations.

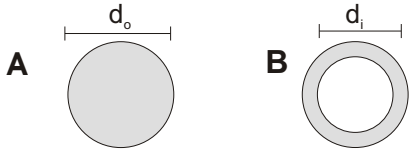

Fig. 3.4: Solid and hollow circle with outer diameter d_o and inner diameter d_i.

The greater *J* is, the greater is the resistance of a structure against torsion around the central axis. **Torsional stiffness** is the product of $G \times J$, where *G* (**Torsional Stiffness Coefficient**) is defined by

$$G = E / (2\ (1+ \upsilon)). \quad (6)$$

A second, complex loading pattern is **bending**. It is the result of two forces acting perpendicular to the axis of a structure, leading to tensile stress at one side of the structure and compressive stress on the opposite side (Fig. 3.3F). The non-stressed plane between both sides is called the **neutral plane**. Bending stiffness and strength can be described in terms of the **area moment of inertia** (*I*). Like the polar moment of inertia, it is a measure of the distribution of material in the cross section of a structure (Fig 3.3). For a solid cross-section *I* is defined as

$$I = \pi\ (d^4/64), \quad (7)$$

for a hollow circle

$$I = \pi/64\ (d_o^{\,4} - d_i^{\,4}). \quad (8)$$

Likewise, the value of *I* of more complex cross-sections can be calculated. The greater *I* is, the greater is the resistance against bending along an axis. **Bending stiffness** is the product of $E \times I$. The **bending moment** is defined as the product of $F \times l$. The **maximum bending stresses** σ_{bmax} can be calculated by the ratio of the bending moment to the **section modulus** *W* where the latter is given as $2I / d$.

The ratio of $(E \times I) / (G \times J)$ is called the **twistiness-to-bendiness-ratio**. The larger this ratio gets, the easier it is to twist a structure relative to bending (Etnier 2001, 2003, Etnier & S. Vogel 2000, S. Vogel 1984, 2003).

Bone is a material which is susceptible to failure by torsional, shear and bending loads. On the other hand, tensile and compressive forces are of little impact because bone has a high **axial stiffness**, defined as the product of $(E \times A) / l$ (A = area of structure, l = length of the structure). If compressive forces exceed the axial stiffness e.g. in relative slender or thin-walled bones, failure by buckling may occur. This takes place in form of **Euler buckling** or as **local buckling**. Whereas Euler buckling is the deflection of the whole structure, local buckling is the local collapse of a structure, seen e.g. when a aluminium beer can is crushed. For Euler buckling, the critical force can be calculated as

$$F_E = (E \times I \times \pi^2) / \ l^2 \quad (9)$$

where l = length of the column for basic case). Local buckling is much more complex than Euler buckling and the formula is rather empirical (Currey 2002). The critical force for local buckling is:

$$F_L = (K \times \pi\ (d_o - d_i)^2 \times E) / 4. \quad (10)$$

K is a semiempirical constant, ranging from 0,5 to 0,8 and depends on the imperfections on the structure at which local buckling can start (Currey 2002). Local buckling is the initial event in compressive failure of a structure. Because in pterosaurs *K* cannot be determined, Euler buckling was calculated as the critical parameter for axial stability.

For the biomechanical investigation of the pterosaurs skulls, the polar and area moment of inertia could be calculated by the dimensions of the reconstructed rostra. For simplification and as detected by sectioning and CT scanning, the rostra were considered to be hollow and the double-tube wall structure (see chapter sectioning) to be massive. Torsional stiffness and bending stiffness was calculated by using material properties of human compact bone, since the exact material properties of pterosaur bone can not be detected. Material properties of structural-analogous bird-bones are not known, too. The forces acting on the rostra were taken from the results yielded by the analysis of lever mechanics at defined coordinates (see chapter 3.3.3). Although this did not permit quantitative results, qualitative predictions could be made, especially by comparing different rostrum types.

In the case of isolated teeth, bending stiffness, bending moment and bending stress could be calculated and compared between the different tooth types. Torsional stress plays a minor role in teeth (see chapter 4) and was neglected in the investigations.

3.3.3 Lever mechanics

The study of lever mechanics is based on the study of a beam along which three elements are identifiable (Fig. 3.5): a) a **fulcrum** or hinge point, b) a point at a distance (l_1) from the fulcrum (**effort arm**) at which the force F_1 is applied, and c) a point at a distance (l_2) from the fulcrum (**load arm**) at which the resulting force F_2 move something (Fig. 3.5). The beam will remain motionless if $F_1 \times l_1 = F_2 \times l_2$. This means, that a body persists in relation to its rotating axis when the sum of the applying forces or moments (product of force and length) is zero. Whereas straight levers are fairly uncommon in organisms, angled levers can be identified at various levels (Fig. 3.5), e.g. the musculoskeletal limb system of vertebrates, which already was studied by Borelli in the 17th century (Schmidt 1706). The angulation is accounted for by including the angle in the basic equation (Fig. 3.5)

$$F_1 \times l_1 \times \sin\alpha 1 = F_2 \times l_2' \times \sin\alpha 2. \quad (11)$$

The ratio of l_1/l_2 is called **mechanical advantage**. In organisms, force arms are often very short whereas load arms are long, leading to a low mechanical advantage. As a consequence, large muscular forces are needed to move even small loads. However, by shortening of the muscles large load arms can be moved as fast as shorter load arms, allowing a more rapid closure e.g. of long jaws relative to shorter jaws.

The basic lever equation is valid only for static systems. For dynamic analyses when acceleration and mass are not neglectable, the equation of motion (principle of d'Alembert) has to be

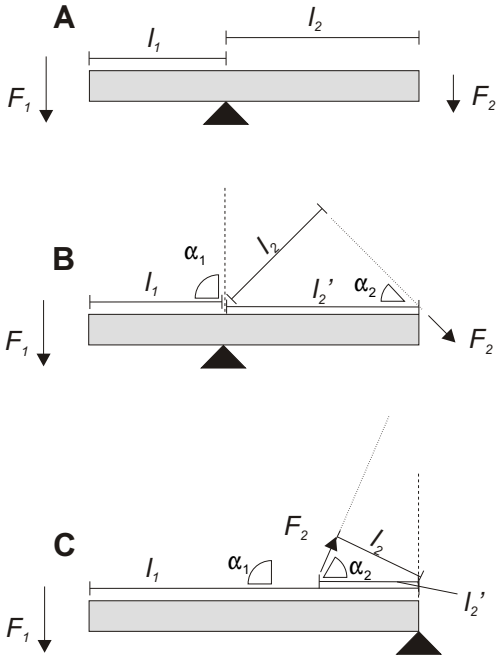

Fig. 3.5: Equilibrium conditions in a lever system: A) Straight lever; B) Angled lever; C) Third class angled lever with $l_2' = l_2 / \sin\alpha_2$; black triangle symbolizing fulcrum, l = lever arms, F = Forces, α = angles.

applied (Aerts 1990). In contrast to e.g. a weight-lifting arm, however, the bite of non-kinetic tetrapods can be viewed as quasi-static because loads are only applied to the upper jaw at the end of the closing phase. A dynamic analysis would only be necessary for the calculation of stresses in the lower jaw but would depend on such unknown parameters as food item weight, acceleration of the jaw e.g. by the jaw adductor muscles and friction of the medium from which the food is caught (water/air). Hence, all analyses in these work are calculated only statically.

A special case of a lever is a **cantilever**, which is fixed at one end and subject to bending moments M_b (Fig. 3.6), calculated as

$$M_b = F \times l. \quad (12)$$

Here the fulcrum is represented by the external surface of the object (= constraint), at which the cantilever is fixed. At this point bending moments and bending stresses reach their maximum.

In direction of the free lever arm, the bending moment approaches zero, whereas in a non-optimised case, the bending stress is zero at the outer end, too (Fig. 3.6A-D). This means, that the outer end is too massively built for the occurring stress. In an optimised lever, the stress remains constant at every point along the lever, which means that the bending moment is identical to the axial resisting moment (Fig. 3.6E-H). This is the case e.g. when the lower profile of the lever reaches the form of a quadratic parabola (Fig 3.6E).

Reducing bending stress is extremely important in bony skeletons, since in these loading regimes bone is very susceptible to failure. Strategies to decrease or neutralise bending stress are the incorporation of an opposing bending, tensile chords or compensation members (Fig. 3.7). The individual elements form a coherent, complex structure, in which local stress concentrations are normally avoided to maintain the operation. However, inherent weak spots are inevitable. Exceeding material strength by bending, torsional forces, or buckling will lead to failure of the structure (e.g. in the femoral neck in humans).

The analysis of the lever mechanics of pterosaur skulls was based on the reconstruction of the vectors of the adductor muscles in each skull. The lever arms of the different adductor muscles could be calculated and force distribution along the rostra could be determined. This permitted a qualitative comparison between different skulls and yielded the basic figures for the calculation of bending and torsional stiffness (see previous chapter). Possible devices for reducing bending stress like soft-tissue compensation by muscles or membranes then could be discussed under the aspect of coherence.

3.3.4 Calculations of biomechanical parameters

To calculate the biomechanical parameters listed in chapters 3.3.1-3.3.2, the reconstructions of the skull constructions were measured using Canvas™ 9 and Canvas™ X (ACD Systems, Inc.). All skull constructions were scaled to the same size with constant height at the level of the lower jaw articulation. The material properties were taken from Tab. 3.2. Internal measurements (wall thickness, size of internal vacuity) were scaled from the CT scans of *Anhanguera sp*, 3895 PAL. Muscle forces were taken as constant for all skull constructions, with values calculated from *Anhanguera sp*, 3895 PAL (Tab. 6.1).

Here, as well as for the 3D-analysis, the incorporation of certain connective tissue types and organs (e.g. skin, hairs, brain, orbita) was omitted because these were assumed to be irrelevant for the biomechanical behaviour during bite or because their material properties and mechanical behaviour could only be assumed by speculations.

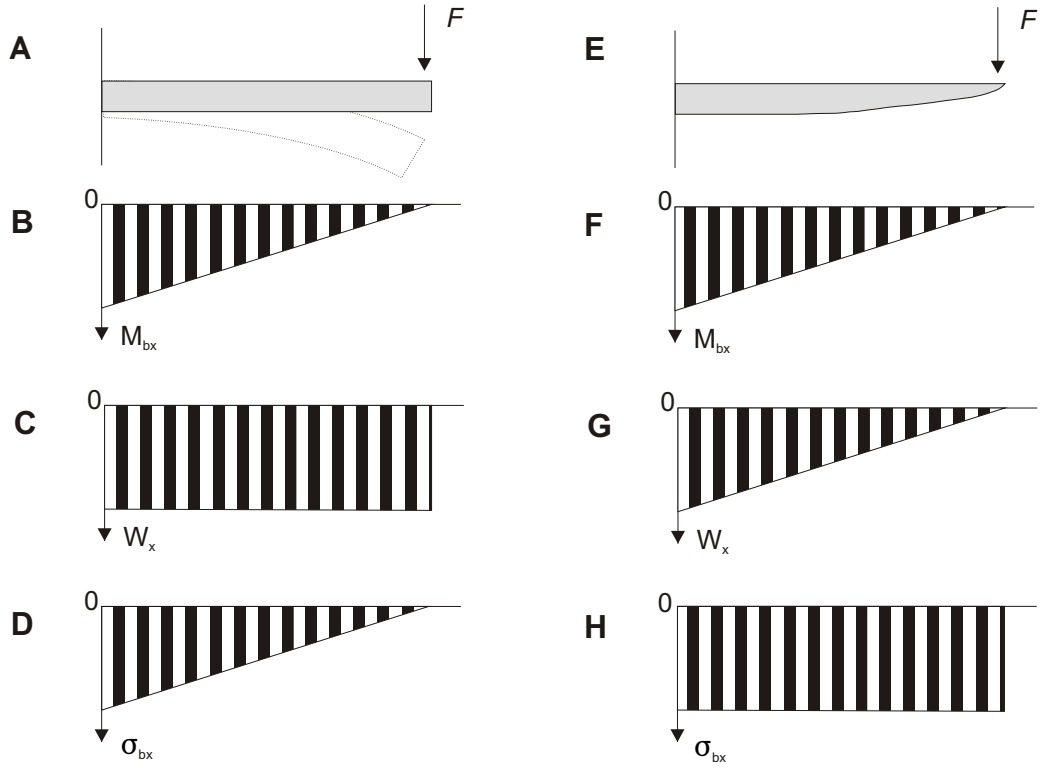

Fig. 3.6: Interrelation between bending moment M_{bx}, section modulus W_x and bending stress σ_{bx} with single load F at outer end: A-D) Non optimised, no moulding; E-H) Optimised with moulding as a quadratic parabola (after Nachtigall 2000).

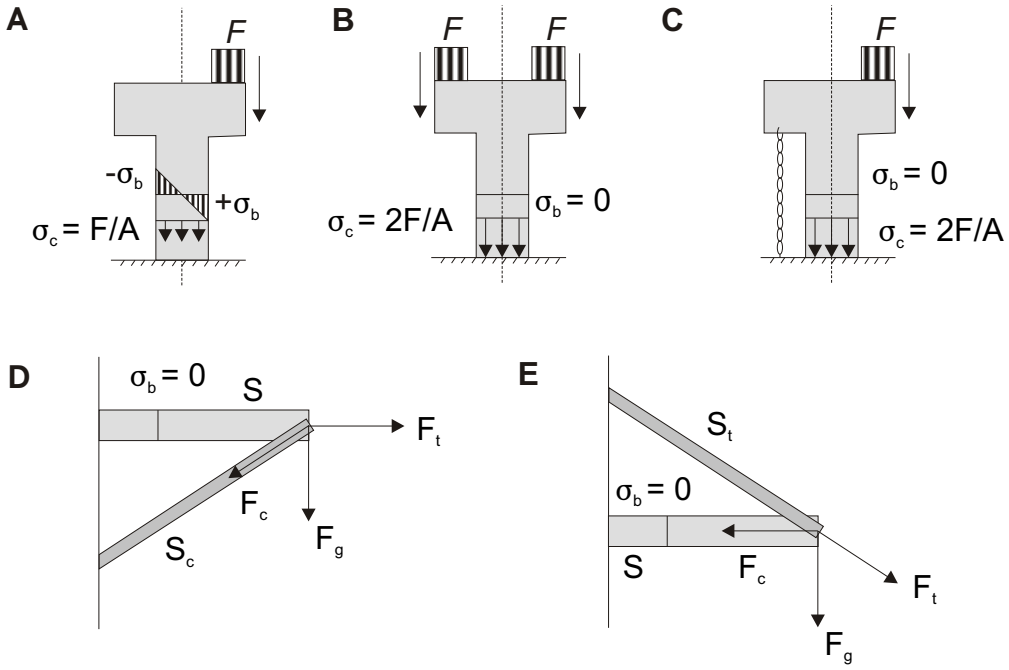

Fig. 3.7: Possible devices for compensation of bending stress: A) Bending loads in a double cantilever arm induced by unilateral loading; B) Neutralizing bending loads by bilateral loading, note doubling of compression loads; C) Reduction of bending loads by insertion of a tensile belt; D) Prevention of bending of a cantilever S induced by gravitation forces F_g by a compressive compensation member S_c, resulting in tensile forces F_t and compressive forces F_c; E) Prevention of bending of a cantilever S induced by gravitation forces F_g by a tensile compensation member S_t, resulting in tensile forces F_t and compressive forces F_c (after Nachtigall 2000). See text for further abbreviations.

3.3.5 Finite element analysis

Finite element analysis (FEA) is based on the elastic theory, which describes the response of a structure to an applied load:

$$\underline{F} = \underline{C} \times \underline{T} \qquad (13)$$

with $\underline{F}$ = force vector, $\underline{C}$ = stiffness matrix = $(E \times A) / l$, $\underline{T}$ = translation vector. As it is not possible to calculate the differential equations for stress and displacement of complex structures, FEA breaks this modelled structure into a limited ("finite") number of subsets ("element"). Each element is defined by a set of coordinates ("nodes"), which can be transformed into a global coordinate system by adding a transformation matrix and in consequence allow to collect the formulation of all elements into a single matrix. The global stiffness matrix then can be formed and stress distribution solved by numerical methods. The boundary conditions are the equilibrium of forces in the nodes and similar deformations at the interconnection between two elements.

In most cases FEA of structures can not be solved by hand and the use of special finite element software packages is needed. In case of the analysis of pterosaur skulls and teeth, ANSYS™ and ABAQUS™ were chosen, because these software packages are quite advanced and were available at the Institut für CAE-Anwendungen of the Fachhochschule für Technik und Gestaltung, Mannheim, which was the co-operation partner for this part of the project.

FEA involved the following steps (Fig. 3.8):

• 1. Simplification of the structure to a geometrical model (pre-process, Fig. 3.8 A)

This was done by creating 3D models of teeth and skulls in the CAD-software PRO/Engineer™ and import in the FE-software via iges-files. Unfortunately, this method caused extensive error-handling due to imperfect import. The Anhanguera skull was imported as stl-file from the 3D software AMIRA™ 2.2.

• 2. Discretisation of the geometric model in elements and nodes (pre-process, Fig. 3.8 B)

For meshing of the skull models, tetrahedron-elements were chosen, because they provided the needed accuracy in contrast to hexahedron elements, which would have been much faster to calculate.

The tooth models were meshed with about 5000 mixed shell/solid elements. As an increase in elements does not necessarily result in an increase of accuracy, less than 20.000 elements were used in meshing of the skull models. Using more elements decreases the accuracy because of multiplication of errors (Fig. 3.8). Characterising the number of elements as a indicator for exactness of the results as in Rayfield et al. (2001) therefore is not advisable, especially if the model is already based on simplified boundary conditions.

• 3. Setting of material properties (pre-process, Fig. 3.8 C)

In this step, the material properties were assigned to the elements. Here it had to be decided whether the properties were chosen as isotropic or anisotropic. The latter is time-consuming because the numerical solution is much more complex to calculate and anisotropic material properties are only poorly known (see chapter 3.3.1). The pterosaur skulls and teeth thus were analysed with isotropic material properties using values of human bone, enamel and dentine for practical purposes. No other method was applicable, because material properties of extinct animals are not ascertainable and properties of recent analogues of pterosaurs (e.g. birds) are not yet determined. In consequence, this decision permitted only qualitative and no quantitative results,

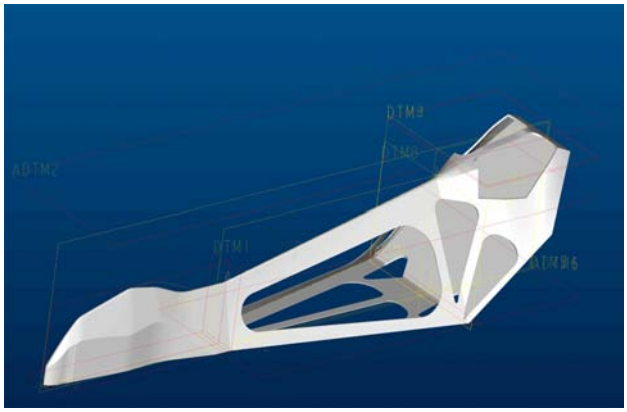

A

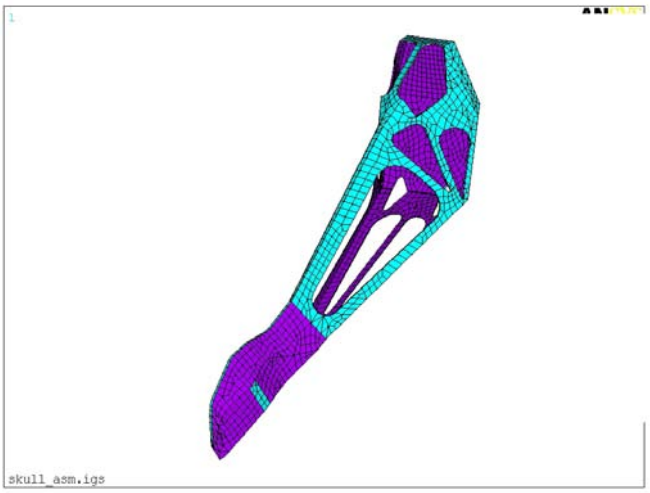

B

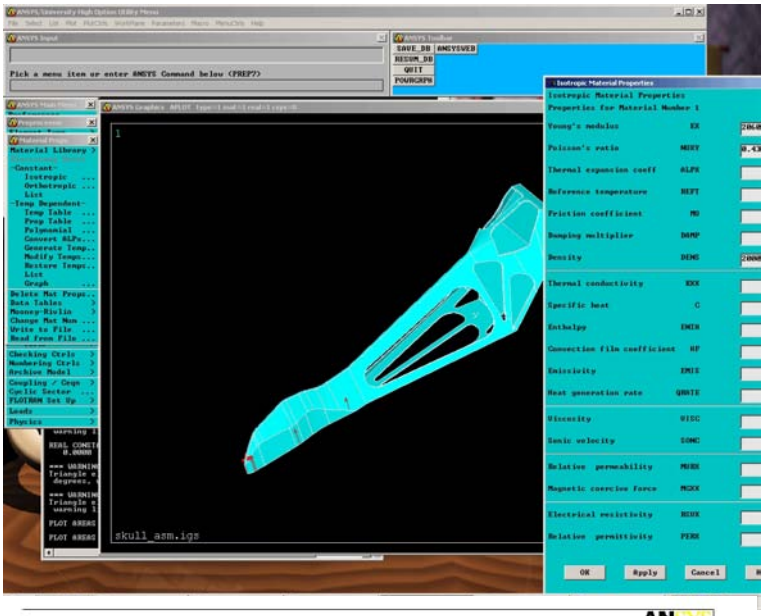

C

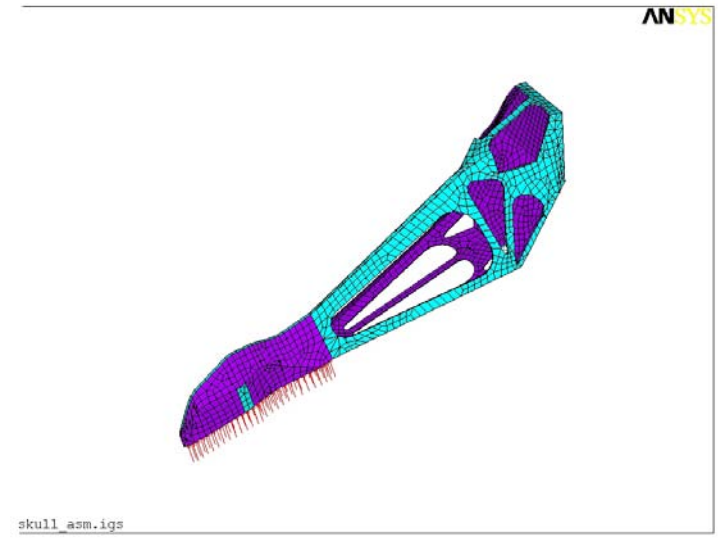

D

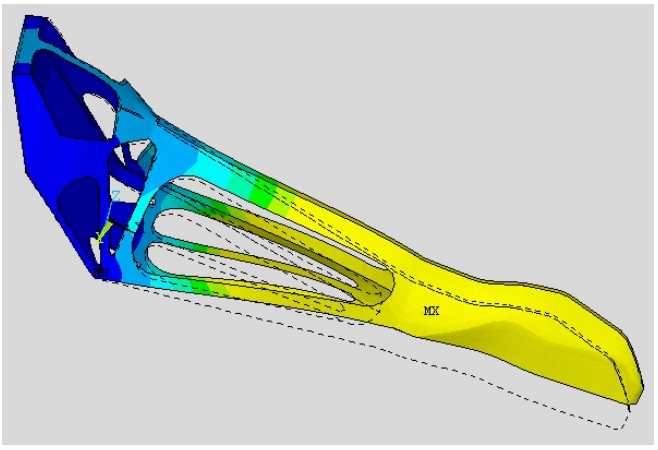

E

Fig. 3.8: Steps in the FEA: A) Geometrical model of a given structure (e.g. pterosaur skull) in PRO/Engineer™; B) Mesh of the model (different colours only for better visualisation) in ANSYS™; C) Application of material properties to the elements; D) Application of boundary conditions to the meshed model, red arrows representing forces; E) Graphical output of calculated values for stress distribution, same colour means same level of deformation whereas brighter colours stand for higher stress values.

because these would be only valid for human skulls shaped like a pterosaur skull[2]. The results were still correct in terms of quality and allowed a comparison of effects of different structural features like crest etc.

• 4. Forming of element stiffness matrices, superposition of all element stiffness matrices to a global stiffness matrix (pre-process)

• 5. Specification of boundary conditions: constraint and load (pre-process, Fig. 3.8 D)

In the tooth models, the constraint was set up at the base of the tooth. Different loading directions were analysed, allowing qualitative comparison between the different loading cases.

The Anhanguera skull model was constrained at the occipital condylus and the lower jaw condyli. Forces were applied at the level of the alveoli in the direction determined in the analysis of the teeth. A fictive force of 100 N was applied to the anterior end of the skull.

All five other skull models were constrained at the occipital and lower jaw condyli and at the level of the teeth, resp. along the jaw line. Forces were applied at the insertions of the adductor musculature, following the reconstructed force vectors and force values.

• 6. Calculation of nodal translations (process)

• 7. Calculation of the wanted values from nodal translations

In all cases, van Mises stresses were calculated. This is a standard stress hypothesis used in engineering (N. Hess 2001, pers. comm.).

• 8. Output and plot of the model (post-process, Fig. 3.8 E)

• 9. Discussion of the results

Because mistakes and simplifications in modelling and elementation will necessarily lead to wrong results ("Trash in, Trash out"), the assumed simplifications and parameters have to be specified for each model.

The 3D modelling of the skulls and teeth in PRO/Engineer™ and the FEA was done by N. Hess-Mohr, A. Berg, G. Schlese and Y. Hamidon (all Institut für CAE-Anwendungen, Fachhochschule für Technik und Gestaltung Mannheim) with the anatomical and boundary conditions input of the author.

2 This pragmatical simplification is crucial for interpreting the results and may explain apparent exceptional mechanical behaviours. Rayfield et al. (2001) analysed an *Allosaurus* skull using bovine material properties and deduced a strikingly high safety factor, which they failed to explain satisfactorily. One of the reasons may have been, that in reality, a bovine skull was analysed, which was shaped like an *Allosaurus* skull. Consequently, quantitative approaches should be avoided *per se* if the material properties can not be gained from the specimen (or from the same species) analysed. Even using values from close-related animals may be erroneous because of the high variability of mechanical properties based on different degrees of mineralisation (Currey 1999).

4. OPERATING REGIME "BITE" IN PTEROSAURS

Because pterosaur skulls are akinetic, no complex manipulating devices like in certain fishes or squamates exist in the pterosaur skull construction. The jaw occlusion (=bite) is a simple hinge-like dorsally directed movement of the lower jaw without any lateral component, caused by contraction of the adductor musculature (M. pseudotemporalis, M. adductor mandibulae, M. pterygoideus anterior and posterior). This type of jaw adduction is typical for reptiles and pterosaur species with screw-like jaw articulations, since the principal direction of jaw movement is not afflicted by this special morphology of quadrate and articular (Bennett 2001b).

The food items are seized with the jaws and fixed with teeth and/or with a rhamphotheca. The enlargement of certain teeth in some pterosaurs indicates that these jaw regions played a more prominent role in the fixation of food items than the rest of the tooth row. If the food item is small it can be swallowed. This may have been supported by cyclic movement of the tongue (De Vree & Gans 1989, 1994), indicated by the well-developed hyolingual apparatus in some pterosaurs, or by inertial feeding which is known in recent reptiles and birds (Bramble & Wake 1985). The ingestion of large food items is only possible when the food item is reduced to smaller pieces either by tearing or inertial reduction by shaking (De Vree & Gans 1994). Both modes may have within the optional operational range of the pterosaurs.

During the jaw occlusion, the loads are transmitted into the jaws through the teeth as punctual forces or in a plane along the jaws in edentulous skulls. This process is independent of the nature and texture of the food. Force transmission via the bony surface of the jaw may only be induced by contact with water and is a result of the difference between water flow (as a vector) and the movement of the jaws in the fluid (as a vector). However, this effect is difficult to quantify and primarily restricted to the lower jaw. It will only be discussed within the scope of filter-feeding, where it may have an influence on the overall skull construction.

During mandibular adduction, mostly vertical loads are applied to the skull. If both jaw margins are loaded simultaneously, compression will result in a vertical plane. It is known from theoretical and experimental studies that shear stress may also occur in an inclined plane and/or dorsoventral bending of the rostrum (Busbey 1995, Preuschoft et al. 1985, Rafferty et al. 2003). For a simple hinge like jaw closure, torsion will only result from unilateral biting (Bolt 1974, Rafferty et al. 2003). Although this may be rather uncommon in pterosaurs because of the relatively narrow jaws, torsional stiffness values of the different jaws can be calculated.

Further possible rostral loadings may be orientated laterally and caused by mediolateral jaw movements. They would generate compression in the side of the direction of the movement, tension on the opposite side and mediolateral bending. Finally, anterorposterior compression parallel to the midline may have played a role during prey-catching, too. However, the latter condition is unusual during normal feeding, and thus neglected in this study.

Especially mediolateral and anteroposterior orientated compressive loading cases mainly act on the devices primarily involved with seizing prey, i.e. dentition and/or a keratinous rhamphotheca, whereas the bony jaws will remain unaffected by the loads. Torsional loads, vertical compressive or shearing forces would be directly transmitted in the skull.

From studies of recent animals (Buckland-Wright 1978, Herring & Mucci 1991, Herring et al. 2001, Rafferty & Herring 1999, Rafferty et al. 2003, Sun et al. 2004) it is known that cranial sutures play an important role in the force transmission patterns of skulls. Butt-ended sutures resist compression but will fail in tension.

Scarf joints with oblique articulating surfaces accommodate tensile and compressive forces in all directions with usually only minor movement (Rafferty & Herring 1999). As a result, tensile and compressive stresses are reduced in magnitude. Interdigitating contacts resist compressive and tensile forces and prevent slipping between adjacent bones. They are not as strong in bending as bone, but absorb up to 100% more energy per volume during impact loading than bone (Jaslow 1990).

In pterosaurs, most skulls have fused bones, showing no sign at best weak sutural impressions. In these pterosaurs the skull is treated as a single unit for biomechanical investigations. In most Upper Triassic and Lower Jurassic pterosaurs, the skulls are composed of a cluster of bones, which tends to disarticulate *post mortem*, indicating rather a composite skull than a single cranial unit. However, this is true mainly for the posterior part of the skull, whereas the rostrum e.g. of *Eudimorphodon*, *Dimorphodon*, *Dorygnathus* or *Campylognathoides* is mostly preserved as a single unit, indicating a rather tight connection between the individual bones in this regions, even if sutures are present. Furthermore, a large part of the rostrum is formed by a single bone, the premaxillary. In consequence, the rostrum is modelled and investigated as a continuous cantilever beam in this study. As the architecture of the orbitotemporal region is more complex than the one of the rostrum, more sophisticated methods like three-dimensional statics (space frame analysis) or FEA have to be applied to calculate the resulting stress patterns.

5. BIOMECHANICS OF PTEROSAUR TOOTH CONSTRUCTIONS

5.1 Basic tooth morphology

Most pterosaurs possess a varying number of thecodont teeth along the jaws, in some cases combined with a keratinous rhamphotheca (Frey et al. 2003b, Wellnhofer 1991a). Generally, the dentition is homodont, but several pterosaurs possess heterodont teeth as far as the shape and size of the teeth are concerned. The teeth are compressed laterally, resulting in an oval cross-section. With only few exceptions (see below), carinae are developed anteriorly and posteriorly. Apart from the upper dentition of *Pterodaustro*, all teeth have single, blunt-conical roots, that may exceed the tooth crown in length. The roots as well as the tooth crowns can be bent either lingually or in posterior direction. The pulp cavity measures about one third of the cross-sectional area of the teeth and extends near the tip of the tooth crown. At the tip of the root, the pulp cavity is visible as a small foramen.

The pattern of enamel and dentine distribution is characteristic for this reptile group (Wellnhofer 1985). The only enamel covering is a cap on the tip of the tooth, exposing the dentine "core" below (Fig. 5.1). The distinct enamel-dentine-boundary (EDB) slopes down at the anterior and posterior carinae but does not reach the alveolar level. Vertical striae are visible on the enamel covering of the tooth. Unlike most other reptiles, the enamel is prismless in pterosaurs (Chiappe & Chinsamy 1996, Dauphin 1988).

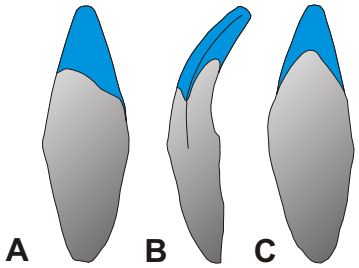

Fig. 5.1: Teeth of *Santanadactylus* (Ornithocheiridae) showing enamel cap (blue) and EDB: A) Lateral view; B) Anterior/posterior view; C) Lingual view. After Wellnhofer (1985).

The tooth replacement in pterosaurs is similar to prolacertiform reptiles, in which the successive tooth erupts posterolingually to its predecessor. In contrast, the typical mode for thecodont vertebrates would be a complete circular resorption of the root of the deciduous tooth by its successor. Fastnacht (1996) demonstrated that the pterosaurian mode of tooth replacement permits to retain the deciduous tooth longer in function. As a consequence, the successive tooth will be relatively larger at the time of shedding, than in the typical thecodont mode. This ensures maintaining the holding or filter efficiency of the dentition. As a result, special grasping devices like in *Coloborhynchus* can be developed, which show a highly coordinated tooth-replacement between the four jaw quadrants, thus avoiding large gaps (Fastnacht 1996).

5.2 Description of principal tooth constructions of pterosaurs

Apart from the general morphology described in 5.1, certain principal tooth construction types can be identified in pterosaurs. In most cases, these construction types are not restricted to a single species. Different construction types may even be present in a single species. However, they do not represent absolute entities, as transformational stages between the different construction types are common.

5.2.1 Eudimorphodon low multicuspid tooth construction (Fig. 5.2)

It is characterised by two to five, anterior-posteriorly arranged cusps. As Wild (1978) demonstrated, teeth with two or four cusps are only partially erupted, so that principally only three- or five-cusped teeth exist. The middle cusp is always the largest and the outer cuspules the smallest. The crown of the teeth are about as high as wide (basal width). All cusps are covered by enamel. The EDB is straight and not distinct sinusoidal like in

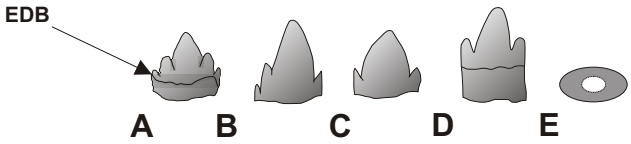

Fig. 5.2: Eudimorphodon low multicuspid tooth construction: A) 5-cusped tooth showing EDB; B) 4-cusped tooth; C) 3-cusped tooth; D) 3-cusped tooth showing EDB; E) Cross-Section, area of pulp cavity hypothetical. After Wild (1978).

typical pterosaur teeth. Although there is no preserved good occlusal view of the teeth, a lateral compression can be proved by measurements of the crown width (Wild 1978).

5.2.2 Eudimorphodon high multicuspid tooth construction (Fig. 5.3)

This constructional type is similar to the former type and bears two to seven cusps. The middle cusp is the largest and about twice as high as the basal width. The EDB is distinctly sinusoidal (Wild 1978).

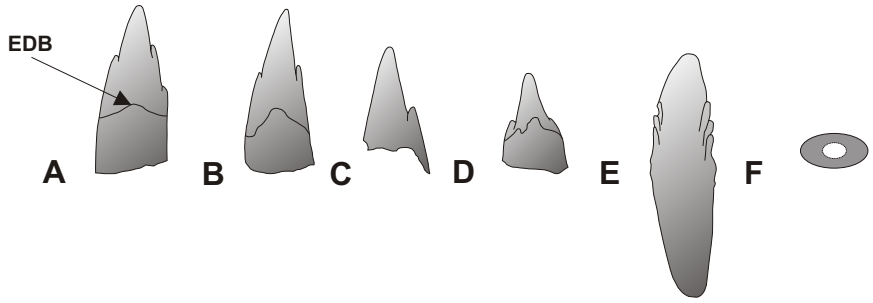

Fig. 5.3: Eudimorphodon high multicuspid tooth construction: A) 4-cusped tooth showing EDB; B) 3-cusped tooth showing EDB; C) 2-cusped tooth; D) 2-cusped tooth showing EDB; E) 7-cusped tooth with root; F) Cross-section, area of pulp cavity hypothetical. After Wild (1978).

5.2.3 Eudimorphodon pseudo-unicuspid tooth construction (Fig. 5.4)

Here, the anterior cusp is the largest and bent in distal direction. The distally proceeding cusps are small-sized and compressed against each other (Wild 1978). The tooth crown is about twice as high as wide and the typical pterosaurian EDB is well-developed (Wild 1978).

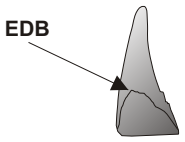

Fig. 5.4: Eudimorphodon pseudo-unicuspid tooth construction showing EDB. After Wild (1978).

5.2.4 Eudimorphodon monocuspid tooth construction (Fig. 5.5)

Only one cusp is present in this tooth construction. The conical tooth crown is bent in posterior direction and about three times as high as the basal width. Unlike all other pterosaurian tooth constructions, the EDB slopes down laterally and not at the carinae (Wild 1978).

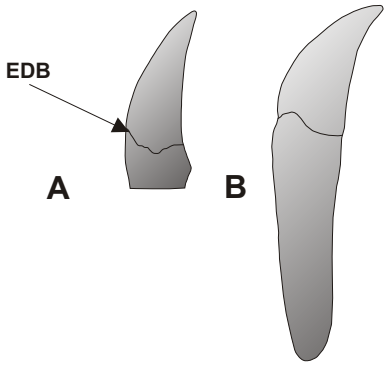

Fig. 5.5: Eudimorphodon monocuspid tooth construction: A) Tooth showing EDB; B) Tooth with EDB and root. After Wild (1978).

5.2.5 Preondactylus tooth construction (Fig. 5.6)

Dalla Vecchia (2003a) reports the occurrence of serrated teeth in a newly prepared specimen of the Upper Triassic pterosaur *Preondactylus*. The upper parts of the mesial and distal carinae of the tooth bear several small, apically orientated cuspules. Following Dalla Vecchia (2003a), this feature is typical for the teeth of the upper jaw of *Preondactylus*. The EDB is sinusoidal on the lateral side of the tooth. A similar pattern is present in *Austriadactylus* where the cuspules extend along the carinae (Dalla Vecchia et al. 2002). The height of the tooth varies from one to two times the basal width.

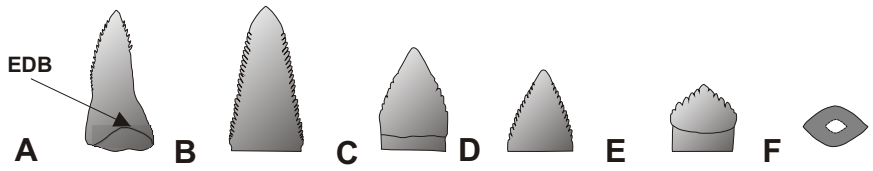

Fig. 5.6: Preondacytlus tooth construction: A) *Preondactylus* tooth with cuspules restricted to the upper part of tooth and EDB (after Dalla Vecchia 2003a); B-E) Teeth of *Austriadactylus* with fully serrated carinae; F) Cross-section. B-F after Dalla Vecchia et al. (2002).

5.2.6 Pterodactylus tooth construction (Fig. 5.7)

Teeth of this constructional type are monocuspid, conical and the crown is about one to three times higher as wide. Higher teeth tend to show a posterior bending similar to the Eudimorphodon monocuspid tooth construction, whereas lower teeth generally are more or less straight. The teeth are compressed laterally and show shallow anterior and posterior carinae. The EDB is well developed.

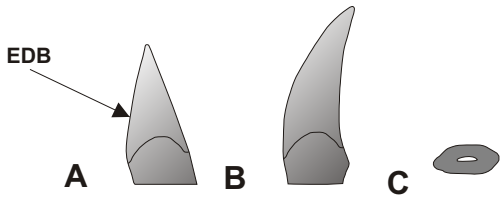

Fig. 5.7: Pterodactylus tooth construction: A) Straight tooth; B) Tooth with posterior curvature; C) Cross-section.

5.2.7 Rhamphorhynchus tooth construction (Fig. 5.8)

The Rhamphorhynchus tooth construction is characterised by its monocuspid, posteriorly curved crown, reaching up to more than eight times in height than the basal width. In some cases, the curvature may be restricted to the upper third of the crown with the lower part being straight. Lateral compression is much more distinctive than in the Pterodactylus tooth construction and the anterior and posterior carinae are well-developed. The EDB is pronounced with the sinus reaching very high in apical direction, leaving much of the dentine of the lateral flanges exposed.

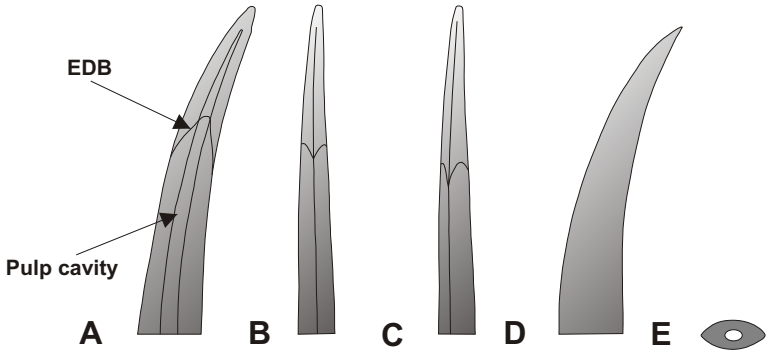

Fig. 5.8: Rhamphorhynchus tooth construction: A) Lateral view of *Rhamphorhynchus* tooth showing EDB and extension of the pulp cavity; B) Anterior view of *Rhamphorhynchus* tooth showing EDB and carinae; C) Posterior view of *Rhamphorhynchus* tooth showing EDB and carinae; D) Tooth of *Austriadactylus*, after Dalla Vecchia et al. (2002); E) Cross-section of *Rhamphorhynchus* tooth.

5.2.8 Ornithocheirus low tooth construction (Figs. 5.1 & 5.9)

The Ornithocheirus low construction resembles the Pterodactylus tooth construction, but the crown is about five times higher than wide. The EDB is asymmetrical with the sinus reaching higher on the lingual side (up to two thirds of the crown height) than on the lateral side. In anterior-posterior direction the tooth crown is straight or only slightly bent, whereas the tooth may be bent up to 90 degrees in lingual direction (Wellnhofer 1985).

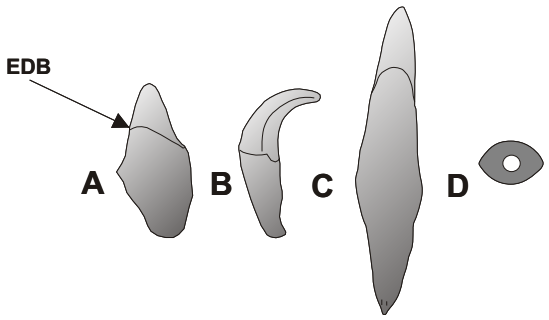

Fig. 5.9: Ornithocheirus low tooth construction: A) Lateral view showing EDB; B) Posterior view showing carinae; C) Lateral view showing EDB; D) Cross-section.

5.2.9 Ornithocheirus high tooth construction (Fig. 5.10)

The teeth are similar to the former constructional type as far as the height is concerned. However, the EDB is situated relatively higher in apical direction, the teeth are much less compressed and anterior or posterior carinae are poorly developed or absent. In anterior view, the teeth are straight, whereas bending may be up to 90 degrees in posterior direction as in *Coloborhynchus* (Fastnacht 1996).

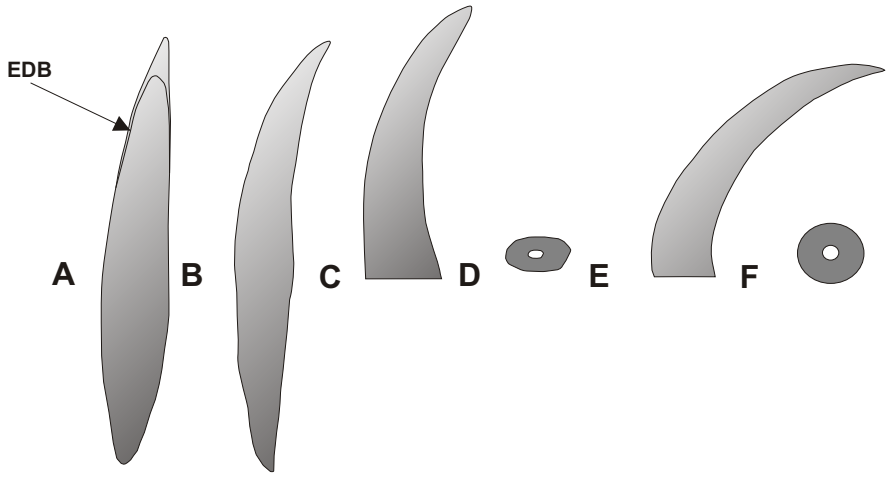

Fig. 5.10: Ornithocheirus high tooth construction: A) Lateral view showing EDB; B) Posterior view; C) Lateral view of curved teeth; D) Cross-section of A)-C); E) Strongly curved tooth of *Coloborhynchus*; F) Cross-section of E. After Fastnacht (1996).

5.2.10 Ctenochasma/Gnathosaurus tooth construction (Fig. 5.11)

The Ctenochasma/Gnathosaurus construction is very high, reaching up to ten times the basal width. The cross-section is circular to oval without mesial or distal carinae and has a very narrow pulp cavity (Wellnhofer 1970). The teeth are bent in distal and lingual directions, the latter as a consequence of the lateral orientation of the alveoli. The EDB is well developed and only the upper part of the tooth is covered by enamel. In *Gnathosaurus* the upper third of the crown is bent in anterior direction, giving the tooth a sigmoid shape in lateral view.

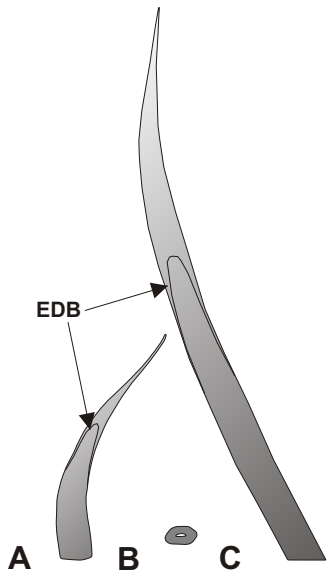

Fig. 5.11: Ctenochasma/Gnathosaurus tooth construction: A) Tooth of *Gnathosaurus*; B) Cross-section of *Ctenochasma* and *Gnathosaurus* tooth; C) Tooth of *Ctenochasma*. Figures scaled x 0,5 than Fig. 2-10.

5.2.11 Pterodaustro high tooth construction (Fig. 5.12)

As Chiappe & Chinsamy (1996) demonstrated, the lower teeth of *Pterodaustro* are real teeth and no keratinous structures as was supposed earlier (Wellnhofer 1991a). They are oval to sub-elliptical in cross-section with a large pulp cavity and reach up to 70 times in height compared to their basal diameter. The orientation of the crown is straight without distal or lingual bending. Following Chiappe & Chinsamy (1996), the teeth are covered by enamel but nothing

can be said about the exact distribution of the EDB. The surface of the teeth is smooth.

5.2.12 Pterodaustro low tooth construction

Not much is known about the teeth in the upper jaw of Pterodaustro and no good drawings or pictures are given. After Chiappe & Chinsamy (1996) the teeth are very small and possess spatulate crowns with slender bases, which are conical in lateral view. Unlike in all other pterosaurs, these teeth are not set in alveoli but probably were embedded in a "corneous structure or a muscular 'lip'" (Chiappe & Chinsamy 1996).

Fig. 5.12: Pterodaustro high tooth construction: A) Tooth of *Pterodaustro*, scaled x 0,1 than Figs. 2-10; B) Cross-section of *Pterodaustro* tooth (after Chiappe & Chinsamy 1996).

5.2.13 Dsungaripterus tooth construction (Fig 5.13)

The teeth of *Dsungaripterus* are poorly known. Young (1964) described short crowned teeth in this species, which are only slightly bent in posterior and lingual directions. Young's drawings of the jaws show roundish-oval alveoli, which indicate teeth with rather circular than lateral compressed cross-section (Frey 2004, pers. comm.). The elevation and thickening of the alveolar bone is characteristic of the implantation of this tooth construction. Wellnhofer (1991) considered the teeth being blunt knobs.

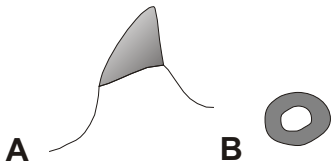

Fig. 5.13: Dsungaripterus tooth construction: A) Tooth with elevated alveolar bone, B) Cross-section of tooth. After Young (1964).

5.3. Biomechanical aspects of morphology of tooth constructions

This chapter is based on the investigation of the geometry of the tooth constructions neglecting the effects of the distribution of the EDB in pterosaur teeth. The consequence of the restricted enamel cover in pterosaur teeth will be described in a separate chapter (see chapter 5.4).

The most basic loading case of a typical conical pterosaur tooth during bite is in line with the central tooth axis. For a simple cylindric crown construction, horizontal tensile and vertical compressive stresses result from vertical loading (Fig. 5.14; Rensberger 2000, Srivastava et al. 1999). Because the ultimate tensile strength of enamel and dentine is much lower than the ultimate compressive strength (Tab. 3.2), the tensile stresses pose more problems than do compressive stresses. Beginning failure would be indicated by microcracks, which may be visible as small vertical irregularities in the enamel.

The resistance against axial loading can be evaluated by the resistance against Euler buckling (Fig. 5.15, Tab. 5.1). In contrast to the low-crowned tooth constructions, in the Rhamphorhynchus, Gnathosaurus, Ctenochasma and Pterodaustro

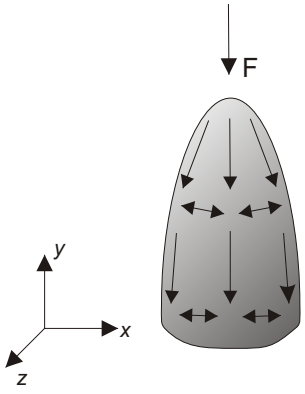

Fig. 5.14: Conical tooth model with apical load *F* causing mediolateral and axial compressive and lateral tensile stresses.

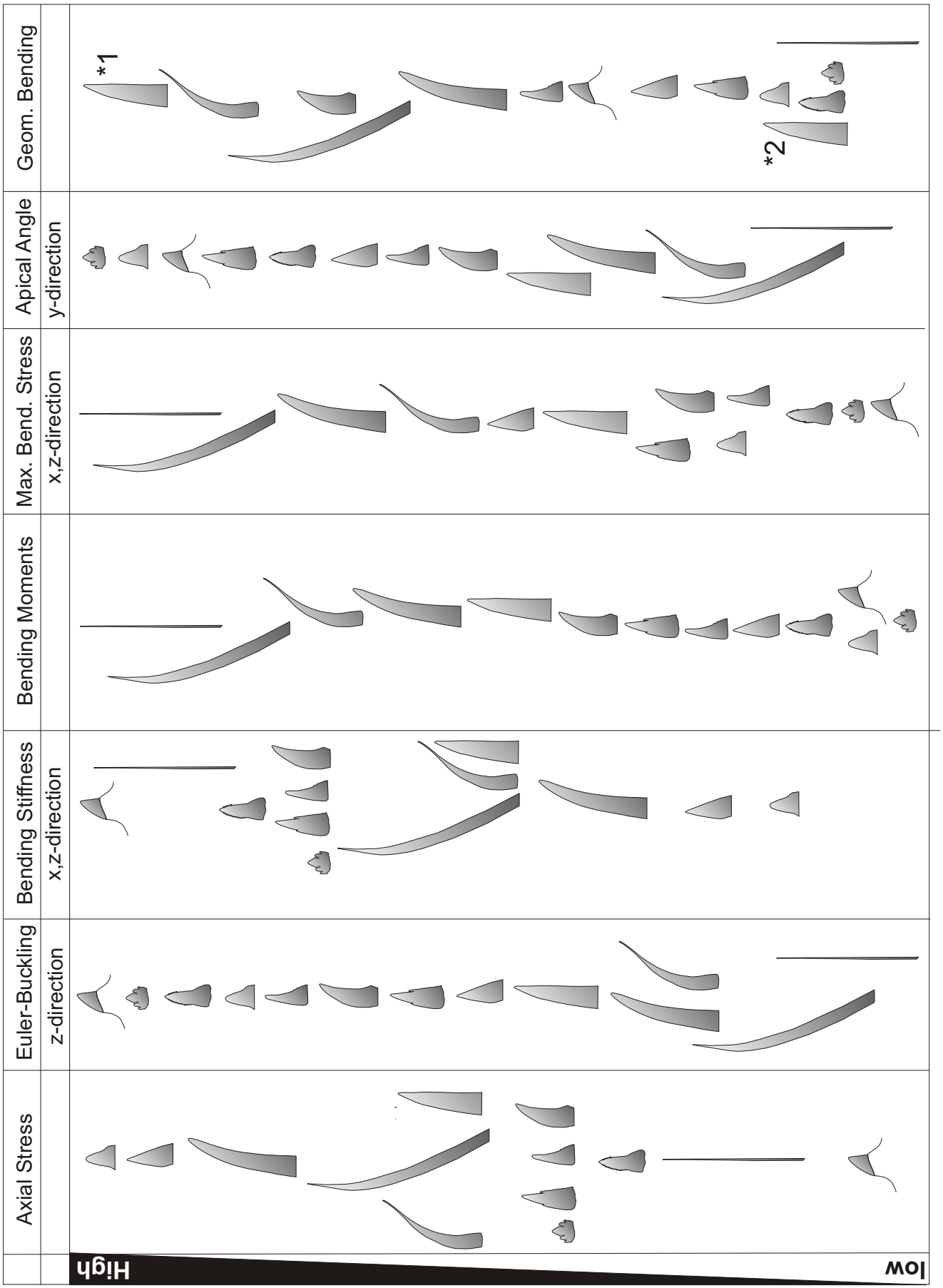

Fig. 5.15: Diagram of different geometrical and mechanical properties of tooth constructions (see also Tab. 5.1). *1 = Bent Ornithocheirus high tooth construction, *2 = Straight Ornithocheirus high tooth construction. Legend see Fig. 5.16.

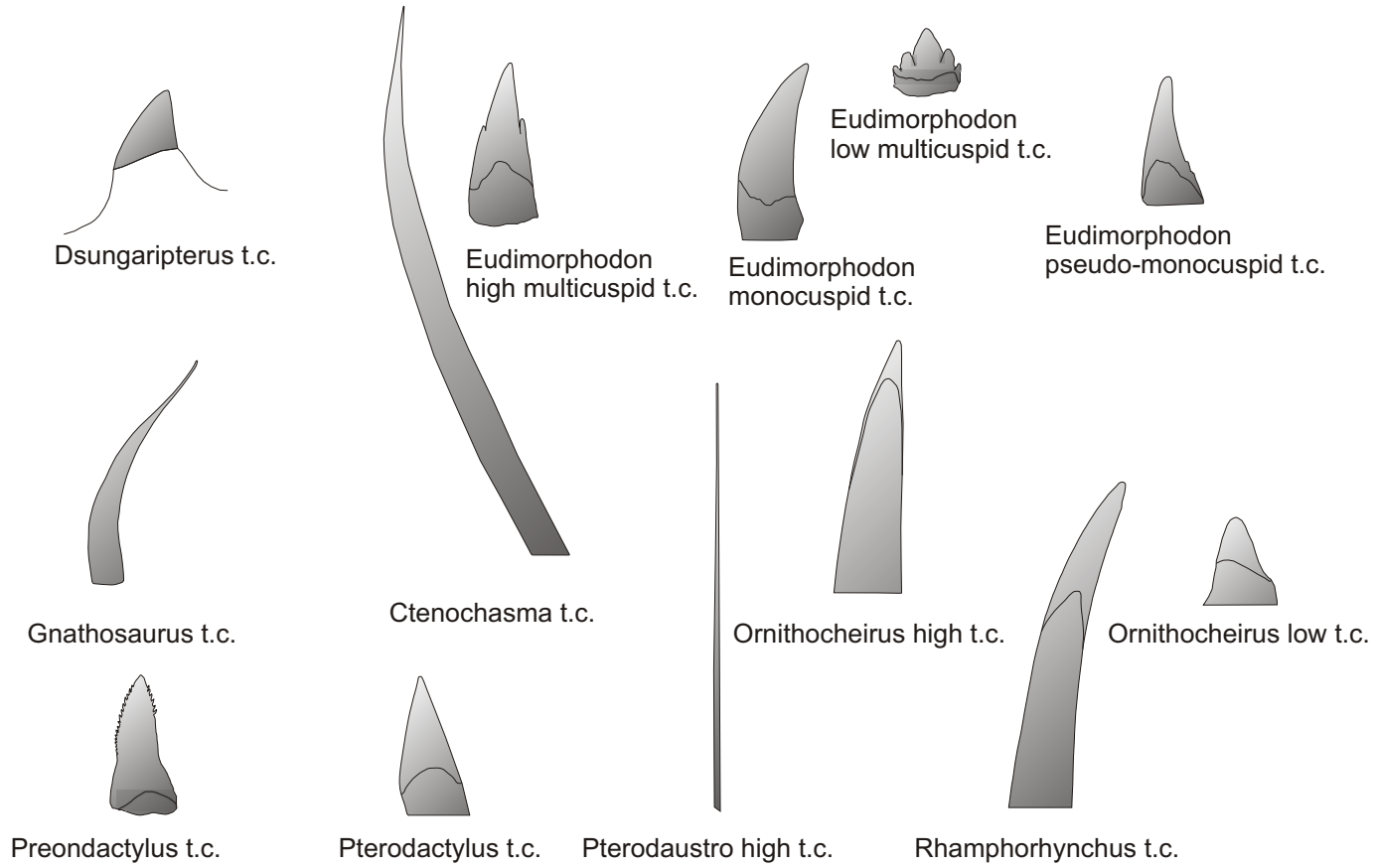

Fig 5.16: Legend for Fig. 5.15. t.c. = tooth construction.

tooth constructions small axial loads will lead to failure of the construction by buckling. The Gnathosaurus tooth construction is also susceptible to buckling, because its sigmoidal shape reflects a "pre-"buckled morphology, similar to sigmoidal bones (Alexander 1981, Bertram & Biewener 1988), rather than a straight column. Within its elastic range, however, the construction can act as a spring and thus buffers a considerable amount of axial load.

Low-crowned tooth constructions have the highest resistance against Euler buckling (Fig. 5.15, Tab. 5.1). This is caused by the low crown height (*l*, see equation 9) and/or by the blunt apex (increase of *A*), so that the forces can be distributed over a larger area than in a high-crowned tooth construction, reducing the axial stress. These low-crowned tooth constructions can resist high loads but allow only minor penetration of the teeth into the food item. On the other hand, a high load can be applied on the food item which can either tightly fixed by active retention of the jaw adduction or can even be crushed if the ultimate stress is reached within the food item.

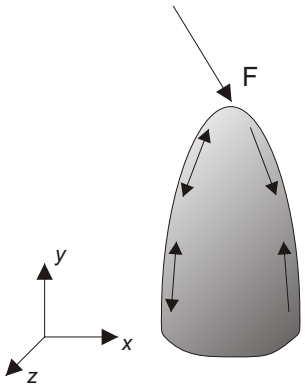

Fig. 5.17: Conical tooth model with oblique load F causing compressive and tensile stresses.

A pure axial loading case may be improbable during bite. Especially struggling, agile food items will result in oblique loads on the tooth construction. These loads consist of a vertical, axial component (y-axis) and two principal horizontal components with forces acting in anterior-posterior (x-axis) and/or lingual-lateral (z-axis) direction (Fig. 5.17). Whereas vertical loads put the tooth construction under compression, horizontal loads will result in bending of the tooth construction. Bending produces much greater stress than pure axial loading, because the loads are restricted to the external part of the tooth construction.

Tooth Construction	Height (mm)	Cross sectional area (mm²)	Apical angle (°)	Degree of bending	Axial stress (N/mm²)	Axial stiffnes
Ctenochasma tc	135.58	38.80	4	15	0.26	0.00
Dsungaripterus tc	11.74	62.99	42	17	0.16	0.02
Eudimorphodon hmtc	23.86	39.98	29	2	0.25	0.01
Eudimorphodon lmtc	9.72	39.98	77	0	0.25	0.04
Eudimorphodon mtc	32	39.98	17	20	0.25	0.01
Eudimorphodon putc	21.41	39.98	26	3	0.25	0.02
Gnathosaurus tc	71.08	38.80	7	22	0.26	0.01
Ornithocheirus htc	40.57	38.80	14	7	0.26	0.01
Ornithocheirus ltc	11.82	26.31	44	3	0.38	0.05
Preondactylus tc	20	49.32	28	0	0.20	0.01
Pterodaustro tc	21.83	27.65	26	7	0.36	0.02
Pterodaustro htc	623	51.76	1	0	0.19	0.00
Rhamphorhynchus tc	51.41	30.32	10	14	0.33	0.01

	Euler buckling (F)		Shear stress (N/mm²)	Bending stiffness	Bending moments
	x	z			
Ctenochasma tc	1.85	0.45	0.26	3443.38	1355.80
Dsungaripterus tc	400.31	257.48	0.16	5590.27	117.40
Eudimorphodon hmtc	61.51	15.94	0.25	3547.94	238.60
Eudimorphodon lmtc	370.63	96.02	0.25	3547.94	97.20
Eudimorphodon mtc	34.20	8.86	0.25	3547.94	320.00
Eudimorphodon putc	76.39	19.79	0.25	3547.94	214.10
Gnathosaurus tc	6.73	1.64	0.26	3443.38	710.80
Ornithocheirus htc	20.65	5.04	0.26	3443.38	405.70
Ornithocheirus ltc	164.96	18.51	0.38	2335.09	118.20
Preondactylus tc	108.01	42.60	0.20	4377.42	200.00
Pterodactylus tc	50.82	6.30	0.36	2453.58	218.30
Pterodaustro htc	0.12	0.05	0.19	4593.50	6230.00
Rhamphorhynchus tc	10.05	1.50	0.33	2690.58	514.10

	Max. bending stress (N/mm²)		Torsional stiffness	Comparison stress (N/mm²)
	F_{ymax}	F_{zmax}		
Ctenochasma tc	56.59	27.96	1031.25	80.40
Dsungaripterus tc	1.86	1.49	3340.79	206.92
Eudimorphodon hmtc	9.38	4.77	1114.59	13.62
Eudimorphodon lmtc	3.82	1.95	1114.59	5.77
Eudimorphodon mtc	12.58	6.40	1114.59	18.15
Eudimorphodon putc	8.42	4.28	1114.59	12.26
Gnathosaurus tc	29.67	14.66	1031.25	42.32
Ornithocheirus htc	16.93	8.37	1031.25	24.32
Ornithocheirus ltc	10.73	3.59	359.72	15.72
Preondactylus tc	5.17	3.24	1890.22	7.60
Pterodactylus tc	17.95	6.32	412.97	25.90
Pterodaustro htc	146.12	96.29	2123.43	80.40
Rhamphorhynchus tc	35.15	13.57	532.67	50.17

Tab. 5.1: List of various mechanical parameters for the different tooth constructions. Anterior-posterior width of tooth constructions set to 10 mm.

All pterosaur tooth constructions have a higher bending stiffness in x-direction than in z-direction (Tab. 5.1). It is assumed, that this disparity reflects the major loading regime during feeding (Van Valkenburgh & Ruff 1987) and is especially present in the Dsungaripterus, Preondactylus, Pterodaustro and the different Eudimorphodon tooth constructions.

The bending moments as well as the maximum bending stresses are lower in the low-crowned than in the high-crowned tooth constructions (Fig. 5.15, Table 5.1). Especially the Ctenochasma and Gnathosaurus tooth constructions will be subject to high bending moments and stress. The Pterodaustro construction marks an exception, because it is very long in relation to its dimension in x- and z-direction. As Currey (1999) demonstrated, it is possible for such a construction to undergo large deflections without generating critical strains on enamel and dentine.

The various tooth constructions show different degrees of curvature, leading to a different behaviour in bending. In a straight construction, loading conditions can change spontaneously especially when loaded during a sudden impact on hard objects. Under this aspect, axial compression can only be considered as a metastable loading condition (Bertram & Biewener 1988) and paraxial loading will lead to buckling of the construction. In contrast to this, curved constructions (e.g. teeth or bones) determine a load predictability in the direction of the curvature. This is a key determinant of a structure's safety factor that must support dynamically variable loads as (Alexander 1981). Under these conditions, a curved tooth constructions thus represents a stable system. Increased loads will result in a change of stress magnitude rather than in the type and distribution of stress, both which are more critical for the structure. Furthermore, a quasi-axial load will result if the curvature of the tooth construction is in line with a circular path around the jaw articulation. In this case, the bending stress is rather low or not present at all (Frey 2004, pers. comm.).

A further effect of a posteriorly curved tooth construction is the restriction of the anterior movement of the food item during jaw occlusion. The food is transfixed and movement without destruction is only possible in posterior direction (e.g. into the oesophagus of the predator). This condition is especially present in the first pair of teeth in Coloborhynchus, which are bent about 90° in posterior direction (Fastnacht 2001). For lesser curved tooth constructions this effect is correspondingly lower.

The efficiency of fixation of food items can also be increased by other means. Possible options are an increase of the overall force of the jaw adductors or to produce greater loads on the food item by enlarging the contact area (e.g. in the Dsungaripterus tooth construction or by replacement of the teeth by a keratinous rhamphotheca). An alternative possibility is to modify the morphology of the tooth crown. The higher the crown is, the deeper it can penetrate into the food item and the more pointed the apex is, the more force is concentrated in this area which is the first to get in contact with the food item. Additionally, a v-pointed profile has less friction than a more blunt, u-shaped profile, because the contact area between the apex and the food item is smaller if its central axis is in line with the force. Consequently, less force is needed for penetration and the compressional loads on the tooth construction will be minimised. These three properties are constrained by the axial stiffness. As shown earlier, the Gnathosaurus, Ctenochasma and Pterodaustro tooth constructions are too susceptible to failure by axial loads to have penetrative capabilities. On the other hand, the Dsungaripterus and Eudimorphodon low multicuspid tooth constructions permit only minor penetration because of their low and broad profile.

Nearly all tooth constructions possess smooth or serrated carinae. Because of their low width, these structures do not significantly increase the area moment of inertia and axial and bending stiffness. Frazzetta (1988) and Abler (1992) demonstrated that smooth or serrated carinae can be interpreted as cutting edges. The experimental data presented by Abler (1992) shows that the force needed for puncturing is much lower in a laterally compressed tooth construction with carinae than without. Such laterally compressed tooth constructions with carinae are present in e.g. the Rhamphorhynchus tooth construction. However, the more circular the cross-section of the tooth-construction gets, the less effect the carinae has. In circular cross-sections (e.g. Pterodaustro tooth construction, some teeth of Ornithocheirus high tooth construction), no carinae are present at all.

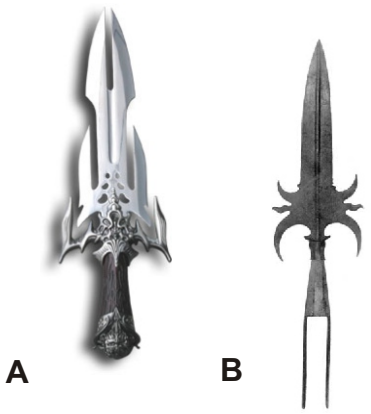

Fig. 5.18: A) Modern fantasy dagger; B) Partizan. Courtesy of www.messerforum.net.

When the tooth construction is pressed against a compliant substrate (=food item), serrations may increase the force needed for penetration if the cuspules are orientated in the line of action. Such types of serrations are typical for the Preondactylus tooth constructions (Fig 5.6). Although multiple cusps are also found in other pterosaur tooth constructions, they do not form strictly serrated carinae because of the low number of cuspules (one to five). A construction with apically orientated serrations resembles present fantasy knives or the partizan/spontoon-blades of early modern pikemen (Fig. 5.18). Although these blade types are often ornamental, they were used in warfare, too. The side-spikes restrict a deeper penetration and sticking of the main spike, at the same time causing more damage to the surface of the food item than a single spike. The same holds true for the Preondactylus tooth construction which needs higher force for a complete penetration than constructions with smooth carinae.

A second difference between both types of carinae becomes evident in cutting movements, although such assumptions strongly depend on the food texture (Frazzetta 1988). Rather than producing a clean cutting, serrations rip open the food item ("grip and rip-hypotheses" cf. Frazzetta 1988). This process requires a large force component perpendicular to the cutting plane, whereas in non-serrated, sharp cutting edges perpendicular forces can be relatively low or even zero in case of razor blades. The ripping mode may be advantageous in case of a very heterogeneous texture or non-compliant food (Vincent & Lillford 1991). Similar structures are found in modern saw blades, but here the teeth are pitched either back- or forward to permit back and forth motion. The Peteinosaurus tooth construction has only apically orientated serrations, making its behaviour dependent on the vertical movement (Fig. 5.19). When the tooth construction sinks

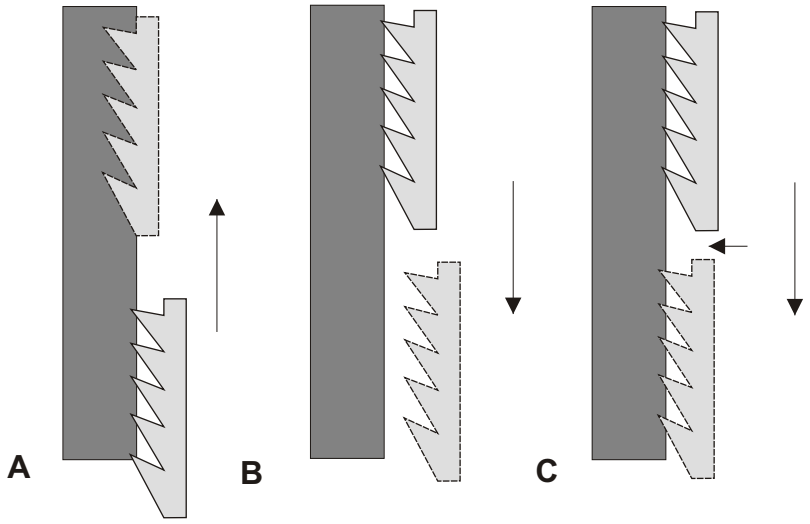

Fig. 5.19: Section of serrated blade (left) and substrate (right), arrows indicating forces and direction of movement: A) Blade acting as a rake, digging in the substrate during movement; B) Blade acting as a saw, disengaging without vertical force component; C) Blade acting as a saw, constant cutting with vertical force component.

into the food item, the serrations act as a rake. The tooth construction will be moved closer to its kerf and set deep into the substrate. Re-moving the tooth construction in the opposite direction leads to a smooth draw cut with the serrations acting as a pitch. This process includes a perpendicular force component preventing a slide-away from the substrate.

In contrast to serrations, tooth constructions with smooth carinae produce clear cuttings, especially in compliant food. A perpendicular force component has to be present in both vertical directions to maintain the contact between the carinae and the substrate. Compared to modern knives, non-serrated pterosaur tooth constructions show strong similarities to the lateral blade profile of rapiers, meat and fillet knives (Fig. 5.20). However, the cross-section resembles a biconvex, Moran grinding with a large blade angle (at least 45°). The optimal angle for a knife would be 30°. This indicates that the cutting ability of pterosaur tooth constructions is rather low, whereas the puncturing/penetrating capacity is well developed.

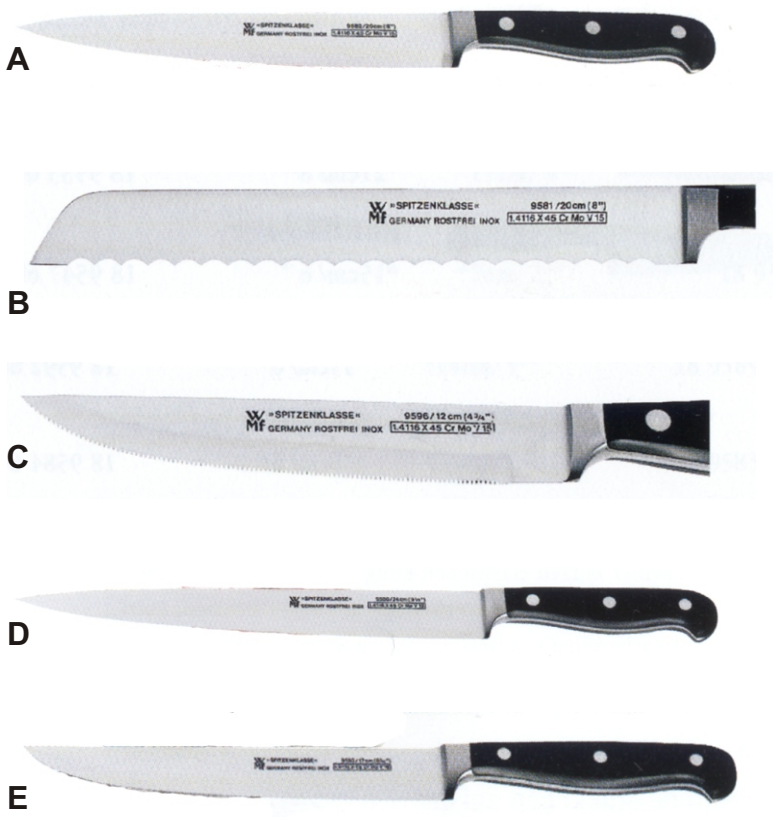

Fig. 5.20: Modern knives as analogues to pterosaur tooth constructions: A) Carver with non-serrated blade, clean cutting of meat fibres (analogue to e.g. Pterodactylus tooth construction); B) Bread knife with a wavy blade edge, ripping of the hard crust of a bread (analogue e.g. to Preondactylus tooth construction); C) Serrated blade edge, eases the cutting of hard rinds and a clear cutting of softer objects (analogue to e.g. Eudimorphodon tooth constructions); D) Slicer with long blade, used for clean cutting of long objects without roving (analogue to e.g. Ornithocheirus high tooth construction); E) Fillet knife with narrow and flexible blade to fillet meat or fish, clean cutting of the fibres (analogue to e.g. Rhamphorhynchus tooth construction). Courtesy of WMF, Geislingen, Germany.

5.4 Biomechanical consequences of the enamel-dentine-boundary (EDB)

Like in most other vertebrates, the teeth of pterosaurs consist of a dentine core of low Young's modulus but high tensile and compressive strength and an external hard and brittle enamel shell with a high Young's modulus. This architecture is analogous to spike-hardened devices in engineering, e.g. gear teeth. As Koenigswald et al. (1987), Marx (1994), Pfretzschner (1986, 1994), Rensberger (1992, 1993, 1995, 2000) and Srivastava et al. (1999) have shown, the ultrastructure of the enamel may influence significantly the overall mechanical behaviour of a tooth. Certain geometrical arrangements of enamel prisms like different amplitudes of folding or an orthogonally alternating configuration complicates the determination of the stress patterns within the tooth. It seems to be generally accepted that the orientation of the enamel prisms is associated with a rein-

forcement of the teeth according to the stress pattern (Pfretzschner 1986). This complex anisotropy makes the determination of the mechanical behaviour especially of mammal teeth difficult. Biomechanical investigations considering the composite nature of pterosaur tooth constructions are much easier, because they lack any ultrastructural differentiations of the enamel.

The analysis of the consequences of the typical pterosaurian EDB is based on the FEA of three different tooth models based on the Rhamphorhynchus tooth construction: (Fig 5.21), A) pure dentine model (CD), B) model with apical enamel cap (CED) and C) model with complete enamel cover (CE). The resulting maximum stresses and deformations for various anterior-posterior orientated loading angles are given in Table 5.2. For all three constructions, the values are lowest, if the model is loaded in line with the bending axis of the tooth construction. When loaded, the CD model will show high strains and stresses (Fig 5.21B). In contrast to this, the CED will result in about 1/4 less deformation and less stress (Fig. 5.21C). In the CE model, there is only half of the strain compared to the CD model but the stress is about twice as high (Fig. 5.21D). The mechanical optimum would be somewhere between the CED and CE models.

As described earlier, most pterosaur tooth construction possess anterior and posterior carinae. Their orientation is congruent with the highest area moment of inertia. Here, the bending strength is the highest and tensile and compressive stresses will occur during anterior-posterior bending. The EDB, which slopes down at the carinae ensures that the total strain of the tooth construction is rather low. Laterally or lingually orientated loads will result in high stresses, because of the low moment of inertia. An enamel covering on the lingual or lateral faces would result in the failure of the tooth construction even if forces are low. As dentine can tolerate much higher stresses than enamel, the tooth construction will react to these forces elastically within a certain range of strain rate. The asymmetry of the EDB between the lingual and lateral sides of the tooth construction indicates that this effect is more pronounced at the lingual side. In most pterosaur tooth constructions, this side is concave and therefore susceptible to tensile loads. Because dentine has a much higher tensile strength than enamel, failure may result in a completely enamel-covered tooth construction. This view was supported by the FEA of a model of the Ornithocheirus high tooth construction (Fig. 5.22), presented by Berg (2002.

5.6 Biomechanical behaviour of teeth *in situ*

The behaviour of a tooth in its alveolus not only depends on the geometry and mechanics of the tooth, but also on its bearing (=implantation) in the jaw. Because pterosaurs possess thecodont teeth (with the exception of the upper jaw dentition in Pterodaustro), the teeth are implanted in a bony sleeve, the alveolus, supported by several trabeculae (Fig. 5.23).

The tissue between tooth and alveolar bone is called the periodontal ligament. It develops from the follicular sac with a matrix consisting of hyaluronic acid, glycoproteins, and proteoglycans (van den Bos & Tonino 1984). Within the ligament, bundles of collagen fibres are aligned perpendicular to the tooth and the bony surface. The fibres are partially embedded into the cementum and the alveolar bone. These mineralised parts of the fibres are the called “Sharpey’s fibres”. The non-mineralised parts form an intertwined meshwork with an orientation perpendicular to the mineralised surfaces of cementum and bone (Walker & Liem 1994). Oxytalan fibres run parallel to the surface of the root.

Even in human dentistry, the mechanical properties of the periodontal ligament is not fully understood. It is obvious that the ligament has considerable influence on the pattern of force transmission during loading of the

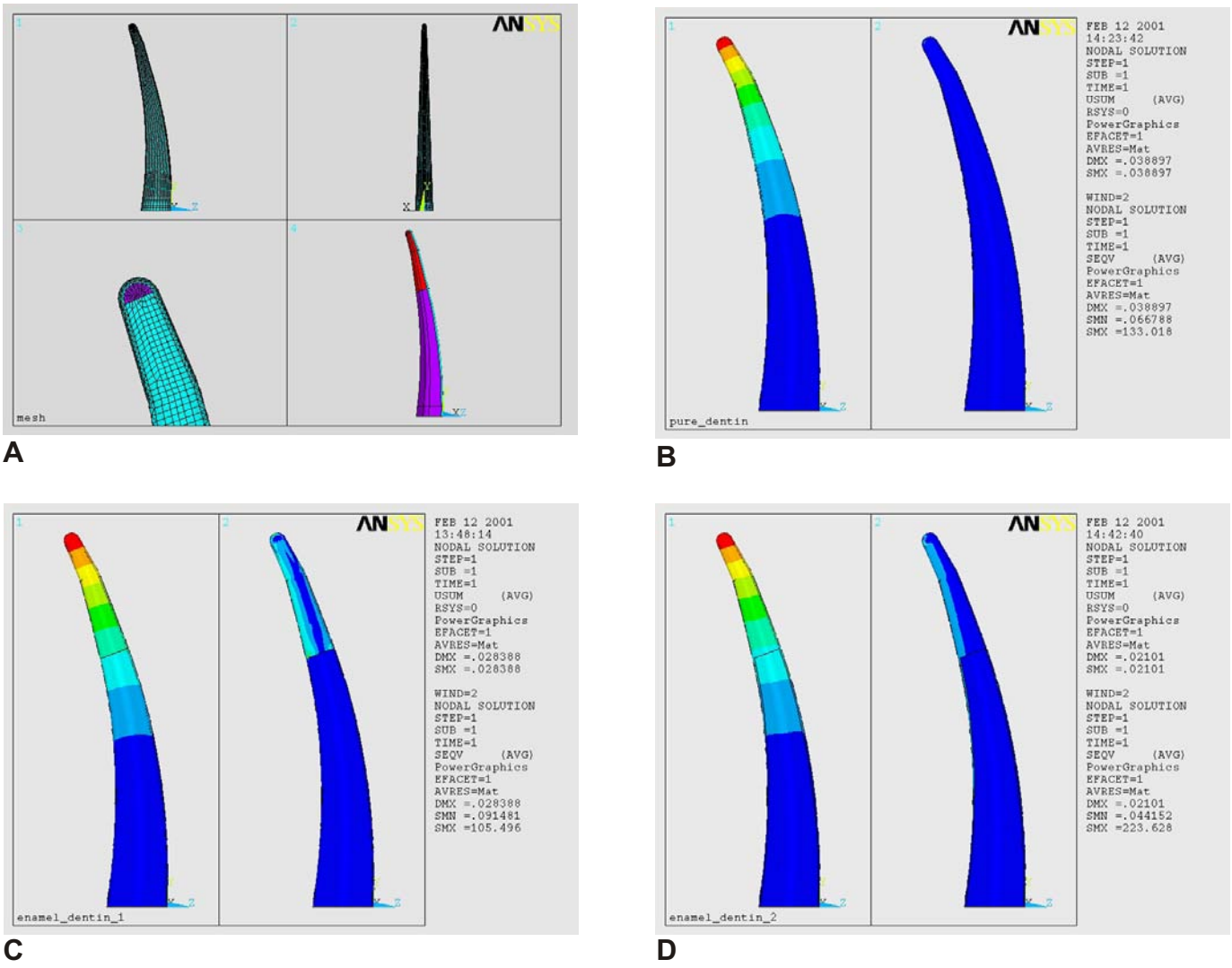

Fig. 5.21: Model of Rhamphorhynchus tooth construction to evaluate the effect of the enamel cover during loading. Same forces applied to all models, same colours mean same level of deformation: A) Model an mesh of tooth with about 5.000 mixed shell/solid elements (upper left window: model in right lateral view, upper right window: model in anterior view, lower left window: detail of the apex of the model, lower right window: model showing enamel cap in red; B) Results of FEA with all elements having properties if dentine CD (left window: deformation, right window: van-Mises-stress); C) Results of FEA with enamel cusp and enamel carinae CED, D) Results of FEA with complete covering by enamel CE. See text for abbreviations.

Loading angle	**0**	**10**	**20**	**30**	**40**	**45**	**50**	**60**	**70**	**90**
Maximum stresses (van Mises)										
CD	433	443	488	528	560	575	587	610	627	612
CED	1340	1226	1114	1018	943	914	891	864	924	1313
Maximum absolute deformation										
usum CD	381	142	104	326	467	549	740	880	935	1370
usum CED	0	66	89	189	280	324	365	4454	525	1000

Tab. 5.2: van Mises-stress (in MPa) and sum of deformation rates (usum) for various loading angles in the CE and CED models of Rhamphorhynchus tooth construction by FEA. See text for abbreviations.

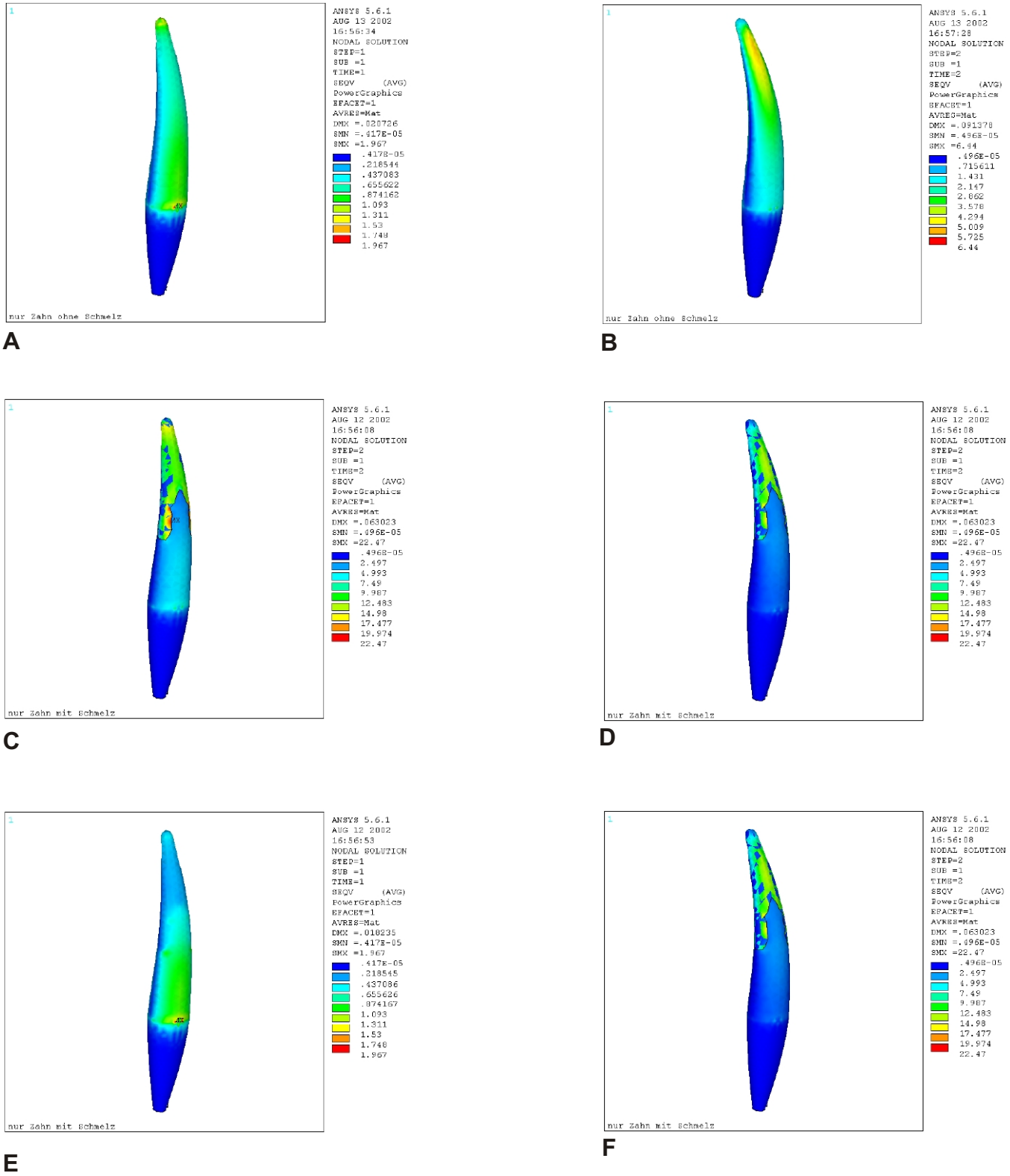

Fig. 5.22: Model of Ornithocheirus high tooth construction to evaluate the effect of the enamel cover during loading from different directions. Same forces applied to all models, same colours mean same level of deformation: A) van-Mises stress in CD model loaded in direction of the tooth's axis; B) Stress in CD model loaded 45° in dorsolingual direction; C) Stresses in CED model loaded in direction of the tooth's axis; D) Stress in CED model loaded 45° in dorsolingual direction; E) Stress in CE model loaded in direction of the tooth's axis; F) Stress in CE model loaded 45° in dorsolingual direction. The highest stresses are found in the CD and CE model at the base of the crown. Oblique loads result in different stress patterns. From Berg (2002). See text for abbreviations.

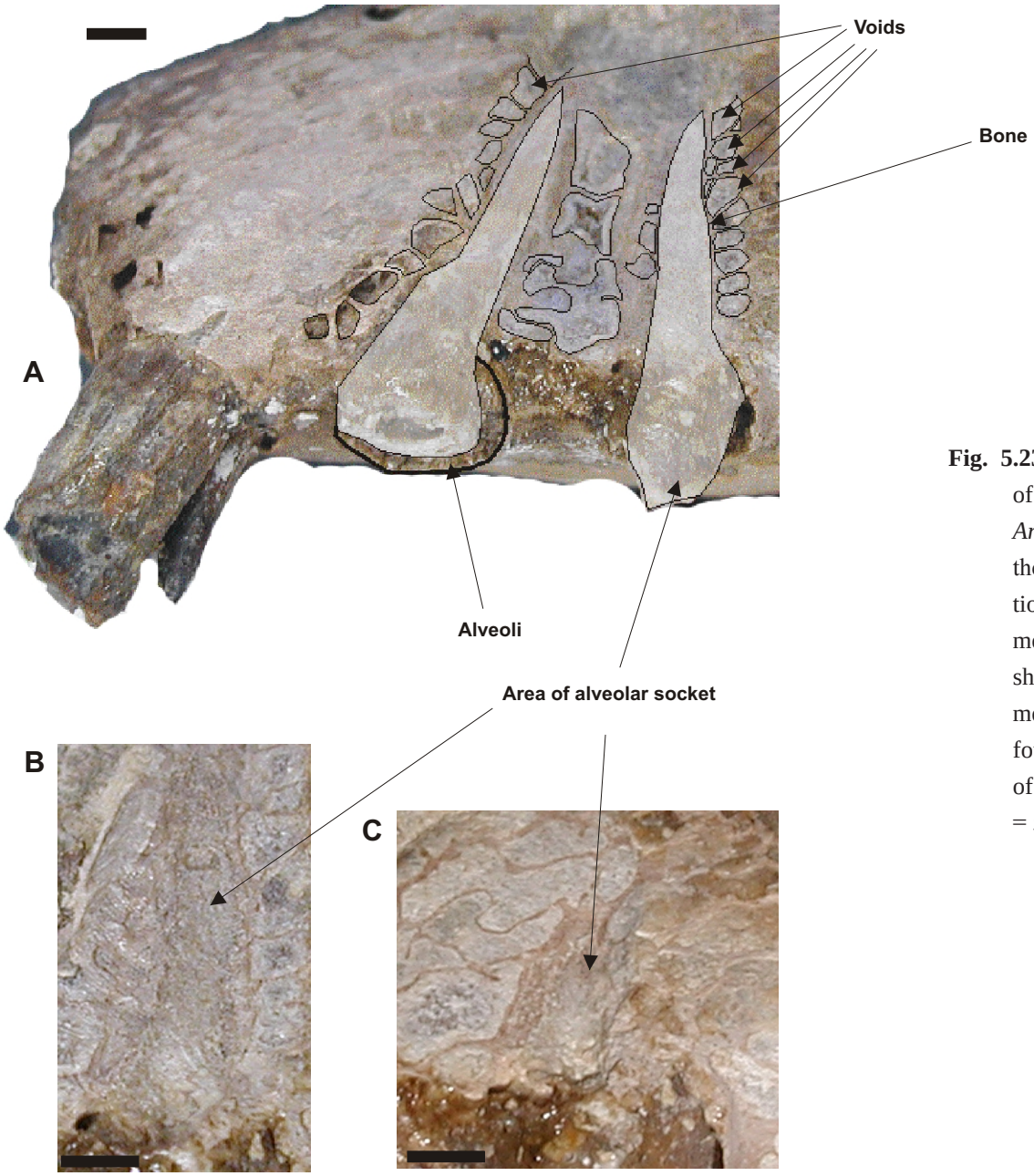

Fig. 5.23: A) Left lateral view of anterior upper jaw of *Anhanguera sp.*, showing the first four tooth positions. Outer bone wall mechanically removed to show interior trabecular meshwork; B) Detail of fourth alveolus; C) Detail of third alveolus. Scale bar = 5 mm.

teeth. To evaluate the influences of the periodontal ligament in pterosaurs, two possible configurations were investigated by Berg (2002) using FEA. The study was based on a FE-model of a typical Ornithocheirus high tooth construction and its surrounding alveolar bone (Fig. 5.24). In the first model, the ligament consists of spars which are capable of transferring only tensile loads (Fig. 5.25), whereas the spars of the second model are able to transfer tensile as well as compressive loads (Fig. 5.26).

The analysis showed that the distribution of tensile stresses in the tooth model is more homogeneous if the ligament transfers only tensile forces. The stress passes more in the direction of the root than in the model with tensile and compressive spars (Berg 2002). Comparing the translation, i.e. the relative motion of the tooth to the alveolar bone during loading, the tensile ligament resulted in bigger translation of the tooth model (Berg 2002). At the same time, the stress at

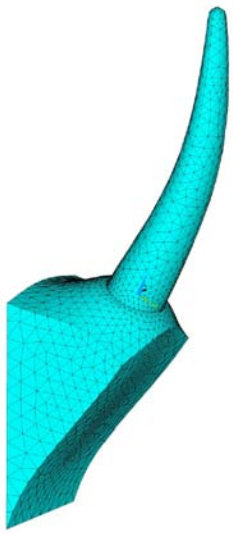

Fig. 5.24: ANSYS™-model of Ornithocheirus high tooth construction implanted in jaw bone. From Berg (2002).

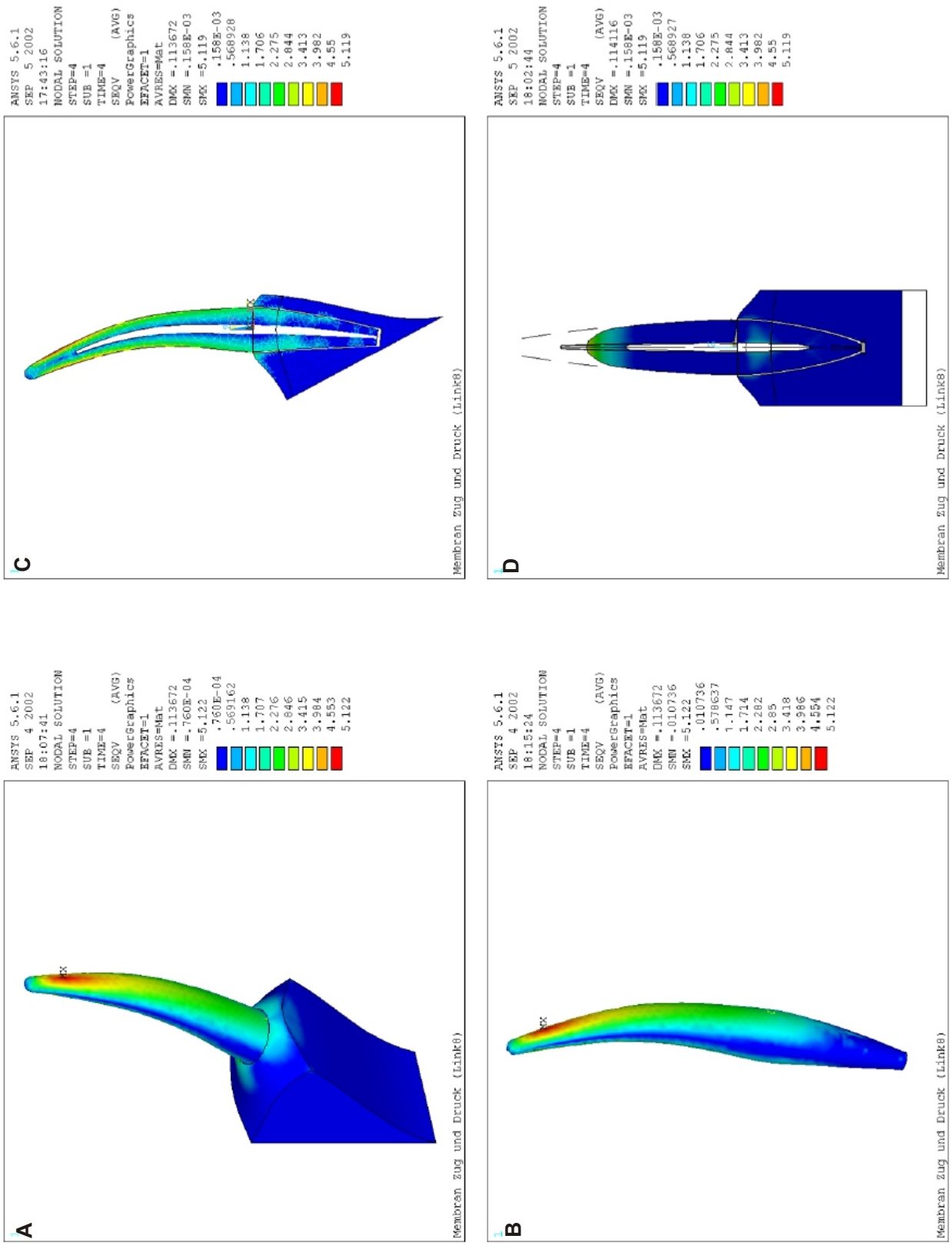

Fig. 5.25: Illustration of stress distribution patterns in the model shown in Fig. 5.24 with tensile-only spars. Same forces applied vertically to all models, same colours mean same level of deformation: A) Antero/posterolateral view of the tooth model including partial jaw model; B) Anterior/posterior view of tooth model A); C) Sagittal section of the tooth/partial jaw model; D) Transverse section of the tooth/partial jaw model. From Berg (2002).

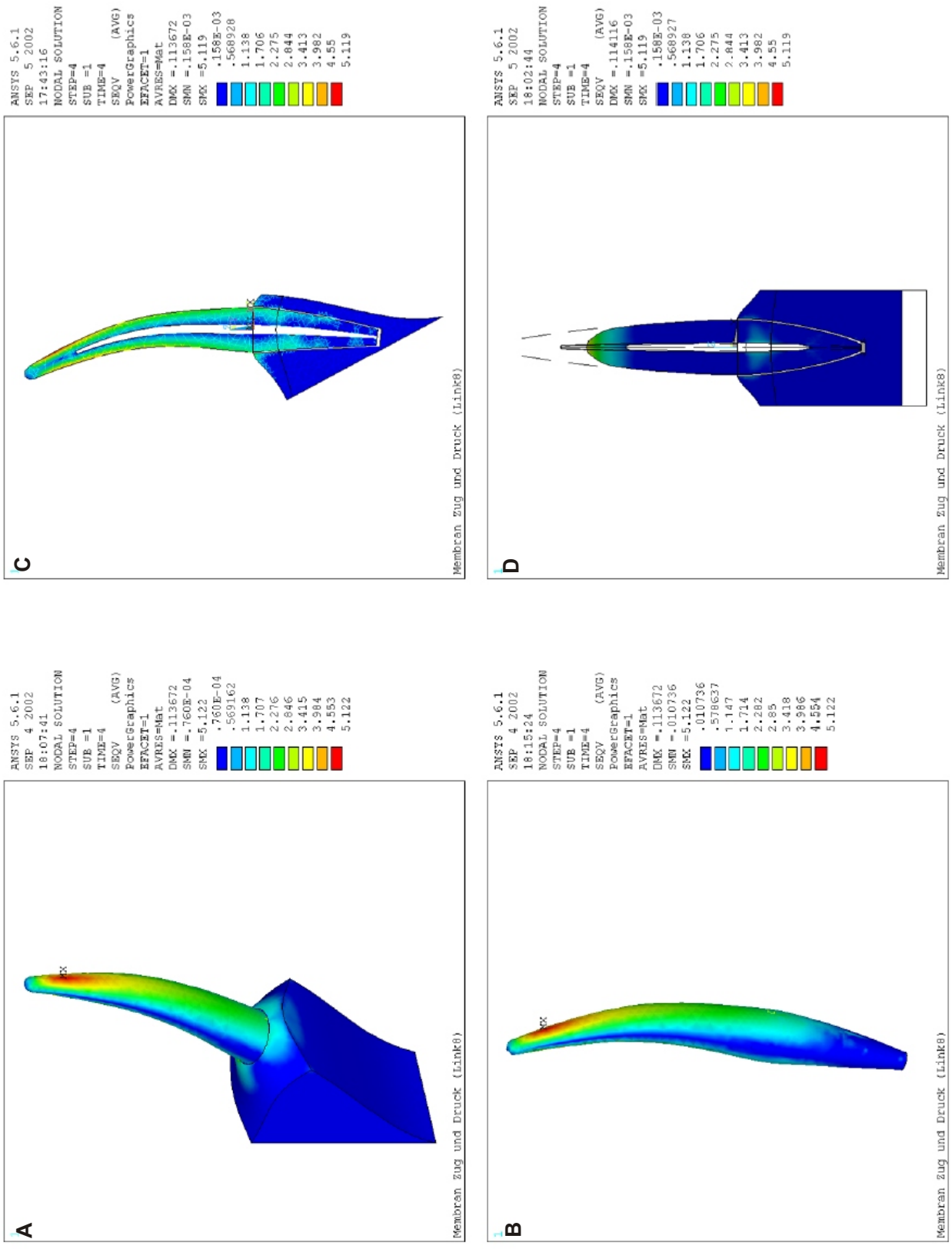

Fig. 5.26: Illustration of stress distribution patterns in the model shown in Fig. 5.24 with tensile and compressive spars. Same forces applied vertically to all models, same colours mean same level of deformation: A)-D) like Fig. 2.25. From Berg (2002).

the circumference of the tooth model is higher in case of a tensile and compressive ligament.

For both configurations, the ligament reacts elastic in the direction of the central root axis and stiff in oblique direction. The former thus represents the optimal direction in which the tooth is loaded, because less force is transmitted into the jaw (damping).

Both models show the same pattern of a global minimum of tensile stresses at the circumference of the alveolar bone around the tooth base. To reach this minimum, the forces have to be applied not exactly in the central axis of the tooth (Berg 2002) but about 18° in lateroventral direction (Fig. 5.27). This condition is similar to a bilateral loading, in which the centre of gravity and the main mass of the food item lie medially between opposing teeth of the same jaw (Fig. 5.28).

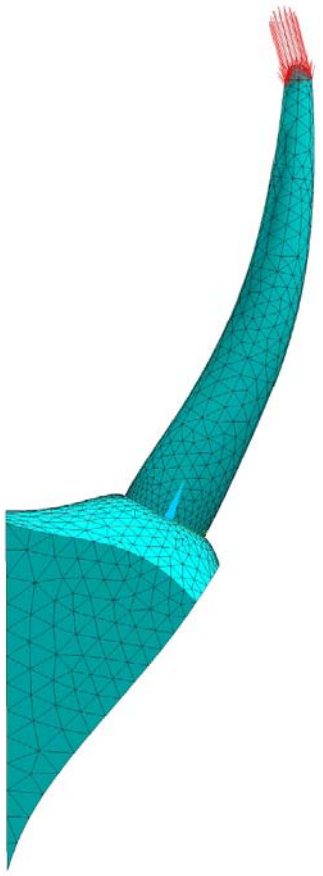

Fig. 5.27: Loading direction of tooth model, in which a global minimum of tensile stresses results in the circumference of alveolar bone around the tooth base. From Berg (2002).

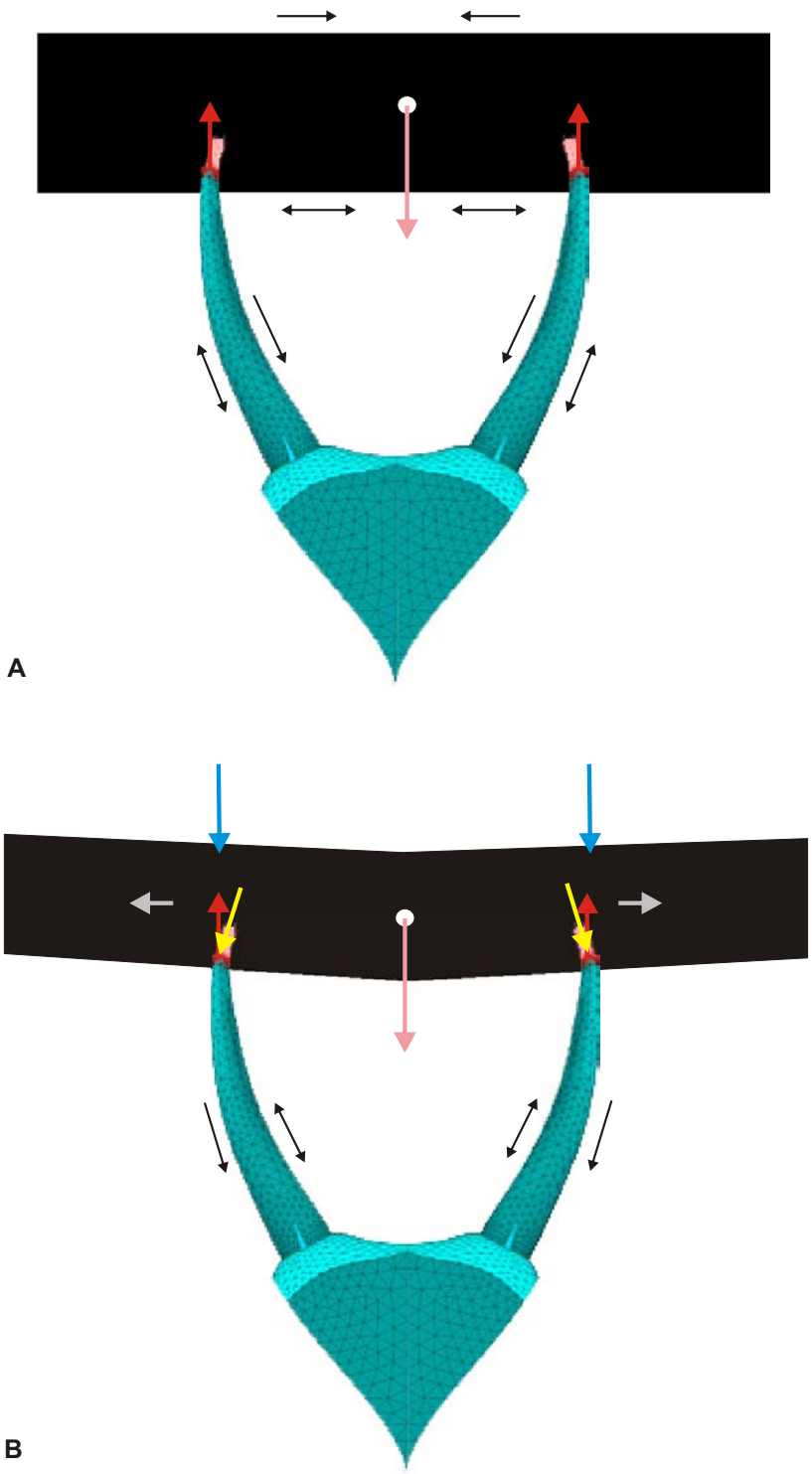

Fig. 5.28: Loads produced during bilateral loading of the tooth/jaw model: A) Loading of the teeth after initial contact of food item by lower jaw. The teeth will react as a statically defined system. The food item will deflect, producing tensile and compressive stresses in the food item. As a result, tensile stresses will result on the lateral side of the tooth and compressive stresses on the lingual side; B) Loading of the teeth after teeth of the upper jaw penetrate the food item. Deflection of the food item is restricted but tends to be deformed in the horizontal plane due to the compressive forces produced by the teeth of upper and lower jaw. The resulting stresses in the teeth are tensile on the lingual side and compressive on the lateral side. The loading leads to translation of the teeth in lateral direction. As a consequence of the overall force pattern, the teeth are not loaded strictly axially but slightly obliquely in medial direction. Blue arrow = forces induced by teeth of upper jaw in the food item, grey arrow = resulting forces within the food item, pink arrow = forces in the centre of mass, red arrow = forces induced by teeth of lower jaw in the food item, yellow arrow = resulting loading of the teeth.

6. CASE STUDY: BIOMECHANICAL ANALYSIS OF THE ANHANGUERA SKULL CONSTRUCTION

6.1 The Anhanguera upper jaw construction

The Anhanguera construction is based on a three-dimensional preserved skull of *Anhanguera sp.*, SMNK 3895 PAL (Fig 6.1). Detailed anatomical description of the skull this genus are given in Campos & Kellner (1985), Kellner & Tomida (2000) and Wellnhofer (1985). Therefore, the external geometry of the skull constructions is described in detail only as far as these aspects are important for the biomechanical behaviour of the construction. To avoid confusion, the standard anatomical nomenclature will be applied.

Fig. 6.1: Skull of *Anhanguera sp.*, SMNK 3895 PAL in right dorsolateral view.

The upper jaw construction is considered to present a continuous structure, without any sutures between individual bones. This is agreement with the condition in the skull of *Anhanguera sp.*, SMNK 2859 PAL (Fig. 6.1) which does not show any visible sutures between the skull bones. However, certain regions in the skull construction will be addressed to by the names of the appropriate bones in the skull of *Anhanguera*, following the descriptions by Campos & Kellner (1985), Kellner & Tomida (2000) and Wellnhofer (1985)

6.1.1 External geometry

The Anhanguera upper jaw construction (Fig 6.2A-D) can be divided into two subunits, an anterior rostrum and the orbitotemporal region. The rostrum reaches from the anterior tip to the line of the lower jaw articulation and bordering bar between the nasoantorbital fenestra and orbita, composed of the processus lacrimalis of the jugal and the processus jugularis of the lacrimal. The rostrum bears 28 tooth pairs, starting at the tip of the rostrum and reaching till about six seventh parts of its length in posterior direction. The first ten pair of teeth are typical for the Ornithocheirus high tooth construction, whereas the posterior ones are of the Ornithocheirus low tooth construction type. The teeth of the anteriormost four tooth positions are bent in posteroventral direction whereas the teeth in subsequent tooth positions are orientated ventrally. The dentition increases in size, starting from the first to the fourth pair of alveoli, the latter bearing the longest teeth of the dentition. In posterior direction, the teeth decrease in height gradually. The teeth of the 17th to 28th alveolus are about one tenth of the height of the longest teeth.

Discounting the crest, the rostrum roughly has a triangular shape in lateral, dorsal and ventral view with the dorsal resp. ventral borders as the largest sides of the triangle. At its anterior end it is about as high as wide. The anterior end of the rostrum is blunt in lateral view and continues into a convex dorsal crest, which reaches until the level of the 12th alveolus. The crest has its greatest height between the 9th and 10th alveolus where the height of the rostrum is increased by about 25% relative to a rostrum that would have a straight margin.

The nasoantorbital fenestra is situated in the posterior one third of the rostrum, reaching from the level of the 20th pair of alveoli to the bordering jugal/lacrimal bar between rostrum and orbita. It is rounded triangular

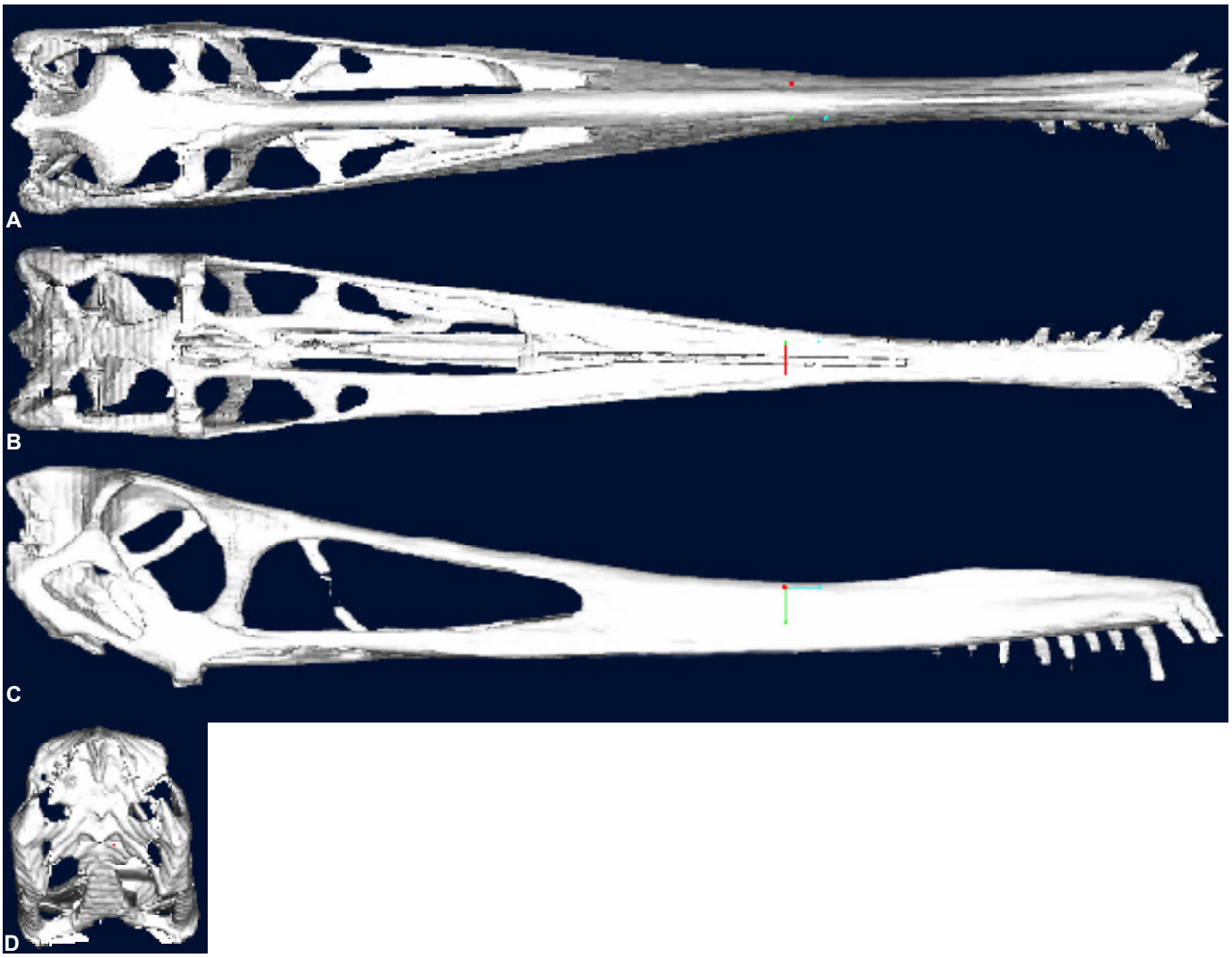

Fig 6.2: Image of the 3D model made from CT scans of *Anhanguera sp.*, SMNK 3898 PAL: A) Dorsal view; B) Ventral view; C) Left lateral view; D) Posterior view.

in outline with two long ventral and dorsal sides and a short posterior side, which is orientated slightly oblique in anterodorsal direction. The height of the nasoantorbital fenestra is about 27% of its length. The dorsal and ventral bordering bars, composed of premaxillary and nasal, respectively maxillary and jugal, taper towards half of the length of the nasoantorbital foramen. Here they reach their lowest height with about one eighth of the height of the rostrum at this level. Posteriorly they increase in height again and merge with the jugal/lacrimal bar.

In ventral view, the anterior part of the facies palatinalis of the rostrum tapers until the level of 8th pair of alveoli. Posterior, the facies palatinalis increases gradually in width and reaches its maximum value at the level of the lower articulation. Six fenestra are visible on the posterior one third of the facies palatinalis. Two of them are situated medially, whereas the others are located pairwise more laterally on each side. The anterior pair of the latter fenestra are bordered anteriorly and medially by the palatine, laterally by the maxillary and posteriorly by the ectopterygoid. The fenestrae are located at the posterior one fifth of the length of the rostrum and are oval-shaped. They are smaller than the other fenestrae on the facies palatinalis, measuring about one sixth of the ventral width of the rostrum at this level. In posterior direction, the rounded-quadrangular shaped subtemporal foramen is situated on each side. It is bordered anteriorly by the ectopterygoid, laterally by the maxillary and jugal, medially by the pterygoid and posteriorly by the quadrate. In length, the subtemporal

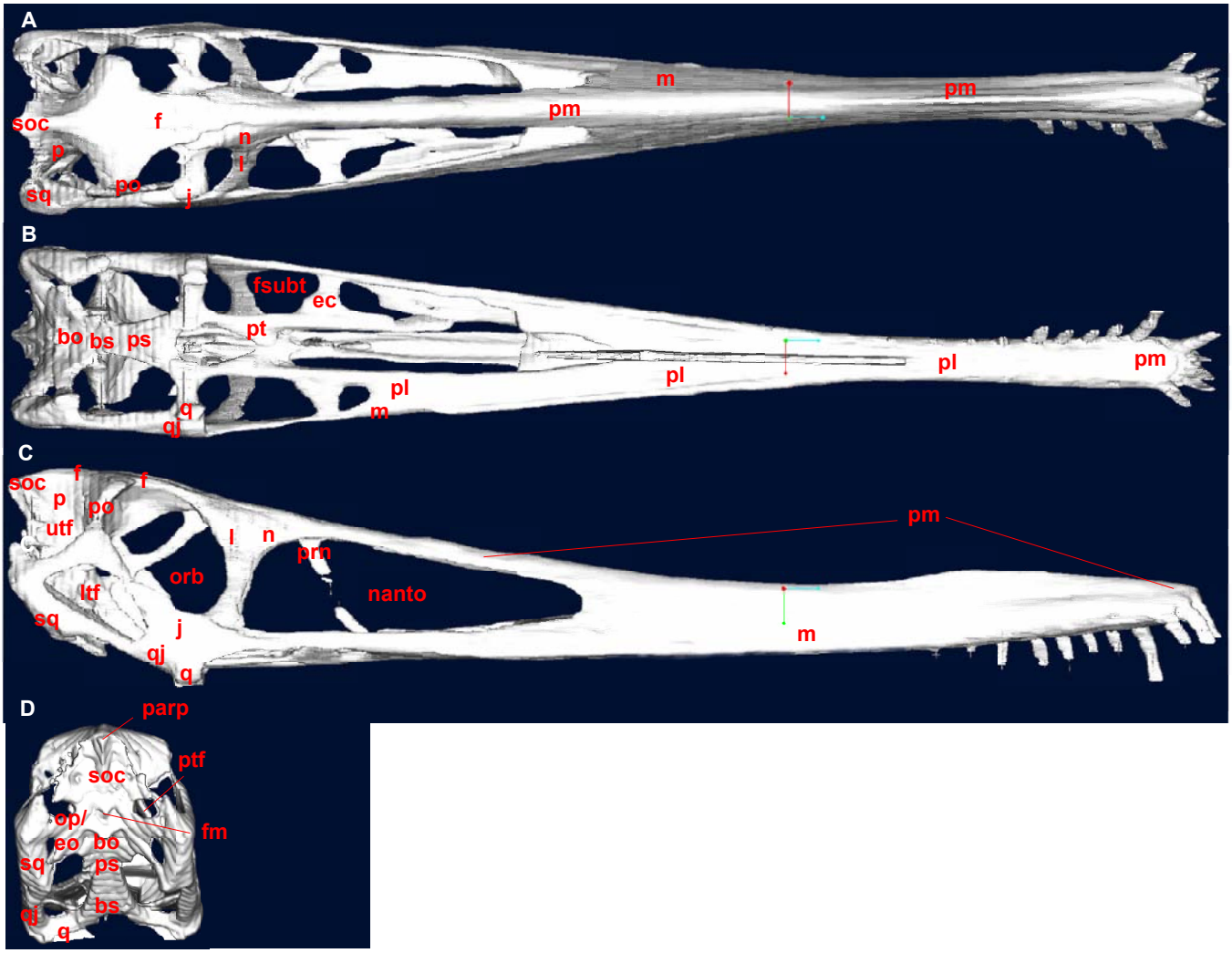

Fig 6.3: Labelling of the areas of the skull bones of *Anhanguera sp.*, SMNP 3895 PAL, according Kellner & Tomida (2000) and Wellnhofer (1985, 1991b). No sutures are visible between individual skull bones. A-D) see Fig. 6.2. Abbreviations: bo basioccipital, bs basisphenoid, ec ectopterygoid, eo exoccipital, f frontal, fm foramen magnum, fsubt foramen subtemporalis, j jugal, l lacrimal, ltf lower temporal fenestra, m maxillary, nanto nasoantorbital fenestra, p parietal, parp paroccipital process, pl palatine, pm premaxillary, po postorbital, prn processus nasalis, orb orbita, op opisthoticum, ps parasphenoid, pt pterygoid, q quadrate, qj quadratojugal, soc supraoccipital, sq squamosal, utf upper temporal fenestra.

foramen measures about one sixth of the total length of the rostrum and in width about one third of the width of the facies palatinalis at this level. Medial to the subtemporal foramen and foramen anterior, two single fenestra are present. The anterior one of these is bordered anterolaterally by the palatine, posterolaterally by the pterygoid and parasphenoid. The fenestra is sub-rectangular in outline and reaches from about the level of the posterior two fifths of the total length of the rostrum to about half of the length of the foramen supratemporalis. The width is about one third of the width of the facies palatinalis at this level. At the posterior end of the anterior medial fenestra, both pterygoids fuse together and form an anteromedial projecting spiny process which extends to the level of the anterior border of the subtemporal foramen. The posteriorly succeeding fenestra is bordered anterolaterally by the pterygoid, posterolaterally by the quadrate and posteriorly by the parasphenoid. It is acute-oval in outline and measures about the same width as the foramen anterior to it and about half of the length of the subtemporal foramen.

Whereas the rostrum forms the anterior part of the skull construction, its posterior part consists of the orbitotemporal region. Here, the largest openings are the orbits, which are situated in the anterior half of the

orbitotemporal region. They are bordered anteriorly by the jugal/lacrimal bar, dorsally by the frontal and posterodorsally by the frontal/postorbital bar. The latter continues into the postorbital/jugal bar which borders the orbita posteroventrally and the jugal ventral to the orbita. The outline of the orbita is oval with the main axis orientated anteroventrally/posterodorsally. In height, the orbita measures about two thirds of the height of the orbitotemporal region and in length about half of the length of the orbitotemporal region.

Together with the quadratojugal, the jugal ventral to the orbita forms a prominent plate-like structure. Its height measures about one third of the total height of the orbitotemporal region at this level.

Posterodorsal to the orbita, the upper temporal fenestra is located. It is surrounded anteriorly by the frontal/postorbital bar, dorsally by the parietal, posterodorsally by the supraoccipital, posteriorly by the squamosal and ventrally by the squamosal/postorbital bar. Medially the ventrally projecting parietal and the braincase border the upper temporal fenestra. The fenestra measures about half of the length and height of the orbitotemporal region.

The lower temporal fenestra is situated posteroventral to the orbita. It is bordered anteriorly by the postorbital process of the jugal and dorsally by the squamosal/postorbital bar. Posteriorly it is enclosed by the quadrate, which is orientated with about 30° in posterodorsal direction, and ventrally by the quadratojugal. The fenestra is rounded-triangular in outline and orientated obliquely with the acute angle located anteroventrally. It has the same height and length as the upper temporal fenestra.

The jugal/lacrimal, postorbital/jugal and the squamosal/postorbital bar all have about the same width, which is about the same as the lateral width of the lower jaw articulation.

In lateral view, the dorsal outline of the orbitotemporal region is convex. The dorsal border is mostly formed by the frontal which forms a rhomboid medial plate in ventral view. Posteriorly the frontal continues into the parietal and the supraoccipital, the latter forming a short, blunt process in posterior direction.

In dorsal as well as in ventral view, the orbitotemporal region is rectangular. The lower jaw articulation is situated ventrally at about the level of one third of the anterior length of the orbita. The articulation forms the ventral support for the construction. The condyles are formed like a helical roll with the long-axis orientated laterally-lingually (Fig. 6.4). They bear a spirical groove, left handed on the right side and right handed on the left side. In medial direction, a short process of the quadrate furnishes the contact with the palatine.

In posterior view, the orbitotemporal region is higher than wide. The occipital condyle, which forms the posterior support of the construction, is situated medially and level with the posterodorsal edge of the lower temporal fenestra. Dorsally to the foramen magnum, the rhomboid supraoccipital is present. The exoccipital and opisthoticum are orientated horizontally at the level of the foramen magnum. They enclose a small fenestra together with the parietal and squamosal. It is roundish and measures about one fourth of the posterior width of the orbitotemporal region.

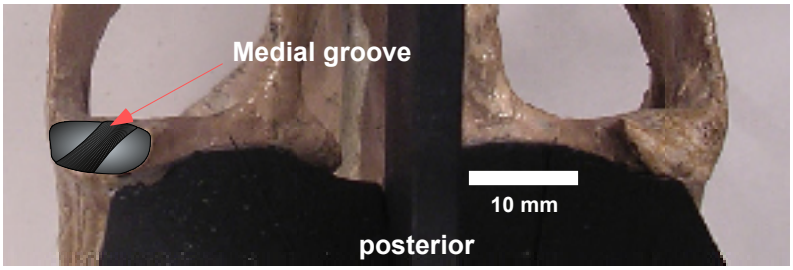

Fig 6.4: Ventral view of lower jaw articulations of *Anhanguera sp.*, SMNK 3895 PAL.

Ventral to the exoccipital/opisthoticum, a second, larger fenestra is developed. Laterally and ventrally it is bordered by the quadrate and medially by the basi- and parasphenoid. Both latter bones are orientated anteroven-

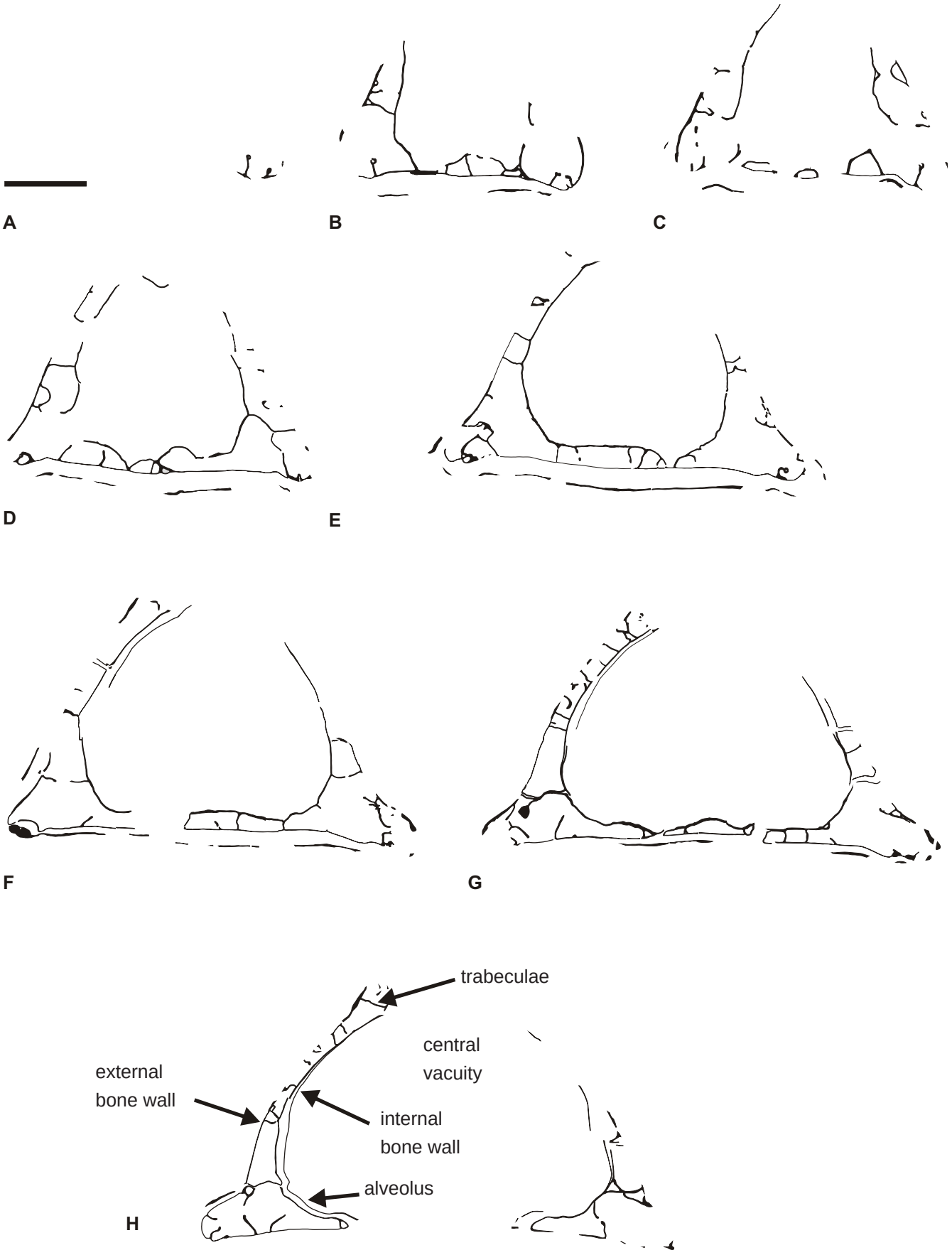

Fig. 6.5: A-I: Drawings of polished cross-sections of ornithocheirid rostrum, taken in 10 mm steps, A = anteriormost cross-section. See Fig 6.6 for interpretational model. Scale bar = 10mm.

trally. The fenestra is oval in ventral view and measures about half of the length and about one third of the width of the orbitotemporal region.

In posterior and lateral view, the squamosal bears a anteroventrally orientated process that is not in contact with other bones. Its tip is level with the ventral extension of the lower temporal fenestra.

6.1.2 Internal geometry

The transversal cross-section through the rostrum is sub-triangular. The external walls are thin compared to the overall width with a mean thickness of 1 mm. Inside the rostrum a second, nearly triangular bone layer is visible, which is slightly thinner than the external wall (Fig 6.5). The two layers are braced by trabeculae which are orientated perpendicular to the layer surfaces. These trabeculae have about the same thickness as the inner layer. Their density is low (roughly 10 trabeculae/side).

The external wall of the rostrum is thickened along the dorsal edge, where the bone thickness is nearly doubled, whereas the thickness of the internal layer remains constant (Fig 6.5). At the ventrolateral edges, the external layer shows ventrolateral projections with an increased trabecular density. This projections form the alveoli and subsidiary interalveolar areas. The external walls of the aveoli are nearly doubled in thickness, like at the dorsal edge of the rostrum.

The overall construction of the rostrum technically represents a hollow triangular tube with a double-layered wall supported by struts (Fig 6.6). Whereas at the anterior rostral region, the internal ventral width w_i is about half of the external ventral width w_o, it increases significantly in posterior direction. At the level of the anterior end of the nasoantorbital fenestra, w_i measures about 6/7 of w_o.

The bars and struts enclosing the nasoantorbital fenestra and forming the orbitotemporal region are composed of an external bone layer with an internal trabecular-filled region (Fig. 6.7). Here, the trabecular density is similar to that of the alveolar region of the anterior rostrum. The orientation of the individual trabeculae varies, but most of them meet the outer layer in angle of about 90°. A number of the trabeculae are not just cylindrical columns but are rather plate-like and wavy. They encircle small voids, giving these bars a spongious cross-section. Also the braincase is enclosed by this spongy bone with only a medial empty space for the brain.

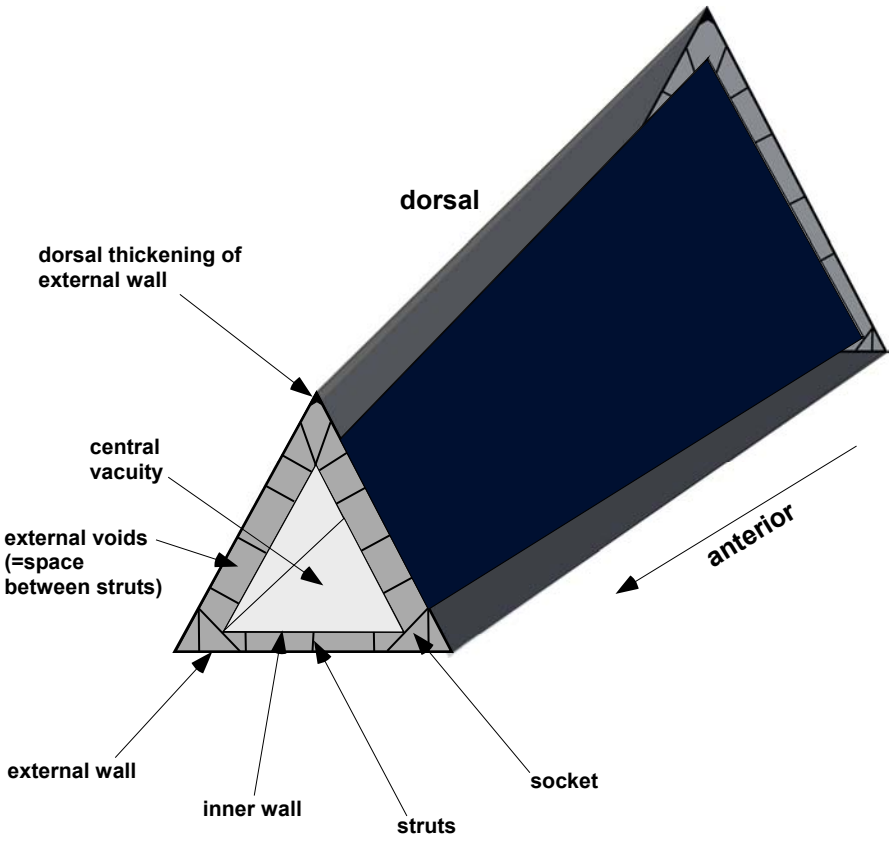

Fig. 6.6: Model for a partial rostrum of *Anhanguera*. Note change in abstract concept, using constructional instead of anatomical terms.

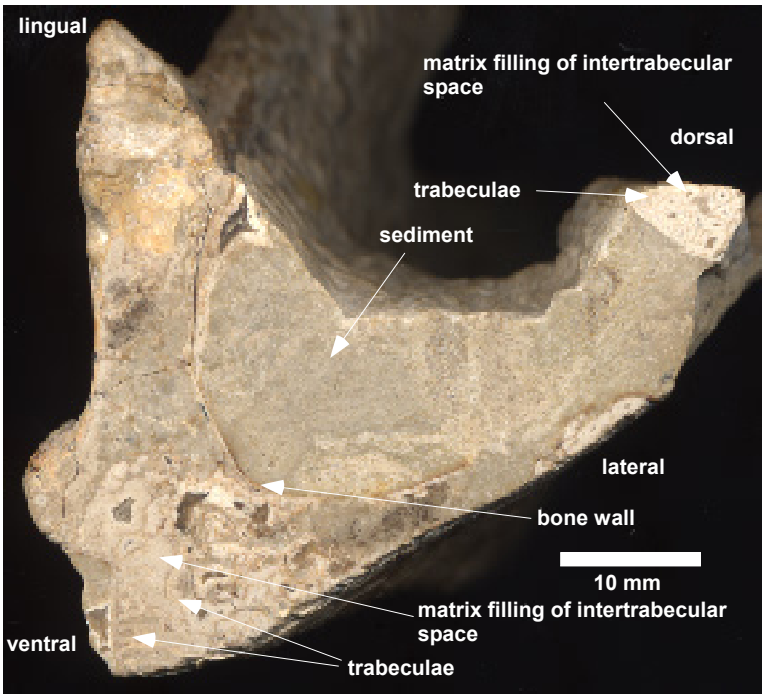

Fig. 6.7: Cross-section through quadratojugal region of an ornithocheirid pterosaur.

6.1.3 Main jaw muscles of the Anhanguera skull

By using comparative anatomy with crocodiles and birds as the closest living relatives, the following main jaw muscles are identified as being importing for jaw closing and opening (Cleuren & DeVree 2000, Schumacher 1973,):

- Musculus adductor mandibulae externus (MAME)
- Musculus adductor mandibulae posterior (MAMP)
- Musculus adductor mandibulae internus (MAMI), subdivided in:
    - M. pterygoideus anterior (MPTA)
    - M. pterygoideus posterior (MPTP)
    - M. pseudotemporalis (MPST)
    - M. intramandibularis (only in lower jaw, therefore omitted here)
- M. depressor mandibulae (MDM)

Their reconstructed origin, course and insertion in the Anhanguera skull are given below and in Fig. 6.8.

• Musculus adductor mandibulae externus & posterior (MAME/P)

Origin: medial side of the upper temporal arch, posterior border of lower temporal fenestra, lateral surface of bony area ventral to orbita and dorsal to quadrate.

Course: passes trough subtemporal foramen in anteroventral direction towards the lower jaw

Insertion: fenestra meckeli and dorsolingual surface of bony area ventral to the F. meckeli

Function: predominantly adduction of mandible

• Musculus pterygoideus anterior (MPTA)

Origin: dorsal surface of the pterygoid, ectopterygoid and palatine at the level of the antorbital fenestra, possibly anterodorsal region of antorbital fenestra (Horner & Lessem 1993, Wellnhofer 1991a).

Course: passes through the anterior region of the subtemporal foramen

Insertion: bony area ventral to the f. meckeli, ventral to the insertion of the MAME/P

Function: predominantly adduction of mandible

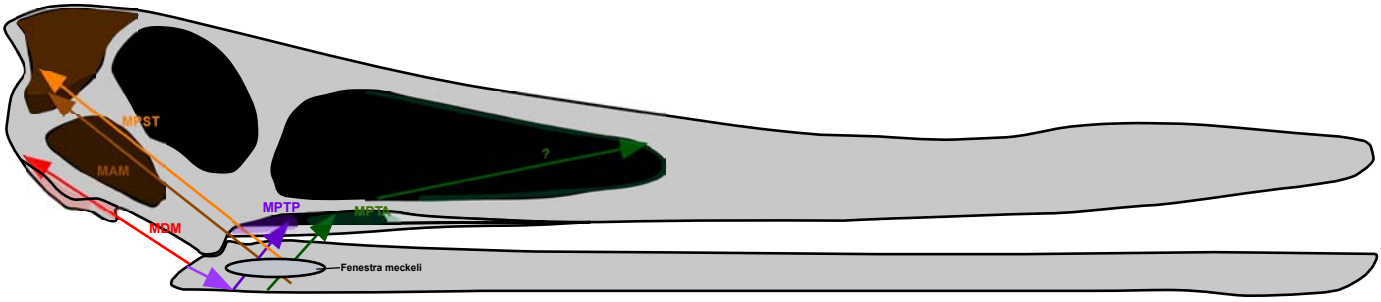

Fig. 6.8: Reconstruction of main jaw muscles, abstraction of stereolithography of *Anhanguera* skull model from Fig. 6.2 and modelled plasticine muscles. Mandible added graphically after own observations on other skulls of *Anhanguera*. Areas of attachment of muscles coloured similar to the colour of the muscles. Abbreviations: MAME/P = Musculus adductor mandibulae (encloses M. adductor mandibulae externus and M. adductor mandibulae posterior), MDM = M. depressor mandibulae, MPST = M. pseudotemporalis, MPTA = M. pterygoideus anterior, MPTP = M. pterygoideus posterior.

• Musculus pterygoideus posterior (MPTP)

Origin: dorsal and ventral surface of the pterygoid

Course: passes latero- and dorsoventrally trough subtemporal foramen

Insertion: ventrolateral, ventral, lingual and dorsolingual area of retroarticular process.

Function: predominantly adduction of mandible

• Musculus pseudotemporalis (MPST)

Origin: from posterodorsal surface of the postorbital/squamosal bar along the lateral side of the parietal to the anterodorsal part of the posterior border of the supratemporal fenestra

Course: passes anteroventrally trough subtemporal foramen

Insertion: anterior end of f. meckeli

Function: predominantly adduction of mandible

• Musculus depressor mandibulae (MDM)

Origin: anterior and posterior facies of the posteroventral squamosal process

Insertion: dorsolateral surface of retroarticular process

Function: abduction of mandible

6.2. Lever mechanics of the Anhanguera construction

For the study of lever mechanics all muscles are treated as acting in a single, sagittal plane. The system represents a third class lever as far as the adductor muscle action is concerned. In contrast to this, the action of the MDM forms a first class lever. The latter is omitted here, because only adductor forces are taken into account. From the measurements taken, it is evident, that the force produced by the MDM during jaw opening is much lower than the forces of the adductor muscles (Tab. 6.1 & 6.2).

The lever arms of the individual jaw closing muscles are shown in Fig. 6.9. The resulting bite forces for an anterior bite are given in Tab. 6.3. Note that the results are calculated for one side only; for a symmetrical bite, the force values have to be doubled because muscles act on both sides of the skull. Damping effects of the food item are neglected.

For the equation given for the conditions of equilibrium in a lever (Sinclair & Alexander (1987)

$$x_B \times F_B \times \sin\alpha_B - \sum l_i \times F_i \times \sin\alpha_i = 0 \ , \qquad (13)$$

Muscle	Length (mm)	Cross-sectional area (mm^2)	Force (N)
MAME/P	90	90	36
MPTA	25	35	14
MPTP	60	220	88
MPST	115	230	92
MDM	70	80	32

Tab. 6.1: Geometrical parameters and resulting force in the major jaw muscles of *Anhanguera sp.*, SMNK 3895 PAL, based on a pennate muscle with muscular force after Martin et al. (1998) of 0,4 N/mm^2.

Muscle	Mass (g)	Estimated force (n)
MAME/P	8.1	27
MPTA	0.88	10.5
MPTP	13.2	66
MPST	26.5	69
MDM	5.6	24

Tab. 6.2: Mass of the major jaw muscles of *Anhanguera sp.*, SMNK 3895 PAL and resulting estimated forces after Sinclair & Alexander (1987).

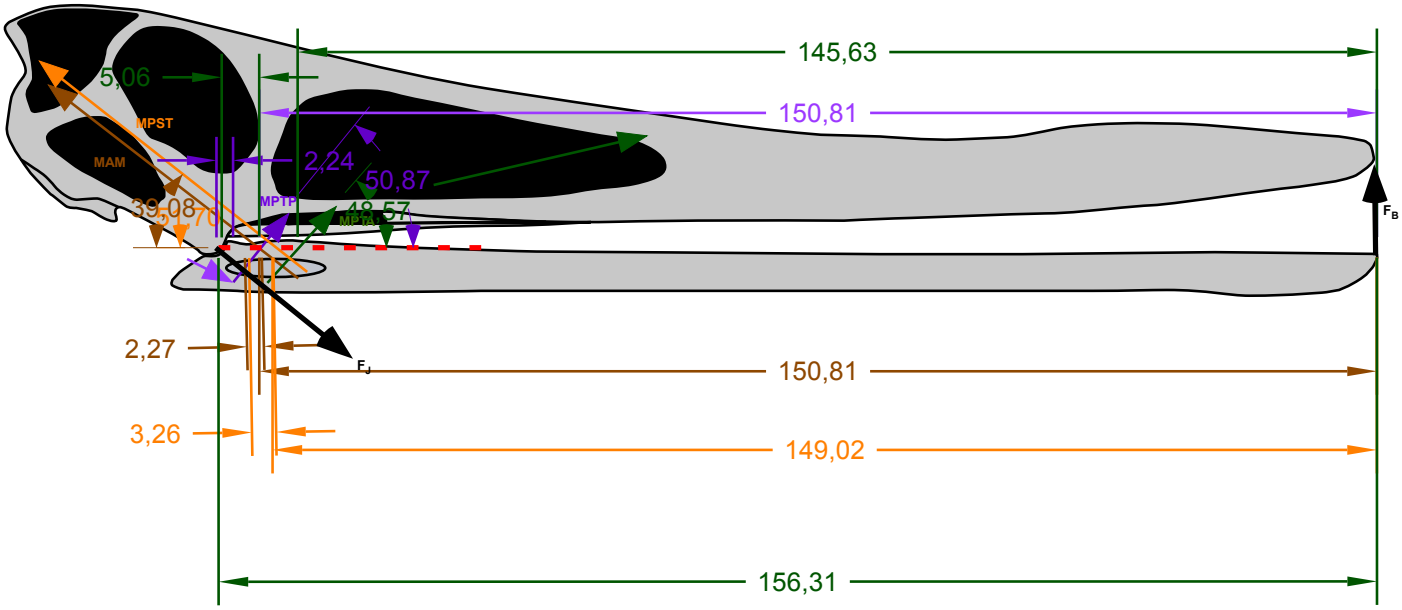

Fig. 6.9: Lever arms of adductors muscles and direction of resulting bite force F_B and joint reaction force F_J for full occlusion in abstraction of stereolithography of *Anhanguera* skull model from Fig. 6.2. Angles in °, distances in mm.

the resulting bite fore F_B is calculated using the values given in Tab. 6.1 as 5.9 N for an anterior bite with an angle of 90°. From this, the resulting joint force (F_J) and its direction is deduced by the equations:

$$F_J \times \sin\alpha_J + F_B \times \sin\alpha_B - \sum(F_i \times \sin\alpha_1) = 0 \ , \quad (14)$$

$$F_J \times \cos\alpha_J + F_B \times \cos\alpha_B + \sum(F_i \times \cos\alpha_1) = 0 \ , \quad (15)$$

For the adductor muscle levers, F_J is 221.9 N and has an angle α_J of 39.83° (Fig. 6.9). The resulting force is roughly in line with the posterior border of the lower temporal fenestra, a relation already premised by Sinclair & Alexander (1987) in other reptiles.

The results above are based on a bite force F_B, which is perpendicular to the jaw. However, the bite force may be as well orientated oblique to the dorsal border of the jaw. If α_B is set as e.g. 70°, F_B results as 6,3 N from equation 13. The resulting joint force F_J is 220.3 N with an angle α_J of 40.2°. If the bite force is orientated parallel to the axes of the anteriormost four tooth pairs (110°), F_B is similar (6.3 N), but F_J increases (223.6 N) and α_J decreases (39.5°). However, these values do not differ significantly from the bite force with an angle of 90° (see above).

The loading conditions can be further varied by considering a more posterior bite, e.g. halfway along the jaw. For a perpendicular bite force the results are F_B = 11.8 N, F_J = 218.2 N and α_J = 38.6° in this case. The bite force is doubled compared to an anterior bite, whereas the joint force remains the same.

In contrast to other longirostrine vertebrates (Preuschoft et al. 1985), F_J in the Anhanguera construction does not exceed the muscular force. The anterior bite forces thus are constrained by the muscular forces and not by F_J.

The sum of the bite forces generated along the jaw from the 1st to the 28th tooth is 349 N. If the teeth were neglected and only the bite force along the jaw bone is considered, the sum of forces is deduced from

$$\sum F_B(x) = \int_{xn}^{xo} \frac{\sum F_i \times l_i \times \sin\alpha_i}{x_B} = (\sum F_i \times l_i \times \sin\alpha_i) \times ((\ln(x_o) - \ln(x_n)) + \frac{1}{x_o}) \quad , \qquad (15)$$

with x_0 being the maximum distance from the lower jaw articulation and x_n the minimum distance from the jaw joint. Setting x_n to 75 mm which corresponds to the last tooth position, $\sum F_B$ is 3353 N. Considering the area of 1st to 8th teeth, the forces are 51 N (teeth) and 365 N (jaw line), respectively (Tab. 6.3).

The calculations made above have only address the final stage of the bite process. To calculate the forces on the lower jaw at the initial stage of the bite, the maximum gape angle has to be reconstructed. This cannot be based solely on the maximum range of the lower jaw articulation because the elongation and functionality of the jaw adductor muscles represents a further constraint. The maximum gape angle of the jaws based on the hard parts alone (40°) would lead to a direct bone-to-bone contact from the facies dorsalis of retroarticular process of the lower jaw with the posterior side of the lower jaw articulation. This is unlikely because this is the insertion site of the MDM, which would be compressed. In this case, the lever arms of MAME/P and MPST have to rotate around the lower jaw articulation to retain contact with the lower jaw. A more reasonable value of the maximum gape angle including the space used by muscles and straight lever arms therefore is about 25°. For this value, the lower jaw is approximately in line with the posterior border of the lower temporal fenestra. Here, the resulting forces and angles are F_B = 5.9 N, F_J = 151.3 N and α_J = 55.6° for an anterior bite (Fig 6.10) and F_B = 10.6 N, F_J = 147 N and α_J = 54.4° for a bite at half of the jaw length. The resulting angles are about in line with the bar between orbita and lower temporal fenestra. However, these forces only occur in the lower jaw, because during this stage, there is no direct contact of lower jaw-food-item-upper jaw.

During the bite process, a clear change in the advantage of the lever arms occurs. In the initial stage, the MPTA and MPTP have the greatest mechanical advantage with a large angle, whereas the MAME/P and MPST produce only small forces. Both latter muscles get important at the terminal stage of the bite for holding

Tooth position	x_a (mm)	x_0 (mm)	F_B	F_J	α_J
1	0	360.97	5.9	221.94	39.83
2	4	356.97	5.97	221.89	39.82
3	11	349.97	6.09	221.82	39.80
4	20	340.97	6.25	221.71	39.77
5	39	321.37	6.61	221.48	39.69
6	37	323.97	6.57	221.51	39.70
7	45	315.97	6.74	221.40	39.67
8	56	304.97	6.98	221.24	39.62
9	70	290.97	7.32	221.03	39.55
10	80	280.97	7.58	220.86	39.5
11	91	269.97	7.89	220.67	39.44
12	110	250.97	8.49	220.29	39.32
13	124	236.97	8.99	219.97	39.22
14	141	219.97	9.68	219.53	39.08
15	153	207.97	10.24	219.18	38.96
16	167	193.97	10.98	218.72	38.81
17	182	178.97	11.90	218.14	38.62
18	195	165.97	12.83	217.56	38.43
19	208	152.97	13.92	216.89	38.21
20	220	140.97	15.11	216.15	37.96
21	230	130.97	16.26	215.45	37.72
22	241	119.97	17.75	214.54	37.40
23	248	112.97	18.85	213.87	37.17
24	256	104.97	20.29	213.01	36.86
25	264	96.97	21.96	212.01	36.50
26	271	89.97	23.67	210.99	36.13
27	278	82.97	25.67	209.82	35.69
28	286	74.97	28.41	208.24	35.07

Tab. 6.3: Resulting resulting bite force F_B and joint reaction force F_J with angle α_J for various tooth positions reconstructed for *Anhanguera sp.*, SMNK 3898 PAL, at final closing stage (occlusion). $\alpha_B = 90°$, x_a = distance from anterior, x_a = distance from lower jaw articulation.

the food item, when these muscles reach their greatest mechanical advantage. At this stage, MPTA and MPTP show a low mechanical advantage.

6.3. Frame analysis of the Anhanguera construction

The Anhanguera construction can be approximated as a frame consisting of struts and rigid joints, in which the former are connected to each other. In contrast to a truss where the struts are joined by pivots and rotation occurs when forces are applied, only deflection is present in a frame (Molnar 1998).

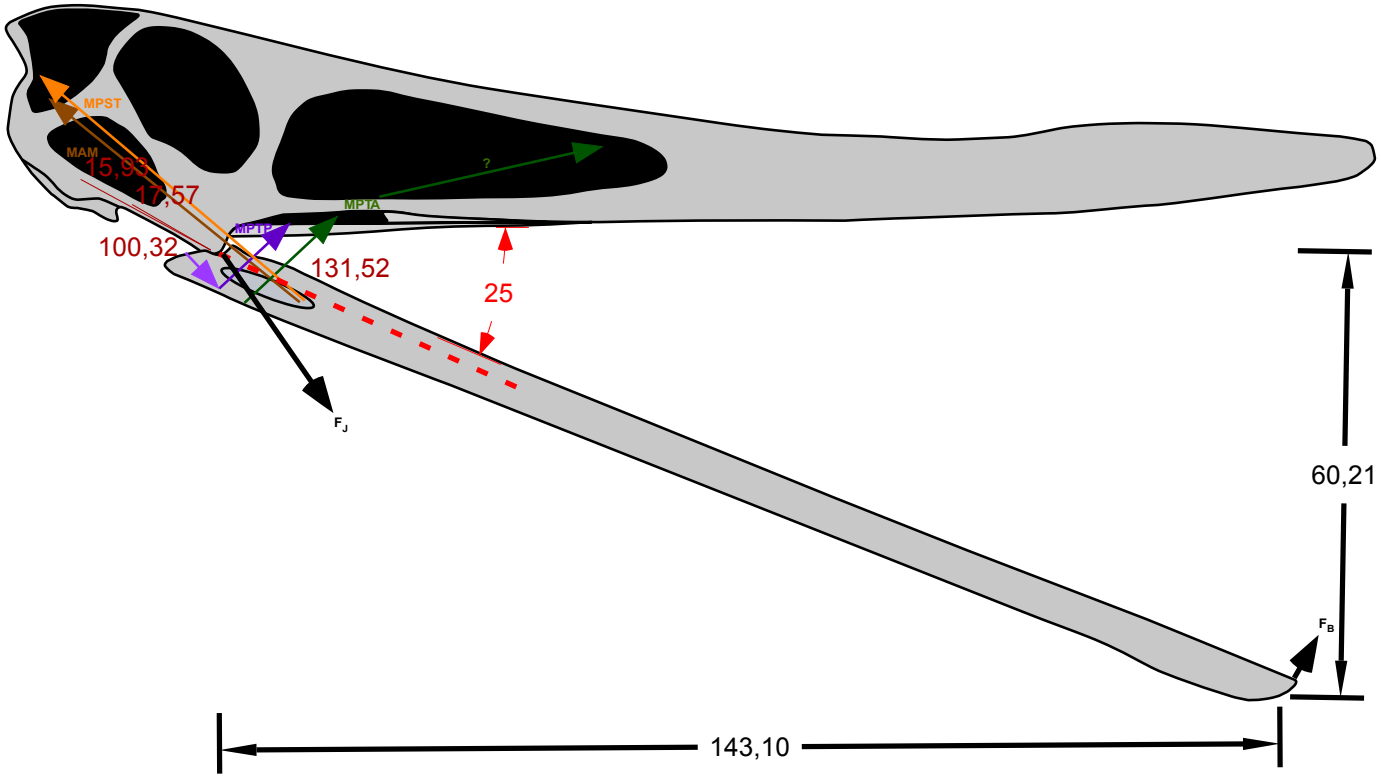

Fig. 6.10: Lever arms of adductor muscles and direction of resulting bite force F_B and joint reaction force F_J for initial occlusion stage in abstraction of stereolithography of *Anhanguera* skull model from Fig. 6.2. Angles in °, distances in mm.

6.3.1 Plane frame analysis

The cross-section of the rostrum is triangular with a dorsally directed paraboloid arch. It can be approximated as a isosceles triangle consisting of three struts. This structure is mechanically stable independent, if it represents a truss or a frame (Bardoux 1966, Molnar 1998).

As the Anhanguera construction has no direct occlusal contact between upper and lower teeth as in mammals, the horizontal force components of the imposed forces are low. Otherwise, the ventral part of the frame triangle would tend to bow and a tensile member would be needed to stabilise the frame (Bardoux 1966).

Applying vertical forces to the plane frame will result in a oppositely directed reaction force which has to be larger than the imposed compressive force. This is caused by the triangular cross-section which, in contrast to a rectangular cross-section, generates horizontal reaction components (Fig. 6.11). The closer the sides of

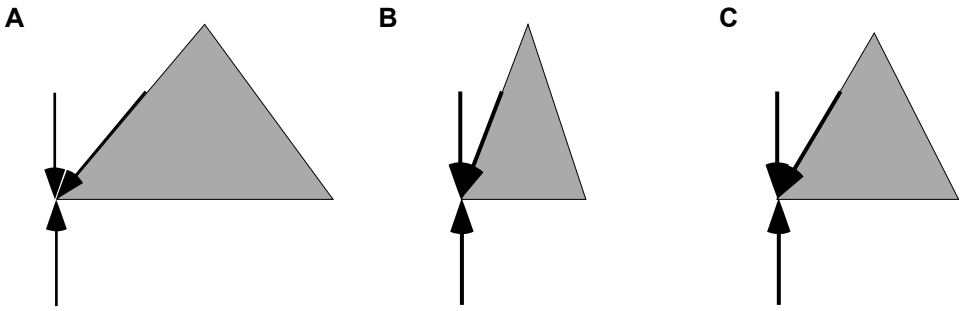

Fig. 6.11: Cross-section of modelled rostrum with bite force and resulting reactions: A) Triangular frame which is wider than high shows relatively high horizontal components (after Molnar 1998); B) Triangular frame which is higher than wide shows relatively low horizontal components (after Molnar 1998); C) Reaction components in a frame typical for the rostrum of the Anhanguera skull construction. Rostrum modelled as being massive.

the triangle are to the vertical line (Fig. 6.11), the lower are the resulting horizontal forces and the more force are absorbed (Molnar 1998).

The plane frame of the Anhanguera skull construction is broad with a mean height/width ratio of 12/11. Forces exerted at the dorsal joints of the plane frame therefore will produce large horizontal reactions. As a consequence, the imposed forces have to be low because otherwise it will fail due to buckling of the ventral bars which correspond the facies palatinalis of the rostrum. More investigations on the cross-section of the construction are given in chapter 6.4 on the beam analysis of the Anhanguera construction.

6.3.2 Space frame analysis

For three dimensional statical analysis, a skull construction can be modelled as a space frame (Badoux 1966, Molnar 1998). For constructing the space frame of the Anhanguera skull construction, triangular and quadrangular units are used. The various bars of the orbitotemporal region are modelled as struts and the rostrum is approximated as a mono frame after the principle of a Pratt truss but with rigid joints. The frame is restrained ventrally by fixed supports at four joints representing the lower jaw articulation and one posterior fixed support representing the occipital condyle for the articulation with the cervical column.

The resulting space frame (Figs. 6.12-6.15) is composed of 60 bars (m), 36 rigid joints (j) and has 15 (r) restraints. For simplification, the stresses of weight support and the force of the food item are neglected, because these can hardly be estimated with confidence. Following the equation given by Hagedorn (2001) for the statical indeterminacy of three dimensional bar structures

$$m + r \geq 3 \times j, \quad (16)$$

the bar structure does not represent a rigid (=coherent) structure as $60 + 15 \leq 108$. This common equation, however, is only valid for trusses (Spillers 1985). If modelled as a truss, distortion of the *Anhanguera* skull model will occur when a vertical force is applied to the joint K1. This would result in rotational movements at the joints K12, K13, K11 and K3 (Fig. 6.15). To prevent this, two further bars spanning from K12 to K3 and K13 to K11 would be needed, making the truss a rigid body (Fig 6.15). However, it still would be no rigid, statically determinate structure after the equation given above.

In contrast to a truss, failure of a space frame is caused by bending of the bars. Using the equation for the statical indeterminancy of space frames (Spillers 1985)

$$6m + r \geq 6 \times j, \quad (17)$$

the space frame model of the *Anhanguera* skull is statically indeterminate to a positive degree as $6 \times 60 + 15 > 6 \times 36$. The frame is stable under the imposed forces (=coherent), but has more members than are needed to guarantee this stability. From the mechanical point of view, the frame thus does not represent an optimal structure but is overbuilt.

For comparative reasons, three loading conditions were analysed:

- single load at the anterior tip of the frame (F_B) without muscular load,
- single load at the anterior tip of the frame (F_B) plus muscular loads (F_i),
- load along the tooth row from the first to the eight pair of teeth (F_B) plus muscular loads (F_i).

Figs. 6.16-6.18 and Tab. 6.4 show the resulting forces along each bar. Material properties of the bars were chosen arbitrarily because of the missing data of pterosaur bone (see chapter 3.2.4). The absolute values of the forces and moments thus should only be used for comparative purposes.

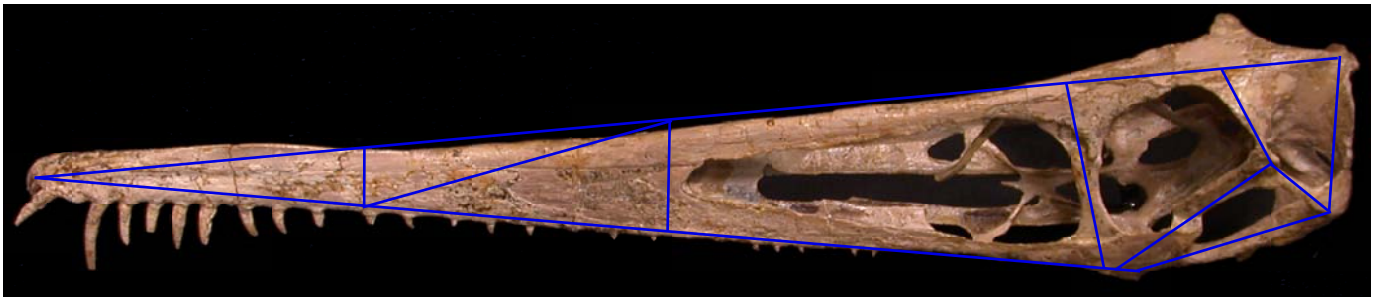

Fig 6.12: Skull of *Anhanguera sp.* SMNK 3895 PAL, with bars of the left lateral side projected into to skull to illustrate approximation of skull by a space frame model.

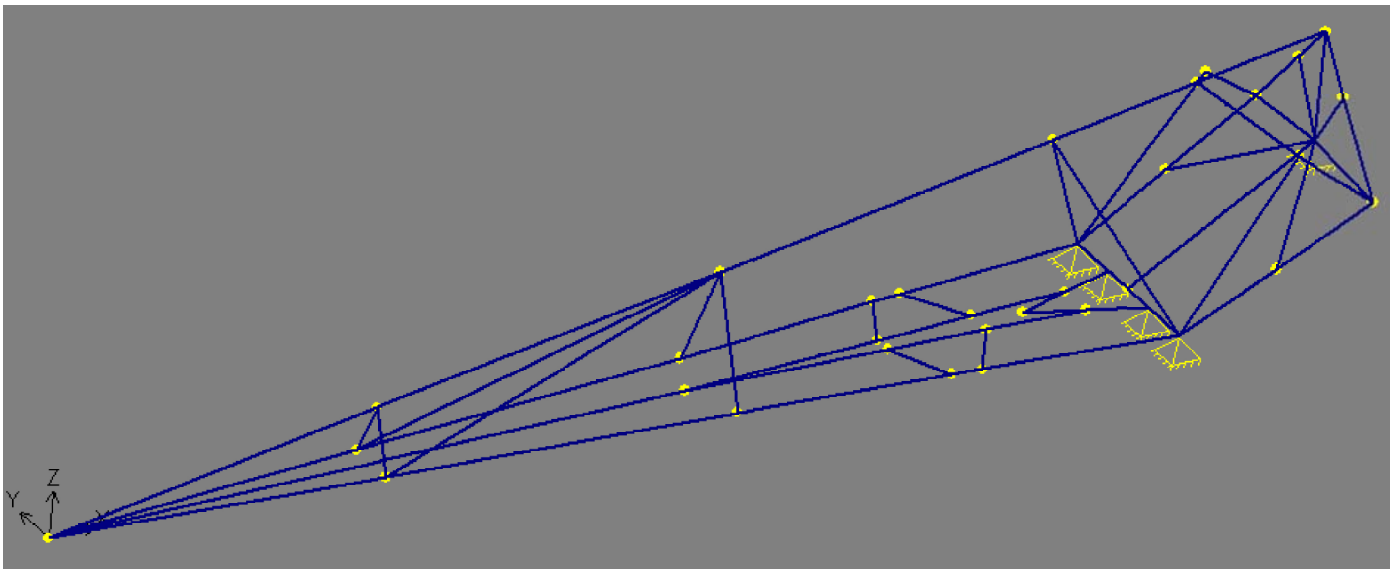

Fig. 6.13: 3D Dorsolateral view of skull of *Anhanguera sp.*, SMNK 3895 PAL, modelled as a space frame. Bars shown in blue colour, nodes in yellow colour and supports as yellow pyramids. Left = anterior.

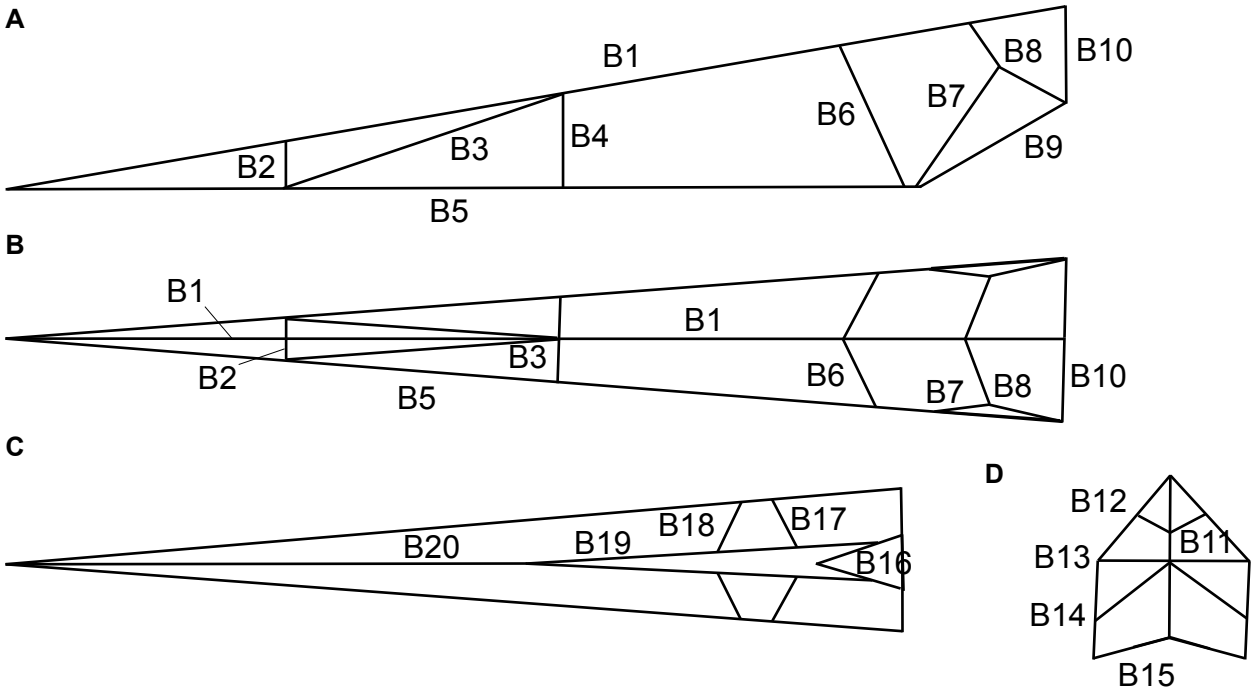

Fig. 6.14: Plane views of space frame model based on the skull of *Anhanguera sp.*, SMNK 3895, with designations of bars of the left side: A) Left lateral view; B) Dorsal view; C) Ventral view; D) Posterior view.

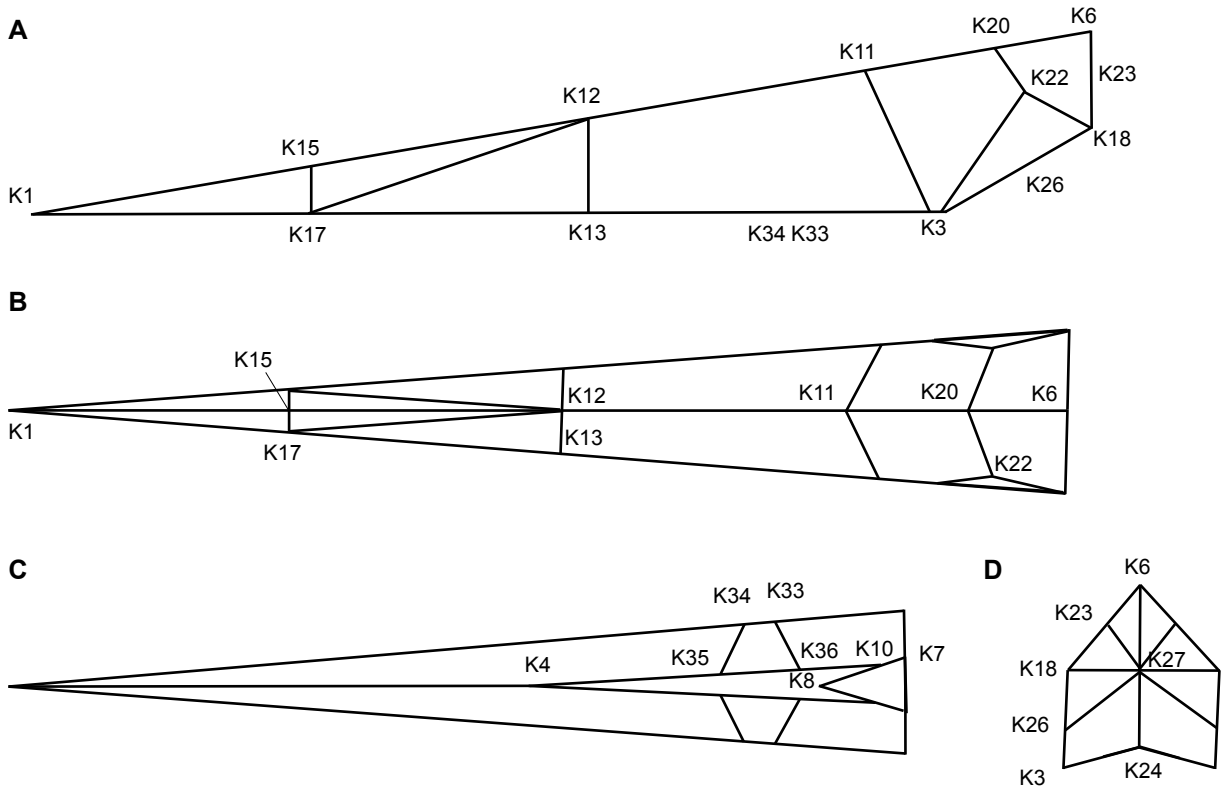

Fig. 6.15: Plane views of space frame model based on the skull of *Anhanguera sp.*, SMNK 3895, with designations of nodes of the left side. For views see Fig. 6.14.

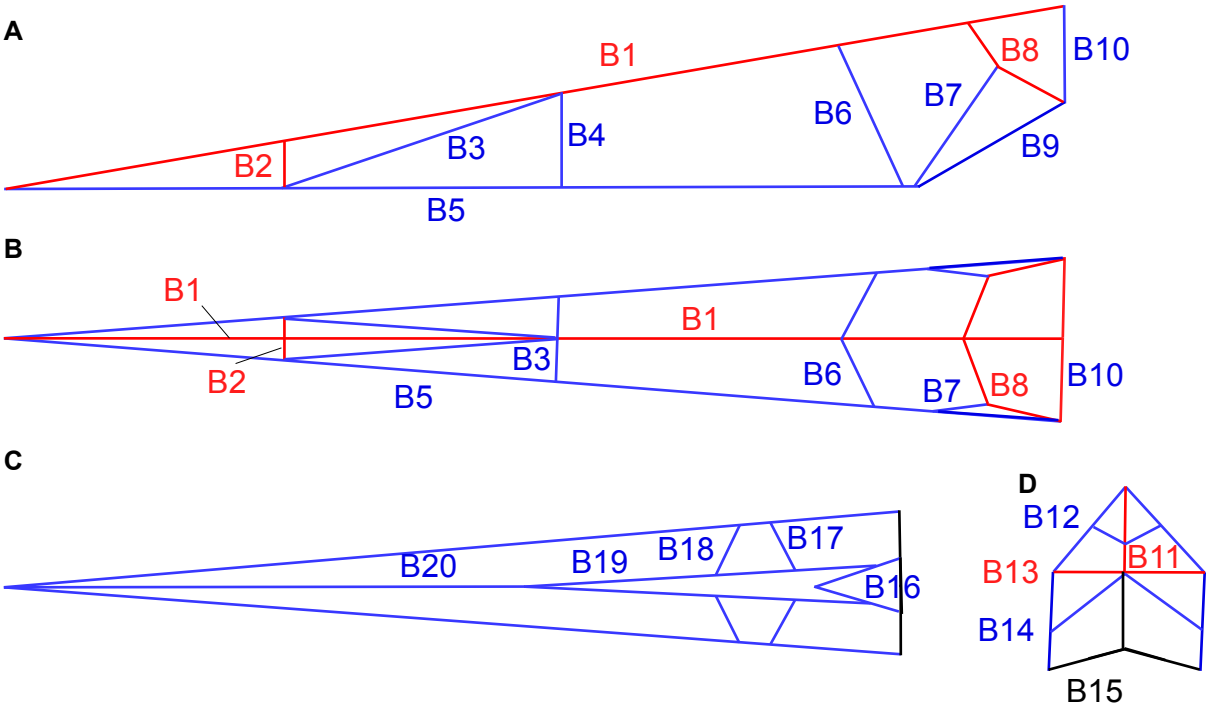

Fig. 6.16: Stress distribution patterns in the space frame model based on the skull of *Anhanguera sp.*, SMNK 3895, under a single anterior load (F_B). For views see Fig. 6.14. Red = compressive stress, blue = tensile stress.

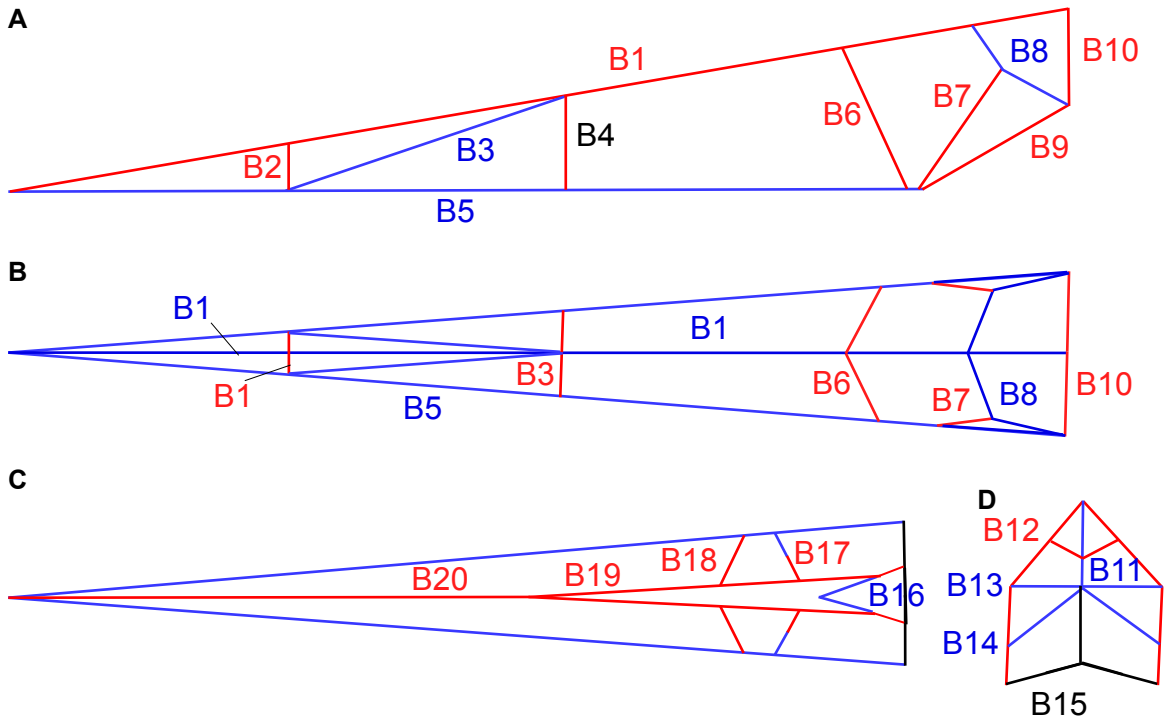

Fig. 6.17: Stress distribution patterns in the space frame model based on the skull of *Anhanguera sp.*, SMNK 3895, under a single anterior (F_B) and muscle (F_i) loads. For views see Fig. 6.14. Red = compressive stress, blue = tensile stress.

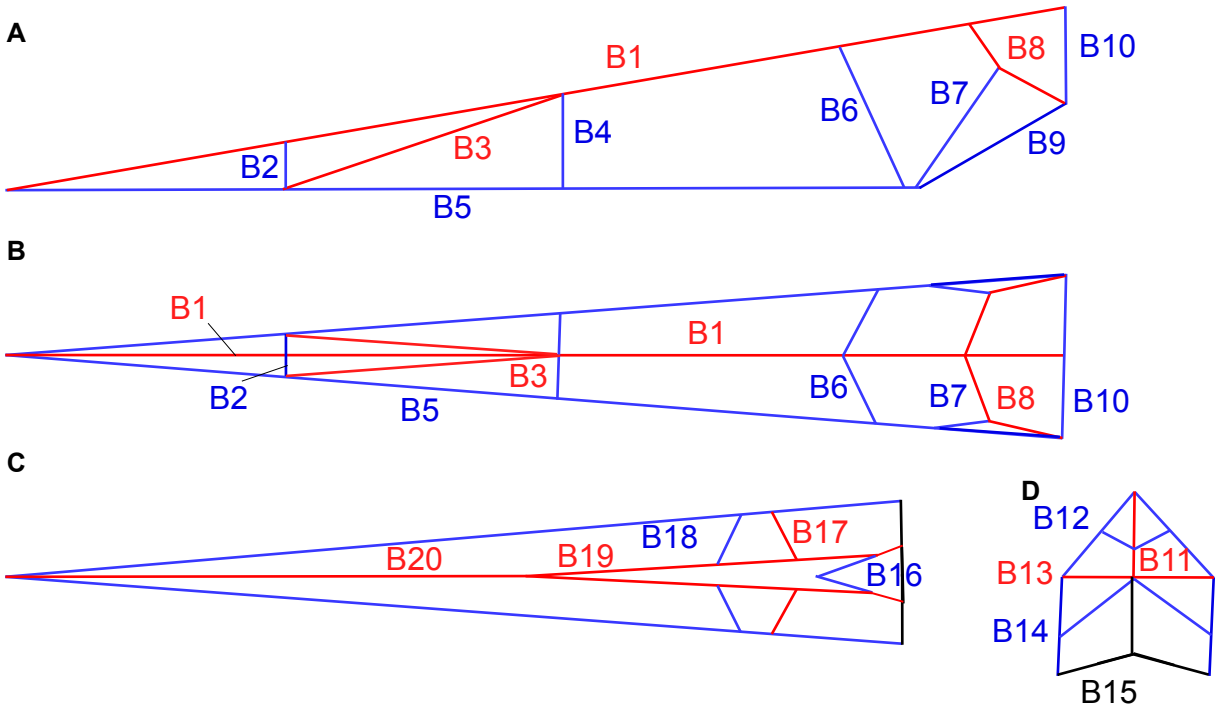

Fig. 6.18: Stress distribution patterns in the space frame model based on the skull of *Anhanguera* sp., SMNK 3895, under a load applied from K1 to K7 on both sides (F_B) and muscle (F_i) loads. For views see Fig. 6.14. Red = compressive stress, blue = tensile stress.

Bar	Single load F_B	Single and muscle load ($F_B + F_i$)	Jaw load and muscle load ($F_B + F_i$)
B1	-33.09 to -4.79	-34.23 to -77.56	-5362.94 to -1657.3
B2	-0.09	-1.02	275.64
B3	0.08	1.85	-1055.54
B4	0.24	-3.46	130.94
B5	14.63 to 15.02	138.01 to 150.75	1437.46 to 2729.43
B6	3.03	-7.72	532.0
B7	11.42	-24.3	1766.15
B8	-12.2 to -12.4	19.06 to 20.7	-1911.84 to -1924.94
B9	6.97 to 7.09	-13.53 to -13.94	1124.62 to 1144.75
B10	17.95 to 18.77	-23.69 to -33.36	2848.2 to 2987.59
B11	-29.45	7.03	-4703.96
B12	4.05	-18.02	621.26
B13	-6.33	12.21	-1008.0
B14	0.18	0.59	31.58
B15	0	0	0
B16	0.37 to 2.36	-127.37 to 4.96	-158.34 to 3.87
B17	0.11	7.52 to -6.6	-18.15 to -24.18
B18	0.09	-0.89	36.05
B19	2.16 to 2.32	-132.33 to -138.88	-107.51 to - 86.3
B20	4.32	-266.34	-170.6

Tab. 6.4: Stress values in the space frame model based on the skull of *Anhanguera sp.*, SMNK 3895, under different loading conditions. Negative values (red) = compressive stress, positive values (blue) = tensile stress.

As seen in Figs. 6.16-6.18 and Tab. 6.4, the nature and magnitude of the forces along the bars vary significantly between the three different loading regimes. Only few congruences exist like in case of the dorsal bar B1 and the ventral bar B5, which are subject to high compressive, respectively tensile stresses in all three loading cases (Figs. 6.16-6.18). The only two other bars which show an identical behaviour are the tensile member B14 and the non-loaded member B15 (Figs. 6.16-6.18). All other members of the space frame differ in their mechanical behaviour as far as the magnitude and nature of the loads are concerned, depending on the loading condition. In most cases, changing the load from a single load at the tip of the frame to a load applied along the tooth row will lead to a reversal of the loading regime, e.g. in the rostral subunit of members B2, B3 and B4 (Figs. 6.16-6.18). Especially in the member B4, the compressive stresses increase significantly during longitudinal load.

Also the orbitotemporal subunit, consisting of the members B6, B7, B8 and B9, reverse the mechanical behaviour from single load to a load along the tooth row plus muscular action (Figs. 6.16-6.18). In all three loading conditions, B8 is the most stressed member of this subunit, followed by B7, B9 and B6 (Figs. 6.16-6.18). The members B6, B7 and B9, which show compressive stresses for a single load, are subject to tensile forces longitudinal forces are applied. Likewise, the member B8 changes from tensile to compressive stresses (Figs. 6.16-6.18). Bending moments may be compensated by the loads induced by the bulging adductor muscles.

The occipital subunit (B10-B14) resembles a Pratt frame commonly used in roof construction (Fig. 6.19). Like previously described from other bars, the resulting loads show a reversal between the three loading conditions. For the third condition, the vertical member B11 and the horizontal member B13 are subject to high compressive loads. In contrast to this, the oblique member B12 as well as B10 show tensile stresses, which in the member B10 are as high as in B1 (Figs. 6.16-6.18).

For a single load without muscular action, the ventral subunit (B16, B17, B18, B19 and B20) is in tension as could be suspected for a simple beam (Fig. 6.16). Adding muscular forces, however, changes the pattern with B18 being the only common tensile member in all three loading cases (Figs. 6.17-6.18). This is caused

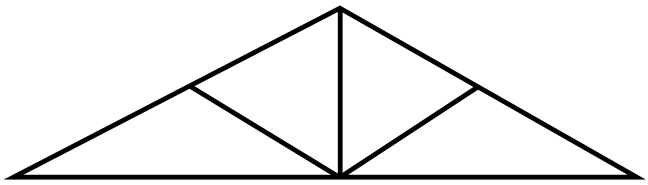

Fig. 6.19: Pratt frame. Note similarity with dorsal part of the posterior view of the space frame model based on the skull of *Anhanguera sp.*, SMNK 3895 PAL (Fig. 6.15D).

mainly by the tensile action of the MPTA and MPTP which lead to compression in all other struts of the ventral subunit. In contrast to the results of the other members, B19 and B20 are subject to higher compressive stresses when the muscular loads are combined with a single force, than with longitudinal loads.

6.4 Cantilever beam model for the rostrum

The rostrum of vertebrates can be approximated as a cantilever, because under common conditions the main loading of the skull is caused by bite forces (Preuschoft et al. 1985). Muscular forces, on the other hand, are restricted to the orbitotemporal region. Therefore, the loadings on the rostral part of the skull can not be compensated by muscular soft-tissue and the bony rostrum has to withstand the forces alone. This model may get more complicated in pterosaurs, where one or two large fenestra exist in the rostrum, which may also have served as attachment areas for muscles, especially for the MPTA (Horner & Lessem 1993, Molnar 1998, Wellnhofer 1991a). To evaluate this effect, the rostrum is first analysed as a continuous cantilever and then the influence of fenestration are discussed (see chapter 6.4.5) and further investigated by using FEA (see chapter 6.5).

The cantilever model encloses the region from the anterior tip of the rostrum to the posterior border of the nasoantorbital fenestra, composed of jugal and lacrimal. The transverse cross-section is triangular and hollow with a mean wall thickness of 3 mm, a value determined by the measurements of CT cross-sections (see chapter 6.1.2). The cross-sectional area increases from anterior to posterior direction. (Fig. 6.20)

After Preuschoft et al. (1985), the incorporation of the alveolar rim into the model results in only minor differences to an analysis, where the rim is omitted. Therefore, the rim was not incorporated in the analysis herein.

6.4.1 Shear stress

Shear stress τ_s is the ratio of shear force against cross-sectional area of the object on which the shear force is applied. In a beam model of a jaw, the shear force corresponds to the bite force F_B, if this load is applied perpendicular to the beam axis. As show in chapter 6.2 about lever mechanics, the bite forces increase in posterior direction. To retain a constant shear stiffness, the cross-sectional area too has to increase.

The shear stress along the rostrum are shown in Fig. 6.21. The values are consistent throughout the rostrum, indicating an identical shear stiffness. The values are the lowest in the area of the dorsal crest and rise hyperbolically in posterior direction.

6.4.2. Bending stress and strength

Applying a load at the anterior end of the rostrum will cause bending moments Mb_y which increase linearly in posterior direction (Fig. 6.22). As was mentioned in chapter 3, the maximum bending stress σ_{bmax} is defined as the ratio of Mb_y/W_y for bending about the y-axis. W_y for a triangular, hollow cross-section with external height (h_o) and basal width (a_o) and internal height (h_i) and basal width (a_i) is given as:

$$Wy = \frac{(h_o \times a_o^{\,2}) - (h_i \times a_i^{\,2})}{24}, \quad (18)$$

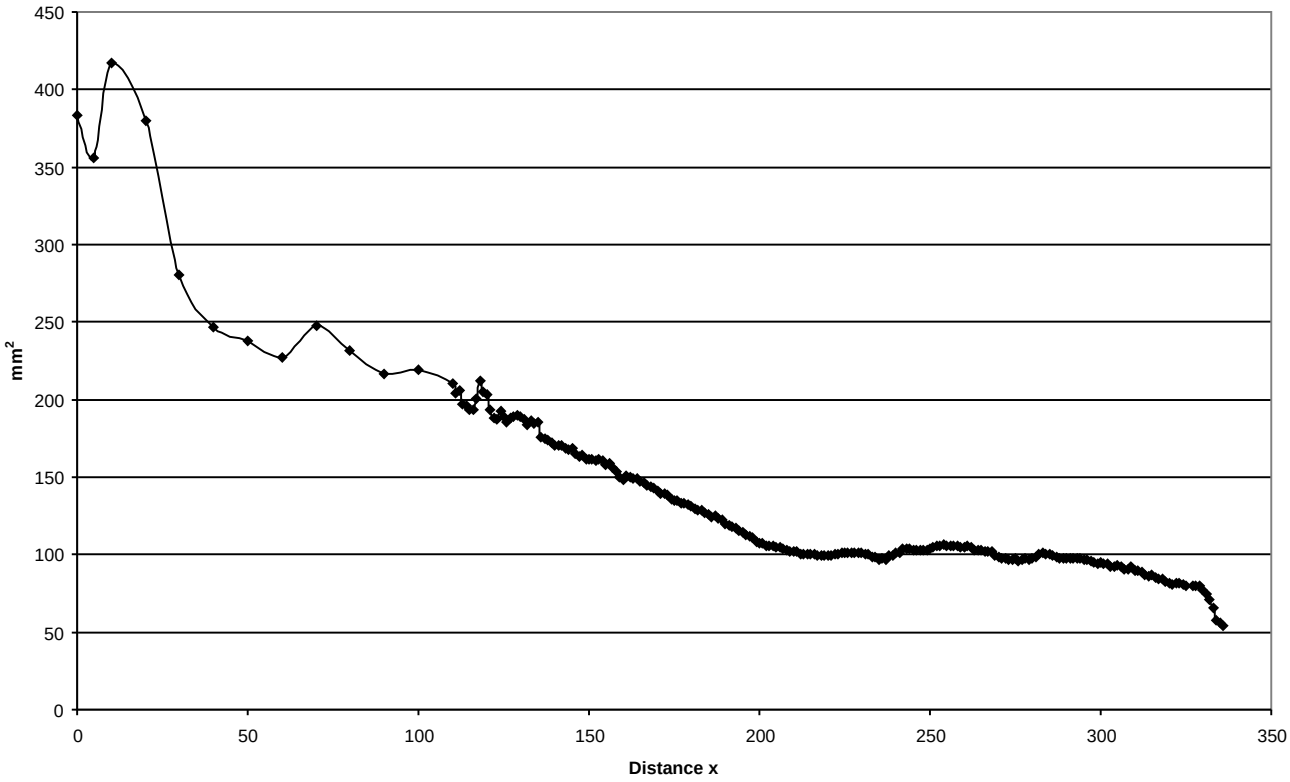

Fig 6.20: Cross sectional area of cantilever beam model for the rostrum of *Anhanguera sp.*, SMNK 3898 PAL. Distance x measured from lower jaw articulation to anterior rostrum.

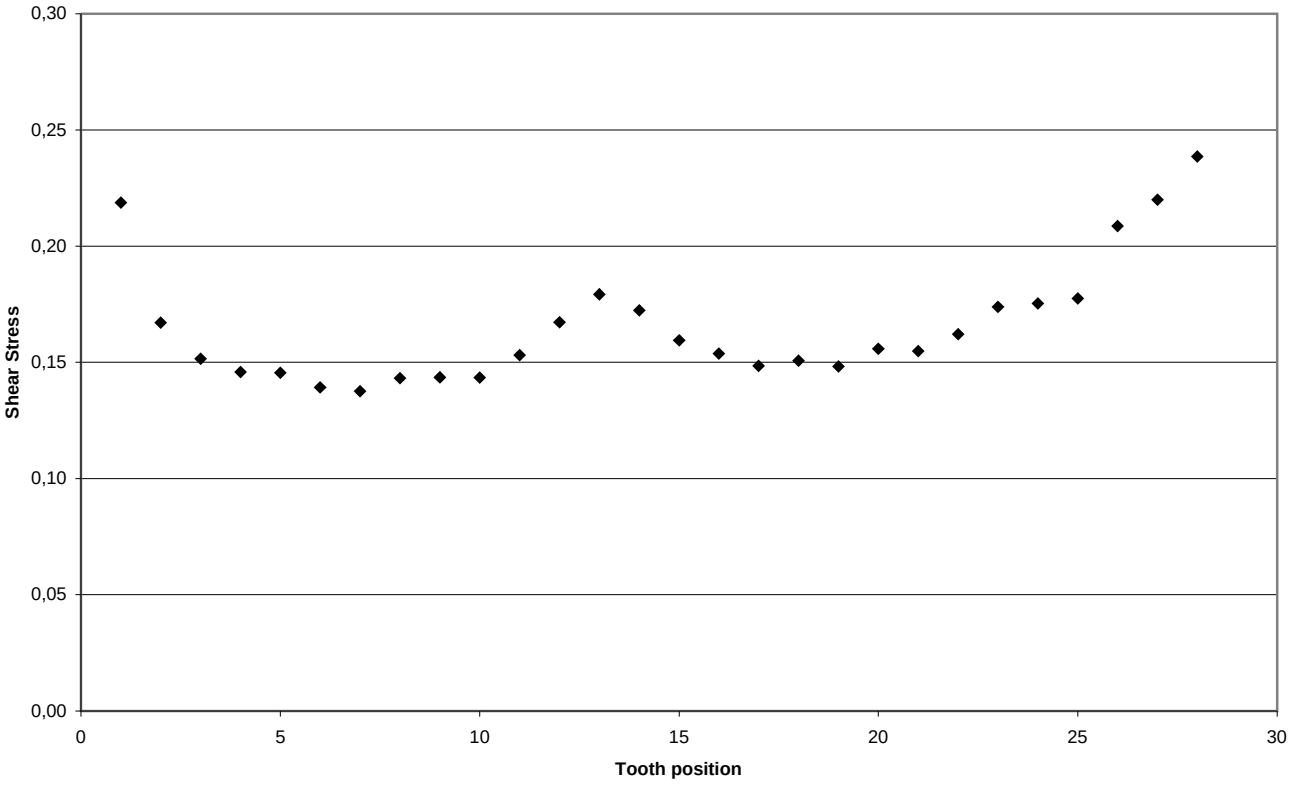

Fig 6.21: Distribution of shear stress τ_s in the cantilever beam model for the rostrum of *Anhanguera sp.*, SMNK 3898 PAL.

The values for W_y and σ_{bmax} along the cantilever model for the rostrum of *Anhanguera sp.*, SMNK 3898 PAL, are shown in Figs. 6.23-6.24. The W_y-curve shows a hyperbolic increase in posterior direction, whereas the values for σ_{bmax} increase from the anterior tip of the cantilever until the posterior end of the crest. Here the absolute maximum of bending stress is reached. Posteriorly the bending stress decreases hyperbolically. The values are lower than in the extant crocodiles *Tomistoma schlegelii* (9.18-14.33 kp/cm2) and *Crocodylus porosus* (0.7-0.58 kp/cm2) (Preuschoft et al. 1985).

The rostrum does not represent an optimal cantilever, since here σ_{bmax} would be constant along the beam (Nachtigall 2000). This is the case, when the cantilever is formed like a quadratic parabola (see chapter 3). Under the aspect of bending resistance, the present cantilever model, thus is overbuilt.

The bending strength of a beam is defined by the area moment of inertia *I*. By modifying equation 8, for bending around the y-axis and a hollow, triangular cross-section I_y is given as:

$$I_y = \frac{(a_o \times h_a^3) - (a_o \times h_i^3)}{36}, \quad (19)$$

The values for the present cantilever model (Fig 6.25) are rather uniform in the anterior part of the rostrum, but increase hyperbolically in posterior direction starting from about the level of the posterior end of the dorsal crest.

During bite, shear forces may also be present in lateral direction, caused by movement of the prey. The magnitude of these transverse components of the bite forces can not be predicted. They are generally low, when the jaws are loaded at their anterior end. Applied to the cantilever model, these forces will result in bending around the z-axis. For this case, by modifying equation 8 the area moment of inertia I_z for a hollow triangular cross-section is defined as:

$$I_z = \frac{(a_o^3 \times h_o) - (a_i^3 \times h_i)}{48}, \quad (20)$$

The values of I_z in the model of the rostrum are constantly low until the posterior end of the dorsal crest, from which they increase hyperbolically in posterior direction (Fig. 6.26).

6.4.3 Torsion

Unilateral loading results in torsion of the beam. The torsional moment (=torque) is the product of the unilateral bite force and the distance of the tooth from the median plane, and is expressed as

$$F \times \frac{a_o}{2}, \quad (21)$$

The greater the distance between tooth row and the median plane is, the greater is the torque. Also a medial inclination of the bite forces reduces the lever arms of the torque (Preuschoft et al. 1985). Fig. 6.27 depicts the values of torque for vertical torsional loads at the various tooth positions. Whereas the torque increases gradually until the 12th tooth position, the values rise exponentially in posterior tooth positions.

For a hollow triangular cross-section the resistance against torsion, the polar moment of inertia (*J*), is given by modifying equation 6 as:

$$J = \frac{ah^3}{36} + \frac{a^3h}{48} = I_x + I_z, \quad (22)$$

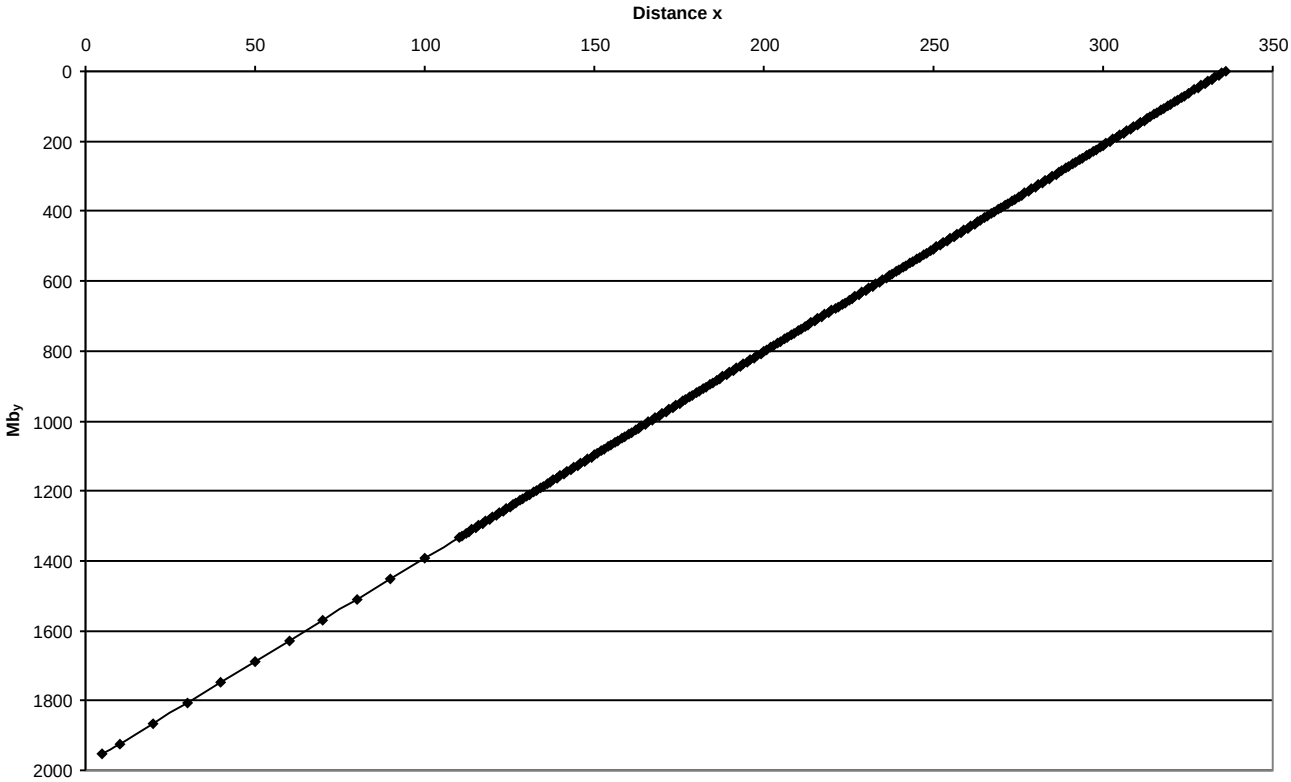

Fig 6.22: Distribution of Mb_y in the cantilever beam model for the rostrum of *Anhanguera sp.*, SMNK 3898 PAL. Note reverse direction of y-axis, following the convention given in Nachtigall (2000).

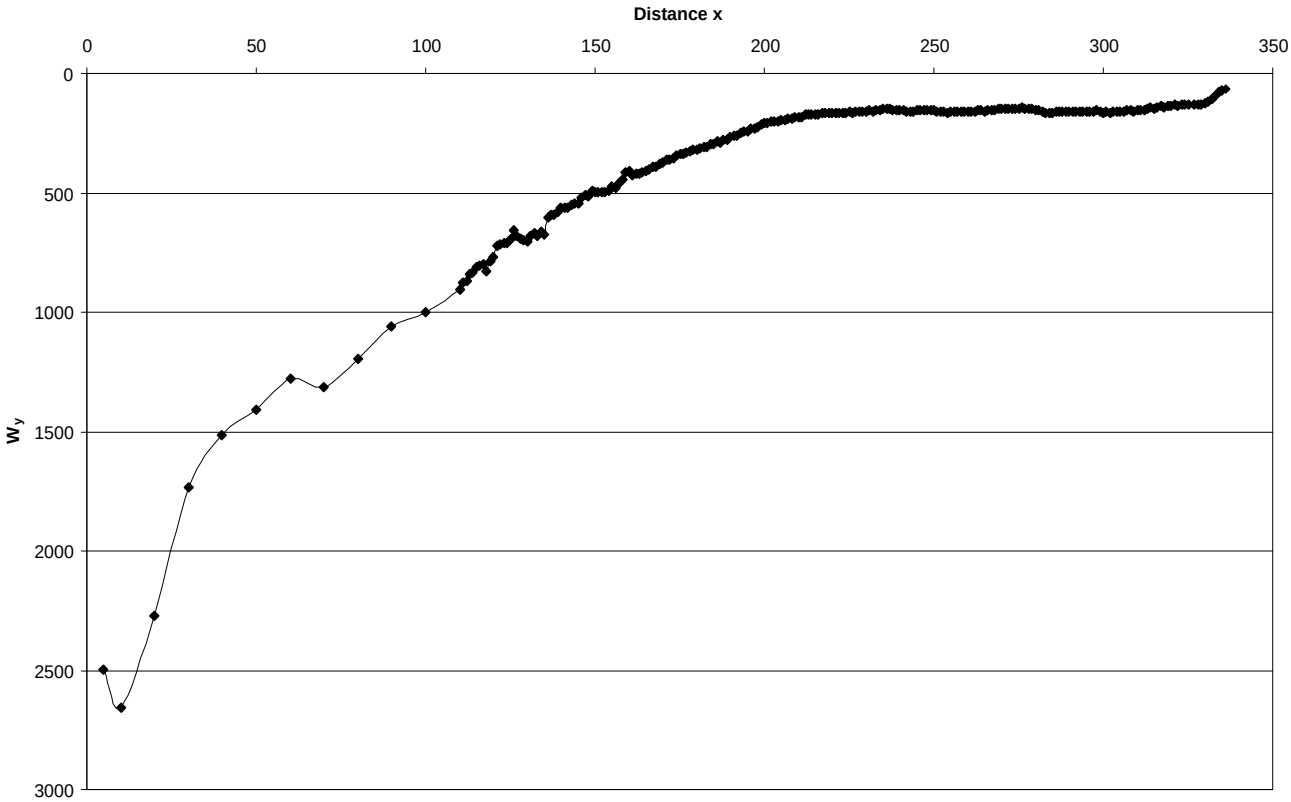

Fig 6.23: Distribution of W_y in the cantilever beam model for the rostrum of *Anhanguera sp.*, SMNK 3898 PAL. Note reverse direction of y-axis, following the convention given in Nachtigall (2000).

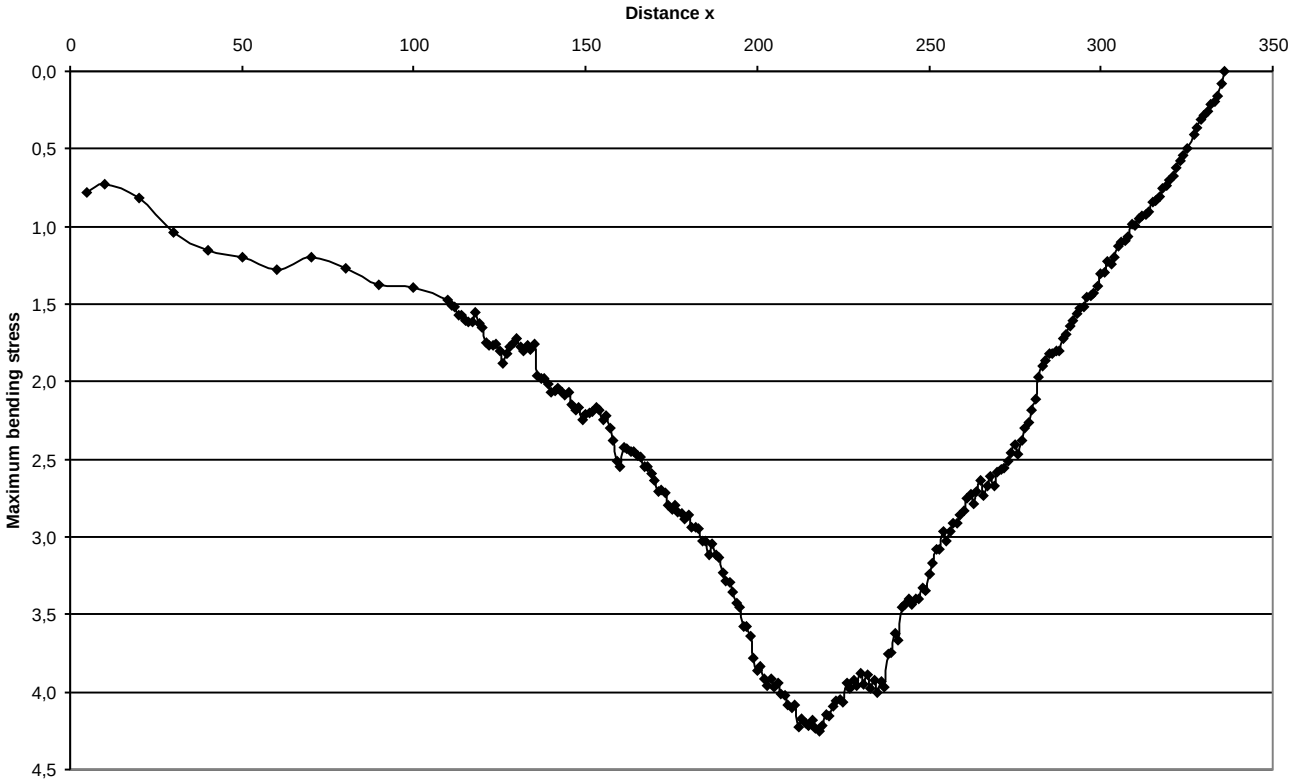

Fig 6.24: Distribution of σ_{bmax} in the cantilever beam model for the rostrum of *Anhanguera sp.*, SMNK 3898 PAL. Note reverse direction of y-axis, following the convention given in Nachtigall (2000).

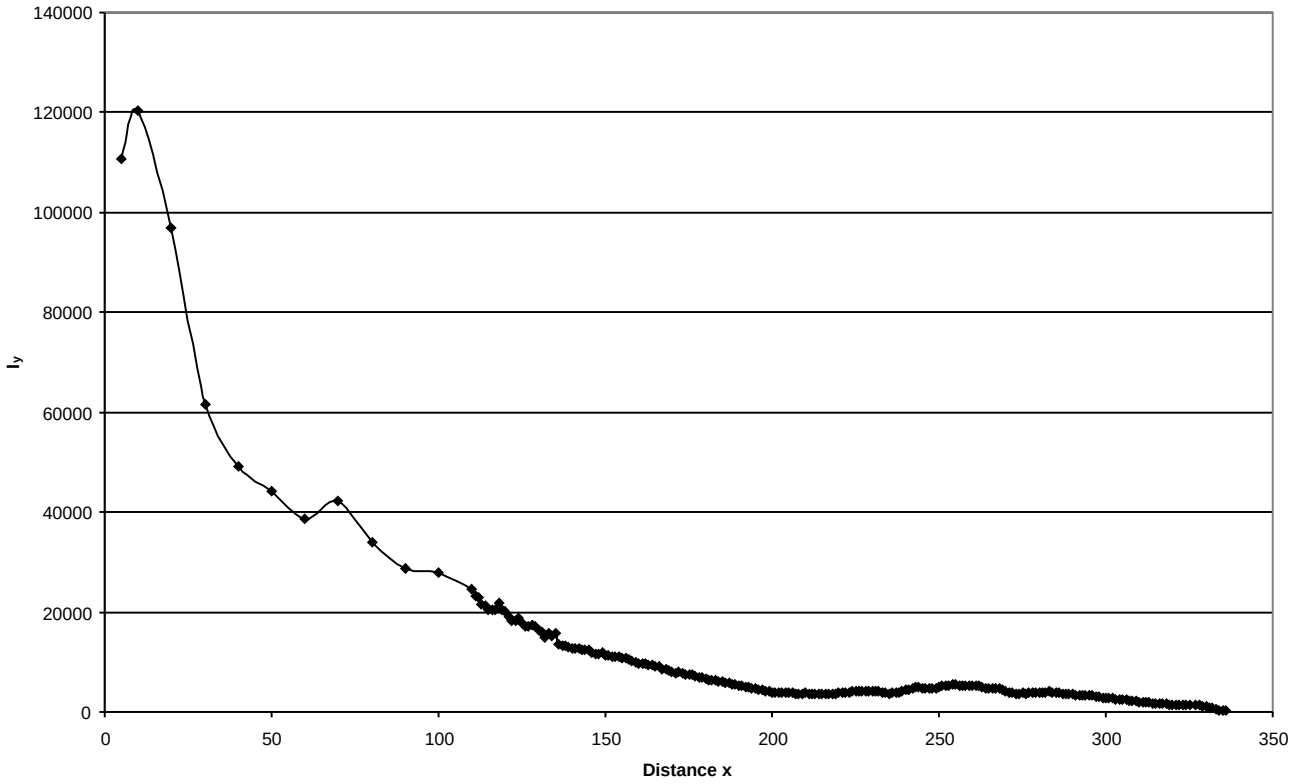

Fig 6.25: Distribution of I_y in the cantilever beam model for the rostrum of *Anhanguera sp.*, SMNK 3898 PAL.

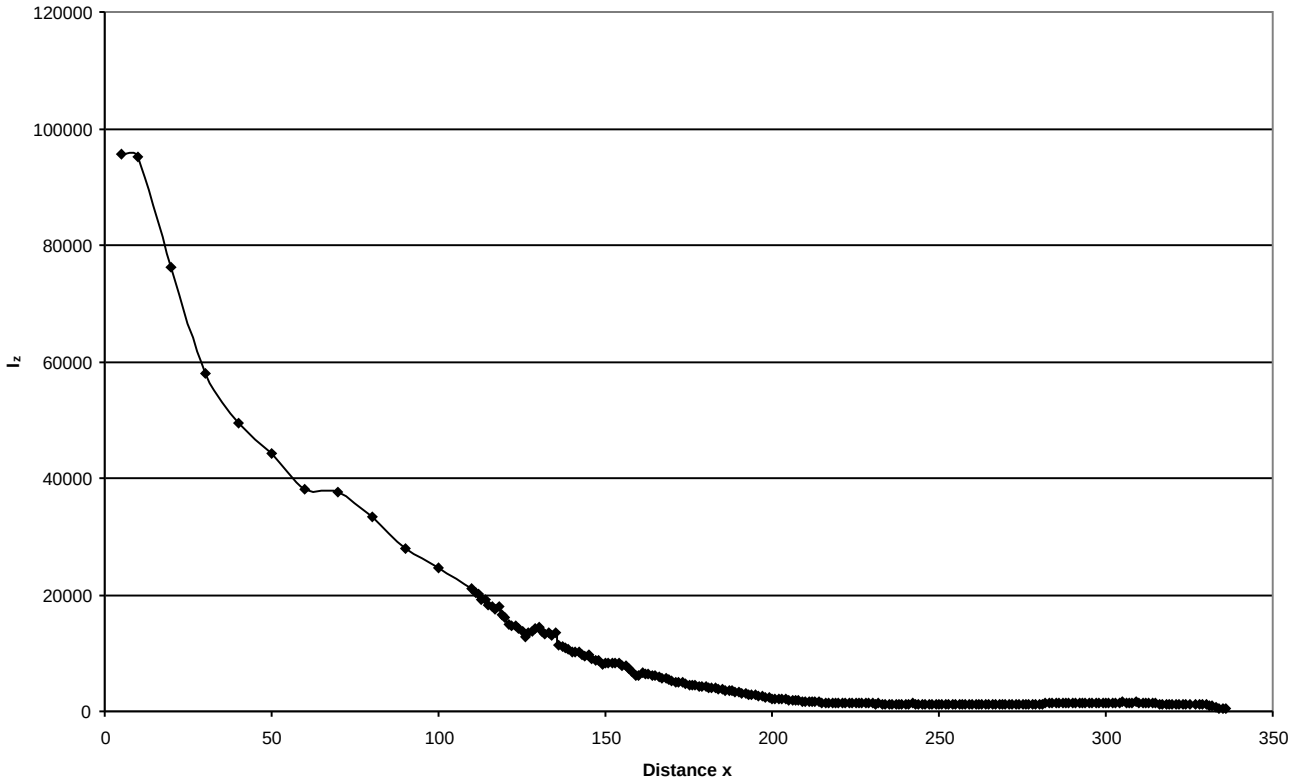

Fig 6.26: Distribution of I_z in the cantilever beam model for the rostrum of *Anhanguera sp.*, SMNK 3898 PAL.

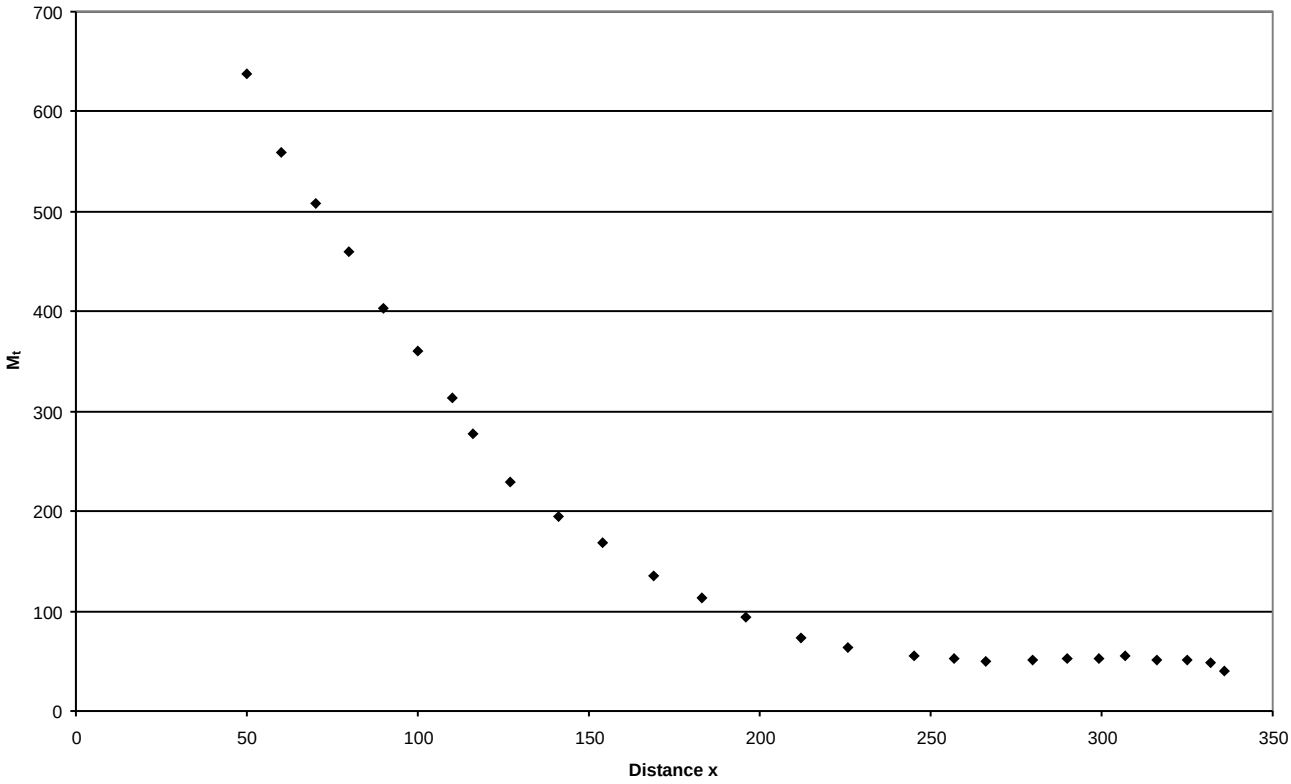

Fig 6.27: Distribution of torque in the cantilever beam model for the rostrum of *Anhanguera sp.*, SMNK 3898 PAL.

The distribution of the polar moment of inertia in the present cantilever model (Fig. 6.28) is similar to the area moment of inertia (Fig. 6.25). It shows an uniform level until about half of the distance between crest and nasoantorbital fenestra, posterior to which the values increase exponentially.

The section modulus for torsion (W_t) is more complicated to estimate. The cross-section of the rostrum can be viewed as closed and thin-walled. In this case, the 1st equation of Bredt can be applied (Böge 2003):

$$W_t = 2 \times A_m \times b_{\min} \ , \quad (23)$$

with A_m = enclosed area by the midline of the wall, b_{min} = minimum thickness of the bone wall. For the given dimensions, the resulting values for W_t show a similar distribution like for torque (Fig. 6.29).

From these calculations, the torsional shear stress τ_t is derived by

$$\tau_t = \frac{M_t}{W_p} \ , \quad (24)$$

The absolute maximum of τ_t in the cantilever model is reached at the 1st to 3rd tooth positions (Fig. 6.30). From here, the values decrease until about half of the distance between posterior border of the crest and nasoantorbital fenestra. Posterior to this, the values remain on the same mean level (Fig. 6.30).

For non-circular profiles in a cantilever, warping of the cross-section will occur, which induces additional normal stress (Preuschoft et al. 1985). This effect increases in direction of the support of the beam, because warping is impeded here. No statements can be made about the intensity of these effects in the present case, because an exact solution for torsion including warping constraints are complex. However, for most applications it was be shown, that the effects are negligible (Beitz & Grothe 1997). Therefore, they are omitted in this study.

6.4.4 Combination of loads

In engineering, the failure of a beam is evaluated by the comparison of the normal and shear stresses. In case of the brittle material bone, the behaviour is best described by the shear stress hypotheses (Böge 2003), which yields a comparison stress σ_v. After Böge (2003), the following equation is applied:

$$\sigma_v = \sqrt{\sigma^2_{res} + 3 \times \tau^2_{res}} , \quad (25)$$

with σ_{res} = bending stress in x-direction and $\tau_{res} = \tau_s + \tau_t$.

Considering an anterior bite, the values of σ_v increase until about the level of the posterior end of the dorsal crest (Fig 6.31). Posteriorly from this, σ_v decreases again.

Other modes of failure than shear are bending and/or torsion, the latter resulting in twisting of the beam around its long axis. The twistiness to bendiness ratio provides information whether a beam is more likely to fail under torsion or under bending. As shown in chapter 3.3.2, both parameters, twistiness (=flexural stiffness) and bendiness (=torsional stiffness), depend on the Young's modulus and Poisson ratio of the material, of which a beam is composed of. Using the values for human bone given in Table 3.2, the ratio was calculated for the given geometry (Fig. 6.32). The beam shows a higher tendency to twist in the region, where the dorsal crest is developed. In contrast, especially in the most anterior region and posterior to the dorsal crest twisting is more probable than bending.

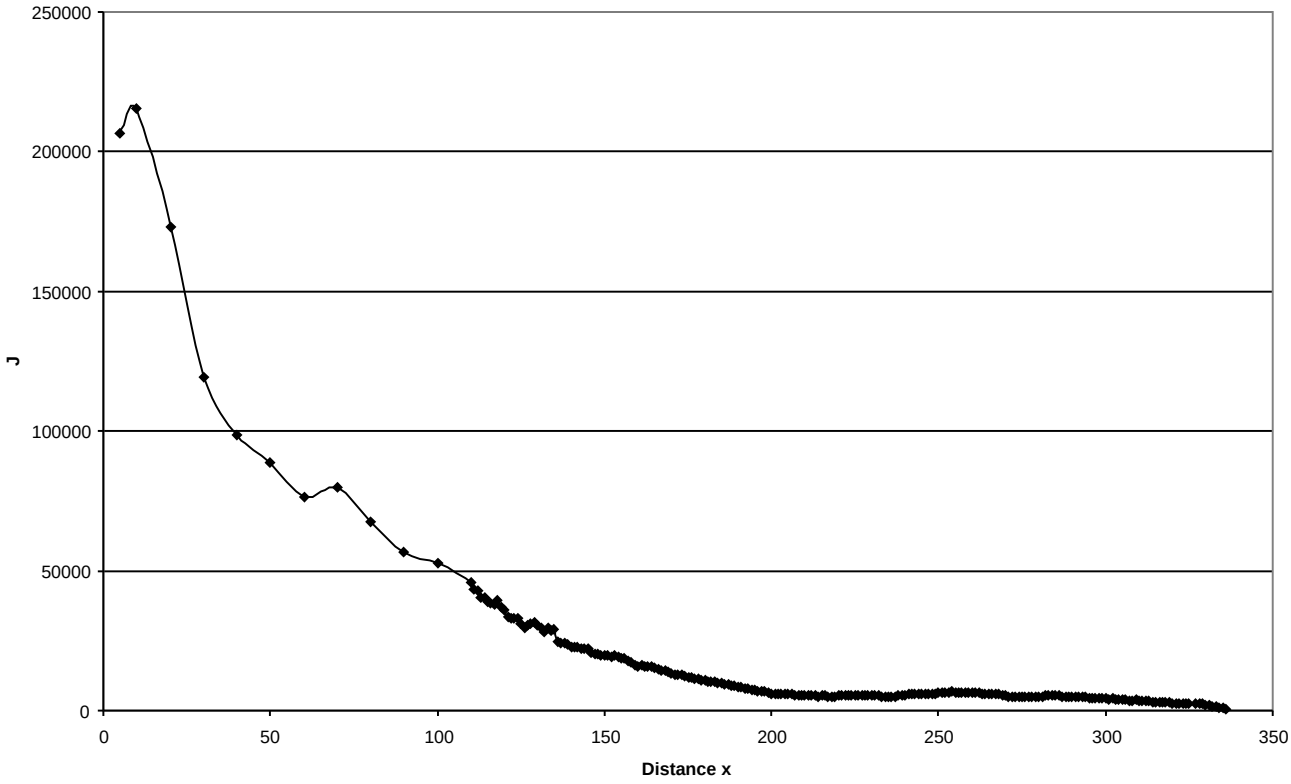

Fig 6.28: Distribution of *J* in the cantilever beam model for the rostrum of *Anhanguera sp.*, SMNK 3898 PAL.

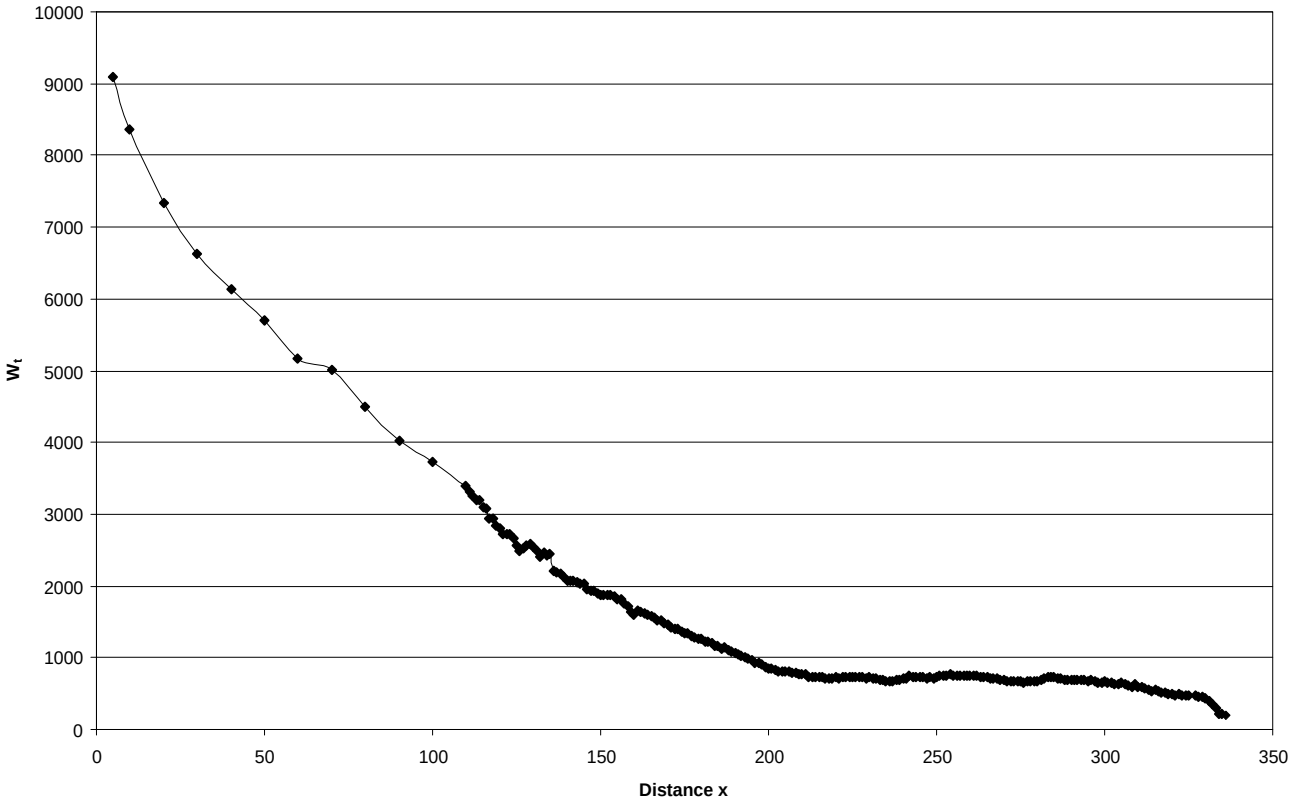

Fig 6.29: Distribution of W_t in the cantilever beam model for the rostrum of *Anhanguera sp.*, SMNK 3898 PAL.

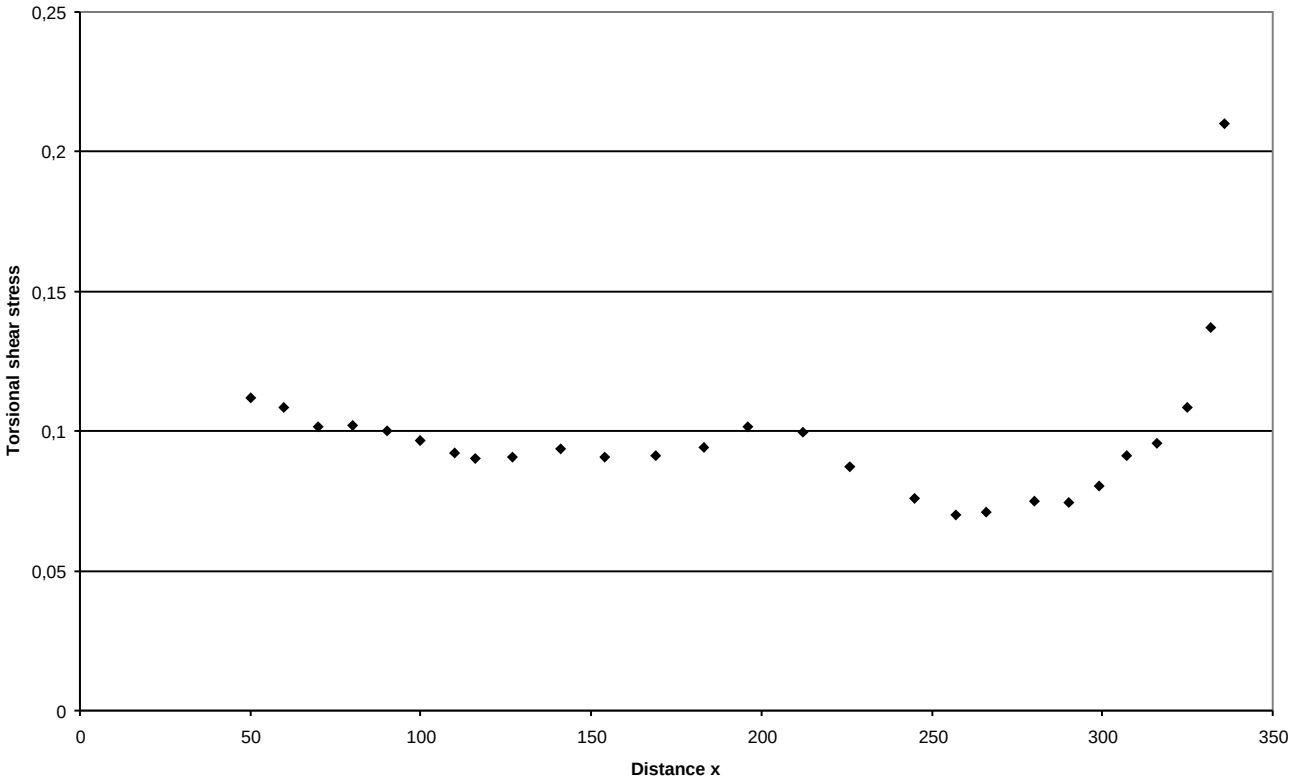

Fig 6.30: Distribution of τ_t in the cantilever beam model for the rostrum of *Anhanguera sp.*, SMNK 3898 PAL.

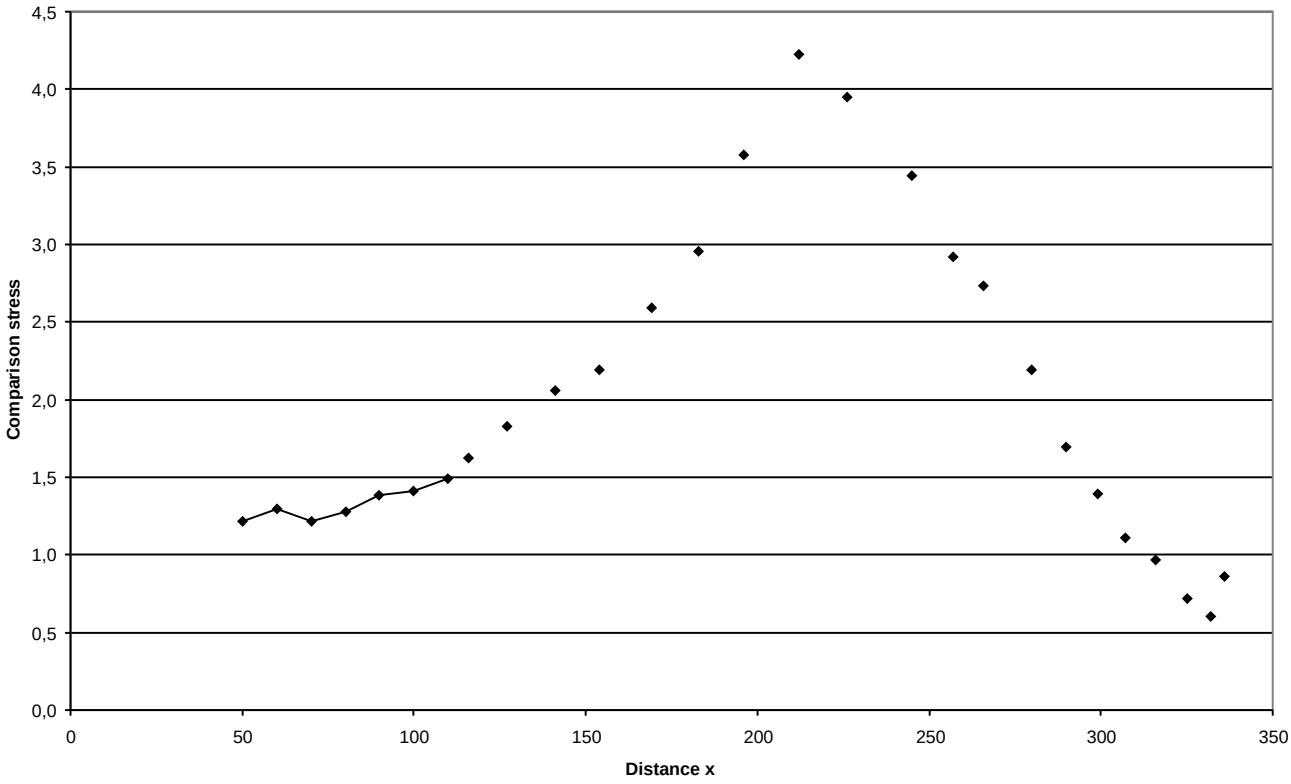

Fig 6.31: Distribution of σ_v in the cantilever beam model for the rostrum of *Anhanguera sp.*, SMNK 3898 PAL.

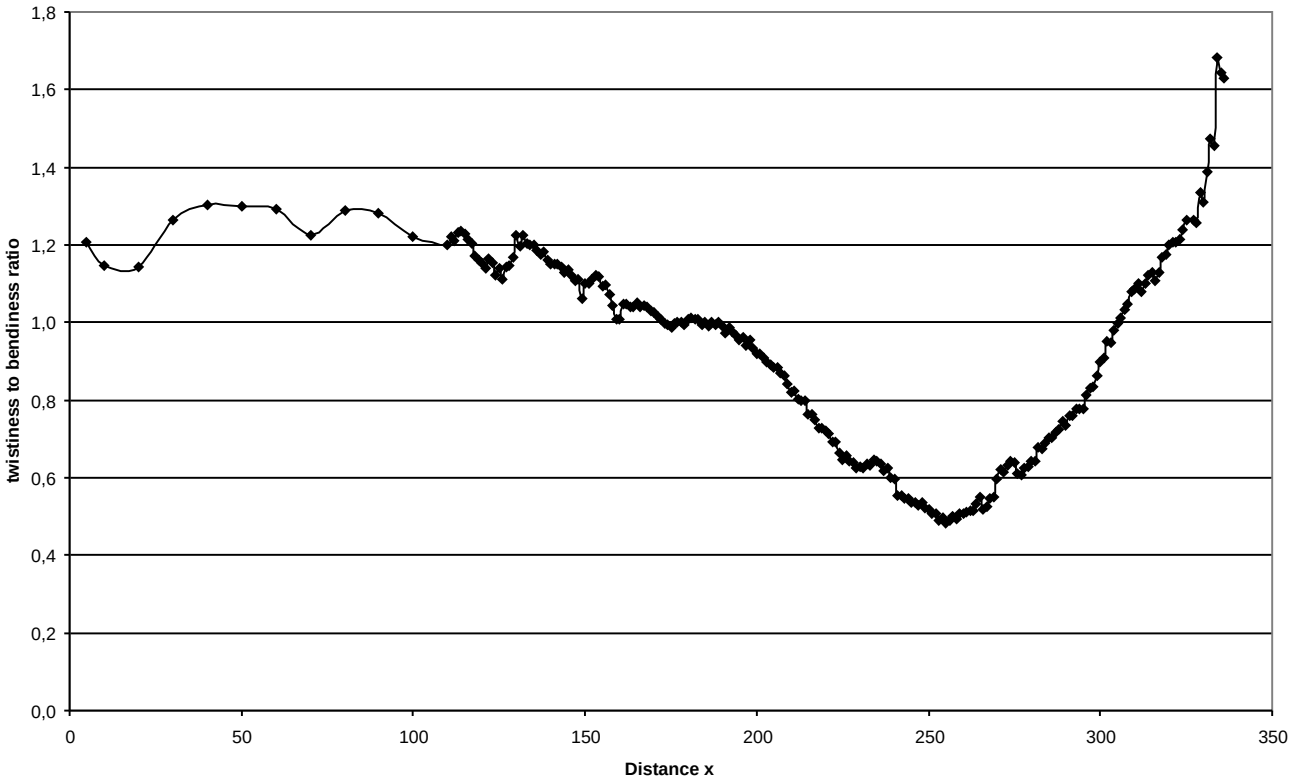

Fig 6.32: Distribution of twistiness to bendiness ratio in the cantilever beam model for the rostrum of *Anhanguera sp.*, SMNK 3898 PAL.

6.4.5 Incorporation of nasoantorbital fenestra in the analysis

When the antorbital fenestra is included into the beam as an empty vacuity, the course of the values of certain parameters changes, because the discontinuity will prevent that the stresses are transmitted all along the surface of the beam. The ventral and dorsal bordering bars of the nasoantorbital fenestra will behave as cantilever beams with relatively small cross-sections compared to the overall rostral beam cross-section.

In case of compressive and tensile stresses, the ventral and dorsal bordering bars will be subject to higher stress concentrations, because the loads are concentrated on a smaller cross-section. These stress concentrations and their position on the bordering bars of the nasoantorbital fenestra is made visible by FEA (Fig. 6.33). The compressive stresses show a local stress concentration halfway along the dorsal bar of the antorbital fenestra. The tensile stresses have their local maximum on the processus maxillaris of the jugal close to the jaw articulation as well as on the pterygoid, ectopterygoid and posterior palatine.

In bending, another effect is the shortening of the distance between vertically opposing points when the bars are bent in dorsal direction (Preuschoft et al. 1985). This is caused by a lower degree of bending in the dorsal bar relative to the ventral members, resulting in a longitudinal shear movement, which causes a posterior displacement of the ventral bars relative to the dorsal bar (Fig. 6.34).

The presence of the nasoantorbital fenestra prevents that shear loads are braced by the opposite side of the cantilever (Preuschoft et al. 1985). Therefore, the cross-sectional area must be divided by two in this region. This leads to an abrupt increase of shear stress here which is in contrast to a continuous cantilever. On the other hand, the torsional stress will be reduced because the profile of the cross-section is not continuous anymore (Romberg & Hinrichs 2003). These effects, however, are valid only if the cross-section is slightly slitted. This is the case, when the ventral vacuities are incorporated in the study alone. Reducing the cross-section to two

ventral and one dorsal bar by including the nasoantorbital fenestra leads to a drastic increase in shear and torsional stresses.

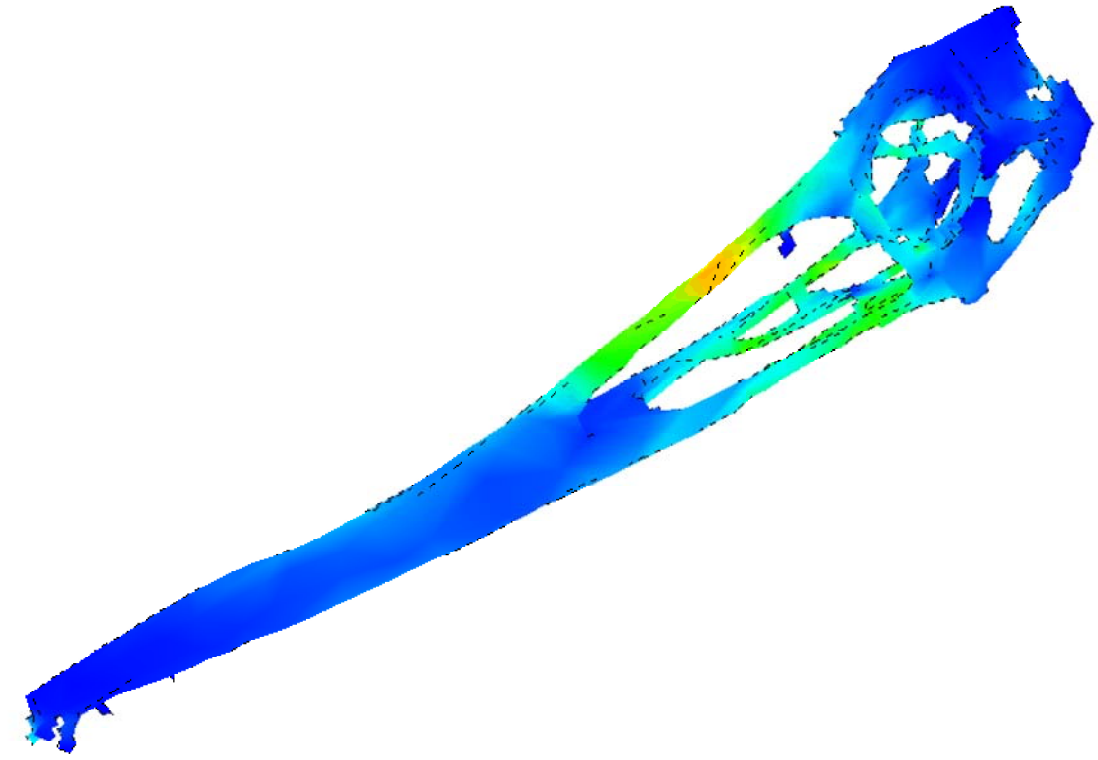

Fig. 6.33: Results of FEA of *Anhanguera* skull model. Lighter colours indicate higher van Mises stresses. F_i not included.

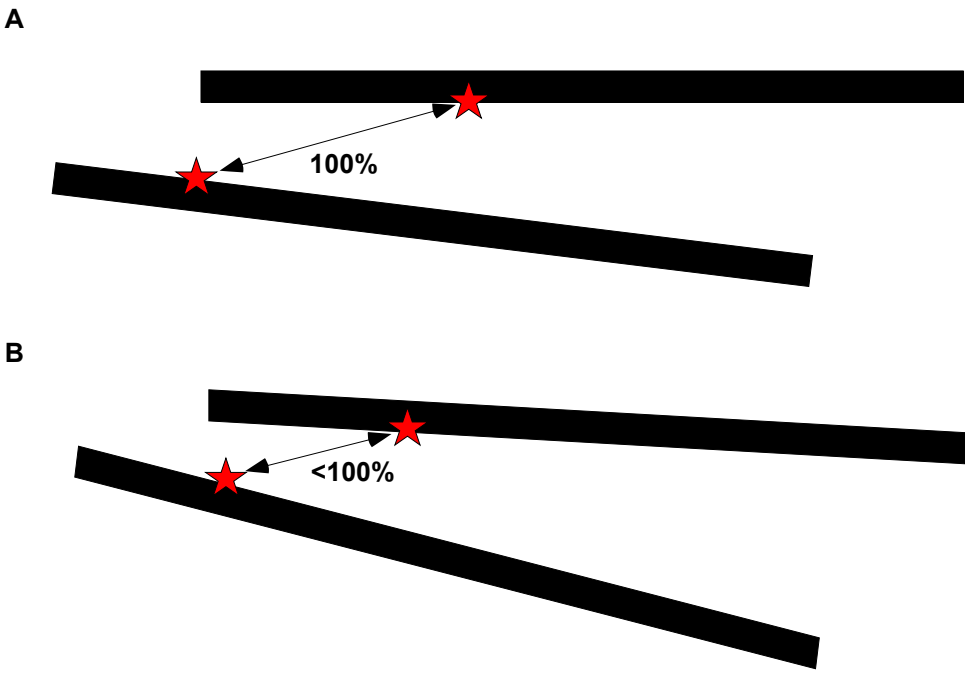

Fig. 6.34: Lateral view of model of a rostrum with dorsal (B1) and ventral (B5) bar with arbitrarily chosen points (stars): A) Neutral position of the bars, distance between points is set as 100%; B) Bending of the bars by implied bite forces leads to relative stronger bending in the ventral bar (B5) than in the dorsal bar (B1) if no vertical orientated member is present, marked point is shifted in posterior direction relative to neutral position, decreasing the distance between both points. After Preuschoft et al. (1985) failure of the rostrum is more likely than in cases where a compressive member is present between the dorsal and ventral bar.

6.5 Summary of internal forces in the Anhanguera skull construction

The internal forces in the skull construction are illustrated by dividing the skull construction into elements in which the main forces and reactions are plotted (Fig. 6.35). The anteriormost rostrum is subject to a dorsal directed bite force, perpendicular to the tooth row. The compressive reaction passes via the dorsal border of the rostrum, respectively the tensile reaction through the ventral surface of the rostrum into the posterior region (Fig. 6.35). Within the rostrum, a vertical orientated shear force is present that tends to shear the anterior portion ventral to the posterior portion (Fig. 6.35). In the pre-nasoantobital part of the rostrum, these shear forces are the highest directly posterior to the dorsal crest.

The rostral area which encloses the nasoantorbital fenestra is interpreted as three bars, a dorsal one and two ventral ones. They are subject to shearing forces anteriorly and posteriorly (Fig. 6.35). The MPTA acts as a tensile member and thus prevents a longitudinal shear movements. Tensile stresses are transmitted via the ventrolateral bars of the nasoantorbital fenestra and compressive stress via the dorsal bar into the orbitotemporal region (Fig. 6.35). The buckling resistance of the dorsal bar is increased by the cross-section of the dorsal bar which is formed like an inverted V. Posteriorly, the shear force tends to shear the posterior rostral element dorsally with respect to the orbitotemporal region.

The posterior region accommodates most of the muscular forces which are directed anteroventrally and mainly act on the braincase and the quadrate region (Fig. 6.35). The joint reaction forces range in their direction between the one of jugal/postorbital bar and the quadrate, both bordering the lower temporal fenestra. The loading regimes of most of the bars surrounding the lower and upper temporal fenestra as well as the laterally orientated bars in the occipital region change depending of the nature of the applied bite forces (Fig 6.16-6.18).

The anterior border of the orbita, and the anterior and posterior bar of the lower temporal fenestra are buttressed against the lower jaw articulation (Fig. 6.35). Here the three bars are joined in the area of the jugal

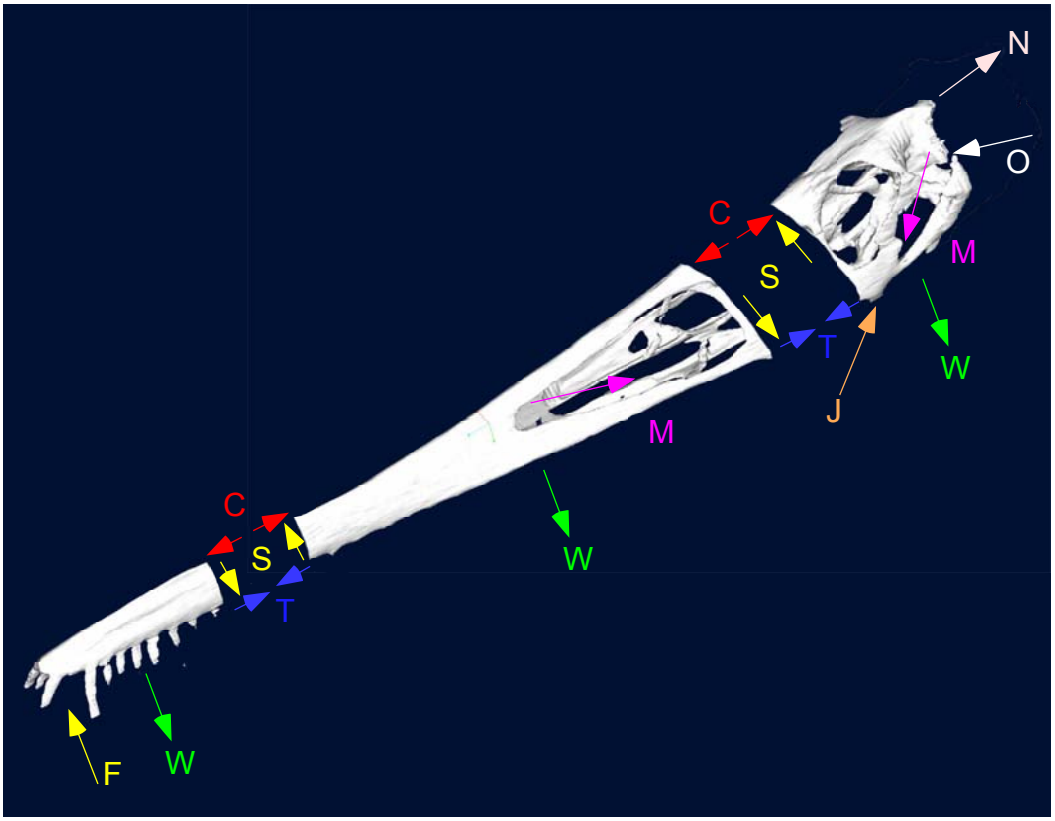

Fig. 6.35: Summary of forces and reactions applied to a model based on the skull of *Anhanguera sp.*, SMNK 3895. C = compression, F = bite, J = joint reaction, M = jaw muscles (MPTA + MAME/P + MPST), N = epaxial musculature, O = support at the occipital condyle, S = shear, T = tensile, W = weight.

dorsal to the condyle. The jaw reaction forces thus counteract the loads transmitted via these members. The compressive stresses of the temporal arch is buttressed by the skull roof and the bars of the occipital region. The high bending moments within this member may be counteracted by laterally imposed forces caused by the bulging of the MPST and MAM.

The compressive reaction, which is transmitted via the broad frontal is passed into the paroccipital process and along the medial bar of the occipital region into the cervical column (Fig. 6.35). Here, supporting forces at the occipital condyle and posteriorly directed forces by the epaxial musculature are present, too. Their action may compensate bending moments which occur in the medial bar in the occipital region.

Apart from the forces induced by a bite and muscular actions, weight forces are also present which are directed perpendicular if the skull construction is orientated horizontally (Fig. 6.35). Furthermore, inertial forces will occur under dynamic conditions, with varying directions and magnitudes.

7. PARAMETRIC STUDY OF PTEROSAUR SKULL CONSTRUCTIONS

The following chapter describes the various skull constructions of pterosaurs (see chapter 3 for details on reconstructions of skulls). The referring results of the muscle reconstruction and the biomechanical behaviour of the rostrum modelled as a cantilever are listed in Appendix A. The chapter includes all known pterosaur genera (state of affair: January 2005), from which enough skull material is known to permit a reliable reconstruction of the skull. For simplification the teeth are not shown here but their position is indicated by arrows. The analysis of the cantilever follows the procedure described in chapter 6.4. As the Anhanguera skull construction already was studied in detail in the last chapter, it is omitted here. Also soft-tissue crest are not incorporated, since their distribution in the pterosaur taxa is strongly dependent on the preservation and they have no mechanical significance for the present discussion.

Next page: Tab. 7.1: List of skull construction with page and figure-numbers in chapter 7 and appendix A.

Skull construction	Page chapter 7	Page appendix A
Angustinaripterus	84, Fig.7.1	A2-4, Figs. A.1-8, Tabs. A.1-2
Anurognathus	85, Fig.7.2	A5-7, Figs. A.9-16, Tabs. A.3-4
Austriadactylus	86, Fig.7.3	A8-10, Figs. A.17-24, Tabs. A.5-6
Batrachognathus	87, Fig.7.4	A11-13, Figs. A.25-32, Tabs. A.7-8
Cacibupteryx	88, Fig.7.5	A14-16, Figs. A.33-40, Tabs. A.9-10
Campylognathoides	89, Fig.7.6	A17-19, Figs. A.41-48, Tabs. A.11-12
Cearadactylus	90, Fig.7.7	A20-22, Figs. A.49-56, Tabs. A.13-14
Coloborhynchus	91, Fig.7.8	A23-25, Figs. A.57-64, Tabs. A.15-16
Criorhynchus	92, Fig.7.9	A26-28, Figs. A.65-72, Tabs. A.17-18
Ctenochasma	93, Fig.7.10	A29-31, Figs. A.73-80, Tabs. A.19-20
Dimorphodon	94, Fig.7.11	A32-34, Figs. A.81-88, Tabs. A.21-22
Dorygnathus	95, Fig.7.12	A35-37, Figs. A.89-96, Tabs. A.23-24
Dsungaripterus	96, Fig.7.13	A38-40, Figs. A.97-104, Tabs. A.25-26
Eudimorphodon	97, Fig.7.14	A41-43, Figs. A.105-112, Tabs. A.27-28
Gallodactylus	98, Fig.7.15	A44-46, Figs. A.113-120, Tabs. A.29-30
Germanodactylus	99, Fig.7.16	A47-49, Figs. A.121-128, Tabs. A.31-32
Gnathosaurus	100, Fig.7.17	A50-52, Figs. A.129-136, Tabs. A.33-34
Huanhepterus	101, Fig.7.18	A53-55, Figs. A.137-144, Tabs. A.35-36
Istiodactylus	102, Fig.7.19	A56-58, Figs. A.145-152, Tabs. A.37-38
Jeholopterus	103, Fig.7.20	A59-61, Figs. A.153-160, Tabs. A.39-40
Ludodactylus	104, Fig.7.21	A62-64, Figs. A.161-168, Tabs. A.41-42
Nyctosaurus	105, Fig.7.22	A65-67, Figs. A.169-176, Tabs. A.43-44
Parapsicephalus	106, Fig.7.23	A68-70, Figs. A.177-184, Tabs. A.45-46
Peteinosaurus	107, Fig.7.24	A71-73, Figs. A.185-192, Tabs. A.47-48
Phobetopter	108, Fig.7.25	A74-76, Figs. A.193-200, Tabs. A.49-50
Plataleorhynchus	109, Fig.7.26	A77-79, Figs. A.201-208, Tabs. A.51-52
Preondactylus	110, Fig.7.27	A80-82, Figs. A.209-216, Tabs. A.53-54
Pteranodon	111, Fig.7.28	A83-85, Figs. A.217-224, Tabs. A.55-56
Pterodactylus antiquus	112, Fig.7.29	A86-88, Figs. A.225-232, Tabs. A.57-58
Pterodactylus elegans	113, Fig.7.30	A89-91, Figs. A.233-240, Tabs. A.59-60
Pterodactylus kochi	114, Fig.7.31	A92-94, Figs. A.241-248, Tabs. A.61-62
Pterodactylus micronyx	115, Fig.7.32	A95-97, Figs. A.249-256, Tabs. A.63-64
Pterodaustro	116, Fig.7.33	A98-100, Figs. A.257-264, Tabs. A.65-66
Quetzalcoatlus	117, Fig.7.34	A101-103, Figs. A.265-272, Tabs. A.67-68
Rhamphorhynchus	118, Fig.7.35	A104-106, Figs. A.273-280, Tabs. A.69-70
Santanadactylus	119, Fig.7.36	A107-109, Figs. A.281-288, Tabs. A.71-72
Scaphognathus	120, Fig.7.37	A110-112, Figs. A.289-296, Tabs. A.73-74
Sinopterus	121, Fig.7.38	A113-115, Figs. A.297-304, Tabs. A.75-76
Sordes	122, Fig.7.39	A116-118, Figs. A.305-312, Tabs. A.77-78
Tapejara	123, Fig.7.40	A119-121, Figs. A.313-320, Tabs. A.79-80
Thalassodromeus	124, Fig.7.41	A122-124, Figs. A.321-328, Tabs. A.81-82
Tupuxuara	125, Fig.7.42	A125-127, Figs. A.329-336, Tabs. A.83-84
Zhejiangopterus	126, Fig.7.43	A128-130, Figs. A.337-344 Tabs. A.85-86

7.1 Angustinaripterus skull construction (see pp. A2-4, Figs. A.1-8, Tabs. A.1-2)

Type species: Angustinaripterus longicephalus Xinlu et al. 1983

Major descriptions of the skull of Angustinaripterus: Wellnhofer (1991a), Xinlu et al. (1983)

Antorbital fenestra / naris: both present

Anterior rostral crest: absent

Medial rostral crest: absent

Orbitotemporal crest: absent

Orientation of occipital region in lateral view relative to vertical plane: ~55°

Keratinous beak: absent

Dentition: nine pair of teeth of Rhamphorhynchus tooth construction, anterior three pair of teeth projecting anteroventrally and enlarged relative to posterior teeth, tooth row ranging from the anterior tip of the rostrum to the level of the anterior third of the antorbital fenestra

Other features: naris oval and elongated in anteroventral/posterodorsal direction, situated anterodorsally to antorbital fenestra and ranging from the level of the 6th to the 9th pair of alveoli, antorbital fenestra subtriangular and about two time of the size of the orbita, ranging from the level of the 8th pair of alveoli to orbita

Cantilever dimensions

Height to length ratio: 1:3.5

Ratio of total length to length of antorbital fenestra & naris: 1:0.48

Ratio of basal Height to basal width: 1:1.13

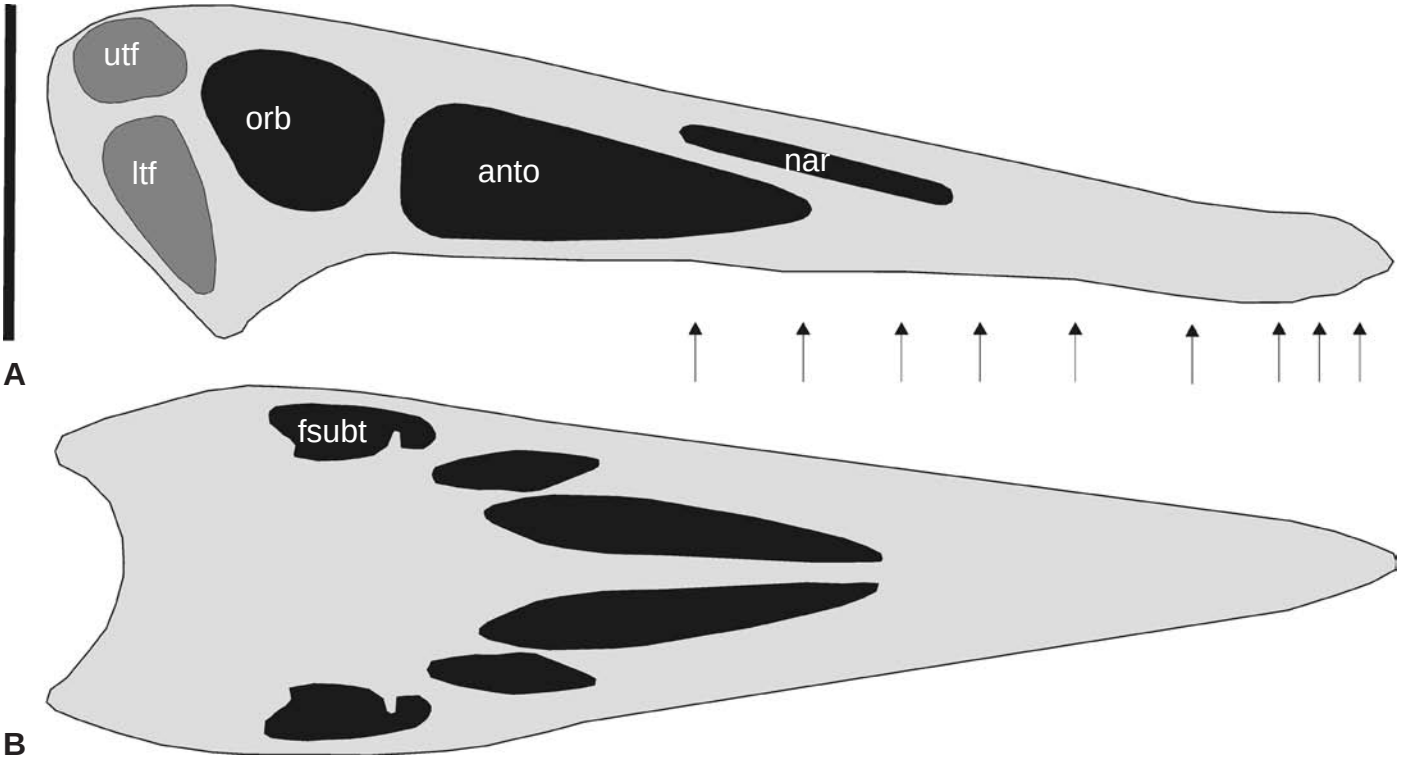

Fig. 7.1: Skull of *Angustinaripterus* in A) right lateral, and B) reconstructed ventral view. Arrows indicate level of alveoli. Scale bar = 70 mm. Abbreviations: anto = antorbital fenestra, fsubt = subtemporal foramen, ltf = lower temporal fenestra, nar = naris, nanto = nasoantorbital fenestra, sof = suborbital fenestra, utf = upper temporal fenestra.

7.2 Anurognathus skull construction (see pp. A5-7, Figs. A.9-16, Tabs. A.3-4)

Type species: Anurognathus ammoni Döderlein 1923

Major descriptions of the skull of Anurognathus: Döderlein (1923), Wellnhofer (1975b, 1978, 1991a)

Antorbital fenestra / naris: both present

Anterior rostral crest: absent

Medial rostral crest: absent

Orbitotemporal crest: absent

Orientation of occipital region in lateral view relative to vertical plane: ~55°

Keratinous beak: absent

Dentition: eight pair of teeth of Pterodactylus tooth construction, projecting ventrally, tooth row ranging from the anterior tip of the rostrum to the level of the anterior border of the orbita

Other features: naris and antorbital fenestra higher than wide, naris triangular and orientated in dorsal/ventral direction, ranging from the anterior tip of the rostrum to the level of the 4th pair of alveoli, antorbital fenestra rectangular and ranging from the level of the 4th to 7th pair of alveoli

Cantilever dimensions

Height to length ratio: 1:1.8

Ratio of total length to length of antorbital fenestra & naris: 1:0.64

Ratio of basal height to basal width: 1:1.51

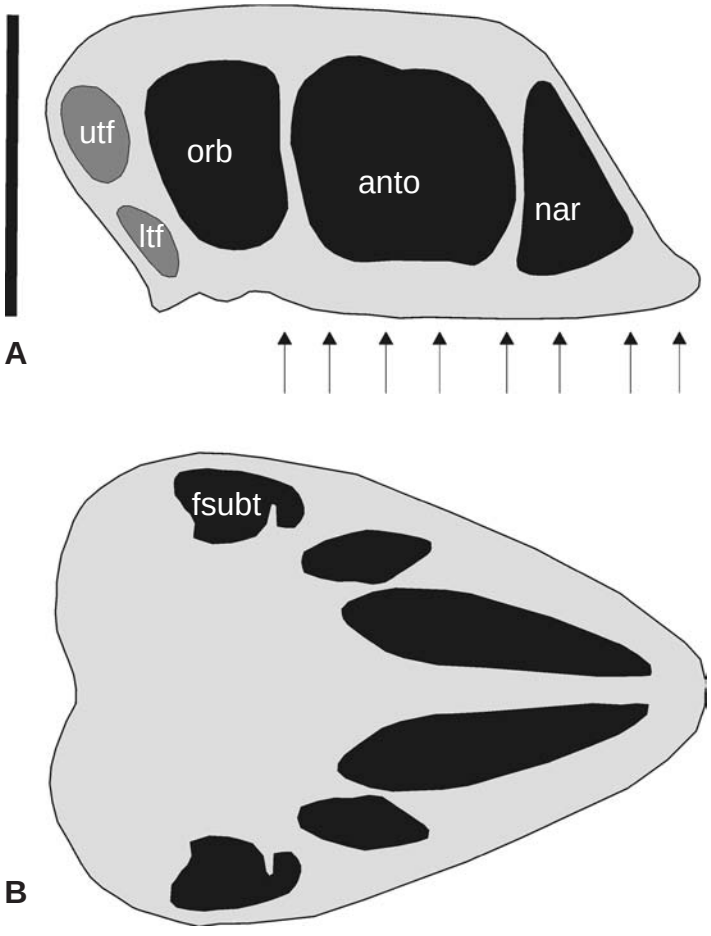

Fig. 7.2: Scaled skull of *Anurognathus* in A) reconstructed right lateral, and B) reconstructed ventral view. Arrows indicate level of alveoli. Scale bar = 70 mm. See Fig. 7.1 for abbreviations.

7.3 Austriadacytlus skull construction (see pp. A8-10, Figs. A.17-24, Tabs. A.5-6)

Type species: Austriadacytlus cristatus Dalla Vecchia et al. 2002

Major descriptions of the skull of Austriadacytlus: Dalla Vecchia et al. (2002, 2003a, 2003b)

Antorbital fenestra / naris: both present

Anterior/medial rostral crest: present, thinner than dorsal border of the rostrum (excluded from analysis), ranging from the anterior tip of the rostrum to the level of half of the length of the orbita.

Orbitotemporal crest: absent

Orientation of occipital region in lateral view relative to vertical plane: ~58°

Keratinous beak: absent

Dentition: fifteen pair of teeth, 1st to 5th pair of teeth of Eudimorphodon monocuspid tooth construction, posterior teeth of Preondactylus tooth construction, all teeth projecting ventrally, tooth row ranging from the anterior tip of the rostrum to the level of the anterior border of the orbita

Other features: naris larger than antorbital fenestra and ranging from the level of the 5th to 10th pair of alveoli, antorbital fenestra rounded triangular and ranging from the level of the 10th to the 15th pair of alveoli

Cantilever dimensions

Height to length ratio: 1:2.82

Ratio of total length to length of antorbital fenestra: 1:0.50

Ratio of basal height to basal width: 1:1.14

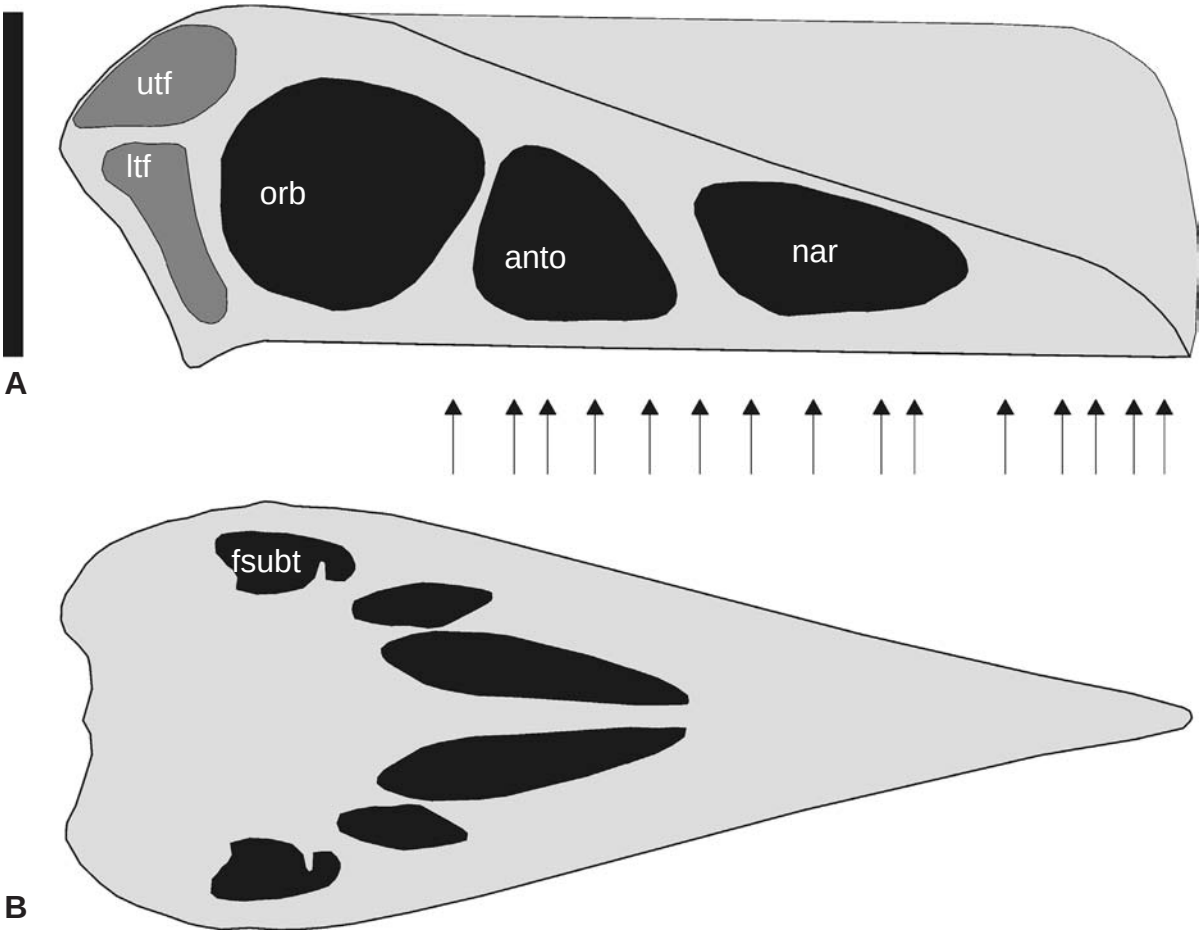

Fig. 7.3: Scaled skull of *Austriadacytlus* in A) right lateral, and B) reconstructed ventral view. Arrows indicate level of alveoli. Scale bar = 70 mm. See Fig. 7.1 for abbreviations.

7.4 Batrachognathus skull construction (see pp. A11-13, Figs. A.25-32, Tabs. A.7-8)

Type species: Batrachognathus volans Rjabinin 1948

Major descriptions of the skull of Batrachognathus: Rjabinin (1948), Wellnhofer (1978, 1991a)

Antorbital fenestra / naris: both present

Anterior rostral crest: absent

Medial rostral crest: absent

Orbitotemporal crest: absent

Orientation of occipital region in lateral view relative to vertical plane: ~55°

Keratinous beak: absent

Dentition: nine to eleven pair of teeth of Rhamphorhynchus tooth construction, all teeth projecting ventrally, tooth row ranging from anterior tip of the rostrum to the level of the anterior border of the orbita

Other features: naris higher than wide, triangular and orientated in dorsal/ventral direction, ranging from the anterior tip of the rostrum to the level of the 4th pair of alveoli position, antorbital fenestra quadratic and ranging from the level of the 4th to 7th pair of alveoli, skull construction paraboloidal in ventral view

Cantilever dimensions

Height to length ratio: 1:1.78

Ratio of total length to length of antorbital fenestra & naris: 1:0.65

Ratio of basal height to basal width: 1:1.55

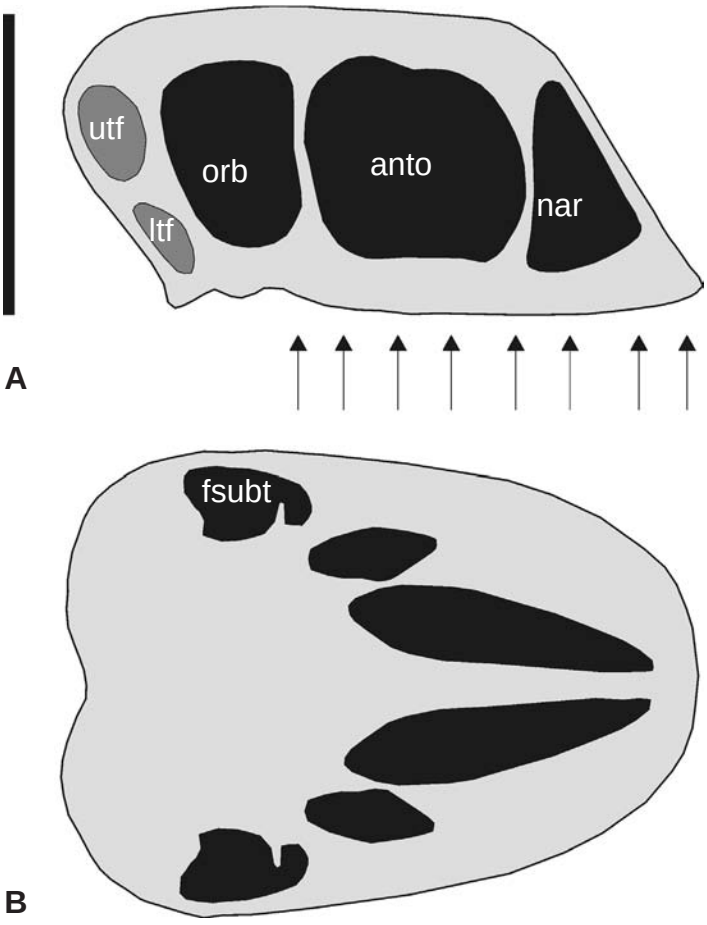

Fig. 7.4: Scaled skull of *Batrachognathus* in A) reconstructed right lateral, and B) reconstructed ventral view. Arrows indicate level of alveoli. Scale bar = 70 mm. See Fig. 7.1 for abbreviations.

7.5 Cacibupteryx skull construction (see pp. A14-16, Figs. A.33-40, Tabs. A.9-10)

Type species: Cacibupteryx caribensis Gasparini et al. 2004

Major descriptions of the skull of Cacibupteryx: Gasparini et al. (2004)

Antorbital fenestra / naris: both present

Anterior rostral crest: absent

Medial rostral crest: absent

Orbitotemporal crest: absent

Orientation of occipital region in lateral view relative to vertical plane: ~85°

Keratinous beak: absent

Dentition: twelve pair of teeth of unknown tooth construction, tooth row ranging from the the anterior tip of the rostrum to the level of the posterior end of the antorbital fenestra

Other features: naris and antorbital fenestra oval in cross section, naris ranging from the level of the 9th to 11th pair of alveoli, orientated anteroventrally/posterodorsally and slightly overlapping the antorbital fenestra in posteroventral direction, antorbital fenestra ranging from the level of the 10th to 12th pair of alveoli

Cantilever dimensions

Height to length ratio: 1:3.07

Ratio of total length to length of antorbital fenestra & naris: 1:0.31

Ratio of basal height to basal width: 1:1.17

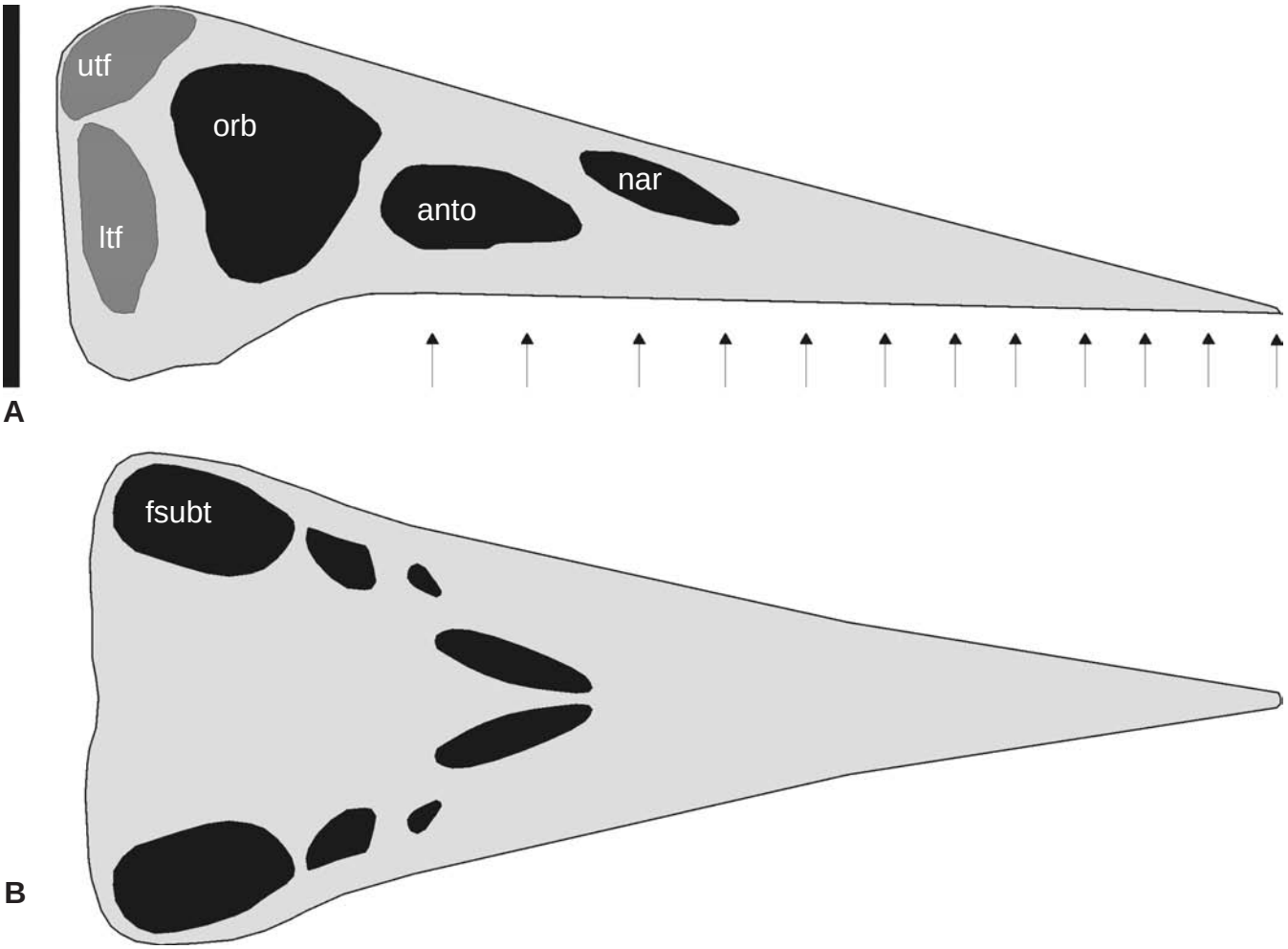

Fig. 7.5: Scaled skull of *Cacibupteryx* in A) reconstructed right lateral, and B) reconstructed ventral view. Arrows indicate level of alveoli. Scale bar = 70 mm. See Fig. 7.1 for abbreviations.

7.6 Campylognathoides skull construction (see pp. A17-19, Figs. A.41-48, Tabs. A.11-12)

Type species: Campylognathus zitteli Plieninger 1895

Major descriptions of the skull of Campylognathoides: Plieninger (1895), Wellnhofer (1974, 1978, 1991a)

Antorbital fenestra / naris: both present

Anterior rostral crest: absent

Medial rostral crest: absent

Orbitotemporal crest: absent

Orientation of occipital region in lateral view relative to vertical plane: ~55°

Keratinous beak: present

Dentition: fourteen pair of teeth of Pterodactylus tooth construction, tooth row ranging from the anterior tip of the rostrum to the level of the anteroventral border of the orbita

Other features: naris and antorbital fenestra about one quarter of the size of orbita, naris ranging from the level of the 4th to 9th pair of alveoli, naris oval, larger than antorbital fenestra and slightly overlapping the antorbital fenestra in posteroventral direction, antorbital fenestra symetrically triangular and ranging from the level of the 8th to 12th pair of alveoli

Cantilever dimensions

Height to length ratio: 1:2.20

Ratio of total length to length of antorbital fenestra: 1:0.40

Ratio of basal height to basal width: 1:0.96

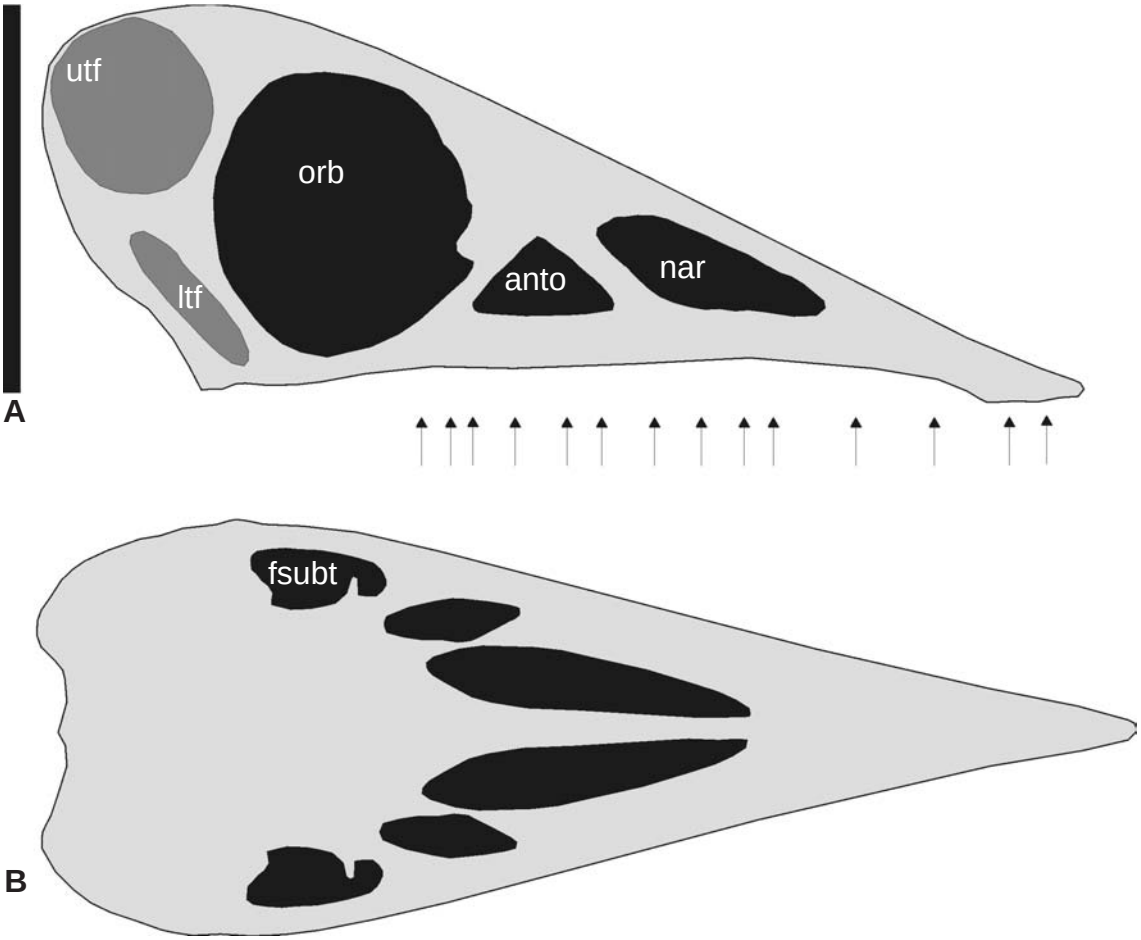

Fig. 7.6: Scaled skull of *Campylognathoides* in A) right lateral, and B) ventral view. Arrows indicate level of alveoli, Scale bar = 70 mm. See Fig. 7.1 for abbreviations.

7.7 Cearadactylus skull construction (see pp. A20-22, Figs. A.49-56, Tabs. A.13-14)

Type species: Cearadactylus atrox Leonardi & Borgomanero 1985

Major descriptions of the skull of Cearadactylus: Leonardi & Borgomanero (1985), Unwin (2002), Wellnhofer (1991b),

Antorbital fenestra / naris: fused into nasoantorbital fenestra

Anterior rostral crest: absent

Medial rostral crest: not present

Orbitotemporal crest: absent

Orientation of occipital region in lateral view relative to vertical plane: ~40°

Keratinous beak present: absent

Dentition: fifteen pair of teeth, anterior four teeth of Ornithocheirus high tooth construction, posterior teeth of Ornithocheirus low tooth construction, tooth row ranging from the anterior tip of the rostrum to the level of the anterior border of the nasoantorbital fenestra

Other features: anterior end of rostrum transversly expanded spatulate and festooned in lateral view from the level of the 1st to 7th pair of alveoli

Cantilever dimensions

Height to length ratio: 1:4.74

Ratio of total length to length of nasoantorbital fenestra: 1:0.43

Ratio of basal height to basal width: 1:0.96

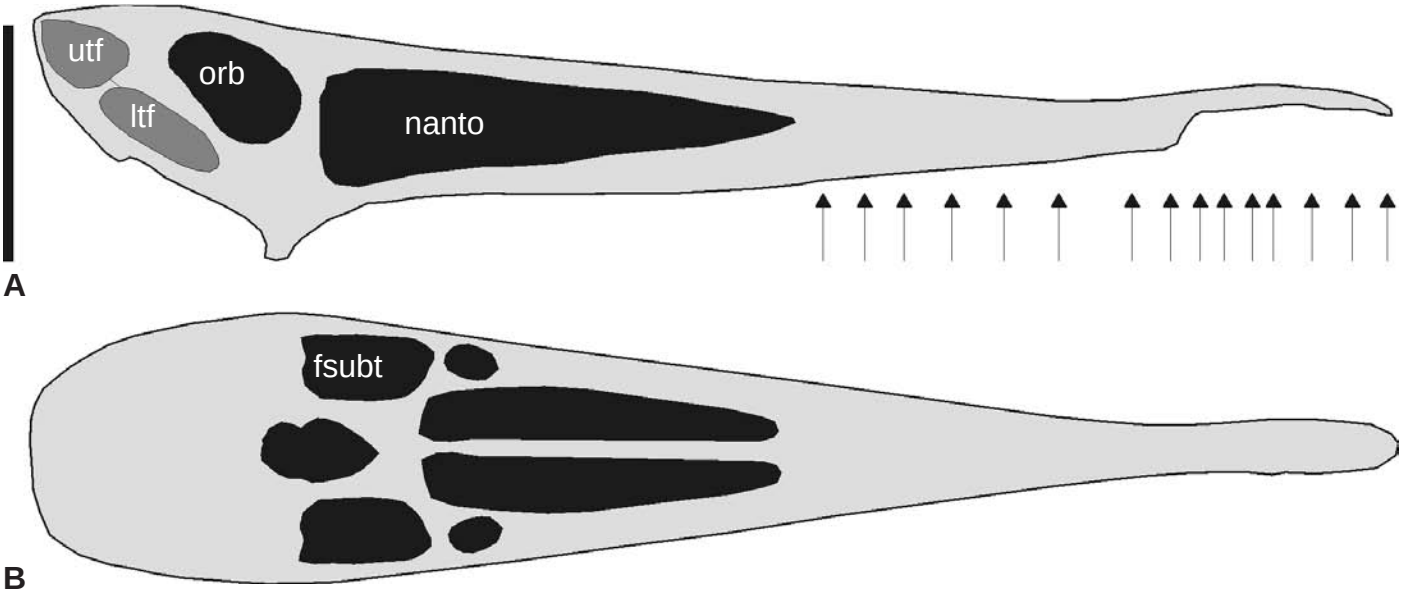

Fig. 7.7: Scaled skull of *Cearadactylus* in A) right lateral, and B) reconstructed ventral view. Arrows indicate level of alveoli. Scale bar = 70 mm. See Fig. 7.1 for abbreviations.

7.8 Coloborhynchus skull construction (see pp. A23-25, Figs. A.57-64, Tabs. A.15-16)

Type species: Coloborhynchus clavirostris Owen 1874

Major descriptions of the skull of Coloborhynchus: Fastnacht (2001), Lee (1994), Owen (1874), Veldmeijer (2003)

Antorbital fenestra / naris: fused into nasoantorbital fenestra

Anterior rostral crest: present, convex in lateral outline, ranging from the anterior tip of the rostrum to the level of the 14th pair of alveoli, reaching its greatest height at about the level of the 10th pair of alveoli.

Medial rostral crest: absent

Orbitotemporal crest: absent

Orientation of occipital region in lateral view relative to vertical plane: ~20°

Keratinous beak: absent

Dentition: eighteen pair of teeth, anterior three pair of teeth of Ornithocheirus high tooth construction, posterior teeth of Ornithocheirus low tooth construction, tooth row ranging from the anterior tip of the rostrum till the level of the anterior third of the nasoantorbital fenestra, 1st pair of alveoli orientated anteriorly, posterior following teeth orientated ventrally

Other features: Anterior end of rostrum transversly expanded spatulate from the level of the 1st to 4th pair of alveoli, nasoantorbital fenestra situated in the posterior half of the rostrum and ranging from the level of the 14th pair of alveoli to the orbita

Cantilever dimensions

Height to length ratio: 1:4.28

Ratio of total length to length of nasoantorbital fenestra: 1:0.45

Ratio of basal height to basal width: 1:1.30

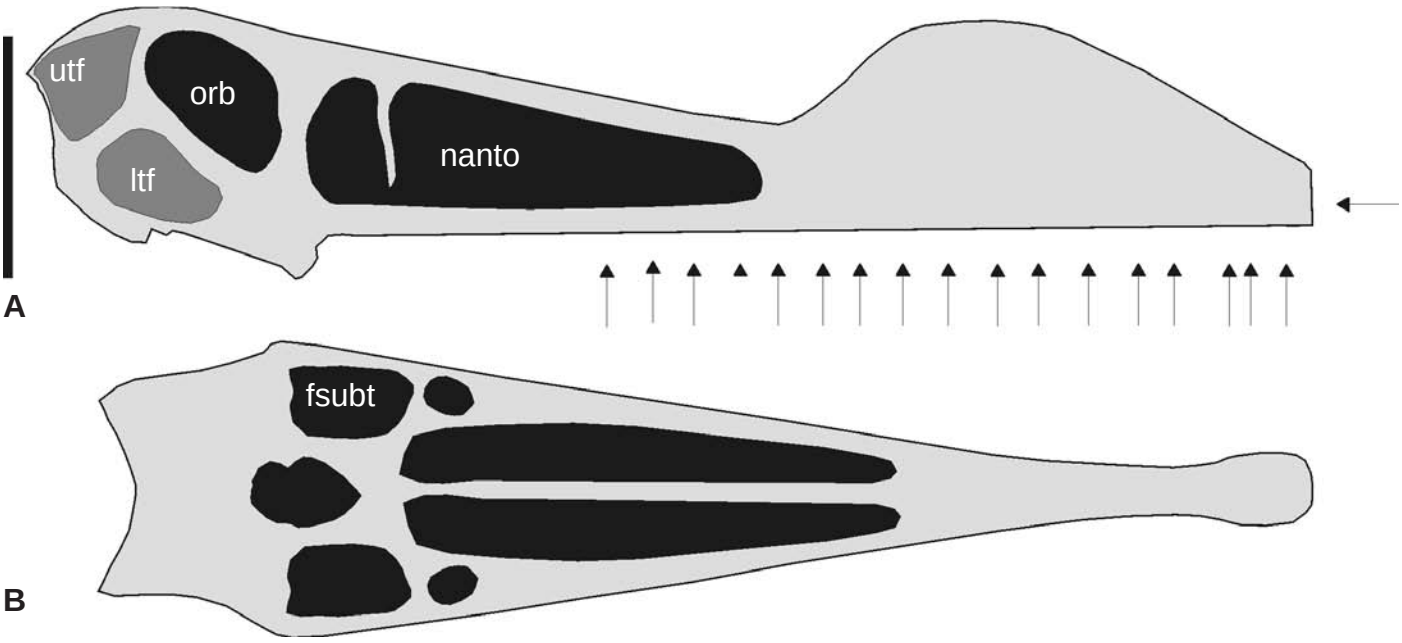

Fig. 7.8: Scaled skull of *Coloborhynchus* in A) right lateral, and B) ventral view. Arrows indicate level of alveoli. Scale bar = 70 mm. See Fig. 7.1 for abbreviations.

7.9 Criorhynchus skull construction (see pp. A26-28, Figs. A.65-72, Tabs. A.17-18)

Type species: Criorhynchus simus Owen 1861

Major descriptions of the skull of Criorhynchus: Owen (1861), Wellnhofer (1987)

Antorbital fenestra / naris: fused into nasoantorbital fenestra

Anterior rostral crest: present, convex in lateral outline, ranging from the anterior tip of the rostrum to the level of the 10th pair of alveoli, reaching its greatest height at about the level between the 7th to 8th pair of alveoli.

Medial rostral crest: absent

Orbitotemporal crest: orbitotemporal region expanded posterodorsally, forming a short blunt process

Orientation of occipital region in lateral view relative to vertical plane: ~20°

Keratinous beak: absent

Dentition: thirteen pair of teeth of Ornithocheirus low tooth construction, tooth row ranging from the anterior tip of the rostrum to the level of the anterior quarter of the nasoantorbital fenestra

Other features: nasoantorbital fenestra situated in the posterior half of the rostrum and ranging from the level of the 12th pair of alveoli to the orbita

Cantilever dimensions

Height to length ratio: 1:4.84

Ratio of total length to length of nasoantorbital fenestra: 1:0.45

Ratio of basal height to basal width: 1:1.38

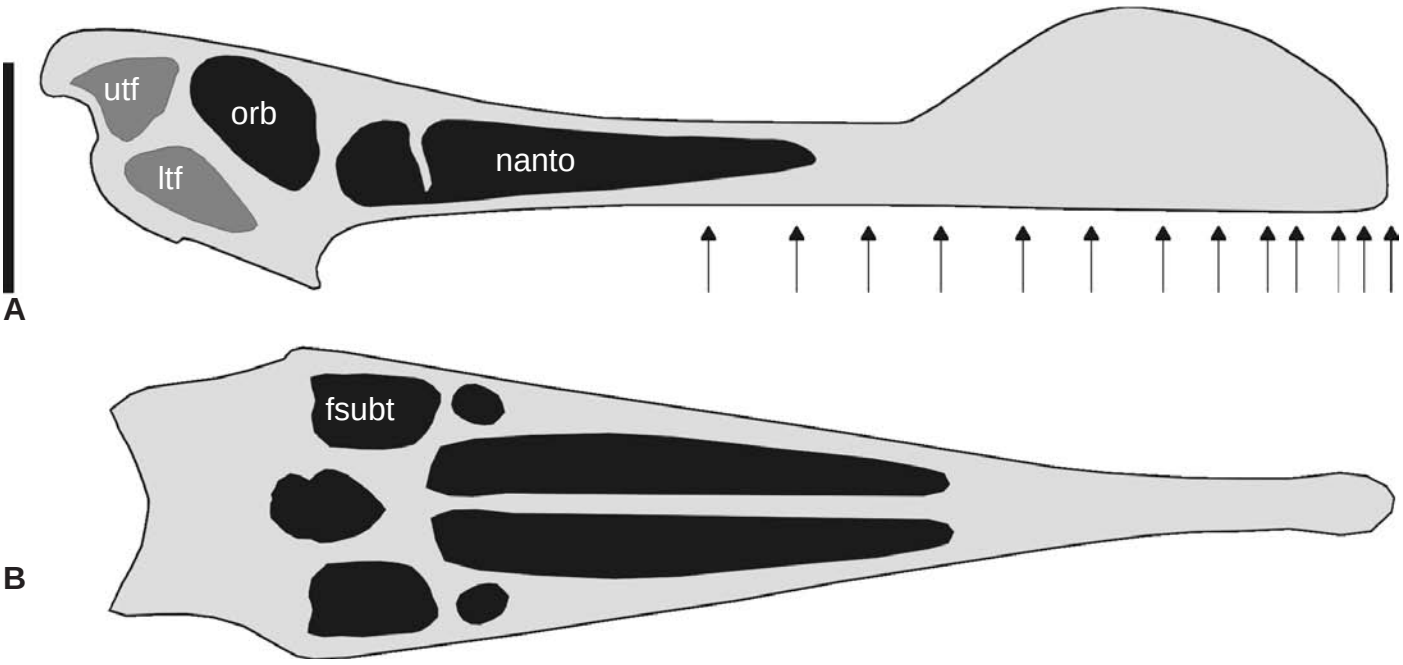

Fig. 7.9: Scaled skull of *Criorhynchus* in A) right lateral, and B) ventral view. Arrows indicate level of alveoli. Scale bar = 70 mm. See Fig. 7.1 for abbreviations.

7.10 Ctenochasma skull construction (see pp. A29-31, Figs. A.73-80, Tabs. A.19-20)

Type species: Ctenochasma roemeri H v. Meyer 1852

Major descriptions of the skull of Ctenochasma: Broili (1936), Buisonjé (1981), Jouve (2004), Meyer (1852), Taquet (1972), Wellnhofer (1970, 1878, 1991a)

Antorbital fenestra / naris: fused into nasoantorbital fenestra

Anterior rostral crest: bony crest absent, soft-tissue crest can not be excluded

Medial rostral crest: bony crest absent, soft-tissue crest can not be excluded

Orbitotemporal crest: bony crest absent, soft-tissue crest can not be excluded

Orientation of occipital region in lateral view relative to vertical plane: ~25°

Keratinous beak: absent

Dentition: up to 90 teeth of Ctenochasma tooth construction, tooth row ranging from the anterior tip of the rostrum to about three quarter of the length of rostrum in posterior direction

Other features: nasoantorbital fenestra rounded triangular, about the same size as orbita and situated in the posterior fifth part of the rostrum

Cantilever dimensions

Height to length ratio: 1:5.85

Ratio of total length to length of nasoantorbital fenestra: 1:0.19

Ratio of basal height to basal width: 1:0.95

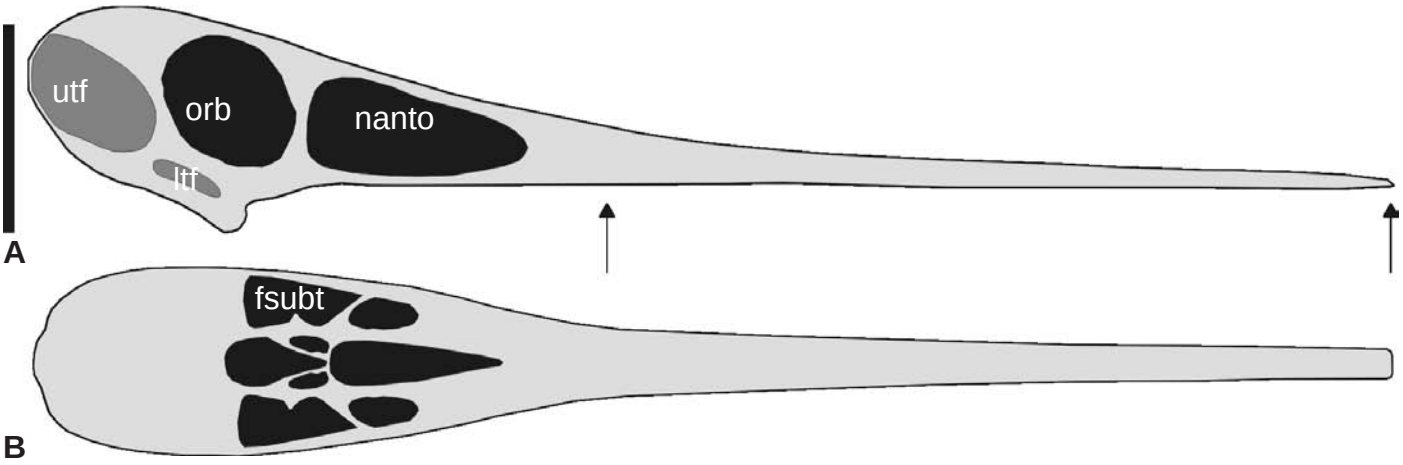

Fig. 7.10: Scaled skull of *Ctenochasma* in A) right lateral, and B) ventral view. Arrows indicate level of the most anterior and most posterior alveoli, Scale bar = 70 mm. See Fig. 7.1 for abbreviations.

7.11 Dimorphodon skull construction (see pp. A32-34, Figs. A.81-88, Tabs. A.21-22)

Type species: Dimorphodon macronyx (Buckland 1829)

Major descriptions of the skull of Dimorphodon: Buckland (1829), Wellnhofer (1978, 1991a)

Antorbital fenestra / naris: both present

Anterior rostral crest: absent

Medial rostral crest: absent

Orbitotemporal crest: absent

Orientation of occipital region in lateral view relative to vertical plane: ~77°

Keratinous beak: absent

Dentition: eighteen pair of teeth of Pterodactylus tooth construction, tooth row ranging from the anterior tip of the rostrum to two thirds of the skull length in posterior direction

Other features: skull with convex dorsal outline in lateral view, naris rounded triangular, larger than antorbital fenestra and ranging from the level of the 4th to 9th pair of alveoli, slightly overlapping the antorbital fenestra in anterodorsal direction, antorbital fenestra rounded triangular ranging from the level of the 8th pair of alveoli to the orbita

Cantilever dimensions

Height to length ratio: 1:2.41

Ratio of total length to length of antorbital fenestra & naris: 1:0.60

Ratio of basal height to basal width: 1:0.83

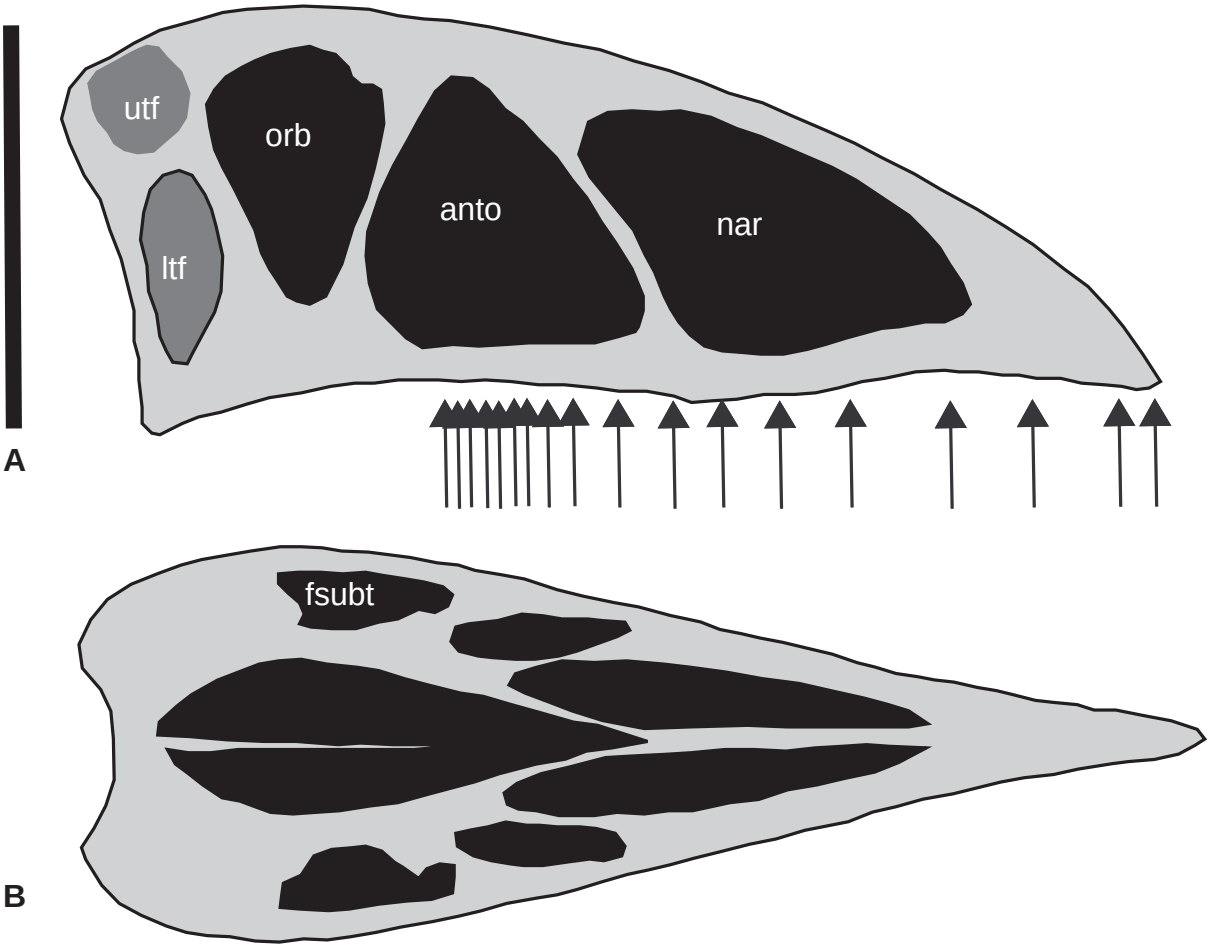

Fig. 7.11: Scaled skull of *Dimorphodon* in A) reconstructed right lateral, and B) reconstructed ventral view. Arrows indicate level of alveoli, Scale bar = 70 mm. See Fig. 7.1 for abbreviations.

7.12 Dorygnathus skull construction (see pp. A35-37, Figs. A.89-96, Tabs. A.23-24)

Type species: Dorygnathus macronyx Theodori 1830

Major descriptions of the skull of Dorygnathus: Wellnhofer (1978, 1991a), Wild (1971), Wiman (1925a)

Antorbital fenestra / naris: both present

Anterior rostral crest: absent

Medial rostral crest: absent

Orbitotemporal crest: absent

Orientation of occipital region in lateral view relative to vertical plane: ~65°

Keratinous beak: absent

Dentition: eleven pair of teeth of Rhamphorhynchus tooth construction, tooth row ranging from the anterior tip of the rostrum to the posterior end of the antorbital fenestra

Other features: naris and antorbital fenestra small relative to the orbita, naris oval, reaching from the level of the 6th to 8th pair of alveoli and slightly overlapping the antorbital fenestra in anterodorsal direction, antorbital fenestra rounded triangular and ranging from the level of the 8th pair of alveoli to the orbita

Cantilever dimensions

Height to length ratio: 1:2.01

Ratio of total length to length of antorbital fenestra: 1:0.32

Ratio of basal height to basal width: 1:0.91

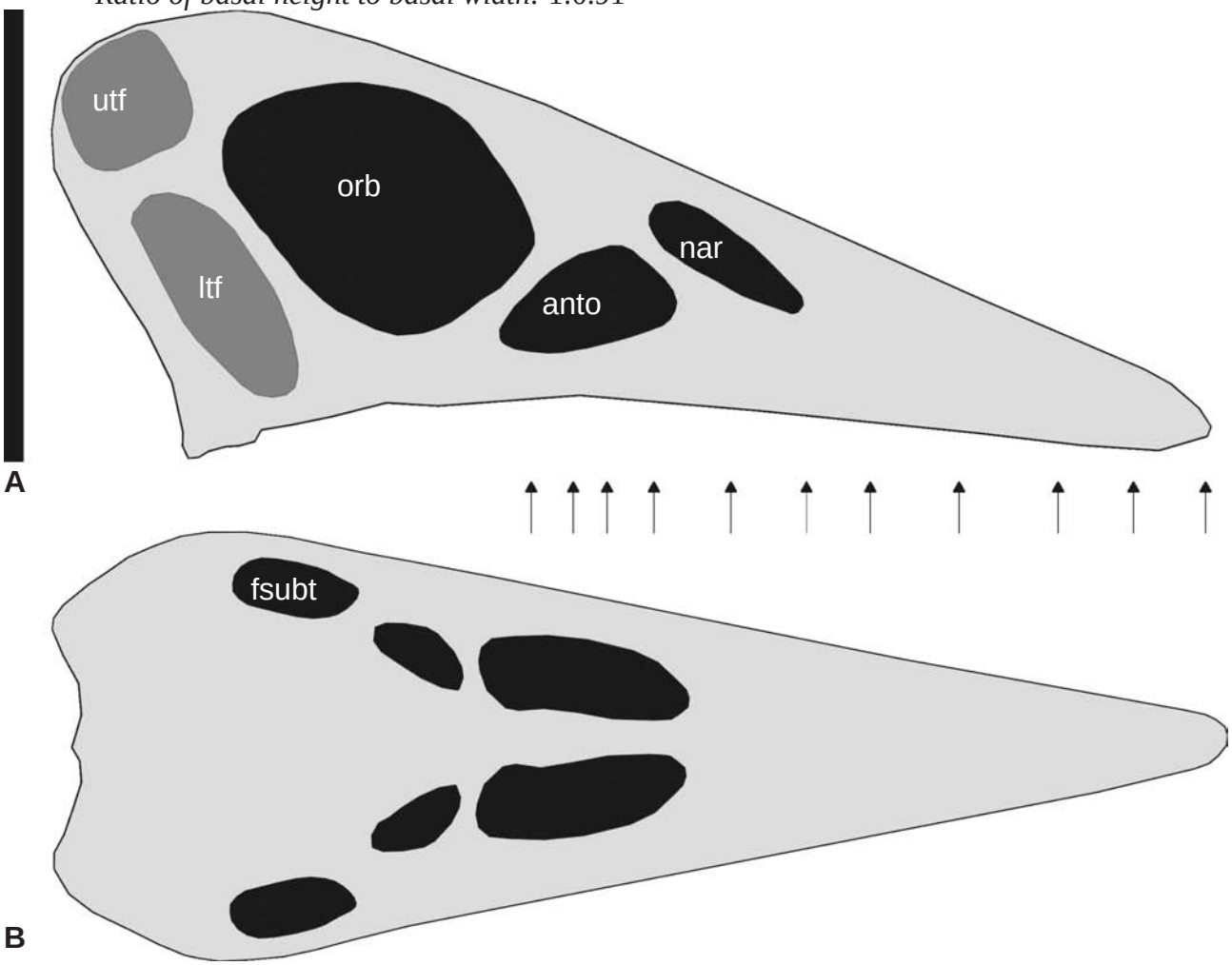

Fig. 7.12: Scaled skull of *Dorygnathus* in A) right lateral, and B) reconstructed ventral view. Arrows indicate level of alveoli. Scale bar = 70 mm. See Fig. 7.1 for abbreviations.

7.13 Dsungaripterus skull construction (see pp. A38-40, Figs. A.97-104, Tabs. A.25-26)

Type species: Dsungaripterus weii Young 1964

Major descriptions of the skull of Dsungaripterus: Wellnhofer (1978, 1991a), Young (1964)

Antorbital fenestra / naris: fused into nasoantorbital fenestra

Anterior rostral crest: absent

Medial rostral crest: present, thinner than dorsal border of the rostrum (excluded from analysis), ranging from the level of the 2nd pair of alveoli to the posterior end of the antorbital fenestra

Orbitotemporal crest: present, short blunt process about the same size at the mean orbital diameter, projecting in posterodorsal direction.

Orientation of occipital region in lateral view relative to vertical plane: ~35°

Keratinous beak: present, covering the anterior rostrum till the 1st pair of alveoli

Dentition: twelve pair of teeth of Dsungaripterus tooth construction, last three pair of alveoli with elevated alveolar walls and smaller interalveolar space than the rest of the tooth row, tooth row ranging from the level of the end of the anterior third of the rostrum to one third of the nasoantorbital fenestra

Other features: nasoantorbital fenestra triangular ranging from the level of the 6th pair of alveoli to the orbita, orbita circular and situated posterodorsal to the antorbital fenestra

Cantilever dimensions

Height to length ratio: 1:3.11

Ratio of total length to length of nasoantorbital fenestra: 1:0.46

Ratio of basal height to basal width: 1:0.61

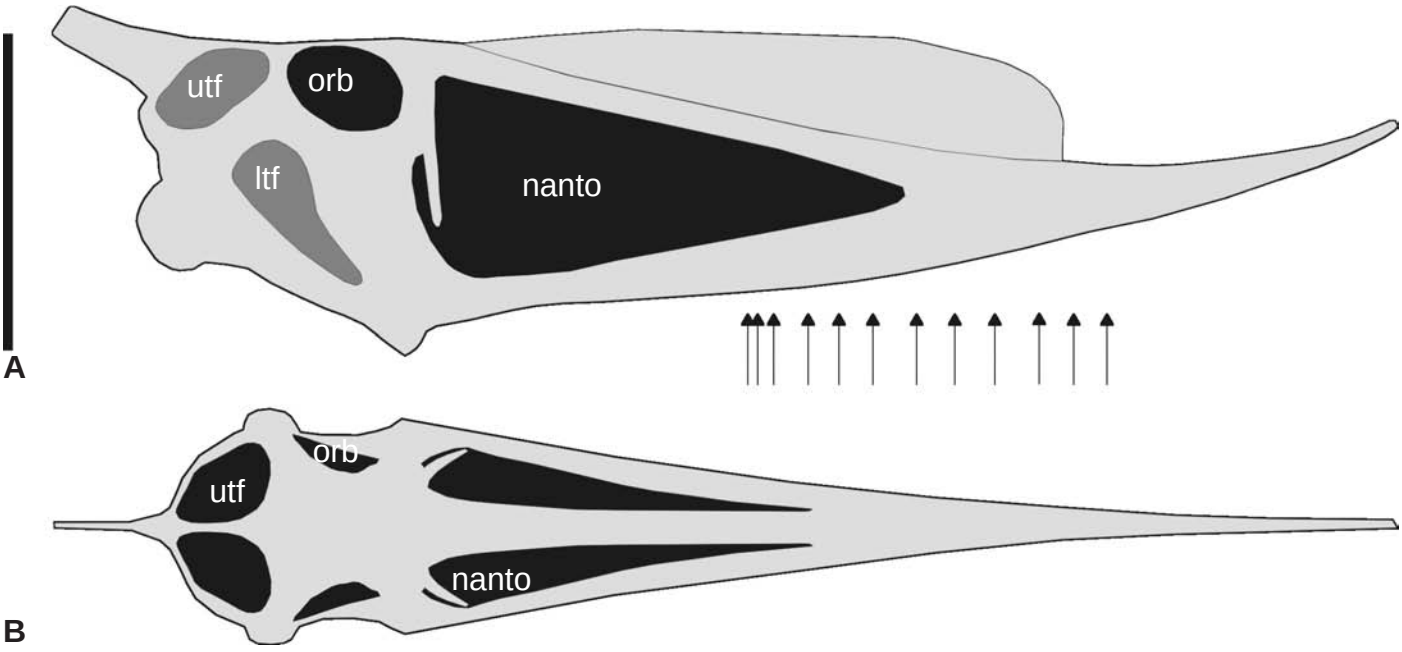

Fig. 7.13: Scaled skull of *Dsungaripterus* in A) right lateral, and B) dorsal view. Arrows indicate level of alveoli. Scale bar = 70 mm. See Fig. 7.1 for abbreviations.

7.14 Eudimorphodon skull construction (see pp. A41-43, Figs. A.105-112, Tabs. A.27-28)

Type species: Eudimorphodon ranzii Zambelli 1973

Major descriptions of the skull of Eudimorphodon: Wellnhofer (1978, 1991b), Wild (1978, 1993), Zambelli (1973)

Antorbital fenestra / naris: both present

Anterior rostral crest: absent

Medial rostral crest: absent

Orbitotemporal crest: absent

Orientation of occipital region in lateral view relative to vertical plane: ~70°

Keratinous beak: absent

Dentition: twenty-nine pair of teeth, 1st to 4th pair of teeth of Eudimorphodon monocuspid tooth construction, 5th pair of Eudimorphodon pseudo-monocuspid tooth construction, posterior following teeth of Eudimorphodon high and posteriorly low multicuspid tooth construction, tooth row ranging from the anterior tip of the jaw to half of the length of the orbita

Other features: naris oval to subtriangular in cross-section, ranging from the level of the 8th to 18th pair of alveoli, naris slightly overlapping antorbital fenestra in posterodorsal direction, antorbital fenestra triangular and ranging from the 18th to 23rd pair of alveoli, naris and antorbital fenestra about one third of the size of the orbita

Cantilever dimensions

Height to length ratio: 1:2.32

Ratio of total length to length of nasoantorbital fenestra: 1:0.36

Ratio of basal height to basal width: 1:1:00

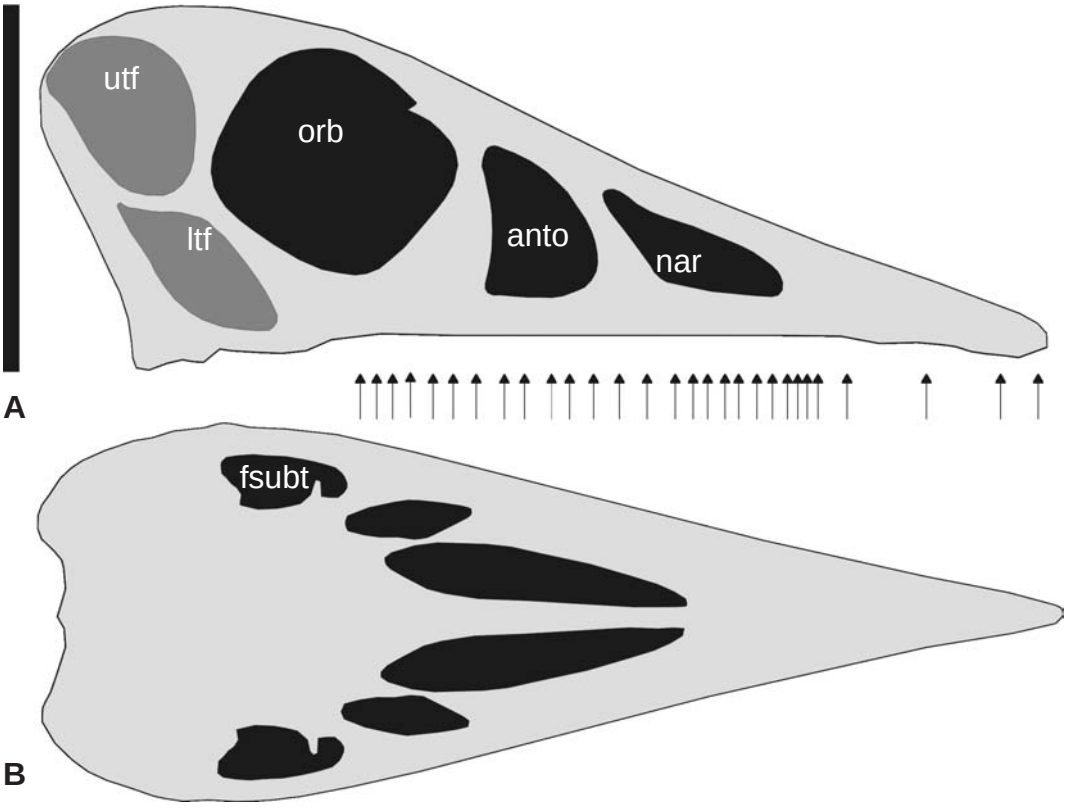

Fig. 7.14: Scaled skull of *Eudimorphodon* in A) right lateral, and B) reconstructed ventral view. Arrows indicate level of alveoli. Scale bar = 70 mm. See Fig. 7.1 for abbreviations.

7.15 Gallodactylus skull construction (see pp. A44-46, Figs. A.113-120, Tabs. A.29-30)

Type species: Gallodactylus canjuersensis Fabre 1976

Major descriptions of the skull of Gallodactylus: Fabre (1976), Meyer (1860), Quenstedt (1855), Plieninger (1907), Wellnhofer (1978, 1991a)

Antorbital fenestra / naris: fused into nasoantorbital fenestra

Anterior rostral crest: absent

Medial rostral crest: absent

Orbitotemporal crest: absent, but dorsal occipital region enlarged in posterodorsal direction

Orientation of occipital region in lateral view relative to vertical plane: ~20°

Keratinous beak: absent

Dentition: eight pair of teeth of Rhamphorhynchus tooth construction, tooth row restricted to anterior fifth part of the rostrum

Other features: nasoantorbital fenestra triangular and situated in the posterior half of the rostrum, upper temporal fenestra enlarged due to posterodorsal expansion of the occipital region

Cantilever dimensions

Height to length ratio: 1:3.31

Ratio of total length to length of nasoantorbital fenestra: 1:0.38

Ratio of basal height to basal width: 1:1.36

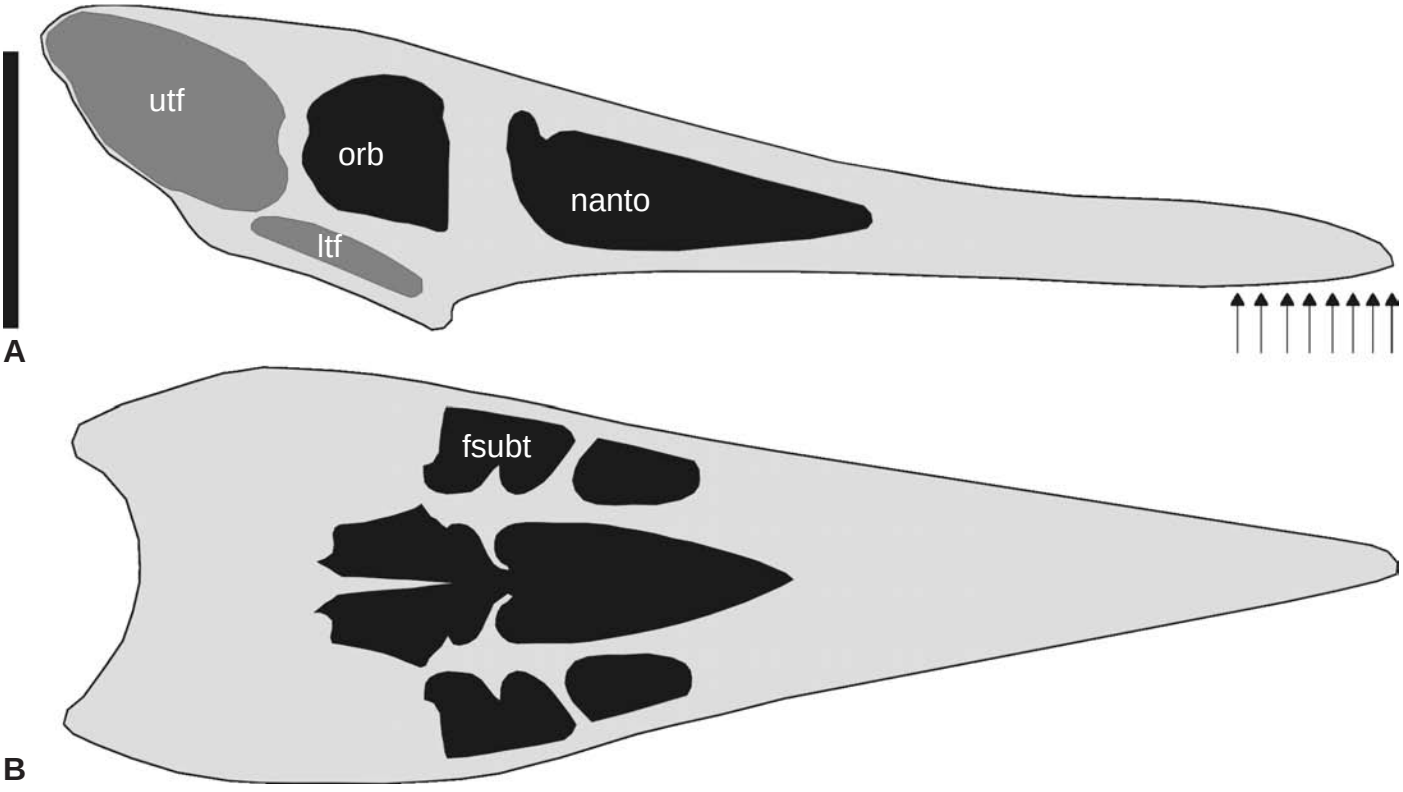

Fig. 7.15: Scaled skull of *Gallodactylus* in A) right lateral, and B) reconstructed ventral view. Arrows indicate level of alveoli. Scale bar = 70 mm. See Fig. 7.1 for abbreviations.

7.16 Germanodactylus skull construction (see pp. A47-49, Figs. A.121-128, Tabs. A.31-32)

Type species: Germanodactylus canjuersensis Young 1964

Major descriptions of the skull of Germanodactylus: Bennett (2002), , Meyer (1860), Wagner (1851), Wellnhofer (1970, 1978, 1991a), Wiman (1925b)

Antorbital fenestra / naris: fused into nasoantorbital fenestra

Anterior rostral crest: absent

Medial rostral crest: present, thinner than dorsal border of the rostrum (excluded from analysis), ranging from the level of the 9th pair of alveoli to one third of the length of the orbita, continuing as soft-tissue crest into orbitotemporal region

Orbitotemporal crest: soft-tissue crest, continued from medial rostral crest

Orientation of occipital region in lateral view relative to vertical plane: ~30°

Keratinous beak: present, covering the anterior rostrum till the 1st pair of alveoli

Dentition: fourteen pair of teeth of Pterodactylus tooth construction, tooth row ranging to half of the length of the nasoantorbital fenestra

Other features: nasoantorbital fenestra triangular and situated in the posterior half of the rostrum, upper temporal fenestra enlarged due to posterodorsal expansion of the occipital region

Cantilever dimensions

Height to length ratio: 1:3.56

Ratio of total length to length of nasoantorbital fenestra: 1:0.43

Ratio of basal height to basal width: 1:1.17

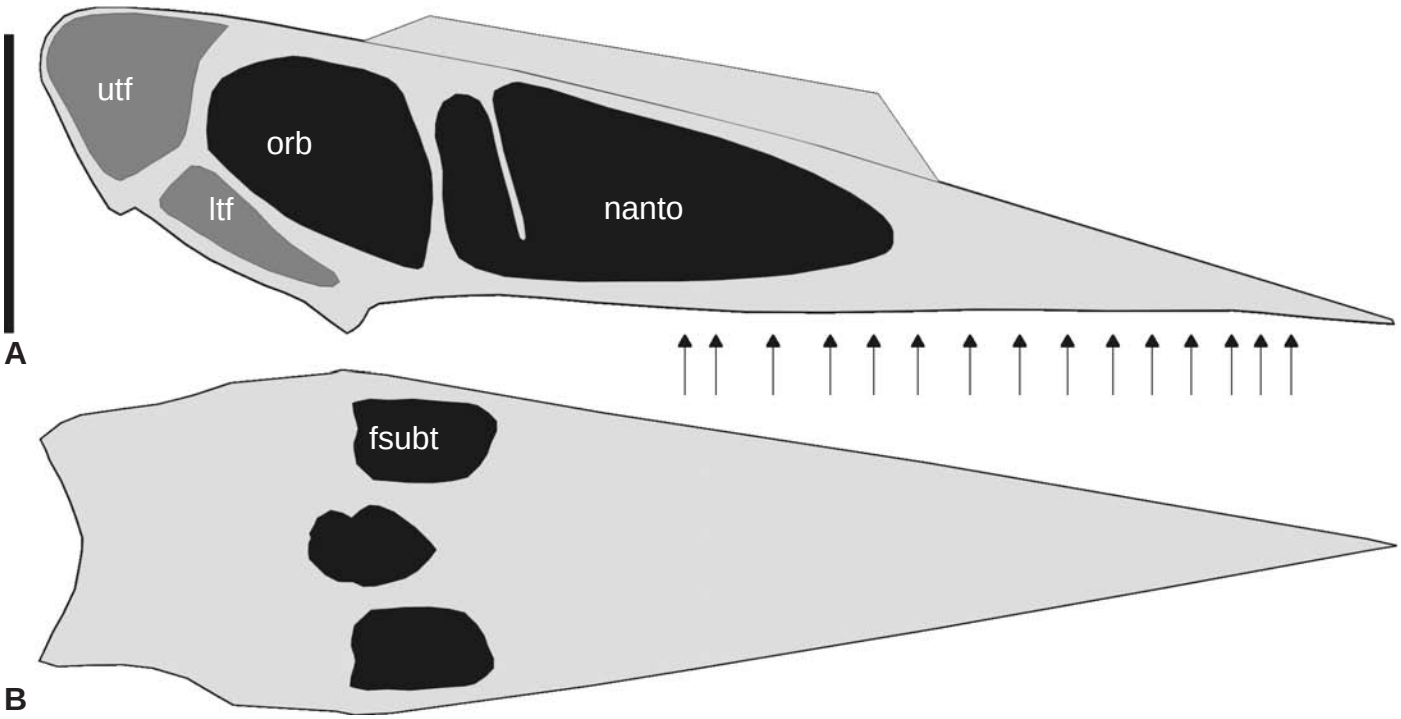

Fig. 7.16: Scaled skull of *Germanodactylus* in A) right lateral, and B) reconstructed ventral view. Arrows indicate level of alveoli. Scale bar = 70 mm. See Fig. 7.1 for abbreviations.

7.17 Gnathosaurus skull construction (see pp. A50-52, Figs. A.129-136, Tabs. A.33-34)

Type species: Gnathosaurus subulatus Meyer 1834

Major descriptions of the skull of Gnathosaurus: Meyer (1834), Wellnhofer (1970, 1978, 1991a)

Antorbital fenestra / naris: fused into nasoantorbital fenestra

Anterior rostral crest: absent

Medial rostral crest: present, thinner than dorsal border of the rostrum (excluded from analysis), ranging from the level of the 21st pair of alveoli to half of the length of the antorbital fenestra, continuing as soft-tissue crest into orbitotemporal region

Orbitotemporal crest: soft-tissue crest, continued from medial rostral crest

Orientation of occipital region in lateral view relative to vertical plane: ~20°

Keratinous beak present: absent

Dentition: thirty-two pair of teeth of Gnathosaurus tooth construction, tooth row ranging from the anterior tip of the rostrum to the level of the anterior end of the nasoantorbital fenestra

Other features: nasoantorbital fenestra subtriangular to oval and situated in the posterior third of the rostrum, anterior rostrum expanded "spatulate" from the level of the 1st to 9th pair of alveoli with largest width at the level of the 4th pair of alveoli

Cantilever dimensions

Height to length ratio: 1:5.56

Ratio of total length to length of nasoantorbital fenestra: 1:0.30

Ratio of basal height to basal width: 1:0.91

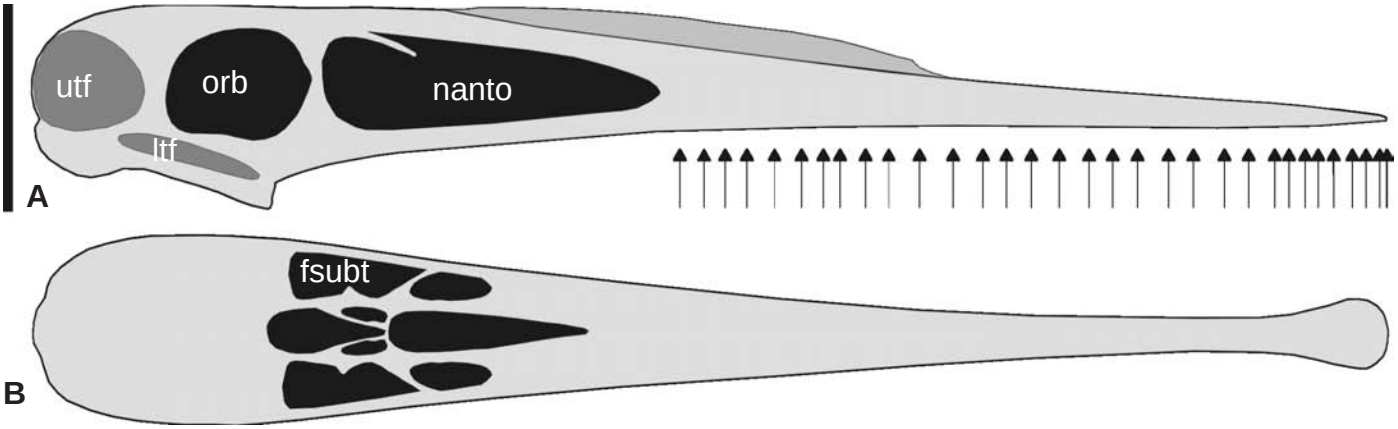

Fig. 7.17: Scaled skull of *Gnathosaurus* in A) right lateral, and B) ventral view. Arrows indicate level of alveoli. Scale bar = 70 mm. See Fig. 7.1 for abbreviations.

7.18 Huanhepterus skull construction (see pp. A53-55, Figs. A.137-144, Tabs. A.35-36)

Type species: Huanhepterus quinyangensis Dong 1982

Major descriptions of the skull of Huanhepterus: Dong (1982)

Antorbital fenestra / naris: fused into nasoantorbital fenestra

Anterior rostral/medial crest: present, thinner than dorsal border of the rostrum (excluded from analysis), ranging from the 7th pair of alveoli to the level of half of the length of the nasoantorbital fenestra, merging into medial rostral crest and continuing as soft-tissue crest into orbitotemporal region)

Orbitotemporal crest: probable soft-tissue crest (Frey et al. 2003b)

Orientation of occipital region in lateral view relative to vertical plane: ~10°

Keratinous beak: absent

Dentition: thirty-two pair of teeth of Rhamphorhynchus tooth construction, tooth row ranging from the anterior tip of the rostrum to the level of the posterior end of the anterior third of the rostrum

Other features: nasoantorbital fenestra triangular to oval and situated in the posterior half of the rostrum, anterior end of rostrum bent in ventral direction from the 1st to 3rd pair of alveoli

Cantilever dimensions

Height to length ratio: 1:4.46

Ratio of total length to length of nasoantorbital fenestra: 1:0.38

Ratio of basal height to basal width: 1:0.73

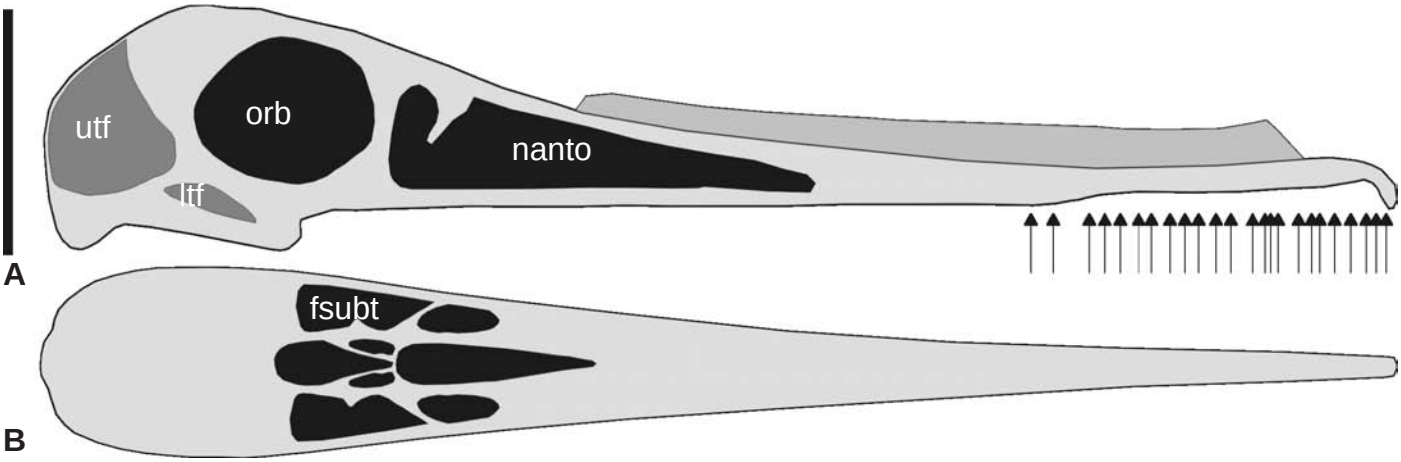

Fig. 7.18: Scaled skull of *Huanhepterus* in A) right lateral, and B) reconstructed ventral view. Arrows indicate level of alveoli. Scale bar = 70 mm. See Fig. 7.1 for abbreviations.

7.19 Istiodactylus skull construction (see pp. A56-58, Figs. A.145-152, Tabs. A.37-38)

Type species: Istiodactylus cluniculus (Seeley 1887)

Major descriptions of the skull of Istiodactylus: Arthaber (1921), Howse et al. (2001), Seeley (1901), Wellnhofer (1978, 1991a)

Antorbital fenestra / naris: fused into nasoantorbital fenestra

Anterior rostral crest: absent

Medial rostral crest: absent

Orbitotemporal crest: absent

Orientation of occipital region in lateral view relative to vertical plane: ~30°

Keratinous beak: absent

Dentition: twelve pair of teeth of Pterodactylus tooth construction, tooth row restricted to the anterior quarter of the rostrum and ranging from the anterior tip of the rostrum to the level of the anterior border of the nasoantorbital fenestra

Other features: nasoantorbital fenestra triangular and situated in the posterior three quarters of the rostrum, orbita expanded posterodorsally relative to the nasoantorbital fenestra, anterior rostrum rounded with an u-shaped outline in ventral view

Cantilever dimensions

Height to length ratio: 1:3.38

Ratio of total length to length of nasoantorbital fenestra: 1:0.76

Ratio of basal height to basal width: 1:0.82

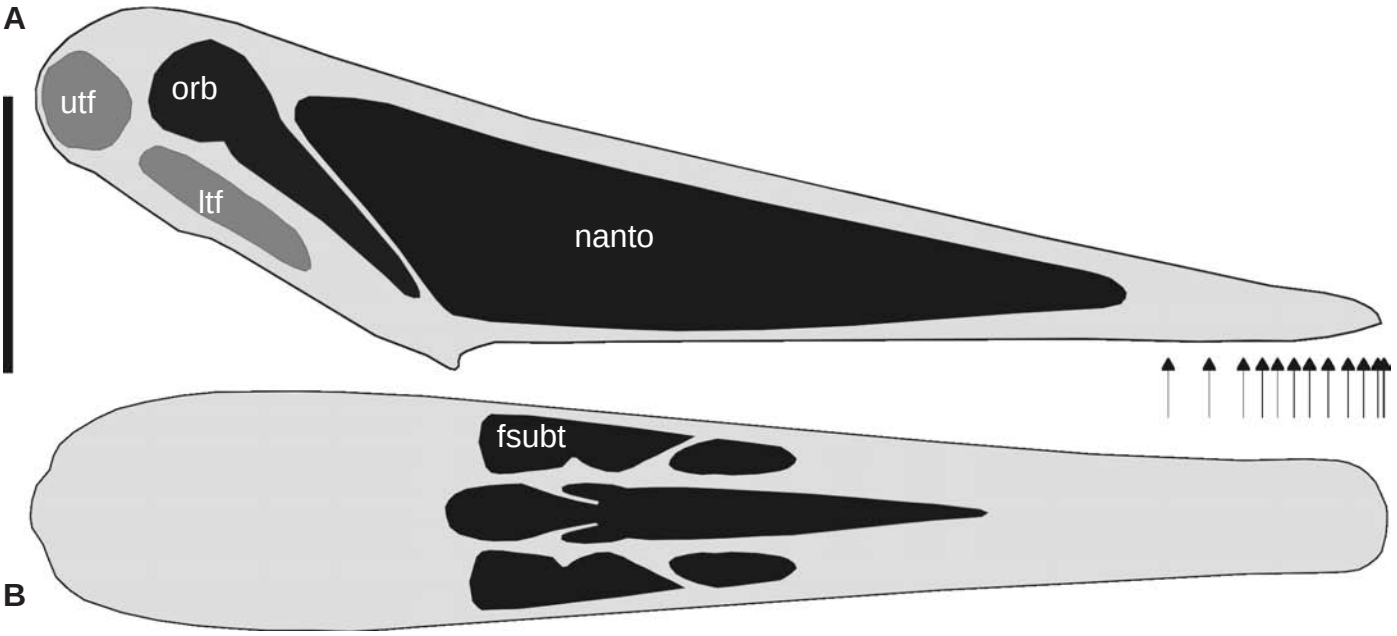

Fig. 7.19: Scaled skull of *Istiodactylus* in A) reconstructed right lateral, and B) reconstructed ventral view. Arrows indicate level of alveoli. Scale bar = 70 mm. See Fig. 7.1 for abbreviations.

7.20 Jeholopterus skull construction (see pp. A59-61, Figs. A.153-160, Tabs. A.39-40)

Type species: Jeholopterus ningchengensis Wang et al. 2002

Major descriptions of the skull of Jeholopterus: Dalla Vecchia (2002), Wang et al. (2002)

Antorbital fenestra / naris: both present

Anterior rostral crest: absent

Medial rostral crest: absent

Orbitotemporal crest: absent

Orientation of occipital region in lateral view relative to vertical plane: ~60°

Keratinous beak: absent

Dentition: nine pair of teeth of Rhamphorhynchus tooth construction, tooth row ranging from the anterior tip of the rostrum to the anterior border of the orbita

Other features: naris and antorbital fenestra higher than wide, naris triangular and orientated in dorsal/ventral direction, ranging from the level of the 3rd pair to 5th pair of alveoli, antorbital fenestra quadratic and ranging from the level of the 5th pair to 9th pair of alveoli, skull construction with a semicircular outline in ventral view

Cantilever dimensions

Height to length ratio: 1:1.38

Ratio of total length to length of nasoantorbital fenestra & naris: 1:0.65

Ratio of basal height to basal width: 1:1.93

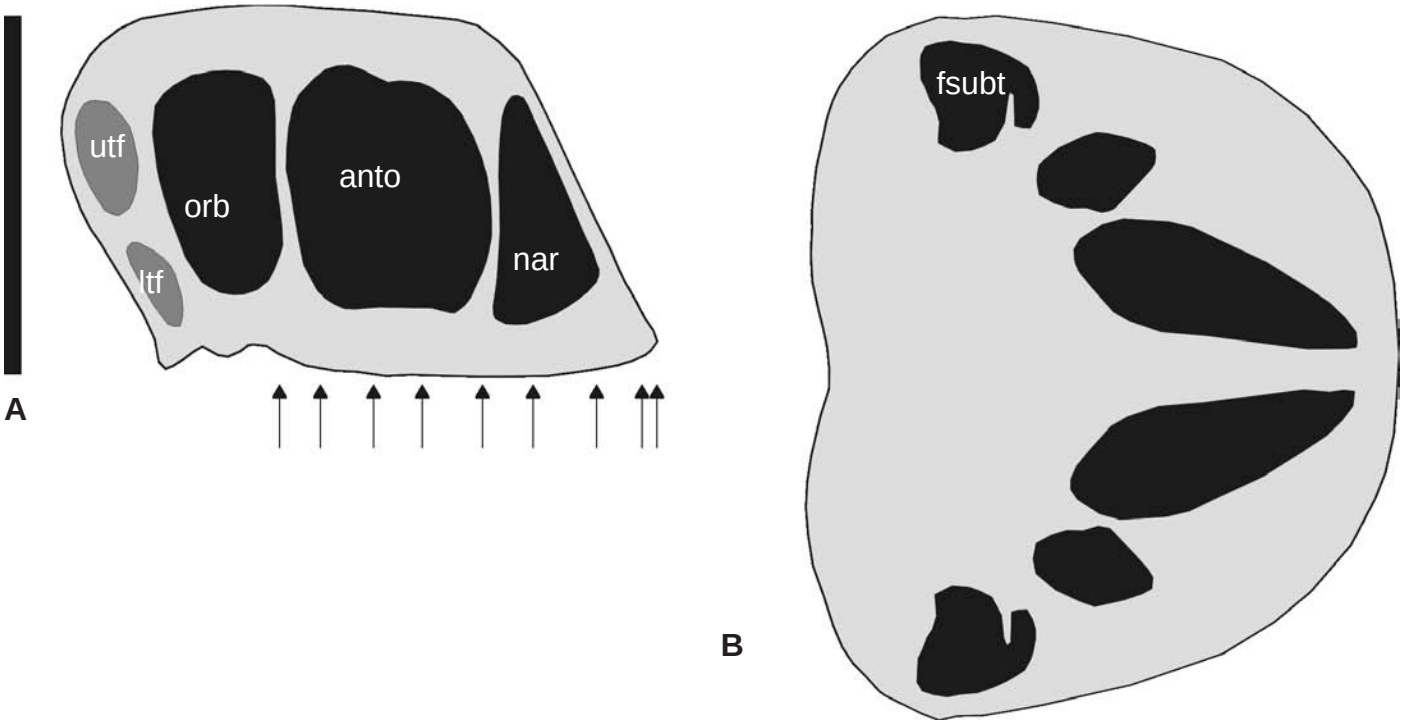

Fig. 7.20: Scaled skull of *Jeholopterus* in A) reconstructed right lateral, and B) reconstructed ventral view. Arrows indicate level of alveoli. Scale bar = 70 mm. See Fig. 7.1 for abbreviations.

7.21 Ludodactylus skull construction (see pp. A62-64, Figs. A.161-168, Tabs. A.41-42)

Type species: Ludodactylus sibbicki Frey et al. 2003a

Major descriptions of the skull of Ludodactylus: Frey et al. (2003a)

Antorbital fenestra / naris: fused into nasoantorbital fenestra

Anterior rostral crest: absent

Medial rostral crest: absent

Orbitotemporal crest: present, bladelike process in posterodorsal direction, extent unknown due to breakage at the only known specimen of this taxon

Orientation of occipital region in lateral view relative to vertical plane: ~33°

Keratinous beak: absent

Dentition: twenty-three pair of teeth, anterior four pair of Ornithocheirus high tooth construction, posterior following of Ornithocheirus low tooth construction, tooth row ranging from the anterior tip of the rostrum to the level of half of the length of the nasoantorbital fenestra

Other features: nasoantorbital fenestra triangular and situated in the posterior third of the rostrum

Cantilever dimensions

Height to length ratio: 1:3.93

Ratio of total length to length of nasoantorbital fenestra: 1:0.37

Ratio of basal height to basal width: 1:1.10

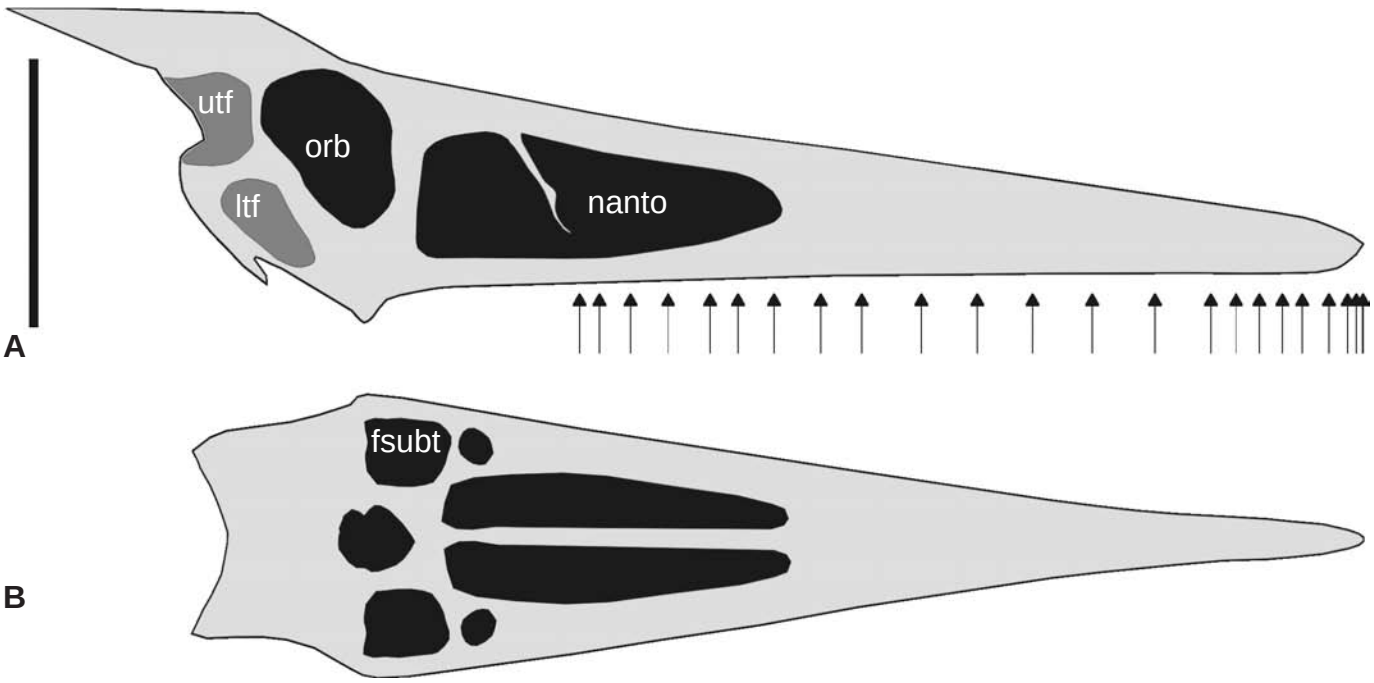

Fig. 7.21: Scaled skull of *Ludodactylus* in A) right lateral, and B) reconstructed ventral view. Arrows indicate level of alveoli. Scale bar = 70 mm. See Fig. 7.1 for abbreviations.

7.22 Nyctosaurus skull construction (see pp. A65-67, Figs. A.169-176, Tabs. A.43-44)

Type species: Nyctosaurus gracilis (Marsh 1876)

Major descriptions of the skull of Nyctosaurus: Bennett (2003), Miller (1972), Wellnhofer (1978, 1991a), Williston (1902)

Antorbital fenestra / naris: fused into nasoantorbital fenestra

Anterior rostral crest: absent

Medial rostral crest: absent

Orbitotemporal crest: absent, although reported by Bennett (2003) from certain skulls of Nyctosaurus, however, there remain uncertainties about the fossil he described, because they are not housed in a public collection and his statements thus can not be verified

Orientation of occipital region in lateral view relative to vertical plane: ~32°

Keratinous beak: most probably present

Dentition: edentulous

Other features: nasoantorbital fenestra triangular, about the same size as the orbita and situated in the posterior fifth part of the rostrum

Cantilever dimensions

Height to length ratio: 1:5.14

Ratio of total length to length of nasoantorbital fenestra: 1:0.15

Ratio of basal height to basal width: 1:0.97

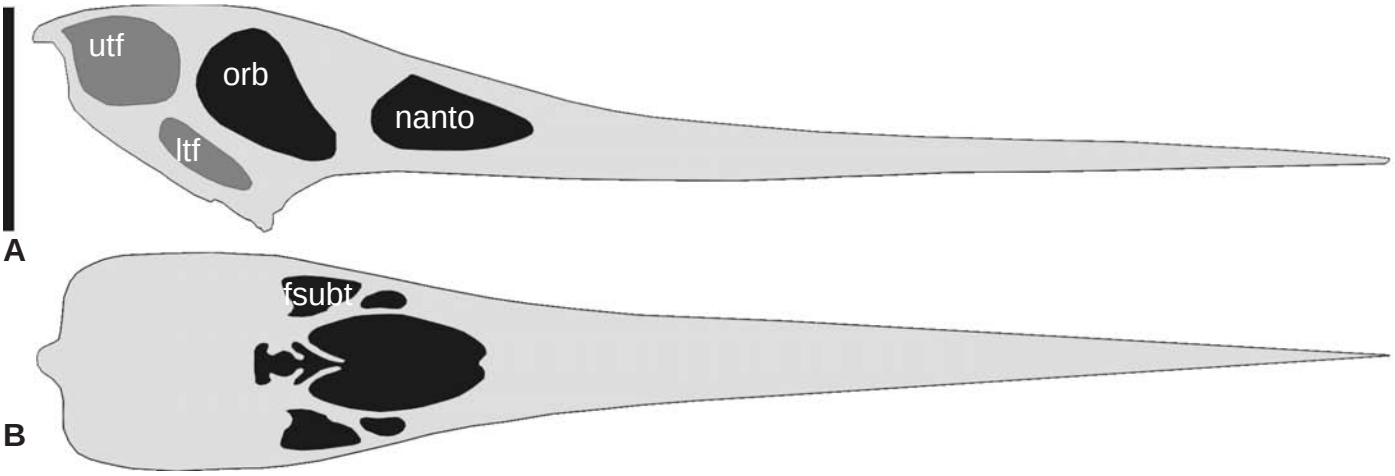

Fig. 7.22: Scaled skull of *Nyctosaurus* in A) right lateral, and B) ventral view. Scale bar = 70 mm. See Fig. 7.1 for abbreviations.

7.23 Parapsicephalus skull construction (see pp. A68-70, Figs. A.177-184, Tabs. A.45-46)

Type species: Parapsicephalus purdoni (Newton 1888)

Major descriptions of the skull of Parapsicephalus: Newton (1888), Wellnhofer (1978, 1991a)

Antorbital fenestra / naris: both present

Anterior rostral crest: absent

Medial rostral crest: absent

Orbitotemporal crest: absent

Orientation of occipital region in lateral view relative to vertical plane: ~50°

Keratinous beak: absent

Dentition: eleven pair of teeth of unknown tooth construction, tooth row ranging from the anterior tip of the rostrum to the level of the anterior end of antorbital fenestra

Other features: naris subrectangular and orientated anteroventrally/posterodorsally, ranging from the level of the 9th pair of alveoli to the level of the anterior third of the antorbital fenestra and overlapping the antorbital fenestra in anterodorsal direction, antorbital fenestra rounded triangular to oval, about twice the size of naris and orbita

Cantilever dimensions

Height to length ratio: 1:3.63

Ratio of total length to length of antorbital fenestra & naris: 1:0.46

Ratio of basal height to basal width: 1:1.31

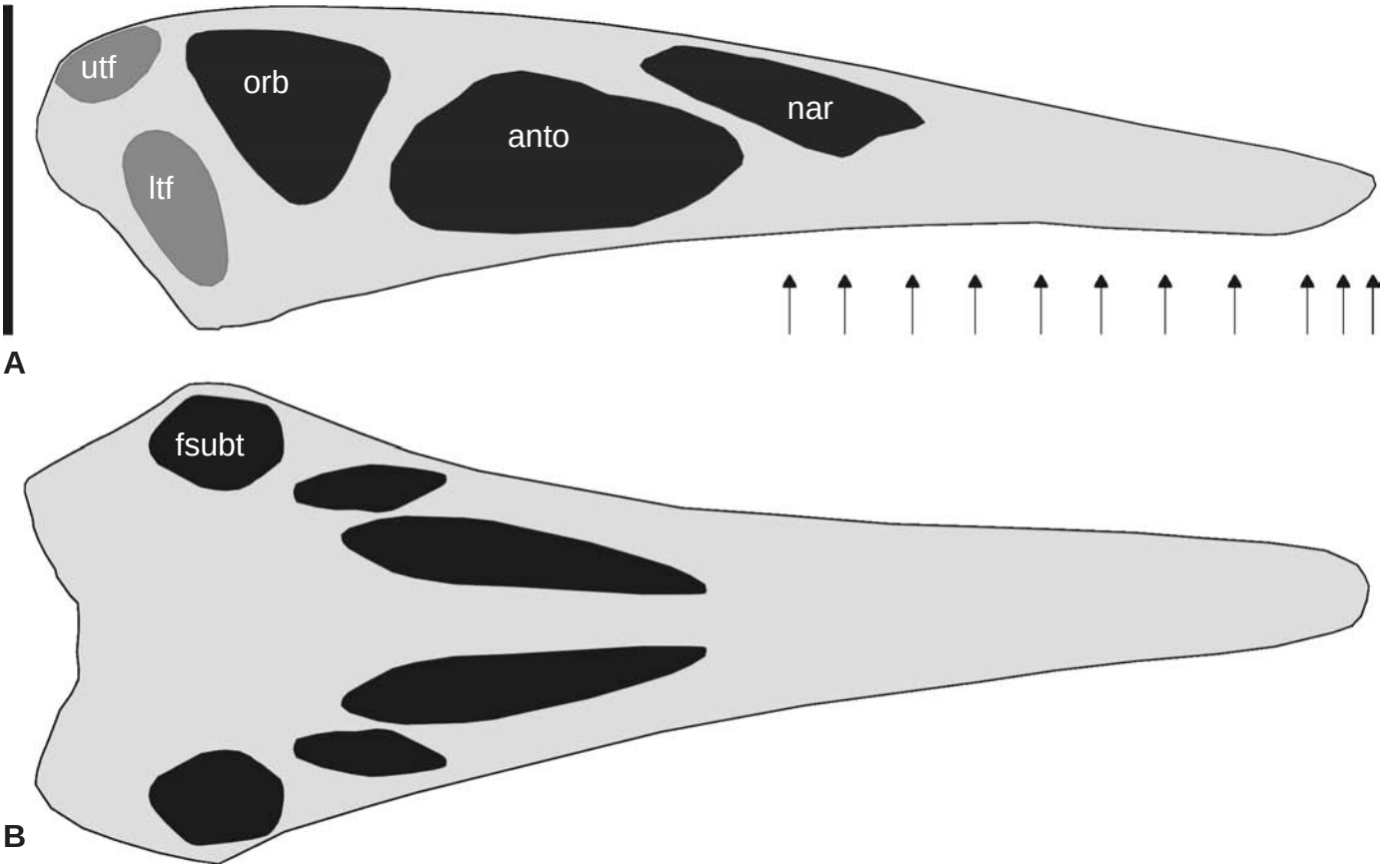

Fig. 7.23: Scaled skull of *Parapsicephalus* in A) right lateral, and B) ventral view. Arrows indicate level of alveoli. Scale bar = 70 mm. See Fig. 7.1 for abbreviations.

7.24 Peteinosaurus skull construction (see pp. A71-73, Figs. A.185-192, Tabs. A.47-48)

Type species: Peteinosaurus zambelli Wild 1978

Major descriptions of the skull of Peteinosaurus: Dalla Vecchia (2003a, 2003b), Wellnhofer (1991a), Wild (1978)

Antorbital fenestra / naris: both present

Anterior rostral crest: absent

Medial rostral crest: absent

Orbitotemporal crest: absent

Orientation of occipital region in lateral view relative to vertical plane: ~75°

Keratinous beak: absent

Dentition: thirty-eight pair of teeth of Pterodactylus tooth construction, tooth row ranging from the anterior tip of the rostrum till the level of the anterior third of the orbita

Other features: skull with convex dorsal outline in lateral view, naris larger than antorbital fenestra, oval-shaped and ranging from the level of the 9th to 26th pair of alveoli, antorbital fenestra triangular and ranging from the level of the 25th to 35th pair of alveoli

Cantilever dimensions

Height to length ratio: 1:2.46

Ratio of total length to length of antorbital fenestra & naris: 1:0.50

Ratio of basal height to basal width: 1:0.99

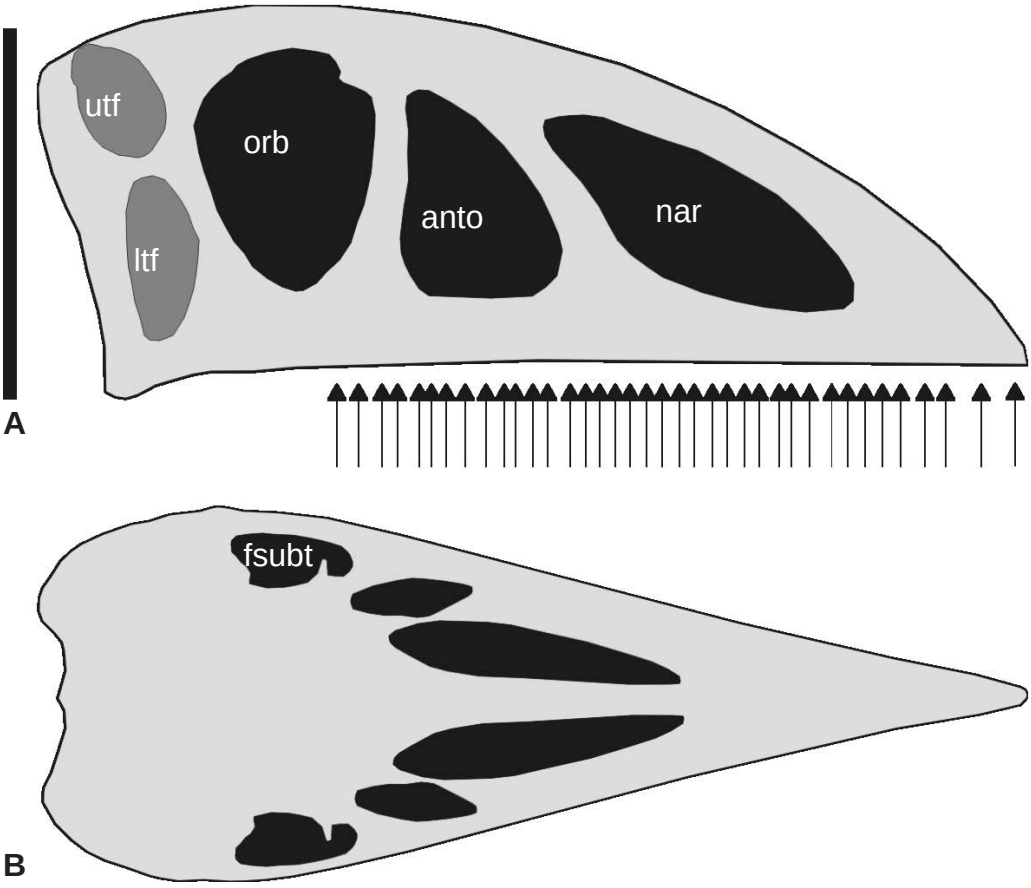

Fig. 7.24: Scaled skull of *Peteinosaurus* in A) reconstructed right lateral, and B) reconstructed ventral view. Arrows indicate level of alveoli. Scale bar = 70 mm. See Fig. 7.1 for abbreviations.

7.25 Phobetopter skull construction (see pp. A74-75, Figs. A.193-200, Tabs. A.49-50)

Type species: Phobetopter parvus (Bakhurina 1982)

Major descriptions of the skull of Phobetopter: Bakhurina (1982), Bakhurina & Unwin (1995), Wellnhofer (1991a)

Antorbital fenestra / naris: fused into nasoantorbital fenestra

Anterior rostral crest: not present

Medial rostral crest: present, thinner than dorsal border of the rostrum (excluded from analysis), ranging from the level of the 2nd pair of alveoli to the level of the posterior end of the antorbital fenestra

Orbitotemporal crest: present, short blunt process about the same size at the orbital diameter, projecting in posterodorsal direction

Orientation of occipital region in lateral view relative to vertical plane: ~45°

Keratinous beak: present, covering the anterior rostrum till the 1st pair of alveoli

Dentition: fourteen pair of teeth of Dsungaripterid tooth construction, 12th and 13th pair of alveoli with elevated alveolar walls, tooth row ranging to the level of the anterior half of nasoantorbital fenestra

Other features: nasoantorbital fenestra triangular ranging from the level of the 7th pair of alveoli to the orbita, orbita circular and situated posterodorsal to the antorbital fenestra, suborbital fenestra present ventral to the orbita

Cantilever dimensions

Height to length ratio: 1:2.75

Ratio of total length to length of nasoantorbital fenestra: 1:0.42

Ratio of basal height to basal width: 1:0.51

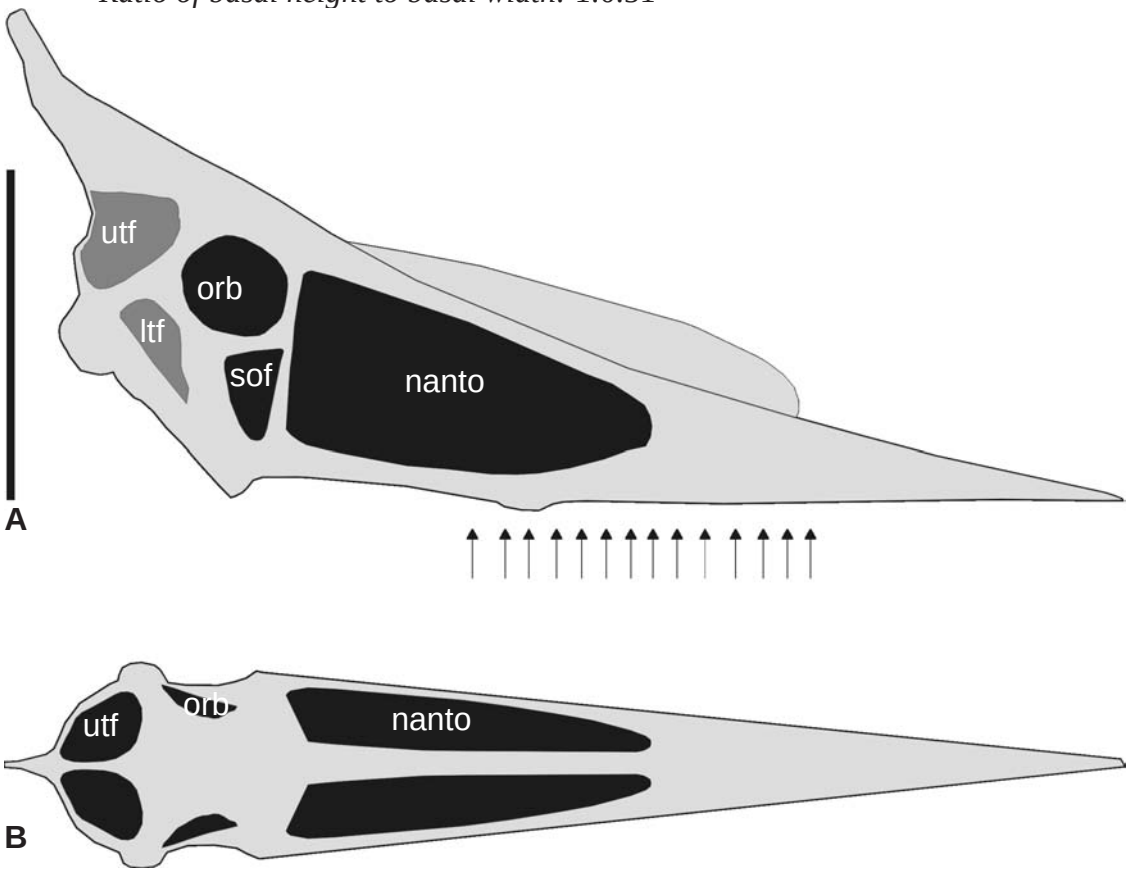

Fig. 7.25: Scaled skull of *Phobetopter* in A) reconstructed right lateral, and B) reconstructed dorsal view. Arrows indicate level of alveoli. Scale bar = 70 mm. See Fig. 7.1 for abbreviations.

7.26 Plataleorhynchus skull construction (see pp. A77-79, Figs. A.201-208, Tabs. A.51-52)

Type species: Plataleorhynchus streptophorodon Howse & Milner 1995

Major descriptions of the skull of Plataleorhynchus: Howse & Milner (1995)

Antorbital fenestra / naris: fused into nasoantorbital fenestra

Anterior rostral crest: absent

Medial rostral/orbitotemporal crest: present, thinner than dorsal border of the rostrum (excluded from analysis), ranging from the level of the 27th pair of alveoli to the level of half of the length of the antorbital fenestra, continuing as soft-tissue crest into orbitotemporal region

Orientation of occipital region in lateral view relative to vertical plane: ~20°

Keratinous beak: absent

Dentition: thirty-nine pair of teeth of Gnathosaurus tooth construction, tooth row ranging from the anterior tip of the rostrum to the level of the anterior end of the nasoantorbital fenestra

Other features: nasoantorbital fenestra rounded triangular to oval and situated in the posterior third of the rostrum, anterior rostrum expanded spatulate from the level of the 1st to 13th pair of alveoli with largest width at the level of the 7th pair of alveoli

Cantilever dimensions

Height to length ratio: 1:5.41

Ratio of total length to length of nasoantorbital fenestra: 1:0.31

Ratio of basal height to basal width: 1:0.93

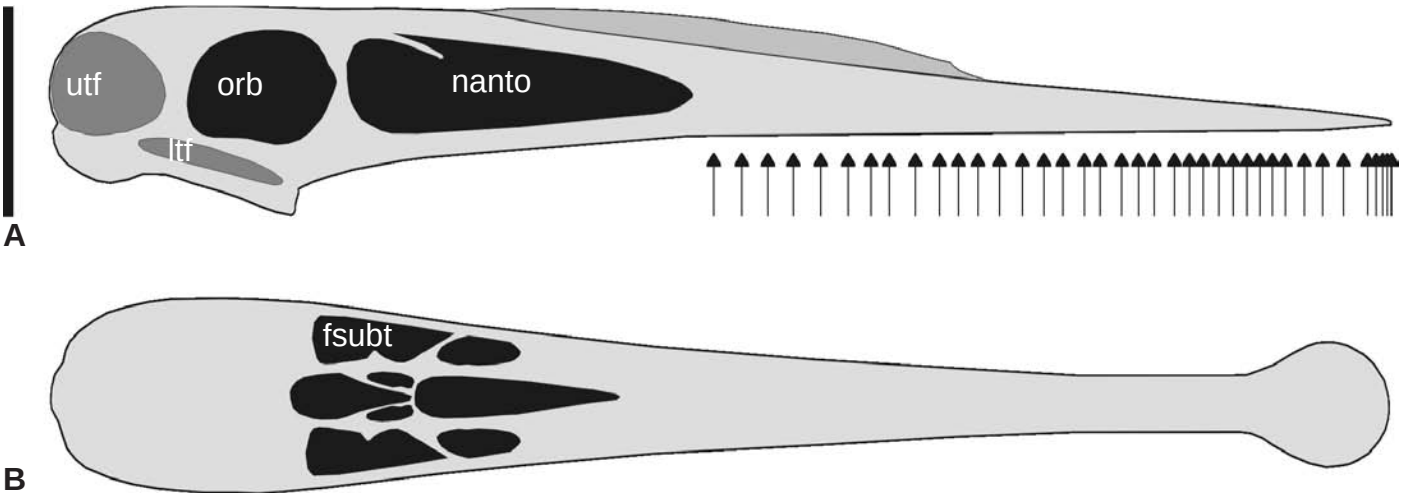

Fig. 7.26: Scaled skull of *Plataleorhynchus* in A) reconstructed right lateral, and B) reconstructed ventral view. Arrows indicate level of alveoli. Scale bar = 70 mm. See Fig. 7.1 for abbreviations.

7.27 Preondactylus skull construction (see pp. A80-82, Figs. A.209-216, Tabs. A.53-54)

Type species: Preondactylus buffarini Wild 1983b

Major descriptions of the skull of Preondactylus: Dalla Vecchia (1998), Wild (1983b)

Antorbital fenestra / naris: both present

Anterior rostral crest: absent

Medial rostral crest: absent

Orbitotemporal crest: absent

Orientation of occipital region in lateral view relative to vertical plane: ~55°

Keratinous beak present: absent

Dentition: twenty-eight pair of teeth of Preondactylus tooth construction, tooth row ranging from the anterior tip of the rostrum to the level of the posterior end of the antorbital fenestra

Other features: naris oval and smaller than antorbital fenestra, situated anterior to the antorbital fenestra and ranging from the level of the 7th pair to the 18th pair of alveoli, antorbital fenestra rounded triangular to sub-oval, about the same size as orbita and ranging from the level of the 19th to 28th pair of alveoli

Cantilever dimensions

Height to length ratio: 1:2.40

Ratio of total length to length of nasoantorbital fenestra & naris: 1:0.55

Ratio of basal height to basal width: 1:1.09

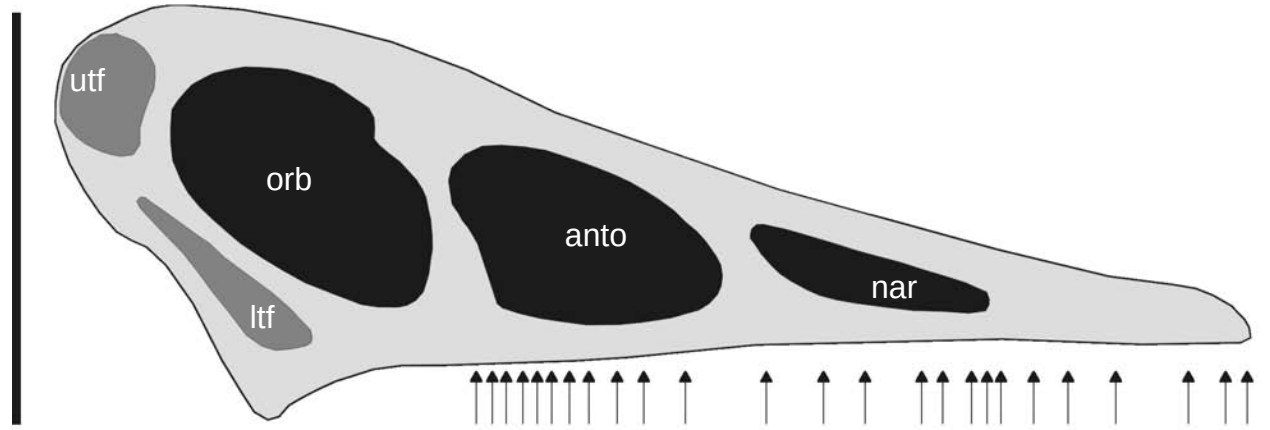

A

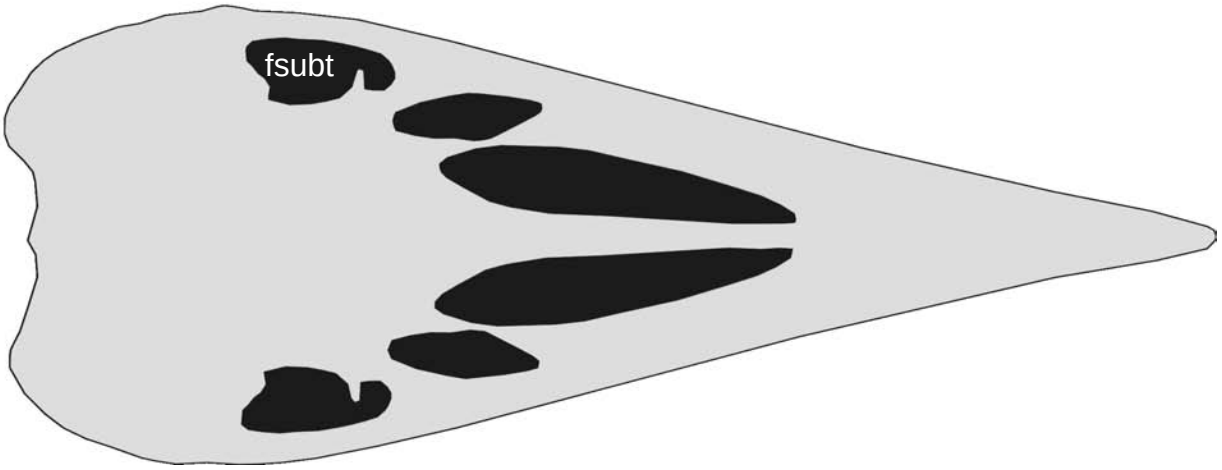

B

Fig. 7.27: Scaled skull of *Preondactylus* in A) reconstructed right lateral, and B) reconstructed ventral view. Arrows indicate level of alveoli. Scale bar = 70 mm. See Fig. 7.1 for abbreviations.

7.28 Pteranodon skull construction (see pp. A83-85, Figs. A.217-224, Tabs. A.55-56)

Type species: Pteranodon longiceps Marsh 1876

Major descriptions of the skull of Pteranodon: Bennett (1992, 1994, 2001a), Eaton (1910), Harkson (1966), Marsh (1872, 1876), Mateer (1975), Wellnhofer (1978, 1991a), Williston (1891)

Antorbital fenestra / naris: fused into nasoantorbital fenestra

Anterior rostral crest: absent

Medial rostral crest: absent

Orbitotemporal crest: bony crest present, extending in posterodorsal direction to about the same length as the rostrum, in *P. sternbergi* bony crest extending in dorsal direction and plate-like

Orientation of occipital region in lateral view relative to vertical plane: ~12°

Keratinous beak: most probably present (Frey et al. 2003c)

Dentition: edentulous

Other features: nasoantorbital fenestra triangular, about twice the size as the orbita and situated in the posterior fifth part of the rostrum

Cantilever dimensions

Height to length ratio: 1:5.21

Ratio of total length to length of nasoantorbital fenestra: 1:0.20

Ratio of basal height to basal width: 1:0.65

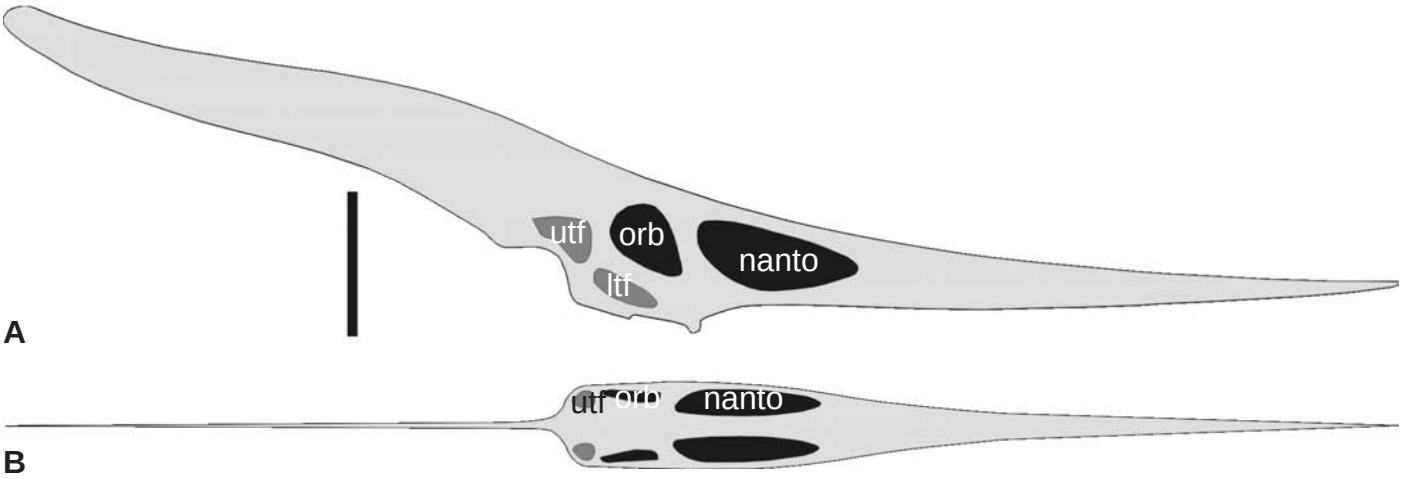

Fig. 7.28: Scaled skull of *Pteranodon* in A) right lateral, and B) reconstructed dorsal view. Scale bar = 70 mm. See Fig. 7.1 for abbreviations.

7.29 Pterodactylus antiquus skull construction (see pp. A86-88, Figs. A.225-232, Tabs. A.57-58)

Type species: Pterodactylus antiquus Soemmerring 1812

Major descriptions of the skull of Pterodactylus antiquus: Cuvier (1801, 1809, 1819, 1824), Meyer (1860, 1861), Soemmering (1812), Wellnhofer (1970)

Antorbital fenestra / naris: fused into nasoantorbital fenestra

Anterior rostral crest: absent

Medial rostral / orbitotemporal crest: soft tissue crest present (Frey et al. 2003c)

Orientation of occipital region in lateral view relative to vertical plane: ~22°

Keratinous beak: present as a keratinous hook in front of the first pair of alveoli (Frey et al. 2003c), not figured here (corresponds to first arrow in Fig. 7.29)

Dentition: eighteen pair of teeth of Pterodactylus tooth construction, tooth row ranging from the anterior tip of the rostrum to the level of the anterior end of the nasoantorbital fenestra

Other features: nasoantorbital fenestra rounded triangular, about twice the size as the orbita and situated in the posterior half of the rostrum

Cantilever dimensions

Height to length ratio: 1:2.57

Ratio of total length to length of nasoantorbital fenestra: 1:0.74

Ratio of basal height to basal width: 1:1.48

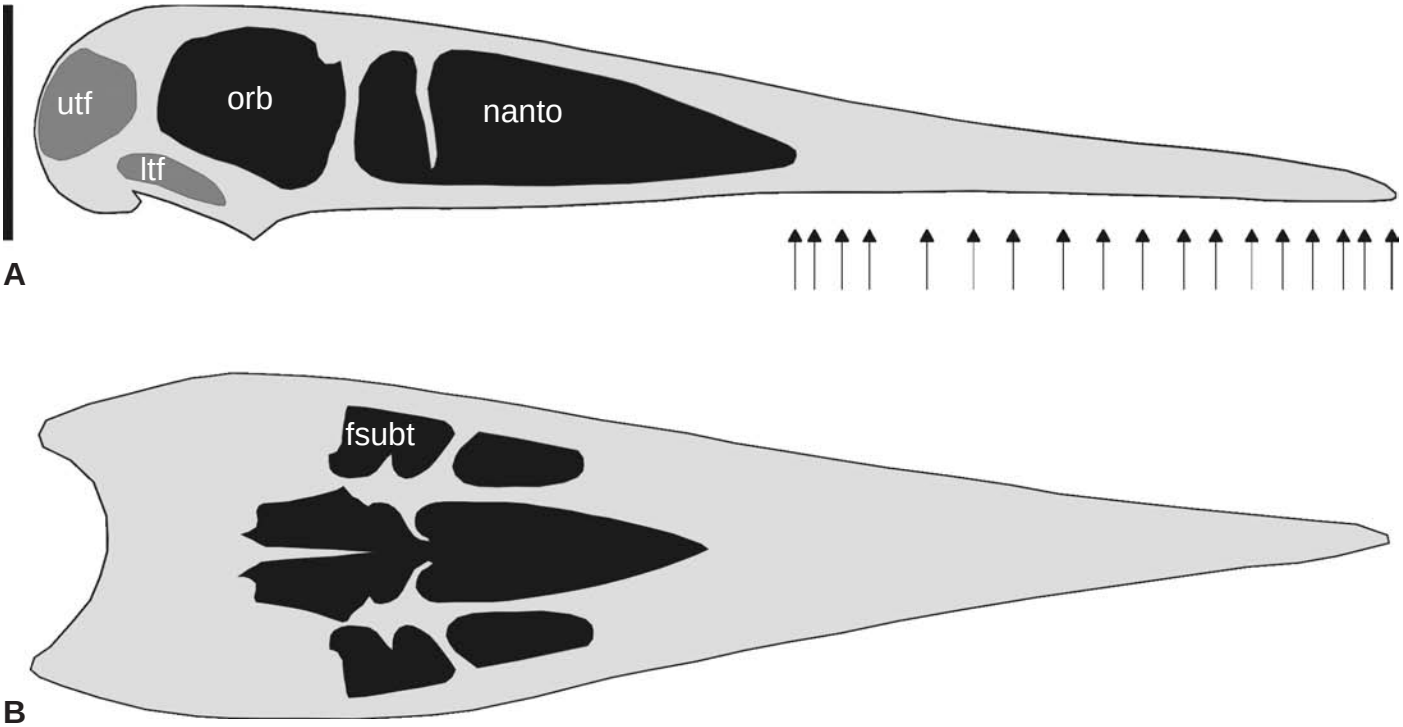

Fig. 7.29: Scaled skull of *Pterodactylus antiquus* in A) right lateral, and B) reconstructed ventral view. Arrows indicate level of alveoli. Scale bar = 70 mm. See Fig. 7.1 for abbreviations.

7.30 Pterodactylus elegans skull construction (see pp. A89-91, Figs. A.233-240, Tabs. A.59-60)

Type species: Pterodactylus elegans Wagner 1861

Major descriptions of the skull of Pterodactylus elegans: Wagner (1861), Wellnhofer (1970, 1978), Zittel (1882)

Antorbital fenestra / naris: fused into nasoantorbital fenestra

Anterior rostral crest: absent

Medial rostral / orbitotemporal crest: soft tissue crest present (Frey et al. 2003c)

Orientation of occipital region in lateral view relative to vertical plane: ~12°

Keratinous beak: present as a keratinous hook in front of the first pair of alveoli (Frey et al. 2003c), not figured here (corresponds to first arrow in Fig. 7.30)

Dentition: seventeen pair of teeth of Pterodactylus tooth construction, tooth row ranging from the anterior tip of the rostrum to the level of the anterior third of the rostrum

Other features: nasoantorbital fenestra rounded triangular, about the same size as the orbita and situated in the posterior half of the rostrum

Cantilever dimensions

Height to length ratio: 1:3.21

Ratio of total length to length of nasoantorbital fenestra: 1:0.34

Ratio of basal height to basal width: 1:1.24

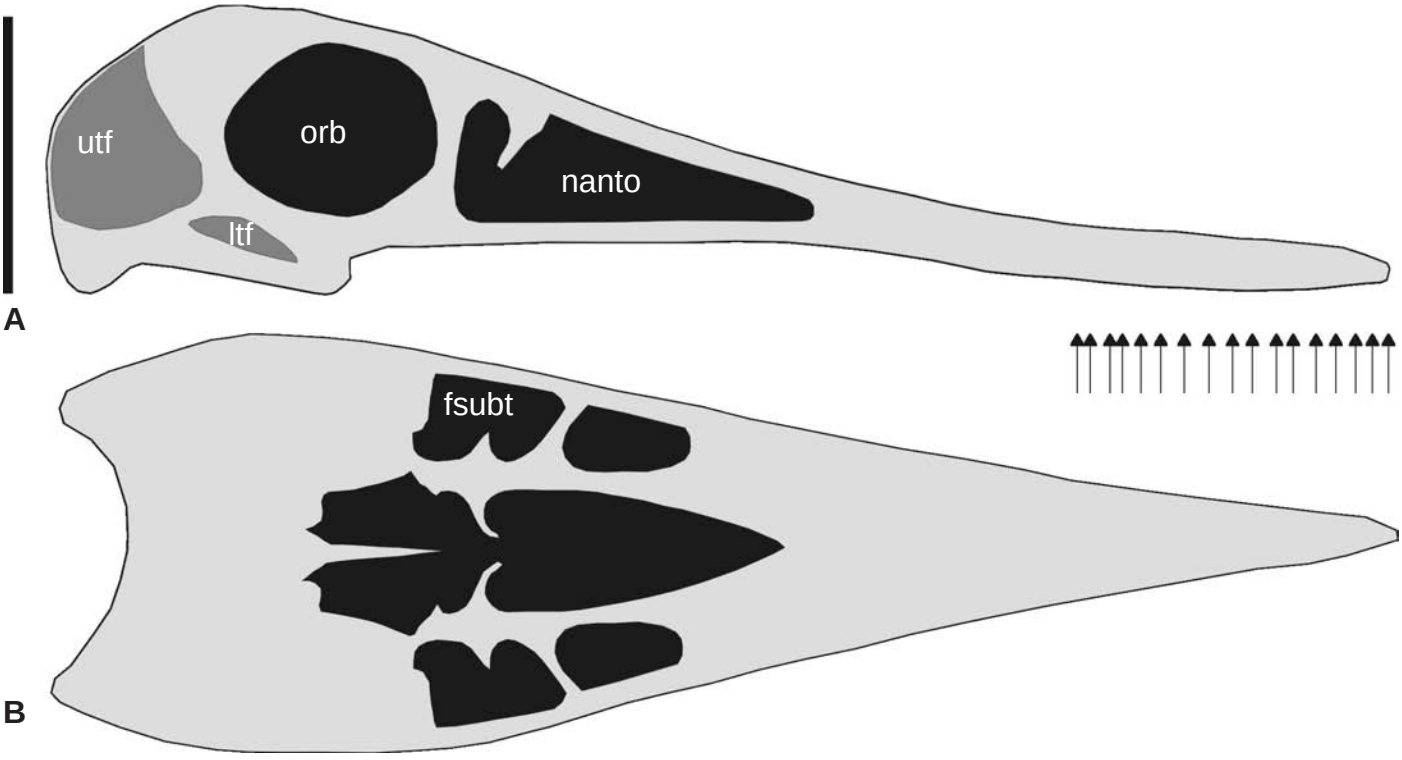

Fig. 7.30: Scaled skull of *Pterodactylus elegans* in A) right lateral, and B) reconstructed ventral view. Arrows indicate level of alveoli. Scale bar = 70 mm. See Fig. 7.1 for abbreviations.

7.31 Pterodactylus kochi skull construction (see pp. A92-94, Figs. A.241-248, Tabs. A.61-62)

Type species: Pterodactylus kochi Wagner 1837

Major descriptions of the skull of Pterodactylus kochi: Meyer (1860), Wagner (1837), Wellnhofer (1970, 1978), Zittel (1882)

Antorbital fenestra / naris: fused into nasoantorbital fenestra

Anterior rostral crest: absent

Medial rostral / orbitotemporal crest: soft tissue crest present (Frey et al. 2003c)

Orientation of occipital region in lateral view relative to vertical plane: ~30°

Keratinous beak: present as a keratinous hook in front of the first pair of alveoli (Frey et al. 2003c), not figured here (corresponds to first arrow in Fig. 7.31)

Dentition: eighteen pair of teeth of Pterodactylus tooth construction, tooth row ranging from the anterior tip of the rostrum to the level of the anterior end of the antorbital fenestra

Other features: nasoantorbital fenestra rounded triangular, about the same size as the orbita and situated in the posterior half of the rostrum

Cantilever dimensions

Height to length ratio: 1:4.22

Ratio of total length to length of nasoantorbital fenestra: 1:0.38

Ratio of basal height to basal width: 1:1.27

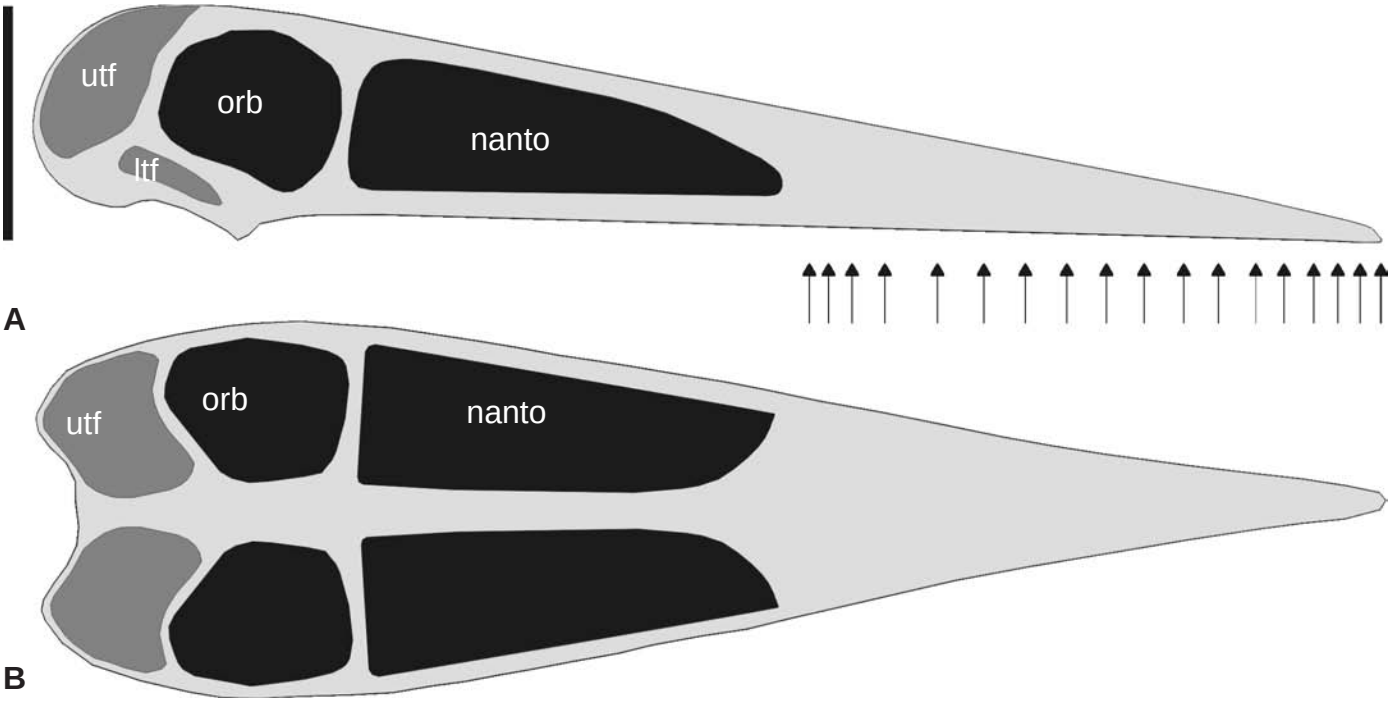

Fig. 7.31: Scaled skull of *Pterodactylus kochi* in A) right lateral, and B) dorsal view. Arrows indicate level of alveoli. Scale bar = 70 mm. See Fig. 7.1 for abbreviations

7.32 Pterodactylus micronyx skull construction (see pp. A95-97, Figs. A.249-256, Tabs. A.63-64)

Type species: Pterodactylus micronyx Meyer 1856

Major descriptions of the skull of Pterodactylus micronyx: Broili (1912), Meyer (1856, 1860), Wellnhofer (1970, 1978)

Antorbital fenestra / naris: fused into nasoantorbital fenestra

Anterior rostral crest: absent

Medial rostral / orbitotemporal crest: soft tissue crest present (Frey et al. 2003c)

Orientation of occipital region in lateral view relative to vertical plane: ~25°

Keratinous beak: present as a keratinous hook in front of the first pair of alveoli (Frey et al. 2003c), not figured here (corresponds to first arrow in Fig. 7.32)

Dentition: eighteen pair of teeth of Pterodactylus tooth construction, tooth row ranging from the anterior tip of the rostrum to the level of the anterior end of the antorbital fenestra

Other features: nasoantorbital fenestra rounded triangular, about the same size as the orbita and situated in the posterior half of the rostrum

Cantilever dimensions

Height to length ratio: 1:2.98

Ratio of total length to length of nasoantorbital fenestra: 1:0.55

Ratio of basal height to basal width: 1:1.61

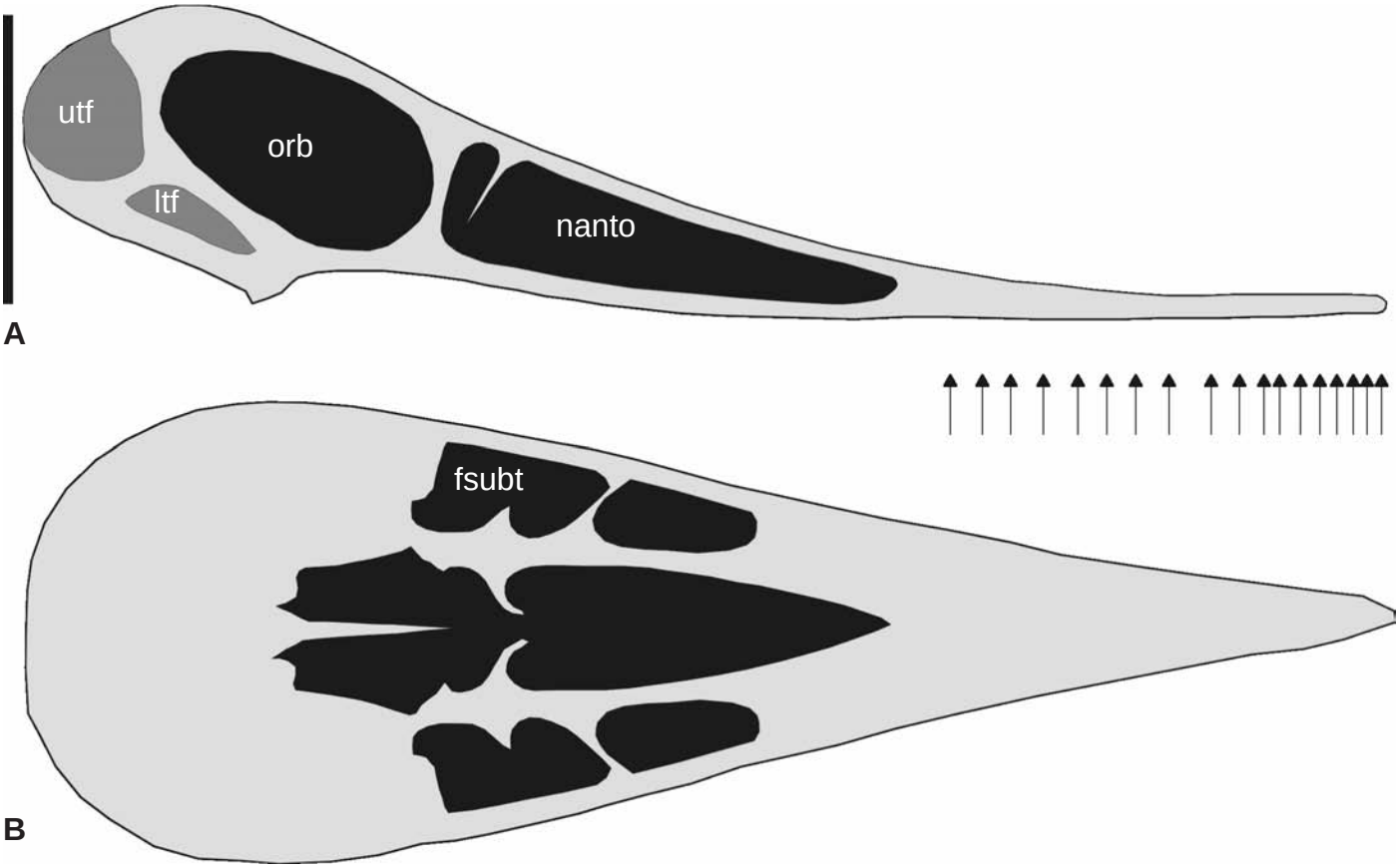

Fig. 7.32: Scaled skull of *Pterodactylus micronyx* in A) right lateral, and B) ventral view. Arrows indicate level of alveoli. Scale bar = 70 mm. See Fig. 7.1 for abbreviations.

7.33 Pterodaustro skull construction (see pp. A98-100, Figs. A.257-264, Tabs. A.65-66)

Type species: Pterodaustro guinazui Bonaparte 1970

Major descriptions of the skull of Pterodaustro: Bonaparte (1970, 1971), Sanchez (1973), Wellnhofer (1978, 1991a)

Antorbital fenestra / naris: fused into nasoantorbital fenestra

Anterior rostral crest: absent

Medial rostral crest: absent

Orbitotemporal crest: absent

Orientation of occipital region in lateral view relative to vertical plane: ~30°

Keratinous beak: absent

Dentition: more than 100 pair of teeth of Pterodaustro low tooth construction, tooth row ranging from the anterior rostrum to the level of about two third of the total rostral length, anteriormost rostrum edentulous, teeth of upper jaw opposed by about 500 pair of teeth of Pterodaustro high tooth construction in the lower jaw, ranging from the anterior tip of the lower jaw to the level of the posterior end of the nasoantorbital fenestra in the upper jaw

Other features: nasoantorbital fenestra rounded triangular, about twice the size as the orbita and situated in the posterior sixth part of the rostrum, rostrum curved in dorsal direction

Cantilever dimensions

Height to length ratio: 1:9.23

Ratio of total length to length of nasoantorbital fenestra: 1:0.14

Ratio of basal height to basal width: 1:0.91

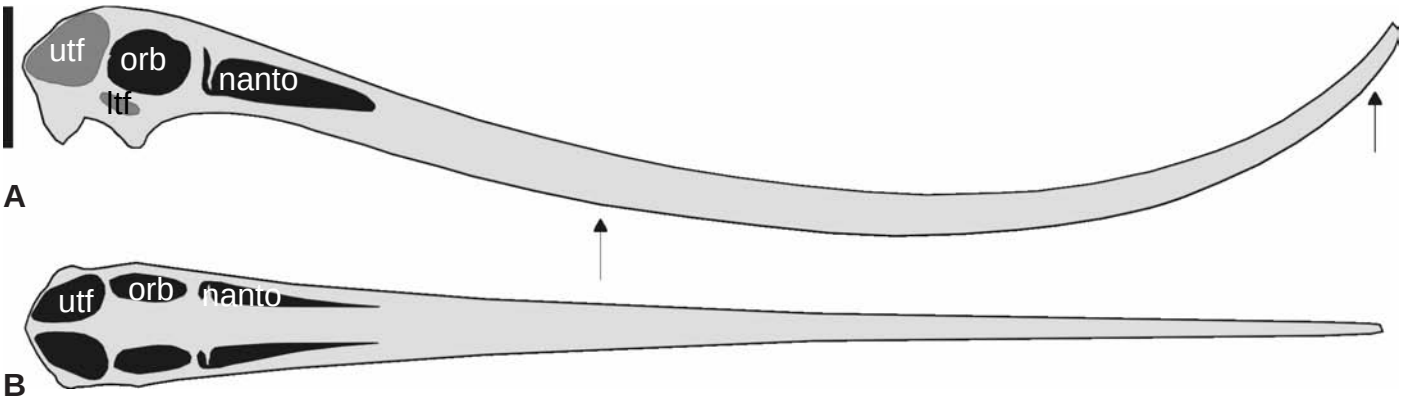

Fig. 7.233: Scaled skull of *Pterodaustro* in A) right lateral, and B) reconstructed dorsal view. Because of the large numbers of teeth, Arrows indicate level of most anterior and most posterior alveoli. Scale bar = 70 mm. See Fig. 7.1 for abbreviations.

7.34 Quetzalcoatlus skull construction (see pp. A101-103, Figs. A.265-272, Tabs. A.67-68)

Type species: Quetzalcoatlus northropi Lawson 1975

Major descriptions of the skull of Quetzalcoatlus: Kellner & Langston (1996)

Antorbital fenestra / naris: fused into nasoantorbital fenestra

Anterior rostral crest: absent

Medial rostral crest: present, beginning at the level of the anterior third of the nasoantorbital fenestra, basal thickness similar to dorsal border of the rostrum (included in analysis), merging into orbitotemporal crest

Orbitotemporal crest: present, short blunt process about the same size as the mean orbital diameter, projecting in posterodorsal direction

Orientation of occipital region in lateral view relative to vertical plane: ~35°

Keratinous beak: most probably present

Dentition: edentulous

Other features: nasoantorbital fenestra oval, situated in the posterior half of the rostrum, rostrum curved in ventral direction

Cantilever dimensions

Height to length ratio: 1:5.72

Ratio of total length to length of nasoantorbital fenestra: 1:0.53

Ratio of basal height to basal width: 1:0.70

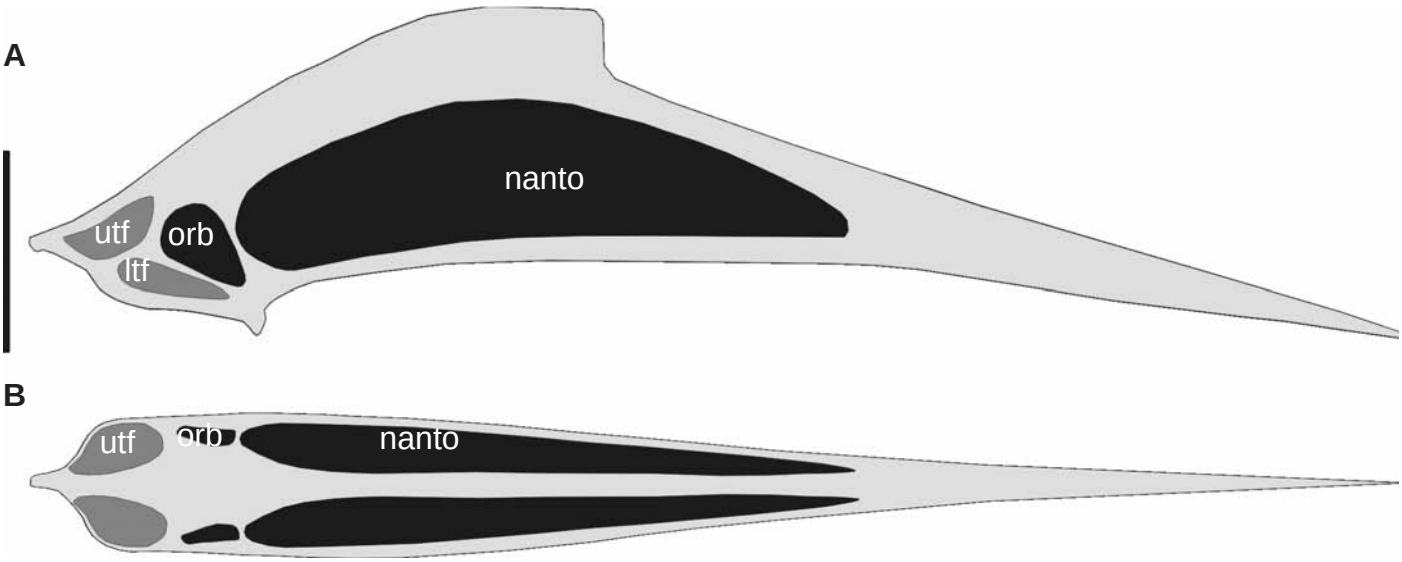

Fig. 7.34: Scaled skull of *Quetzalcoatlus* in A) reconstructed right lateral, and B) reconstructed ventral view. Scale bar = 70 mm. See Fig. 7.1 for abbreviations

7.35 Rhamphorhynchus skull construction (see pp. A104-106, Figs. A.273-280, Tabs. A.69-70)

Type species: Rhamphorhynchus longicaudus Münster 1839

Major descriptions of the skull of Rhamphorhynchus: Bennett (1996a), Goldfuss (1831), Koh (1937), Meyer (1847, 1860), Smith-Woodward (1902), Stolley (1936), Wagner (1851, 1861), Wellnhofer (1975a, 1975b, 1978, 1991a), Wiman (1925a), Zittel (1882)

Antorbital fenestra / naris: both present

Anterior rostral crest: absent

Medial rostral crest: absent

Orbitotemporal crest: absent

Orientation of occipital region in lateral view relative to vertical plane: ~40°

Keratinous beak: most probably present as keratinous sheat at the anterior end of the rostrum (Wellnhofer 1991a)

Dentition: ten pair of teeth of Rhamphorhynchus tooth construction, tooth row ranging from the posterior end of the anterior fifth part of the rostrum to the level of the posterior end of the antorbital fenestra, all teeth projecting anteroventral

Other features: naris and antorbital fenestra oval and about the same size and small in comparison with orbita, naris and antorbital fenestra situated in the posterior half of the rostrum, naris ranging from the level of the 6th to 8th pair of alveoli, antorbital fenestra ranging from the level of the 8th to 10th pair of alveoli

Cantilever dimensions

Height to length ratio: 1:3.07

Ratio of total length to length of nasoantorbital fenestra: 1:0.28

Ratio of basal height to basal width: 1:1.10

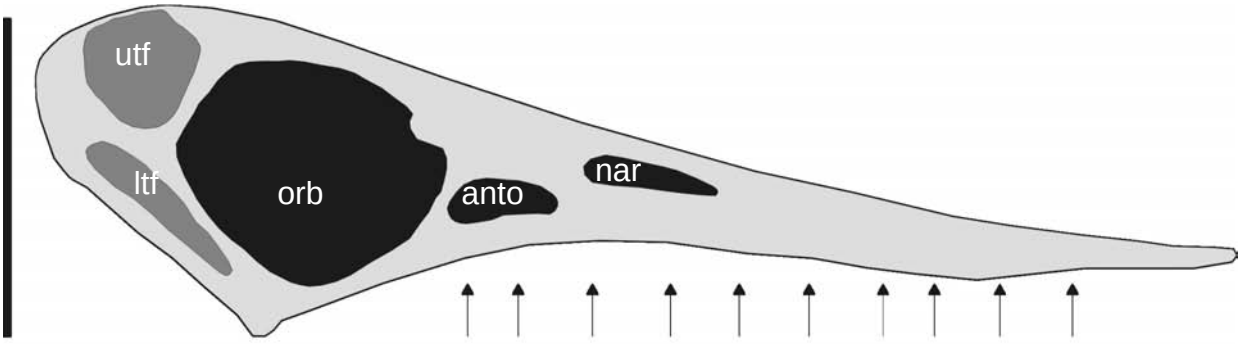

A

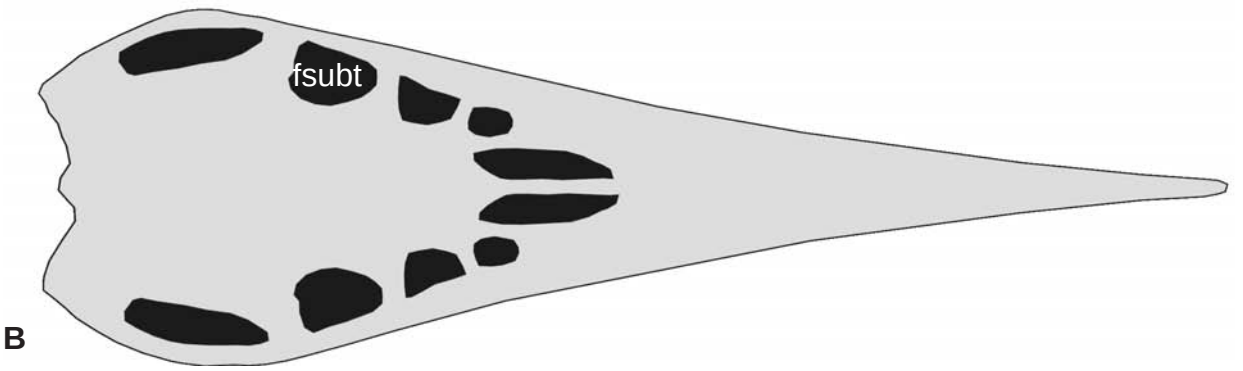

B

Fig. 7.35: Scaled skull of *Rhamphorhynchus* in A) right lateral, and B) ventral view. Arrows indicate level of alveoli. Scale bar = 70 mm. See Fig. 7.1 for abbreviations.

7.36 Santanadactylus skull construction (see pp. A107-109, Figs. A.281-288, Tabs. A.71-72)

Type species: Santanadactylus brasiliensis Buisonjé 1980

Major descriptions of the skull of Santanadactylus: Buisonjé (1980), Wellnhofer (1985)

Antorbital fenestra / naris: fused into nasoantorbital fenestra

Anterior rostral crest: absent

Medial rostral crest: absent

Orbitotemporal crest: orbitotemporal region expanded posterodorsally forming a short blunt process

Orientation of occipital region in lateral view relative to vertical plane: ~20°

Keratinous beak: absent

Dentition: eighteen pair of teeth of Ornithocheirus low tooth construction, tooth row ranging from the anterior tip of the rostrum to the level of the anterior quarter of the nasoantorbital fenestra

Other features: nasoantorbital fenestra rounded triangular, situated in the posterior half of the rostrum and ranging from the level of the 12th pair of alveoli to the orbita

Cantilever dimensions

Height to length ratio: 1:4.84

Ratio of total length to length of nasoantorbital fenestra: 1:0.45

Ratio of basal height to basal width: 1:1.38

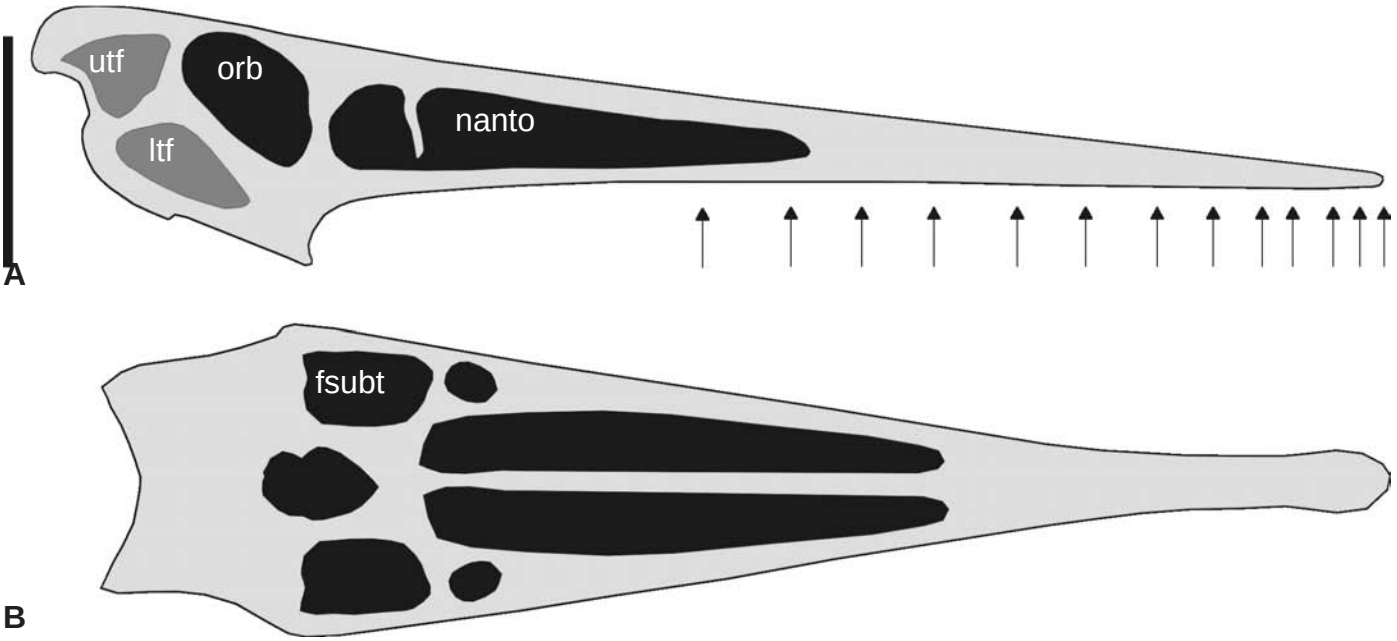

Fig. 7.36: Scaled skull of *Santanadactylus* in A) reconstructed right lateral, and B) reconstructed ventral view. Arrows indicate level of alveoli, Scale bar = 70 mm. See Fig. 7.1 for abbreviations.

7.37 Scaphognathus skull construction (see pp. A110-112, Figs. A.289-296, Tabs. A.73-74)

Type species: Scaphognathus crassirostris Goldfuss 1831

Major descriptions of the skull of Scaphognathus: Goldfuss (1831), Meyer (1860), Wellnhofer (1975b, 1978, 1991a)

Antorbital fenestra / naris: both present

Anterior rostral crest: absent

Medial rostral crest: absent

Orbitotemporal crest: absent

Orientation of occipital region in lateral view relative to vertical plane: ~60°

Keratinous beak: absent (?)

Dentition: nine pair of teeth of Rhamphorhynchus tooth constructions, tooth row ranging from the anterior rostrum to the level of half of the length of the antorbital fenestra

Other features: naris oval and situated anterodorsal to antorbital fenestra, ranging from the level of the 5th to 7th pair of alveoli, antorbital fenestra triangular, about twice the size of the naris and the same size as orbita

Cantilever dimensions

Height to length ratio: 1:2.40

Ratio of total length to length of nasoantorbital fenestra: 1:0.45

Ratio of basal height to basal width: 1:1.00

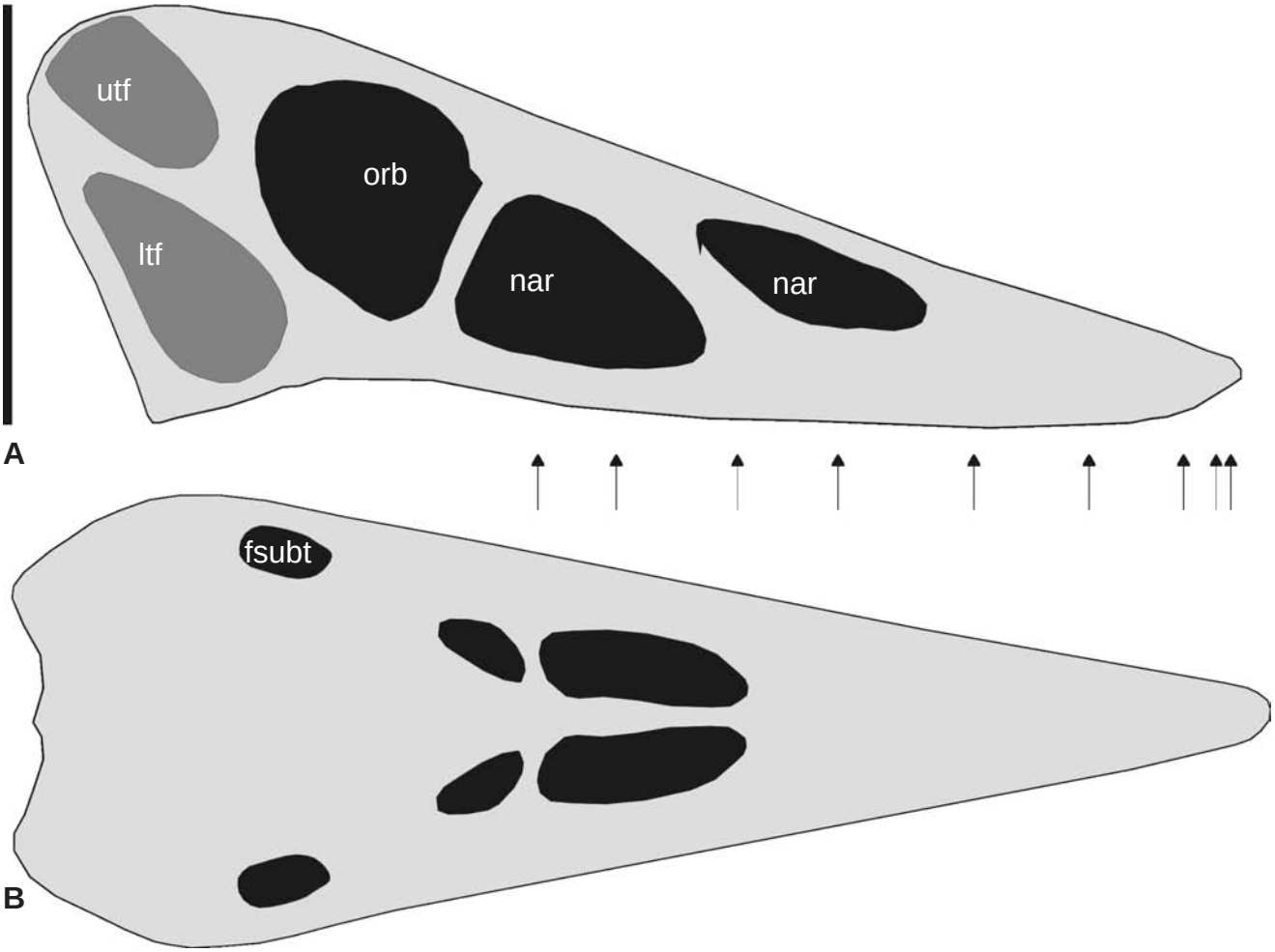

Fig. 7.37: Scaled skull of *Scaphognathus* in A) right lateral, and B) reconstructed ventral view. Arrows indicate level of alveoli. Scale bar = 70 mm. See Fig. 7.1 for abbreviations.

7.38 Sinopterus skull construction (see pp. A113-115, Figs. A.297-304, Tabs. A.75-76)

Type species: Sinopterus dongi Wang & Zhou 2003

Major descriptions of the skull of Sinopterus: Wang & Zhou (2003)

Antorbital fenestra / naris: fused into nasoantorbital fenestra

Anterior rostral crest: bony crest present, continuing into medial rostral crest.

Medial rostral crest: crest present as bony spline, beginning at the posterior end of the nasoantorbital fenestra and continuing parallel to orbitotemporal crest in posterior/posterodorsal direction, same width as orbitotemporal crest

Orbitotemporal crest: present, short blunt process about the same size at the orbital height, projecting in posterodorsal direction and situated ventral to the spline formed by the medial crest

Orientation of occipital region in lateral view relative to vertical plane: ~50°

Keratinous beak: most probably present

Dentition: edentulous

Other features: nasoantorbital fenestra about four times as large as the orbita, situated centrally in the rostrum

Cantilever dimensions

Height to length ratio: 1:3.54

Ratio of total length to length of nasoantorbital fenestra: 1:0.43

Ratio of basal height to basal width: 1:0.76

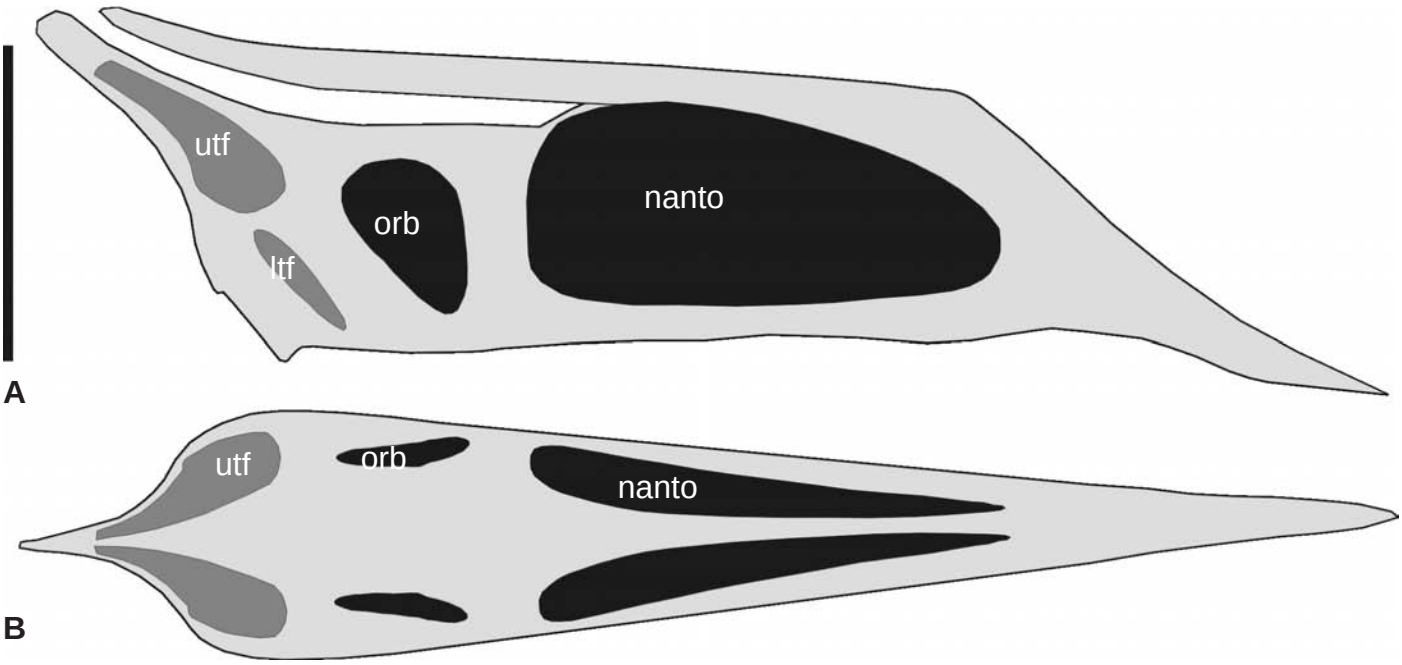

Fig. 7.38: Scaled skull of *Sinopterus* in A) right lateral, and B) reconstructed ventral view. Scale bar = 70 mm. See Fig. 7.1 for abbreviations.

7.39 Sordes skull construction (see pp. A116-118, Figs. A.305-312, Tabs. A.77-78)

Type species: Sordes pilosus Sharov 1971

Major descriptions of the skull of Sordes: Sharov (1971), Wellnhofer (1978)

Antorbital fenestra / naris: both present

Anterior rostral crest: absent

Medial rostral crest: absent

Orbitotemporal crest: absent

Orientation of occipital region in lateral view relative to vertical plane: ~40°

Keratinous beak: absent

Dentition: eight pair of teeth of Pterodactylus tooth construction, tooth row ranging from the anterior end of of the rostrum to the level of the posterior third of the antorbital fenestra

Other features: naris oval, about one third of the size of the antorbital fenestra and situated anterodorsal to the antorbital fenestra, ranging from the level of the 6th to 7th pair of alveoli, antorbital fenestra triangular and about half the size of the orbita, naris and antorbital fenestra situated in the posterior half of the rostrum

Cantilever dimensions

Height to length ratio: 1:2.85

Ratio of total length to length of nasoantorbital fenestra: 1:0.29

Ratio of basal height to basal width: 1:1.37

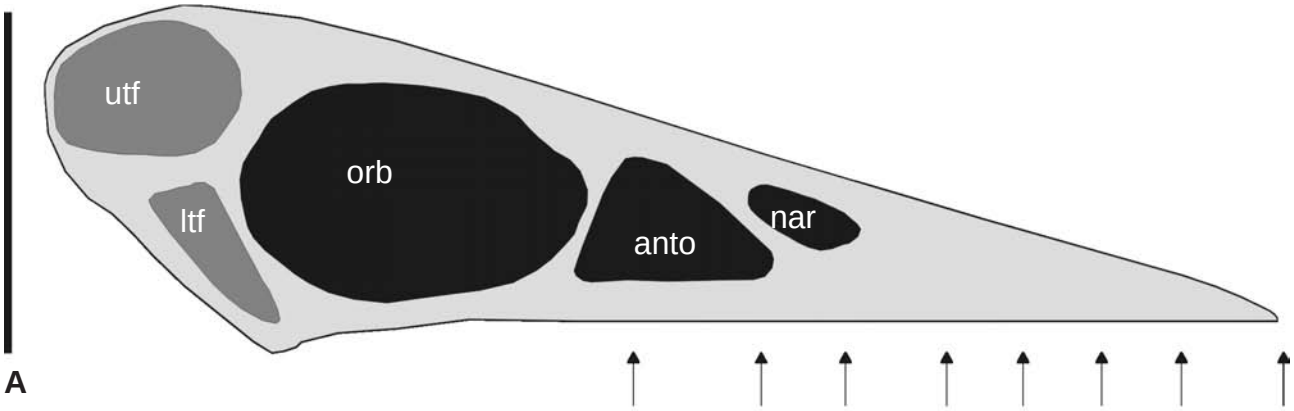

A

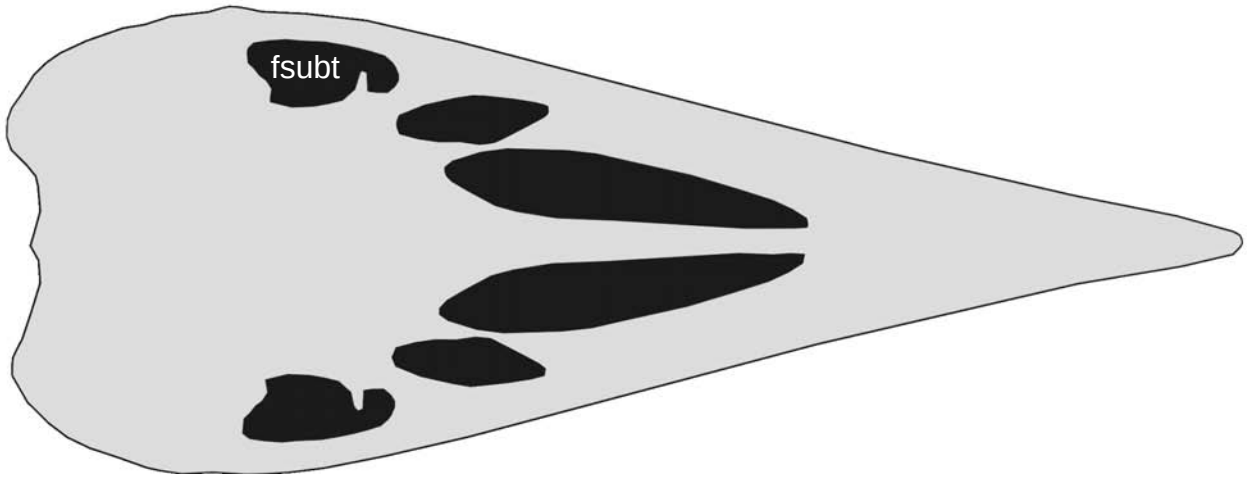

B

Fig. 7.39: Scaled skull of *Sordes* in A) right lateral, and B) reconstructed ventral view. Arrows indicate level of alveoli. Scale bar = 70 mm. See Fig. 7.1 for abbreviations.

7.40 Tapejara skull construction (see pp. A119-121, Figs. A.313-320, Tabs. A.79-80)

Type species: Tapejara wellnhoferi Kellner 1989

Major descriptions of the skull of Tapejara: Campos & Kellner (1997), Frey & Tischlinger (2000), Frey et al. (2003b, 2003c), Kellner (1989, 1996b), Wellnhofer (1991a), Wellnhofer & Kellner (1991)

Antorbital fenestra / naris: fused into nasoantorbital fenestra

Anterior rostral crest: bony crest present, continuing into medial rostral crest. In *T. navigans* and *T. imperator* accompanied by soft tissue crest (Campos & Kellner 1997, Frey et al. 2003b) which extends dorsally in height to about twice of the length of the skull, in *T. imperator* the soft-tissue crest extends posteriorly doubling the length of the bony skull

Medial rostral crest: crest present as bony spline, beginning at the posterior end of the nasoantorbital fenestra and continuing parallel to orbitotemporal crest in posterior/posterodorsal direction, same width as orbitotemporal crest. After Frey (2005, pers. comm.), this spline is fused to the orbitotemporal crest in adult animals

Orbitotemporal crest: present, short blunt process about the same size at the orbital height, projecting in posterodorsal direction and situated ventral to the spline formed by the medial crest

Orientation of occipital region in lateral view relative to vertical plane: ~45°

Keratinous beak: most probably present (Frey et al. 2003c)

Dentition: edentulous.

Other features: nasoantorbital fenestra rounded triangular, about four times as large as the orbita, situated at the posterior two thirds of the rostrum

Cantilever dimensions

Height to length ratio: 1:1.67

Ratio of total length to length of nasoantorbital fenestra: 1:0.58

Ratio of basal height to basal width: 1:0.57

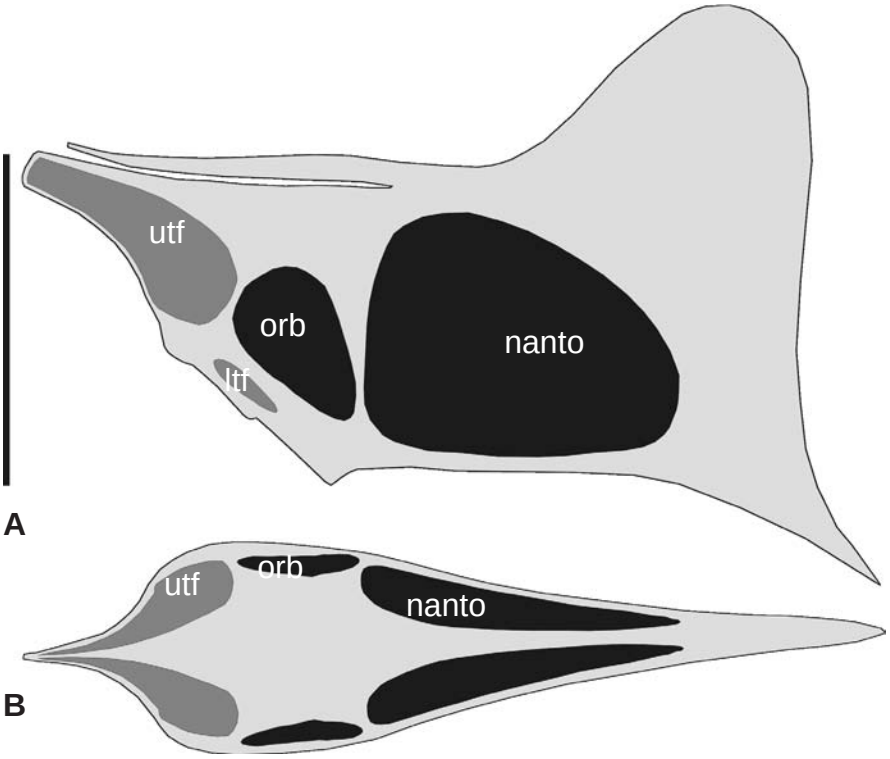

Fig. 7.40: Scaled skull of *Tapejara* in A) right lateral, and B) reconstructed ventral view. Scale bar = 70 mm. See Fig. 7.1 for abbreviations.

7.41 Thalassodromeus skull construction (see pp. A122-124, Figs. A.321-328, Tabs. A.81-82)

Type species: Thalassodromeus sethi Kellner & Campos 2002

Major descriptions of the skull of Thalassodromeus: Kellner & Campos (2002)

Antorbital fenestra / naris: fused into nasoantorbital fenestra

Anterior rostral / medial crest: thinner than dorsal border of the rostrum (excluded from analysis), beginning at the anterior tip of the rostrum and continuing into orbitotemporal crest

Orbitotemporal crest: bony crest continuing from anterior/medial rostral crest and merging with posterodorsal extension of the temporal region, extending in posterodorsal direction to about two thirds of the length of the rostrum and doubling the height of the skull

Orientation of occipital region in lateral view relative to vertical plane: ~50°

Keratinous beak: most probably present

Dentition: edentulous.

Other features: nasoantorbital fenestra rounded triangular and situated in the posterior two thirds of the rostrum, about two times higher than orbita

Cantilever dimensions

Height to length ratio: 1:2.74

Ratio of total length to length of nasoantorbital fenestra: 1:0.56

Ratio of basal height to basal width: 1:0.59

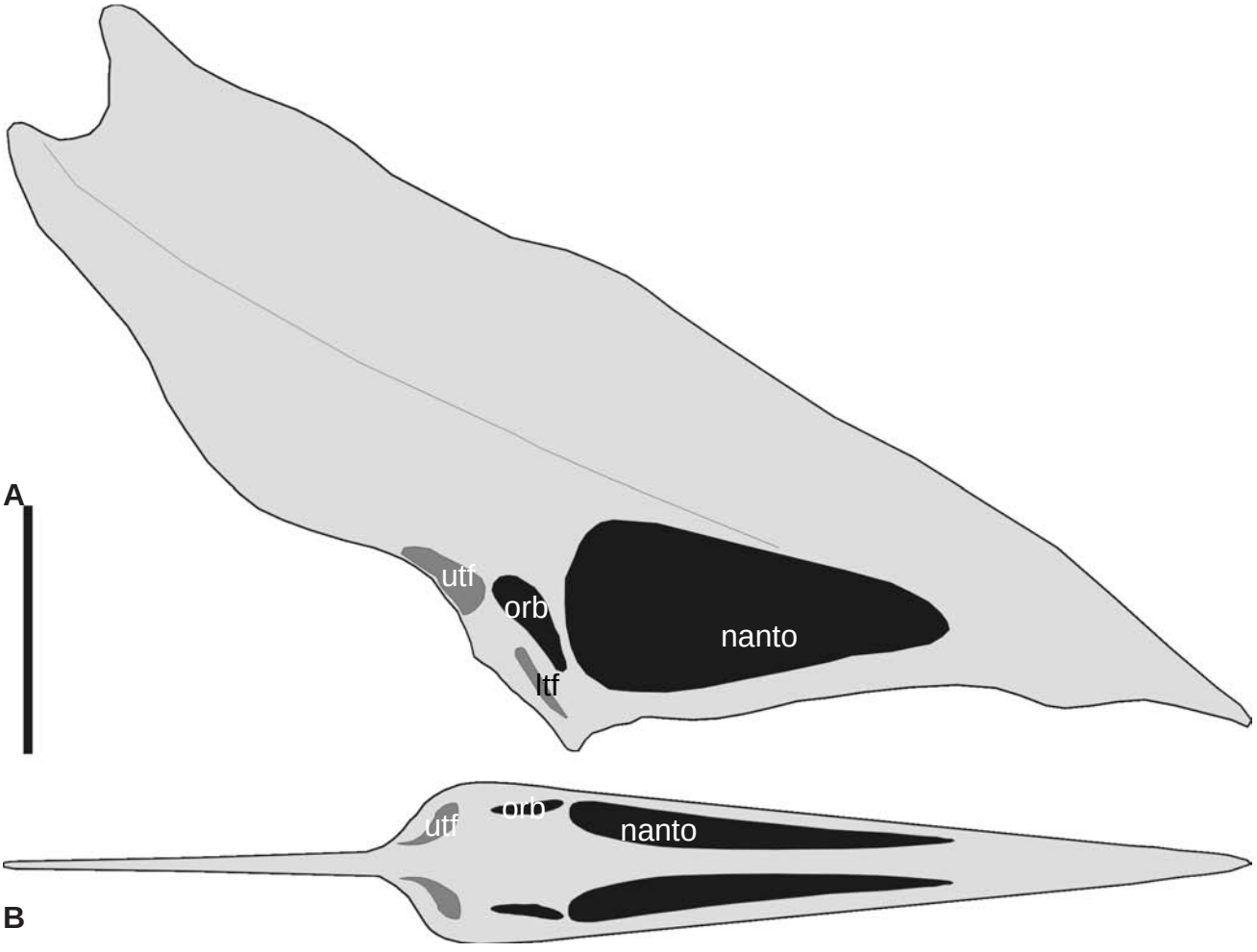

Fig. 7.41: Scaled skull of *Thalassodromeus* in A) right lateral, and B) reconstructed dorsal view. Scale bar = 70 mm. See Fig. 7.1 for abbreviations.

7.42 Tupuxuara skull construction (see pp. A125-127, Figs. A.329-336, Tabs. A.83-84)

Type species: Tupuxuara cristata Kellner & Campos 1989

Major descriptions of the skull of Tupuxuara: Kellner & Campos (1988, 1994), Wellnhofer (1991a)

Antorbital fenestra / naris: fused into nasoantorbital fenestra

Anterior rostral / medial crest: thinner than dorsal border of the rostrum (excluded from analysis), beginning at the anterior tip of the rostrum and continuing into orbitotemporal crest

Orbitotemporal crest: bony crest continuing from anterior/medial rostral crest and merging with posterodorsal extension of the temporal region, extending in posterodorsal direction to about one third of the length of the rostrum and doubling the height of the skull

Orientation of occipital region in lateral view relative to vertical plane: ~40°

Keratinous beak: most probably present

Dentition: edentulous.

Other features: nasoantorbital fenestra rounded triangular and filling the posterior two thirds of the rostrum , about two times higher than orbita

Cantilever dimensions

Height to length ratio: 1:2.74

Ratio of total length to length of nasoantorbital fenestra: 1:0.62

Ratio of basal height to basal width: 1:0.57

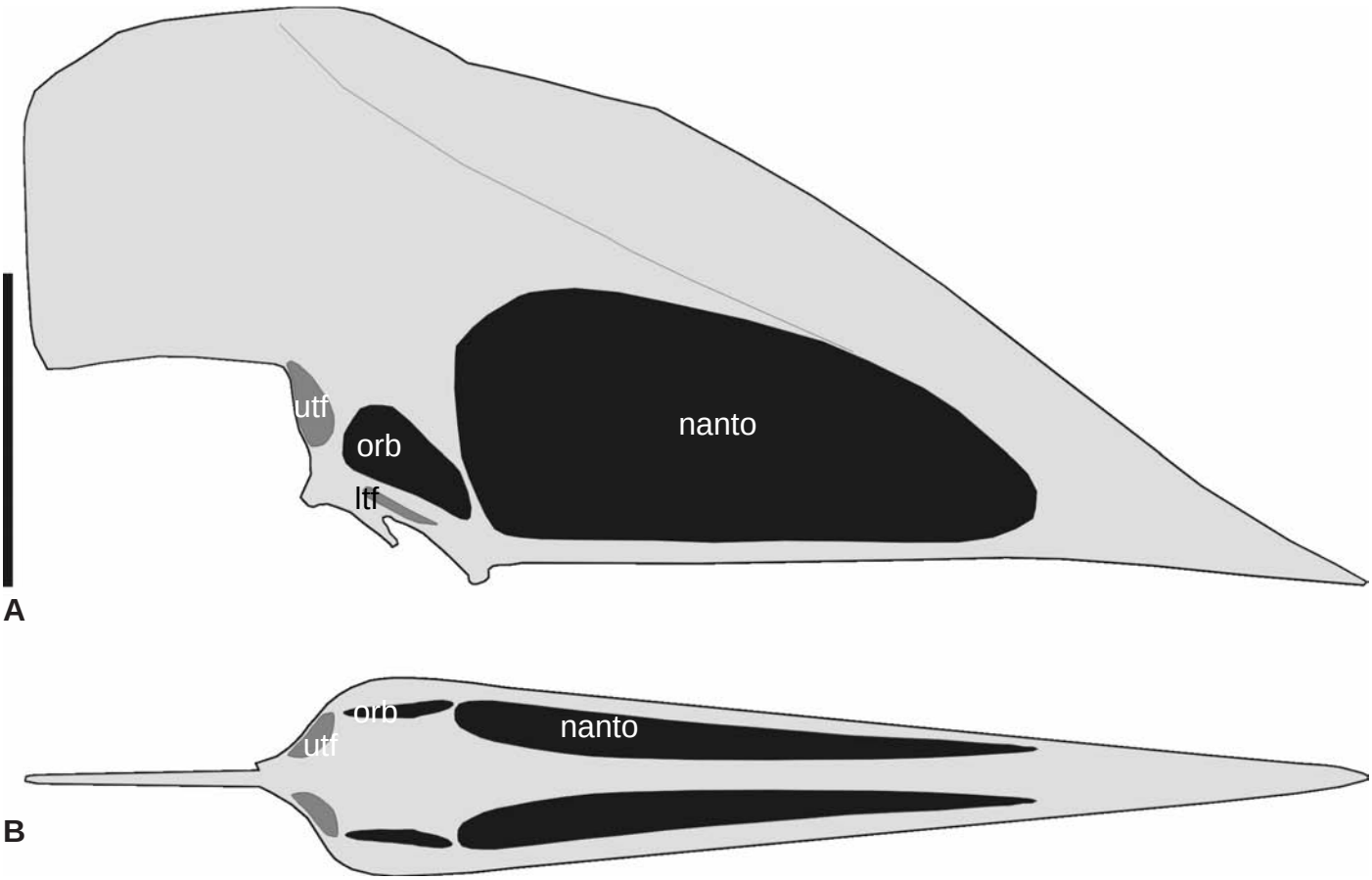

Fig. 7.42: Scaled skull of *Tupuxuara* in A) right lateral, and B) reconstructed dorsal view. Scale bar = 70 mm. See Fig. 7.1 for abbreviations.

7.43 Zhejiangopterus skull construction (see pp. A128-130, Figs. A.337-344 Tabs. A.85-86)

Type species: Zhejiangopterus linhaiensis Cai & Wei 1994

Major descriptions of the skull of Zhejiangopterus: Cai & Wei (1994)

Antorbital fenestra / naris: fused into nasoantorbital fenestra

Anterior rostral crest: absent

Medial rostral crest: absent

Orbitotemporal crest: absent

Orientation of occipital region in lateral view relative to vertical plane: ~25°

Keratinous beak: most probably present

Dentition: edentulous

Other features: nasoantorbital fenestra oval and situated in the posterior half of the rostrum, orbita circular and situated posteromedial to nasoantorbital fenestra, orbitotemporal region curved in ventral direction leading to a convex dorsal outline in this area

Cantilever dimensions

Height to length ratio: 1:5.13

Ratio of total length to length of nasoantorbital fenestra: 1:0.46

Ratio of basal height to basal width: 1:0.58

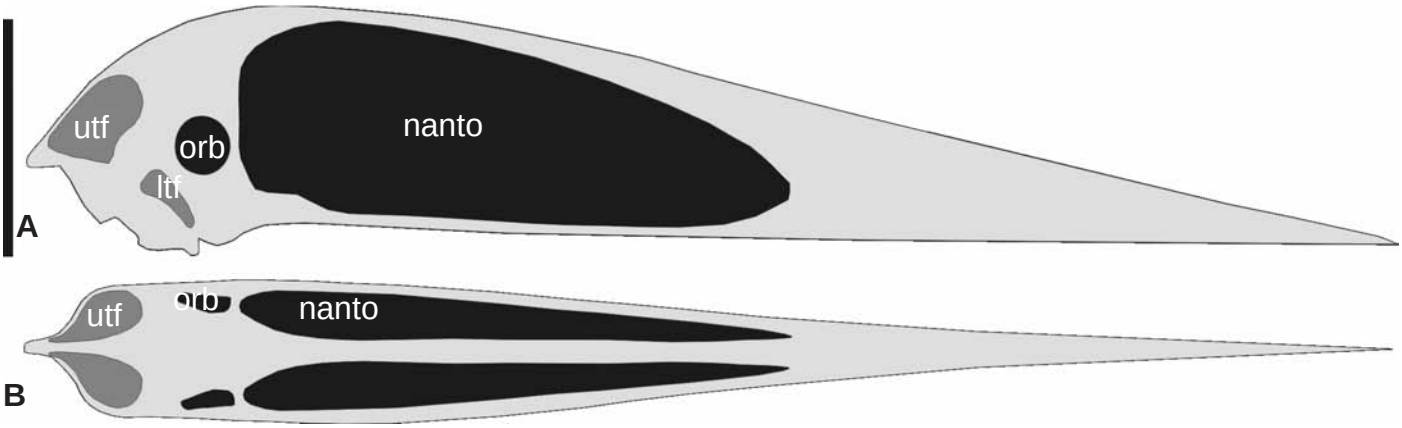

Fig. 7.43: Scaled skull of *Zhejiangopterus* in A) right lateral, and B) reconstructed dorsal view. Scale bar = 70 mm. See Fig. 7.1 for abbreviations.

8. FEM-ANALYSES OF MODELS FOR SELECTED SKULLS

8.1 *Dimorphodon* (Figs. 8.1-8.6)

The FE-model for the *Dimorphodon* skull shows minor differences in stress distribution between an anterior loading case (Fig. 8.1) and a loading along the entire lateral margin of the rostrum (Fig. 8.3). Stress concentrations are found at the postorbital-squamosal bar, at the posterodorsal and ventral border of the orbita and at the lower jaw articulation (Figs. 8.4 & 8.6). Minor differences between both loading cases occur at the ectopterygoid bar and at the anterior border of the antorbital fenestra, where higher stress results in case of an anterior bite. The other parts of the skull construction show a low uniform stress distribution. The highest stress is located at the lower jaw articulation and are about ten times higher than the values in the anterior rostrum.

However, the resulting stress pattern is different in case of a posterior loading case, which analyses a bilateral bite at the last tooth positions, ventral to the antorbital fenestra (Fig. 8.2). Compared to the other two loading cases, the stress is increased around the orbita, around the upper temporal fenestra, around the antorbital fenestra and at the lower jaw articulation where the highest stress values occur (Fig. 8.5). The rostrum anterior to the antorbital fenestra as well as the area around the lower temporal fenestra, the dorsal premaxillary-frontal bar and the anterior-posterior orientated ventral bars show the same uniform, low stress values as in both other loading cases.

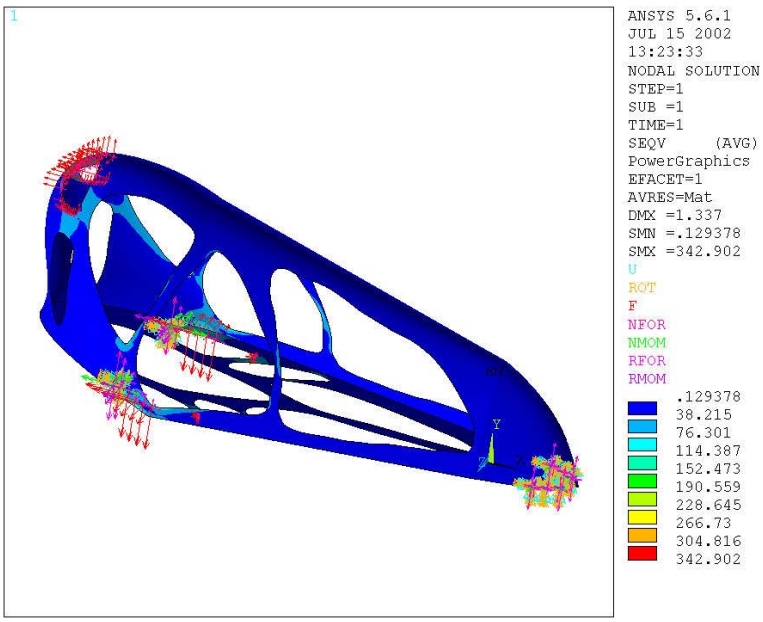

Fig. 8.1: Constraints in the FE-model for the *Dimorphodon* skull, analysing an anterior bite.

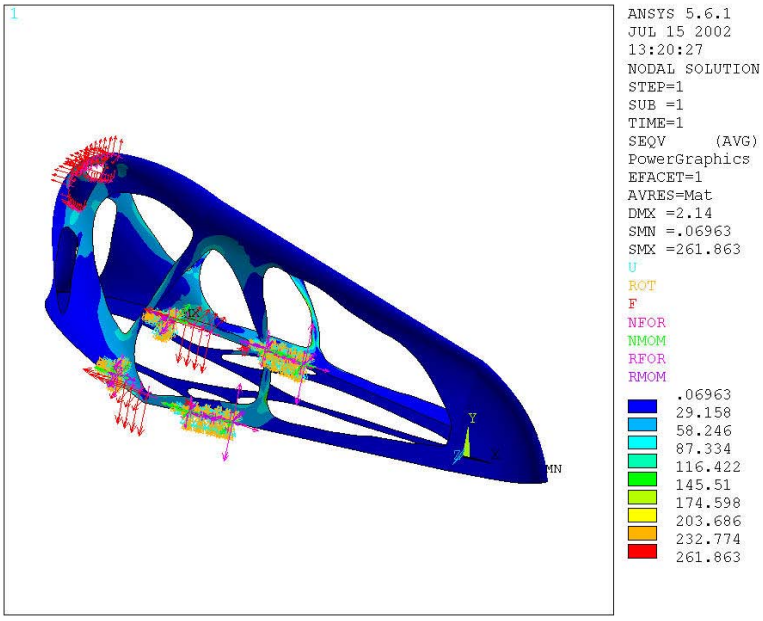

Fig. 8.2: Constraints in the FE-model for *Dimorphodon* skull, analysing a posterior bite.

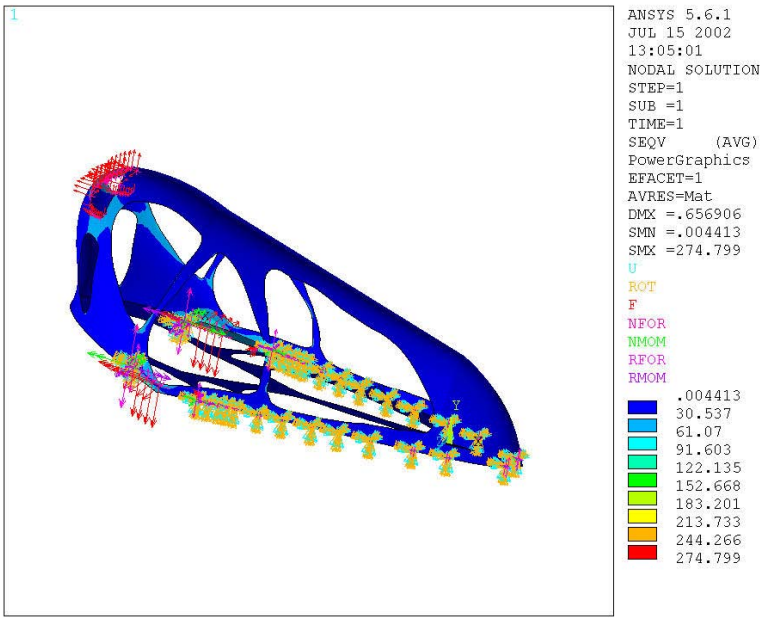

Fig. 8.3: Constraints in the FE-model for the *Dimorphodon* skull, analysing a bite along the entire lateral margin of the rostrum.

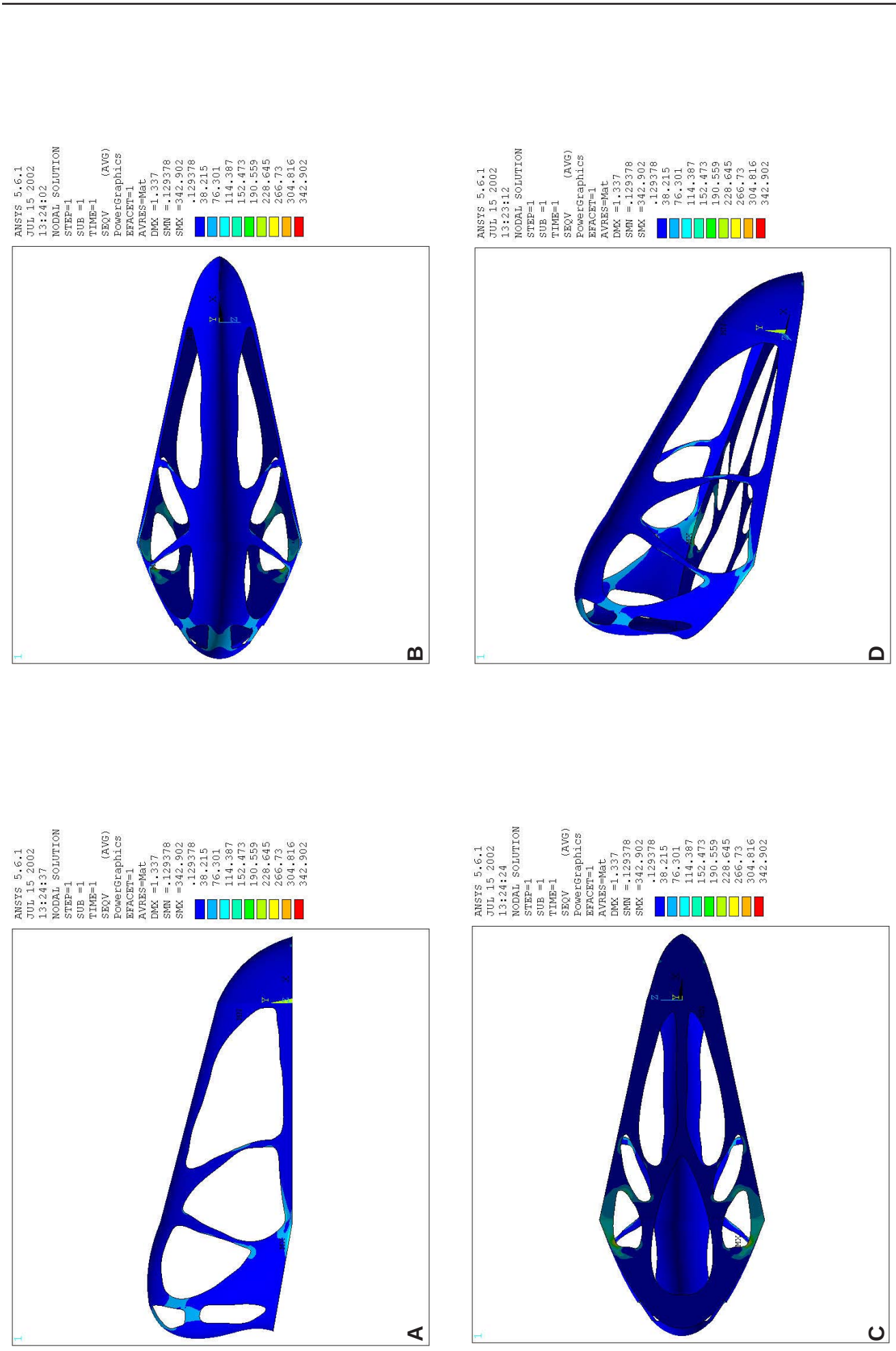

Fig. 8.4: van Mises stress in the FE-model for the *Dimorphodon* skull, analysing an anterior bite: A) Right lateral view; B) Dorsal view; C) Ventral view; D) Right dorsolateral view. Same colours mean same level of deformation.

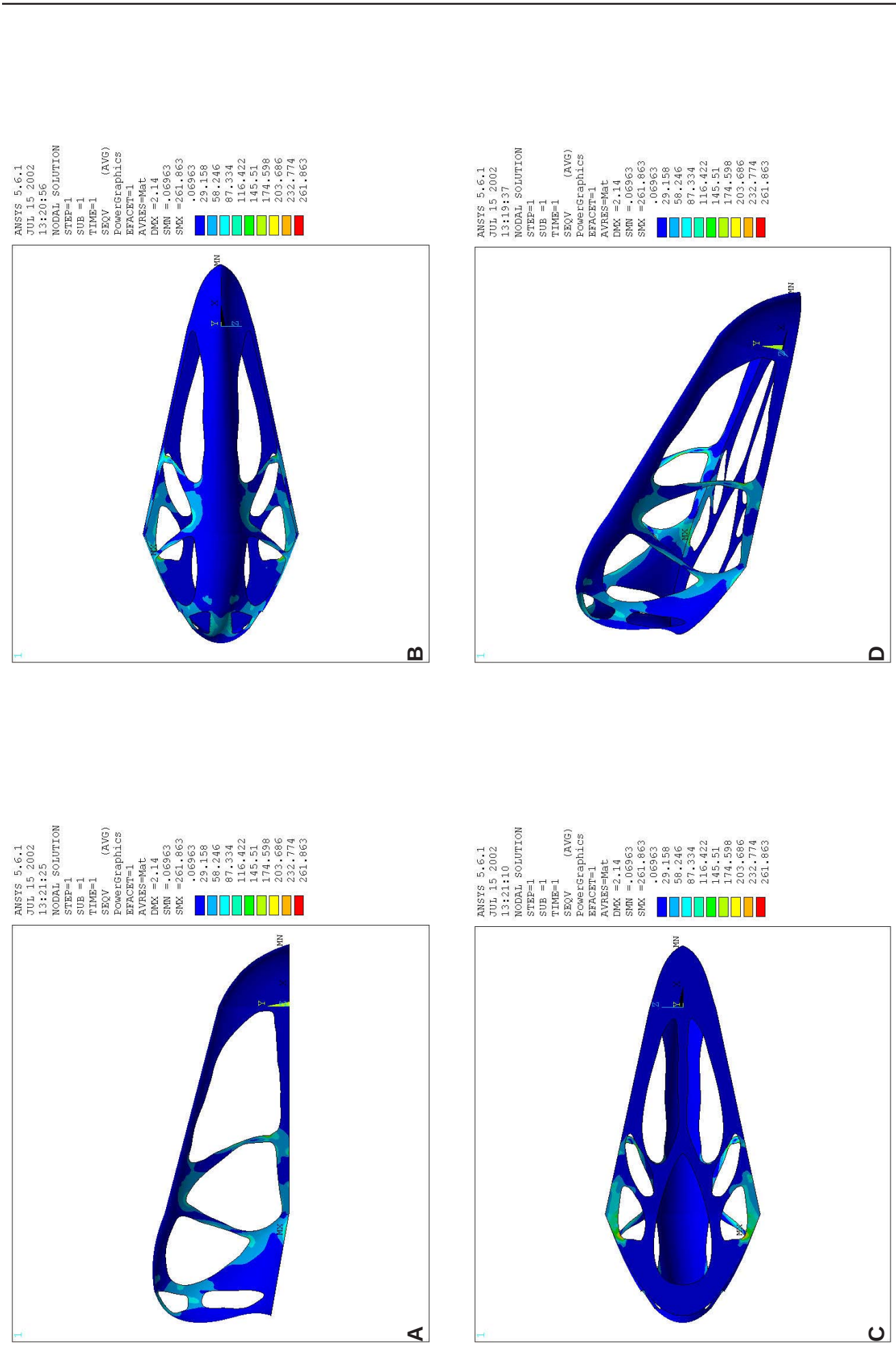

Fig. 8.5: van Mises stress in the FE-model for the *Dimorphodon* skull, analysing an posterior bite: A) Right lateral view; B) Dorsal view; C) Ventral view; D) Right dorsolateral view. Same colours mean same level of deformation.

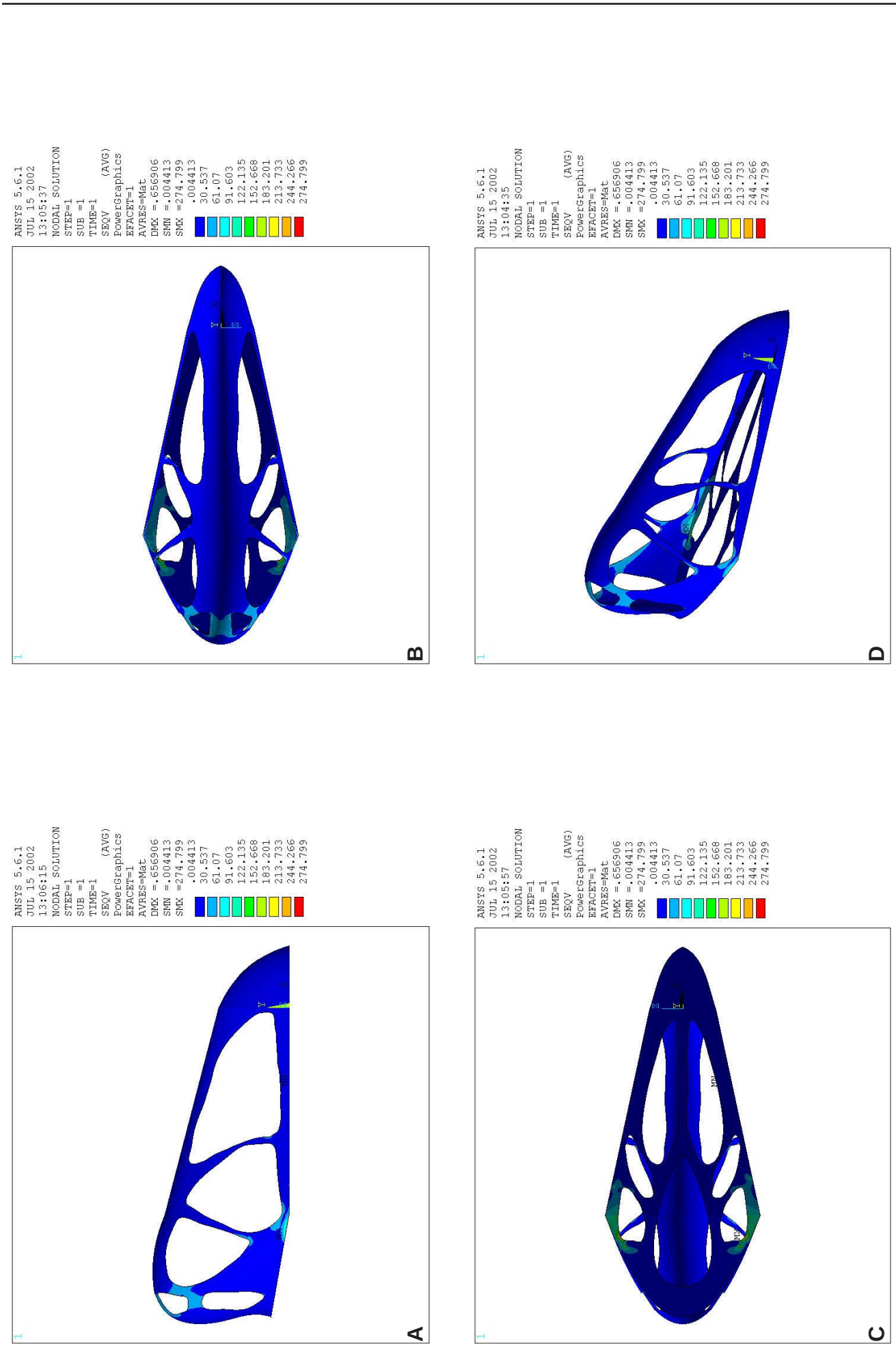

Fig. 8.6: van Mises stress in the FE-model for the *Dimorphodon* skull, analysing a bite along the entire lateral margin of the rostrum: A) Right lateral view; B) Dorsal view; C) Ventral view; D) Right dorsolateral view. Same colours mean same level of deformation.

8.2 *Pterodactylus* (Figs. 8.7-8.12)

The FE-model for the *Pterodactylus* skull shows a nearly similar pattern of stress distribution for all three loading cases (Figs. 8.7-8.9). Increased stress values are located around the upper temporal fenestra, around the orbita with the exception of the anterodorsal region, at the posterior and anterodorsal border of the antorbital fenestra, the ectopterygoid, the pterygoid-palatine bar and at the lower jaw articulation (Figs. 8.10-8.12). Here, the average stress values are about four times higher than in the anterior rostrum. The highest stress are found at the lower jaw articulation where the stress values are about ten times higher than in the anterior rostrum.

Low, uniform stress values result at the rostrum including the ventral and dorsal borders of the nasoantorbital fenestra, the posteroventral border of the lower temporal fenestra and the ventral elements with the exception of the ectopterygoid and pterygoid-palatine bar (Figs. 8.10-8.12).

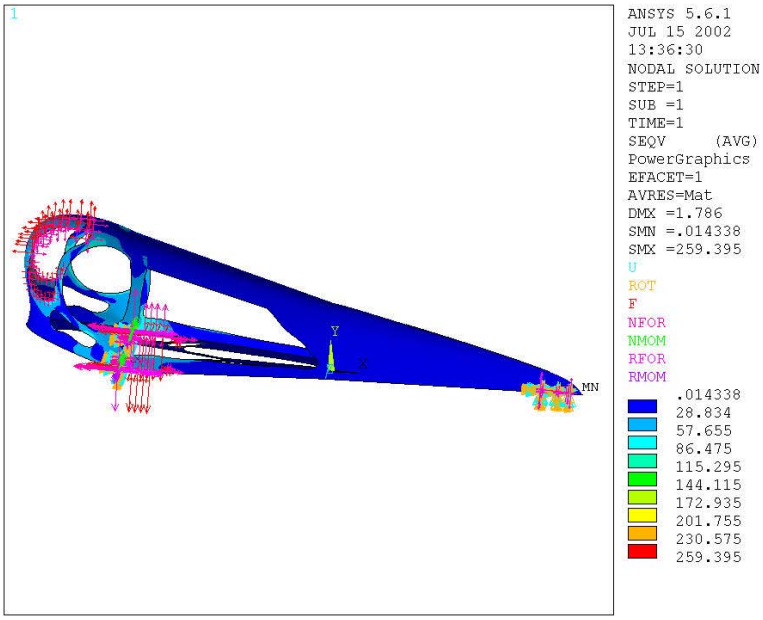

Fig. 8.7: Constraints in the FE-model for the *Pterodactylus* skull, analysing an anterior bite.

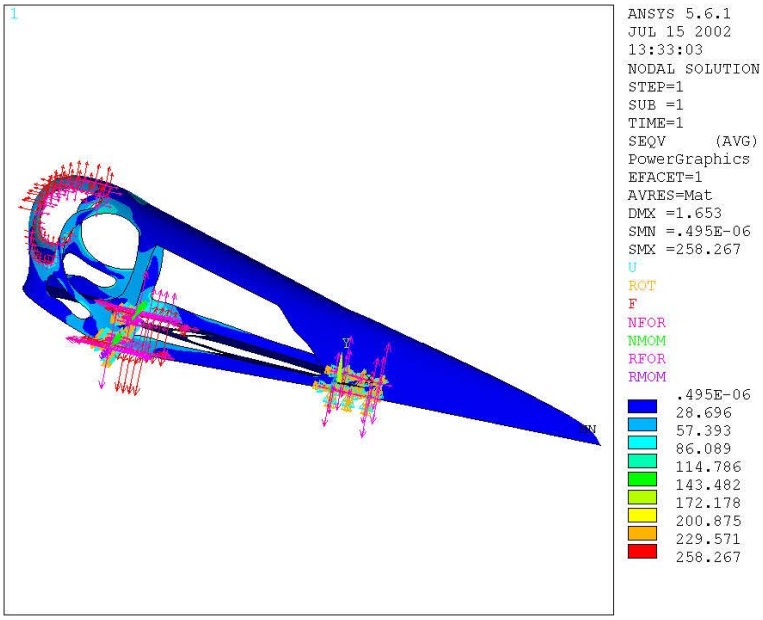

Fig. 8.8: Constraints in the FE-model for the *Pterodactylus* skull, analysing a posterior bite.

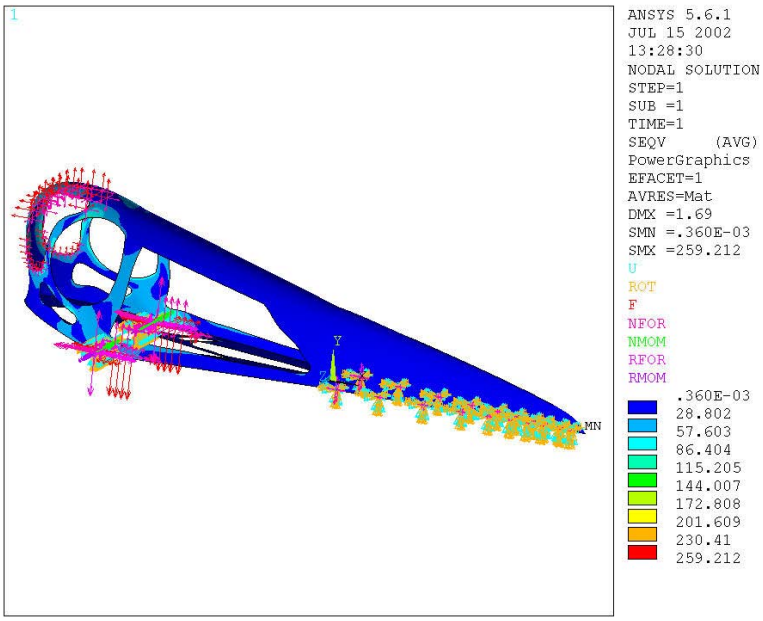

Fig. 8.9: Constraints in the FE-model for the Pterodactylus skull, analysing a bite along the entire lateral margin of the rostrum.

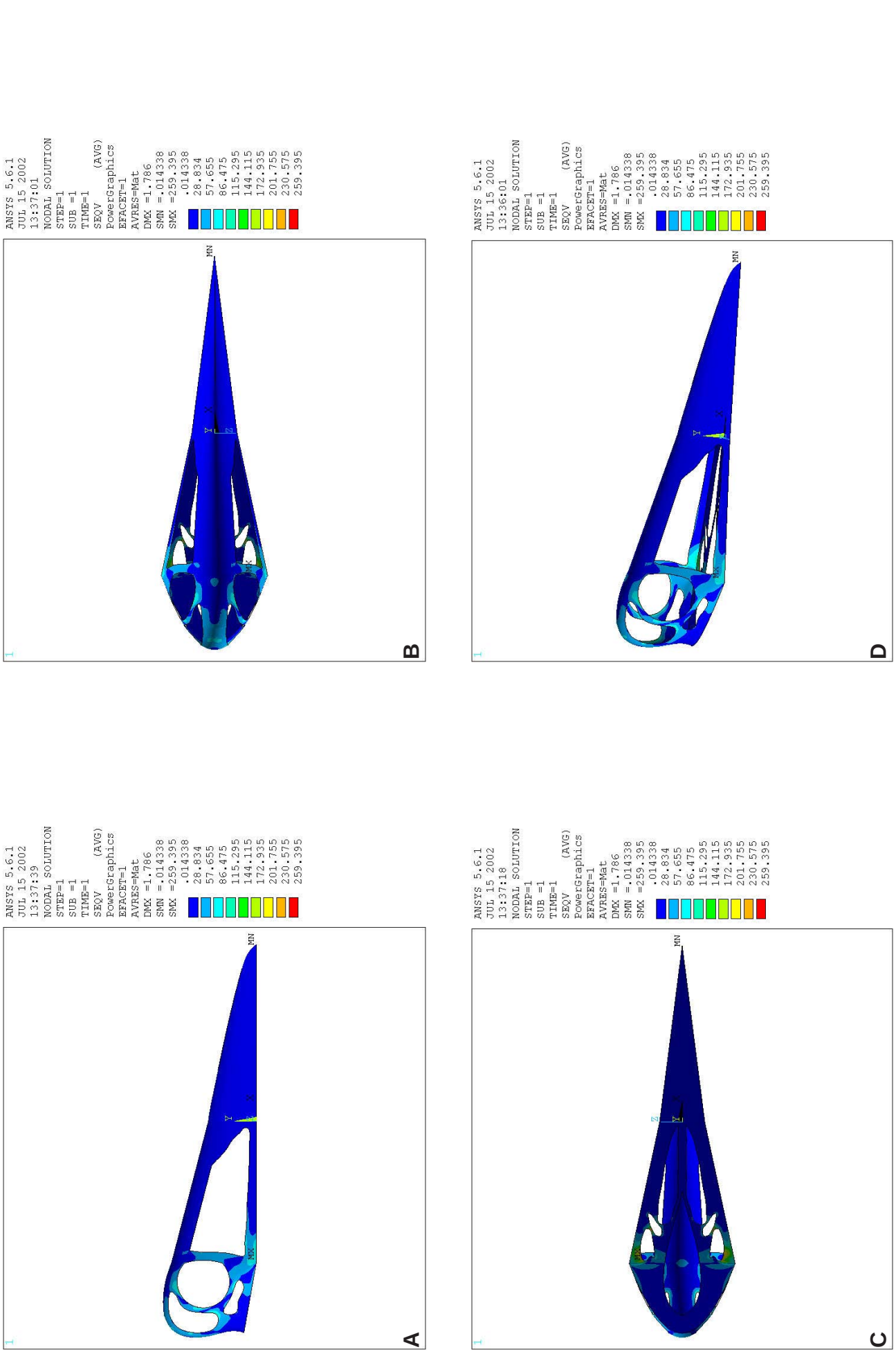

Fig. 8.10: van Mises stress in the FE-model for the *Pterodactylus* skull, analysing an anterior bite: A) Right lateral view; B) Dorsal view; C) Ventral view; D) Right dorsolateral view. Same colours mean same level of deformation.

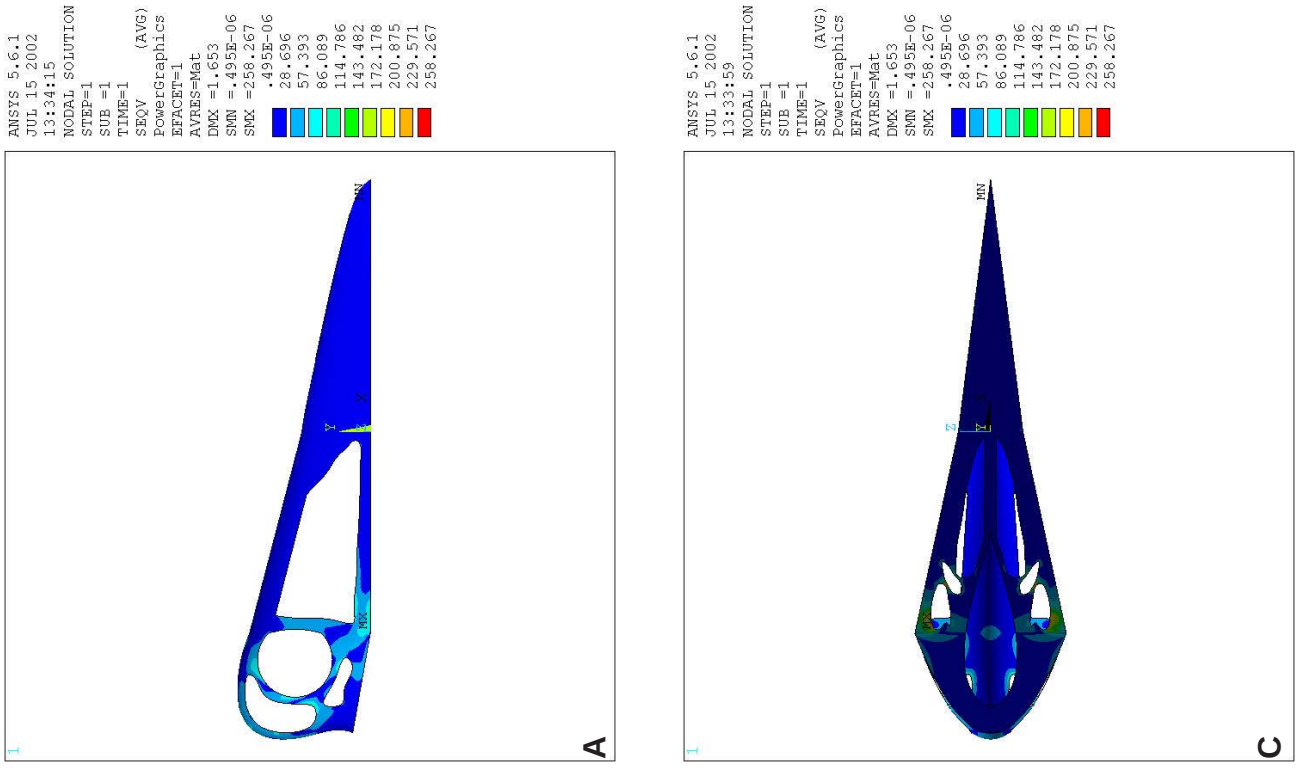

Fig. 8.11: van Mises stress in the FE-model for the *Pterodactylus* skull, analysing an posterior bite: A) Right lateral view; B) Dorsal view; C) Ventral view; D) Right dorsolateral view. Same colours mean same level of deformation.

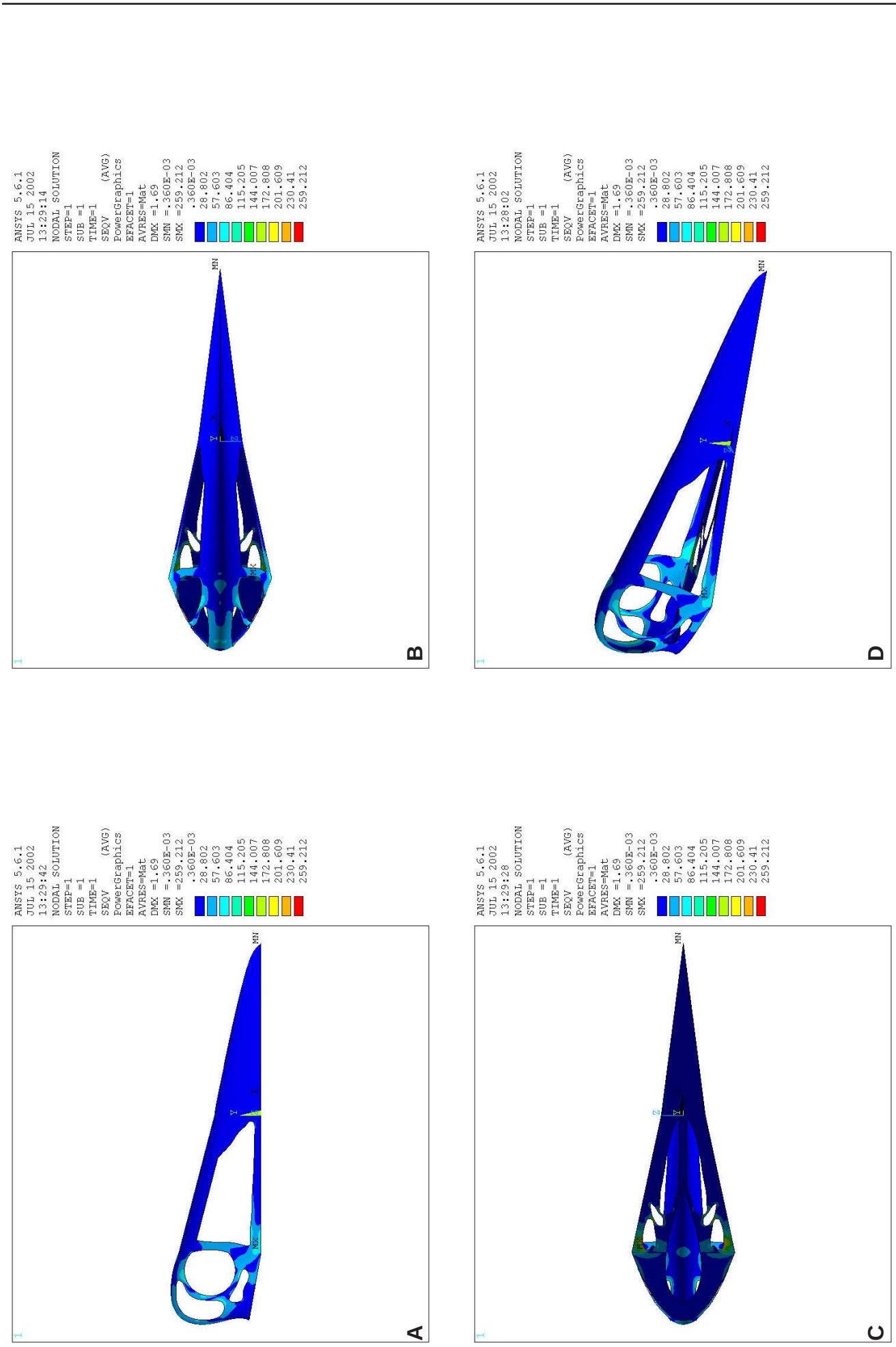

Fig. 8.12: van Mises stress in the FE-model for the *Pterodactylus* skull, analysing a bite along the entire lateral margin of the rostrum: A) Right lateral view; B) Dorsal view; C) Ventral view; D) Right dorsolateral view. Same colours mean same level of deformation.

8.3 *Santanadactylus* (Figs. 8.13-8.18)

Like in the previous model, the stress distribution in the FE-model for the *Santanadactylus* skull shows no significant differences for all three loading cases (Figs. 8.13-8.15).

Increased stress values are present around the upper temporal fenestra, at the posteroventral and anteroventral region of the orbita, the anterodorsal region of the nasoantorbital fenestra, ectopterygoid bar and at the lower jaw articulation (Figs. 8.16-8.18). The mean values in these areas are about six times higher than in the anterior rostrum, which - like the remaining areas - show low, uniform stress values (Figs. 8.16-8.18).

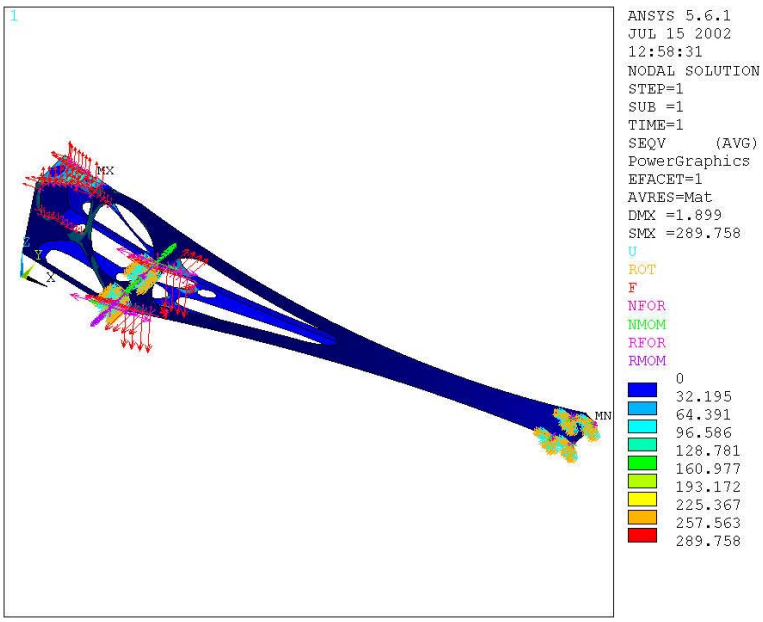

Fig. 8.13: Constraints in the FE-model for the *Santanadacytlus* skull, analysing an anterior bite.

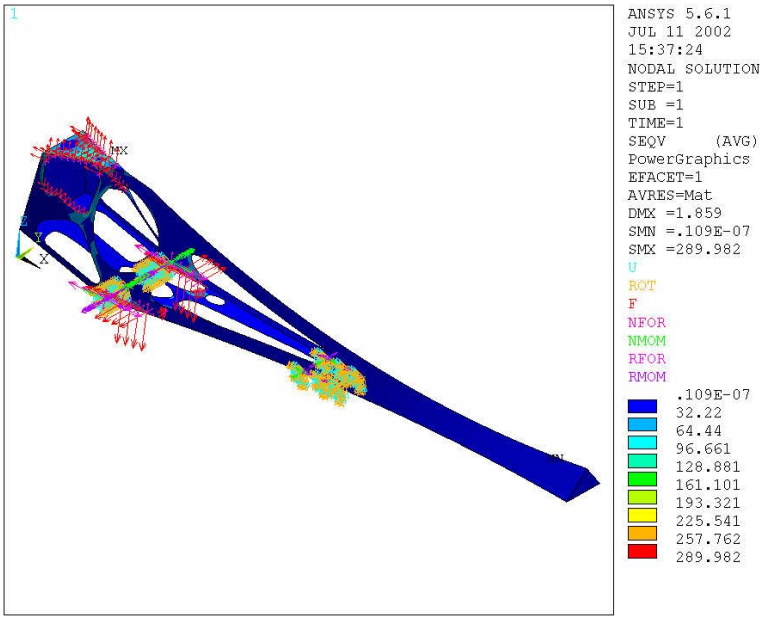

Fig. 8.14: Constraints in the FE-model for the *Santanadactylus* skull, analysing a posterior bite.

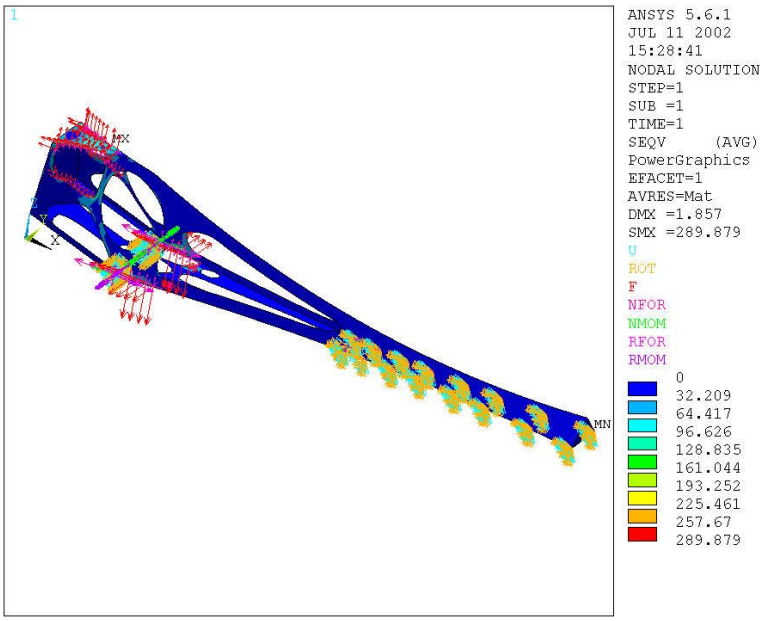

Fig. 8.15: Constraints in the FE-model for the *Santanadactylus* skull, analysing a bite along the entire lateral margin of the rostrum.

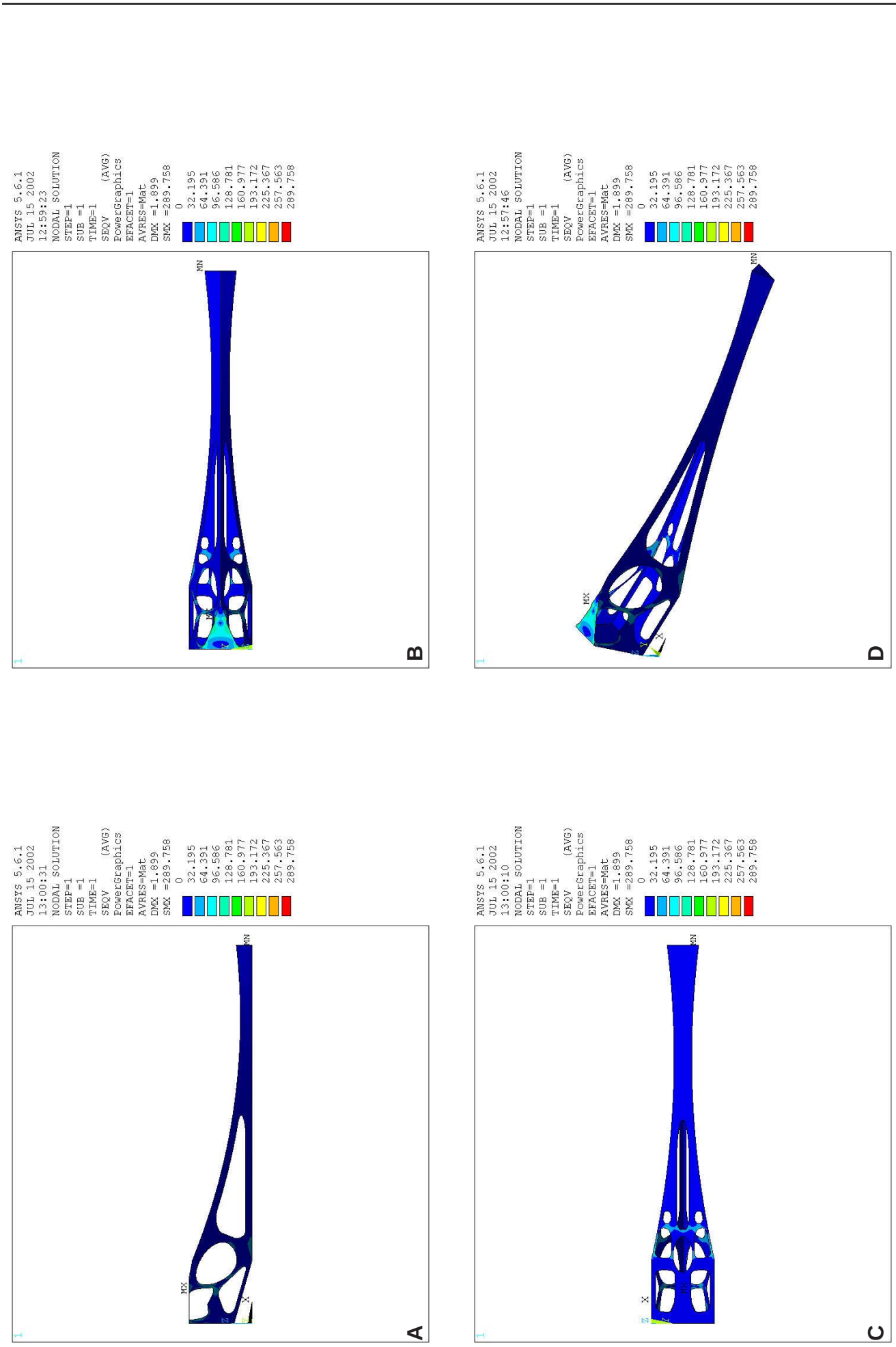

Fig. 8.16: van Mises stress in the FE-model for the *Santanadactylus* skull, analysing an anterior bite: A) Right lateral view; B) Dorsal view; C) Ventral view; D) Right dorsolateral view. Same colours mean same level of deformation.

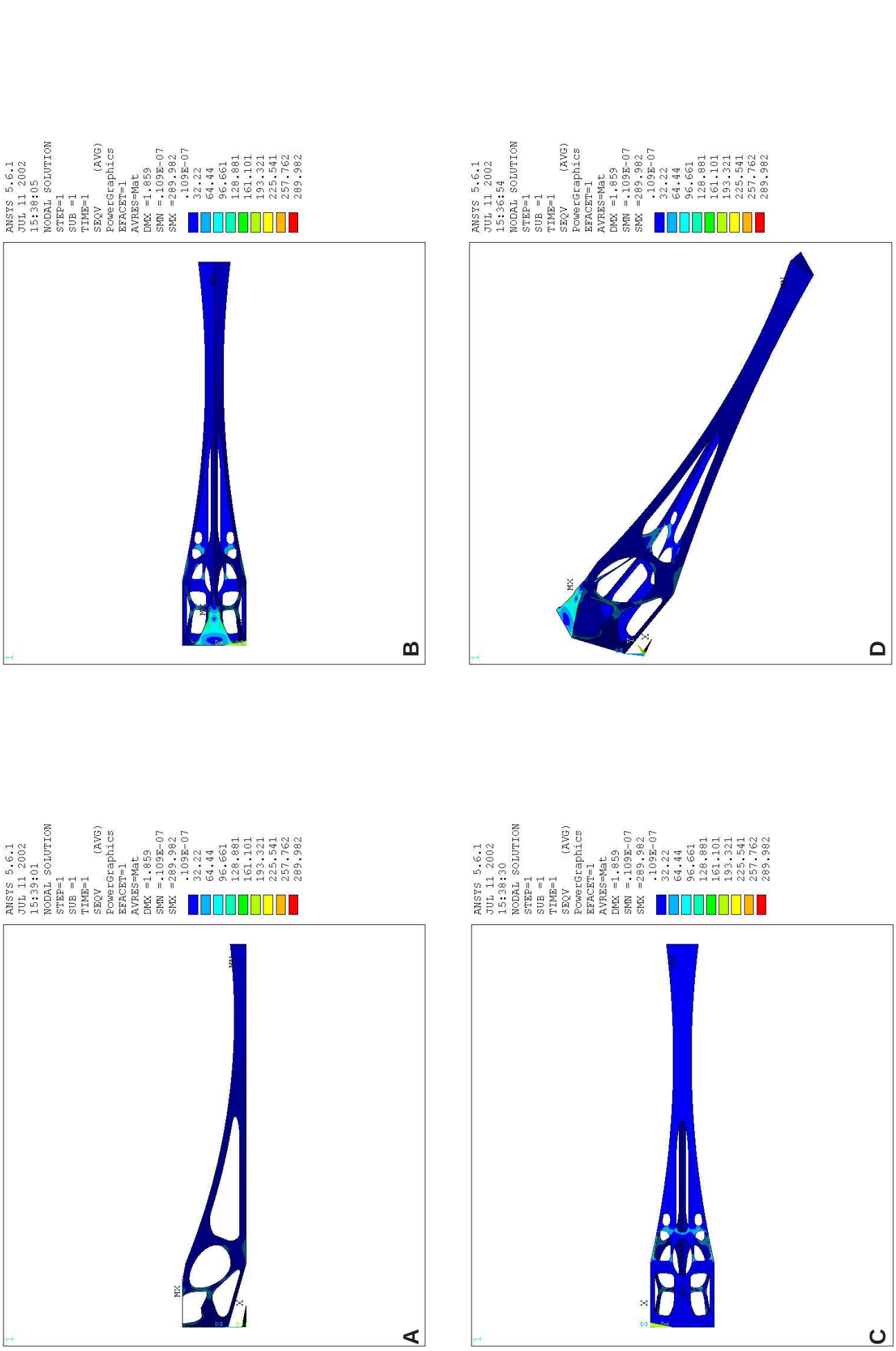

Fig. 8.17: van Mises stress in the FE-model for the *Santanadactylus* skull, analysing an posterior bite: A) Right lateral view; B) Dorsal view; C) Ventral view; D) Right dorsolateral view. Same colours mean same level of deformation.

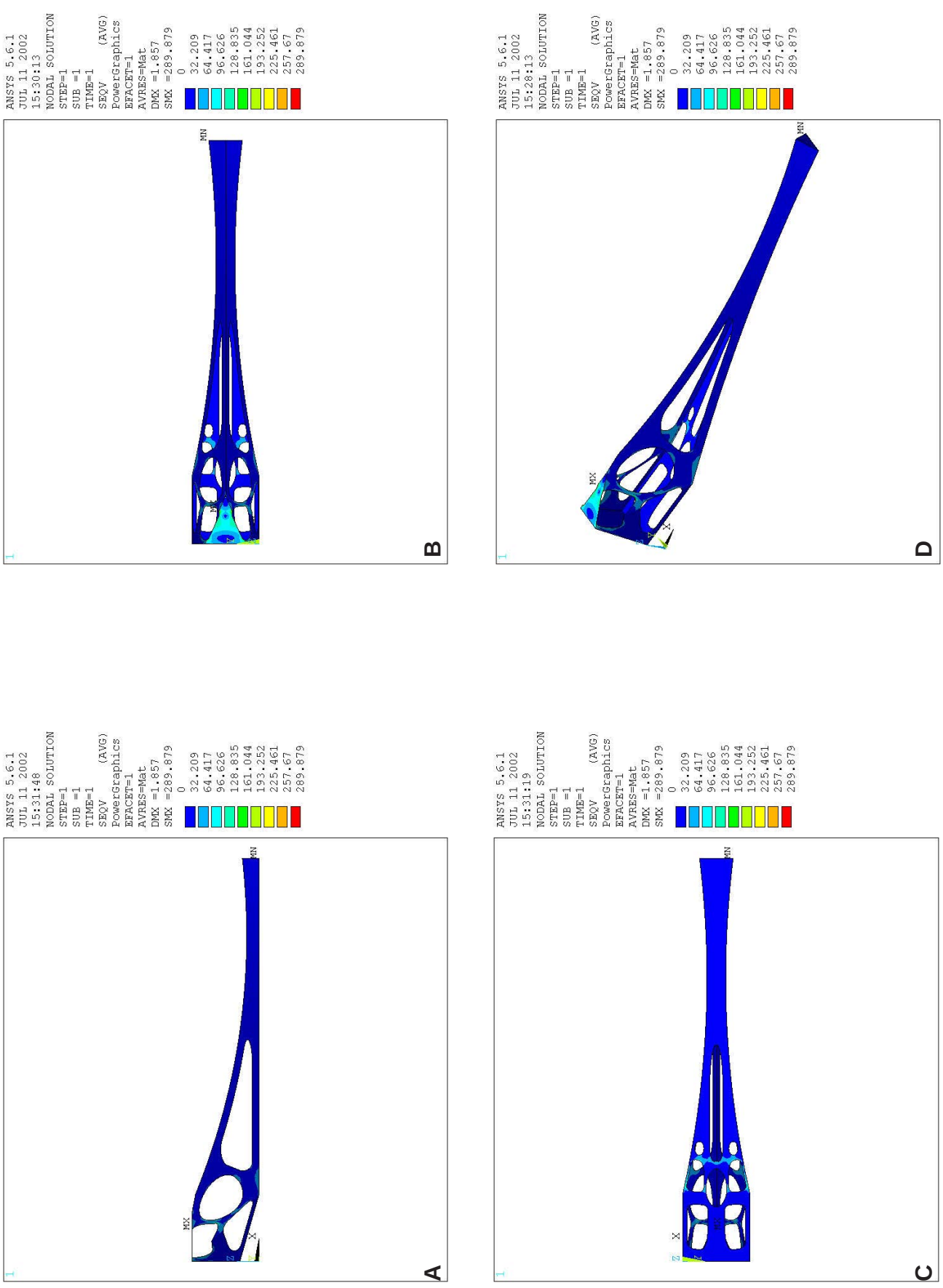

Fig. 8.18: van Mises stress in the FE-model for the *Santanadactylus* skull, analysing a bite along the entire lateral margin of the rostrum: A) Right lateral view; B) Dorsal view; C) Ventral view; D) Right dorsolateral view. Same colours mean same level of deformation.

8.4 *Coloborhynchus* (Figs. 8.19-8.24)

In the FE-model of the skull for *Coloborhynchus*, all three loading cases (Figs. 8.19-8.21) show an identical pattern of stress distribution. Stress concentrations are found around the upper temporal fenestra with the exception of the postorbital bar, the anteroventral region of the orbita, posteroventral region of the nasoantorbital fenestra and around the subtemporal foramen (Figs 8.22-8.24). The stresses are the highest in case of a bilateral bite along the entire lateral margin of the rostrum, where they are up to seven times higher than in the anterior rostrum.

Low, uniformly distributed stress values occur in the remaining areas of the rostrum including the anterior rostrum and the dorsal and ventral borders of the nasoantorbital fenestra as well as the postorbital bar, the area around the lower temporal fenestra and most of the ventral bars (Figs 8.22-8.24).

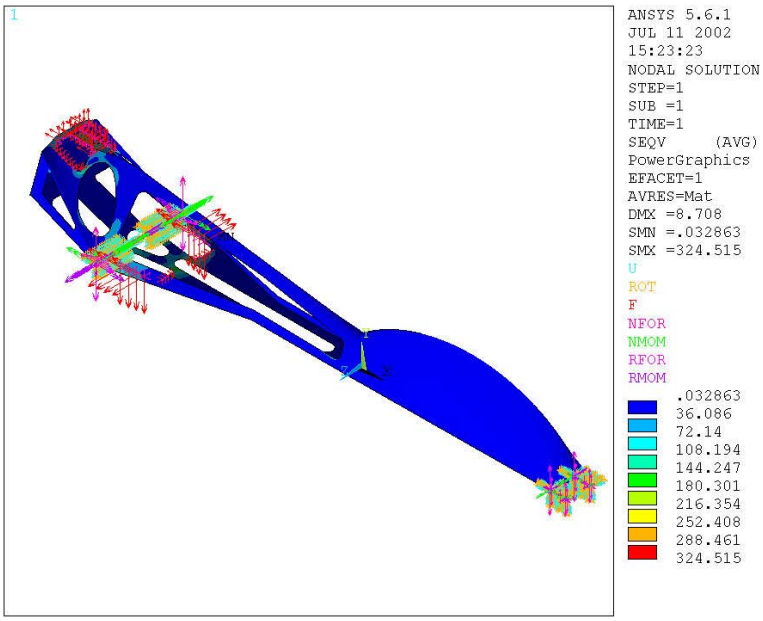

Fig. 8.19: Constraints in the FE-model for the *Coloborhynchus* skull, analysing an anterior bite.

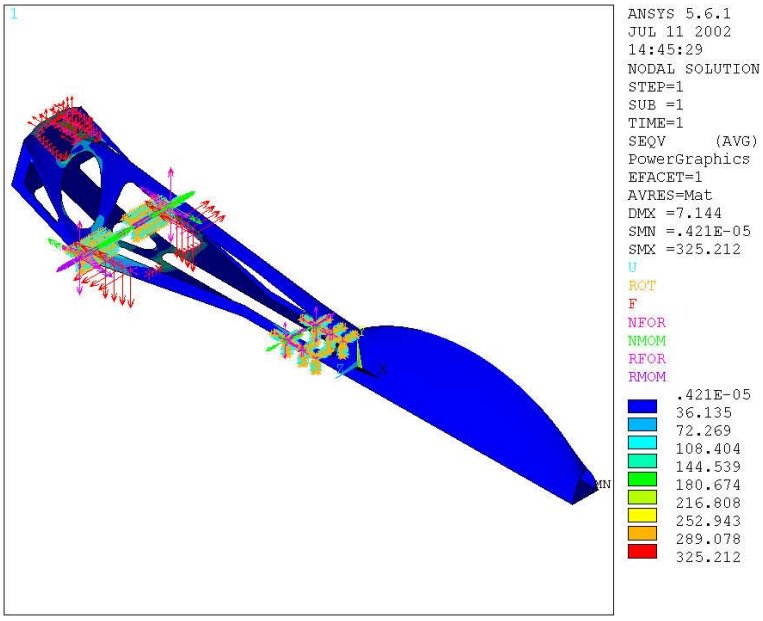

Fig. 8.20: Constraints in the FE-model for the *Coloborhynchus* skull, analysing a posterior bite.

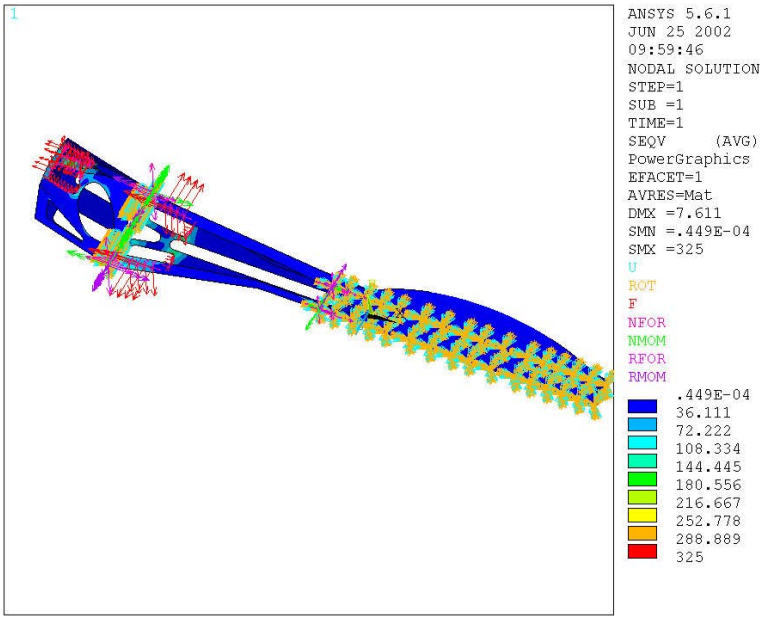

Fig. 8.21: Constraints in the FE-model for the Coloborhynchus skull, analysing a bite along the entire lateral margin of the rostrum.

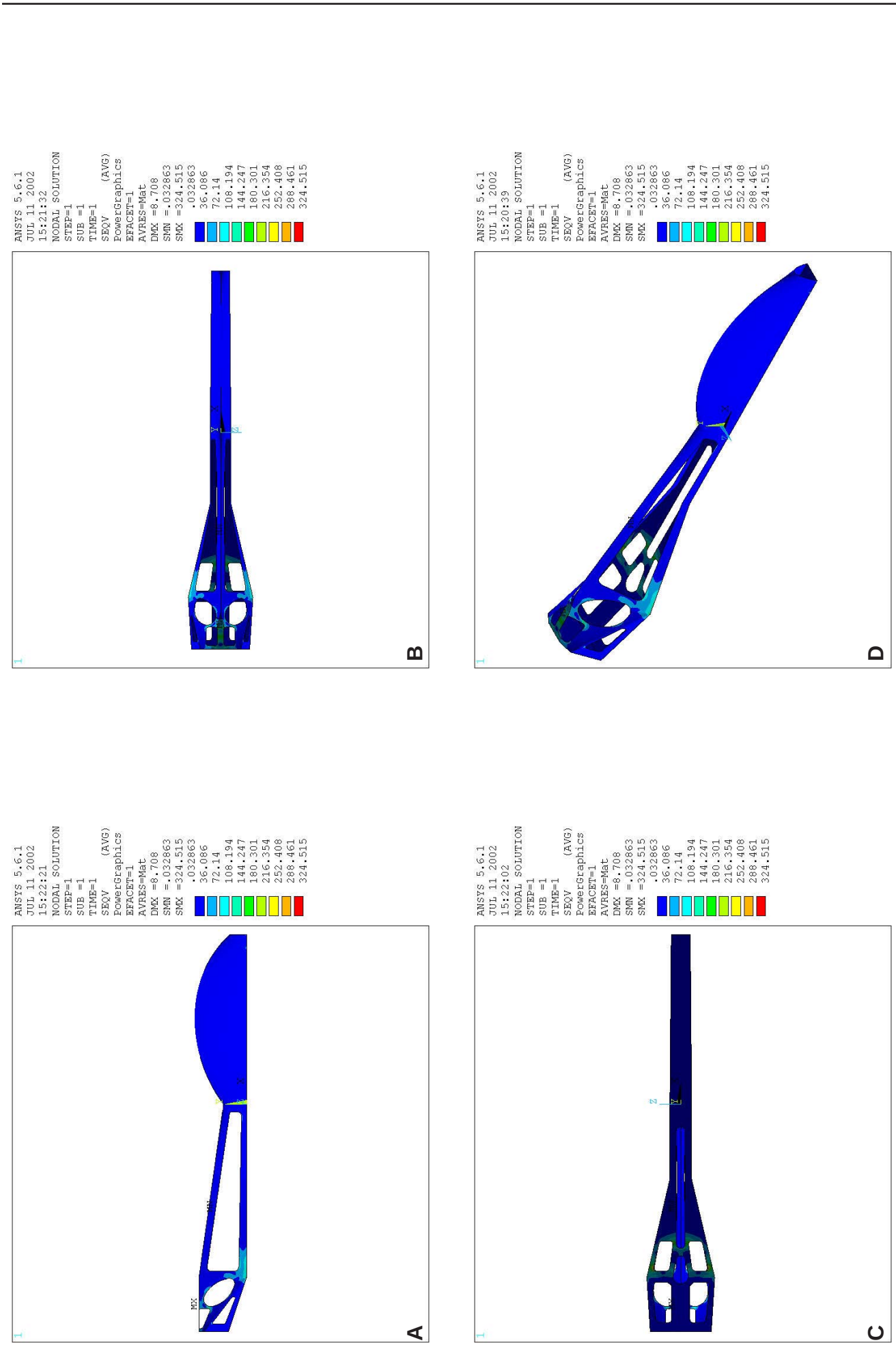

Fig. 8.22: van Mises stress in the FE-model for the *Coloborhynchus* skull, analysing an anterior bite: A) Right lateral view; B) Dorsal view; C) Ventral view; D) Right dorsolateral view. Same colours mean same level of deformation.

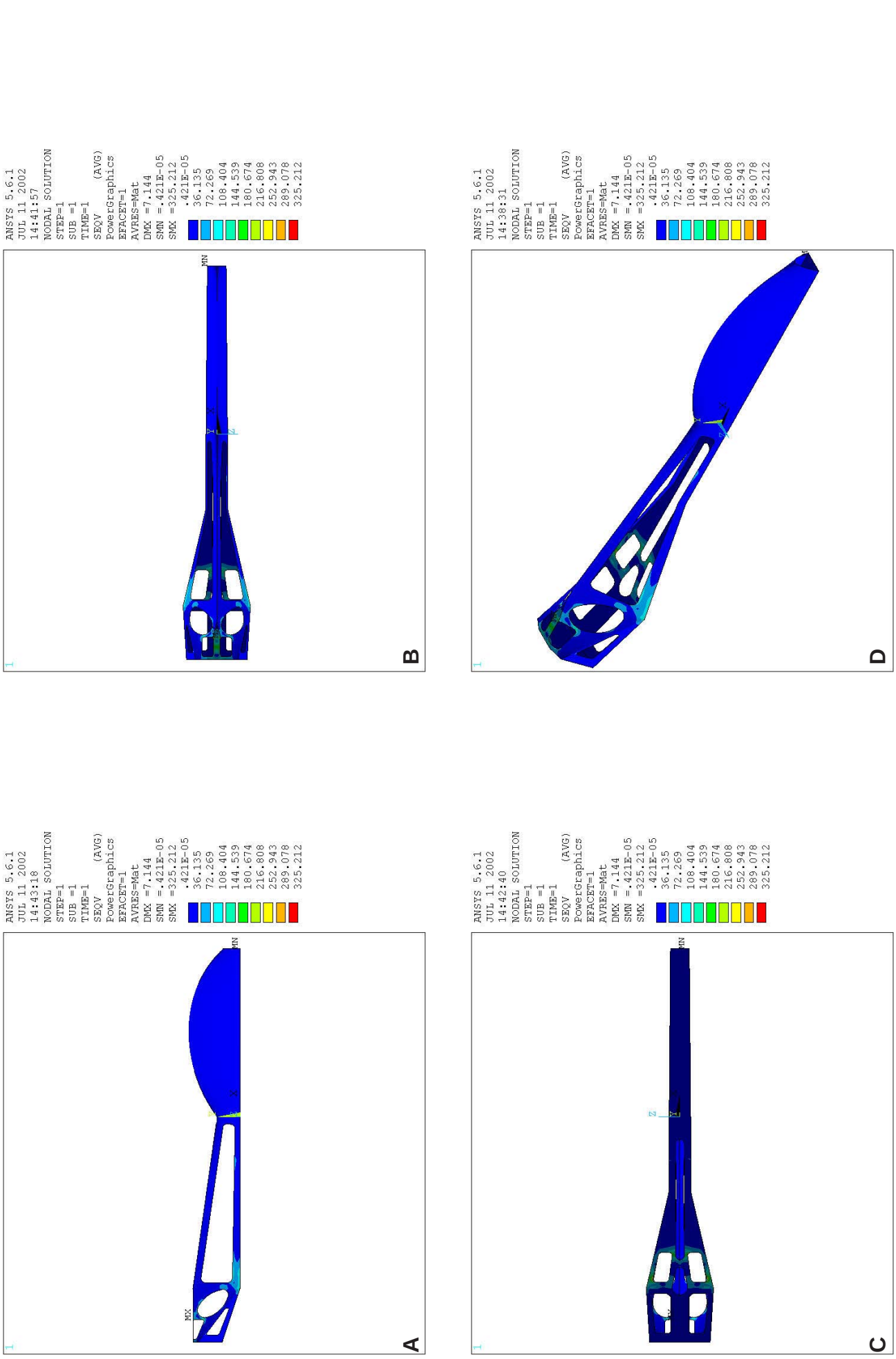

Fig. 8.23: van Mises stress in the FE-model for the *Coloborhynchus* skull, analysing an posterior bite: A) Right lateral view; B) Dorsal view; C) Ventral view; D) Right dorsolateral view. Same colours mean same level of deformation.

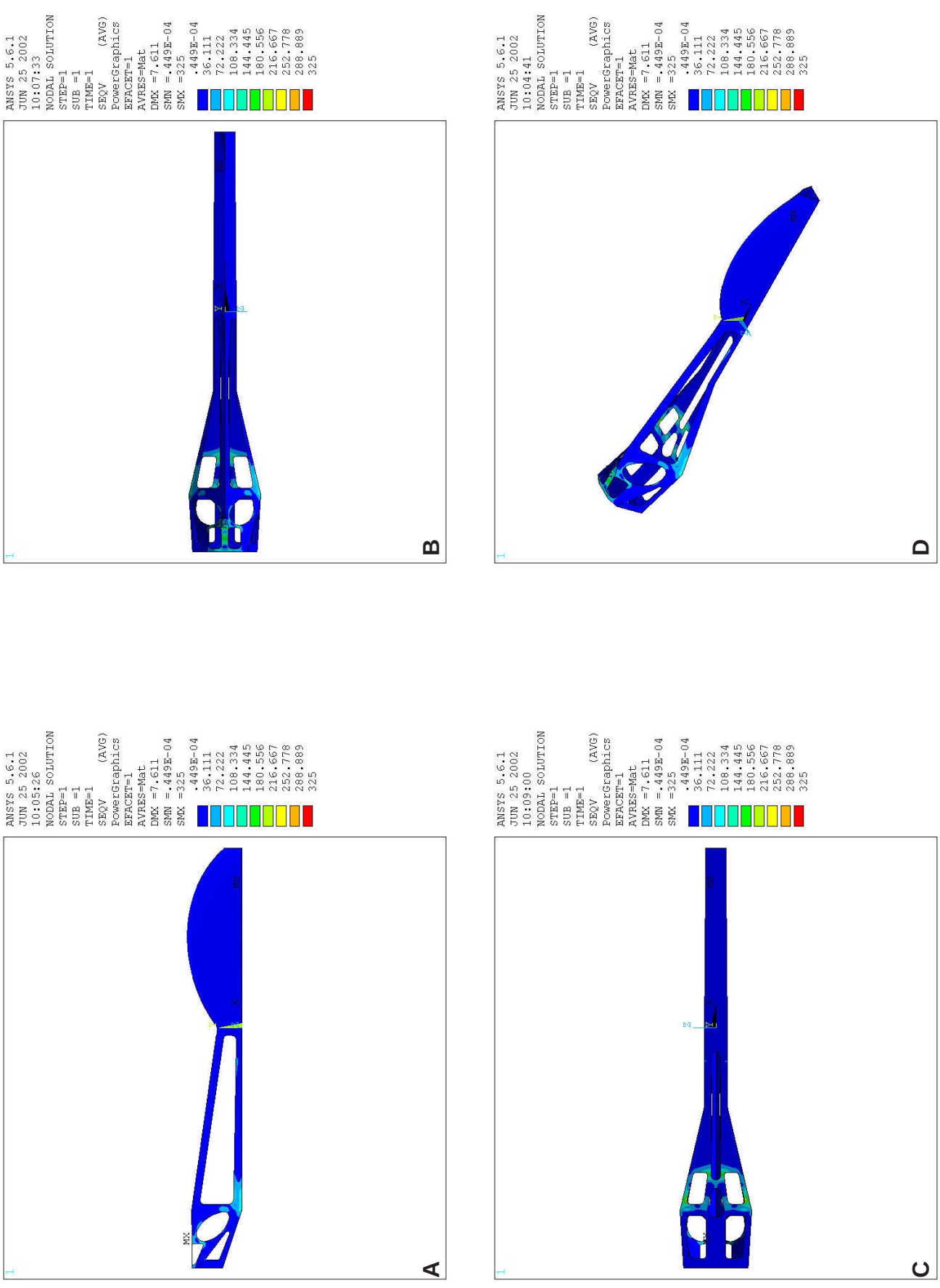

Fig. 8.24: van Mises stress in the FE-model for the *Coloborhynchus* skull, analysing a bite along the entire lateral margin of the rostrum: A) Right lateral view; B) Dorsal view; C) Ventral view; D) Right dorsolateral view. Same colours mean same level of deformation.

8.5 *Pteranodon* (Figs. 8.25-8.33)

No significant differences for all three loading cases (Figs. 8.25-8.27) are visible for the stress distribution in the FE-model for the *Pteranodon* skull. High stresses are concentrated around the orbita, the postorbital bar as well as the posterodorsal region of the lower temporal fenestra, the posteroventral region of the nasoantorbital fenestra, the dorsomedial region between both orbitae and the lower jaw articulation (Figs.8.28-8.33). The mean stress values are about five times higher than in the remaining parts including the orbitotemporal crest, which shows a low, uniform stress pattern. As in the previous skull constructions, the highest stresses in the FE-models for the *Pteranodon* skull occur at the lower jaw articulation where the stresses are up to ten times higher than in the anterior rostrum (Figs.8.28-8.33).

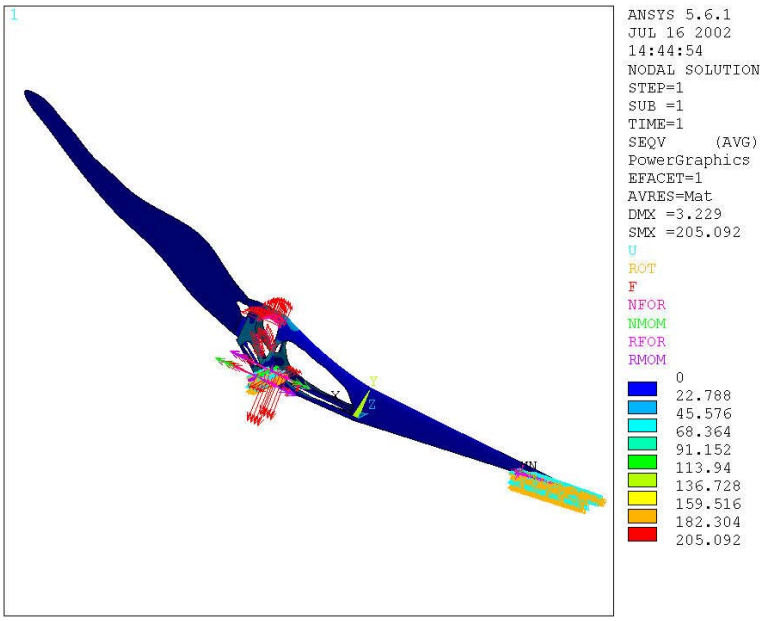

Fig. 8.25: Constraints in the FE-model for the *Pteranodon* skull, analysing an anterior bite.

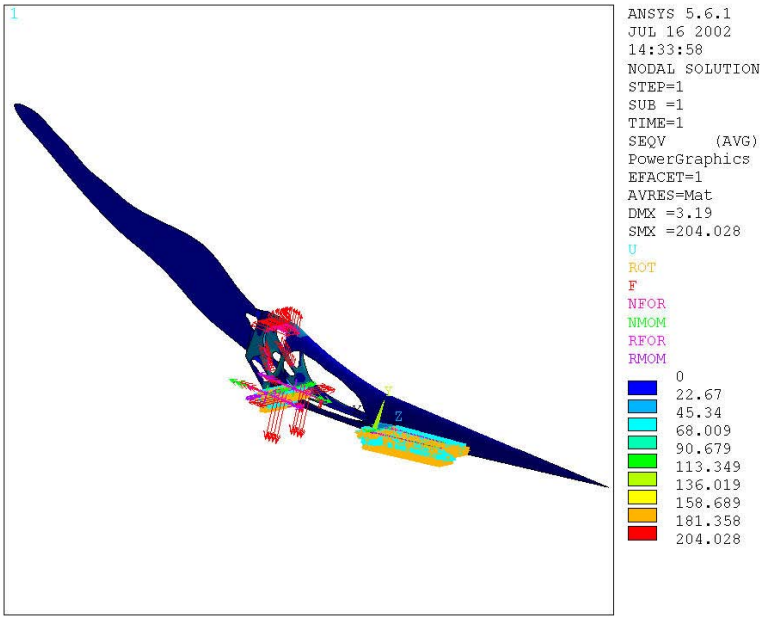

Fig. 8.26: Constraints in the FE-model for the *Pteranodon* skull, analysing a posterior bite.

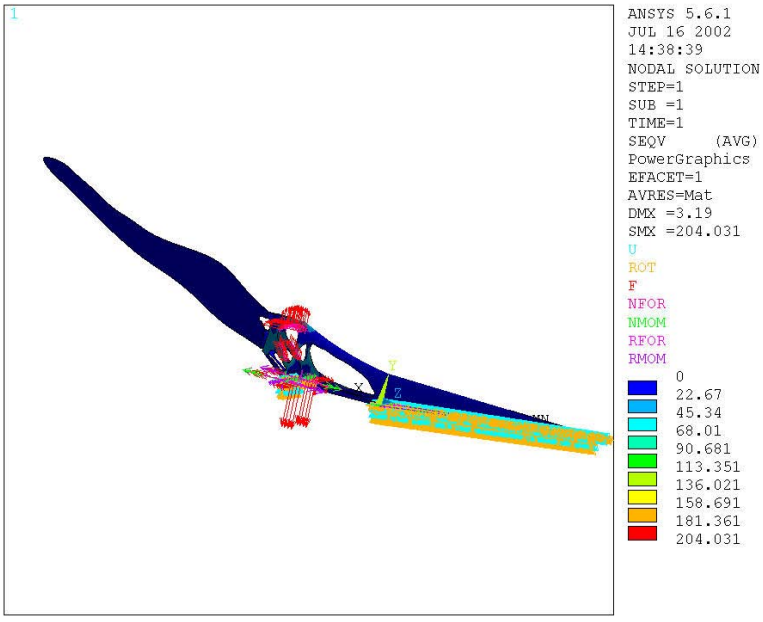

Fig. 8.27: Constraints in the FE-model for the *Pteranodon* skull, analysing a bite along the entire lateral margin of the rostrum.

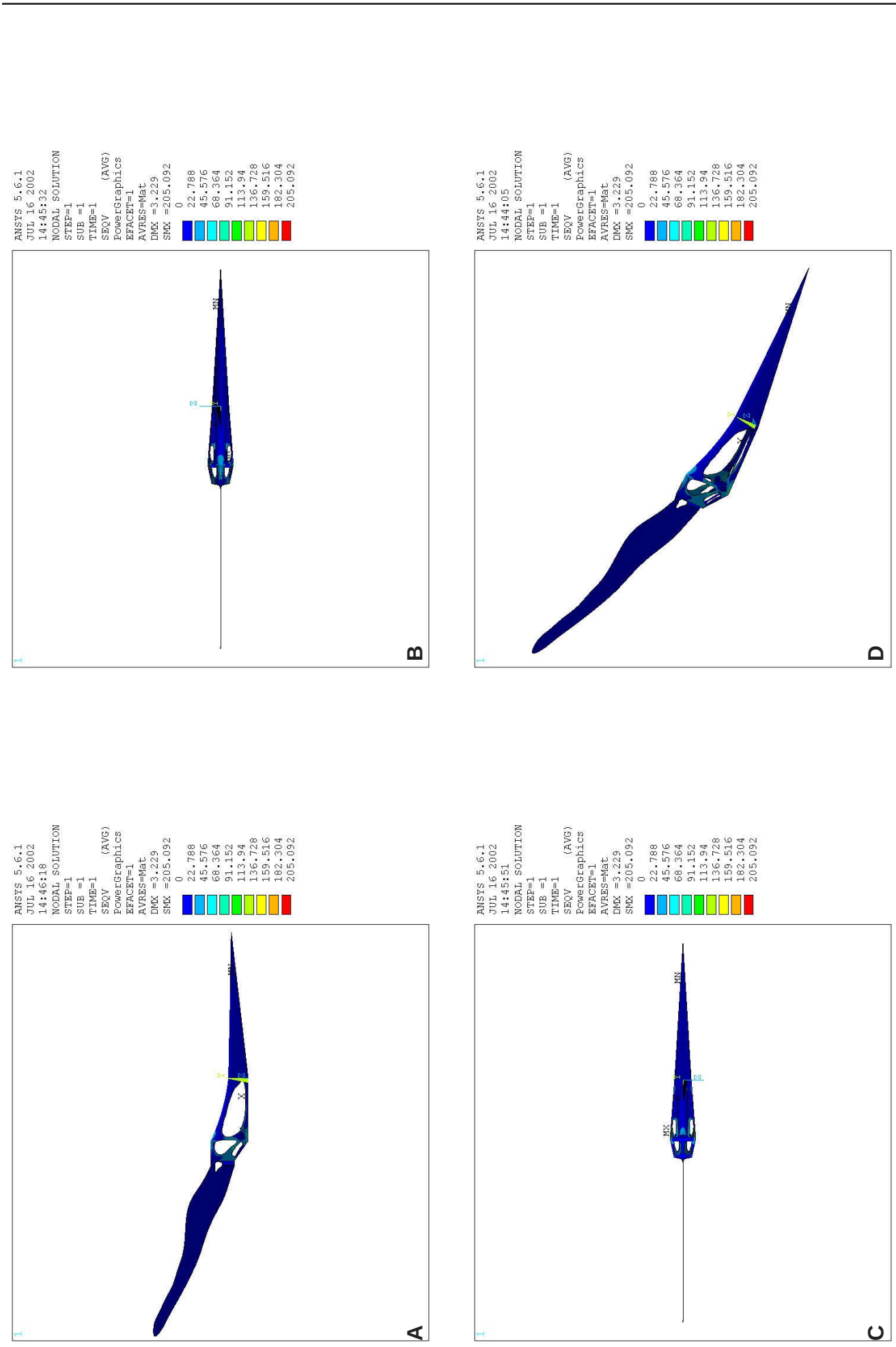

Fig. 8.28: van Mises stress in the FE-model for the *Pteranodon* skull, analysing an anterior bite: A) Right lateral view; B) Dorsal view; C) Ventral view; D) Right dorsolateral view. Same colours mean same level of deformation.

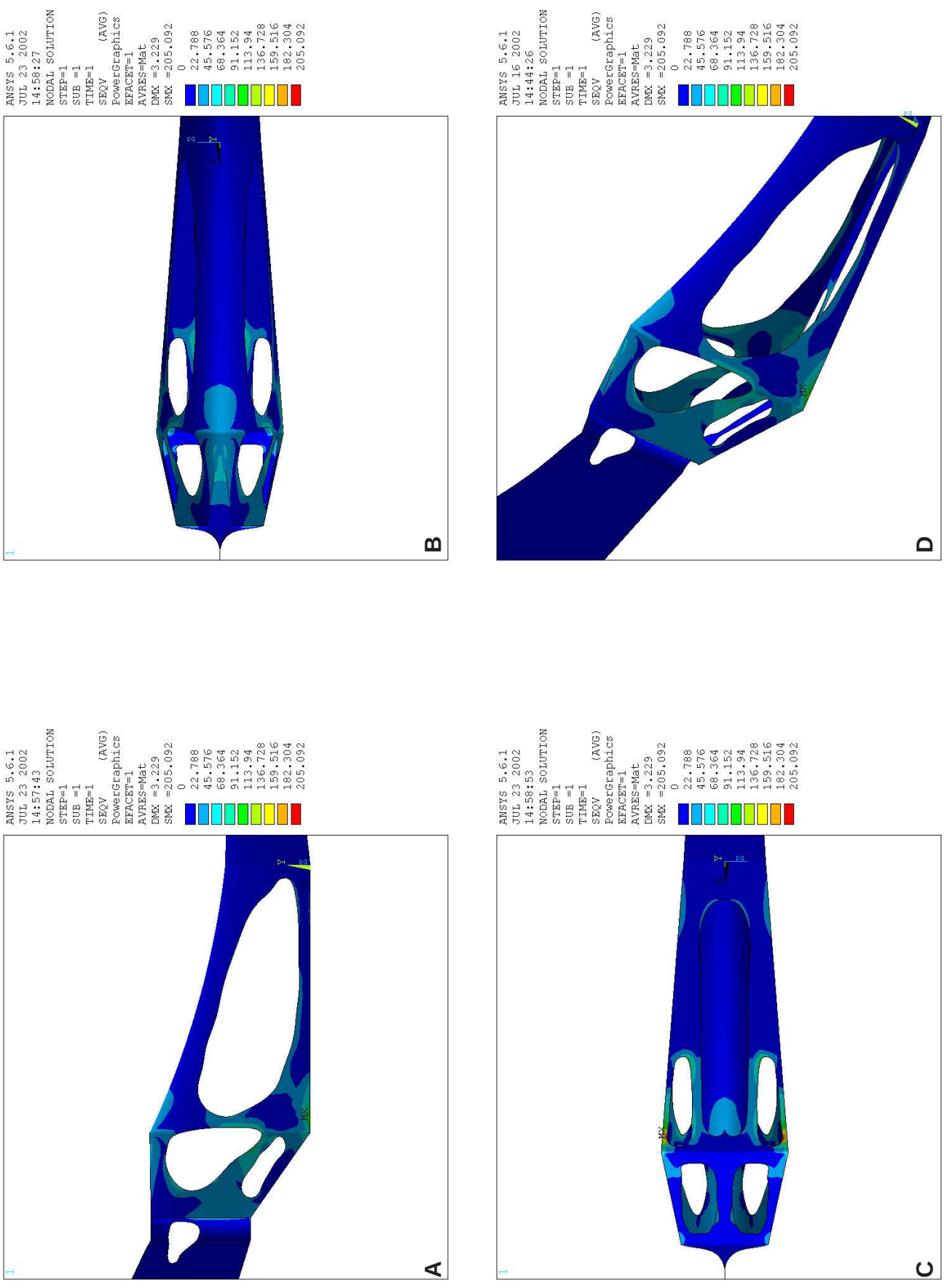

Fig. 8.29: van Mises stress in the FE-model for the *Pteranodon* skull, analysing an anterior bite: A) Detail of right lateral view; B) Detail of dorsal view; C) Detail of ventral view; D) Detail of right dorsolateral view. Same colours mean same level of deformation.

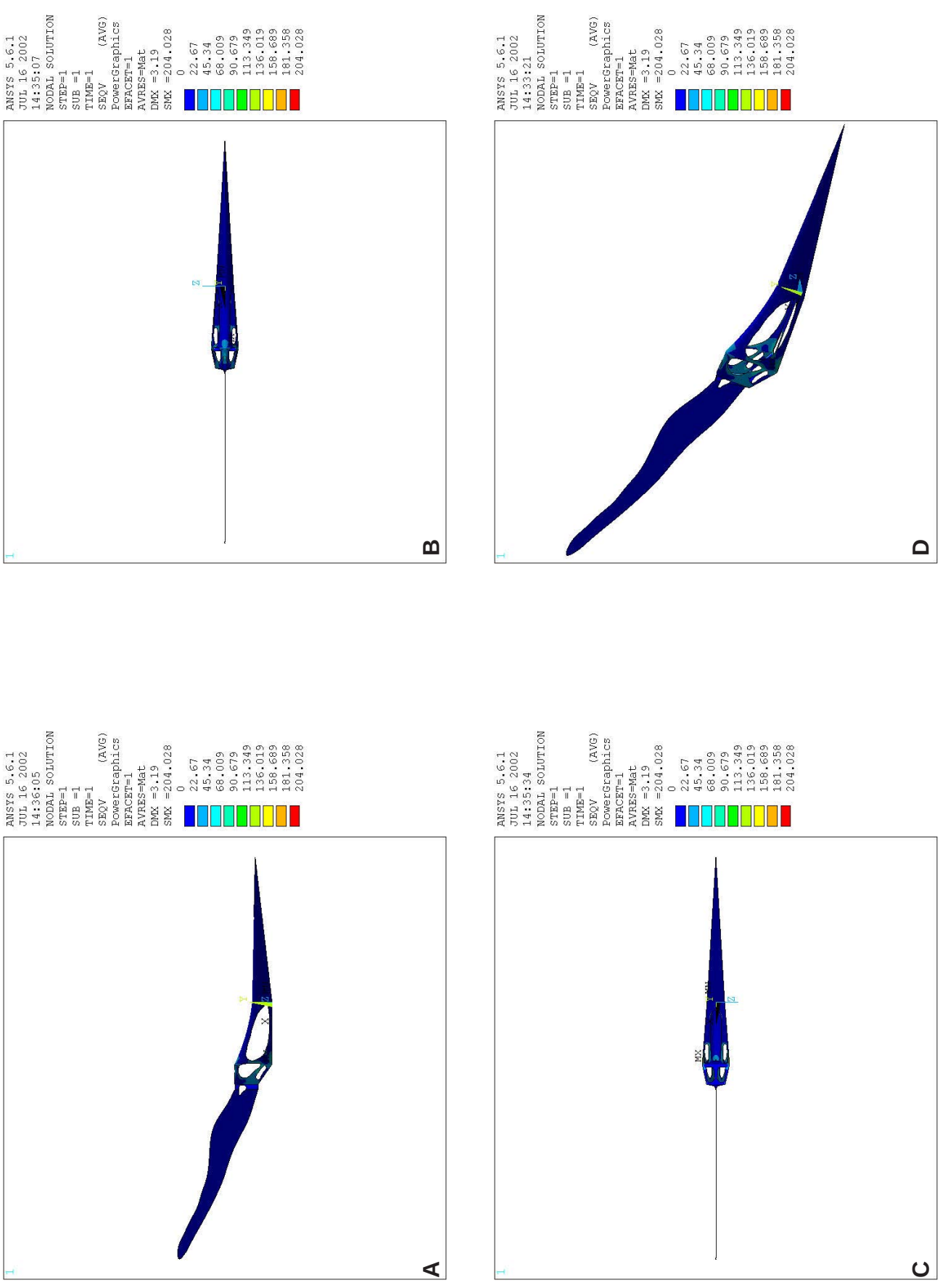

Fig. 8.30: van Mises stress in the FE-model for the *Pteranodon* skull, analysing an posterior bite: A) Right lateral view; B) Dorsal view; C) Ventral view; D) Right dorsolateral view. Same colours mean same level of deformation.

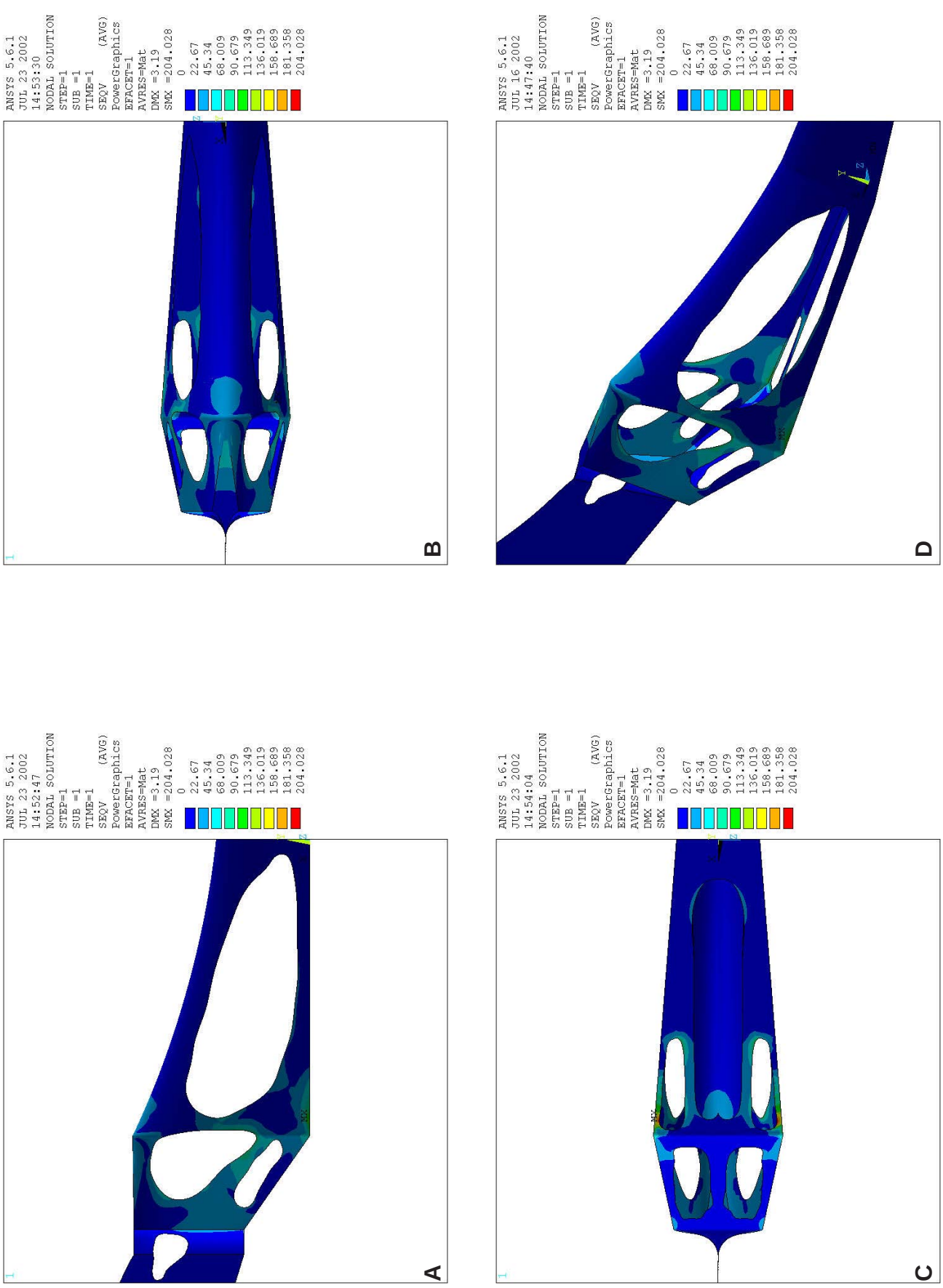

Fig. 8.31: van Mises stress in the FE-model for the *Pteranodon* skull, analysing an posterior bite: A) Detail of right lateral view; B) Detail of dorsal view; C) Detail of ventral view; D) Detail of right dorsolateral view. Same colours mean same level of deformation.

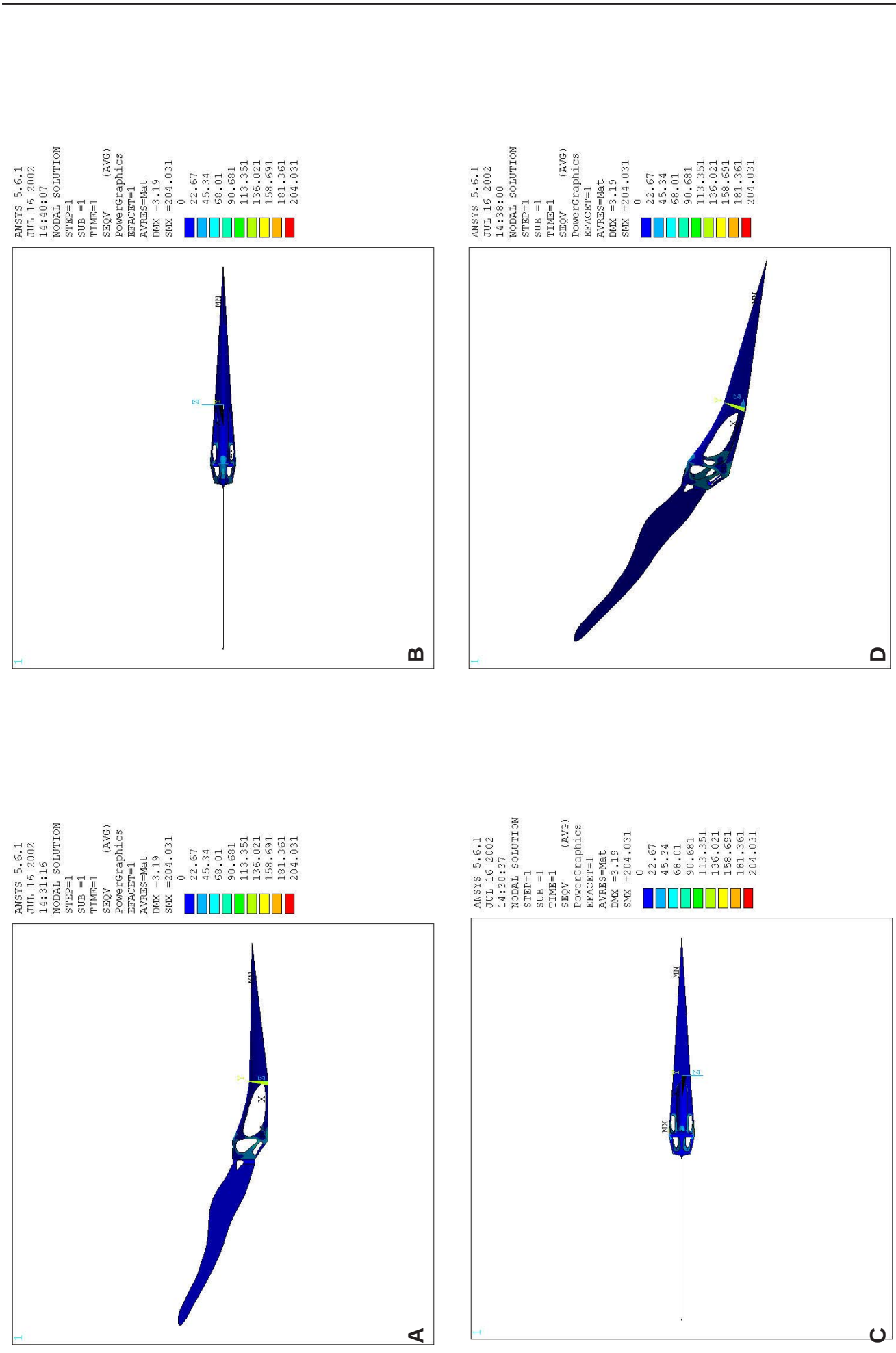

Fig. 8.32: van Mises stress in the FE-model for the *Pteranodon* skull, analysing an bite along the entire lateral margin of the rostrum: A) Right lateral view; B) Dorsal view; C) Ventral view; D) Right dorsolateral view. Same colours mean same level of deformation.

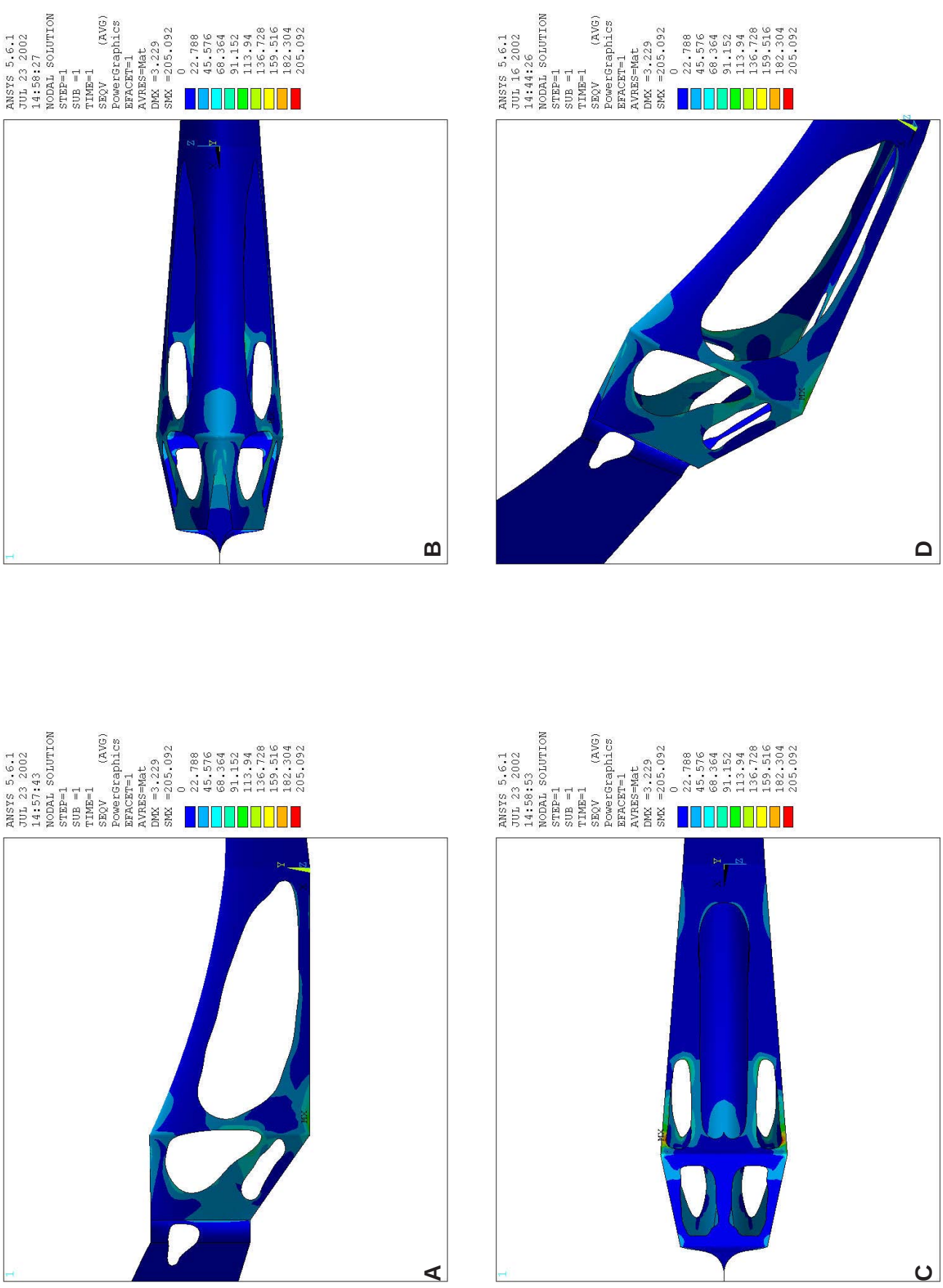

Fig. 8.33: van Mises stress in the FE-model for the Pteranodon skull, analysing a bite along the entire lateral margin of the rostrum: A) detail of right lateral view, B) detail of dorsal view, C) detail of ventral view and D) detail of right dorsolateral view. Same colours mean same level of deformation.

9. DISCUSSION

Based on the mechanical investigations made in the previous chapters, close affinities are present between the different pterosaur tooth and skull constructions. This allows to determine possible transformations between the tooth constructions, leading to an evolutionary pathway diagram of tooth constructions but without irreversible transformations. Likewise, the skull constructions are grouped into certain constructional types, from which major transformations are established. These processes are discussed for their biomechanical consequences and will thus yield conclusive criteria for the functional interpretation of the different constructional levels as well as for the direction of possible evolutionary pathways between the skull constructions/levels. Then pathways are compared to cladograms representing actual views of the phylogenetic systematic of pterosaurs and differences are discussed. Finally, scaling effects of the bite of pterosaurs will be addressed to.

9.1 Possible evolutionary pathways of pterosaur tooth constructions

The possible evolutionary pathways of the pterosaur tooth constructions are based on a monocuspid, conical preconstruction (Fig. 9.1: node A) which represents the typical reptilian tooth pattern (Edmund 1969). All pterosaur tooth constructions described above can be derived from this, partially by multiple evolutionary pathways (Fig. 9.1). Alternatively, the monocuspid preconstruction could be succeeded by a subsequent preconstruction which has three cusps and affinities to certain types of the Eudimorphodon low multicuspid tooth construction.

9.1.1 Main basal pathways

Adding side-cusps to the preconstruction like in the Eudimorphodon low multicuspid tooth construction results in an increase of axial and bending stiffness and thus decrease of axial and bending stress in x-direction (see also Fig. 5.15 & Tab. 9.1). In a next step, the neck of the tooth construction is heightened, exposing the dentine and permitting a deeper penetration into the food item (Fig. 9.1). For axial loads, the dentine neck act as an absorber, because of the higher ultimate compressive strength and lower Young's modulus than enamel. This also prevents high strain rates in the neck due to a bending in z-direction, in which the axial moment of inertia is very low. Adding further side cusps increases the axial stiffness in x-direction while still retaining low bending moments and leads to a greater occlusional surface with the opposing tooth (Fig. 9.1: node B). This allows the tight fixation of even small food items which cannot be penetrated by the tooth construction. A further increase (Fig. 9.1: node B to C) of the crown-height results in the option of a deeper penetration into the food item. In consequence, the bending moments and stress increase. At this level, the EDB begins to curve, leading to a greater flexibility in z-direction which counteracts the higher bending stress in this direction. In the following step, the efficiency of the penetration is increased due to a reduction of the friction by scaling down the side cusps (Fig. 9.1: node C) leading to a monocuspid tooth construction with a well developed EDB (Pterodactylus tooth construction). It is derived either by reducing the side-cusps symmetrically (Eudimorphodon high multicuspid tooth construction) or by the loss of the anterior cusps and slight curvature

Next page: Fig. 9.1: Possible evolutionary pathways of pterosaur tooth constructions and functional implications. Note that the Pterodaustro low tooth construction is omitted from this diagram because of the fragmentary data. A-F: Branching nodes, hypothetical constructions with black background. Double arrow indicates possible reversals. See text for further details.

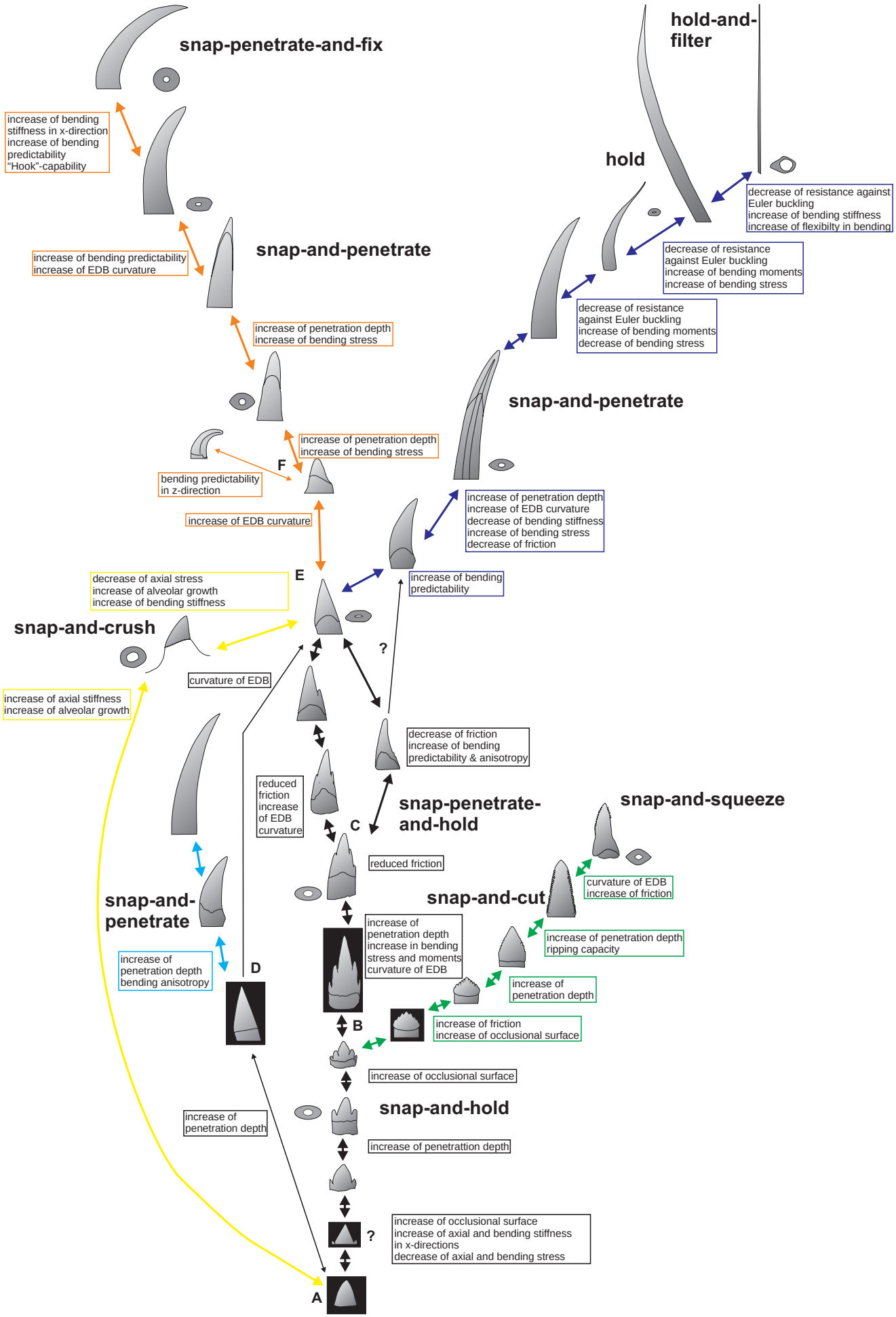
snap-penetrate-and-fix
increase of bending stiffness in x-direction
increase of bending predictability
"Hook"-capability
increase of bending predictability
increase of EDB curvature
snap-and-penetrate
increase of penetration depth
increase of bending stress
F
increase of penetration depth
increase of bending stress
bending predictability in z-direction
increase of EDB curvature
hold-and-filter
hold
decrease of resistance against Euler buckling
increase of bending stiffness
increase of flexibilty in bending
decrease of resistance against Euler buckling
increase of bending moments
increase of bending stress
decrease of resistance against Euler buckling
increase of bending moments
decrease of bending stress
snap-and-penetrate
increase of penetration depth
increase of EDB curvature
decrease of bending stiffness
increase of bending stress
decrease of friction
E
increase of bending predictability
decrease of axial stress
increase of alveolar growth
increase of bending stiffness
snap-and-crush
?
curvature of EDB
increase of axial stiffness
increase of alveolar growth
decrease of friction
increase of bending predictability & anisotropy
reduced friction
increase of EDB curvature
snap-penetrate-and-hold
C
snap-and-squeeze
reduced friction
curvature of EDB
increase of friction
snap-and-cut
snap-and-penetrate
increase of penetration depth
increase in bending stress and moments
curvature of EDB
increase of penetration depth
ripping capacity
increase of penetration depth
bending anisotropy
D
increase of penetration depth
B
increase of friction
increase of occlusional surface
increase of occlusional surface
snap-and-hold
increase of penetration depth
increase of penetrattion depth
?
increase of occlusional surface
increase of axial and bending stiffness
in x-directions
decrease of axial and bending stress
A

of the tooth crown (Eudimorphodon pseudo-monocuspid tooth construction) In both pathways, the bending moments are reduced, but the axial and bending stress increase. The latter effects are counter-acted by the increased curvature of the EDB on the lateral sides of the tooth construction. The level of the Pterodactylus tooth construction is also derived directly via a hypothetical tooth construction (Fig. 9.1: node D) from a mono-cuspid preconstruction by increasing the height of the neck and curvature of the EDB (thin black arrows). Such a hypothetical tooth construction could as well give rise to the Eudimorphodon monocuspid tooth construction (see below).

9.1.2 Lower branching pathways

The Eudimorphodon monocuspid tooth construction cannot be derived from most other pterosaur tooth constructions because the EDB is developed different with a downward curvature on the lateral sides of the tooth construction. This indicates greater flexibility in x-direction than in z-direction. It is derived from the hypothetical tooth construction at node D (Fig. 9.1) by increasing the penetration depth (heightening of the tooth crown and decreasing the apical angle) and the curvature of the tooth construction. It leads to greater bending moments and bending stress but at the same time an increased bending predictability in the anterior x-direction. The reversely curved EDB indicates a lower lateral flexibility in z-direction relative to the typical curved tooth constructions.

At node B (Fig. 9.1) the Eudimorphodon low multicuspid tooth construction is transformed into the serrated Preondactylus tooth construction. This pathway is characterised by high bending stiffness in x as well as z-direction. Heightening of the crown permits a deeper penetration, however, due to the addition of cuspules, the occlusional surface and the penetrational friction is increased. These changes increase the capacity of fracturing fibrous or hard-textured food items (Jeronimidis 1991, Purslow 1991). On the other side, the bending stress and moments increase, while the axial stress decreases. The penetration efficiency is increased by a shifting of the cuspules to the lower parts of the carinae, so that the apex is formed by a single, larger cusp. This reduces the friction in y-direction but retains a high friction in x-direction. In the possible end-construction of this pathway, the lower cuspules are completely reduced and the apical ones are orientated vertically, increasing the penetrational friction drastically. This tooth construction is less capable of piercing and ripping of food items but allows to squeeze food items, which is supported by the low axial stress present in this tooth construction (Fig. 5.15, Tab 5.1). The EDB is curved, resulting in an increased bending stability in z-direction, which counteracts the decrease of bending stiffness in x-direction.

9.1.3 Upper branching pathways

The Pterodactylus tooth construction forms the base for multiple evolutionary pathways (Fig. 9.1: node E). One leads to the Dsungaripterus tooth construction by prolonged alveolar growth. The alveolar bone enfolds the tooth neck, so that the crown is low and broad, resulting in low axial stress. The bending stiffness in x- and z-directions is increased and bending moments and stress are low, because the pulp cavity is wide and the cross-section is nearly circular. This tooth construction is also derived directly from a monocuspid preconstruction by added alveolar growth and geometrical bending.

A second pathway based on the Pterodactylus tooth construction combines the Ornithocheirus tooth constructions (Fig. 9.1: node E). It shows a successive increase in height and decrease of the apical angle leading

to a greater penetration depth. However, the higher the crown is in this pathway, the greater the bending stiffness is. On the other hand, the bending moments and bending stress increase. The latter effect is counteracted in z-direction to a certain degree by the EDB which is situated very high on the tooth-crown. The high bending moments are absorbed in the curved Ornithocheirus high tooth construction which shows a clear bending predictability in anterior x-direction. The end-construction with its 90° curvature in posterior direction not only has the capacity to act as hook but also resists greater lateral forces than the preceding tooth constructions because of its higher bending stiffness in x-direction. Node F (Fig. 9.1) shows the division between this main pathway, and a side-pathway in which the Ornithocheirus low tooth construction gets bent in medial z-direction, resulting in a greater bending predictability for this direction.

The third pathway branching from the Pterodactylus tooth construction leads via the Rhamphorhynchus tooth construction, Gnathosaurus tooth construction, Ctenochasma tooth construction to the Pterodaustro tooth construction (Fig. 9.1: node E). The initial transformational step is the curvature of the tooth construction leading to a better bending predictability in anterior x-direction. The progressive curvature of the EDB allows an increased lateral flexibility, so that the diameter in z-direction can be further reduced, providing less resistance in profile of the tooth construction during penetration. However, a further heightening of the crown like in the Gnathosaurus tooth construction and Ctenochasma tooth construction leads to a decrease in axial stiffness and increase in tendency for Euler buckling, bending stiffness and moments (Fig. 5.15 & Tab. 5.1). Finally, the Pterodaustro high tooth construction has a very low axial stiffness but high bending stiffness and flexibility due to its large height compared with its diameter.

9.1.4 Summary of main processes and functional implications of tooth constructions

The main canalising processes in the basal parts of the evolutionary pathway diagram (Fig. 9.1) are the increase of the occlusional surface by adding of cusps, increasing the holding capacity for a dentition with complete occlusion (–> snap-and-hold). Therefore, even small food items can be snatched. Larger food items, however, generate larger forces and therefore need a firmer hold which could either result from larger adductor muscles or by a deeper penetration of the food. The latter originates from heightening of the tooth crown and reduction of the apical angle (–> snap-penetrate-and-hold). This process results in high bending moments and stress, especially in z-direction. A greater stability against this loading regime is achieved by the typical pterosaurian curvature of the EDB, which in turn permits a stronger lateral compression and therefore less resistance in profile of the tooth construction.

A second process is based on increasing the resistance in x-direction (and therefore the need of larger adductor muscle forces for penetration) by cuspules and serrated carinae. This permits a higher cutting efficiency of fibrous and hard-textured food items (–> snap-and-cut). This pathway ends in a fork-like tooth construction which has a rather low cutting capacity in x-direction but a high cutting capacity in y-direction with a low penetration depth (–> snap-and-squeeze). Analogue to this, the main direction of the forces in the Dsungaripterus tooth construction are also orientated in y-direction. The low apical angle and height of the tooth construction prevents a deep penetration of the food item. Due to the low axial stress and low tendency for Euler buckling it permits to put large loads on the food item (–> snap-and-crush).

In the upper parts of the evolutionary pathway diagram, the penetration depth is further increased (–> snap-and-penetrate). As a consequence, the bending moments and stress in x and z-direction increase. This

is accompanied by an increased height of the curvature of the EDB and of the overall tooth constructions, leading to a greater bending stability in anterior x-direction. As a consequence, the movements of the food items in anterior direction are restricted, especially in the tooth constructions with 90° curved tooth crowns (–> snap-penetrate-and-fix). In the second pathway leading to the Ctenochasma tooth construction, the axial stiffness and the resistance against Euler buckling decrease so that the penetrational capability of these high tooth construction gets low. Instead, bending loads due to perpendicular loads are more important as indicated by the great flexibility of the Pterodaustro tooth construction in x and z-direction (–> hold/hold-and-filter).
In contrast to these rather constraining processes, the variation in bending stiffness in x-direction, demonstrates that the diameter in x-direction as well as the expansion of the pulp cavity are highly variable and may show several reversals.

9.2 Categorisation of skull constructions

The skull constructions listed in chapter 7 are grouped in 24 major constructional types, based on their architecture, biomechanical behaviour of the teeth and skull (see Figs.A.345-A.359 in Appendix B for definitions of the criteria for relativity). Whereas some skull categories are represented by a single skull construction, others comprise a number of skull constructions in which the differences between individual skull constructions are not significant (see also Tab A.85 in Appendix B for summary).

9.2.1 Angustinaripterus constructional type (AngusCT)

Included skull constructions: Angustinaripterus, Parapsicephalus
Main characteristics: relatively large antorbital fenestra and naris which are situated in the posterior two thirds of the rostrum, jugal/lacrimal bar between antorbital fenestra and naris orientated slightly oblique, crest absent, obliquely orientated occipital region (50°-55°), tooth row ranging from anterior end of rostrum to posterior end of antorbital fenestra, consisting of Rhamphorhynchus tooth constructions (assumed here for Parapsicephalus skull construction), rostrum long (low basal height to length ratio), medium basal width (medium basal height to width ratio), medium F_B, high to medium F_J, orientated from -40° to -50°, high maximum bending moments, low to medium bending stress, low shear and comparison stress, high average twistiness to bendiness ratio.

9.2.2 Anurognathus constructional type (AnuroCT)

Included skull constructions: Anurognathus, Batrachognathus, Jeholopterus
Main characteristics: relatively large antorbital fenestra and naris which are nearly similar sized to rostrum, jugal/lacrimal bar between naris and antorbital fenestra orientated vertically, crest absent, obliquely orientated occipital region (55°), tooth row ranging from anterior end of rostrum to posterior end of antorbital fenestra, consisting of Pterodactylus tooth construction, rostrum very short (very high basal height to length ratio), large basal width (low basal height to width ratio), high F_B, medium F_J, orientated from -37° to -40°, high maximum bending moments, low anterior bending stress, very low anterior shear and comparison stress, high average twistiness to bendiness ratio.

9.2.3 Azhdarchidae constructional type (AzdarchCT)

Included skull constructions: Quetzalcoatlus, Zheijangopterus

Main characteristics: relatively medium-sized nasoantorbital fenestra which is situated in the posterior half of the rostrum, medial bony crest obligatory present, rostrum straight to ventrally bent, obliquely orientated occipital region (25-35°), edentulous with keratinous beak, rostrum long (low basal width to height ratio), low basal width (high basal height to width ratio), low F_B, high F_J, orientated from -40 to -45°, medium to high maximum bending moments, very high bending, shear and comparison stress, very low to low average twistiness to bendiness ratio.

9.2.4 Cacibupteryx constructional type (CaciCT)

Included skull construction: Cacibupteryx

Main characteristics: relatively small antorbital fenestra and naris which are situated in the posterior half of the rostrum, jugal/lacrimal bar between antorbital fenestra and naris orientated oblique, bony crest absent, vertical orientated occipital region (85°), tooth row ranging from anterior end of rostrum to posterior end of antorbital fenestra, tooth constructions unknown, rostrum of medium length (medium basal height to length ratio), medium basal width (medium basal height to width ratio), high F_B, low F_J, orientated about -52°, very high maximum bending moments, very high bending stress, high shear stress, medium comparison stress, high average twistiness to bendiness ratio.

9.2.5 Campylognathoides constructional type (CampCT)

Included skull construction: Campylognathoides

Main characteristics: relatively large antorbital fenestra and naris which are situated in the posterior two thirds of the rostrum, jugal/lacrimal bar between antorbital fenestra and naris orientated obliquely, bony crest absent, slightly obliquely orientated occipital region (55°), tooth row ranging from anterior end of rostrum to posterior end of antorbital fenestra, consisting of Pterodactylus tooth construction, rostrum short (high basal width to height ratio) and anteriorly with keratinous cover, medium basal width (medium basal height to width ratio), high F_B, low F_J, orientated about -43°, high maximum bending moments, high bending, shear and comparison stress, high average twistiness to bendiness ratio.

9.2.6 Cearadactylus constructional type (CearaCT)

Included skull construction: Cearadactylus

Main characteristics: relatively medium-sized nasoantorbital fenestra which is situated in the posterior half of the rostrum, bony crest absent, obliquely orientated occipital region (20°), tooth row consisting of Ornithocheirus tooth construction and restricted to the anterior fifth of the rostrum, rostrum long (low basal width to height ratio) and festooned, medium basal width (medium basal height to width ratio), medium F_B, high F_J, orientated about -40°, high maximum bending moments, medium bending stress, low shear and comparison stress, high average twistiness to bendiness ratio.

9.2.7 Ctenochasma constructional type (CtenoCT)

Included skull construction: Ctenochasma

Main characteristics: relatively small nasoantorbital fenestra which is situated in the posterior fifth part of the rostrum, bony crest absent, soft-tissue crest optional, obliquely orientated occipital region (25°), tooth row ranging from anterior end of rostrum to posterior end of nasoantorbital fenestra of Ctenochasma tooth construction, rostrum very long (low basal width to height ratio), medium basal width (medium basal height to width ratio), low F_B, high F_J, about -40°, high maximum bending moments, low bending stress, medium shear stress, medium comparison stress, very high average twistiness to bendiness ratio.

9.2.8 Dimorphodon constructional type (DimoCT)

Included skull constructions: Dimorphodon, Peteinosaurus

Main characteristics: relatively large antorbital fenestra and naris which are nearly similar sized to rostrum, jugal/lacrimal bar between naris and antorbital fenestra orientated vertically, bony crest absent, slightly obliquely orientated occipital region (75°-77°), tooth row ranging from anterior end of rostrum to posterior end of antorbital fenestra, consisting of Pterodactylus tooth construction, convex dorsal outline of skull construction, rostrum short (high basal height to length ratio), medium basal width (medium basal height to width ratio), high F_B, very low F_J, orientated about -50°, high maximum bending moments, medium anterior bending, shear and comparison stress, low average twistiness to bendiness ratio.

9.2.9 Dsungaripterid constructional type (DsungCT)

Included skull constructions: Dsungaripterus, Phobetopter

Main characteristics: relative medium-sized nasoantorbital fenestra which is situated in posterior half of rostrum, medial and orbitotemporal crest present, possibly combined with a soft-tissue crest, linking the bony crests, obliquely orientated occipital region (35°-45°), edentulous anterior rostrum with keratinous beak, tooth row situated posteriorly in the rostrum, consisting of Dsungaripterus tooth construction, orbita circular and situated posterodorsal to nasoantorbital fenestra, rostrum of medium length (medium basal height to length ratio), low basal width (high basal height to basal width ratio), medium F_B, high F_J, orientated from -55° to -48°, medium to high anterior bending moments, very high anterior bending and comparison stress, low to medium anterior shear stress, low average twistiness to bendiness ratio.

9.2.10 Eudimorphodon constructional type (EudiCT)

Included Skull construction: Eudimorphodon

Main characteristics: relatively medium-sized antorbital fenestra and naris, which are situated in the posterior half of the rostrum, jugal/lacrimal bar between antorbital fenestra and naris orientated steeply oblique, bony crest absent, slightly obliquely orientated occipital region (70°), tooth row of Eudimorphodon tooth constructions, rostrum short (high basal width to height ratio), medium basal width (medium basal height to width ratio), high F_B, medium F_J, orientated about -45°, high maximum bending moments, high bending stress, medium shear and comparison stress, high average twistiness to bendiness ratio.

9.2.11 Gallodactylus constructional type (GalloCT)

Included skull construction: Gallodacytlus

Main characteristics: relatively medium-sized nasoantorbital fenestra which is situated in the posterior half of

the rostrum, bony crest absent, obliquely orientated occipital region (40°), tooth row of Ornithocheirus high (anterior) and low (posterior) tooth construction, restricted to anterior fifth part of rostrum, rostrum long (low basal width to height ratio), medium basal width (medium basal height to width ratio), medium F_B, medium F_J, orientated about -37°, high maximum bending moments, medium bending, shear and comparison stress, high average twistiness to bendiness ratio.

9.2.12 Gnathosaurus constructional type (GnathoCT)

Included skull constructions: Gnathosaurus, Plataleorhynchus

Main characteristics: relatively small nasoantorbital fenestra which is situated in the posterior third of the rostrum, medial bony crest present, obliquely orientated occipital region (20°), tooth row of Gnathosaurus tooth construction ranging from the anterior end of the rostrum till anterior border of nasoantorbital fenestra, rostrum very long (low basal width to height ratio) and anteriorly expanded, medium basal width (medium basal height to width ratio), low F_B, high F_J, about -30°, high maximum bending moments, low bending stress, low to medium shear stress, medium comparison stress, very high average twistiness to bendiness ratio.

9.2.13 Huanhepterus constructional type (HuanCT)

Included skull construction: Huanhepterus

Main characteristics: relatively small nasoantorbital fenestra which is situated in the posterior third of the rostrum, medial bony crest present, obliquely orientated occipital region (10°), tooth row of Rhamphorhynchus tooth construction restricted to the anterior third of the rostrum, rostrum long (low basal width to height ratio), medium basal width (medium basal height to width ratio), low F_B, high F_J, about -40°, very high maximum bending moments, high bending stress, low shear stress, medium comparison stress, low average twistiness to bendiness ratio.

9.2.14 Istiodactylus constructional type (IstioCT)

Included skull construction: Istiodactylus

Main characteristics: relatively large nasoantorbital fenestra which is nearly similar sized to rostrum, bony crest absent, obliquely orientated occipital region (30°), tooth row of Ornithocheirus low tooth construction restricted to the anterior quarter of the rostrum, rostrum long (low basal width to height ratio) and rounded anteriorly in ventral view, medium basal width (medium basal height to width ratio), medium F_B, high F_J, about -32°, medium maximum bending moments, low bending stress, high shear stress, medium comparison stress, high average twistiness to bendiness ratio.

9.2.15 Ornithocheirid constructional type (OrnithoCT)

Included skull constructions: Anhanguera, Coloborhynchus, Criorhynchus, Ludodactylus, Santanadactylus

Main characteristics: relatively medium-sized nasoantorbital fenestra which is situated in the posterior half of the rostrum, anterior or orbitotemporal crest optional, obliquely orientated occipital region (20°-33°), tooth row ranging from anterior end of rostrum to posterior end of antorbital fenestra consisting of Ornithocheirus high (anterior) and low (posterior) tooth constructions, rostrum long (low basal height to length ratio), large to average basal width (low to medium basal height to width ratio), low F_B, high F_J, orientated from -30° to -40°,

average to high maximum bending moments, low bending stress, very low shear and comparison stress, low twistiness to bendiness ratio in crested regions of the rostrum, otherwise high twistiness to bendiness ratio.

9.2.16 Preondactylus constructional type (PreonCT)

Included skull constructions: Austriadactylus, Preondactylus

Main characteristics: relatively large antorbital fenestra and naris, which are situated in the posterior two thirds of the rostrum, jugal/lacrimal bar between antorbital fenestra and naris orientated steeply oblique, bony crest absent, medial soft-tissue crest optional, slightly obliquely orientated occipital region (55°-58°), tooth row of Preondactylus tooth construction and partially anteriorly of Eudimorphodon monocuspid tooth construction, rostrum of medium length to short (medium to high basal width to height ratio), medium basal width (medium basal height to width ratio), high F_B, medium F_J, orientated from -45° to -50°, high maximum bending moments, high bending and shear stress, medium to high comparison stress, high average twistiness to bendiness ratio.

9.2.17 Pteranodontid constructional type (PteranoCT)

Included skull constructions: Pteranodon, Nyctosaurus

Main characteristics: relatively small nasoantorbital fenestra which is situated in the posterior fifth of the rostrum, orbitotemporal bony crest obligatory present, obliquely orientated occipital region (12°-32°), edentulous with keratinous beak, rostrum long (low basal width to height ratio) and narrow (medium to high basal height to width ratio), low F_B, high F_J, orientated from -35° to -50°, low to medium maximum bending moments, very high bending, shear and comparison stress, low average twistiness to bendiness ratio in Pteranodon skull construction, high in Nyctosaurus skull construction.

9.2.18 Pterodactylus constructional type (PteroCT)

Included skull constructions: Germanodactylus, Pterodactylus antiquus, Pt. elegans, Pt. kochi, Pt. micronyx

Main characteristics: relatively medium-sized nasoantorbital fenestra which is situated in the posterior half of the rostrum, medial bony crest present in Germanodactylus skull construction, soft-tissue crest possibly present in all five skull constructions, soft-tissue orbitotemporal spline possibly present, obliquely orientated occipital region (12°-30°), keratinous hook (Pterodactylus skull construction) or beak (Germanodactylus skull construction) present on anterior rostrum, tooth row consisting of Pterodactylus tooth construction and ranging from the post-beaked rostrum to the posterior end of the nasoantorbital fenestra (Germanodactylus skull construction) to restricted to the anterior third of the post-beaked rostrum (Pt. elegans skull construction), rostrum of medium length to long (medium to low basal height to length ratio), large to medium basal width (low to medium basal height to width ratio), low to medium F_B, high F_J, orientated from -20° to -35°, medium to high maximum bending moments, bending, shear and comparison stress, high average twistiness to bendiness ratio.

9.2.19 Pterodaustro constructional type (PterodauCT)

Included skull construction: Pterodaustro

Main characteristics: relatively small nasoantorbital fenestra which is situated in the posterior sixth of the

rostrum, bony crest absent, obliquely orientated occipital region (30°), tooth row of Pterodaustro tooth construction (see chapters 5.2.10-5.2.11 for more detailed description on Pterodaustro tooth construction and differences between upper and lower jaw), rostrum very long (very low basal width to height ratio), medium basal width (medium basal height to width ratio), low F_B, high F_J, about -40°, high maximum bending moments, low bending stress, low to medium shear stress, medium comparison stress, very high average twistiness to bendiness ratio.

9.2.20 Rhamphorhynchus constructional type (RhamCT)

Included skull construction: Rhamphorhynchus

Main characteristics: relatively small antorbital fenestra and naris, which are situated in the posterior third of the rostrum, jugal/lacrimal bar between antorbital fenestra and naris orientated slightly oblique, bony crest absent, obliquely orientated occipital region (40°), tooth row of Rhamphorhynchus tooth construction, rostrum of average length (medium basal width to height ratio) and covered with keratinous rhamphotheca, average basal width (medium basal height to width ratio), medium F_B, high F_J, orientated about 43°, medium maximum bending moments, high bending stress, medium shear stress, high comparison stress, high average twistiness to bendiness ratio.

9.2.21 Scaphognathus constructional type (ScaphoCT)

Included skull constructions: Dorygnathus, Scaphognathus

Main characteristics: relatively large antorbital fenestra and naris, which are situated int eh posterior two thirds of the rostrum, jugal/lacrimal bar between antorbital fenestra and naris orientated oblique, bony crest absent, slightly obliquely orientated occipital region (60°-65°), tooth row of Rhamphorhynchus tooth construction, rostrum short (high basal width to height ratio), medium basal width (medium basal height to width ratio), high F_B, medium F_J, orientated from -47° to -49°, high maximum bending moments, medium bending stress, medium to high shear stress, low to high comparison stress, high average twistiness to bendiness ratio.

9.2.22 Sordes constructional type (SordCT)

Included skull construction: Sordes

Main characteristics: relatively small antorbital fenestra and naris, which are situated in the posterior third of the rostrum, jugal/lacrimal bar between antorbital fenestra and naris orientated oblique, bony crest absent, slightly obliquely orientated occipital region (40°), tooth row of Pterodactylus tooth construction, rostrum of average length (medium basal width to height ratio), large basal width (low basal height to width ratio), medium F_B, low F_J, orientated about -47°, high maximum bending moments, medium bending, shear and comparison stress, high twistiness to bendiness ratio

9.2.23 Tapejarid constructional type (TapeCT)

Skull constructions: Tapejara, Sinopterus

Main characteristics: relatively large nasoantorbital fenestra, which is situated in the posterior two thirds of the rostrum, bony crest present anteriorly and continuing into orbitotemporal region as spline parallel to blunt orbitotemporal crest (spline absent in *T. navigans*), soft tissue crest present from the antorbital to orbitotem-

poral region dorsal to bony crest, obliquely orientated occipital region (45°-50°), edentulous with keratinous beak, rostrum short (high basal width to height ratio), low basal width (high basal height to width ratio), medium to high F_B, high F_J, orientated about 40°, very high maximum bending moments in Sinopterus skull construction, low in Tapejara skull construction, high bending, shear and comparison stress, low to very low twistiness to bendiness ratio.

9.2.23 Tupuxuarid constructional type (TupCT)

Included skull constructions: Thalassodromeus, Tupuxuara

Main characteristics: relatively large nasoantorbital fenestra which is situated in the posterior two thirds of rostrum, bony crest reaching from the anterior tip of the rostrum to the orbitotemporal region, continuing dorsally into a soft-tissue crest, obliquely orientated occipital region (40°-50°), edentulous with keratinous beak, rostrum of medium length (medium basal height to length ratio), low basal width (high basal height to basal width ratio), medium F_B, high F_J, orientated from -42° to -51°, low to medium anterior bending moments, high bending, shear and compressive stress, low average twistiness to bendiness ratio.

9.3 Transformation processes

By comparing the different skull constructions, the following variations are observed:

- longirostrine *versus* brevirostrine skull constructions
- vertically *versus* obliquely orientated occipital regions
- antorbital fenestra with separate naris vs. nasoantorbital fenestra
- tooth row ranging from anterior end of rostrum to posterior end of antorbital fenestra vs. reduced dentition or edentulous jaws with keratinous rhamphotheca
- non-crested *versus* crested skull constructions
- soft tissue crests *versus* bony crests
- non-curved *versus* curved jaws

These observations will be discussed here for their mechanical consequences, because they will yield information on possible transformation processes.

9.3.1 Longirostrine *versus* brevirostrine jaws

Based on lever mechanics (see chapter 6.2), a direct relation exists between rostral length and the bite force F_B. The longer the rostrum is, the lower values for F_B will result at the anterior tip of the jaw, if the muscular configuration is set constant. This relation also depends on the attachment angle of the adductor muscles (= angle of the muscles forces) and orientation of the occipital region, which varies between the different skull constructions. The result, therefore, is a more scattered relation, than for the simple relation mentioned above (Fig. 9.2). The lowest values for F_B occur in the Pteranodon skull construction, the highest in the brevirostrine Jeholopterus skull construction. The Batrachognathus, Anurognathus and Tapejara skull constructions are similar to the latter as far as the length of the rostra are concerned. Their bite forces, however, are different due to the different angles of the jaw muscle forces. This relation also accounts for the fact that although the Pterodaustro skull construction has the longest rostrum of all pterosaur skull constructions, it shows a higher F_B than the shorter Pteranodon skull construction.

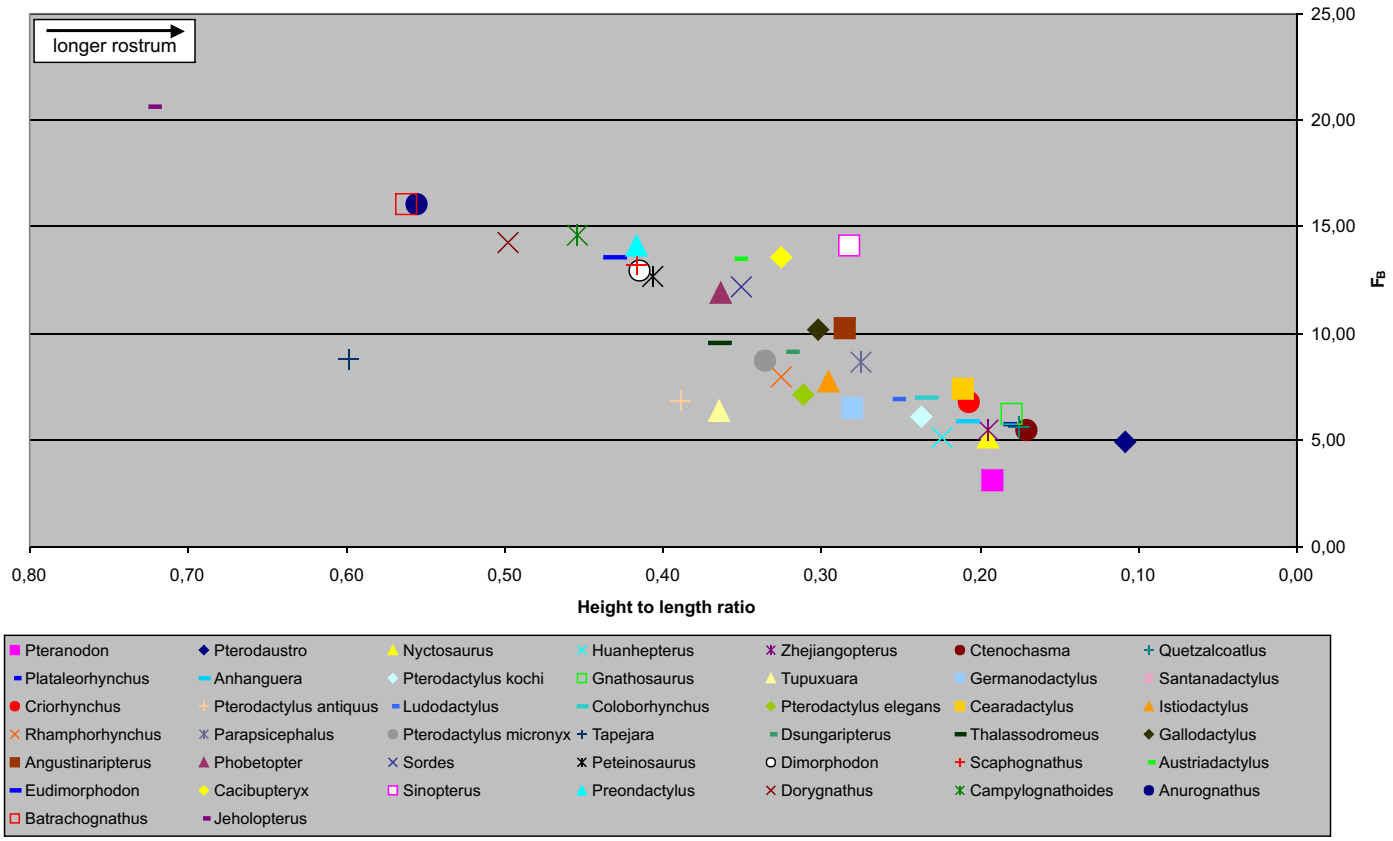

Fig. 9.2: Illustration of relationship between height to length ration and bite force F_B for the investigated skull constructions. Note decreasing bite force F_B with increasing length of the rostrum.

A further consequence of an elongated rostrum is an increase of the resulting joint reaction force, F_J. Like F_B, this relation is influenced by the different orientations of the occipital region (e.g. Dimorphodon constructional type vs. Scaphognathus constructional type). The values of F_J, however, vary only about 5% for all skull constructions. This value is even lower in cases of a bite at the level of half of the rostral length.

For all skull constructions considered in this study, F_J does exceed F_B multiple time. The ratio between both forces is the highest in the Jeholopterus skull construction where F_J is ten times higher than F_B. This pattern is similar to the one observed in *Caiman* (Cleuren et al. 1995 , Sinclair & Alexander 1987) and corresponds to the analysis by FEM (see chapter 8), in which the major stress concentrations occur at the region of the lower jaw articulation and not at the anterior end of the rostrum.

The length of the rostrum also determines the velocity of jaw occlusion (Fig. 9.3). No quantitative electromyography is possible on pterosaur jaw muscles, because of the lack of biological data in the fossil record. Therefore, this approach has to rely on the assumptions that all muscles are considered to be fully active and thus act simultaneously. However, it is obvious, that these assumptions are questionable (De Vree & Gans 1994). In the pterosaur skull construction, a shift in mechanical advantage is present during closing of the jaws, starting from the MPTA via the MPTP to the MAME/P and MPST in the final closing stage (see chapter 9.3.2 for explanation) This pattern results in a complex dynamic rather than a static jaw closing system, with different activation times for each muscle group. The consequences of an elongated rostrum, however, are identical whether such a dynamic or a more simplified, static system is analysed. This is caused by the fact, that jaw closing muscles of the same muscular architecture contract in the same time independent of the length of the rostrum (for alteration of muscular architecture leading to different contraction times see chapter 9.3.2). Therefore, a longirostrine jaw closes in the same time as a short rostrum does. Assuming an identical gaping

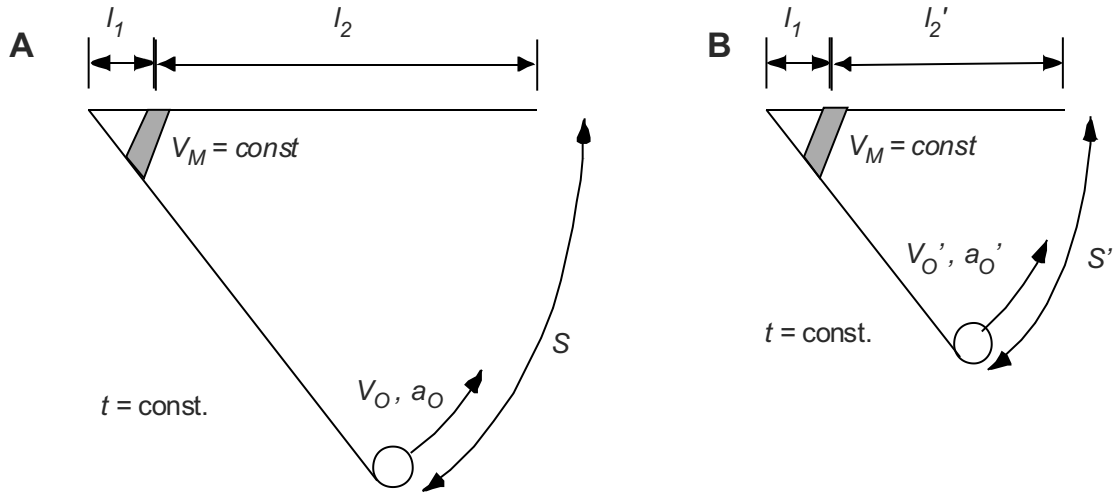

Fig. 9.3: Illustration of relationship between rostral length and acceleration of jaws: A) Short jaw with l_1=moment arm of muscle (force arm), l_2=moment arm of load (load arm), v_M = shortening velocity of muscle, t = shortening time of muscle, s = way of the anteriormost point of the lower jaw till closure of jaws, v_o = velocity of food item, a_o = acceleration of food item; B) Same situation as in A) but $l_2' < l_2$ leading to $s' < s$ and $v_o', a_o' < v_o, a_o$.

angle, however, a point at the anterior end of a longirostrine lower jaw has to be moved a relatively longer way than in the brevirostrine jaw because of its greater distance to the jaw articulation (Fig. 9.3). In consequence, such a point will be subject to an increased acceleration (Currey 2002) and the jaws will close faster relative to brevirostrine jaws (but still at the same time). For such longirostrine, high-accelerated jaw constructions, the main position for prey-grasping is shifted to the anterior end of the jaws because this is the place of the highest velocity/acceleration on the lower jaw. Special structures (e.g. enlarged teeth, lateral expansion of the anterior end of the rostrum, beaks) can be expected here to increase the grasping efficiency. The acceleration is less important in brevirostrine jaws and this position may be situated anywhere along the whole dentition or even be concentrated in their posterior part where the highest values for F_B are reached.

Furthermore, the acceleration of the lower jaws may be increased by storing elastic energy in the rami of the lower jaw during jaw opening and release during the closing process. This is the case for jaws with helical jaw articulations, present in pterodactyloid skull constructions and therefore in most longirostrine pterosaurs. Abduction of the lower jaw leads to the elastic spreading of both mandibular rami by a ventrolateral bulging. If the tonus of the depressor musculature is decreased, the rami unbend and release the stored energy as acceleration of the lower jaw.

Two further specialisations of longirostrine jaws are known from avian feeding mechanisms (Zweers 1991). The first is lengthening of the jaws for improved penetration of small holes or a viscous substrate. Again, the anterior end of the jaws plays a major role for grasping of prey items here. However, reducing the drag coefficient, i.e. reduction of the cross-sectional area, is necessary for ensuring the efficiency (= reduced compressional forces along the jaws) of such a structure, thus allowing penetration of small holes or viscous substrate (Stark 1979).

The second specialisation in birds relates to the filter-feeding (Zweers 1991). In combination with some sort of jaw rim filter device, longirostrine jaws will increase filter capacity along the jaw rami due to an enlarged filter area (although this is hard to quantify in absolute terms). In avians, such filter devices exist in form of a number a small notches and lamellar systems in the keratinous beaks of certain bird species, e.g. Anatidae (Hildebrand & Goslow 2004). For pterosaur skull constructions two options are possible, either the

development of notches on the anterior part of rhamphotheca similar to birds or by an increased number of teeth. So far large keratinous beaks in pterosaurs are mostly documented by impressions on the bones. Frey et al. (2003c), however, report interdigitating ridges from the rhamphotheca of a specimen of *Tapejera*. The second option is present in the Pterodaustro, Ctenochasma, Huanhepterus and Gnathosaurus skull construction and possibly in the Istiodactylus skull construction. Transitional stages between these options may be possible but lack the direct evidence of a notched or lamellar keratinous rhamphotheca.

9.3.2 Inclination of occipital region

A number of skull constructions possess occipital regions which are obliquely orientated in posterodorsal/anteroventral direction. In some skull constructions these regions approach nearly horizontal conditions with an occipital angle of about 10° (e.g. Huanhepterus skull construction), whereas others are nearly vertically orientated (e.g. Cacibupteryx or Dimorphodon skull construction type). This difference in orientation has consequences for the architecture of the adductor and abductor muscles and their force output. These muscles usually have the greatest mechanical advantage when their inserting tendon forms a rectangular angle with the lower jaw (Currey 2002, S. Vogel 2003). This relationship is deduced from lever mechanics (see chapter 3.3.3), because for an angle α between tendon and lower jaw of 90° $\sin\alpha$ reaches its maximum value of 1, and the muscle can transfer a maximum of its force (e.g. the MPST and MAME/P in occluded jaws of some skull constructions). All angles lower than 90° will lead to a lower mechanical advantage[3].

In pterosaurs, a low mechanical advantage is seen in the M. pterygoideus, where both compartments insert at an oblique angle at the lower jaw. However, this is only true for occluded jaws and different if the initial state of the closing cycle with wide opened jaws is analysed (see reconstruction of muscles in chapter 6 and Fig. 6.10). Considering an average gaping angle of about 25° to a theoretical maximum amount of 40°, it is apparent, that lower jaw and M. pterygoideus form a first class lever system with a high mechanical advantage. The more the jaw occlude, the less this mechanical advantage gets. In contrast to this, the third class lever systems between the jaw and the MAME/P respectively MPST show an increase of the mechanical advantage during occlusion. Most pterosaur skull constructions, however, have an obliquely orientated occipital region, resulting in a low mechanical advantage of the latter muscles. Especially in longirostrine skull constructions, there is a strong tendency for such an inclination (Fig 9.4), whereas, the shorter the rostrum is, the more do both muscles approach the mechanical optimum of an angle α of 90°.

To understand the effect of inclination of the occipital region, the previous discussion of elongated jaws (see chapter 9.3.1) will contribute. The latter were interpreted in the light of an increased closing velocity and acceleration of the jaws. This process is amplified by increasing the moment arm of the muscles relative to the jaw joint due to elongation of the muscles. By doing so, a high initial acceleration and velocity is produced, leading to a high average velocity of the lower jaw (Currey 2002).

Three options are possible to elongate a muscle in the orbitotemporal skull region. The first is to increase the height of the skull. However, this would lead to an increase of drag, which is disadvantageous during flight. The second is to keep the height of the skull constant but to shift the insertion area of the adductor muscles at the orbitotemporal region in posterodorsal direction, leading to an inclined occipital region. This results in a low mechanical advantage and lower forces relative to the first option. Looking at the pterosaur

3 Note that this relation considers only the relation between tendon and lower jaw, NOT the different direction of muscle fibres at the insertion e.g. in the upper temporal fenestra.

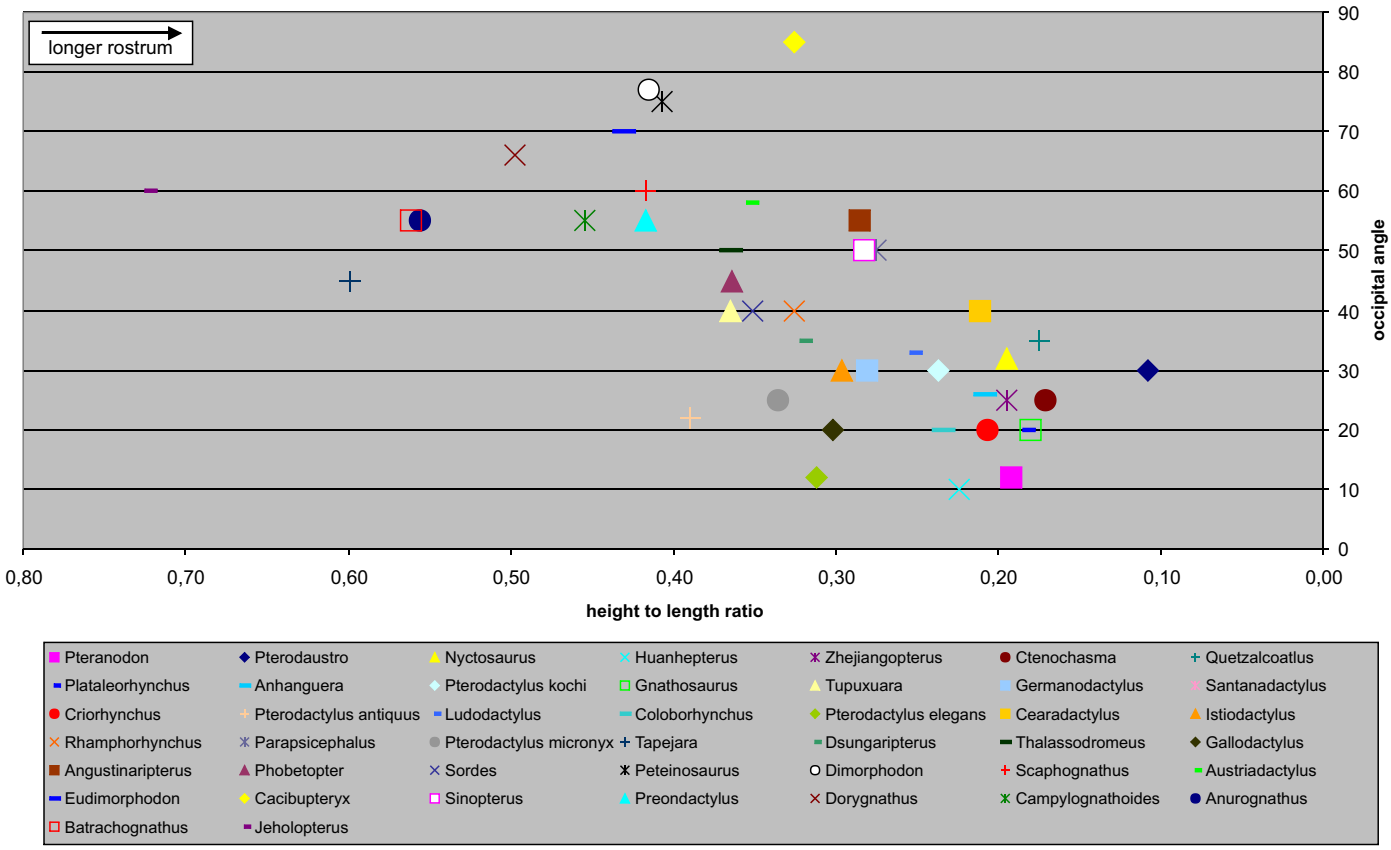

Fig. 9.4: Illustration of relationship between height to length ration and occipital angle for the investigated skull constructions. Note tendency of lower occipital angle with increasing length of the rostrum.

skull constructions the main constraints seem to favour the second option. In some skull constructions with a bony orbitotemporal crest, the length of the orbitotemporal muscles may even have been increased by extending the attachment area onto the basal parts of the crest. The third option is to arrange a muscle as a pulley. This is present in case of the MPTA (see reconstruction in chapter 6), where the posteroventral ridge of the retroarticular process acts as a deflection pulley. A similar pulley system is not present in other pterosauria jaw adductor muscles

Elongated muscles show a disadvantage for the amount of force production: during shortening, the force that such a muscle can apply, will fall off, caused by the relative shorter sarcomeres than in short muscles (Currey 2002). In the graph of the Hill equation, giving the relation between velocity and load of a muscle, the muscle will rapidly “slide” down the curve (Currey 2002). However, as muscles are composed of a large numbers of individual muscle fibres, a broad range of fibre directions is possible at the attachment area, especially when the latter is as large as that of the MPST in the upper temporal fenestra. Assuming a time-dependant cascade of activation of individual fibres from anterior to posterior in the MPST and possibly the MAME/P, may partially compensate the effects of decreasing forces. Although this scenario can not be verified on pterosaur skulls, such cascades are known from extant animals like the scincid *Trachydosaurus* (Gans & De Vree 1987).

A further effect of an inclined occipital region concerns the lower jaw articulation with the joint reaction and joint forces. Assuming a bilateral bite, the joint forces are compressive and orientated in posterodorsal direction as demonstrated in chapter 6. For skull constructions with a vertical orientated occipital region, these compressive forces acting on the quadrate can not be absorbed by the quadrate, jugal/postorbital or jugal/lac-

rimal bars of the occipital region. In case of an inclined occipital angle, however, the joint force direction corresponds well with the angle of inclination. For a more posterior bite as well as for the pre-occlusion stages of the jaws the vector of the joint force has a greater inclination than when the jaws are fully closed (Cleuren et al. 1995). Considering this, it is obvious that for such inclined skull constructions the quadrate bar posterior to the lower temporal fenestra as well as the jugal/postorbital bar are subject to axial and bending loads and thus stabilise the quadrate region. An enlargement of the area ventrolateral to the orbita thereby increase its stabilising efficiency. For a posterior bite, also the jugal/lacrimal bar will be subject to high loads caused by the joint forces.

The stress patterns, which results from the loads at the lower jaw articulation is observed in the FE analyses of pterosaur skull models (see chapter 8 for description) in the regions described above. Similar stabilising devices for joint forces like inclination of the occipital region or buttressing by orbitotemporal bars have already been described from various reptile groups, e.g. in *Caiman* (Sinclair & Alexander 1987, Cleuren et al. 1995).

9.3.3 Development of the nasoantorbital fenestra

Some skull constructions like e.g. those of Anurognathus, Batrachognathus and Jeholopterus possess a naris, which is separated from the antorbital fenestra by a vertical orientated bar, composed of maxillary and nasal. In others like e.g. the Dimorphodon or Sordes skull construction, this bar is orientated more oblique in posterodorsal/anteroventral direction, whereas in the Angustinaripterus skull construction it is gently inclined and the naris is slit-like and situated anterodorsal to the antorbital fenestra. In most other skull constructions, however, the antorbital fenestra and naris are fused, and form a nasoantorbital fenestra anterior to the orbita. All longirostrine skull constructions bear a nasoantorbital fenestra, whereas most brevirostrine skull have a separate naris and antorbital fenestra.

The first results of a FEM approach using a virtual synthesis *sensu* Witzel & Preuschoft (2005) shows, that in the Anhanguera skull construction the area of the nasoantorbital fenestra is not stressed (Witzel 2005, pers. comm.). In consequence, there is no need for any mineralized connective tissue in this area, which is supposed to make the skull lighter (Wellnhofer 1991a). However, the contribution to the reduction of the overall weight may be less significant or even lead to heavier skulls, because certain types of connective tissue have a higher density than bone tissue (Frey 2005, pers. comm.).

There is evidence, that the length of the antorbital/nasoantorbital fenestra is related to the posterior extension of the tooth row. Especially in longirostrine skull constructions, the dentition is restricted to the area of the rostrum anterior to the antorbital/nasoantorbital fenestra or only rather small teeth are present level with the antorbital/nasoantorbital fenestra. Whereas in the first case, loading in the area of the antorbital/nasoantorbital fenestra is less likely to occur than in the anterior end of the jaw, only minor forces are induced in the latter case. As these minor forces can be absorbed by other load-bearing structural units like the dorsal (premaxillary/nasal) or ventral (maxillary/jugal) enclosing bars of the nasoantorbital fenestra, the bony bar between naris and antorbital fenestra thus can be reduced if the antorbital fenestra is extended in anterior direction. The only exception from this may be the Dsungaripterus and Phobetopter skull constructions. Both will be discussed in the following chapter 9.4.

Together with the type and size of the dentition, the extension of the nasoantorbital fenestra thus yields information at which levels of the jaws loads were applied during bite. This may also hold true for edentulous

jaws and point to differences in feeding styles for e.g. the Pteranodon skull construction with a long rhamphotheca versus e.g. the Tupuxuara skull construction with a rather short rhamphotheca, as assumed by the size of the nasoantorbital fenestra.

In case of separated naris and antorbital fenestra, the effects of a change in direction and subsequent loss of the separating bony bar is tested by using the space frame analysis (Tab. 9.1). In a skull construction with short rostrum and vertical orientated bar B4 between naris and antorbital fenestra, the main stress occurs in the compressive dorsal member B1. For such a case, B2 is subject to compressive forces and bending. Moving B4 into a more oblique angle, the bar gets subject to compression only, although the amount of compressive forces increase significantly. In consequence, the bar B2 switches from tensile to compressive loads. While B1 shows an increase in compressive loads, the tensile loads in the ventral bar B5 are decreased. Removing B4 altogether, leads to an insignificant increase in compressive load of B1, whereas it doubles in B2; although the overall loads in the latter are small. In this scenario, the tensile forces in B5 reach its maximum.

In those brevirostrine skulls with large fenestrations, a vertical or oblique member B4 would be a structural analogue to the bony nasal septum of crocodiles. The latter acts as a compressive resistant member and thus prevents a differential bending of the palatinal plate and the dorsal roof of the skull (Preuschoft et al. 1985).

Modell	B1	B5	B2	B4	B6	B7	B8	B9	B10
snarav	-800	280	32	-14	137	389	-375	270	674
snaravpt	-802	277	32	-15	136	390	-375	273	680
snarao	-895	263	-48	-109	161	403	-389	266	700
snaraopt	-898	263	-48	-108	159	405	-390	278	702
snasa	-906	200	-89	-	162	377	-386	284	686
snasapt	-903	203	-92	-	160	376	-384	282	684
lnarav	-3549	1964	-151	-15	492	1741	-1586	1137	2880
lnaravpt	-3550	1960	-151	-17	480	1742	-1586	1137	2881
lnarao	-3655	1548	-822	-178	533	1758	-1609	1156	2919
lnaraopt	-3658	1550	-822	-178	530	1760	-1610	1156	2922
lnasa	-3655	2049	-920	-	561	1718	-1622	1177	2924
lnasapt	-3699	2041	-917	-	558	1717	-1620	1176	2922

Tab. 9.1: Comparison of the loads in various bar models. Loads in N, compressive loads negative (red), tensile loads positive (blue). Abbreviations: b1-b10: bars, see Fig. 6.16, snarav = short rostrum, antorbital fenestra, naris and vertical orientated bar b4; snaravpt = same as snarav but with tensile loads at anterordorsal edge of antorbital fenestra, simulating possible insertion of MPTA; snaral = short rostrum, antorbital fenestra, naris and oblique orientated bar b4; snaraopt = same as snarao but with tensile loads at anterordorsal edge of antorbital fenestra, simulating possible insertion of MPTA; snasa = short rostrum, nasoantorbital fenestra, naris and vertical orientated bar b4; snasapt = same as snasa but with tensile loads at anterordorsal edge of nasoantorbital fenestra, simulating possible insertion of MPTA; lnarav = long rostrum, antorbital fenestra, naris and vertical orientated bar b4; lnaravpt = same as lnarav but with tensile loads at anterordorsal edge of antorbital fenestra, simulating possible insertion of MPTA; lnaral = long rostrum, antorbital fenestra, naris and oblique orientated bar b4; lnaraopt = same as lnarao but with tensile loads at anterordorsal edge of antorbital fenestra, simulating possible insertion of MPTA; lnasa = long rostrum, nasoantorbital fenestra, naris and vertical orientated bar b4; lnasapt = same as lnasa but with tensile loads at anterordorsal edge of nasoantorbital fenestra, simulating possible insertion of MPTA.

The space frame analysis described so far differs from that for longirostrine skulls. For the latter (Tab. 9.1), the effects on the dorsal bar B1 are similar to the one mentioned above, but a minimum in tensile loads in B5 is reached, when an oblique bar B4 is present. Whereas the lowest stress values are present in B2 when B4 is vertically orientated, they show a maximum when B4 is removed. However, the values in all other compressive members are far lower than the maximum compressive load, present in bar B1. Assuming that the ultimate compressive stress is even higher than these values, removing the member B4 is possible without subsequent failure of the entire space frame. In longirostrine jaws, this area is actually much less stressed than in short skull constructions. The function of preventing the differential bending between the ventral and dorsal members of the rostrum mentioned above, is mostly taken over by the walls of the rostral section anterior to the nasoantorbital fenestra[4]. Alternatively, it would be achieved by a tensile member which could have been theoretically present in the nasoantorbital fenestra. Such a tensile member was proposed by Wellnhofer (1991a), by reconstructing the insertion point of the MPTA on the anterodorsal end of the antorbital, respectively nasoantorbital fenestra. This would lengthen the muscle as well as increase the mechanical advantage of the muscle fibres by a greater attachment angle due to the insertion on a fascia overlying the nasoantorbital fenestra. However, in this case the overall weight of the skull is enlarged relative to a skull without a large MPTA.

Although no direct evidence for the hypotheses proposed by Wellnhofer (1991a) exists in form of scars or rugosities in the potential insertion areas, it is possible with the space frame analysis to test, which effects such a muscle has on the stress distribution. The effects of an enlarged insertion area of the MPTA are rather neglectable as far as the stress pattern in the space frame is concerned (Tab. 9.1). As the overall stresses are only insignificantly higher, the same assumptions can be made as in the previous cases. Replacing the compressive bar B4 by a tensile member (e.g. the MPTA) thus will not result in failure of the space frame unless the ultimate compressive strength is reached in the member B1 or alternatively the ultimate tensile strength in B5. This means that the reconstruction of Wellnhofer (1991a) is neither verified through any attachment marks nor falsified by mechanical investigations and therefore has to remain hypothetical.

9.3.4 Reduction of dentition and replacement by a keratinous beak

One of the main processes during pterosaur evolution is the complete reduction of the dentition. Different stages of reduction are present in the pterosaur skull constructions:

- fully developed dentition (= dentition extending from anterior tip of the jaw to at least half of the length of the antorbital/nasoantorbital fenestra)
- dentition restricted to pre-nasoantorbital rostrum, partly with enlarged anterior teeth
- dentition restricted to anterior end of rostrum
- fully developed dentition but keratinous hook present at the anterior end of the rostrum
- keratinous beak (rhamphotheca) at the anterior end of rostrum, teeth restricted to posterior part of the rostrum

- edentulous jaws, rhamphoteca covering most part of the jaws

The occurrence of keratinous hooks at the anterior part of the rostrum has only been recently proven by studies using ultraviolet-light (Tischlinger & Frey 2001, Frey et al. 2003c). As the detection of such structures heavily relies on the preservation of the specimen, it is unclear in how many pterosaurs such a keratinous hook

4 A similar pattern is seen in the results from the virtual synthesis of the skull of *Anhanguera* (Witzel 2005, pers. comm.).

was present. The toothless anterior rostrum like e.g. in *Campylognathoides* or *Rhamphorhynchus* may be an indirect indicator for such a configuration. A keratinous hook is unlikely in those pterosaurs with teeth present at the anteriormost end of the rostrum like e.g. *Coloborhynchus* or *Gnathosaurus.* In these skull constructions the main point of loading of the skull is not at the anteriormost end of the rostrum, but about three to four tooth positions posteriorly as can be deduced by the size of the teeth. A keratinous hook thus would have only minor effects.

Frey et al (2003c) argued that a keratinous hook would operate like a tooth and that for an increase in size the torsional forces become progressively smaller. This assumption is oversimplified as only a small keratinous hook functionally does only operate like a single tooth when it is very small. However, the torsional loads produced at the anteriormost end of the rostrum are very low; from a strict mechanical point they are even zero at this level by definition (Bögge 2003). If the hook gets larger e.g. like in *Germanodactylus* as proposed by Frey et al (2003c) it will act more similar to a pair of teeth and thus rarely will be loaded symmetrically, although the loads will be distributed over a larger area and not as two point loads like in the case of a tooth pair. This will cause bending of the hook and thus also puts torsional loads on the rostrum. Torsional resistance is much more constrained by the jaw architecture, e.g. the more narrow the rostrum is the less is the resulting torque. Apart from a mechanical point of view, a single hook-like structure at the anterior end of the rostrum yields the option to use this structure as a peg to catch or manipulate small objects, although the functional difference to an anterior pair of teeth is only minor. However, this is use is speculative because of the fossil evidence for such a behaviour (see discussion on biological in chapter 2.1.2).

A significant difference is seen in the material properties of teeth and keratin. Whereas especially enamel - a very hard but brittle material - has a very high Young's modulus (about 60.000 MPa), keratin reacts much more flexible to loads (Young's modulus about 4000, S. Vogel 2003). This means, that it resists compression well and stores a lot of compressive energy relative to its weight, so that the loads are only partially transmitted to the bony rostrum. The larger a rhamphotheca is, the more energy it can store and the less loads are transmitted to the bone. Mechanically the keratinous rhamphotheca acts like shock absorption device for the rostrum, an effect which is especially important during an impact bite.

Enlarging the keratinous hook to a rhamphotheca, covering the premaxillary (and possibly the maxillary) bone, leads to a reduction of the number of teeth, and finally to a complete loss of teeth. Because of the difference in specific weight between keratin and teeth, the development of edentulous jaws thus results in a reduction of the overall weight. However, it is questionable whether this represents the main constraint for the reduction of the dentition as - in contrast to birds - the main weight in the skull of pterosaurs is caused by the mass of the relatively large muscles. The overall weight-reducing effects therefore may be rather low.

More important than weight-saving are the consequences for the mechanical regime in the rostrum during bite. In a toothed rostrum, the loads are applied as single point-loads through the teeth. Despite the presence of special shock absorption devices (see chapter 5), this may be critical especially for impact bites which produce very high loads. In edentulous jaws, the loads generally are distributed over a larger area due to the presence of a rhamphotheca, either along the jaw margins or even the entire ventral surface in the upper jaw, respectively dorsal surface in the lower jaw. This leads to a more homogenous load on the underlying bony attachment surface which is transmitted via connective tissue in between. Furthermore, due to the shock absorption effect of the keratin, the loads are significantly lower than without a keratinous rhamphotheca.

A second effect is the reduction of the probability of torsional loads, although this effect is lower than supposed by Frey et al. (2003c) because of the reasons given above. Torque still is possible during bite (and is also present in birds), but is less pronounced. This is the result of a more homogeneous pressure on the food item by the occlusal surfaces of the rhamphotheca which also will bring the load vectors more to the midline than for a bite at the jaw margins. This effect is lower in a rhamphotheca with raised lateral margins. As pointed out previously, however, the jaw geometry is of greater significance for the reduction of torque. Most pterosaur skull constructions are narrow relative to their height, thus reducing more significantly the amount of torsional loads (see chapter 6.3.5 for a more detailed discussion on this subject) than may be expected from a rhamphotheca alone.

The presence of the rhamphotheca as a damping device may explain the very high shear, maximum bending and comparison stresses, which are observed in all toothless skull constructions (see chapter 7). These stress values are multiple times higher than in toothed skull constructions. Assuming that these stress do not approach the ultimate stress values, leading to failure of the constructions, this means that the toothed pterosaur skull constructions are overbuilt multiple times. However, this is uncommon for biological structures which typically have safety factors of 2-4 (S. Vogel 2003). This disparity is resolved, when the energy-storing effects of the keratin described above are considered. This leads to an absorption of the high stresses by the rhamphotheca and to a safety-factor typical for toothed pterosaur skull constructions. In consequence, the presence of a rhamphotheca has to be considered a necessary prerequisite for the development of the narrow, edentulous skull constructions seen in Pteranodon, Quetzalcoatlus or Tapejara.

Reduction of the dentition by the replacement with a keratinous beak leads to a loss of friction (Frey et al. 2003c). If such friction is important for feeding, this relation has to be compensated e.g. by a relief on the internal side of the beak (as seen in *Tapejara* as longitudinal interdigitating ridges), sharp or rough margins or a terminal hook at the rostrum. Similar devices are known from certain birds, which additionally like all birds possess kinetic skulls to accommodate the problem of a forward pointing force component produced by the closing jaws on the food item (Starck 1979). Similar relief structures are also known from turtles which possess keratinous beaks, too (Starck 1979). The reason why these are only poorly documented in pterosaurs may be taphonomic with actually only a few Lagerstätten like Solnhofen and the Crato Formation in Brasil or Liaoning in China yielding information on soft-tissue structures.

The dimensions of the rhamphotheca may only be limited by the location of the naris or the nasoantorbital fenestra. Since direct imprints are not visible, the beak of *Pteranodon* may therefore have covered the whole pre-nasoantorbital rostrum (see Wellnhofer 1991: 139 for reconstruction). In pterosaurs with a large nasoantorbital fenestra like *Quetzalcoatlus*, it may have been smaller than in *Pteranodon* but additionally may have covered the ventral and dorsal borders (not the fenestra itself) of the nasoantorbital fenestra as sheaths, similar to birds (Starck 1979). However, the shock-absorbing effects are less than in the pre-nasoantorbital region because of the small cross-section of these sheaths. The extension of the nasoantorbital fenestra thus may be closely coupled with the dimension of the rhamphotheca and - in analogue to birds - reflect different feeding habits.

In some skull constructions like the Dsungaripterus or Phobetopter skull construction, teeth still are prominent despite the fact that an anterior rhamphotheca is present. This is deduced from the fact that the most posterior teeth are the largest and most robust teeth of the whole dentition (Wellnhofer 1991a). This pattern is contrary to all other toothed pterosaur skull constructions where the teeth decrease in size posteriorly. This fact

will be discussed more detailed in the chapter on the functional implications of the skull construction types (chapter 9.4).

Whereas, the development of a rhamphotheca leads to a reduction of the dentition from anterior, there is a second, seeming tendency to reduce the dentition from posterior. This is visible in the Istiodactylus skull construction, where teeth are only present in the anterior quarter of the rostrum. Also the dentition of the Pterodactylus elegans skull construction is restricted to the anterior third of the rostrum. This may be explained either by a reduction in tooth count or by an anterior shifting of the expression loci of the odontogenetic cells. Both processes may be caused by an elongation of the rostrum. This tendency to shift the teeth in the pre-naris/pre-nasoantorbital region of the rostrum has been mentioned earlier and interpreted in a mechanical context. Only in the Pterodactylus elegans and Gallodactylus skull construction the posterior end of the dentition is situated in some distance anterior to the level of the anterior end of the nasoantorbital fenestra. As in the former there is no reduction in absolute numbers of tooth pairs relative to other pterosaur skull constructions, there is no reduction of tooth count in a strict sense. Considering the presence of a keratinous hook and its development into a rhamphotheca, which extends in posterior direction, a rapid evolutionary loss of the complete dentition is possible on the basis of this level (Pt. elegans skull construction). In contrast to this, the Gallodactylus skull constructions shows a reduction of the tooth count with large anterior teeth and smaller posterior teeth. It represents the only skull type in which a reduction of the dentition from posterior without a rhamphothecal stage is present.

Contrary to the reduction of the dentition, some pterosaur skull constructions show an enlargement of the anterior tooth pairs (e.g. in the Anhanguera, Coloborhynchus or Angustinaripterus skull construction) or an increase in tooth count (e.g. Gnathosaurus or Plataleorhynchus skull construction). In most cases, the anterior part of the rostrum is elongated, too. Such structures and tendencies were predicted earlier (see chapter 9.3.1) especially for longirostrine jaw constructions because of their increase of the efficiency of the anterior rostrum in snap-feeding. Both strategies lead to different feeding options, as will be discussed in the chapter on the constructional categories.

9.3.5 Development of crests

The presence of crest at the skulls of pterosaurs can be discussed based on the biomechanical investigations made herein. However, it has to kept in mind, that the resulting effects may not have been the main reason that these crests evolved. Other effects like the consequences for the aerodynamic and hydrodynamic performance or for thermoregulation due to the increased surface area may have been important factors, too. In contrast to these ideas, which can be tested by numerical analysis, the idea that the crests were used as signal devices (Bennett 1992, Wellnhofer 1991a) can not by verified and thus is only speculative.

For the following discussion, four types of dorsal crests are distinguished: a bony anterior (= anterior to naris/nasoantorbital fenestra), bony medial (= dorsal to nasoantorbital fenestra), bony orbitotemporal crest and a soft-tissue crest. The latter may be present at the anterior, medial and/or orbitotemporal region. The effects of anterior bony crests are visible by comparing a crested *versus* a similar crestless skull construction (e.g. Santanadactylus, vs. Criorhynchus and Coloborhynchus skull construction). The results are identical for an anterior crest and a medial-crested skull construction.

No significant difference are seen for the resulting bite force F_B of the crested and non-crested skull constructions mentioned above (Fig. A.348). This is caused by the similar muscular and occipital architecture which is - of course - is not influenced by a anterior or medial crest. In case of the bending moments, lower values are present in the crested skull construction (Fig A.351). Similar results are found for the maximum bending, shear and comparison stress (Figs. A.352-A.357). It is evident, however, that the values are only lower than for the non-crested skull construction in the region where a crest is present. Even more striking is the difference in the twistiness to bendiness ratio (Figs. A.358-A.359). The crestless Santanadactylus skull construction shows an overall tendency for twisting rather than bending. In the crested Coloborhynchus and Criorhynchus skull constructions, this ratio is reduced significantly below the critical value of 1.0 where bending will get easier twisting (Etnier 2001, 2003, Etnier & S. Vogel 2000, S. Vogel 1984, 2003). Keeping in mind, that bone is much more susceptible to fail under torsional loads than in bending, the effect of an anterior crest is to mechanically stabilise the skull constructions against failure during bite. This adds to the effect of a hollow rostrum, which can be interpreted as a anti-bending, anti-torsional strategy similar to the use of hollow steel tubes used in mechanical engineering or architecture (Fastnacht 2005). Similar results are present in case of a massive, medial crest, e.g. by the comparison of the crested Quetzalcoatlus skull construction with the non-crested Zheijangopterus skull constructions (Figs. A.345-A.359). However, in these edentulous forms the overall stress-reducing effects are rather neglectable because here the values for shear, maximum bending and comparison stress are *per se* much higher than in toothed skull constructions, a phenomenon which has been discussed earlier (chapter 9.3.4). Again, the consequences of a crest are most obvious in the twistiness to bendiness ratio with a decrease of the values in the region of the crest. As for anterior crests, these effects are more pronounced, the closer the loads are applied to the level of the crest.

The thinner a crest is, the less effect it has on the mechanical behaviour of the skull construction during bite. A thin bony lamella which is present dorsomedially e.g. in the Germanodactylus skull construction thus is mechanically negligible, although it may serve as an attachment area for a soft-tissue crest or may form the mineralised part of a soft-tissue crest (Frey et al. 2003b, 2003c). Theoretically such a soft-tissue crest could act as a tensile member and - similar to the bracing in a suspension bridge - unload the dorsal border of the skull construction which is subject to high compressive stresses. However, for an effective bracing system, a compressive member similar to the pillar of suspension bridges is needed. This is only present in case of the Tapejara skull construction where a dorsally directed bony spline is developed at the anterodorsal end of the rostrum (Frey et al. 2003b). The mineralised bases of the crest fibres at the dorsal margin present in specimens like *Tapejara imperator,* SMNK PAL 2839, which show an angular insertion relative to the horizontal plane supporting this hypothesis. Although previously interpreted in the light of aerofoils and the aerodynamic effects of the crest (Frey et al. 2003c), there is potential at least in some soft-tissue crest for stabilising effects under the loading regimes investigated herein. Further work, e.g. by using FEM is needed to test this hypotheses.

The effects of orbitotemporal crest can not be evaluated by using the beam model used in chapter 6, because it only comprises the rostral part of the skull construction. The results of the FEM study (see chapter 8) shows, that these crest are not stressed and therefore not obligatory to stabilise the skull construction during bite. Also the virtual FEM synthesis does not yield any necessity of a bony structure in this area (Witzel 2005, pers. comm.). As pointed out in chapter 9.3.2, however, such a crest can serve as an enlarged attachment area

for the adductor muscles originating in the upper temporal fenestra, e.g. in the Pteranodon skull construction. This may also explain the blunt supraoccipital process present in the posterodorsal temporal regions in some ornithocheirid pterosaurs (e.g. *Anhanguera*, *Criorhynchus*). Yet, the attachment area of the adductor muscles is restricted to the base of the crest. The elongation of the crest in *Pteranodon* or possibly even more pronounced in *Nyctosaurus* (Bennett 2003) therefore must be controlled by different constrains like e.g. signal function (Bennett 1992, Wellnhofer 1991a).

9.3.6. Curvature of jaws

A few pterosaur skull constructions possess curved jaws, either in anterodorsal (Pterodaustro and Dsungaripterus skull construction) or in anteroventral direction (Quetzalcoatlus and to a lesser degree Tapejara skull construction). Although these skull constructions were analysed using beam theory as being straight in chapter 7, the curvature will have an influence on the loading during jaw occlusion.

In case of the dorsally concave rostrum of the Dsungaripterus skull construction, Frey et al. (2003c) proposed an increase of friction during bite. Such an effect is obviously present in the Pterodaustro skull construction. Looking at the mechanical consequences, both, Dsungaripterus and Pterodaustro skull are curved in the direction, in which the bite forces would tend to deform the skull constructions. Such "pre-bent" structures are known from other skeletal elements like long bones e.g. the femur (Currey 2002). The reason for this has been the topic of some debate (Alexander 2003, Bertram & Biewener 1988, 1992, Cubo et al. 1999, Currey 2002). However, both stages are not directly comparable because - in contrast to long bones - no counter-bending muscles exist in the skull region.

The Pterodaustro skull construction shows only low loads at its rostrum because of its great length. Interpreting the Pterodaustro skull construction in terms of filter-feeding (see next chapter), the lower jaw would act as a shovel and therefore would increase its efficiency by a dorsal curvature, which leads to a corresponding curvature of the upper jaw.

For the Dsungaripterus skull construction the major loads seem to be applied in the region of the posterior teeth and not at the anterior rostrum This is deduced from the size of the teeth, which are the largest at the posterior end of the rostrum, a state that is not present in others pterosaurs. Wellnhofer (1991a) proposed that the rostrum may have been used as a manipulating device similar to sea birds. An increase in friction as proposed by Frey et al. (2003c) would be in accordance with this foraging mode, where the curved rostrum - in combination with a keratinous rhamphotheca - may have been used as a lever by a dorsal movement of the skull (e.g. to detach food items from the substrate). The curved rostrum would strengthen the skull construction against the reaction forces produced during this action because the stiffness is increased relative to a non-curved rostrum in the direction of the curvature (Bertram & Biewener 1988). Also compressive forces in direction of the rostrum are possible in this foraging mode, a loading configuration in which curved jaws would be more stable than straight jaws (Bertram & Biewener 1988).

Only the Ctenochasma and Pterodaustro skull constructions possess relatively longer rostra than the Quetzalcoatlus skull construction. Both former skull constructions are associated with filter feeding (see next chapter), an option from which evidence is missing in the Quetzalcoatlus skull construction. Theoretically the rhamphotheca could have been used as a filter device in *Quetzalcoatlus*, but because this structure is not yet directly documented in the fossil record of *Quetzalcoatlus*, a typical pterosaurian bite must be considered to

be more plausible. Also the Tapejara skull construction show a anteroventral curving of the rostrum, although it is less prominent than in the Quetzalcoatlus skull construction.

In birds anteroventrally curved upper jaws are present in a number of groups, e.g. the Bucerotidae, Nectariidae or in *Numenius arquatus*. In most cases these jaws are slender and therefore different from the rostrum of the Quetzalcoatlus or Tapejara skull construction, which resemble more the beaks of the Bucerotidae. This bird group is mostly frugivorous, although a couple of genera are omnivorous (Elliott 1887-1892), and all genera possess dorsomedial crest on their beaks. By studying living hornbills in the zoo, it is apparent that the anteroventrally curved beak reduces the friction and thus often leads to a loss of the food item due to gravitational forces. The same has to be assumed for anteroventrally curved jaws of pterosaurs. On the other hand, an anteroventrally curved rostrum would counteract the high bending stress acting during bite, similar to discussion of curved tooth constructions (see chapter 5). Further work including studies on the jaw mechanics of hornbills is needed to clarify and quantify the effects of anteroventrally curved jaws.

9.4 Functional implications of the constructional types

Based on the previous discussions, functional implications for feeding are assigned to the different skull constructional types. This approach follows and enhances the concept by Frey et al. (2003c). The skull constructional types are only listed in those cases, where they operate with a high efficiency, as deduced by the discussion in chapter 7 and in this chapter (see above). In most cases, other options are possible aside with lower efficiency, yielding the optional operational range of the jaw construction. However, some skull types are excluded by their morphology and biomechanical behaviour. The sequence of functional implications is chosen arbitrarily.

9.4.1 Snap-and-penetrate

Mechanical characteristics: deep penetration of food items by teeth, high torsional and bending loads.
Assigned constructional types: Angustinaripterus CT, Cacibupteryx CT, Cearadactylus CT, Ornithocheirid CT, Gallodactylus CT, Huanhepterus CT, Rhamphorhynchus CT, Scaphognathus CT
Characteristics of assigned constructional types: toothed rostra with long teeth, medium-sized to longirostrine jaws, leading to high acceleration/velocity of the jaws during occlusion, high torsional and bending stiffness.
Excluded constructional levels: Azhdarchidae CT, Ctenochasma CT, Gnathosaurus CT, Dsungaripterus CT Huanhepterus CT, Pteranodon CT, Pterodaustro CT, Tapejaraid CT, Tupuxuarid CT
Characteristics of excluded constructional types: absence of teeth, respectively low crowned teeth or tooth constructions with low resistance against Euler buckling
Remarks: Penetration causes high bending moments on the teeth which will be reduced due to the enamel/dentine-distribution and the energy absorption effects of the periodontal ligament. An extended rostrum will lead to an increase of the acceleration of the jaws and thus increase the impact energy on the food item (Currey 2002, S. Vogel 2003).

The presence of an anterior or medial bony crest reduces torsional and bending stress. Based on the size and morphology of the lower jaw symphysis, skimming is an option for the Cearadactylus and Ornithocheirus CT.[5] In the Rhamphorhynchus CL, the torque is much reduced due to the narrow jaws. In contrast to the other

5 Note that this refers to the skull construction alone and not to the posterior, postcranial construction in Ornithocheirids. If the neck construction is considered, skimming is problematic in Ornithocheirids (Frey 2005, pers. comm.)

constructional levels listed here, the main holding function is not performed by the teeth but by the keratinous anterior beak if a full occlusion is possible at this level. Again, skimming is within the optional range of this skull construction.

9.4.2 Snap-and-lock

Mechanical characteristics: high F_B, high torsional loads, high shear loads and low bending loads
Assigned constructional levels: Anurognathus CT, Tapejarid CT
Characteristics of assigned constructional types: brevirostrine rostrum
Excluded constructional levels: Ctenochasma CT, Gnathosaurus CT, Huanhepterus CT, Pterodaustro CT
Characteristics of excluded constructional types: Tooth constructions with low resistance against Euler buckling or filter-feeding constructions
Remarks: The skulls of the Anurognathus CT are broad and box-like. Either the resulting torsional loads are low due to the intake of only small-sized food or absorbed by a possible cranial kinesis (see below). In contrast to this, the Tapejara CT allows a selective grasping with the anterior end of the rostrum covered by a rhamphotheca. Torsional loads are low due to the lateral narrow skull constructions and the presence of the rhamphotheca. Furthermore, the upper jaw is curved anteroventrally thus forming some sort of plier together with the anterodorsally curved lower jaw. Although Wellnhofer (1991) proposed a frugivorous diet for *Tapejara*, the narrow skull construction shows a high torsional stiffness which is not needed for such food items. Torsional loads typically are produced e.g. by food items of low Young's modulus (Vincent & Littford 1991). In some skulls of *Sinopterus* and juvenile specimens of *Tapejara* (Frey 2005, pers. comm.) the dorsal bony border of the nasoantorbital is continued into a posterodorsally orientated spline which is not firmly attached to the orbitotemporal region. Especially in *Sinopterus* a gap is present between the spine and the orbital region, permitting some mobility between the bones and thus absorption of especially the high shear stress analogue to the cranial kinesis present in birds. A similar effect of kinetic areas for the stress distribution has also been described from Tyrannosaurus rex (Rayfield 2004, 2005).

9.4.3 Hold-and-filter

Mechanical characteristics: high twistiness to bendiness ratio
Assigned constructions levels: Ctenochasma CT, Gnathosaurus CT, Huanhepterus CT, Istiodactylus CT (?), Pterodaustro CT
Characteristics of assigned constructional types: longirostrine jaws with high tooth count and low interalveolar space, tooth construction mostly with low resistance against Euler buckling, expanded anterior rostrum optional
Excluded constructional levels: Angustinaripterus CT, Anurognathus CT, Azhdarchidae CT, Cacibupteryx CT, Cearadactylus CT, Dsungaripterus CT, Ornithocheirus CT, Gallodactylus CT, Huanhepterus CT, Pteranodon CT, Rhamphorhynchus CT, Scaphognathus CT, Tapejarid CT, Tupuxuarid CT
Characteristics of excluded constructional types: absence of teeth (assuming that the rhamphotheca is not used for filtering), brevirostrine skulls, large interalveolar areas, heterodont dentition as far as the height of teeth is concerned (e.g. Ornithocheirus high vs. low tooth construction), low twistiness to bendiness ratio
Remarks: the filter apparatus is formed by dentition with a high number of teeth, situated in an elongated

rostrum. The size of the food items which can be filtered is constrained by the denseness of the teeth. It is therefore smaller in the Pterodaustro CT than for the other skull constructional types. A high amount of the muscular energy will be used when the lower jaw has to be moved against the drag of the water. Curvature of the jaws in dorsal direction increases the amount of fluid which can be gathered similar to a shovel in comparison with a spade (as a model for a straight rostrum). This is independent whether the water-flow is orientated medial-laterally or posterior-laterally.

In the Istiodactylus skull construction, the morphology of the anterior part of the rostrum resembles that of ducks with a broad, rounded beak. Together with the tight occlusion of the teeth of the upper and lower jaws, this indicates the capacity to take hold of even small food items. The latter would be advantageous for the Istiodactylus skull construction with its low torsional stiffness, because such food items do not produce significant torsional loads. As this represents a necessary prerequisite for filtering, the skull construction is listed here, although annotated with a question mark.

9.4.4 Snap-and-hold

Mechanical characteristics: high velocity/acceleration of lower jaw, high F_B, low penetrational depth
Assigned constructional levels: Campylognathoides CT, Dimorphodon CT, Istiodactylus CT, Pterodactylus CT, Sordes CT
Characteristics of assigned constructional types: medium to long rostrum, low to medium height of tooth construction (e.g. Pterodactylus tooth construction), high twistiness to bendiness ratio
Excluded constructional levels: Pterodaustro CT
Characteristics of excluded constructional types: low resistance of tooth constructions against Euler buckling and bending
Remarks: Basal feeding strategy. Size of food items is constrained by the width of the alveolar space, respectively interlocking of lower and upper jaw teeth (e.g. low width in Dimorphodon CT, large width in Campylognathoides CT). The presence of a keratinous hook increases manipulation of the food items and results in lower bending and secondary torsional loads.

9.4.5 Snap-hold-and-slice

Mechanical characteristics: high velocity/acceleration of lower jaw, high F_B, low penetrational depth, highly fibrous food items
Assigned constructional levels: Eudimorphodon CT, Preondactylus CT
Characteristics of assigned constructional types: relatively short rostrum, average to high F_B, teeth with serrated edges
Excluded constructional levels: all other constructional levels
Characteristics of excluded constructional types: non-serrated teeth or edentulous jaws
Remarks: similar to snap-and-hold, but with slicing component added by serration of teeth (see chapter 5.3), allowing a firm grasp of fibrous food items. In contrast to the Preondactylus CT, the Eudimorphodon CT has the option to hold very small food items due to the tight interlocking of upper and lower teeth and the small interalveolar spaces. Large food items can be fixed with the four anterior tooth pairs or with the enlarged multicuspid teeth ventral to the nasal/maxillary bar which separates naris and antorbital fenestra. A bite in this

region causes large loads because of the high values of F_B at this level. These loads will be transmitted via the nasal/maxillary bar into the dorsal region of the skull construction and onward into the orbitotemporal region. Applying an asymmetrical load at the level of the nasal/maxillary bar will result in high torsional loads.

9.4.6 Snap-and-squeeze

Mechanical characteristics: high velocity/acceleration of lower jaw, high F_B, low penetrational depth, high axial loads on tooth constructions

Assigned constructional levels: Dsungaripterus CT

Characteristics of assigned constructional types: increase of friction at anterior rostrum by rhamphotheca, largest teeth at posterior part of dentition, high resistance of tooth constructions against Euler buckling or bending

Excluded constructional levels: Angustinaripterus CT, Cacibupteryx CT, Cearadactylus CT, Ctenochasma CT, Gnathosaurus CT, Ornithocheirus CT, Gallodactylus CT, Huanhepterus CT, Pterodaustro CT, Rhamphorhynchus CT, Scaphognathus CT

Characteristics of excluded constructional types: low F_B, tooth constructions with low bending stiffness and resistance against Euler buckling

Remarks: The anterior part of the rostrum with its low and narrow profile can be used as a manipulating device for food items as discussed in chapter 9.3.6. The construction of the posterior teeth shows a high bending stiffness and resistance against Euler buckling (see chapter 5.3). In combination with the high values of F_B at the level of the posterior teeth, this indicates option for crushing hard-textured food-items. The resulting high loads from a bite at this level are absorbed by the raised alveolar walls of the posterior teeth as well as the enlarged jugal area ventral of the orbita. The buttressing function of the suborbital jugal area leads to a putative shifting of the orbita in dorsolateral direction via a stage with a suborbital fenestra (Phobetopter skull construction) to the Dsungaripterus skull construction.

Untypical for pterosaurs skull constructions, the largest teeth are situated ventral to the nasoantorbital fenestra where in other pterosaur skulls no or only small teeth are present. For the latter condition, failure of the skull construction can be expected if large loads are applied here, caused by the thin bone walls and low cross-sectional diameter of the ventrally bordering bars of the nasoantorbital fenestra. This may not be the case in *Dsungaripterus* if the thick bone walls typical for dsungariptid pterosaur long bones are present in the skull, too. In this case, the stability of the ventral bars would be increased against compressive loads orientated perpendicular to the long axis of the bar (Fastnacht 2005).

9.4.7 Snap-squeeze-and-cut

Mechanical characteristics: high velocity/acceleration of lower jaw, planar loading of the rostum, low torsional loads

Assigned constructional levels: Azhdarchidae CT, Pteranodon CT, Tupuxuarid CT

Characteristics of assigned constructional types: dentition replaced by rhamphotheca, narrow skull constructions in dorsal view, medium to long rostrum

Excluded constructional levels: all other constructional levels except Tapejarid CT

Characteristics of excluded constructional types: toothed rostra, high twistiness to bendiness ratio

Remarks: The Snapping efficiency is increased by elongation of the rostrum. Torsion and bending stiffness are low due to the narrow skull construction, shear stresses, however, are very high relative to all other pterosaur skull constructions (see chapter 7). The presence of a rhamphotheca reduces the shear stress and leads to a more uniform distribution of loads, assuming that this area is the preferred region for taking hold of food items. The restriction of the rhamphotheca to the anterior end of the rostrum - as deduced for the Azhdarchidae and Tupuxuara CT (see chapter 9.3.4) - thus points to a more selective grasping than in the Pteranodon CT, where the rhamphotheca is much larger and food items can be grasped along 4/5 of the entire jaw length.

The Tupuxuara and Thalassodromeus skull constructions do not imply a skimming mode of foraging similar to the extant *Rhynchops* as assumed by Kellner & Campos (2002). In the extant Black Skimmer fishes are caught along the whole area of the jaws (Zusi 1962) and both upper and lower jaws are mostly covered by a keratinous rhamphotheca. The lower jaws possess a very large and narrow symphysis which is unlike the condition of the symphysis in the lower jaw of *Thalassodromeus*, which is very short. Although the Tupuxuara and Thalassodromeus skull constructions are very narrow too, they are much higher than wide, resulting in very high bending, shear and comparison stress. In *Rhynchops* the skull is only about twice as high as wide and the loads on the skull are absorbed by cranial kinesis as well as special absorbing devices (Zusi 1962) from which none is present in these pterosaur skull constructions. Further arguments against a skimming mode of *Tupuxuara* and *Thalassodromeus* concern the pressure on the cervical vertebra (Frey, 2005, pers. comm.), which, however, is beyond the topic of this study.

9.5 Possible evolutionary pathways

9.5.1 Determination of possible transformations

Transformations between two constructions are characterised by irreversible changes of the construction (Herkner 1999). The resulting constructional level must retain its bionomic coherence and must be operable, i.e. must not fail. The reduction of teeth or extremities are examples for such irreversible transformations (D.S. Peters 1985b). Within a construction level, possible variations may occur (D.S. Peters 1985b), which may be the base for subsequent constructional levels. Both, transformation and variations, rely on the *Ökonomieprinzip* (D.S. Peters 1985b , D.S. Peters & Gutmann 1971), which was described more closely in chapter 3.1.1.

Based on the discussion so far, only two processes are considered as irreversible transformations. This is the complete reduction of the dentition and replacement by a keratinous rhamphotheca and the fusion of the antorbital fenestra and naris. The first transformation is based on the loss of the potential of odontogenetic proliferation in the area of the rhamphotheca (Mitsiadis 2003). In consequence, the reduction of the dentition from anterior has to be considered as irreversible. Likewise, the loss of the separating maxillary/nasal bar between naris and antorbital fenestra is irreversible because it implies a re-mineralisation along a pre-formed connective tissue e.g. tendon or ligament (Fastnacht et al. 2002, Müller 2003). However, there is no direct evidence for such a structure in the pterosaur skull construction. From a mechanical point of view, a tensile member in this area, which is orientated like the separating bony bar, is non-functional since it is not loaded in tension but in compression during bite (see chapter 6 and 9.3.3). Tensile members would only operate in anterodorsal/posteroventral direction. An alternative compressive member would be cartilage, which has to be ruled out due its low axial stiffness.

Apart from these two irreversible transformations, some of the processes described in chapter 9.3 lead to variations within a constructional level. They have to be interpreted under the aspect of the *Ökonomieprinzip* described in chapter 3.1.1 with respect to a certain function. In case of present study, theses are the different feeding implications discussed in chapter 9.4.

The referring processes are:

- elongation of the rostrum –> increased acceleration and velocity of occlusion
- shortening of the rostrum –> increased bite forces
- inclination of the occipital region –> increased acceleration and velocity of occlusion, buttressing against joint reaction forces
- increased height of tooth constructions –> deeper penetration depth
- increased number of teeth –> higher filter capacity
- presence of anterodorsal crest –> reduction of torque, shear and comparison stress
- presence of mediodorsal crest –> reduction of torque, shear stress and comparison stress, tendency for bending instead of twisting, stabilises dorsal bordering bar of nasoantorbital fenestra
- presence of orbitotemporal crest –> increased acceleration and velocity of occlusion

Some of these processes induce other, subsequent processes:

- shifting of posterior end of tooth row in anterior direction, induced by elongation of rostrum; food item is grasped more anteriorly
- shifting of the orientation of the separating maxillary/nasal bar between antorbital fenestra and naris, induced by elongation of rostrum because of the decreased stress in the bar
- narrowing of the skull construction, induced by edentulous jaws with rhamphotheca, which absorbs the high shear, bending and comparison stress resulting from such a morphology
- size of rhamphotheca, constrained by size of nasoantorbital fenestra

All these processes increase the efficiency of the skull construction but do not necessarily reduce the complexity of the skull construction, a fact which is also described by the *Ökonomieprinzip* (D.S. Peters 1985b, D.S. Peters & Gutmann 1971). Since these processes are assumed to be directed under the aspect of economisation, they are not irreversible and thus do not constitute a constructional level on their own. Therefore they are treated as structural variations within a certain constructional level, and changes are marked in Figs 9.5-9.11with a double arrow to make clear, that reversal are possible. The derivation from other skull constructions or types is constructed by using a parsimonious number of changes, minimising the number of overall changes in morphology and transformations needed and maintaining the mechanical coherence.

9.5.2 Determination of a possible preconstruction

A preconstruction forms the base for a transformation series with functional transitional stages, leading to end-constructions (Herkner 1999). This preconstruction may be either hypothetical or may be derived from extant or fossil animals.

Based on the common characteristics of pterosaur skull constructions and the discussion above, certain features are derived for the pterosaur skull preconstruction. These are:

- diapsid temporal fenestra
- separated naris and antorbital fenestra

• short rostrum
• vertical occipital region
• tooth row ranging from anterior end of rostrum to level with orbit
• homodont, monocuspid tooth construction
• low interalveolar space

In mechanical terms this skull construction shows high torsional and shear stresses, low bending stress and moments and has high bite forces. In functional terms, this hypothetical preconstruction represents a typical snap-and-hold construction.

The phylogeny of pterosaurs has been topic of some controversy. Whereas some authors argue for a close relationship between dinosaurs and pterosaurs (Bennett 1996b, Benton 1999, Padian 1984, Sereno 1991, 1996), others concluded a descendance from eosuchians or prolacertiformes (Benton 1985, D. Peters 2000, Wild 1983a, 1984). The latter view is supported from the presence of multicuspid teeth in juvenile specimens of *Tanystropheus* (Wild 1973), which resemble the teeth of the Triassic pterosaur *Eudimorphodon* (Wellnhofer 1991a, Wild 1978, 1983a, 1984). However, the known skulls from these reptile groups, e.g. *Tanystropheus* (as shown in Wild 1973) or *Prolacerta* (as shown in Modesto & Sues 2004) lack the antorbital fenestra present in archosaurs and possess some features which is supposed to be ancestral like palatinal teeth (Modesto & Sues 2004). The characteristics of the pterosaur skull preconstruction given above matches more closely that of *Scleromochlus taylori* as reconstructed by Benton (1999), although differences are present in case of the orbitotemporal region which is very slender and slightly inclined in posterodorsal direction.

For these reasons, a hypothetical preconstruction is chosen herein instead of using the skulls of the taxa mentioned above as a model. A more thorough analysis of the entire pterosaur construction and the bionomic reorganisation from terrestrial locomotion to flight might clarify whether a more specific diapsid taxon might be used as a model for a pterosaur preconstruction. The presence of multicuspid teeth is not a character, present in the pterosaur skull preconstruction, but is derived as stated in the discussion on pterosaur tooth constructions (see chapter 9.1).

9.5.3 Basal rhamphorhynchoid skull constructional level

This constructional level contains all shamphorhynchoid skull construction types, excluding the Campylognathoides and Rhamphorhynchus skull constructions. Within this level, three different tendencies of changing morphology of the skull constructions are constructed, using the criteria given in chapter 9.5.1. The end-constructions of these three pathways can not be transferred directly into each other, only by a reversal of structural changes. A soft-tissue crest may be present in all skull constructions oft this level, although it is only documented from *Angustinaripterus* and from an undescribed rhamphorynchoid pterosaur from China (Frey 2005, pers. comm.). However, in contrast to some pterodactyloid pterosaurs, the crest is not supported by a mediodorsal bony crista and therefore is not considered to have any influence on the skull mechanics during bite.

The Eudimorphodon skull constructional type is derived from the Proto-pterosaur skull construction by elongation of the rostrum and a more obliquely orientated occipital region. (Fig. 9.5). The changes lead to an increase in snap efficiency (= increased jaw closing velocity) as well as some buttressing of the bars anterior and posterior to the lower temporal fenestra against the joint reaction forces (see chapter 9.3.2). In conse-

quence, the maxillary/nasal bar between antorbital fenestra and naris is orientated steeply oblique and retains a main supporting role for the loads imposed by a bite as the level of this bar. Here some of the largest teeth are present, resulting in the probability of high loads because of the high bite force F_B present here. A complete reduction of the bar is thus not possible without a shifting of the loads in a more anterior direction (see chapter 9.3.3).

Further modifications are found in the dentition where the interalveolar space between the four premaxillary teeth is increased due to the elongation of the premaxillary part of the rostrum. Im comparison to the preconstruction, these four tooth pairs are enlarged and curved, increasing the penetrational depth as well as the bending stability (see chapter 9.1). Posteriorly, due to the increase of the occlusional surface of the teeth by addition of anterior and posterior cusps (see chapter 9.1), the dentition is very dense and has no significant interalveolar space. This is different from the two other pathways within this constructional level, in which the skull construction possess simple, monocuspid teeth, either of Pterodactylus or Rhamphorhynchus tooth construction with large interalveolar space (Figs. 9.6-9.7).

These changes are continued into the Preondactylus constructional level in which the rostrum is further elongated and the occipital region more obliquely orientated than in the Eudimorphodon constructional level (Fig. 9.5). The anteriormost four tooth pairs and the two tooth pairs ventral to the bar between naris and antorbital fenestra are still the largest teeth, but the teeth are more widely-spaced than in the Eudimorphodon constructional level, restricting the possibility to hold small objects here. Nearly all teeth are serrated leading to an increase of friction and ripping capacity during penetration of the food item (see chapter 5). Like in the Eudimorphodon construction level, high torsional loads will result from an asymmetrical bite.

A second evolutionary pathway is constructed based on the hypothetical Proto-pterosaur skull construction, leading via the Dimorphodon to the Anurognathus skull construction type (Fig. 9.6). Here, the main changes are the bulging of the dorsal bar, a reduction in number of teeth, broadening of the skull and shortening of the pre-orbital part of the rostrum. These changes increase the snap-and-hold, respectively snap-and-lock efficiency. They lead to an increase of torque and shear stresses, but decrease in bending moments. Due to the mechanical regime present in this pathway, the occipital region and the bar between antorbital fenestra and naris are more or less vertical, therefore maintaining the high mechanical advantage of the jaw musculature, acting at the same time as one of the main supports of the skull construction (see chapter 9.3.3). In contrast to most other pterosaurs, fossil skulls of *Anurognathus*, *Batrachognathus* and *Jeholopterus* indicate an incomplete fusion of the bones. From studies of recent animals (e.g. Buckland-Wright 1978, Herring & Mucci 1978, Rafferty & Herring 1999, Rafferty et al 2003, Sun et al. 2004), it is known that sutures play an important role in absorbing much of the strain energy put on bones. In the skulls of pterosaurs with rather short rostra, the incomplete fusion of bony elements thus may be a direct mechanical consequence of the high strains present in such skulls.

The third evolutionary pathway based on the proto-pterosaur skull construction shows an increase of the jaw closing acceleration by lengthening of the rostrum and/or inclination of the occipital region (Fig 9.7). Both processes may have occurred simultaneously or in successive steps. The presence of the Cacibupteryx skull construction with a longer rostrum than in the preconstruction and vertically orientated occipital region, indicates that the inclination is subsequent to the elongation of the rostrum. Due to the increase in rostral length, bending moments increase and the maxillary/nasal bar between antorbital fenestra and naris gets obliquely

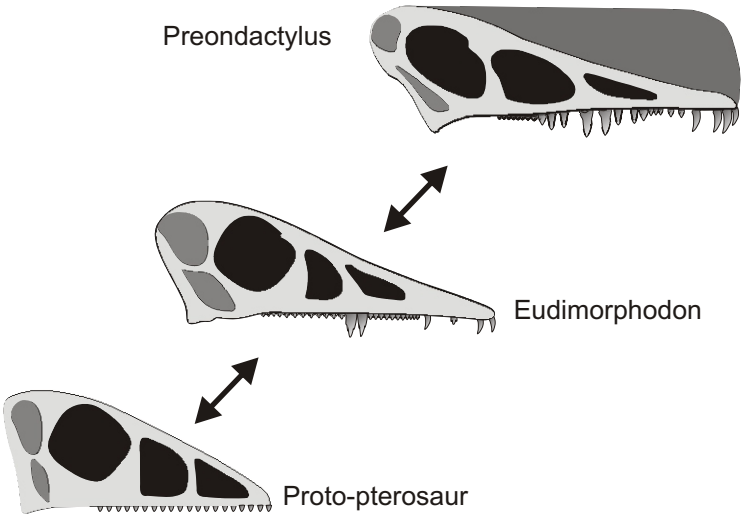

Fig. 9.5: First evolutionary pathway described in the text with skull constructions derived from a hypothetical Proto-pterosaur skull construction. See text for explanation of transformational processes.

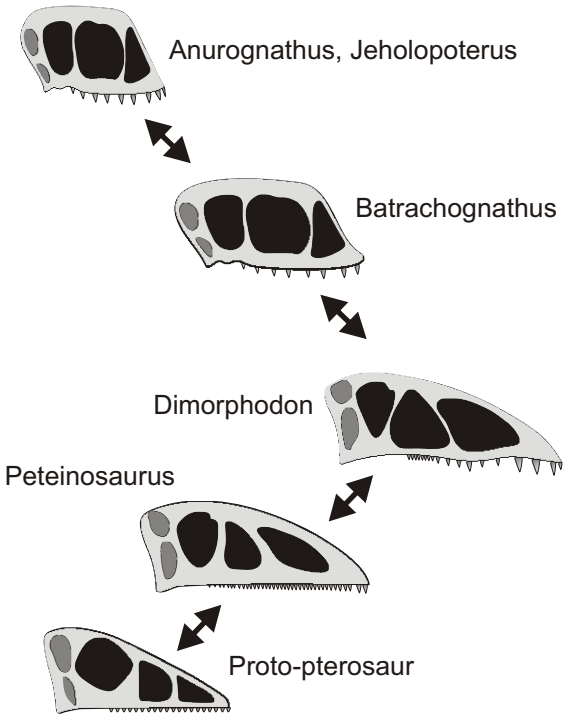

Fig. 9.6: Second evolutionary pathway described in the text with skull constructions derived from a hypothetical Proto-pterosaur skull construction. See text for explanation of transformational processes.

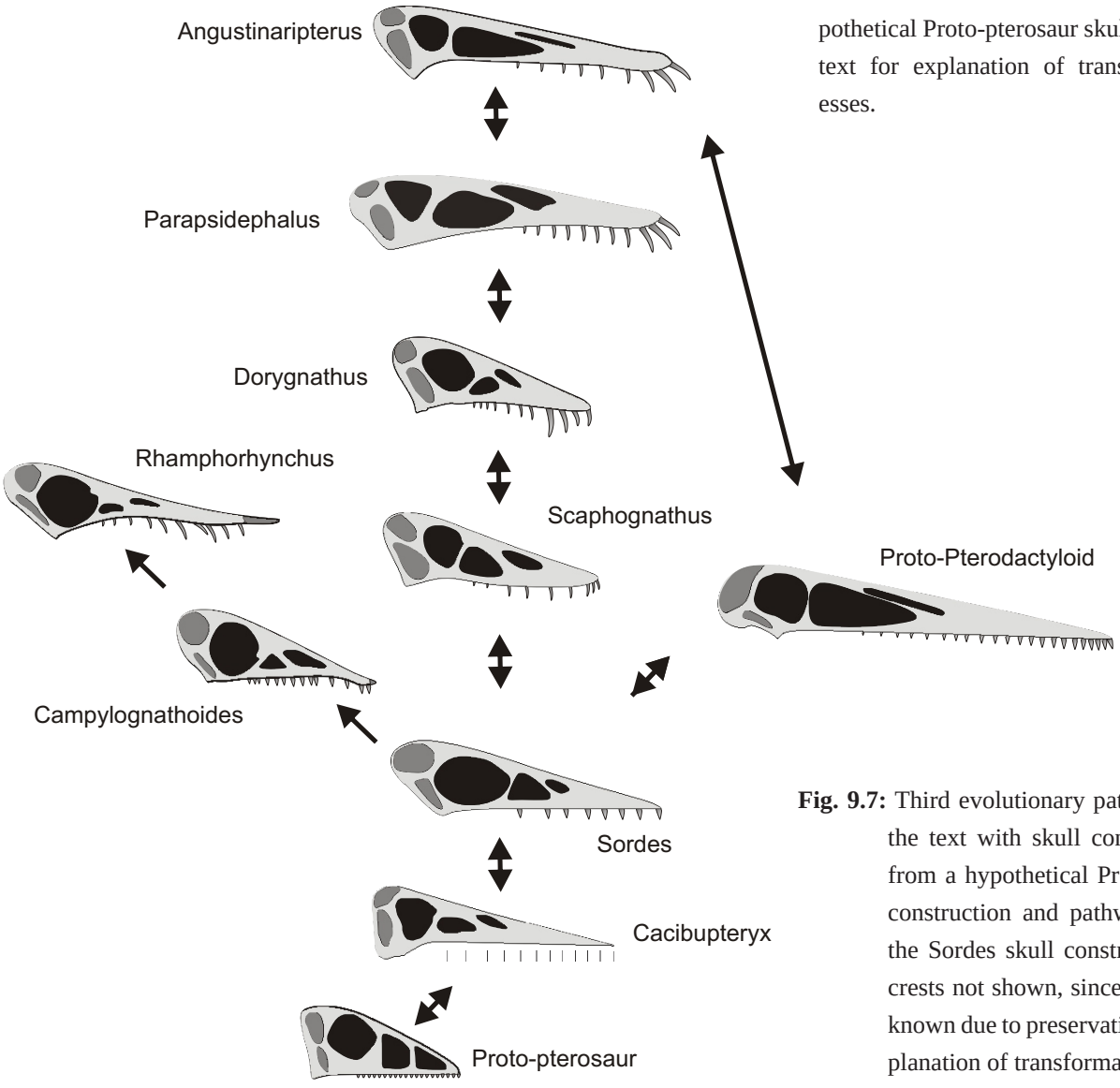

Fig. 9.7: Third evolutionary pathway described in the text with skull constructions derived from a hypothetical Proto-pterosaur skull construction and pathways derived from the Sordes skull construction. Soft-tissue crests not shown, since distribution is unknown due to preservation. See text for explanation of transformational processes.

orientated. The latter change is caused by the high occlusional loads at the elongated rostrum, where the support of the skull construction is maximised by an inclined bar. As a further, second step, the occipital region gets inclined, leading to the Sordes skull construction, from which three different lineages are derived (Fig 9.7). The first lineage leads to the Rhamphorhynchus skull constructional. As this represents another constructional level, it is described separately (see chapter 9.5.4).

The second pathway based on the Sordes skull construction leads via the Scaphognathus to the Parapsicephalus constructional level (Fig 9.7). The first step is the development of vertically orientated, enlarged teeth of Rhamphorhynchus tooth constructional type. The Sordes skull construction is thus transformed from a snap-and-hold into a snap-and-penetrate construction (see chapter 9.4). As a second step, the rostrum is elongated, increasing the snapping efficiency due to the increased occlusional velocity. As a mechanical consequence, the maxillary/nasal bar between antorbital fenestra and naris is low-angled against the horizontal plane, but still acts as a support for the skull construction (see chapter 9.3.3). This results in an anterodorsal orientation of the naris relative to the antorbital fenestra and a slit-like shape of the naris, present in the Angustinaripterus skull construction (Fig. 9.7).

To get to a hypothetical Proto-Pterodactyloid skull construction within the basal rhamphorhynchoid skull constructional level, two pathways are possible to construct (Fig. 9.7). One is the derivation from the Angustinaripterus skull construction. Here, the changes needed are a further inclination of the occipital region, leading to a low angle against the horizontal plane, and a change of the dentition type from Rhamphorhynchus (snap-and-penetrate) to Pterodactylus (snap-and-hold) tooth construction. The latter step may be more unlikely than constructing a pathway leading from the Sordes skull construction to the Proto-Pterodactyloid skull construction (Fig. 9.7), because of the higher number of changes needed. Similar to the pathway described in the previous paragraph, the rostrum is enlarged, the occipital region further inclined in posterodorsal direction and the maxillary/nasal bar orientated in posterodorsal direction with a low angle. However, there is no need for a change of the dentition type here, because the Sordes skull construction also possess teeth of Pterodactylus tooth construction. As both, Sordes and Proto-Pterodactyloid skull construction, are snap-and-hold constructions, the efficiency is increased in the latter skull construction (see chapter 9.3.1).

The Proto-Pterodactylus skull construction forms the base for all other constructional levels, except the Rhamphorhynchus skull constructional level (Figs. 9.8-9.11).

9.5.4 Rhamphorhynchus skull constructional level

The pathway leading to this level is based on the Sordes skull construction. It is characterised by the formation of non-hook-like keratinous beak (Fig. 9.7), present at the toothless anterior rostrum of the Campylognathoides skull construction. As this transformation is irreversible (see chapter 9.5.1), it constitutes the Rhamphorhynchus skull construction level. The keratinous beak is further enlarged in the Rhamphorhynchus skull construction (Fig 9.7).

In this pathway, the snapping efficiency is increased by an enlarged rostrum (see chapter 9.3.1). High bending moments occur and shear and comparison stresses are reduced due to presence of the rhamphotheca (see chapter 9.3.4) The size of the nasoantorbital fenestra and the naris retains small, and both remain orientated inline to each other. In the Rhamphorhynchus skull construction, the anteroventrally projecting teeth of Rhamphorhynchus tooth constructional type increase the penetration depth of the teeth while the torque is reduced

due to the narrowing of the rostrum. The enlarged anterior beak becomes responsible for holding of the food item, although a complete occlusion is questionable in *Rhamphorhynchus* (Frey 2005, pers. comm.).

9.5.5 Pterodactylus skull constructional level

This constructional level is derived from the hypothetical Proto-Pterodactyloid skull construction by fusion of naris and antorbital fenestra and development of an anterior keratinous hook. Both transformations are irreversible (see chapter 9.5.1) and lead to the Pterodactylus antiquus/kochi skull construction (Fig. 9.8). The formation of the nasoantorbital fenestra is induced by the low loads on the maxillary/nasal bar between naris and antorbital fenestra due to an increase in rostral length. This leads to the reduction of the bar (see chapter 9.3.3). The consequences of keratinous hook are discussed in detail in chapter 9.3.4. Its presence results in a reduction of the dentition from anterior. In this skull construction, a soft-tissue crest is present, but without any bony support in form of a mediodorsal crest.

The Pterodactylus antiquus/kochi skull construction forms the base for two alternative pathways (Fig. 9.8). The changes leading via the Germanodactylus skull construction to the Dsungaripterus skull construction type is caused by an increase in size of the rhamphotheca. Whereas a keratinous hook acts more or less similar to teeth, this increase leads to the reduction of torque and absorption of shear and comparison stress (see chapter 9.3.4). The dentition is not entirely shifted in posterior direction on the rostrum but reduced from anterior. This process is irreversible. As shown previously (see chapter 9.3.4), the absorbing effects of the rhamphotheca permits the narrowing of the skull, which further reduces the torque. Such a narrowing is seen in the Germanodactylus skull construction and more distinct in the Dsungaripterus skull constructional type.

The decrease of friction due to the loss of the teeth may be accounted for by a curvature of the jaws as seen in the Dsungaripterus skull construction type or by a relief on the internal surface of the beak (Frey at al. 2003c). However, in contrast to the tapejarids (Frey at al. 2003c), no fossil evidence exists for the latter scenario in *Germanodactylus*, *Phobetopter* or *Dsungaripterus*.

In contrast to the Pterodactylus kochi/Pt. elegans skull construction, the Dsungaripterus skull constructional type has a relatively shorter rostrum, increasing the bite forces. Furthermore, as shown in chapter 9.4.6, high loads may be common in this skull construction type due to a bite at the posterior end of the dentition. This induces high joint reaction forces F_J in the Dsungaripterus skull constructions. These forces are buttressed by the enlarged jugal area ventral to the orbita, which leads to a reduction of the suborbital fenestra and the size of the orbita (see chapter 9.3.2).

Parallel to the development of a rhamphotheca, the soft-tissue crest present in the skull constructions of this pathway is supported by a thin, bony mediodorsal crista (Fig. 9.8). This structure is developed for the first time in the Germanodactylus skull construction and situated dorsal to the nasoantorbital fenestra. The genesis of these crest, which also occurs in other constructional levels has been discussed in detail in Frey et al. (2003c), where they were interpreted as a mineralised support for a soft-tissue crest. Furthermore, the crista has also a stabilising effect for the dorsal premaxillary/nasal bar against torsional and high compressive loads present in this area (see chapter 9.3.5). This crest is thicker in the Dsungaripterus skull construction type, where even higher loads than in the Germanodactylus skull construction can be expected due posterior bites (see chapter 9.4.6).

In the Pterodactylus as well as the Germanodactylus skull construction, the posteroventral part of the soft-tissue crest is supported by an occipital cone, formed by fibrous-elastic connective tissue (Frey et al. 2003c). In the Dsungaripterus constructional level, the medial crest is more mineralised and the cone is replaced by a bony crest at the posterodosal occipital region. It is not clear whether this bony crest is formed by the supraoccipital and parietal bones or by mineralised soft-tissue.

The second pathway within the Pterodactylus skull construction level, leading to the Pterodactylus elegans/Pt. micronyx skull constructions shows a reduction of the dentition in posterior direction (Fig. 9.8). A keratinous hook is present at the anterior tip of the rostrum. The posterior teeth are reduced because they do not form an essential part of the dentition for snap-and-hold function. The grasping of food items is instead concentrated on the anterior part of the rostrum. The results are low torsional loads, but high bending moments. These have to be accommodated for by the anterior rostrum which is of low height. The size of the nasoantorbital fenestra is constrained by this low profile and thus do not extend to the level the posterior end of the dentition as in most other pterosaur skull constructions (Fig. 9.7). Otherwise, the load bearing capacity of the rostrum would be reduced drastically (see chapter 9.3.3).

If the dentition is further reduced, the keratinous hook gets more prominent, and may be enlarged to form a rhamphotheca. This transformation is irreversible. It decreases the loads and leads to a more uniform distribution of stresses. Two different skull construction levels are derived by this transformation from the Pterodactylus micronyx skull construction, depending on the size of the nasoantorbital fenestra and the length of the rostrum. Both, the hypothetical proto-azhdarchoid as well as the Pterandon skull construction (Fig. 9.8) are described in separate chapters below.

9.5.6 Azhdarchoid skull constructional level

The Proto-azhdarchoid skull construction is derived from the Pterodactylus micronyx skull construction by the complete reduction of the dentition from posterior and enlargement of the keratinous hook to a rhamphotheca (Fig. 9.9). The mechanical effects of the rhamphotheca (see chapter 9.3.4) permits the option of a more narrow skull construction than in the toothed Pterodactylus constructional level. A soft-tissue crest may be present in this skull construction, as well as a mediodorsal crista, which is common in most azdharchoids .

The two pathways which are derived from this hypothetical skull construction (Fig. 9.9) are characterised by different proportions of the nasoantorbital fenestra and rhamphotheca. In the Azhdarchoid skull construction type, the rostrum is enlarged, therefore increasing the velocity of the occlusion (snap-squeeze-and-cut, see chapter 9.4.7). Due to the large rostral area anterior to the nasoantorbital fenestra, food items can be grasped over a large area along the jaw. The resulting torsional, shear and comparisons stress are low due to the presence of the rhamphotheca (see chapter 9.3.4) . However, large bending moments are present, which are counteracted by the curvature of the rostrum in the Quetzalcoatlus skull construction (see chapter 9.3.6). Here, the bony mediodorsal crest stabilises the dorsal bordering bar of the nasoantorbital fenestra against the high compressive forces during occlusion.

In contrast to the pathway leading to the azhdarchid skull construction type the rostrum is not significantly enlarged in the Tupuxuarid skull construction type. However, the region of the rostrum anterior to the nasoantorbital fenestra, and therefore the rhamphotheca, measures only one third of the overall length of the rostrum.

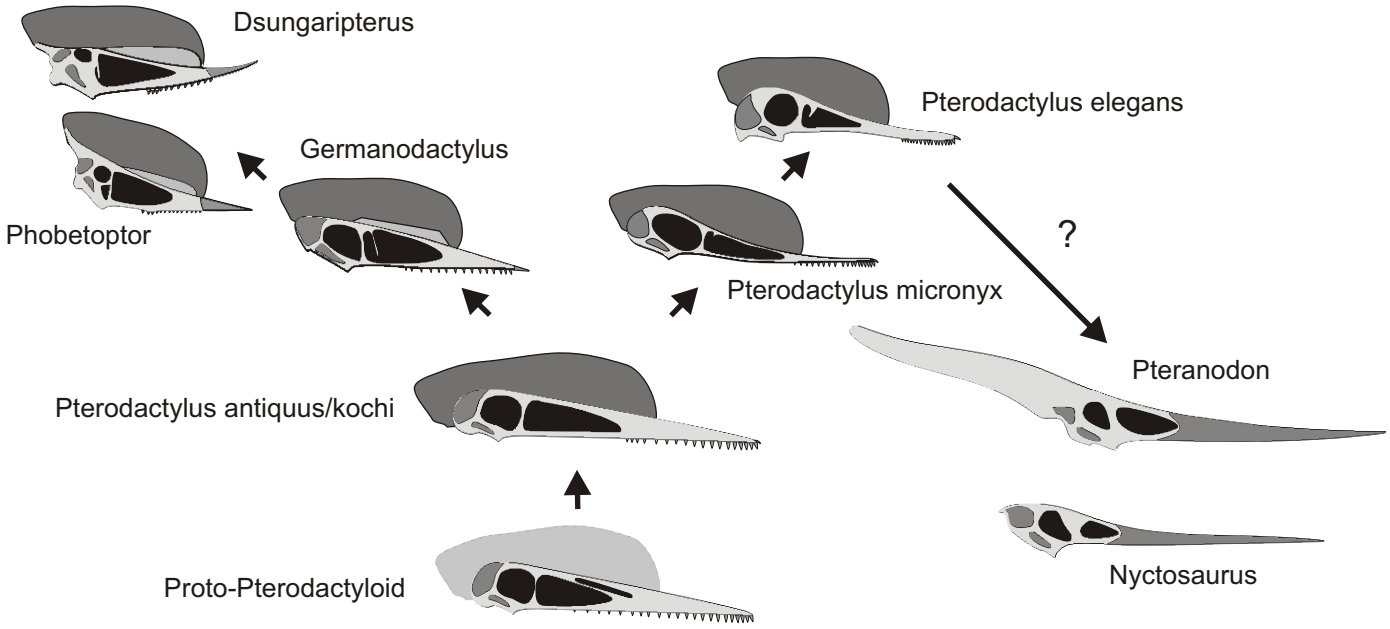

Fig. 9.8: First evolutionary pathways described in the text with skull constructions derived from a hypothetical Proto-pterodactyloid skull construction, respectively from the Pterodactylus antiquus/kochi skull construction. See text for explanation of transformational processes.

Fig. 9.9: Second evolutionary pathways described in the text with skull constructions derived from the Pterodactylus elegans skull construction. See text for explanation of transformational processes.

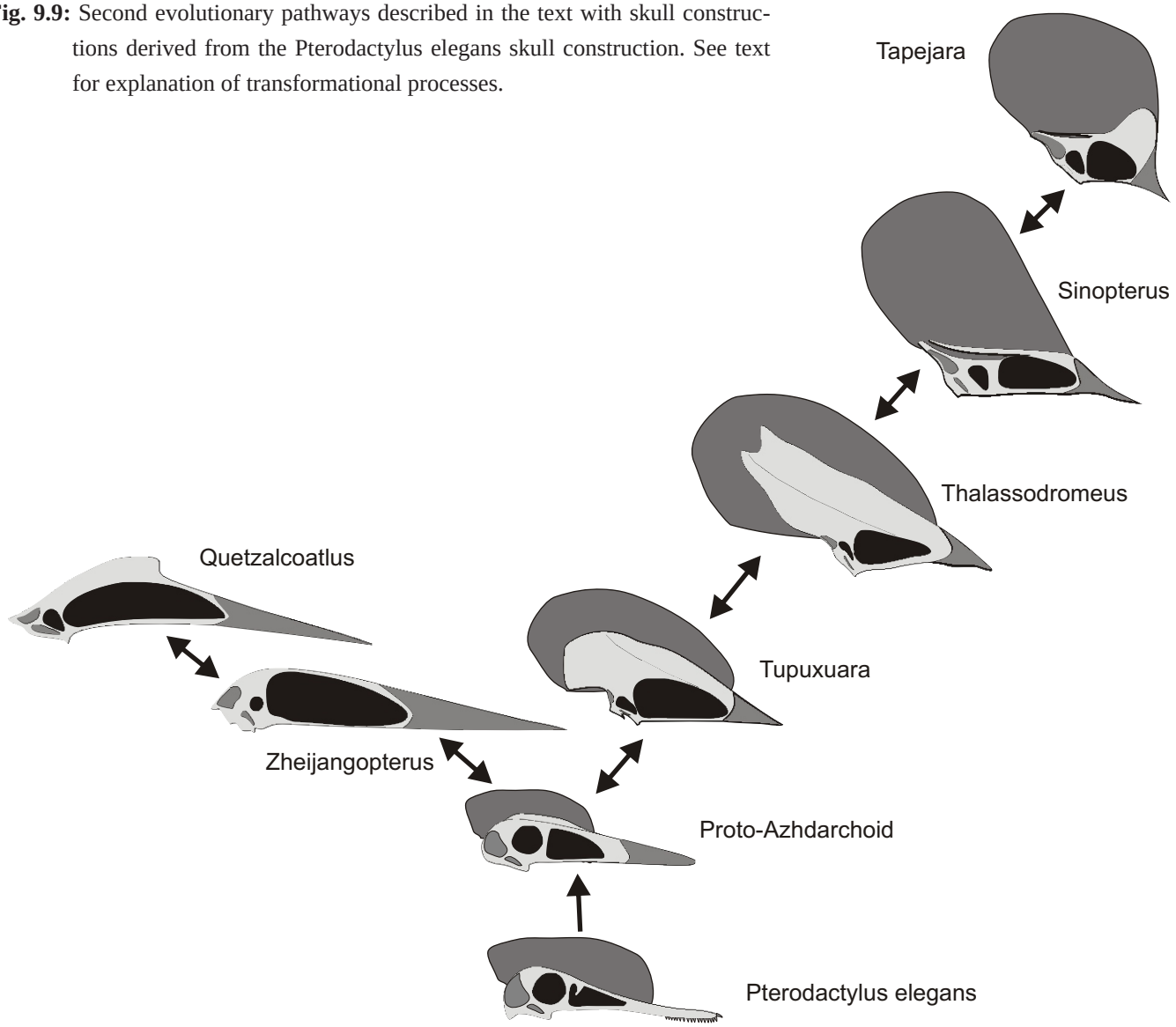

This is contrary to the situation in the Azhdarchid skull construction type (see above) and thus is considered a second, different tendency of change within the Azhdarchoid skull constructional level here (Fig. 9.9).

Like the Azhdarchid skull construction type the Tupuxuarid skull construction type exhibits snap-squeeze-and-cut characteristics (see chapter 9.4.7). However, in the latter type, the rhamphotheca is relatively short which indicates, that grasping of the food items is also concentrated on the anterior third of the rostrum and therefore on a smaller area than in the Azhdarchid skull construction type. This implies a more precise and directed bite. The thin, striated crest which extends from the anterior rostrum to the orbitotemporal region indicates the presence of a large soft-tissue crest (Frey et al. 2003c). It stabilises the entire dorsal margin of the rostrum against loads (see chapter 9.3.5).

The changes leading from the Proto-Azhdarchoid to the Tupuxuarid skull construction type parallel the changes needed to derive the Tapejarid skull construction type. It is therefore reasonable to assume a connection between both latter types, although a parallel modification can not be ruled out (Fig. 9.9). As the Tapejarid skull construction type is brevirostrine, it is more parsimonious to derive it from the longirostrine Tupuxuarid skull construction than *vice versa*. Shortening of the rostrum leads to an increase of the anterior bite forces and decreased occlusion velocity of the jaws. In consequence, the bending moments decrease, but shear, torsional and comparisons stresses increase. However, the latter stress types are significantly reduced due to the presence of the anterior bony crest (see chapter 9.3.5). This the main difference to the Anurognathid and Dimorphodontid skull constructional type, described earlier, which are also brevirostrine and possess a rostrum with large fenestrations. Here, the vertically orientated jugal/lacrimal and maxillary/nasal bars in the rostrum act as supports for the rostrum. The latter bar is not present in the Tapejarid skull construction and stabilising of the rostrum is achieved by the stress-reducing effect of the crest and rhamphotheca. Furthermore, a constricted connection between the orbitotemporal region and the dorsal bordering bar of the nasoantorbital may decrease the stresses in the Tapejarid skull constructional type. In contrast to the Tupuxuarid skull construction type, a steeper angulation is present in the anterior rostrum of the Tapejard skull construction type (Fig. 9.9). This indicates different foraging modes. Assuming e.g. a piscivorous diet for pterosaurs of this type, the dipping depth is much less in Tapejara (100 mm) than in Tupuxuara (400 mm, Frey 2005, pers. comm.).

9.5.7 Ornithocheirid/Chasmatoid skull constructional level

In contrast to the latter pathways which are derived from the Pterodactylus constructional level, all pathways described in this chapter lack the formation of a keratinous hook. One possible option here is to increase the size of the anterior tooth pairs and thus to develop a special prey-catching device at the anterior end of the rostrum. This increases the snap-and-hold efficiency due to the deeper penetration of the food item (–> snap-and-penetrate, see chapter 9.4.1). The changes lead to a skull constructions with Ornithocheirus tooth constructions (Fig. 9.10) and the Ornithocheirus constructional level. It is derived from the hypothetical Proto-Pterodactyloid skull construction by lengthening of especially the pre-nasoantorbital part of the rostrum and loss of the soft-tissue crest (Santanadactylus skull construction). This leads to higher acceleration of the jaws but increases bending and torsional loads. The development of an anterior bony crest as in the Anhanguera, Coloborhynchus and Criorhynchus skull constructions (Fig. 9.10) has the effect of increasing bending and torsional stiffness and decreasing the comparison stress.

Fig. 9.10: Third evolutionary pathway described in the text with skull constructions derived from the hypothetical Proto-Pterodactyloid skull construction. See text for explanation of transformational processes.

An alternative pathway leads to the Ludodactylus skull construction where a crest is present, too (Fig. 9.25). It is situated posterodorsally to the orbitotemporal region, presumably enlarging the moment arm of the muscles originating at the upper temporal fenestra (see chapter 9.3.5). Whether the Cearadactylus skull construction is derived from the latter or from the Santanadactylus skull construction is unclear (Fig. 9.10). The festoonation of the jaw margin present in this skull construction leads to high shear stress and a clear tendency for twisting (see chapter 7.7) due to high torque. This is contrary to the development seen in most other skull constructions of the Ornithocheirus constructional level. A similar condition is seen in the Istiodactylus skull construction, which also has a high tendency for twisting (see chapter 7.19). However, although of Ornithocheirus constructional type, the teeth of the latter skull construction are not enlarged as in the Ornithocheirus constructional level and show a tight occlusional indenting with the teeth of the lower jaw. Furthermore, the nasoantorbital fenestra is enlarged so that most of the rostrum is occupied by the fenestra. The tooth row is restricted row to the short, laterally expanded and rounded pre-nasoantorbital part of the rostrum. Since the overall tooth count is high, this does not represent a reduction of the dentition. Due to the large rostrum of the Istiodactylus skull construction, a high occlusive acceleration and velocity of the jaws is present. However, the "duck-like" anterior rostrum with occlusion of teeth indicates a filter-feeding option or a use comparable to a spaghetti fork. The Istiodactylus constructional level can be derived either directly from the Santanadactylus skull construction by reducing the height of the teeth, enlarging the nasoantorbital fenestra and expanding the anterior tip of the rostrum or alternatively from the Cearadactylus constructional level (Fig. 9.10). In the latter skull construction, high torsional loads are present due the large teeth and the unusual morphology of the anterior rostrum with the festoonation and the laterally expanded tip (see above). Decreasing the height of the teeth leads may reduce the loads in this part of the rostrum, by implying smaller food items. As a consequence, the nasoantorbital fenestra can be increased in size and the jugal/lacrimal bar can be reduced in cross-sectional area because it is much lower stressed. Alternative to this pathway, the Istiodactylus could be derived directly from a hypothetical Proto-Pterodactyloid skull construction by enlarging of the nasoantorbital fenestra and anterior shifting of the dentition.

The second pathway which is derived from the Proto-Pterodactyloid skull construction also includes the elongation of the rostrum (Fig. 9.11). Similar to pathways described above, this leads to an increased acceleration of the jaws but reduced anterior bite forces. However, in contrast to the latter pathways, the number and slenderness of the teeth increase drastically. In consequence, the size of the nasoantorbital fenestra remains small. Such a hypothetical Proto-Ctenochasmatoid skull construction (Fig. 9.11) may also bear a soft-tissue crest, which is combined with a fibrous crista on the dorsal bar of the rostrum, and facilitates the stabilising against compressive and torsional loads. This hypothetical skull constructions gives rise to the Gnathosaurus skull construction and moreover, the Ctenochasma skull construction by a further increase of the number of teeth and thus smaller food items and/or an increased filter-option of the jaws (Fig. 9.11). In the Ctenochasma skull construction, a fibrous crista is missing, suggesting that the loads in the dorsal bar are lower than in the preceding skull constructions. With an ongoing increase in tooth count and elongation of the pre-nasoantorbital part of the rostrum a transformation into the Pterodaustro skull construction is possible (Fig. 9.11). These processes increase the filtering capacity of the jaws. However, here an increase in tooth height only takes place in the lower jaw, whereas in the upper jaw the teeth are shortened. Otherwise, the filter device would not be operable, because of the tight dentition in the lower jaw which makes interdigitating with the teeth from the

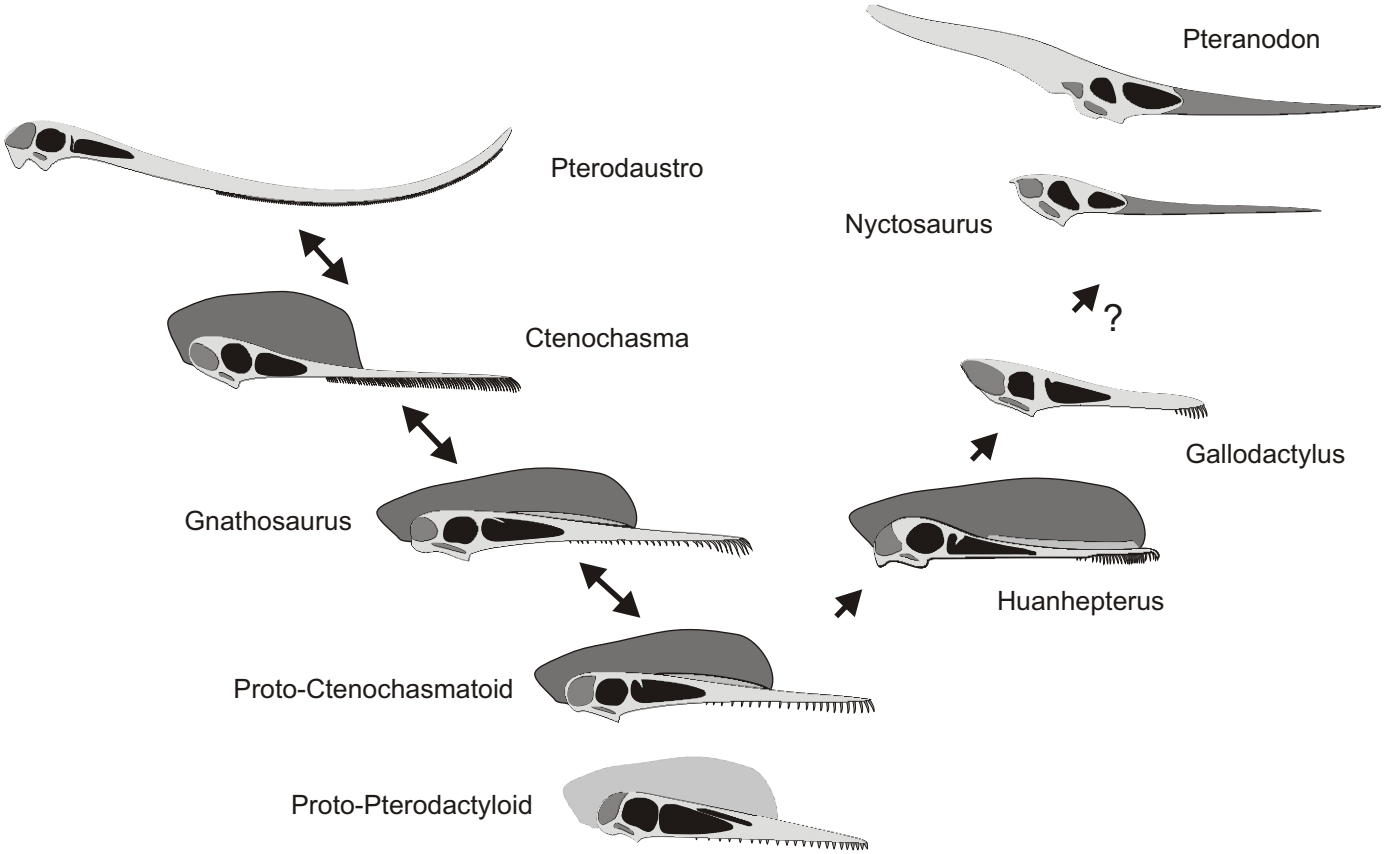

Fig. 9.11: Fourth evolutionary pathway described in the text with skull constructions derived from the hypothetical Proto-Pterodactyloid skull construction. See text for explanation of transformational processes.

lower jaw impossible. Lengthening the teeth of the upper jaw while shortening the lower teeth on the other hand would permit food items to drop out of the jaw. The bending of the jaws are interpreted as increasing the efficiency of "shovelling" of large masses of water filled with food items/particles and conducting them in the direction of the oesophagus. This independent whether the water flow is in posterior direction or in ventral direction.

A second pathway, leading from the Proto-Ctenochasmatoid to the Huanhepterus skull construction (Fig. 9.11), includes a reduction of a number of posterior tooth positions and like in the Cearadactylus skull construction a festoonation of the anterior rostrum. This festoonation leads to a greater torque, which, however, may be compensated by the presence of a mediodorsal crista, which extends near the anterior tip of the jaw. From this level, the Gallodactylus skull construction is derived by a further reduction of the posterior dentition and a lateral expansion of the anterior rostrum (Fig. 9.11), analogue to the pathway leading from the Cearadactylus to the Istiodactylus skull construction (Fig. 9.10). This expansion leads to a decrease of the torsional stiffness. The reduction of the bony crista may indicate that the overall torsional loads caused by the food items are rather low so that no additional stabilising devices are needed.

9.5.7 Pterandontid skull constructional level

While all the evolutionary pathways described so far are biomechanically conclusive, the transformational processes leading to the Pteranodon constructional level are ambiguous (see also Frey et al. 2003c). The presence of a keratinous rhamphotheca may indicate a derivation from the Pterodactylus elegans skull construction. Both share a nasoantorbital fenestra which is small compared with the overall size of the rostrum and a

slender, tapering rostrum. As the dentition is restricted to the anterior third of the rostrum in the Pterodactylus elegans skull construction, the transformation of the keratinous hook into a rhamphotheca may lead to the complete reduction of the dentition. The other transformations would include a lengthening of the pre-nasoantorbital rostrum, loss of dentition and development of an orbitotemporal crest (Fig. 9.8). Mechanically, these changes would decrease the shear, torsion and comparison stress, whereas the bending moments are increased.

A second possibility would be a transformation from the Gallodactylus skull construction (Fig. 9.11). Here, the teeth are restricted to the anterior end of the rostrum. A reduction of the dentition, lengthening and tapering of the rostrum as well as the development of a rhamphotheca and occipital crest could lead to the Pteranodon constructional level.

As a third possibility, the Ludodactylus skull construction could serve as a preconstruction for the Pteranodon constructional level (Fig. 9.10) because of the presence of a orbitotemporal crest, a structure which does not occur in any other pterosaur skull construction. Again, the complete reduction of the dentition, lengthening and tapering of the rostrum would be the major processes here.

Especially, the latter scenario seems more unlikely than the former two scenarios because one of the changes leading to the Ludodactylus skull construction is the lengthening of the anterior tooth pairs. Reduction of the teeth would reverse this trend. Although further alternative preconstructional levels (Dsungaripterus, Azhdarchid, Pterodaustro or Istiodactylus constructional level) can be constructed, these include more and rather complicate changes than for the three alternative possibility described above. Only the first pathway is based on a preconstruction which already possesses a keratinous hook (Pterodactylus micronyx skull construction), whereas in the other two pathways such a structure has to arise independently. The first scenario is therefore considered to be the most plausible.

9.6 Comparison of the evolutionary pathways with recent cladograms

Although a couple of attempts had been made, to analyse the phylogentic systematics of pterosaurs (Bennett 1989, 1994, Howse 1986, Kellner 1995, 1996a, Unwin 1992, 1995, Viscardi et al. 1999), only two thorough analyses exist which contain most of the pterosaur species known so far (Kellner 2003, Unwin 2003). Both analyses differ in the position of certain higher groups (e.g. Dsungaripteridae, Dimorphodontidae and Anurognathidae) and will therefore discussed separately. For comparative purposes, the evolutionary pathways constructed in the previous chapters are transferred into a dendrogram illustration (Fig. 9.12).

9.6.1 Comparison with cladogram by Kellner (2003)

Congruencies between the cladogram (Fig 9.13) and the evolutionary pathways constructed here (Fig. 9.12) exist in case of the position of the monophyletic group containing the Dsungaripteridae, Azhdarchidae, *Tupuxuara* and *Tapejara* (Fig. 9.13: 1) as well as the group with *Germanodactylus*, *Pterodactylus kochi*/*Pt. antiquus*, *Ctenochasma*, *Pterodaustro* and *Gallodactylus* (Fig. 9.13: 2) and the position of *Scaphognathus* and *Dorygnathus* (Fig. 9.13: 3), both taxa which are assigned to the *Scaphognathus* skull construction type (see 9.2.21). Also the relationship of *Rhamphorhynchus* and *Campylognathoides* resembles the evolutionary pathway dendrogram (Fig. 9.12). Although some species are missing in the cladogram, the relation between these

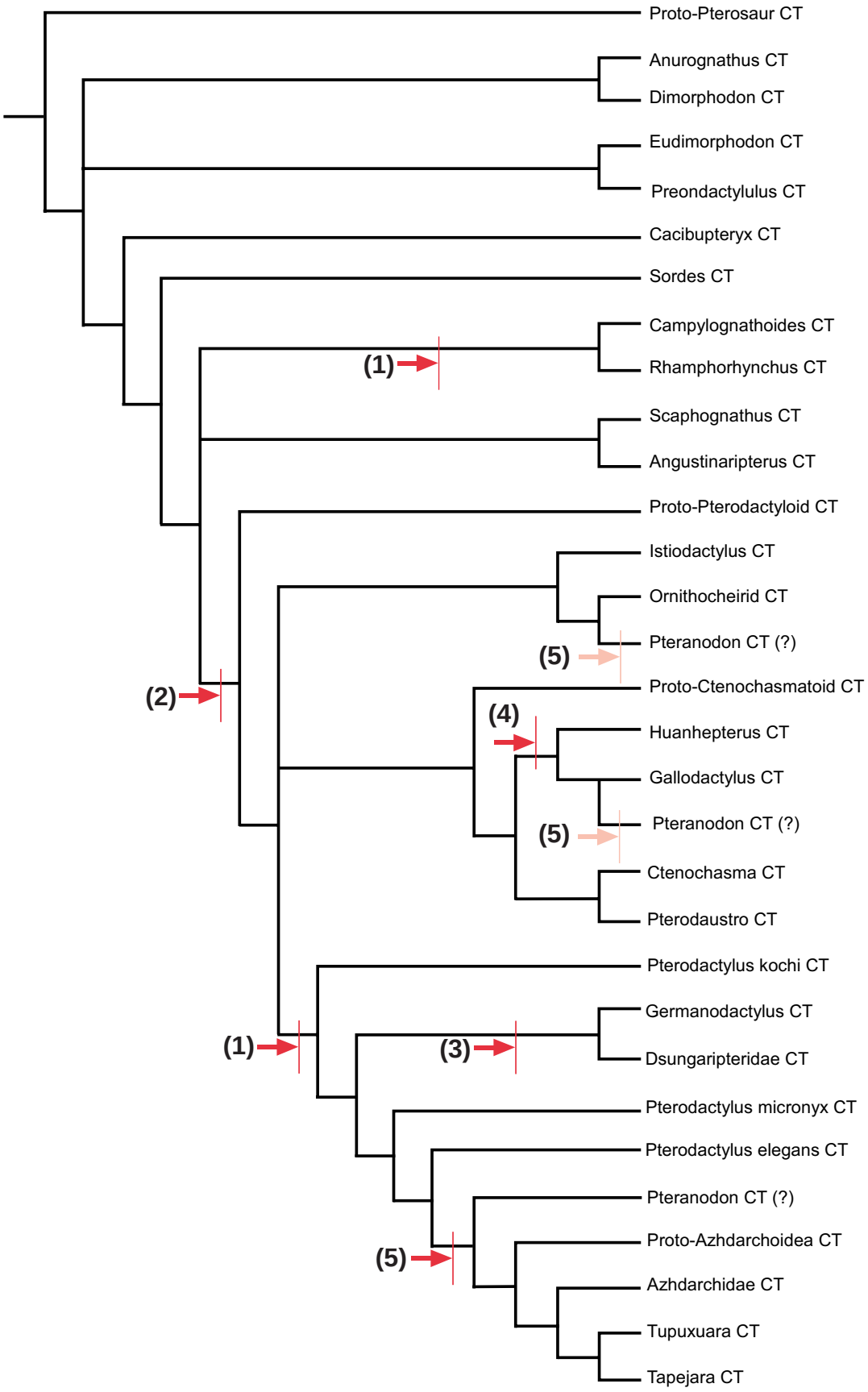

Fig. 9.12: Dendrogram illustrating the evolutionary pathways described herein. Red arrows = irreversible transformations, pink arrows = irreversible transformation for alternative positions of the Pteranodon CT. (1) = Keratinous hook/sheet at the anterior end of the rostrum; (2) = Nasoantorbital fenestra (–> Pterodactyloidea skull constructions); (3) = Rostrum with teeth and keratinous anterior rhamphotheca; (4) = Reduction of dentition from posterior; (5) = Edentulous rostrum.

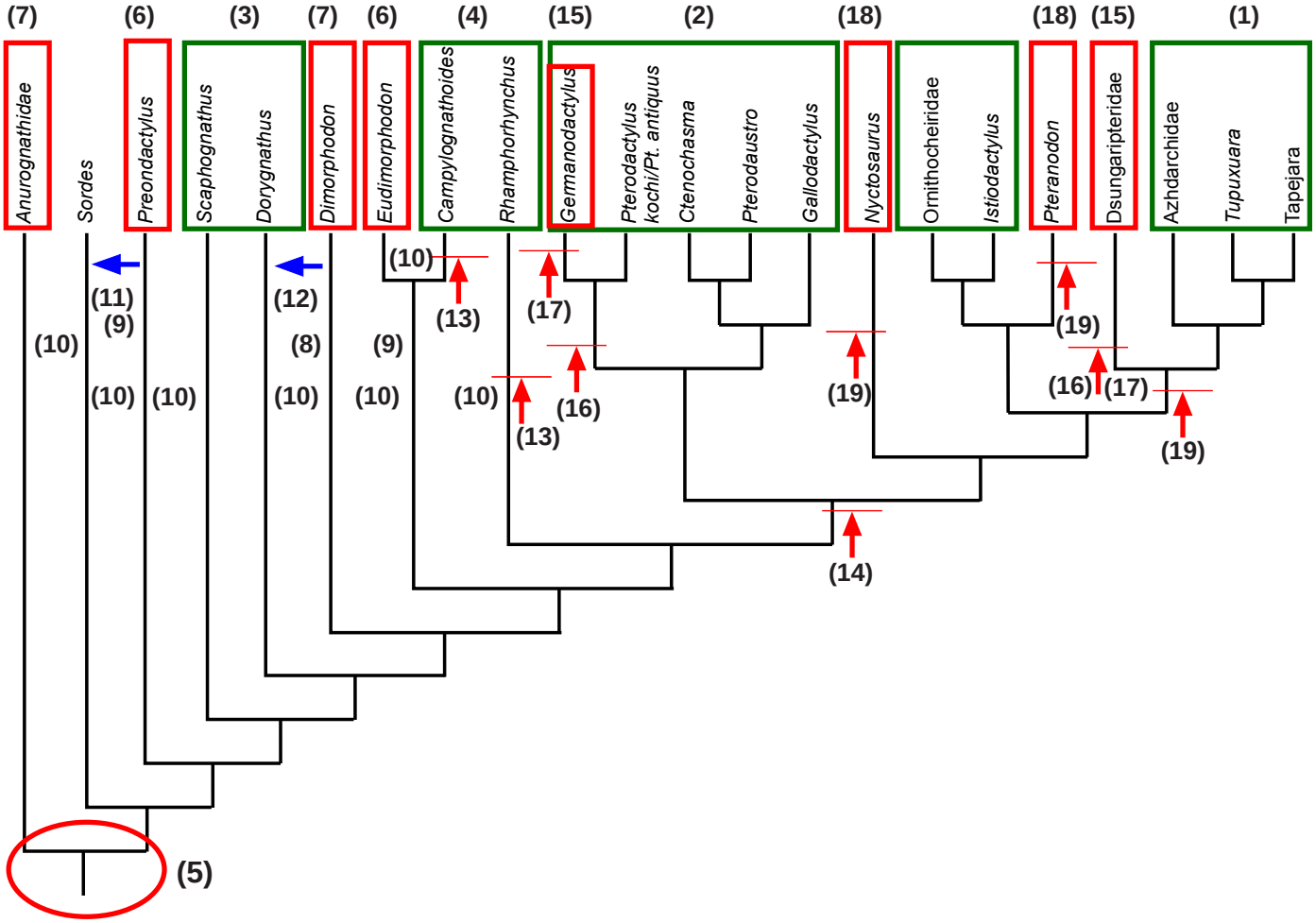

Fig. 9.13: Cladogram proposed by Kellner (2003). Blue arrows = reversal of changes, red arrows = irreversible transformation, green rectangles = similarities to evolutionary pathway diagram, red rectangle/ellipse = differences to evolutionary pathway diagram. Numbers see text.

different taxa follows the evolutionary transformations and changes within a constructional level changes constructed in the previous chapter.

However, there are a number of differences between the evolutionary pathway diagram and the cladogram by Kellner (2003). At the base of the cladogram a dichotomy is present (Fig. 9.13: 5) which does not match the polytomy seen in the dendrogram (Fig. 9.12). As deduced by the dendrogram, *Anurognathus* and *Dimorphodon* should form a single group with *Eudimorphon*/*Preondactylus* and all other taxa as sister-groups, whereas in the cladogram by Kellner (2003) the positions of these taxa are scattered (Fig. 9.13: 6+7). This can only be explained if an independent development of certain skull constructional types is assumed. In this case, a high numbers of reversals occur, although none of them violates irreversible transformations. One of these reversals is the reduction of the skull length in *Dimorphodon* (Fig. 9.13: 8), if *Anurognathus* with a brevirostrine skull is considered to be plesiomorphic (Kellner 2003). Also multicuspid teeth would develop two times (Fig. 9.13: 9) and the dentition changes multiple times (Fig. 9.13: 10). The views that *Sordes* is plesiomorphic to *Preondactylus* (Fig. 9.13: 11) and *Dorygnathus* to *Dimorphodon* (Fig. 9.13: 12) are not supported by the evolutionary pathways, and can only be explained by a reversal of the changes between the different skull construction types (see chapter 9.5.3). Another case of an independent development of skull constructional types in the cladogram by Kellner (2003) are *Campylognathoides* and *Rhamphorhynchus* (Fig. 9.13: 4) where

a keratinous beak at the anterior end of the rostrum occurs two times (Fig. 9.13: 13). Furthermore, the position of the latter taxon is problematic, because it is plesiomorphic to the Pterodactyloidea (Fig. 9.13: 14). In the evolutionary pathway diagram, the possession of a keratinous beak forms an irreversible transformation (Fig. 9.12). The position within the cladogram thus can be only be explained if this character is apomorphic, making the use of Rhamphorhynchus as the closest taxa to the Pterodactyloidea (Fig. 9.13: 14) questionable.

Similar to the evolutionary pathway diagram, the Pterodactyloidea form a single group, which is characterised by the fusion of the nasoantorbital fenestra as an irreversible transformation (Fig. 9.13: 14). The relationship within the Pterodactyloidea (Fig 9.28) resembles more the pattern seen in the evolutionary pathway diagram (Fig. 9.12) than in the non-pterodactyloid pterosaurs. However, the position of *Germanodactylus* and *Dsungaripteridae* (Fig. 9.13: 15) does not correspond to the position in the dendrogram and would lead two times to the development of a keratinous hook (Fig. 9.13: 16) and reduction of the dentition from anterior (Fig. 9.13: 17).

The position of the Dsungaripteridae as a sister-group of the Azhdarchoidea (Fig. 9.13: 15) and its relation to the group comprising *Pteranodon* and the Ornithocheiroidea is irreproducible in terms of biomechanical founded changes and transformations. These paraphyletic groups are furthermore problematic, because of the outgroup position of *Nyctosaurus*, meaning, that the *Pteranodon* skull construction type is developed two times independently (Fig. 9.13: 18). Considering *Nyctosaurus* as an outgroup is problematic because the complete reduction of the dentition and replacement by a keratinous rhamphotheca represents an irreversible transformation and thus does not permit to derive a toothed skull construction from it. If the edentulous beak is assumed to be apomorphic to *Nyctosaurus*, this would require an independent development of a keratinous hook/beak four times independently (Fig. 9.13: 19).

In summary, the cladogram by Kellner (2003) includes a high number of reversals and the multiple development of certain skull construction types and transformations. Therefore, it is not very parsimonious with respect of biomechanical transformation. In two cases (*Rhamphorhynchus* and *Nyctosaurus*) violations against irreversible transformations are present, if the reduction of teeth is not considered to be apomorphic to these taxa. The latter assumption, however, makes their outgroup relationship to other groups (Pterodactyloidea, respectively *Pteranodon* + Ornithocheiroidea + Dsungaripteridae + Azhdarchoidea) questionable.

9.6.2 Comparison with cladogram by Unwin (2003)

In contrast to the cladogram by Kellner (2003) most steps in this cladogram (Fig 9.14) are supported by the changes and transformations seen in the evolutionary pathway diagram. However, some differences exist, e.g. in case of the basal dichotomy (Fig. 9.14: 1) instead of the polytomy present in the dendrogram (Fig. 9.12). Therefore, the Dimorphodontidae and Anurognathidae are sister-groups (Fig. 9.14: 2), and do not form a monophyletic group like indicated in the dendrogram.

The monophyly of the Rhamphorhynchinae and Scaphognathinae (Fig. 9.14: 3) is not consistent with the evolutionary pathway diagram. It can only be accomplished by a reversal in the development of an anterior keratinous beak, present in *Campylognathoides* but not in *Scaphognathus*. As this would violate against an irreversible transformation, the independent appearance of a keratinous beak at the anterior rostrum (Fig. 9.14: 4) is be the only alternative. Like shown in the previous chapter, due to the presence of the rhamphotheca, Rhamphorhynchus can not be considered a direct outgroup for the Pterodactyloidea. Here, the position of

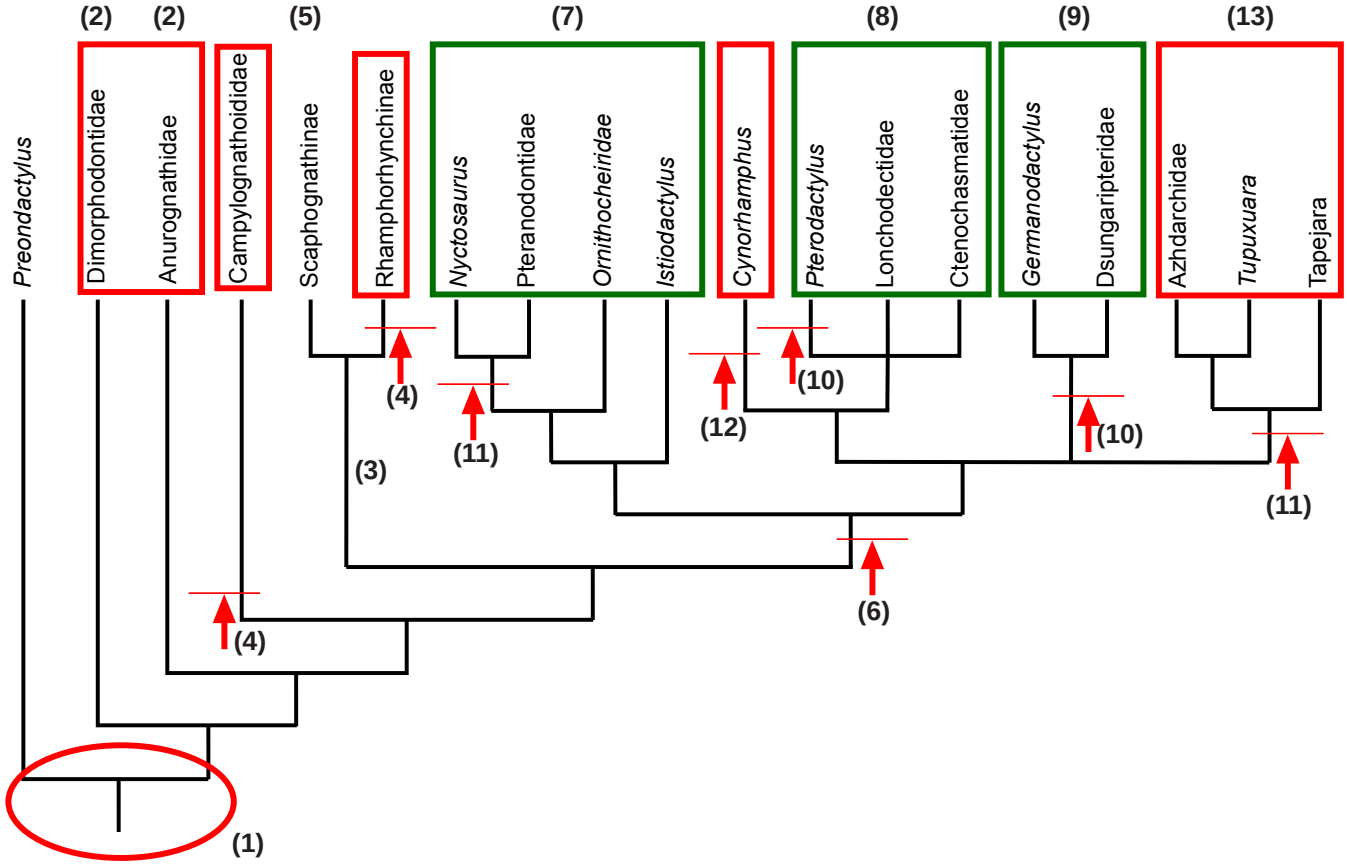

Fig. 9.14: Cladogram proposed by Unwin (2003). Blue arrows = reverse changes, red Arrows = irreversible transformation, green rectangles = similarities to evolutionary pathway diagram., red rectangle/ellipse = differences to evolutionary pathway diagram. Numbers see text.

Scaphognathus (Fig. 9.14: 5) is much more in accordance with the evolutionary pathway dendrogram (Fig. 9.12).

Like in the cladogram by Kellner (2003), the Pterodactyloidea is defined by the presence of a nasoantorbital fenestra as an irreversible transformation (Fig. 9.14: 6) in the cladogram by Unwin (2003). Within the Pterodactyloidea, the position of the group comprising *Nyctosaurus*, Pteranodontidae and the Ornithocheiroidea (Fig. 9.14: 7) resembles the pattern in the dendrogram (Fig 9.28). The grouping of *Nyctosaurus* and *Pteranodon* (Fig. 9.14: 7) is in agreement with the determination of a biomechanically founded Pteranodon constructional level (although postcranial characters might not support this monophyly, E.Frey 2005, pers. comm.). The sister-group relationship with the Ornithocheirids has already been proposed as one alternative in the evolutionary pathway diagram (see chapter 9.5.7).

The monophyly between *Germanodactylus* and Dsungaripteridae (Fig. 9.14: 8), respectively *Pterodactylus*, Lonchodectidae and Ctenochasmatidae (Fig. 9.14: 9) is supported by the evolutionary pathway diagram, although Unwin (2003) was not able to solve the polytomy between the latter groups. Here, the position of *Pterodactylus* corresponds to the position of the hypothetical proto-pterodactyloid in the evolutionary pathway diagram. As a result, a keratinous hook (Fig. 9.14: 10), respectively keratinous rhamphotheca (Fig. 9.14: 11) would have developed four times independently within the Pterodactyloidea. However, the existence of a keratinous hook has not been included in the cladistic analysis by Unwin (2003), so that the position of *Pterodactylus* might be subject to change if this character would be accounted for. This might also explain

the position of *Gallodactylus* (*Cynorhamphus*), in which the dentition is reduced from posterior (=irreversible transformation) (12) and thus is not be considered to be plesiomorphic.

A further difference is found in case of the position of *Tapejara* which is considered to be a plesiomorphic taxon relative to *Tupuxuara* and the Azhdarchidae (13). If the latter are taken as sister-groups, than lengthening of the rostrum is a secondary phenomenon relative to *Tapejara* and therefore a reversal relative to the evolutionary pathway diagam (Fig. 9.12).

Despite the differences described above, the cladogram proposed by Unwin (2003) is much more parsimonious in terms of the biomechanical transformations needed than the cladogram by Kellner (2003). Although some reversals are needed to explain the pattern of the cladogram, no irreversible transformations are violated if the presence of a keratinous anterior beak in *Rhamphorhynchus* is not considered as a plesiomorphic character for this taxon. Furthermore, the resulting pattern is quite similar to the biomechanical evolutionary pathway diagrams (Fig 9.26). However, it has to be stated, that the cladogram by Unwin (2003) includes less taxa than the one by Kellner (2003) which in consequence reduces the amount of possible discrepancies.

9.7 Scaling effects of pterosaur skulls

In the discussion made so far, pterosaur skulls were viewed as skull constructions, independent of the real size of the original skulls. Considering the wide range in size, beginning from juvenile specimens of *Pterodactylus* with skull as small as 30 mm to the skull of *Quetzalcoatlus* with a size of about 1,5 m, it is apparent, that the absolute bite forces are very different, too. Although the scaling of bite forces cannot be measured directly, it is known from other vertebrate groups like birds or crocodiles, that bite forces scale positively with jaw muscle and body mass (Erickson et al. 2003, van der Meij & Bout 2004). This means, that an increase in skull-size and an elongated rostrum does not inevitably result in relative lower anterior bite forces F_B. However, these effects are not yet studied in detail in living animals. On the other hand, increasing the size of the skull clearly leads to a an extension of the optional prey-spectrum to larger food items. Of course this does not necessarily means the denial of smaller-sized food items, which is obvious in extant animals (e.g insectivory in gulls, prey spectra of crocodiles, arachnivory in house cats etc.) .

Whereas most Triassic and Jurassic pterosaurs possess nearly similar-sized skulls, a drastic increase in skull-length is present in the dsungaripterid, azhdarchoid, ornithocheirid and pteranodontid pterosaurs, all dating from the Cretaceous. In these pterosaurs, the optional prey spectra includes much larger food items than for the smaller sized species and specimens. Due to the positive allometry of the bite forces against the size and dimensions of the skull, however, the loads applied during bite also increase relative to a smaller-sized skull. Therefore, especially in the large-headed pterosaurs compensation by the development of a rhamphotheca (and reduction of weight by the loss of teeth) or a crest are essential for the stability (=coherence) of the skull. For the skulls of *Quetzalcoatlus*, *Zheijangopterus*, *Tupuxuara*, *Tapejara*, *Thalassodromeus* and *Sinopterus*, the keratinous hook present in *Pterodactylus* is the necessary pre-requisite for the development of large skulls. This may hold true also for *Pteranodon* as well as *Nyctosaurus*. In the large-headed ornithocheirids crests are developed, with a highly variable morphology but identical, stress-reducing mechanical effects.

However, the increase in skull size also leads to an increase in absolute skull weight and more significant in muscle mass because of the positively allometric relation between muscle mass and size of the animal. This results in the need for weight-reduction elsewhere. Besides its mechanical effect, the fusion of the antorbital

fenestra and the naris could contribute to this effect, but only if the nasoantorbital fenestra is not filled by connective-tissue, even heavier than bone. It is apparent, that the pterosaur with the largest skull (*Quetzalcoatlus northropi*) also has a large nasoantorbital fenestra. However, the skull of *Pteranodon*, which is about one fourth smaller than the one of *Quetzalcoatlus* possess a small nasoantorbital fenestra, which may point to a greater mechanical than weight-saving constraint in the proportion of this fenestra. More effective weight-saving strategies are be the reduction of teeth, reduction of bone-wall thickness and the reduction of internal bony mineralisations.

10. CONCLUSIONS AND PERSPECTIVES

The combined approach using, lever and cantilever mechanics, space frame analysis and FEM has proven successful for analysing the mechanical effects of various pterosaur tooth and skull constructions for the operational regime “bite”. Especially both latter methods allows to discuss alternative scenarios or properties of structures (e.g. the material properties of the periodontal membrane). The combined analysis can be used as a standardised method for other research into skull mechanics of vertebrates. Because of the lack of data in the fossil record (e.g. material properties, boundary conditions), however, these methods can not yield quantitative correct results similar to the study of recent animals.

The different morphologies of pterosaur tooth construction determine different operational ranges, in which the teeth perform best (= greatest resistance against failure). The incomplete enamel-covering of pterosaur tooth constructions with a distinct enamel-dentine-boundary thereby leads to a reduction of strain and stress and to a greater lateral elasticity of the teeth than for a complete enamel cover. This permits the development of high and lateral compressed teeth like e.g. the Rhamphorhynchus tooth construction. Further stress-absorption occurs in the periodontal membrane, although its exact mechanical behaviour can not be clarified unambiguously.

As can be deduced from the analysis of the skull of Anhanguera, the jaw reaction force F_J determines the stability of the skull construction. The large jugal area dorsal to the orbita and the inclined occipital region act as buttresses against these high loads. In contrast to the orbitotemporal region, which is subject to varying loading conditions, the pattern in the rostrum is less complex. Here, mainly bending in dorsal direction and torsion occur. The hollow rostrum leads to a reduction of weight of the skull and to a high bending and torsional resistance.

By comparison of the morphology and mechanical behaviour of various pterosaur skull constructions, specific variations are determined:

• A longer rostrum leads to higher velocity and acceleration of the lower jaw during occlusion. This is further amplified by an elastic recoil of the spread lower jaw rami during occlusion. Also the inclined occipital region increases the velocity and acceleration of the lower jaw during occlusion due to the lengthening of the MAME/P and MPST. A similar muscle-lengthening effect may be deduced from the presence of an orbitotemporal crest. Brevirostrine skull constructions on the other hand show a higher bite force F_B at the anterior end of the rostrum with a lower velocity and acceleration of the lower jaw during occlusion.

• The presence of an anterior bony crest leads to a reduction of the shear and comparison stress and to a higher tendency for bending than twisting, which decreases the tendency of failure of the skull construction. A similar effect is proved for a medial bony crest, which furthermore stabilises the premaxillary-nasal member dorsal to the nasoantorbital fenestra against the high compressive loads during occlusion. The effects of soft-tissue crests for the operating regime “bite” are neglectable.

• Fusion of naris and antorbital fenestra is the consequence of an elongated rostrum in which this area is less stressed than in brevirostrine skull construction. Whereas in the latter, the bars bordering the naris and antorbital fenestra stabilise the skull construction against failure, the separating maxillary-nasal bar between both fenestra gets more and more oblique and less-stressed the longer the rostrum is. This leads to a complete reduction of this bar and formation of the nasoantorbital fenestra.

• With the exception of the Gallodactylus skull construction, the reduction of the dentition follows the development of an anterior keratinous hook at the anterior end of the rostrum. This hook and furthermore, the formation of a keratinous rhamphotheca leads to a reduction of especially torsional and shear loads and has a shock-absorbing effect. Subsidiary, the overall weight of the skull is reduced. The presence of a rhamphotheca permits the lateral narrowing of the skull construction.

These mechanical considerations allow to narrow down the optional operational regimes of the skull constructions to seven main functional implications: snap-and-penetrate, snap-and-lock, hold-and-filter, snap-and-hold, snap-hold-and-slice, snap-and-squeeze and snap-squeeze-and-cut. Here, most pterosaur skull constructions show local optima of performance for certain implications, whereas in some cases they can be excluded from others. Due to the missing fossil stomach content of pterosaurs no special food items are assigned to these functional categories.

The results of the comparison of the mechanical behaviour of the skull constructions allows to determine possible irreversible transformations. These are the reduction of the dentition and replacement by a keratinous rhamphotheca and the fusion of naris and antorbital fenestra. The transformations allow to construct an evolutionary pathway diagram with specific constructional levels, in which structural variations are possible. Based on a hypothetical, generalised diapsid skull preconstructions the following levels are derived: Basal Rhamphorhynchoid skull constructional level, Rhamphorhynchus skull constructional level, Pterodactylus skull constructional level, Azhdarchoid skull constructional level, Ornithocheirid/Chasmatoid skull constructional level and Pteranodon skull constructional level. Whereas all other levels are based on biomechanical conclusive steps, the latter level can not be derived unambiguously.

By comparison with the possible processes and transformation in the evolutionary pathway diagram, cladograms reflecting the phylogenetic systematic of pterosaurs can be evaluated. The cladograms by Kellner (2003) and Unwin (2003) show a high number of similarities to the evolutionary pathway diagram. However, the cladogram by Kellner (2003) shows a high number of reversals and is less parsimonious in terms of changes needed. Violations against irreversible transformations exist in both cladograms in case of the presence of the keratinous hook at the anterior end of the rostrum. In both cladograms this can only be dissolved if the character is apomorphic for those taxa which are considered to be outgroups for certain groups within the pterosaurs.

The present study has shown the use of constructional morphology for determining the optional operational range of the skull constructions during bite and as well for the evaluation of phylogenetic systematics. Likewise, other vertebrate skull constructions can be analysed and their optional operational range confined on a nonomologic-deductive rather than on a narrative-speculative basic principle. However, to understand the bionomic coherence of the overall pterosaur construction, further investigations are needed. At the skull region this mainly considers the aero-/hydrodynamics in which e.g. soft-tissue crests play a much more important role than during bite. Subsequently the construction of the cervical column has to studied more closely because its operational range constrains considerably the range of motion of the skull. And furthermore the whole postcranial construction has to be incorporated in the evolutionary pathway diagram to permit a more exhaustive comparison to the cladograms.

ACKNOWLEDGMENTS

During the last year, a couple of people accompanied this work. In the first place these were my supervisors, Jürgen Boy and Dino Frey, whose enthusiasm about palaeontology (each on their own way) shows, that working on “old, dead bones” is not just a job but a mission. I also learned a different look at fossils from working together with mechanical engineers and enjoyed it - after we finally found a common language. My thanks go to Natascha Hess-Mohr, Ralf Mohr, Andreas Berg, Y. Hamidon, S. Schlese, Ulrich Witzel and Hans-Peter Weiser. Interdisciplinary work really is fun!

Many thanks also for all those people who gave me access to “their” collections and specimens: Sandra Chapman (BMNH), Sankar Chatterjee (CM), Chris Collins (AMNH), Dino Frey (SMNK), Wann Langston Jr.. (TMM), Andreas Matzke (GPIT), Helmut Mayr (BSP), Angela Milner (BMNH), Anna Paganoni (MCSNB), M. Norell (AMNH), Tim Rowe (TMM), Rainer Schoch (SMNS), Peter Wellnhofer, (BSP), RupertWild (SMNS), Andre Veldmeijer (RGM), Günter Viohl (SOS) and Jan de Vos (RGM).

The CT scanning would not have been possible with the master of the Somatom S, Stephan Boor. It’s always like Christmas to sit in this dark-room, just a couple of moments before the first picture emerges on the screen.

R. Kastner & M. Maus did a great job on preparing the pterosaur material. I guess I never will be patient enough for such a job!

What is science without dispute and discussion? I savour discussing pterosaur stuff and else with Natascha Bakhurina, Anusuya Chinsamy, Jim Cunningham, Don Henderson, Bernd Herkner, Gerald Mayr, Johannes Müller, David Peters, Holger Preuschoft, Oliver Rauhut, Steve Salisbury, Herbert Schick, Daniela Schwarz, Norbert Schmidt-Kittler and Dave Unwin,

This work would not have been possible without the support of colleagues and friends. I benefited much from you! And thanks for listening to my philosophical excesses ;-) And sometimes giving me new ideas (although most of them are too crazy). Dietrich Berg, Thomas Brachert, Gaby Försterling, Sandra. Gehner, Thomas Grießemer, Kirsten Grimm, Reiner Käsberger, Wolfgang Kathe, Nils Knötschke, Karsten Kroeger, Rupert Krömer, Klaus Meyer zu Uptrup, Eric Milsom, Inken Mueller-Töwe, Markus Reuter, Beatrix Spahn, Alexander Streb, Sabine Theis-Krömer and Maren Wolter. And especially Kerstin Müller for all her patience with me (too much to list here)! I know, it’s hard sometimes...

This work would not have been possible without a funding. I thank Dino Frey and Hans-Peter Weiser for taking the risk of starting the DFG-project as part of this theses was done during the DFG-project FR 1314/2-1. Also the people at the Südwestrundfunk, especially Klaus Weis and Carsten Klinck for making it possible to work while working. Thanks to Norbert Schmidt-Kittler for giving me the opportunity of doing something I like most - teaching students. And this not just for fun. And last but not least, my parents which gave me the possibility for my way of life.

And for all of you whom I forgot: Shame on me!

LITERATURE

Abler, W.L. (1992): The serrated teeth of tyrannosaurid dinosaurs, and biting structures in other animals. - Paleobiology, **18**(2): 161-183.

Ablondi, F. (1998): Automata, Living and Non-Living: Descartes' Mechanical Biology and His Criteria for Life. - Biology and Philosophy, **13**: 179-186.

Aerts, P. (1990): Mathematical Biomechanics and the "what", "how" and "why" in functional morphology. - Netherlands Journal of Zoology, **40**(1-2): 153-172.

Alexander, R.M. (1968): Animal Mechanics. - Sidgwick & Jackson (London), 356 p.

Alexander, R.M. (1981): Factors of Safety in the structure of animal. - Sci. Prog., **67**: 109-130.

Alexander, R.M. (1985): The ideal and the feasible: physical constraints on evolution. - Biological Journal of the Linnean Society, **26**: 345-358.

Alexander, R.M. (2003): Principles of Animal Locomotion. - Princeton University Press (Princeton), 371 p.

Amundson, R. & Lauder, G.V. (1993-94): Function without Purpose: The Uses of Causal Role Function in Evolutionary Biology. - Biology and Philosophy, **9**: 443- 469.

Arramon, Y.P. & Cowin, S.C. (1997): Hydraulic Stiffening of Cancelious [!*sic*] Bone. - Forma, **12**(3, 4): 209-221.

Arthaber, G. von (1921): Über Entwicklung, Ausbildung und Absterben der Flugsaurier. - Paläontologische Zeitschrift, **4**: 1-47.

Bardoux, D.M. (1966): Framed structures in the mammalian skull. - Acta Morphologica Neerlando-Scandinavica, **6**: 239.-250.

Bagge, M. (2000): A model of bone adaptation as an optimization process. - Journal of Biomechanics, **32**: 1349-1357.

Bakhurina, N.N. (1982): A pterodactyl from the Lower Cretaceous. - Palaeontologicheskii Zhurnal, **4**: 104-108.

Bakhurina, N.N. & Unwin, D.M. (1995): A survey of pterosaurs from the Jurassic and Cretaceous of the Former Soviet Union and Mongolia. - Historical Biology, **10**: 197-245.

Barghusen, H.R. (1968): The lower jaw of cynodonts (Reptilia, Therapsida) and the evolutionary orign of mammal-like adductor jaw musculature. - Postilla, **116**: 1-49.

Barghusen, H.R. (1973): The adductor jaw musculature of *Dimetrodon* (Reptilia, Pelycosauria). - Journal of Paleontology, **47**: 823-834.

Barel, C.D.N., van der Meulen, J.W. & Berkhoudt, H. (1977): Kinematischer Transmissionskoeffizient und Vierstangensystem als Funktionsparameter und Formmodell für Mandibulare Depressionsapparate bei Teleostiern. - Anatomischer Anzeiger, **142**: 21-31.

Barthel, K.W, Swinburne, N.H.M, & Morris, S.C. 1990. Solnhofen: A Study in Mesozoic Palaeontology. - Cambridge University Press (Cambridge), 236 p..

Beecher, R.M. (1977): Function and Fusion at the Mandibular Symphysis. - American Journal of Physical Anthropology, **47**: 325-336.

Beitz, W. & Grote, K.-H. (1997): Dubbel - Taschenbuch für den Maschinenbau. - Springer Verlag (Berlin), 1832 p.

Bennett, C.S. (1989): A pteranodontid pterosaur from the Early Cretaceous of Peru, with comments on the relationship of Cretaceous Pterosaurs. - Journal of Paleontology, **63**(5): 669-677.

Bennett, C.S. (1992): Sexual dimorphism of *Pteranodon* and other pterosaurs, with coments on cranial crests. - Journal of Vertebrate Paleontology, **12**(4): 422-434.

Bennett, C.S. (1994): Taxonomy and systematics of the Late Cretaceous Pterosaur *Pteranodon* (Pterosauria, Pterodactyloidea). - Occasional Papers of the Natural History Museum, University of Kansas, **169**: 1-20.

Bennett, C.S. (1996a): A statistical study of *Rhamphorhynchus* from the Solnhofen Limestone of Germany: year-classes of a single large species. - Journal of Paleontology, **69**(3): 569-580.

Bennett, C.S. (1996b): The orign of pterosaurs and their systematic position within the Diapsida. - Journal of Vertebrate Paleontology, **16**(3): 22A.

Bennett, C.S. (2001a): The Osteology and Functional Morphology of the Late Cretaceous Pterosaur *Pteranodon* - Part I. General Description of Osteology. - Palaeontographica, Abteilung A, **260**(1-6): 1-112.

Bennett, C.S. (2001b): The Osteology and Functional Morphology of the Late Cretaceous Pterosaur *Pteranodon* - Part II. Size and Functional Morphology. - Palaeontographica, Abteilung A, **260**(1-6): 113-153.

Bennett, S.C. (2002): Soft tissue preservation of the cranial crest of the pterosaur *Germanodactylus* from Solnhofen. - Journal of Vertebrate Paleontology, **22**(1): 43-48.

Bennett, S.C. (2003): New crested specimen of the Late Cretaceous pterosaur *Nyctosaurus*. - Paläontologische Zeitschrift, **77**(1): 61-75.

Benton, M.J. (1985): Classification and phylogeny of the diapsid reptiles. - Zoological Journal of the Linnean Society, **84**: 97-194.

Benton, M.J. (1999): *Scleromochlus taylori* and the orign of dinosaurs and pterosaurs. - Philosophical Transactions of the Royal Society London, Series B, **354**: 1423-1446.

Berg, A. (2002): FEM-Analyse des Einflusses der periodontalen Membran auf die Übertragung der Beißkraft beim Pterosaurier Coloborhynchus [!*sic*]. - Studienarbeit am Insitut für CAE-Anwendungen, Fachhochschule für Technik und Gestaltung Mannheim, 45 p. [unpublished]

Bertram, J.E.A. & Biewener, A.A. (1988): Bone Curvature: Sacrificing Strength for Load Predictabiliy?. - Journal of Theoretical Biology, **131**: 75-92.

Bertram, J.E.A. & Biewener, A.A. (1992): Allometry and curvature in the long bones of quadrupedal animals. - Journal of Zoology, **226**: 455-467.

Bertram, J.E.A. & Swartz, S.M. (1991): The „Law of Bone Transformation": A Case of Crying Wolff?. - Biological Review, **66**: 245-273.

Biewener, A.A. (2003): Animal Locomotion. - Oxford University Press (Oxford), 281 p.

Bock, W.J. (1959): Preadaptation and multiple evolutionary pathways. - Evolution, **13**: 194-211.

Bock, W.J. (1964): Kinetics of Avian Skull. - Journal of Morphology, **114**: 1-42.

Bock, W.J. (1966): An approach to the functional analysis of bills shape. - *Auk*, **83**: 10-51.

Bock, W.J. (1989): Organisms as Functional Machines: A Connectivity Explanation. - American Zoologist, **29**: 1119-1132.

Bock, W.J. (1991): Explanations in Konstruktionsmorphologie and Evolutionary Morphology. - In: Schmidt-Kittler, N. & Vogel, K. (eds.), Constructional Morphology and Evolution, Springer Verlag (Berlin), 9-29.

Bock, W.J. (1999): Cranial Kinesis Revisited. - Zoologischer Anzeiger, **238**: 27-39.

Bock, W.J. & Kummer, B. (1986): The Avian Mandible as a Structural Glider. - Journal of Biomechanics, **1**: 89-96.

Bock, W.J. & von Wahlert, G. (1965): Adaptation and the form-function complex. - Evolution, **19**: 269-299.

Bögge, A. (2003). Technische Mechanik. - Friedr. Vieweg & Sohn Verlagsgesellschaft (Braunschweig), 428 p.

Bolt, J.R. (1974): Evolution and functional interpretations of some suture patterns in paleozoic labyrinthodont amphibians and other lower tetrapods. - Journal of Paleontology, **48**(3): 434-458.

Bonaparte, J.F. (1970): *Pterodaustro guiñazui* gen. et sp. nov. - Pterosaurio de la formacion Lagarcito, Provincia de San Luis, Argentinia y su significado en la geologia regional. - Acta Geologica Lilloana, **10**(10): 209-225.

Bonaparte, J.F. (1971): Descripción del Cráneo y Mandibulas de *Pterodaustro guinazui* de la fromación Lagarcito, San Luis, Argentinia. - Publicaciones del Museo Municipal de Ciencias Naturales de Mar del Plata, **1**(9): 263-272.

Bonik, K. (1976): Quantitative Betrachtungen zur Gallertoid-Hydroskelett-Theorie. - In: Aufsätze und Reden der senckenbergischen naturforschenden Gesellschaft, **29**: 22-38.

Bonik, K.(1977): Quantitative Aspekte hydraulischer Systeme in Metazoen-Konstruktionen. I. Die Statik von Hydroskelett-Konstruktionen. - Courier Forschungs-Institut Senckenberg, **23**: 1-79.

Bonik, K., Grasshoff, M. & Gutmann, W.F. (1976a): Die Evolution der Tierkonstruktion (I). Problemlage und Prämissen. - Natur und Museum, **106**(5): 129-143.

Bonik, K., Grasshoff, M. & Gutmann, W.F. (1976b): Die Evolution der Tierkonstruktion (III). Vom Gallertoid zur Coelomhydraulik. - Natur und Museum, **106**(6): 178-188.

Bonik, K., Grasshoff, M. & Gutmann, W.F. (1976c): Die Evolution der Tierkonstruktion (IV). Die Entwicklung der Ringelwürmer und ihre Aufgliederung in Vielborster, Wenigborster und Egel. - Natur und Museum, **106**(10): 303-316.

Bonik, K., Grasshoff, M. & Gutmann, W.F. (1977a): Die Evolution der Tierkonstruktion (V). Die Entwicklung des Zentral-Nerven-Systems in Abhängigkeit von der Biomechanik der Rahmen-Konstruktion (Bauplan). - Courier Forschungs-Institut Senckenberg, **22**: 1-66.

Bonik, K., Grasshoff, M. & Gutmann, W.F. (1977b): Die Evolution der Tierkonstruktion (VI). Von der segmentalen Wurmhydraulik zum Außenskelett-Muskelsystem der Gliederfüßer. - Natur und Museum, **107**(5): 131-140.

Bonik, K., Gutmann, W.F. & Peters, D.S. (1977c): Optimierung und Ökonomisierung im Kontext von Evolutionstheorie und Phylogenetischer Rekonstruktion. - Acta Biotheoretica, **26**: 75-119.

Bout, R.G. & Zweers, G.A. (2001): The role of cranial kinesis in birds. - Comparative Biochemistry and Physiology, Part A, **131**: 197-205.

Bowman, S.M., Keaveny, T.M., Gibson, L.J., Hayes, W.C. & McMahon, T.A. (1994): Compressive creep behavior of bovine trabercular bone. - Journal of Biomechanics, **27**(3): 301-310.

Boy, J.A. (1998): Möglichkeiten und Grenzen einer Ökosystem-Rekonstruktion am Beispiel des spätpaläozoischen lakustrinen Paläo-Ökosystems. - Paläontologische Zeitschrift, **72**(1/2): 207-240.

Boy, J.A. (2003): Paläoökologisch Rekonstruktion von Wirbeltieren: Möglichkeiten und Grenzen. - Paläontologische Zeitschrift, **77**(1): 123-152.

Boyde, A. (2003): The real response of bone to exercise. - Journal of Anatomy, **203**: 173-189.

Bramble, D.M. (1978): Orign of the mammalian feeding complex: models and mechanisms. - Paleobiology, **4**(3): 271-301.

Bramble, D.M. & Wake, D.B. (1985): Feeding Mechanisms of Lower Tetrapods. - In: Hildebrand, M., Bramble, D.M., Liem, K.F. & Wake, D.B. (eds.), Functional Vertebrate Morphology, The Belknap Press of Harvard University Press, Cambridge MA, 230-261.

Bramwell, C.D. & Whitfield, G.R. (1974): Biomechanics of *Pteranodon*. - Philosophical Transactions of the Royal Society London, Series B, **267**: 503-581.

Broili, F. (1912): Über *Pterodacytlus micronyx* H. v. Meyer. - Zeitschrift der Deutschen geologischen Gesellschaft, **64**(3): 492-500.

Broili, F. (1936): *Ctenochasma gracile* Oppel. - Geognostische Jahreshefte, **29/30**: 299-306.

Brown, B. (1943): Flying Reptiles. - Natural History, **52**: 104-111.

Brown, T.D. (2001): Devices and Techniques for in Vitro Mechanical Stimulation of Bone Cells. - In: Cowin, S.C. (ed.), Bone Mechanics Handbook, CRC Press (Boca Raton), 26-1 - 26-31.

Buckland, W. (1829): Proceedings of the Geological Society, **1**: 127.

Buckland-Wright, J.C. (1978): Bone Structure and the Patterns of Force Transmission in the Cat Skull (*Felis catus*). - Journal of Morphology, **155**: 35-62.

Buisonjé, de P.H. (1980): *Santanadactylus brasiliensis* nov. gen., nov. sp., a long-necked, large pterosaurier from the Aptien of Brasil. - Proceedings of the Koninklijke Nederlandse Akademie van Wetenschappen B, **83**(2): 145-172.

Buisonjé, de P.H. (1981): *Ctenochasma porocristata* nov.sp. from the Solnhofen Limestone with some remarks on other Ctenochasmatidae. - Proceedings of the Koninklijke Nederlandse Akademie van Wetenschappen B, **84**(4): 411-436.

Bürger, R. (1986): Constraints for the evolution of functionally coupled characters: A nonlinear analysis of a phentoypic model. - Evolution, **40**: 182-193.

Burger, E.H. (2001): The False Premise in Wolff`s Law. - In: Cowin, S.C. (ed.), Bone Mechanics Handbook, CRC Press (Boca Raton), 28-1 - 28-16.

Busbey III, A.B. (1995): The structural consequence of skull flattening in crocodilians. - In: Thomason J.J. (ed.), Functional Morphology in Vertebrate Paleontology, Cambridge University Press, pp. 173-192.

Cai, Z. & Wei, F. (1994): *Zhejiangopterus linhaiensis* (Pterosauria) from the Upper Cretaceous of Linhai, Zhejiang, China. - Vertebrata PalAsiatica, **33**(2): 181-194.

Campos, D.A. & Kellner, A.W.A. (1985): Panorama of the Flying Reptiles Study in Brazil and South America. - Annais Academia brasileira de Cîencias **57**(4): 453-466.

Campos, D. A. & Kellner, A.W.A. (1997): Short Note on the First Occurence of Tapejaridae in the Crato Member (Aptian), Santana Formation, Araripe Basin, Northeast Brasil. - Annais Academia brasileira de Cîencias, **69**(1): 83-87.

Carter, D.R., Mikic, B. & Padian, K. (1998): Epigenetic mechanical factors in the evolution of long bone epiphyses. - Zoological Journal of the Linnean Society, **123**: 163-178.

Chapman, G. (1974): Versatility in Hydraulic Systems. - Journal of Experimental Zoology, **194**: 249-270.

Chiappe, L.M. & Chinsamy, A. (1996): *Pterodaustro*'s true teeth. - Nature, **379**: 211-212.

Clark, R.B. & Cowey, J.B. (1958): Factors controlling the Change of Shape of certain Nemertean and Tubellarian Worms. - Journal of Experimental Biology, **35**: 731-748.

Cleuren, J. & De Vree, F. (2000): Feeding in Crocodilians. - In: Schwenk, F. (ed.), Feeding: Form, Function, and Evolution in Tetrapod Vertebrates, Academic Press (San Diego), 337-358.

Cleuren, J., Aerts, P. & De Vree, F. (1995): Bite and Joint Force Analysis in *Caiman crocodilus*. - Belgian Journal of Zoology, **125**(1): 79-94.

Cowin, S.C. (1997): The False Premise of Wolff's Law. - Forma, **12**(3,4): 247-262.

Cowin, S.C. (2001): The False Premise in Wolff`s Law. - In: Cowin, S.C. (ed.), Bone Mechanics Handbook, CRC Press (Boca Raton), 30-1 - 30-15.

Cowin, S.C. & Hart, R.T. (1990): Errors in the orientation of the principal stress axes if bone tissue is modeled as isotropic. - Journal of Biomechanics, **23**: 349-352.

Cowin, S.C. & Moss, M.L. (2001): Mechanosensory Mechanisms in Bone. - In: Cowin, S.C. (ed.), Bone Mechanics Handbook, CRC Press (Boca Raton), 29-1 - 29-17.

Crompton, A.W, (1995): Masticatory function in nonmammalian cynodonts and early mammals**. -** In: Thomason J.J. (ed.), Functional Morphology in Vertebrate Paleontology, Cambridge University Press**,** 55-75.

Crompton, A.W. & Hotton III, N. (1967): Functional morphology of the masticatory apparatus of two dicynodonts (Reptilia, Therapsida). - Postilla, **109**: 1-51.

Cubo, J., Menten, L. & Casinos, A. (1999): Sagittal long bone scurvature in birds. - Annales des Sciences Naturelles, **20**(4): 153-159.

Currey, J.D. (1984): The Mechanical Adaptation of Bones. - Princeton University Press, 294 p.

Currey, J.D. (1999): The design for mineralised hard tissues for their mechanical functions. - The Journal of Experimental Biology, **202**: 3285-3294.

Currey, J.D. (2002): Bones - Structures and Mechanics. - Princeton University Press (Princeton), 436 p.

Cuvier, G. (1801): Reptile volant. Extrait d'un ouvrage etc., an **9**: 6.

Cuvier, G. (1809): Mémoire sur le squelette fossile d'un reptile volant des environs d'Aichstedt, que quelques naturalistes ont pris pour un oiseau, et donc nous formons un genre de Sauriens, sous le nom de Ptero-Dactyle. Annales des Musée d'Histoire naturelle, **13**: 424.

Cuvier, G. (1819): (*Pterodactylus antiquus*). Oken's Isis, 1126 und 1788.

Cuvier, G. (1924): Recherches sur les ossements fossiles. **5**(2): 382.

Dalla Vecchia, F.M. (1993): *Cearadactylus*? *ligabuei* nov. sp., a new early Cretaceous (Aptian) pterosaur from Chapada do Araripe (Northeastern Brazil). - Bolletino del Societa Paleontologia Italiana **32**(3): 401-409.

Dalla Vecchia, F.M. (1998): New observations on the osteology and taxonomic status of *Preondactylus buffarinii* Wild, 1984 (Reptilia, Pterosauria). - Bolletino della Società Paleontologica Italiana, **36**(3): 355-366.

Dalla Vecchia, F.M. (2002): Observations on the non-Pterodacytloid Pterosaur *Jeholopterus ningchengensis* from the Early Cretaceous of China. - Natura Nascosta, **24**: 8-27.

Dalla Vecchia, F.M. (2003a): New morphological observations on Triassic pterosaurs. - In: Buffetaut E. & Mazin J.-M. (eds.), Evolution and Palaeobiology of Pterosaurs, Geological Society Special Publications, **217**: 23-44.

Dalla Vecchia, F.M. (2003b): A review of the Triassic pterosaur record. - Rivista del Museo Civico di Scienze Naturali "E. Caffi", **22**: 13-29.

Dalla Vecchia, F.M., Wild, R., Hopf, H. & Reitner, J. (2002): A crested rhamphorhynchoid pterosaur from the Late Triassic of Austria. - Journal of Vertebrate Paleontology, **22**(1): 196-199.

Daniel, W.J. & McHenry, C. (2000): Bite force to skull stress correlation - modelling the skull of *Alligator mississippiensis*. - In: Grigg, G.C., Seebacher, F. & Franklin, C.E. (eds.), Crocodilian Biology and Evolution, Franklin Surrey Beatty & Sons, 135-143.

Dauphin, Y. (1988): L'email dentaire des reptiles actuels et fossiles: repartition de la strcuture prismatique, son role, ses implications. - Palaeontographica, Abt A., **203**(4-6): 171-84.

DeMar, R. & Barghusen, H.R. (1972): Mechanics and Evolution of the synapsid jaw. - Evolution, **26**: 622-637.

De Vree, F. & Gans, C. (1989): Functional morphology of the feeding mechanisms in lower tetrapods. - Fortschritte der Zoologie, **35**: 115-127.

De Vree, F. & Gans, C. (1994): Feeding in tetrapods. - Advances in Comparative & Environmental Physiology, **18**: 93-118.

Doblaré, M. & García, J.M. (2002): Anisotropic bone remodelling based on a continuum damage-repair theory. - Journal of Biomechanics, **35**: 1-17.

Döderlein, L. (1923): *Anurognathus Ammoni*, ein neuer Flugsaurier. - Sitzungs-Berichte der Bayerischen Akademie der Wissenschaften, mathematisch-naturwissenschafliche Klasse, 117-164.

Dong, Z. (1982): A new pterosaur (*Huanhepterus quingyangensis* gen. et sp. nov.) from Ordos, China. - Vertebrata PalAsiatica, **20**(2): 115-121.

Dong, Z. & Lü, J.-C. (2005): A new Ctenochasmatid Pterosaur from the Early Cretaceous of Liaoning Province. - Acta Geologica Sinica, **79**(2): 164-167.

Driesch, H. (1935): Die Maschine und der Organismus. Bios, **4:** 1-76.

Druzinsky, R.E. & Greaves, W.S. (1979): A Model to Explain the Posterior Limit of the Bite Point in Reptiles. - Journal of Morphology, **160**: 165-168

Dullemeijer, P. (1956): The functional morphology of the head of the common viper, *Vipera berus* (L.). - Archives neerlandaises de zoologie, **12**: 1-11.

Dullemeijer, P. (1959): A comparative functional-anatomical study of the heads of some Viperidae. Morphologisches Jahrbuch, **99**: 882-944.

Dullemeijer, P. (1991): Evolution of Biological Constructions: Concessions, Limitations, and Pathways. - In: Schmidt-Kittler, N. & Vogel, K. (eds.), Constructional Morphology and Evolution, Springer Verlag (Berlin), pp. 313-329.

Dullemeijer, P. (2001): An Introduction to Vertebrate Morphology. - In: Dutta, H.M. & Munshi, J.S.D. (eds.), Vertebrate functional morphology: horizon of research in the 21st century, Science Publishers (Enfield), 1-9.

Eaton, G.F. (1910): Osteology of *Pteranodon*. Memoirs of the Conneticut Academy of Arts and Sciences, **2**: 1-38.

Edlinger, K. (1992): Nervensysteme als integrale Bestandteile mechanischer Konstruktionen. - Aufsätze und Reden der senckenbergischen Naturforschenden Gesellschaft, **38**: 131-155.

Edlinger, K. (1994): Das Spiel der Moleküle - Reicht das Organismusverständnis des molekularbiologischen Reduktionismus?. - Natur und Museum, **124**(6): 199-206.

Edmund, A.G. (1969): Dentition. - In: Gans, C. (ed.), Biology of the Reptilia - Volume 1: Morphology A, Academic Press, pp. 117-200.

Elliott, D.G. (1887-1892): Monograph of Hornbills. - [reprint 1995 Fundacef-Verlag (Seibersbach)].

Erlach, K. (1994): Anthropologische Aspekte des Maschinenbegriffs. - In: Maier, W. & Zoglauer T. (eds.), Technomorphe Organismuskonzepte: Modellübertragung zwischen Biologie und Technik, problemata, **128**: 134-161.

Erickson, G.M., Lappin, A.K. & Vliet, K.A. (2003): The ontogeny of bite-force performance in American alligator (*Alligator mississippiensis*). - Journal of Zoology, **260**: 317-327.

Etnier, S.A. (2001): Flexural and Torsional Stiffness in Multi-Joined Biological Beams. - Biological Bulletin, **200**: 1-8.

Etnier, S.A. (2003): Twisting and Bending of Biological Beams: Distribution of Biological Beams in a Stiffness Mechanospace. - Biological Bulletin, **205**: 36-46.

Etnier, S.A. & Vogel, S. (2000): Reorientation of Daffodil (*Narcissus*: Amazyllidaceae) flowers in wind: drag reduction and torsional flexibility. - American Journal of Botany, **87**(1): 29-32.

Fabre, J.A. (1976): Un nouveau Pterodactylidae du Gisement de Canjuers (Var) *Gallodactylus canjuersensis* nov. gen., nov. sp.. - Annales de Paléontologie (Vert.), **62**(1): 35-70.

Fastnacht, M. (1996): Zum Zahnwechsel zweier Pterosaurierfunde aus der Chapada do Araripe. - Unpublished Diploma Thesis, Johannes Gutenberg-Universität , 122 p.

Fastnacht, M. (2001): First record of *Coloborhynchus* (Pterosauria) from the Santana Formation (Lower Cretaceous) of the Chapada do Araripe, Brazil. - Paläontologische Zeitschrift, **75**(1): 23-36.

Fastnacht, M. (2005): The first dsungaripterid pterosaur from the Kimmeridgian of Germany and the biomechanics of pterosaur long bone. - Acta Palaeontologica Polonica, **50**(2): 273-288.

Fastnacht, M., Hess, N., Frey, E. & Weiser, H.-P. (2002): Finite Element Analysis in Vertebrate Palaeontology. - Senckenbergiana lethaea, **82**(1): 195-206.

Frazzetta, T.H. (1988): The mechanics of cutting and the form of shark teeth (Chondrichthyes, Elasmobranchii). Zoomorphology, **108**: 93-107.

Frey, E. & Martill, D.M. (1994): A new Pterosaur from the Crato Formation (Lower Cretaceous, Aptian) of Brazil. - Neues Jahrbuch für Geologie und Paläontologie, Abhandlungen, **194**(2/3): 379-412.

Frey, E. & Martill, D.M. (1998): Late ontogenetic fusion of the processus tendinis extensoris in Cretaceous pterosaurs from Brazil. - Neues Jahrbuch für Geologie und Paläontologie, Monatshefte, **1998**(10): 587-594.

Frey, E. & Tischlinger, H. (2000): Weichteilanatomie der Flugsaurierfüße und Bau der Scheitelkämme: Neue Pterosaurierfunde aus den Solnhofener Schichten (Bayern) und der Crato-Formation (Brasilien). - Archaeopteryx, **18**: 1-16.

Frey, E., Herkner, ,B., Schrenk, F. & Seiffert, C. (1993): Reconstructing Organismic Constructions and the Problem of *Leptictidium*'s Locomotion. - Kaupeia, **3**: 89-95.

Frey, E., Martill, D.M. & Buchy, M.-C. (2003a): A new crested ornithocheirid from the Lower Cretaceous of northeastern Brazil and the unsual death of an unusual pterosaur. - In: Buffetaut, E. & Mazin, J.-M. (eds.), Evolution and Palaeobiology of Pterosaurs, Geological Society Special Publications, **217**: 55-63.

Frey, E., Martill, D.M. & Buchy, M.-C. (2003b): A new species of tapejarid pterosaur with soft-tissue head crest. - In: Buffetaut, E. & Mazin, J.-M. (eds.), Evolution and Palaeobiology of Pterosaurs, Geological Society Special Publications, **217**: 65-72.

Frey, E., Tischlinger, H., Buchy, M.-C. & Martill, D.M. (2003c): New specimens of Pterosauria (Reptilia) with soft-parts with implications for pterosaurian anatomy and locomotion. - In: Buffetaut, E. & Mazin, J.-M. (eds.), Evolution and Palaeobiology of Pterosaurs, Geological Society Special Publications, **217**: 233-266.

Fung, Y.C. (1990): Biomechanics - Motion, Flow, Stress, and Growth. - Springer (Berlin), 569 p.

Gans, C. & De Vree, F. (1987): Functional Bases of Fiber Length and Angulation in Muscles. - Journal of Morphology, 192: 63-85.

Gasparini, Z., Fernández, M: & De La Fuente, M. (2004): A new Pterosaur from the Jurassic of Cuba. - Palaeontology, **47**(4): 919-927.

Gingerich, P.D. (1971): Functional significance of mandibular translation in vertebrate jaw mechanics. - Postilla, **152**: 1-10.

Gingerich, P.D. (1979): The Human Mandible: Lever, Link, or Both?. - American Journal of Physical Anthropology, **51**: 135-138.

Gläser, H.-J. (1995): Man soll das Kind nicht mit dem Bade ausschütten: zur Kritik der Gutmannschen Evolutionskonzeption. - Ethik und Sozialwissenschaften, **6**(3): 320-322.

Graber, V. (1886a): Die äußeren mechanischen Werkzeuge der Tiere. I. Wirbeltiere. - G. Freytag (Leipzig), 224 p.

Graber, V. (1886b): Die äußeren mechanischen Werkzeuge der Tiere. II. Wirbellose Tiere. - G. Freytag (Leipzig), 224 p.

Goldfuss, A. (1831): Beträge zur Kenntnis verschiedener Reptilien der Vorwelt. - Nova acta Academiae Leopoldino-Carolinae, **15**: 61-128.

Gooch, K.J. & Tennant, C.J. (1997): Mechanical Forces: Their Effects on Cells and Tissues. Springer Verlag (Berlin), 182 p.

Goodship, A.E. & Cunningham, J.L. (2001): Pathophysiology of Functional Adaptation of Bone in Remodeling and Repair in Vivo. - In: Cowin, S.C. (ed.), Bone Mechanics Handbook, CRC Press (Boca Raton), 26-1 - 26-31.

Gould, S.J. (1989): A developmental constraint in *Cerion*, with comments on the definition and interpretation of constraints in evolution. - Evolution, **43**(3): 516-539.

Gould, S.J. (2002): The Structure of Evolutionary Theory. - Belknap Press (Cambridge, Ma), 2433p.

Gould, S.J. & Vrba, E.S. (1982): Exadaptation - a Missing Term in the Science of Form. - Paleobiology, **8**(1): 4-15.

Gould, J.S. & Lewontin, R.C. (1979): The Sprandels of San Marco and the Panglossian Paradigma - a critique of the adaptionist program. - Proceedings of the Royal Society London, Series B, **205**: 381-398.

Greaves, W.S. (1982): A mechanical limitation on the position of the jaw muscles of mammals: the one-third rule. - Journal of Mammalogy, **63**(2): 261-266.

Greaves, W.S. (1985a): The generalized carnivore jaw. - Zoological Journal of the Linnean Society, **85**: 267-274.

Greaves, W.S. (1985b): The mammalian post-orbital bar as a torsion-resisting helical strut. - Journal of Zoology, **207**: 125-136.

Greaves, W.S. (1988a): The maximum average bite force for a given jaw length. - Journal of Zoology, **214**: 295-306.

Greaves, W.S. (1988b): A Functional Consequence of an Ossified Mandibular Symphysis. - American Journal of Physical Anthropology, **77**: 53-56.

Greaves, W.S. (1991a): A relationship between premolar loss and jaw elongation in selenodont artiodactyls. - Zoological Journal of the Linnean Society, **101**: 121-129.

Greaves, W.S. (1991b): The orientation of the force of the jaw muscles and the length of the mandible in mammals. - Zoological Journal of the Linnean Society, **102**: 367-374.

Greaves, W.S. (1995): Functional predictions from theoretical models of the skull and jaws in reptiles and mammals. - In: Thomason, J.J. (ed.), Functional Morphology in Vertebrate Paleontology, Cambridge University Press, 99-115.

Greaves, W.S. (2000): Location of the Vector of Jaw Muscle Force in Mammals. - Journal of Morphology, **243**: 293-299.

Gudo, M. & Ammar, M. (2001): Embryologie des Menschen - hydraulische Mechanismen der Entwicklung. - Natur und Museum, **131**(2): 33-45.

Guillet, A., Doyle, W.S. & Rüther, H. (1985): The combination of photogrammetry and finite elements for a fine grained functional analysis of anatomical structures. - Zoomorphology, **105**: 51-59.

Gutmann, M. (1996): Evolutionstheorie und ihr Gegenstand - Beitrag zur Methodischen Philosophie zu einer konstruktiven Theorie der Evolution. - Verlag für Wissenschaft und Bildung (Berlin), 332 p.

Gutmann, M. & Herkner, B. (1992): Konstruktion und Energie oder: Der vermittelte Widerspruch. - Aufsätze und Reden der senckenbergischen naturforschenden Gesellschaft, **38**: 68-79.

Gutmann, W.F. (1972): Die Hydroskelett-Theorie. - Aufsätze und Reden der senckenbergischen naturforschenden Gesellschaft, **21**: 1-91.

Gutmann, W.F. (1973): Der Konstruktionsplan der Cranioten: ein phylogenetisches Modell und seine methodisch-theoretischen Konstituenten. - Courier Forschungs-Institut Senckenberg, **3**: 1-36.

Gutmann, W.F. (1987): Organismus und Konstruktion: I. Das energetisch getriebene System und die Evolution. - Natur und Museum, **117**(6): 165-172.

Gutmann, W.F. (1989): Die Evolution hydraulischer Konstruktionen. - Verlag Waldemar Kramer (Frankfurt am Main), 201 p.

Gutmann, W.F. (1992): Organismus und Energie. - Aufsätze und Reden der senckenbergischen Naturforschenden Gesellschaft, **38**: 9-25.

Gutmann, W.F. (1994): Evolution von Konstruktionsreihen: die Frankfurter Theorie. In: Gutmann, W.F., Mollenhauer, D. & Peters, D.S., Morphologie und Evolution, Senckenberg-Buch **70**, 317-338.

Gutmann, W.F. (1996a): Gibt es Alternativwege für die Entwicklung der Organisation von Lebewesen I. - Natur und Museum, **126**(8): 250-261.

Gutmann, W.F. (1996b): Gibt es Alternativwege für die Entwicklung der Organisation von Lebewesen II. - Natur und Museum, **126**(9): 283-297.

Gutmann, W.F. & Bonik K. (1981): Kritische Evolutionstheorie: Ein Beitrag zur Überwindung altdarwinistischer Dogmen. - Gerstenberg Verlag (Hildesheim), 227 p.

Gutmann, W.F. & Edlinger, K. (1994a): Morphodynamik und Maschinentheorie: die Grundlage einer kausalen Morphologie. - In: Gutmann, W.F., Mollenhauer, D. & Peters, D.S., Morphologie und Evolution, Senckenberg-Buch **70**, 177-200.

Gutmann, W.F. & Edlinger, K. (1994b): Konstruktion und Verhalten von Maschinen. Zur Modellgrundlage von Morphologie und Evolutionstheorie. - In: Maier, W. & Zoglauer T. (eds.), Technomorphe Organismuskonzepte: Modellübertragung zwischen Biologie und Technik, problemata, **128**: 162-173.

Gutmann, W.F. & Weingarten, M. (1988): Organismus und Konstruktion: III. Mechanische Arbeit von lebenden Konstruktionen sichert das thermodynamische Nicht-Gleichgewicht. - Natur und Museum, **118**(3): 83-92.

Gutmann, W.F. & Weingarten, M. (1991): Maschinentheoretische Grundlagen der organismischen Konstruktionslehre . - Philosophia Naturalis, **28**: 231-256.

Gutmann, W.F. & Weingarten, M. (1992): Grundlagen von Konstruktionsmorphologie und organismischer Konstruktionsmorphologie. - Aufsätze und Reden der senckenbergischen Naturforschenden Gesellschaft, **38**: 51-68.

Hagedorn, P. (2001): Technische Mechanik Band 1: Statik. - Verlag Harri Deutsch (Frankfurt am Main), 326 p.

Harkson, J.C. (1966): *Pteranodon sternbergi*, a new pterodactyl from the Niobrara Formation of Kansas. - Proceedings of the South Dakota Academy of Science, **45**: 74-77.

Harris, J.E. & Crofton, H.D. (1957): Structure and Function in the Nematodes: Internal Pressure and Cuticular Structure in *Ascaris*. - Journal of Experimental Biology, **34**: 116-130.

Hazelwood, S.J., Martin, R.B., Rashid, M.M. & Rodrigo, J.J. (2001): A mechanistic model for internal bone remodeling exhibits different dynamic responses in disuse and overload. - Journal of Biomechanics, **34**: 299-308.

Herkner, B. (1989): Die Entwicklung der saltatorischen Bipedie bei Säugetieren innerhalb der Tetrapodenevolution. - Courier Forschungs-Institut Senckenberg, **111**: 1-102.

Herkner, B. (1999): Über die evolutionäre Entstehung des tetrapoden Lokomotionsappartes der Landwirbeltiere: Ein konstruktionsmorphologisches Transformationsmodell auf evolutionstheoretischer Grundlage. - Carolinea, Beiheft **13**: 1-353.

Herrel, A., De Grauw, E. & Lemos-Espinal, J.A. (2001): Head Shape and Bite Performance in Xenosaurid Lizards. - Journal of Experimental Zoology, **290**: 101-107.

Herring, S.W. (1994): Functional Properties of the Feeding Musculature. - In: Bels, V.L., Chardon, M. & Vandewalle, P., Biomechanics of Feeding in Vertebrates, Advances in Comparative & Environmental Physiology, **18**: 5-28.

Herring, S.W. & Mucci, R.J. (1991): *In Vivo* Strain in Cranial Sutures: The Zygomatic Arch. - Journal of Morphology, **207**: 225-239.

Herring, S.W., Rafferty, K.L., Liu, Z.J. & Marshall, C.D. (2001): Jaw muscles and skull in mammals: the biomechanics of mastication. - Comparative Biochemistry and Physiology, Part A, **131**: 207-219.

Hildebrand, M. & Goslow, G.E. (2004): Vergleichende und funktionelle Anatomie der Wirbeltiere. - Springer (Berlin), 709 p.

Horner, J.R. & Lessem, D. (1993): The complete *T. rex*. - Simon & Schuster (New York), 239 p.

Howse, S.C.B. (1986): On the cervical vertebrae of the Pterodactyloidea (Reptilia: Pterodacytloidea). - Zoological Journal of the Linnean Society, **88**: 307-328.

Howse, S.C.B. & Milner, A.R. (1995): The pterodactyloids from the Purbeck Limestone Formation of Dorset. - Bulletin of the Natural History Museum London (Geology), **51**(1): 73-88.

Howse, S.C.B., Milner, A.R. & Martill, D.M. (2001): Pterosaurs. - In: Martill, D.M. & Naish, D. (eds.), Dinosaurs of the Isle of Wight, Palaeontological Association Field Guide to Fossils, **10**: 324-335.

Huiskes, R. & Chao, E.Y.S. (1983): A survey of finite element analysis in orthopedic biomechanics: the first decade. - Journal of Biomechanics, **16**(6): 385-409.

Hylander, W.L. (1979a): An Experimental Analysis of Temporomandibular Joint Reaction Force in Macaques. - American Journal of Physical Anthropology, **51**: 433-456.

Hylander, W.L. (1979b): Mandibular Function in *Galago crassicaudatus* and *Macaca fascicularis*: an *In Vivo* Approach to Stress Analysis of the Mandible. - Journal of Morphology, **159**: 253-296.

Hylander, W.L. (1985): Mandibular Function and Biomechanical Stress and Scaling. - American Zoologist, **25**: 315-330.

Jaslow, C.R. (1990): Mechanical properties of cranial sutures. - Journal of Biomechanics, **23**(4): 313-321.

Jenkins, I., Thomason, J.J. & Norman, D.B. (2002): Primates and Engineering Principles: Applications to Craniodental Mechanisms in ancient Terrestrial Predators. - Senckenbergiana lethaea, **82**(1): 223-240.

Jeronimidis, G. (1991): Mechanical and fracture properties of cellular and fibrous materials. - In: Vincent, J.F.V. & Lillford, P.J. (eds.), Feeding and the Texture of Food, Society for Experimental Biology Seminar Series, **44**: 1-17.

Ji, S. & Ji, Q. (1988): A new species of pterosaur from Liaoning, *Dendrorhynchus curvidentatus*, gen. et sp. nov.. - Jiangsu Geology **22**(4): 199-206.

Ji, S. & Ji, Q. (1997): The first discovery of a pterosaur from western Liaoning Province (*Eosipterus yangi* gen. et sp.nov.). - Acta Geologica Sinica **71**(1): 1-6.

Ji, S. & Ji, Q. (1998): A New Fossil Pterosaur (Rhamphorhynchoidea) from Liaoning. - Jiangsu Geology **22**(4): 199-206.

Ji, S. & Padian, K. (1999): Biostratigraphy of new pterosaurs in China. - Nature, **398**: 573-574

.

Jouve, S. (2004): Description of a skull of *Ctenochasma* (Pterosauria) from the Latest Jurassic of eastern France, with a taxonomic revision of European Tithonian Pterodactyloidea. - Journal of Vertebrate Paleontology, **24**(3): 542-554.

Kabel, J., van Rietbergen, B., Dalstra, M., Odgaard, A. & Huiskes, R. (1999): The role of an effective isotropic tissue modulus in the elastic properties of cancellous bone. - Journal of Biomechanics, **32**: 673-680.

Kafka, V. (1983): On Hydraulic Strengthening of Bones. - Biorheology, **20**: 789-793.

Kellner, A.W.A. (1984): Ocorrência de uma mandíbula de Pterosauria (*Brasileodactylus araripensis*, nov. gen.; nov. sp.) Na Formação Santana, Cretáceo da Chapada do Araripe, Ceará - Brasil. - Anais XXXIII Congr.Brasil.Geologia **2**: 578-590.

Kellner, A.W.A. (1989): A New Edentate Pterosaur of the Lower Cretaceous from the Araripe Basin, Northeastern Brazil. - Annais Academia brasileira de Cîencias, **61**(4): 439-446.

Kellner, A.W.A. (1995): The relationships of the Tapejaridae (Pterodactyloidea) with comments on pterosaur phylogeny. - In: Sun, A. & Wang, Y. (eds.), Sixth Symposium on Mesozoic Terrestrial Ecosystems and Biota, China Ocean Press (Beijing), 73-77.

Kellner, A.W.A. (1996a): Pterosaur Phylogeny. - Journal of Vertebrate Paleontology, **16**(3): 45A.

Kellner, A.W.A. (1996b): Description of the Braincase of Two Early Cretacous Pterosaurs (Pterodactyloidea) from Brazil. - American Museum Novitates, **3175**: 1-34.

Kellner, A.W.A. (2001): A review of the pterosaur record from Gondwana. - Strate, Série 1, **11**: 51-53.

Kellner, A.W.A. (2003): Pterosaur phylogeny and comments on the evolutionary history of the group. - In: Buffetaut, E. & Mazin, J.-M. (eds.), Evolution and Palaeobiology of Pterosaurs, Geological Society Special Publications, **217**: 105-137.

Kellner, A.W.A. & Campos, D.A. (1988): Sobre um novo pterosauro com crista sagittal da Bacia do Araripe, Cretacéo Inferior de nordeste do Brasil. - Annais Academia brasileira de Cîencias, **60**: 459-469.

Kellner, A.W.A. & Campos, D.A. (1994): A New Species of *Tupuxuara* (Pterosauria, Tapejaridae) from the Early Cretaceous of Brazil. - Annais Academia brasileira de Cîencias, **66**(4): 467-473.

Kellner, A.W.A. & Campos, D.A. (2002): The Function of the Cranial Crest and Jaws of a Unique Pterosaur from the Early Cretaceous of Brazil. Science, **297**: 389-392.

Kellner, A.W.A. & Langston, W. Jr. (1996): Cranial remains of *Quetzalcoatlus* (Pterosauria: Azhdarchidae) from Late Cretaceous sediments of Big Bend National Park, Texas. - Journal of Vertebrate Paleontology, **16**(2): 222-231.

Kellner, A.W.A. & Tomida, Y. (2000): Description of a New Species of Anhangueridae (Pterodactyloidea) with Comments on the Pterosaur Fauna from the Santana Formation (Aptian-Albian), Northeastern Brazil. - National Science Museum Monographs, **17**: 1-135

Kier, W.M. (1982): The Functional Morphology of the Musculature of Squid (Loliginidae) Arms and Tentacles. - Journal of Morphology, **172**: 179-192.

Kier, W.M. (1985): The Musculature of Squid Arms and Tentacles: Ultrastructural Evidence for Functional Differences. - Journal of Morphology, **185**: 223-239.

Kier, W.M. (1992): Hydrostatic skeleton and muscular hydrostats. - In: Biewener, A.A. (ed.), Biomechanics - Structures and Systems: A Practical Approach, IRL Press (Oxford), 205-231.

Kier, W.M. & Smith, K.K. (1985): Tongues, tentacles and trunks: the biomechanics of movement in muscular-hydrostats. - Zoological Journal of the Linnean Society, **83**: 307-324.

Klaauw, C.J. v.d. (1945): Cerebral skull and facial skull. - Archives neerlandaises de zoologie, **7**: 16-37.

Koehl, M.A.R., Quillin, K.J. & Pell, C.A. (2000): Mechanical Design of Fiber-Wound Hydraulic Skeletons: The Stiffening and Straightening of Embryonic Notochords. - American Zoologist, **40**: 28-41.

Koenigswald, W. von, Rensberger, J.M. & Pfretzschner, H.-U. (1987): Changes in tooth enamel of early Paleocene mammals allwoing increased diet diversity. - Nature, **328**: 150-152.

Koh, T.-P. (1937): Untersuchungen über die Gattung *Rhamphorhynchus*. - Neues Jahrbuch für Mineralogie, Geologie und Paläontologie, Beilage-Band, **77**: 455-506.

Kripp, D. von (1932): Die Kaubewegung von *Edmontosaurus spec*. auf Grund der mechanisch-konstruktiven Analyse. - Palaeobiologica, **5**: 409-422.

Kripp, D. von (1933a): Der Oberschnabel-Mechanismus der Vögel. - Jahrbuch für Morphologie, Abteilung 1, **71**: 469-544.

Kripp, D. von (1933b): Beiträge zur mechanischen Analyse des Schnabelmechanismus. - Jahrbuch für Morphologie, Abteilung 1, **72**: 541-566.

Kripp, D. von (1933c): Die Spezialisationsreihe der Störche, Reiher und Kormorane vom konstruktiven und biotechnischen Standpunkt. - Jahrbuch für Morphologie, Abteilung 1, **72**: 60-92

Kripp, D. von (1935a): Die mechanische Analyse der Schnabelkrümmung und ihre Bedeutung für die Anpassungsforschung. - Jahrbuch für Morphologie, Abteilung 1, **76**: 448-494.

Kripp, D. von (1935b): Der Unterkiefer der Vögel als Eisenbetonkonstruktion. - Jahrbuch für Morphologie, Abteilung 1, **76**: 659-662.

Kripp, D. von (1943): Ein Lebensbild von *Pteranodon ingens* auf flugtechnischer Grundlage. - Nova Acta Leopoldina, Neue Folge, **12**(83): 217-246.

Kull, U. (1994): Turgeszens, Hydraulik, Information und das Maschinenkonzept in der Biologie. - In: Maier, W. & Zoglauer, T. (eds.), Technomorphe Organismuskonzepte: Modellübertragung zwischen Biologie und Technik, problemata, **128**: 199-212.

Kummer, B. (1961): Die Torsion der unteren Extremität, ihre Entstehung und funktionelle Bedeutung. - Verhandlungen der Deutschen Orthopädischen Gesellschaft, **49**: 115-135.

Langenbach, G.E.J., Zhang, F., Herring, S.W. & Hannam, A.G. (2002): Modelling the masticatory biomechanics of a pig. - Journal of Anatomy, **201**: 383-393.

Lauder, G.V. (1981): Form and Function: structural analysis in evolutionary morphology. - Palaeobiology, **7**(4): 430-442.

Lauder, G.V. (1995): On the inference of function from structure. - In: Thomason, J.J. (ed.), Functional Morphology in Vertebrate Paleontology, Cambridge University Press, 1-18.

Lawson, D.A. (1975): Pterosaur from the Latest Cretaceous of West Texas: Discovery of the Largest Flying Creature. - Science, **187**: 947-948.

Lee, T.C., Staines, A. & Taylor, D. (2002): Bone adaptation to load: microdamage as a stimulus for bone remodelling. - Journal of Anatomy, **201**: 437-446.

Lee, Y.-N. (1994): The Early Cretaceous pterodactyloid pterosaur *Coloborhynchus* from North America. - Palaeontology, **37**(4): 755-763.

Leonardi, G. & Borgomanero, G. (1985): *Cearadactylus atrox* nov.gen., nov.sp. novo Pterosauria (Pterodactyloidea da Chapada do Araripe, Ceará, Brasil. - D.N.P.M. Coletânea de Trabalhos Paleontológicos, Séria Geológica, **27**: 75-80.

Lewens, T. (2002): Adaptationism and Engineering. - Biology and Philosophy, **17**: 1-31.

Levinton, J.S. (2001): Genetics, paleontology and evolution. - Cambridge University Press (Cambridge), 617 p.

Lü, J.-C. (2002): Soft-tissue in an Early Cretaceous pterosaur frim Liaoning Province, China. - Memoir of the Fukui Prefectural Dinosaur Museum **1**: 19-28.

Lü, J.-C. (2003): A new pterosaur: *Beipiaopterus chenianus*, gen. et sp. nov. (Reptilia: Pterosauria) from Western Liaoning Province of China. - Memoir of the Fukui Prefectural Dinosaur Museum, **2**: 153-160.

Lü, J.-C. & Ji, Q. (2005): A New Ornithocheirid from the Early Cretaceous of Liaoning Province, China. - Acta Geologica Sinica, **79**(2): 157-163.

Mahner, M. & Bunge, M. (2000): Philosophische Grundlagen der Biologie. - Spinger Verlag (Berlin), 402 p.

Marinelli, W. (1938): Der Schädel von *Smilodon*, nach der Funktion des Kieferapparates analysiert. - Palaeobiologica, **6**: 246-271

Marsh, O. (1872): Discovery of additional remains of Pterosauria etc.. - American Journal of Science and Arts, **3**: 241.

Marsh, O. (1876): Principal characters of American pterodactyls. - American Journal of Science and Arts, **12**: 479.

Martill, D.M. & Frey, E. (1998): A new pterosaur Lagerstätte in N. E. Brazil (Crato Formation; Aptian, Lower Cretaceous) : preliminary observations. - Oryctos **1**: 79-85.

Martill, D.M. & Unwin, D.M. (1989): Exceptionally well preserved pterosaur wing membrane from the Cretaceous of Brazil. - Nature **340**: 138-140.

Martin, R.B., Burr, D.B. & Sharkey, N.A. (1998): Skeletal Tissue Mechanics. - Springer (Berlin), 392 p.

Marx, A. (1994): Simulationsrechnungen und Untersuchungen zum physikalischen Verhalten hypsodonter Herbivoren. - Unpublished dissertation Rheinische Friedrich Wilhelm-Universität Bonn, 98 p..

Mateer, N.J. (1975): A study of *Pteranodon*. - Bulletin of the Geological Institut of the University of Uppsala, New Series, **6**: 23-33.

Maynard Smith, J., Burian, J., Kauffman, S., Alberch, P., Campbell, J., Goodwin, B., Lande, R., Raup, D. & Wolpert, L. (1985): Developmental constraints and evolution. - Quarterly Review of Biology, **60**: 2656-287.

McShea, D. (2000): Functional Complexity in Organisms: Parts as Proxies. - Biology and Philosophy, **15**: 641-668.

Meers, M.B. (2002): Cross-sectional geometric properties of the crocodylian humerus: an exception to Wolff's Law. - Journal of Zoology, **258**: 405-418.

Meyer, H. von (1834): *Gnathosaurus subulatus*, ein Saurus aus dem lithographischen Schiefer von Solnhofen. - Museum Senckenbergianum, **I**: 3.

Meyer, H. von (1847): *Homoeosaurus maximiliani* und *Rhamphorhynchus* (*Pterodactylus*) *longicaudus*, zwei fossile Reptilien aus dem Kalkschiefer von Solnhofen - Schmerber (Frankfurt), 22 p.

Meyer, H. von (1852): *Ctenochasma Roemeri*. - Palaeontographica, **2**: 82-84.

Meyer, H. von (1854): Briefliche Mitteilungen an Professor Bronn. - Neues Jahrbuch für Mineralogie, Geologie und Paläontologie, **1854**: 47-58.

Meyer, H. von (1856): Briefliche Mitteilungen an Professor Bronn. - Neues Jahrbuch für Mineralogie, Geologie und Paläontologie, **1856**: 826.

Meyer, H. von (1860): Zur Fauna der Vorwelt. Reptilien aus dem lithographischen Schiefer des Jura in Deutschland und Frankreich. - Verlag Heinrich Keller (Frankfurt am Main), 142 p.

Meyer, H. von (1861): *Pterodactylus spectabilis* aus dem lithographischen Schiefer von Eichstätt. - Palaeontographica, **10**: 1-10.

Miller, H.W. (1972): The taxonomy of the *Pteranodon* species from Kansas. - Transactions of the Kansas Academy of Science, **74**(1): 1-19.

Mitsiadis, T.A., Chéraud, Y., Sharpe P. & Fontaine-Pérus, J. (2003): Development of teeth in chick embryos after mouse neural crest transplantations. - Proceedings of the National Academy of Sciences, **100**(11):6541–6545.

Modesto, S.P. & Sues, H.-D. (2004): The skull of the Early Triassic archosauromorph reptile *Prolacerta broomi* and its phylogenetic significance. - Zoological Journal of the Linnean Society, **140**: 335-351.

Molnar, R.E. (1998): Mechanical factors in the design of the skull of *Tyrannosaurus rex* (Osborn, 1905). - Gaia, **15**: 193-218.

Morgan, E.F., Bayraktar, H.H. & Keaveny, T.M. (2003): Trabecular bone modulus-density relationships depend on anatomic site. - Journal of Biomechanics, **36**: 897-904.

Moss, M.L. & Young, R.W. (1960): A functional approach to craniology. - American Journal of Physical Anthropology, **18**: 281-292.

Müller, J. (2003): Early loss and multiple return of the lower temporal arcarde in diapsid reptiles. - Naturwissenschaften, **10**: 473-476.

Münster, G. zu (1839): Über einige neue Versteinerungen in den lithographischen Schiefern von Baiern. - Neues Jahrbuch Mineralogie, Geologie und Paläontologie: 676-682.

Nachtigall, W. (1991): Functional Aspects of Morphology. - In: Schmidt-Kittler, N. & Vogel, K. (eds.), Constructional Morphology and Evolution, Springer Verlag (Berlin), 31-40.

Nachtigall, W. (2000): Biomechanik. - Friedr. Vieweg & Sohn Verlagsgesellschaft mbH, Braunschweig, 459 p.

Neander, K. (1991): Functions as selected effects: the conceptual analyst's defense. - Philosophy of Science, **58**: 168-184.

Newton, E.T. (1888): On the skull, brain and auditory organ of a new species of Pterosaurian (*Scaphognathus Purdoni*) from the Upper Lias near Whitby, Yorkshire. - Philosophical Transactions of the Royal Society, **179**: 503-537.

Nida-Rümelin, J. (1994): Reduktionismus und Holismus. - In: Maier, W. & Zoglauer, T. (eds.), Technomorphe Organismuskonzepte: Modellübertragung zwischen Biologie und Technik, problemata, **128**: 25-46.

Nobiling, G. (1977): Die Biomechanik des Kieferapparates beim Stierkopfhai (*Heterodontus portusjacksoni* = *Heterodontus philippi*). - Advances in Anatomy, Embryology and Cell Biology, **52**: 1-52.

Odgaard, A. (1997): Three-Dimensional Methods for Quantification of Cancellous Bone Architecture. - Bone (New York), **20**(4): 315-328.

Olson, E.C. (1961): Jaw Mechanisms: Rhipidistians, Amphibians, Reptiles. - American Zoologist, **1**: 205-215.

Otto, F. (1995): Pneu und Knochen. - Mitteilungen des Instituts für leichte Flächentragwerke (IL) Universität Stuttgart, **35**: 1-254.

Owen, R. (1861): Monograph of the fossil Reptilia of the Cretaceous Formations. Supplement III. - Palaeontographical Society Monograph, **12**: 1-25.

Owen, R. (1874): Monograph of the fossil Reptilia of the Mesozoic Formations. I. Pterosauria. - Palaeontographical Society Monograph, **27**: 1-14.

Padian, K. (1984): The Orign of Pterosaurs. - In: Reif, W.E. & Westphal, D. (eds.), Third Symposium on Mesozoic Terrestrial Ecosystems, Attempto-Verlag (Tübingen), pp. 163-168.

Padian, K. (1995): Form versus function: the evolution of a dialectic. - In: Thomason J.J. (ed.), Functional Morphology in Vertebrate Paleontology, Cambridge University Press, 264-277.

Pauwels, F. (1980): Biomechanics of the Locomotor Apparatus - Contributions on the Functional Anatomy of the Locomotor Apparatus. - Springer Verlag (Berlin), 518 p.

Penzlin, H. (1994): Der Reduktionismus und das Lebensproblem. - In: Maier, W. & Zoglauer, T. (eds.), Technomorphe Organismuskonzepte - Modellübertragungen zwischen Biologie und Technik, problemata, frommann-holzboog (Stuttgart), **128**: 47-66.

Peters, D.S. (2000): A Reexamination of four Prolacertiformes with Implications for Pterosaur Phylogenies. - Rivista Italiana di Paleontologia e Stratigrafia, **106**(3): 239-336.

Peters, D.S. (1972): Das Problem konvergent entstandener Strukturen in der anagenetischen und genealogischen Systematik. - Zeitschrift für zoologische Systematik und Evolutionsforschung, **10:** 161-173.

Peters, D.S. (1985a): Mechanical constraints canalyzing the evolutionary transformations of tetrapod limbs. - Acta Biotheoretica, **34**: 157-164.

Peters, D.S. (1985b): Erneut vorgestellt: Das “Ökonomieprinzip” - Aufsätze und Reden der Senckenbergischen Naturforschenden Gesellschaft, **35**: 143-153.

Peters, D.S. & Gutmann, W.F. (1971): Über die Lesrichtung von Merkmals- und Konstruktionsreihen. - Zeitschrift für zoologische Systematik und Evolutionsforschung, **9**: 237-263.

Peters, D.S. & Gutmann, W.F. (1973): Modellvorstellungen als Hauptelement phylogenetischer Methodik. - Aufsätze und Reden der senckenbergischen naturforschenden Gesellschaft, **24**: 26-38.

Pfretzschner, H.-U. (1986): Structural Reinforcement and Crack Propagation in Enamel. - In: Russel, D.E., Santoro, J.-P. & Sigogneau-Russel, D. (eds.), Teeth Revistited, Proceedings of the 7th International Symposium on Dental Morphology, Mémoire du Musée national Histoire naturelle Paris (série C), **53**: 133-143.

Pfretzschner, H.-U. (1994): Biomechanik der Schmelzmikrostruktur in den Backenzähnen von Grossäugern. - Palaeontographica Abt.A, **234**(1-3): 1-88.

Pigliucci, M. & Kaplan, J. (2000): The fall and rise of Dr Pangloss: adaptionism and the Spandrels 20 years later. - Trends in Ecology and Evolution, **15**(2): 66-70.

Plieninger, F. (1895): *Campylognathoides Zitteli*. Ein neuer Flugsaurier aus dem Oberen Lias Schwabens. - Palaeontographica, **41**: 19-22.

Plieninger, F. (1907): Die Pterosaurier der Juraformation Schwabens. - Palaeontographica, **53**: 209-213.

Prendergast, P.J. & van der Meulen, M.C.H. (2001): Mechanics of Bone Regeneration. - In: Cowin, S.C. (ed.), Bone Mechanics Handbook, CRC Press (Boca Raton), 32-1 - 32-13.

Preuschoft, H. (1989): Biomechanical approach to the evolution of the facial skeleton of hominoid primates. - Fortschritte der Zoologie, **35**: 421-431.

Preuschoft, H. & Witzel, U. (2002): Biomechanical investigations on the Skulls of Reptiles and Mammals. - Senckenbergiana lethaea, **82**(1): 207-222.

Preuschoft, H., Demes, B., Meier, M. & Bär H.F. (1985): Die biomechanischen Prinzipien im Oberkiefer von langschnäuzigen Wirbeltieren. - Zeitschrift für Morphologie und Anthropologie, **76**(1): 1-24.

Price, L.I. (1971): A Presença de Pterosauria no Cretáceo Inferior da Chapada do Araripe, Brasil. - Annais Academia brasileira de Cîencias, **43**(Supplement): 415-461.

Purslow, P.P. (1991): Measuring meat texture and understanding its structural basis. - In: Vincent, J.F.V. & Lillford, P.J. (eds.), Feeding and the Texture of Food, Society for Experimental Biology Seminar Series, **44**: 35-56.

Quenstedt, F.A. (1855): Über *Pterodactylus suevicus* im lihtographischen Schiefer Württembergs. - 52 p.

Rafferty, K.L. & Herring, S.W. (1999): Craniofacial Sutures: Morphology, Growth, and in Vivo Masticatory Strains. - Journal of Morphology, **242**: 167-179.

Rafferty, K.L., Herring, S.W. & Marshall, C.D. (2003): Biomechanics of the Rostrum and the Role of Facial Sutures. - Journal of Morphology, **257**: 33-44.

Ramtani, S. & Zidi, M. (2001): A theoretical model of the effect of continuum damage on a bone adaptation model. - Journal of Biomechanics, **34**: 471-479.

Ravosa, M.J., Johnson, K.R. & Hylander, W.L. (2000): Strain in the Galago Facial Skull. - Journal of Morphology, **245**: 51-66.

Rayfield, E.J. (2004): Cranial mechanics in *Tyrannosaurus rex*. - Proceedings of the Royal Society London, B, **271**: 1451-1459.

Rayfield, E.J. (2005): Using finite-element analysis to investigate suture morphology: A case study using large carnivorous dinosaurs. - The Anatomical Record Part A: Discoveries in Molecular, Cellular, and Evolutionary Biology, **283A**(2): 349-365.

Rayfield, E.J., Norman, D.B., Horner, C.C, Horner, J.R., Smith, P.M., Thomason, J.J. & Upchurch, P. (2001): Cranial design and function in a large theropod dinosaur. - Nature, **409**: 1033-1037.

Reif, W.-E. (1975): Lenkende und limitierende Faktoren in der Evolution. - Acta Biotheoretica, **24**(3-4): 136-162.

Reif, W.-E. (1982): Functional morphology on the procrustean bed of the neutralism-selectionism debate. - Notes on the Constructional Morphology approach. - Neues Jahrbuch für Geologie und Paläontologie, Abhandlungen, **164**: 46-59.

Reif, W.-E. (2002): Evolution of Organ Systems: Phylogeny, Function and Reciprocal Illumination. - Senckenbergiana lethaea, **82**(1): 195-206

.

Reif, W.-E. (2003): Inferences of function in fossils: The case of moas' leg bones. - Neues Jahrbuch für Geologie und Paläontologie, Monatshefte, **2003**(3): 129-144.

Reif, W.-E., Thomas, R.D.K. & Fischer, M.S. (1985): Constructional morphology: an analysis of constraints in evolution. - Acta Biotheoretica, **34**: 233-248.

Rensberger, J.M. (1992): Relationship of chewing stress and enamel microstructure in rhinocerotoid cheek teeth. - In: Smith, P. & Tchernov, E. (eds.), Structure, Function and Evolution of Teeth, Freund Publishing House (London), 163-183.

Rensberger, J.M. (1993): Adaptation of Enamel Microstructure to Differences in Stress Intensity in the Eocene Perissodactyl Hyracotherium. - In: Kobayashi, I., Mutvei, H. & Sahni, A. (eds.), Structure, Formation and Evolution of Fossil Hard Tissues, Tokai University Press (Tokyo), 131-145.

Rensberger, J.M. (1995): Determination of stresses in mammalian dental enamel and their relevance to the interpretation of feeding behaviours in extinct taxa. - In: Thomason, J.J. (ed.), Functional Morphology in Vertebrate Paleontology, Cambridge University Press, 151-172.

Rensberger, J.M. (2000): Pathways to functional differentiation in mammalian enamel. - In: Teaford, M.F., Smith, M.M. & Ferguson, M.W.J. (eds.), Development, Function and Evolution of Teeth, Cambridge University Press (Cambridge), 252-268.

Rieß, J., Frey, E., Begenat, R. & Weber, E. (1989): Über die Schwierigkeit, aus Form- und Funktionsreihen stammesgeschichtliche Abläufe zu rekonstruieren. - In: Edlinger, K. (ed.), Form und Funktion - Ihre stammesgeschichtlichen Grundlagen, WUV - Universitätsverlag (Wien), 97-109.

Rjabinin, A.N. (1948): Bemerkung über ein Flugreptil aus dem Jura des Kara-Tau [in russian]. - Trudy Akademia Nauk, Palaeontological Institute, **15**(1): 86-93.

Romberg, O. & Hinrichs, N. (2003): Keine Panik vor Mechanik!. - Friedr. Vieweg & Sohn Verlagsgesellschaft (Braunschweig), 343 p.

Rudwick, M.J.S. (1964): The Inference of Function from Structure in Fossils. - The Bristish Journal for the Philosophy of Science, **15**: 27-40.

Russell, A.P. & Thomason, J.J. (1993): Mechanical Analysis of the Mammalian Head Skeleton. - In: Hanken, J. & Hall, B.K. (eds.), The Vertebrate Skull - Vol.3: Functional and Evolutionary Mechanisms, University of Chicago Press, 345-383.

Salisbury, S.W. (2001): A biomechanical transformation model for the evolution of the eusuchian bracing system. - Unpublished PhD thesis, University of New South Wales, 504 p.

Salisbury, S.W. & Frey, E. (2001): A biomechanical transformation model for the evolution of semi-spheroidal articulations between adjoining vertebral bodies in crocodilians. - In: Grigg, G.C. & Franklin C.F. (eds.), Crocodilian Biology and Evolution, Surrey Beatty & Sons (Chipping Norton), 85-134.

Sanchez, T.M. (1973): Redescripcion del Craneo y Mandibulas de *Pterodaustro guiñazui* Bonaparte (Pterodactyloidea, Pterodaustriidae). - Ameghinia, **10**(4): 313-325.

Sander, P.M. (1999): The Microstructure of Reptilian Tooth Enamel: Terminology, Function, and Phylogeny. - Münchner Geowissenschaftliche Abhandlungen, Reihe A (Geologie und Paläontologie), **39**: 1-102.

Sansom, R. (2002): Constraining the adaptationism debate. - Biology and Philosophy, **18**: 493-512.

Scapino, R.P. (1965): The Third Joint of the Canine Jaw. - Journal of Morphology, **116**: 23-50.

Schmidt, S.H. (1706): Giovanni Alfonso Borelli: Von der wundersamen Macht der Muskeln. - Curt R. Vincentz Verlag Hamburg, 77 p. [Reprint 1978].

Schumacher, G.-H. (1973): The Head Muscles and Hyolaryngeal Skeleton of Turtles and Crocodilians. - In: Gans, C. & Parsons, T.S. (eds.), Biology of the Reptilia, Vol. 4, Academic Press (San Diego), 101-109.

Schwenk, F. (ed.) (2000): Feeding: Form, Function, and Evolution in Tetrapod Vertebrates. - Academic Press (San Diego), 537 p.

Seeley, H..G. (1887): On a sacrum apparently indicating a new type of bird, *Ornithodesmus cluniculus*. - Quarterly Journal of the Geological Society, **43**: 206.

Seeley, H.G. (1901): Dragons of the air. An account of flying reptiles. - Methuen & Co. (London), 239 p.

Seilacher, A. (1970): Arbeitskonzept zur Konstruktionsmorphologie. - Lethaia, **3**: 393-396.

Sereno, P.C. (1991): Basal Archosaurs: Phylogenetic Relationships and Functional Implications. - Journal of Vertebrate Paleontology, Supplement **11**(4): 1-53.

Sereno, P.C. (1996): The phylogenetic position of pterosaurs within Archosauria. - Journal of Vertebrate Paleontology, **16**(3): 64A.

Sharov, A.G. (1971): (New flying reptiles from the Mesozoic of Kazhakstan and Kirgisia). - Akad. Nauk SSSR Trudy Palaeont. Inst., **130**: 104-113. [in Russian]

Simpson, G.G. (1953): The Major Features of Evolution. - Columbia University Press (New York), 434 p.

Sinclair, A.G. & Alexander, R. M. (1987): Estimates of forces exerted by the jaw muscles of some reptiles. - Journal of Zoology, **213**: 107-115.

Smith-Woodward, A. (1902): On two skulls of the Ornithosaurian *Rhamphorhynchus*. Annual Magazine of Natural History, (7), **9**: 1-5.

Soemmering, S. Th. von (1812): Über einen *Ornithocephalus brevirostris* der Vorwelt. - Denkschriften der Königlich-Bayerischen Akademie der Wissenschaften, mathematisch-physikalische Classe, **3**: 89-158.

Spillers, W.R. (1985): Introduction to Structures. - Ellis Horwood Limited (Chichester), 262 p.

Srivastava, R., Ahmad, A. & Rao, V.R. (1999): Stress patterns in conical teeth of reptiles and mammals: experimental and finite element analysis. - Revista Espanola de Palaeontología, **14**(2): 269-277.

Starck, D. (1935): Kaumuskulatur und Kiefergelenk der Ursiden. - Jahrbuch für Morphologie, Abteilung 1, **76**: 104-147.

Starck, D. (1940): Beobachtungen an der Trigeminusmuskulatur der Nashornvögel nebst Bemerkungen über einige Besonderheiten des Vogelschädels und über die Kiefermuskulatur im allgemeinen. - Gegenbaurs Morphologisches Jahrbuch, **84**(4): 585-623.

Starck, D. (1979): Vergleichende Anatomie der Wirbeltiere auf evolutionsbiologischer Grundlage. Band 2. Das Skeletsystem - Allgmeines, Skeletsubstanzen, Skelet der Wirbeltiere einschließlich Lokomotionstypen. - Springer Verlag (Berlin), 776 p.

Stolley, E. (1936): *Odonthorhynchus aculeatus* n. g. n. sp., ein neuer Rhamphorhynchide von Solnhofen. - Neues Jahrbuch für Mineralogie, Geologie und Paläontologie, Beilage-Band, Abt. B., **75**: 543-563.

Sun, Z., Lee, E. & Herring, S.W. (2004): Cranial Sutures and Bones: Growth and Fusion in Relation to Masticatory Strain. The Anatomical Record, Part A, **276A**: 150-161.

Swartz, S.M. (1991): Strain Analysis as a Tool for Functional Morphology. - American Zoologist, **21**: 655-669.

Taquet, P. (1972): Un crâne de *Ctenochasma* (Pterodactyloïdea) du Portlandien inférieur de la Haute-Marne, dans les collections du Musée de Saint-Dizier. - Comptes rendus de l'Academie des Sciences Paris, Série D, **274**: 362-364.

Teng, S. & Herring, S.W. (1998): Compressive Loading on Bone Surfaces From Muscular Contraction: An *In Vivo* Study in the Miniature Pig, *Sus scrofa*. - Journal of Morphology, **238**: 71-80.

Theodori, C. (1830): Knochen von *Pterodactylus* aus der Liasformation von Banz. - Frorieps Notzizen für Natur- und Heilkunde, **632**: 101.

Thomason, J.J. (1991): Cranial strength in relation to estimated biting forces in mammals. - Canadian Journal of Zoology, **69**: 2326-2333.

Thomason, J.J. & Russell, A.P. (1986): Mechanical Factors in the Evolution of the Mammalian Secondary Palate: A Theroretical Analysis. - Journal of Morphology, **189**: 199-213.

Thomason, J.J., Tsui, P. & Russell, A.P. (1995): Mechanical function of the mammalian secondary palate: a finite element analysis. - Journal of Vertebrate Paleontology, **15**(3): 56A.

Tischlinger, H. & Frey, E. (2001): "Mit Haut und Haar!" Flugsaurier-Neufunde mit Weichteilerhaltung. - Fossilien, **2001**(3): 151-158.

Tittel, K. (1994): Beschreibende und funktionelle Anatomie des Menschen. - Gustav Fischer Verlag (Jena), 374 p.

Tucker, R. (1954): Studies in Functional and Analytical Craniology I-VI. - Australian Journal of Zoology, **2**: 382-430.

Tucker, R. (1955): Studies in Functional and Analytical Craniology VII-X. - Australian Journal of Zoology, **3**: 513-546.

Turner, C.H. (1992): On Wolff's Law of trabercular architecture. - Journal of Biomechanics, **25**(1): 1-9.

Unwin, D.M. (1992): The phylogeny of the Pterosauria. - Journal of Vertebrate Paleontology, **12**(3): 57A.

Unwin, D.M. (1995): Preliminary results of a phylogenetic analysis of the pterosauria (Diapsida: Archosauria). - In: Sun, A.& Wang, Y., Sixth Symposium of Mesozoic Terrestrial Ecosystems and Biota, China Ocean Press (Beijing), 69-72.

Unwin, D.M. (2002): On the systematic relationships of *Cearadactylus atrox*, an enigmatic Early Cretaceous pterosaur from the Santana Formation of Brazil. - Mitteilungen des Naturkundlichen Museums Berlin, Geowissenschaftliche Reihe, **5**: 239-263.

Unwin, D.M. (2003): On the phylogeny and evolutionary history of pterosaurs. - In: Buffetaut, E. & Mazin, J.-M. (eds.), Evolution and Palaeobiology of Pterosaurs, Geological Society Special Publications, **217**: 139-190.

Unwin, D.M., Lü, J. & Bakhurina, N.N. (2000): On the systematic and stratigraphic significance of pterosaurs from the Lower Cretaceous Yixian Formation (Jehol Group) of Liaoning, China. - Mitteilungen des Naturkundlichen Museums Berlin, Geowissenschaftliche Reihe, **3**: 108-126.

van den Bos, T. & Tonino, G.J. (1984): Composition and metabolism of the extracellular matrix in the periodontal ligament of impeded and unimpeded rat incisors. - Archives of Oral Biology, **29**(11): 893-897.

van der Meij, M.A.A. & Bout, R.G. (2004): Scaling of jaw muscle size and maximal bite force in finches. - The Journal of Experimental Biology, **207**:2745-2753.

Van Valkenburgh, B. & Ruff, C.B. (1987): Canine tooth strength and killing behaviour in large canivores. - Journal of Zoology, **212**: 379-397.

Veldmeijer, A. (2002): Pterosaurs from the Lower Cretaceous of Brazil in the Stuttgart Collection. - Stuttgarter Beiträge zur Naturkunde, Serie B (Geol. Paläont.) **327**: 1-27.

Veldmeijer, A. (2003): Description of *Coloborhynchus spielbergi* sp. nov. (Pterodactyloidea) from the Albian (Lower Cretaceous of Brazil). - Scripta Geologica, **125**: 35-139.

Vincent, J.F.V. (1982): Structural Biomechanics. - The Macmillan Press Ltd. (London), 206 p.

Vincent, J.F.V. & Lillford, P.J. (eds.) (1991): Feeding and the Texture of Food. - Society for Experimental Biology Seminar Series, **44**: 1-247.

Viscardi, P., Dyke, G.J., Wilkinson, M., & Ranyer, J.M. (1999): Missing data and the phylogeny of the Pterosauria. - Journal of Vertebrate Palaeontology, **19**(3): 83A.

Vogel, K. (1989a): Konstruktionsmorphologie und Rekonstruktion der Stammesgeschichte. - In: Edlinger K. (ed.), Form und Funktion - Ihre stammesgeschichtlichen Grundlagen, WUV - Universitätsverlag (Wien), 55-67.

Vogel, K. (1989b): Constructional morphology and the reconstruction of phylogeny. - In: Schmidt-Kittler, N. & Willmann, R. (eds.), Phylogeny and the Classification of Fossil and Recent Organisms, Abhandlungern des Naturwissenschaftlichen Vereins Hamburg, (NF), **28**: 255-264.

Vogel, K. (1991): Concepts of Constructional Morphology. - In: Schmidt-Kittler, N. & Vogel, K. (eds.), Constructional Morphology and Evolution, Springer Verlag, Berlin, 55-68.

Vogel, S. (1984): Drag and Flexibility in Sessile Organisms. - American Zoologist, **24**: 37-44.

Vogel, S. (2001): Prime Mover - A Natural History of Muscles. - W.W. Norton Company & Inc. (New York), 307 p.

Vogel, S. (2003): Comparative Biomechanics - Life's Physical World. - Princeton University Press (Princeton), 580 p.

Wagner, A. (1837): Beschreibung eines neuentdeckten *Ornithocephalus*, nebst allgemeinen Bemerkungen über die Organisation dieser Gattung. - Abhandlungen der Bayerischen Akademie der Wissenschaften, mathematisch-physikalische Classe, **2**: 165-198.

Wagner, A. (1851): Beschreibung einer neuen Art von *Ornithocephalus*, nebst allgemeinen Bemerkungen über die Organisation dieser Gattung. - Abhandlungen der Bayerischen Akademie der Wissenschaften, mathematisch-physikalische Classe, **6**: 1-64.

Wagner, A. (1861): Charakteristik einer neuen Flugeidechse, *Pterodactylus elegans*. - Sitzungsberichte der Bayerischen Akademie der Wissenschaften, mathematisch-physikalische Classe: 363-365.

Wainwright, S.A. (1970): Design in Hydraulic Organisms. - Naturwissenschaften, **57**(7): 321-326.

Wainwright, S.A., Biggs, W.D., Currey, J.D. & Gosline, J.M. (1976): Mechanical Design in Organisms. - Edwald Arnold (London), 423 p.

Walker, W.F. Jr. & Liem, K.F. (1994): Functional Anatomy of Vertebrates: An Evolutionary Perspective. - Saunders College Publishing (Fort Worth), 830 + XXIp.

Wang, X. & Lü, J. (2001): Discovery of a pterodactyloid pterosaur from the Yixian Formation of western Liaoning, China. - Chinese Science Bulletin **46**(13): 1112-1117.

Wang, X. & Zhou, Z. (2003): A new pterosaur (Pterodacytloidea, Tapejaridae) from the Early Cretaceous Jiufotang Formation of western Liaoning, China and its implications for biogeograohy. - Chinese Science Bulletin, **48**(1): 16-23.

Wang, X., Zhou, Z., Zhang, F. & Xu, X. (2002): A nearly completely articulated rhamphorhynchoid pterosaur with well preserved wing membranes and "hairs" from Inner Mongolias, northeast China. - Chinese Science Bulletin, **47**(3): 226-230.

Wang, X., Wang, X., Jin, F., Xu, X. & Wang, Y. (1999): Vertebrate assemblages of the Jehol Biota in western Liaoning, China. - In: Wang, Y. & Deng, T. (eds.), Proceeding of the Seventh Annual Meeting of the Chinese Society of Vertebrate Paleonology, China Ocean Press,. Beijing 1999, 1-12.

Weber, H. (1958): Konstruktionsmorphologie. - Zoologisches Jahrbuch, Abteilung Allgemeine Zoologie, **68**: 1-112.

Weijs, W.A. & Van Ruijven, L.J. (1990): Models of Masticatory Mechanics: their reliability, Resolving Power and Usefulness in Functional Morphology. - Netherlands Journal of Zoology, **40**(1-2): 136-152.

Weijs, W.A., Brugman, P. & Klok, E.M. (1987): The Growth of the Skull and Jaw Muscles andf Its Functional Consequences in the New Zealand Rabbit (*Oryctolagus cuniculus*). - Journal of Morphology, **194**: 143-161.

Weingarten, M. (1994): Konstruktion und Verhalten von Maschinen. Zur Modellgrundlage von Morphologie und Evolutionstheorie. - In: Maier, W. & Zoglauer, T. (eds.), Technomorphe Organismuskonzepte: Modellübertragung zwischen Biologie und Technik, problemata, **128**: 162-173.

Weishampel, D.B. (1993): Beams and Machines: Modeling Approaches to the Analysis of Skull Form and Function. - In: Hanken, J. & Hall, B.K. (eds.), The Vertebrate Skull - Vol.3: Functional and Evolutionary Mechanisms, University of Chicago Press, 303-344.

Wellnhofer, P. (1970): Die Pterodactyloidea (Pterosauria) der Oberjura-Platenkalke Süddeutschlands. - Abhandlungen der Bayerischen Akademie der Wissenschaften, Neue Folge, **141**: 1-133.

Wellnhofer, P. (1974): *Campylognathoides liassicus* (Quenstedt), an Upper Liassic pterosaur from Holzmaden - The Pittsburgh Specimen. - Annals of the Carnegie Museum of Natural History, **45**: 5-34.

Wellnhofer, P. (1975a): Die Rhamphorhynchoidea (Pterosauria) der Oberjura.-Plattenkalke Süddeutschlands. Teil II - Allgemeine Skelettmorphologie. - Palaeontolographica, Abt. A, **148**(1-33): 1-33.

Wellnhofer, P. (1975b): Die Rhamphorhynchoidea (Pterosauria) der Oberjura.-Plattenkalke Süddeutschlands. Teil II - Systematische Beschreibung. - Palaeontolographica, Abt. A, **148**(4-6): 132-186.

Wellnhofer, P. (1978): Handbuch der Paläoherpetologie - Teil 19: Pterosauria. - Gustav Fischer Verlag (Stuttgart), 82 p.

Wellnhofer, P. (1980): Flugsaurierreste aus der Gosau-Kreide von Muthmannsdorf (Niederösterreich) - ein Beitrag zur Kiefermechanik der Pterosaurier. - Mitteilungen der Bayerischen Staatssammlung für Paläontologie und historische Geologie, **20:** 95-112.

Wellnhofer, P. (1983): Solnhofer Plattenkalk: Urvögel und Flugsaurier. - Museum beim Solnhofer Aktien-Verein, Maxberg, 64 p.

Wellnhofer, P. (1985): Neue Pterosaurier aus der Santana-Formation (Apt) der Chapada do Araripe, Brasilien. - Palaeontographica, Abt A., **187**(4-6): 105-182.

Wellnhofer, P. (1987): New Crested Pterosaurs from the Lower Cretaceous of Brazil. - Mitteilungen der Bayerischen Staatssammlung für Paläontologie und historische Geologie, **27**: 175-186.

Wellnhofer, P. (1991a): The Illustrated Encyclopedia of Pterosaurs. Crescent Books (New York), 192 p.

Wellnhofer, P. (1991b): Weitere Pterosaurierfunde aus der Santana-Formation (Apt) der Chapada do Araripe, Brasilien. - Palaeontographica Abt.A, **215**(1-3): 43-101.

Wellnhofer, P. (1991c): The Santana Formation Pterosaurs. - In: Maisey, J.G. (ed.), Santana fossils: an illustrated atlas, T.F.H. Publications (New Jersey), 351-371.

Wellnhofer, P. & Kellner, A.W.A. (1991): The Skull of *Tapejara wellnhoferi* Kellner (Reptilia, Pterosauria) from the Lower Cretaceous Santana Formation of the Araripe Basin, Northeastern Brazil. - Mittteilungen der Bayerischen Staatssammlung für Paläontologie und historische Geologie, **31**: 89-106.

Wild, R. (1971): *Dorygnathus mistelgauensis* n.sp., ein neuer Flugsaurier aus dem Lias Epsilon von Mistelgau (Fränkischer Jura). - Geologisches Blatt Bayern, **21**(4): 178-195.

Wild, R. (1973): Die Triasfauna der Tessiner Kalkalpen. XXIII. *Tanystropheus longobardicus* (Bassani) (Neue Ergebnisse). - Schweizer Paläontologische Abhandlungen, **95**: 1-162.

Wild, R. (1978): Die Flugsaurier (Reptilia, Pterosauria) aus der Oberen Trias von Cene bei Bergamo, Italien. - Bolletino del Societa Paleontologia Italiana, **17**(2): 176-256.

Wild, R. (1983a): Über den Ursprung der Flugsaurier. - Weltenburger Akademie, Erwin Rutte-Festschrift: 231-238.

Wild, R. (1983b): A new pterosaur (Reptilia, Pterosauria from the Upper Triassic (Norian) of Friuli, Italy. - Gortania - Atti Museo Friuli di Storia Naturale, **5**: 45-62.

Wild, R. (1984): Flugsaurier aus der Obertrias von Italien. - Naturwissenschaften, **71**: 1-11.

Wild, R. (1993): A juvenile specimen of *Eudimorphodon ranzii* Zambelli (Reptilia, Pterosauria) form the Upper Triasasic (Norian) of Bergamo. - Rivista del Museo Civico di Scienze Naturali "E.Caffi" Bergamo, **16**: 95-120.

Williston, S.W. (1891): The Skull and Hind Extremity of *Pteranodon*. - The American Naturalist, **25**: 1124-1126.

Williston, S.W. (1902): On the Skull of *Nyctodactylus*, an Upper Cretaceous Pterodactyl. - Journal of Geology, **10**(5): 520-531.

Wiman, C. (1925a): Über *Dorygnathus* und andere Flugsaurier. - Bulletin of the Geological Institut of the University of Uppsala, **19**: 23-54.

Wiman, C. (1925b): Über *Pterodactylus Westmanni* und andere Flugsaurier. - Bulletin of the Geological Institut of the University of Uppsala, **20**: 1-38.

Witmer, L.M. & Rose, K.D. (1991): Biomechanics of the jaw apparatus of the gigantic Eocene bird *Diatryma*: implications for diet and mode of life. - Paleobiology, **17**(2): 95-120.

Witzel, U. & Preuschoft, H. (2005): Finite-element model construction for the virtual synthesis of the skulls in vertebrates: Case study of Diplodocus. - The Anatomical Record Part A: Discoveries in Molecular, Cellular, and Evolutionary Biology, **283A**(2): 391-401.

Wolff, J. (1892): Das Gesetz der Transformation der Knochen. - A. Horschwald (Berlin), 152 p.

Xinghua, Z., He, G., Dong, Z. & Bingzhao, G. (2002): A study of the effect of non-linearities in the equation of bone remodeling. - Journal of Biomechanics, **35**: 951-960.

Xinlu, H., Daihuan, Y. & Chunkang, S. (1983): A new pterosaur from the Middle Jurassic of Dashanpu, Zigong, Sichuan. - Journal of the Chengdu College of Geology, Supplement **1**: 27-33.

Young, C. (1964): On a new pterosaurian from Sinkiang, China. - Vertebrata Palasiatica, **8**: 221-256.

Zambelli, R. (1973): *Eudimorphodon ranzii* gen.nov., sp.nov., uno pterosauro triassico. - Rend.Sci.Inst.Lomb. B, **107**: 27-32.

Zhou, Z., Barrett, P.M. & Hilton, J. (2003): An exceptionally preserved Lower Cretaceous ecosystem. - Nature, **421**: 807-814.

Zittel, K.A. (1882): Über Flugsaurier aus dem lithographischen Schiefer Bayerns. - Palaeontographica, **29**: 47-80.

Zusi, R.L. (1959): The Function of the Depressor Mandibulae in Certain Passerine Birds. - Auk, **76**: 537-539.

Zusi, R.L. (1962): Structural adaptations of the head and neck in the Black Skimmer *Rynchops nigar* Linnaeus. - Publications of the Nuttall Ornithological Club, **3**: 1-101.

Zusi, R.L. (1967): The Role of the Depressor Mandibulae in Kinesis of the Avian Skull. - Proceedings of the United States National Museum, Smithsonian Institution, **123**: 1-28.

Zweers, G.A. (1985): Greek classicism in living Structure? Some deductive pathways in animal morphology. - Acta Biotheoretica, **34**: 249-276.

Zweers, G.A. (1991): Transformation of avian feeding mechanisms: a deductive method. - Acta Biotheoretica, **39**: 15-36.

JAW MECHANICS OF THE PTEROSAUR SKULL CONSTRUCTION AND THE EVOLTUION OF TOOTHLESSNESS

Michael Fastnacht

APPENDIX A: BIOMECHANICAL PARAMETER OF PTEROSAUR SKULL CONSTRUCTIONS

A.1. Angustinaripterus skull construction (see also chapter 7.1)

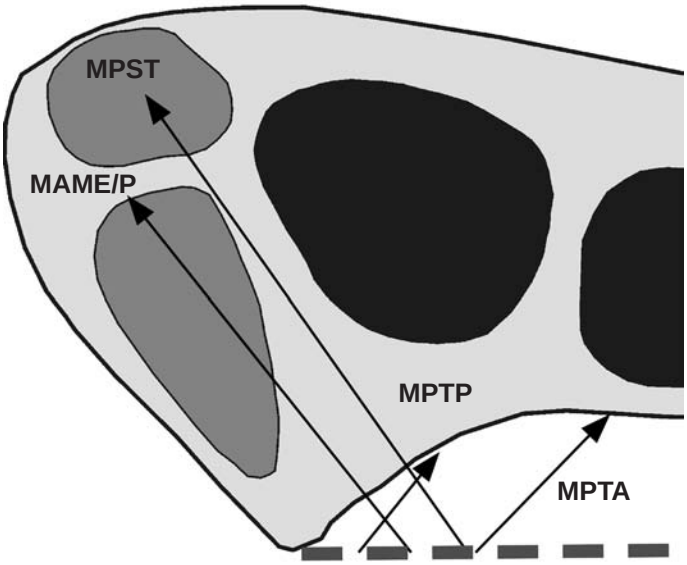

Fig. A.1: Reconstruction of the principal pulling direction of the main adductor muscles in the skull of *Angustinaripterus*. See chapter 6 for abbreviations.

Muscles	F_1	l_1	α_1	F_2	l_2	α_1
MAME/P	36	13.24	51	2.06	231.43	129
MPST	92	19.92	54	8.15	224.75	126
MPTA	14	21.84	46	1.37	222.92	134
MPTP	88	6.37	51	2.35	238.3	129

Tab. A.1: Reconstructed lever parameters for the scaled Angustinaripterus skull construction. See chapter 6.2 for abbreviations.

	F_B	F_J	α_J
1st tooth position	10.25	221.87	-50.26
1st to 4th tooth position	43.15	884.85	-50.17
last tooth position	31.27	206.15	-46.53
average	16.51	217.14	-49.18

Tab. A.2: Reconstructed bite and joint reaction forces and angle of joint reaction force in the scaled Angustinaripterus skull construction. Negative angle values mean anterodorsal direction of force. See chapter 6.2 for abbreviations.

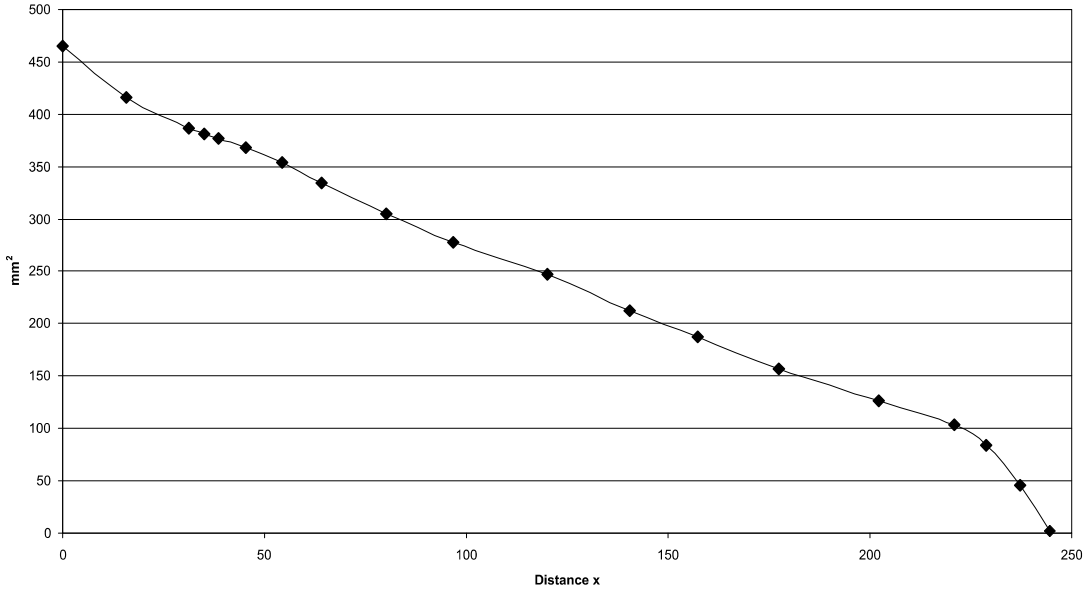

Fig. A.2: Cross-sectional area of the Angustinaripterus rostrum construction. See chapter 6.4 for legend.

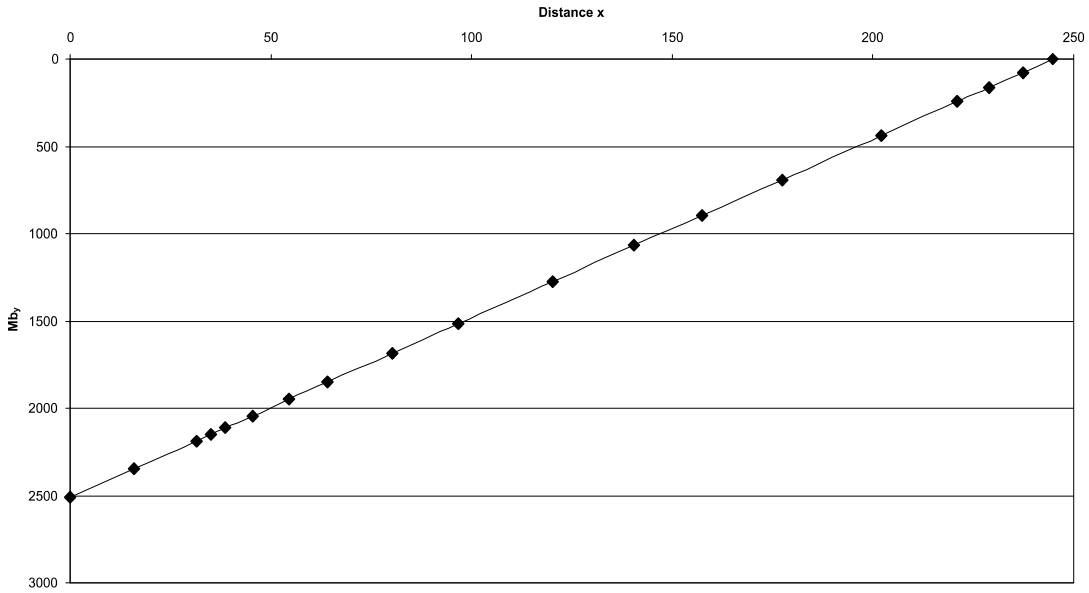

Fig. A.3: Bending moments in the Angustinaripterus rostrum construction. See chapter 6.4 for legend.

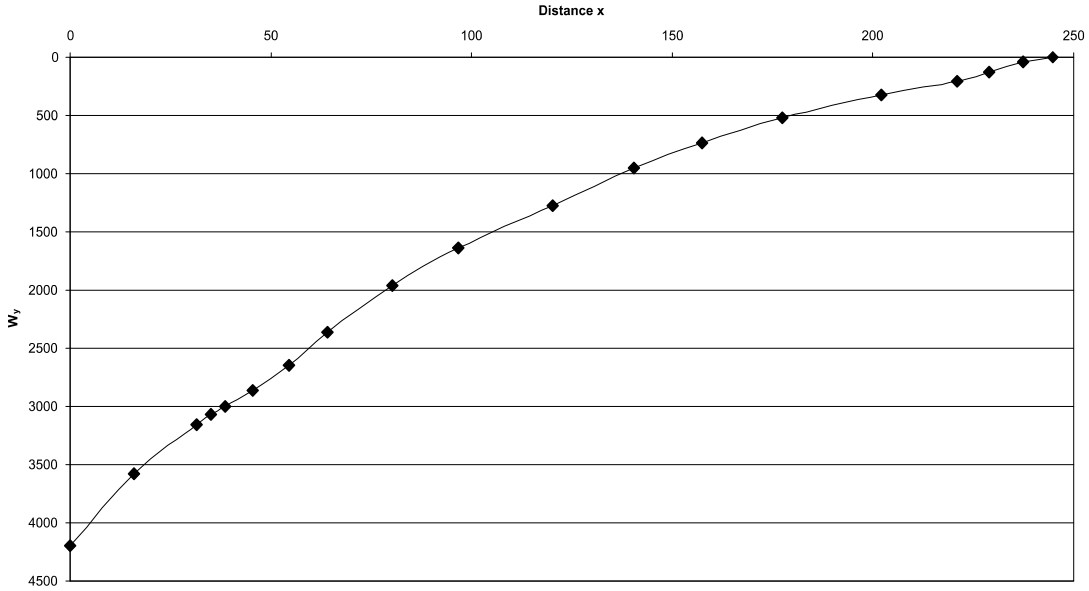

Fig. A.4: Section modulus in the Angustinaripterus rostrum construction. See chapter 6.4 for legend.

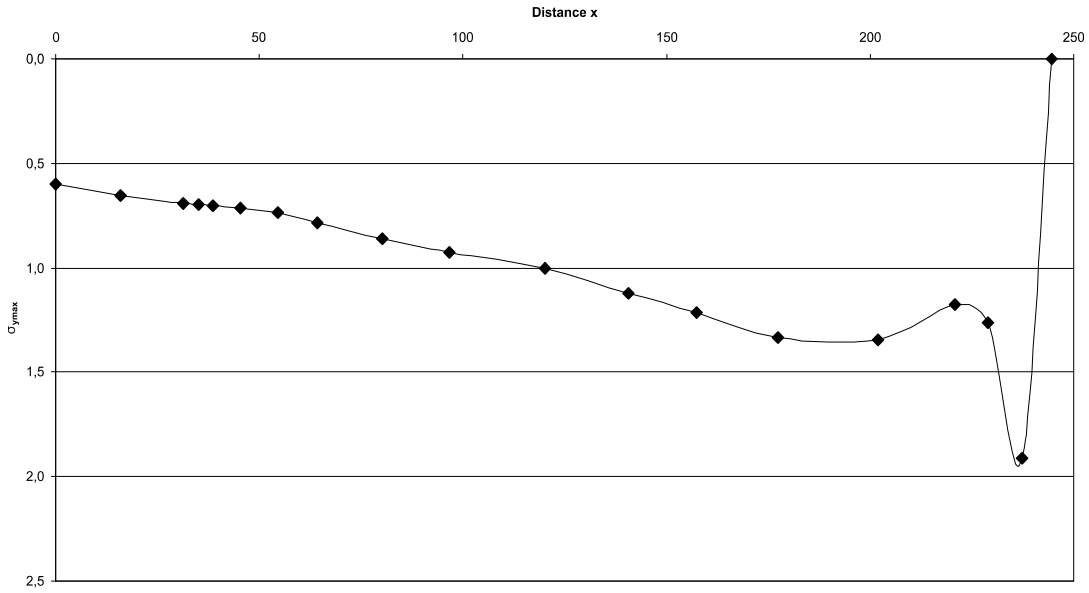

Fig. A.5: Maximum bending stress in the Angustinaripterus rostrum construction. See chapter 6.4 for legend.

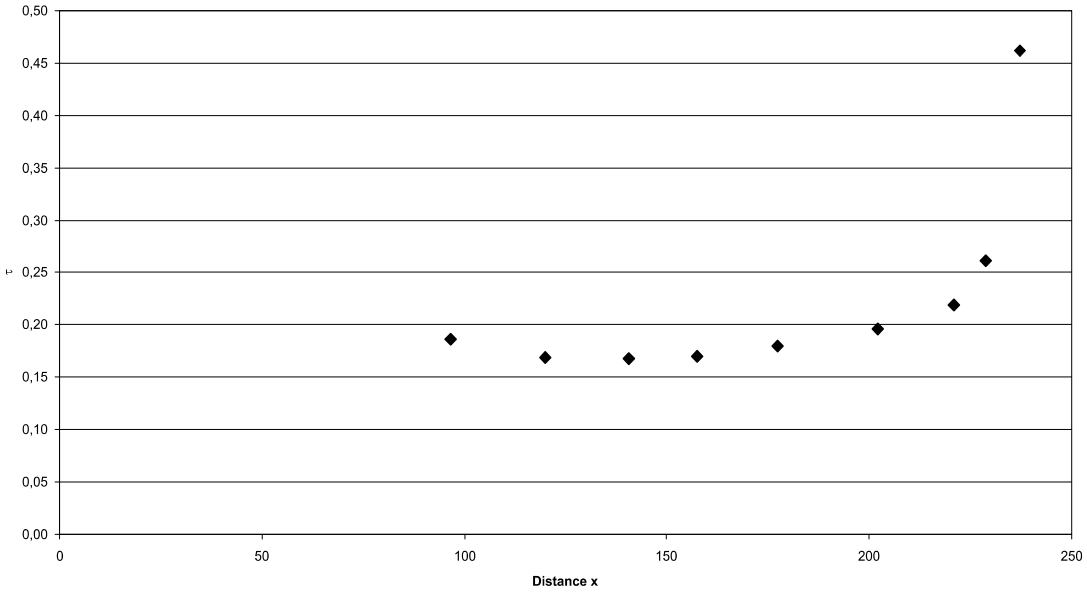

Fig. A.6: Shear stress in the Angustinaripterus rostrum construction. See chapter 6.4 for legend.

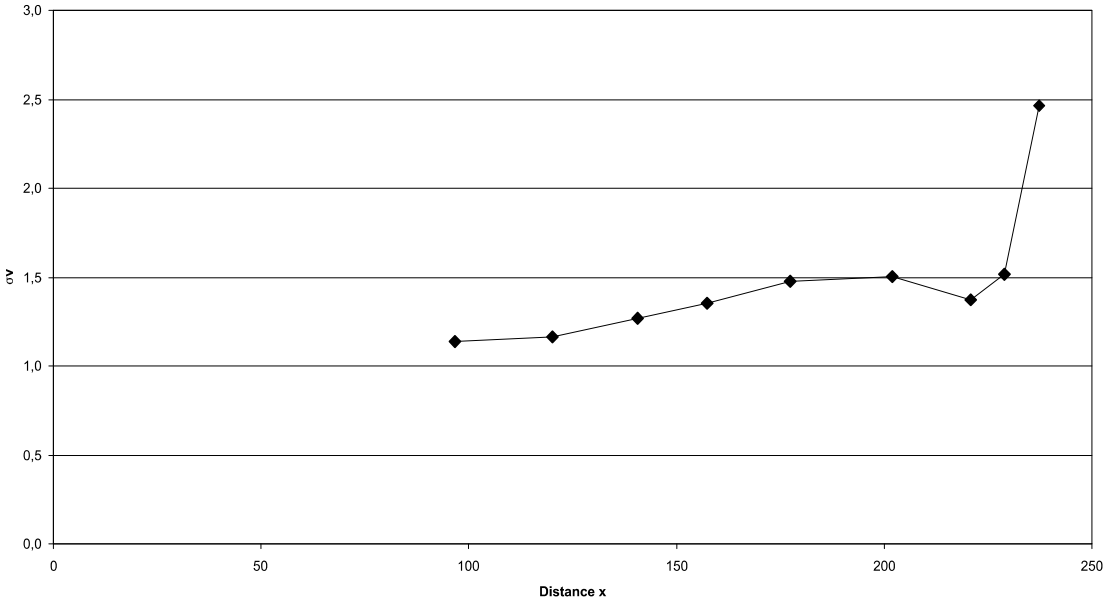

Fig. A.7: Comparison stress in the Angustinaripterus rostrum construction. See chapter 6.4 for legend.

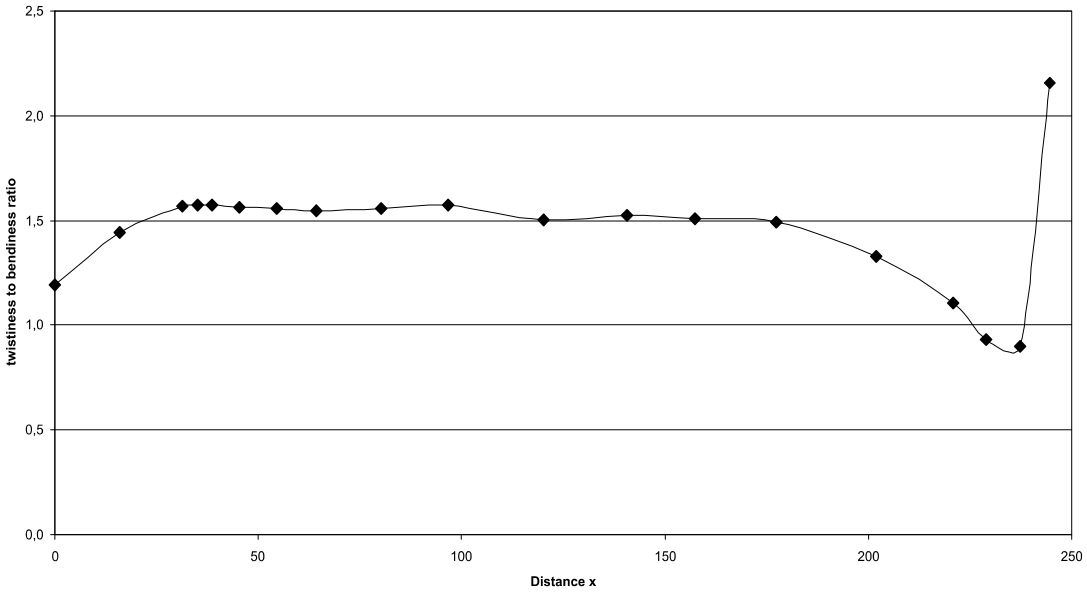

Fig. A.8: Twistiness to bendiness ratio in the Angustinaripterus rostrum construction. See chapter 6.4 for legend.

A.2. Anurognathus skull construction (see also chapter 7.2)

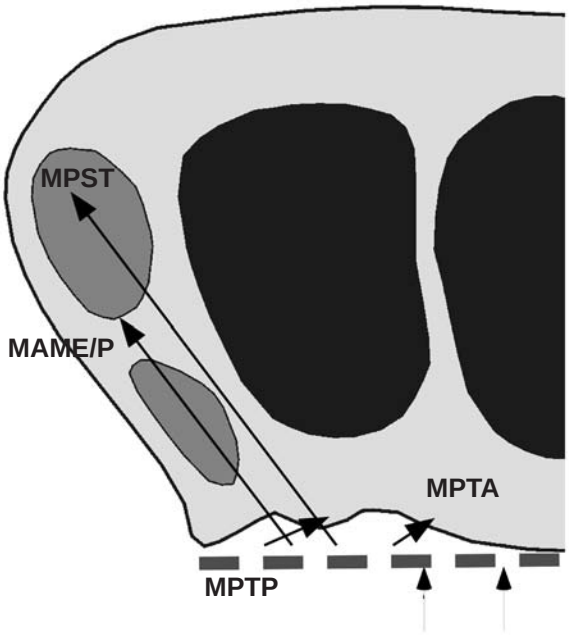

Fig. A.9: Reconstruction of the principal pulling direction of the main adductor muscles in the skull of *Anurognathus*. See chapter 6 for abbreviations.

Muscles	F_1	l_1	α_1	F_2	l_2	α_1
MAME/P	36	10.86	53	3.44	113.69	127
MPST	92	16.88	53	14.42	107.68	127
MPTA	14	24.22	33	3.38	100.34	147
MPTP	88	7.48	24	5.62	117.07	156

Tab. A.3: Reconstructed lever parameters for the scaled Anurognathus skull construction. See chapter 6.2 for abbreviations.

	F_B	F_J	α_J
1st tooth position	16.10	213.07	-37.44
1st to 4th tooth position	72.99	847.11	-36.98
last tooth position	70.50	185.11	-29.02
average	32.25	204.20	-33.64

Tab. A.4: Reconstructed bite and joint reaction forces and angle of joint reaction force in the scaled Anurognathus skull construction. Negative angle values mean anterodorsal direction of force. See chapter 6.2 for abbreviations.

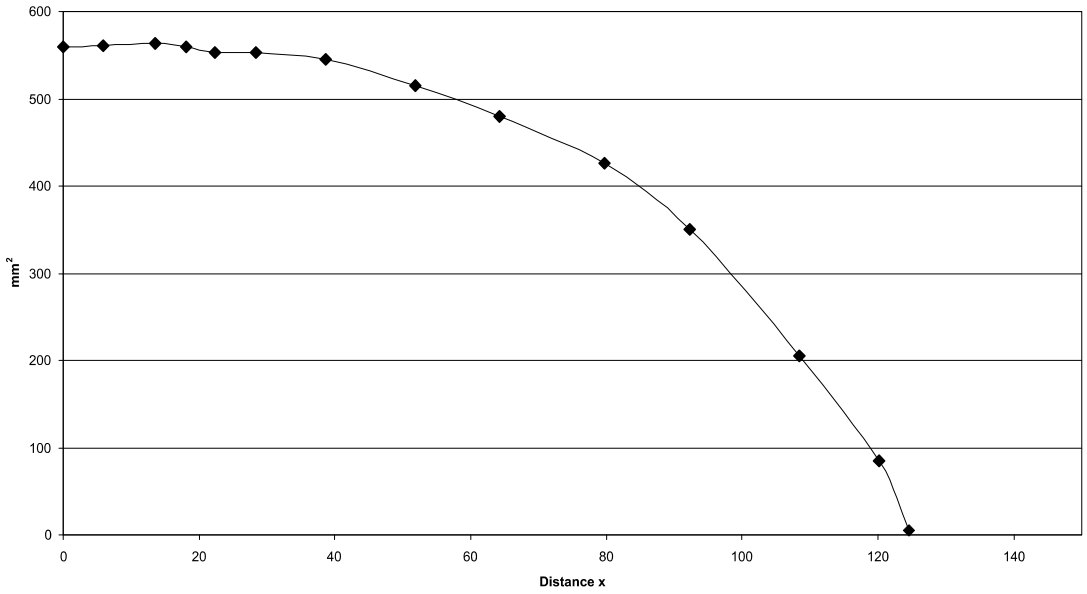

Fig. A.10: Cross-sectional area of the Anurognathus rostrum construction. See chapter 6.4 for legend.

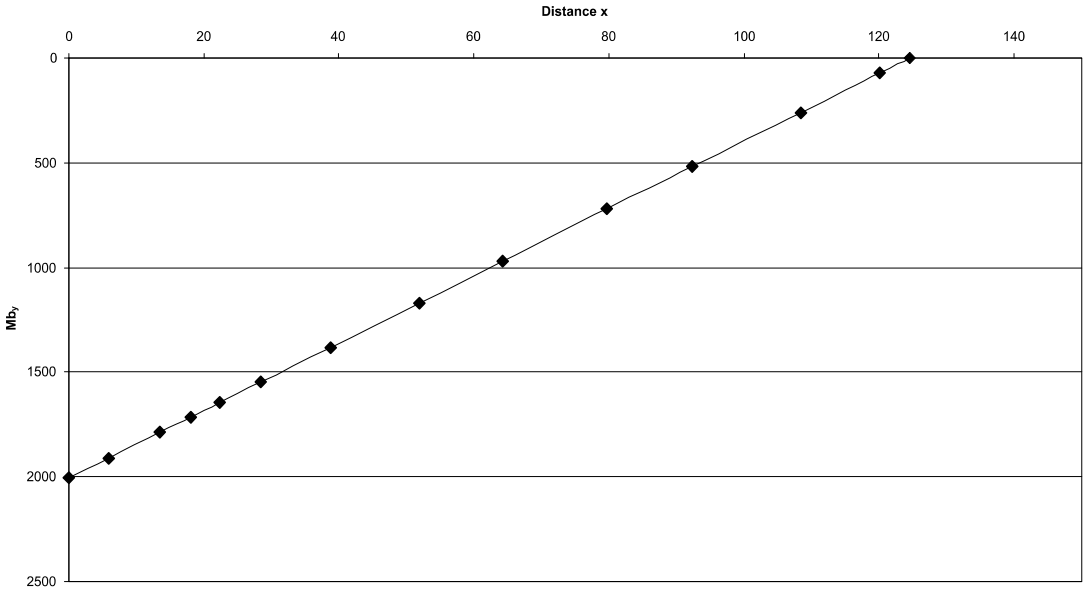

Fig. A.11: Bending moments in the Anurognathus rostrum construction. See chapter 6.4 for legend.

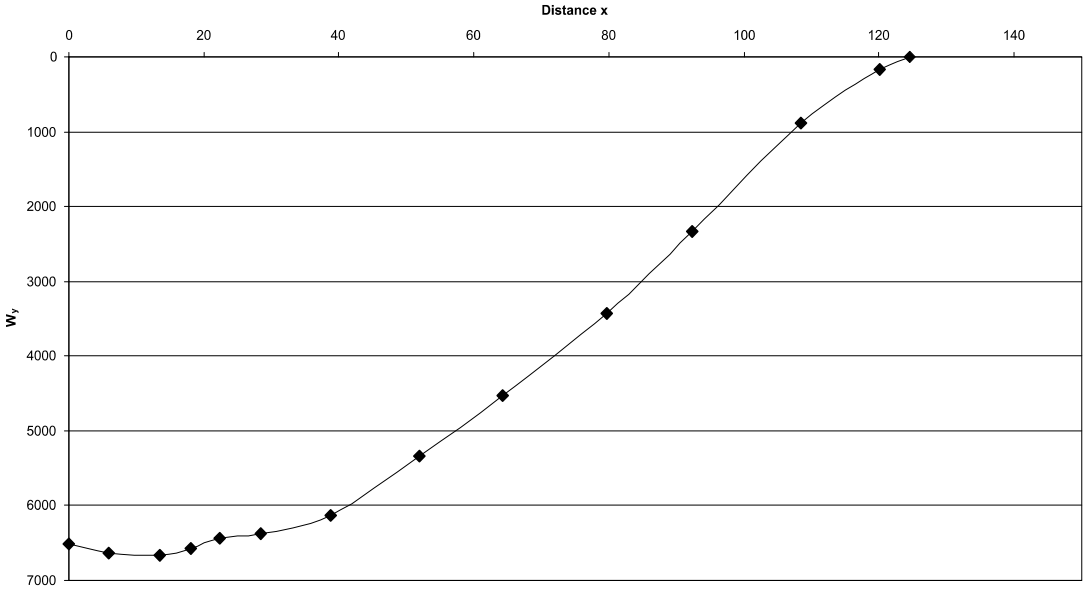

Fig. A.12: Section modulus in the Anurognathus rostrum construction. See chapter 6.4 for legend.

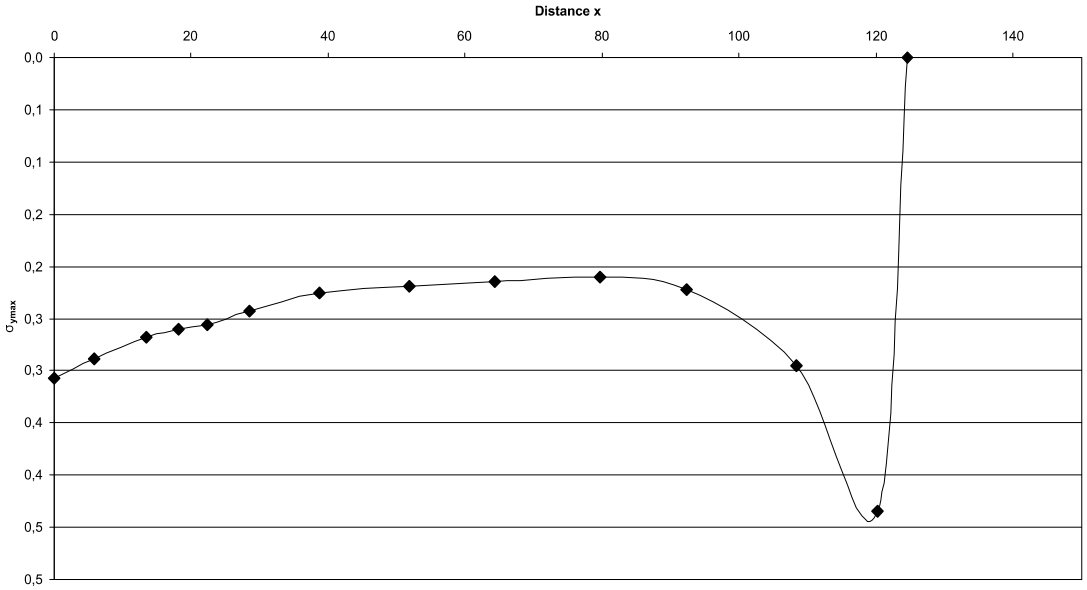

Fig. A.13: Maximum bending stress in the Anurognathus rostrum construction. See chapter 6.4 for legend.

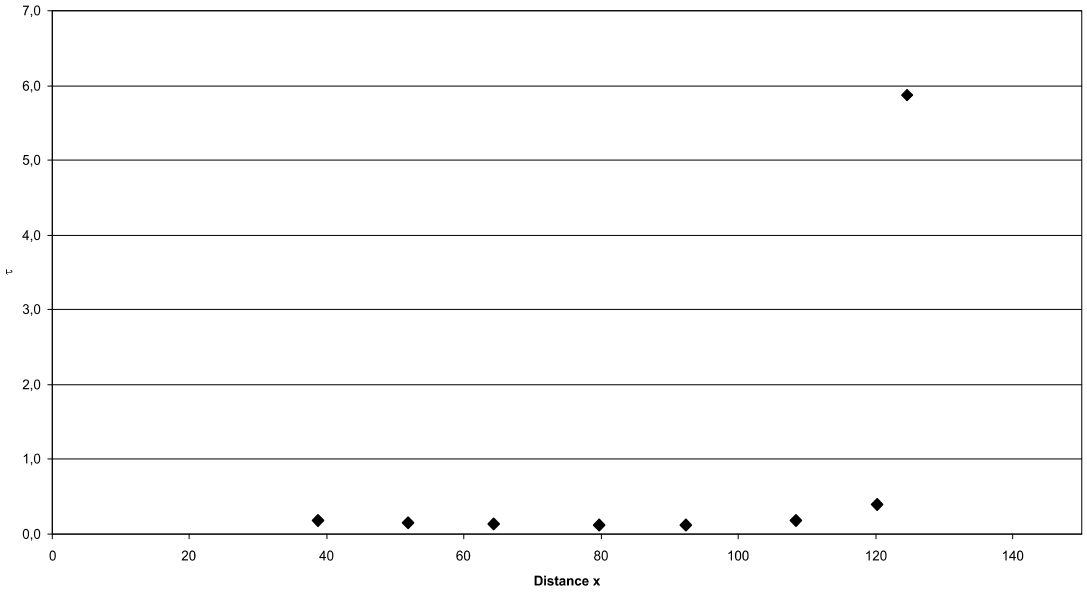

Fig. A.14: Shear stress in the Anurognathus rostrum construction. See chapter 6.4 for legend.

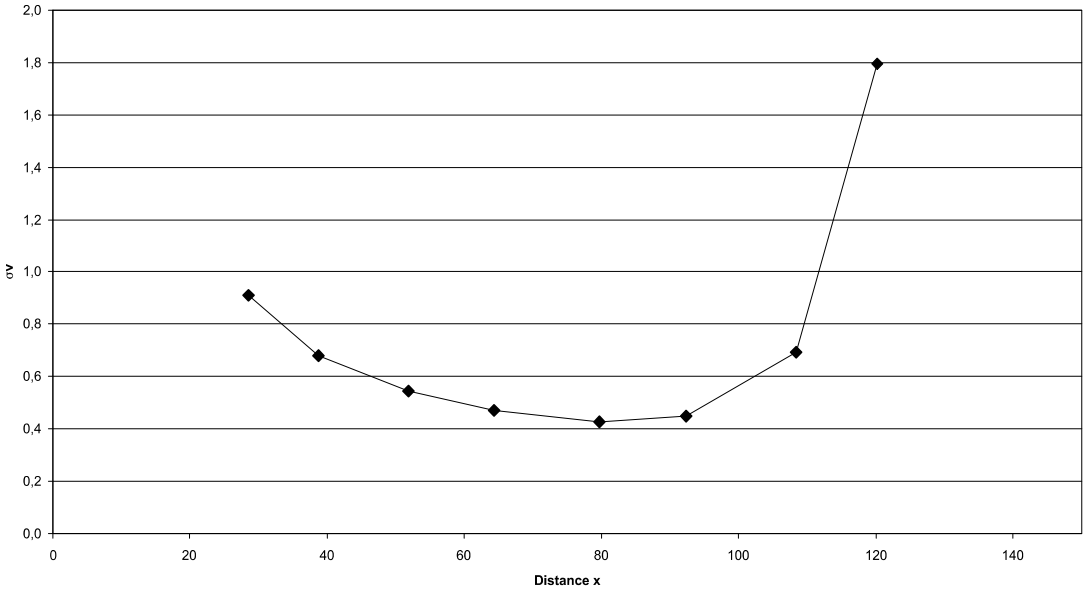

Fig. A.15: Comparison stress in the Anurognathus rostrum construction. See chapter 6.4 for legend.

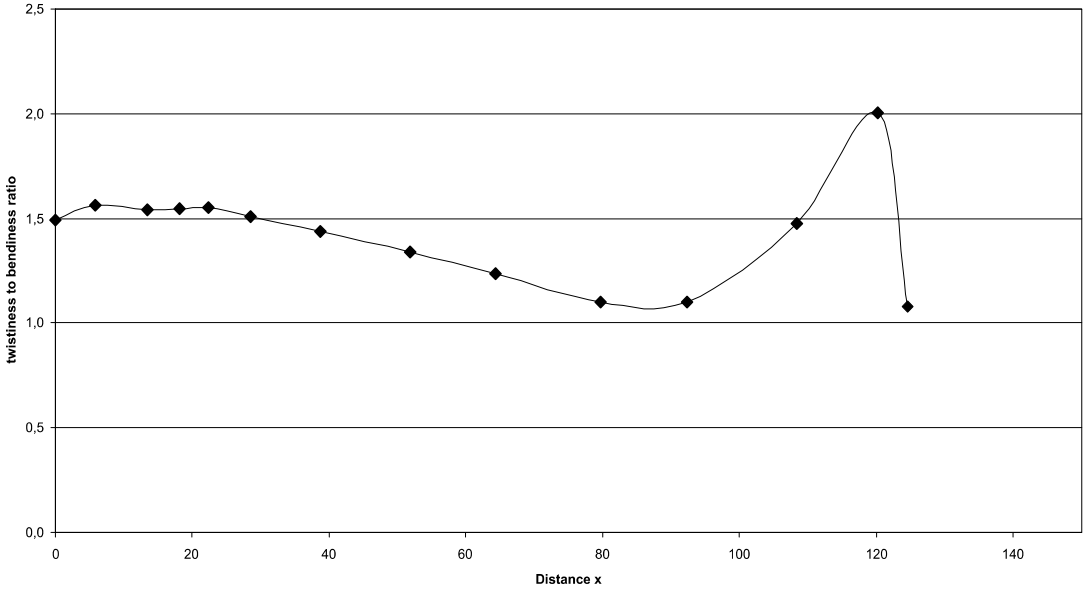

Fig. A.16: Twistiness to bendiness ratio in the Anurognathus rostrum construction. See chapter 6.4 for legend.

A.3. Austriadacytlus skull construction (see also chapter 7.3)

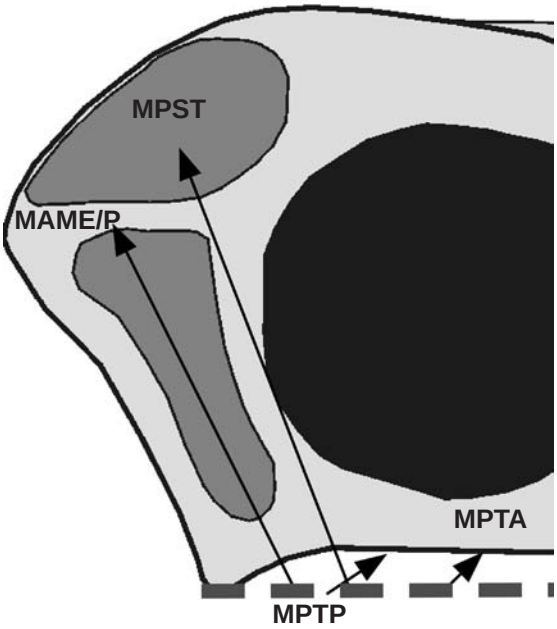

Fig. A.17: Reconstruction of the principal pulling direction of the main adductor muscles in the skull of *Austriadacytlus*. See chapter 6 for abbreviations.

Muscles	F_1	l_1	α_1	F_2	l_2	α_1
MAME/P	36	9.77	63	1.88	187.52	117
MPST	92	16.45	69	8.37	180.84	111
MPTA	14	27.25	45	9.90	170.04	135
MPTP	88	13.62	34	6.53	183.66	146

Tab. A.5: Reconstructed lever parameters for the scaled Austriadacytlus skull construction. See chapter 6.2 for abbreviations.

	F_B	F_J	α_J
1st tooth position	13.90	209.00	-50.99
1st to 4th tooth position	56.66	839.12	-50.95
last tooth position	50.78	182.81	-45.69
average	24.53	201.97	-49.01

Tab. A.6: Reconstructed bite and joint reaction forces and angle of joint reaction force in the scaled Austriadacytlus skull construction. Negative angle values mean anterodorsal direction of force. See chapter 6.2 for abbreviations.

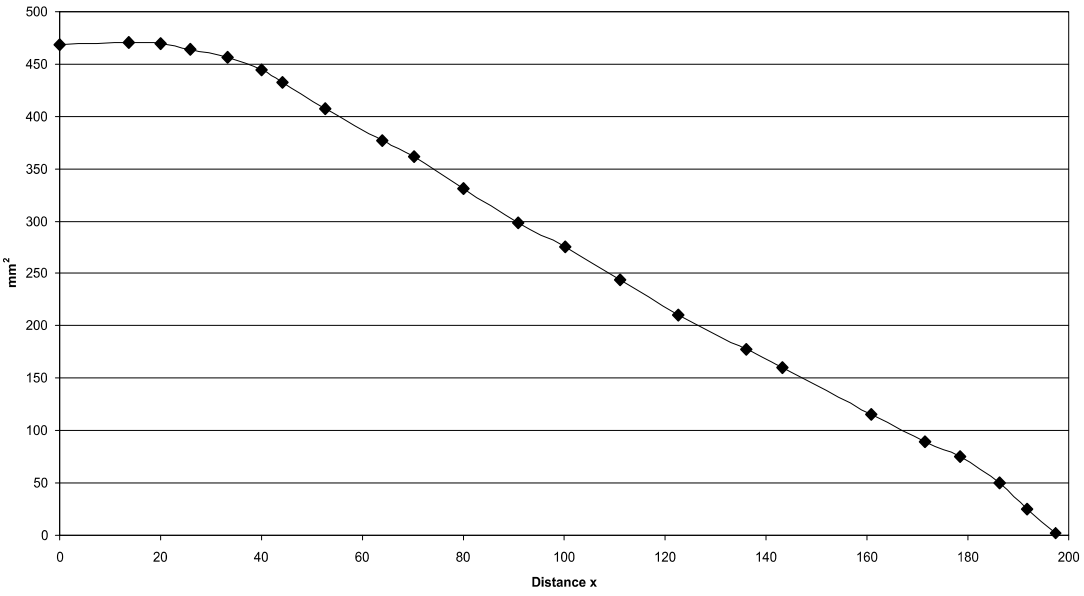

Fig. A.18: Cross-sectional area of the Austriadacytlus rostrum construction. See chapter 6.4 for legend.

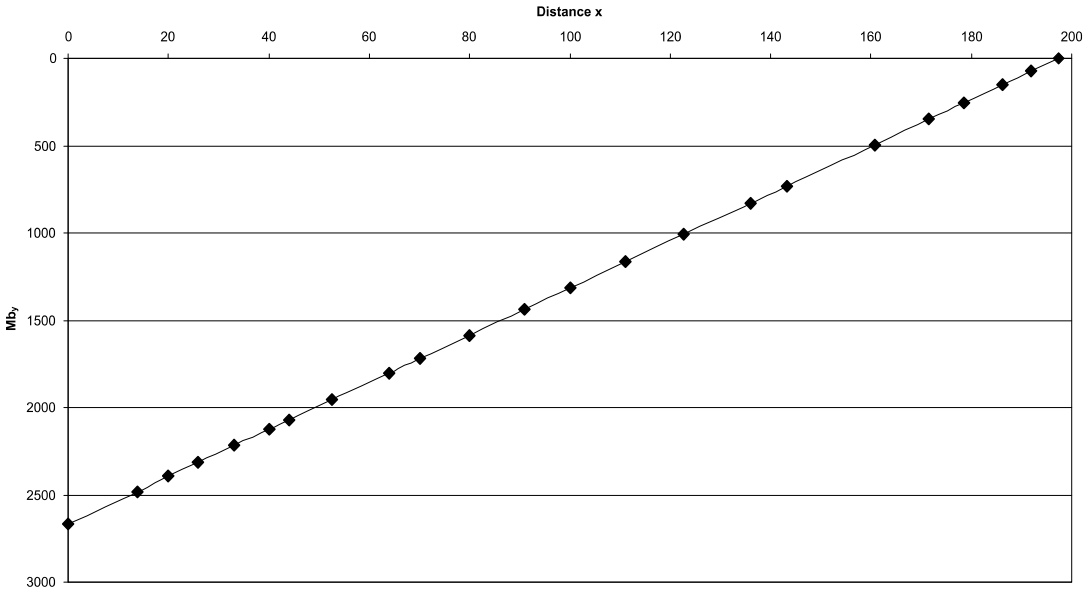

Fig. A.19: Bending moments in the Austriadacytlus rostrum construction. See chapter 6.4 for legend.

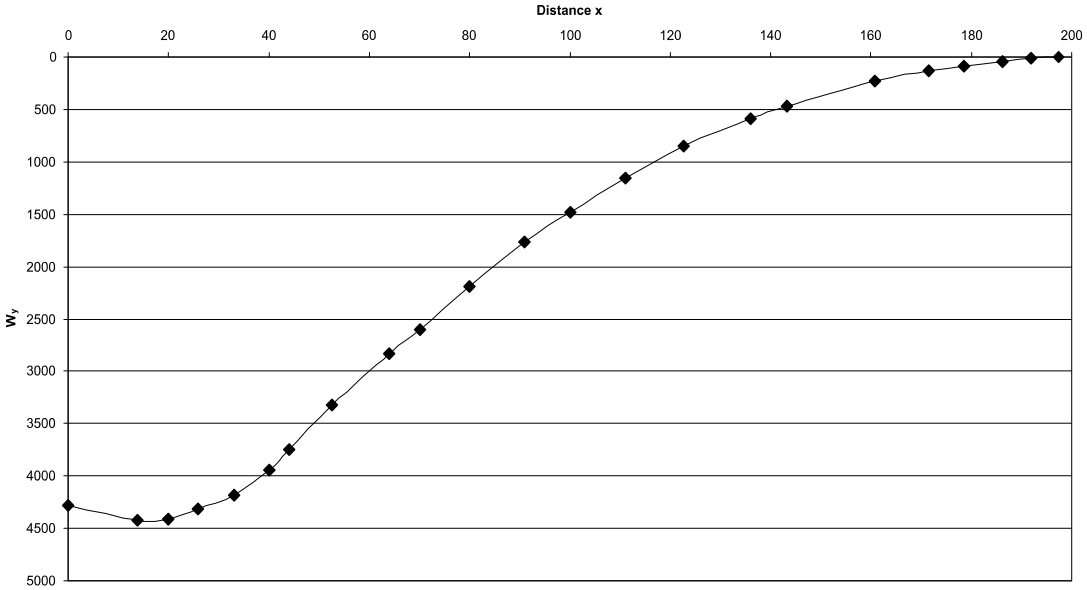

Fig. A.20: Section modulus in the Austriadacytlus rostrum construction. See chapter 6.4 for legend.

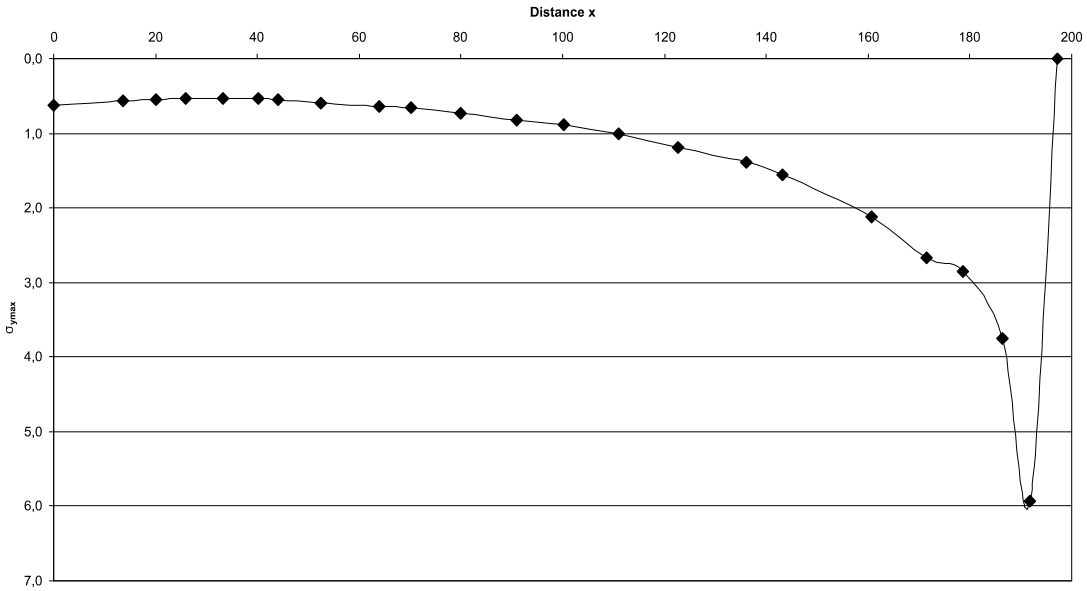

Fig. A.21: Maximum bending stress in the Austriadacytlus rostrum construction. See chapter 6.4 for legend.

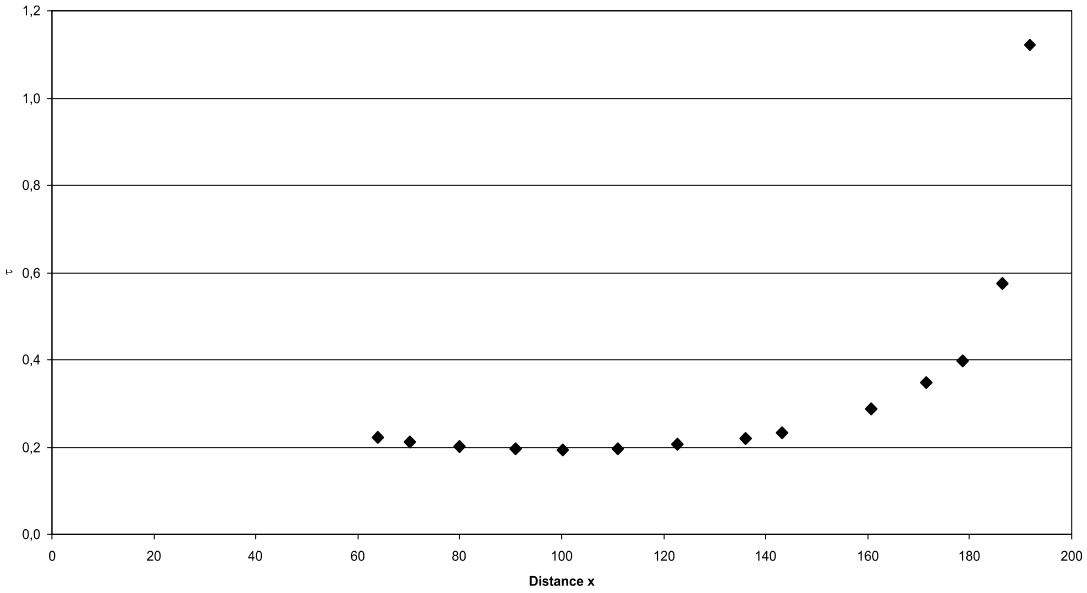

Fig. A.22: Shear stress in the Austriadacytlus rostrum construction. See chapter 6.4 for legend.

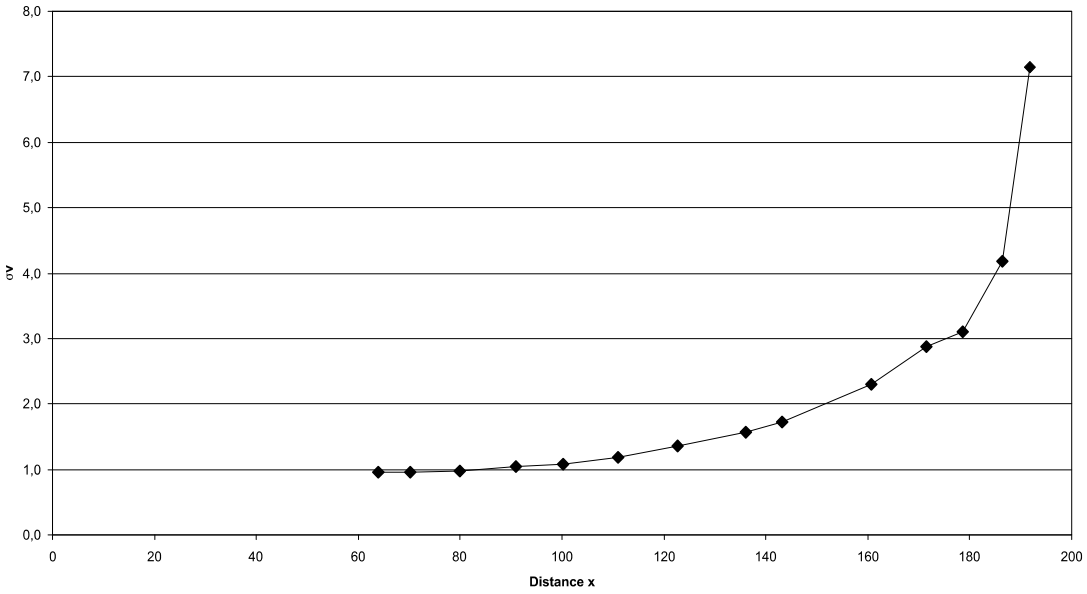

Fig. A.23: Comparison stress in the Austriadacytlus rostrum construction. See chapter 6.4 for legend.

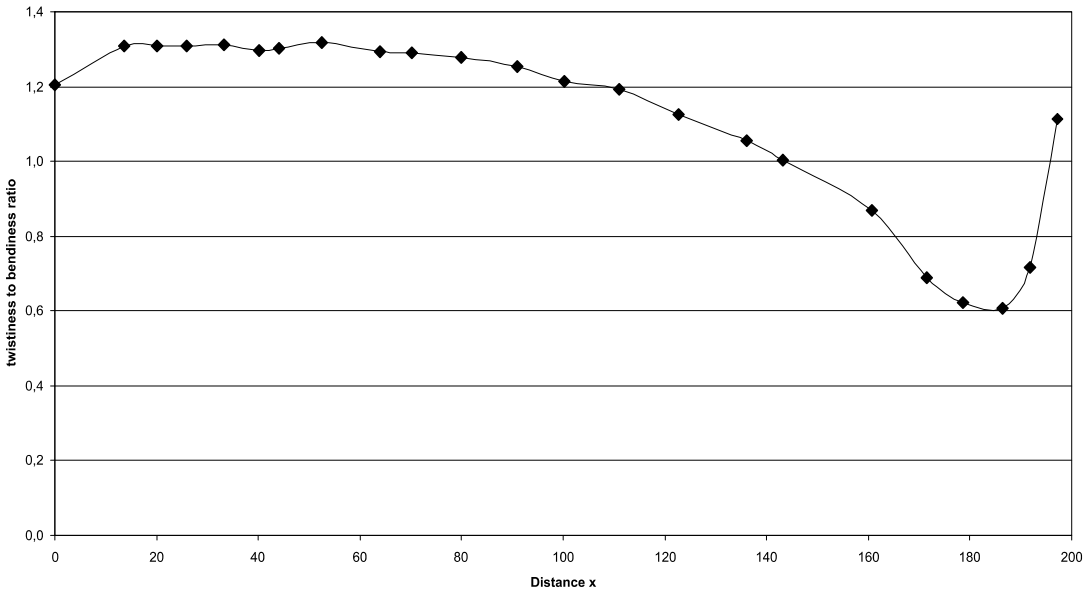

Fig. A.24: Twistiness to bendiness ratio in the Austriadacytlus rostrum construction. See chapter 6.4 for legend.

A.4. Batrachognathus skull construction (see also chapter 7.4)

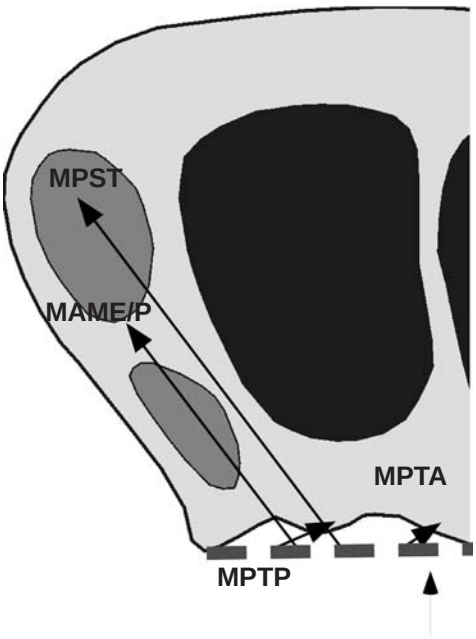

Fig. A.25: Reconstruction of the principal pulling direction of the main adductor muscles in the skull of *Batrachognathus*. See chapter 6 for abbreviations.

Muscles	F_1	l_1	α_1	F_2	l_2	α_1
MAME/P	36	10.86	53	3.44	113.69	127
MPST	92	16.88	53	14.42	107.68	127
MPTA	14	24.22	33	3.38	100.34	147
MPTP	88	7.48	24	5.62	117.07	156

Tab. A.7: Reconstructed lever parameters for the scaled Batrachognathus skull construction. See chapter 6.2 for abbreviations.

	F_B	F_J	α_J
1st tooth position	16.10	213.07	-37.44
1st to 4th tooth position	72.88	847.18	-36.99
last tooth position	70.25	185.21	-24.02
average	32.21	204.22	-33.65

Tab. A.8: Reconstructed bite and joint reaction forces and angle of joint reaction force in the scaled Batrachognathus skull construction. Negative angle values mean anterodorsal direction of force. See chapter 6.2 for abbreviations.

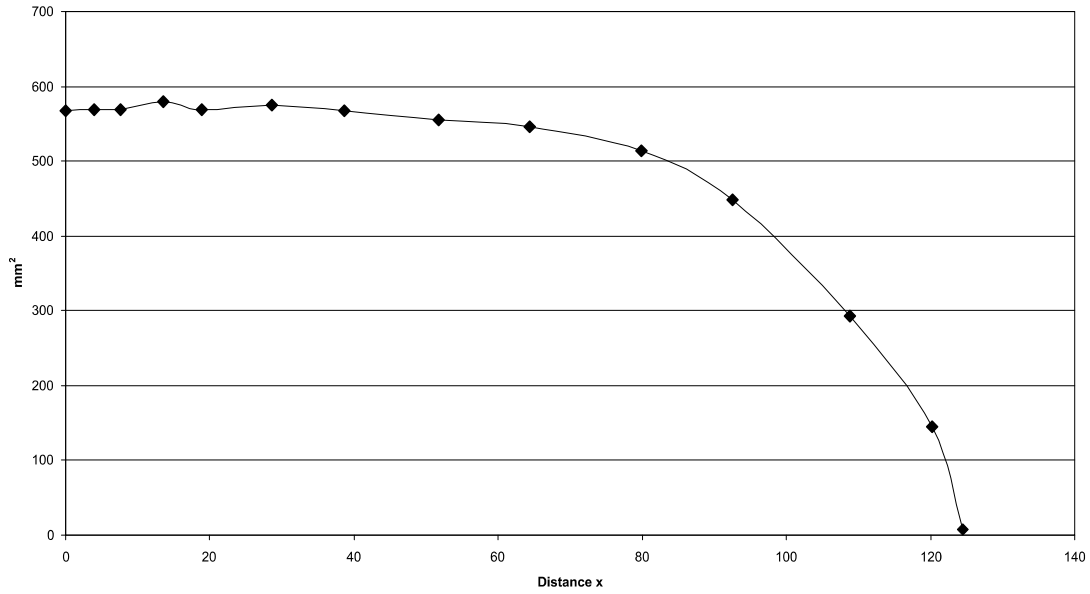

Fig. A.26: Cross-sectional area of the Batrachognathus rostrum construction. See chapter 6.4 for legend.

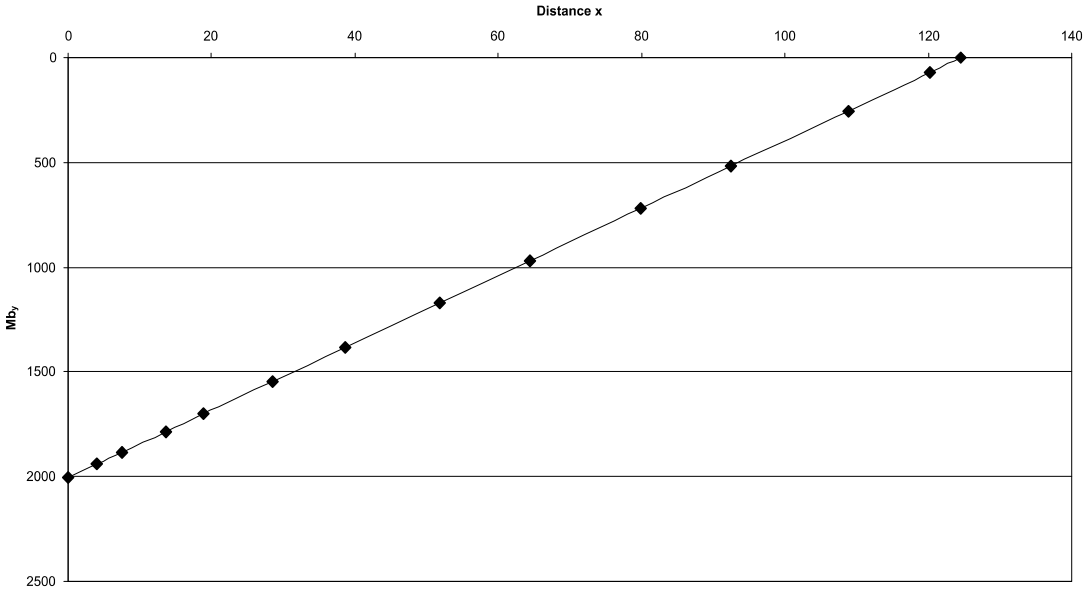

Fig. A.27: Bending moments in the Batrachognathus rostrum construction. See chapter 6.4 for legend.

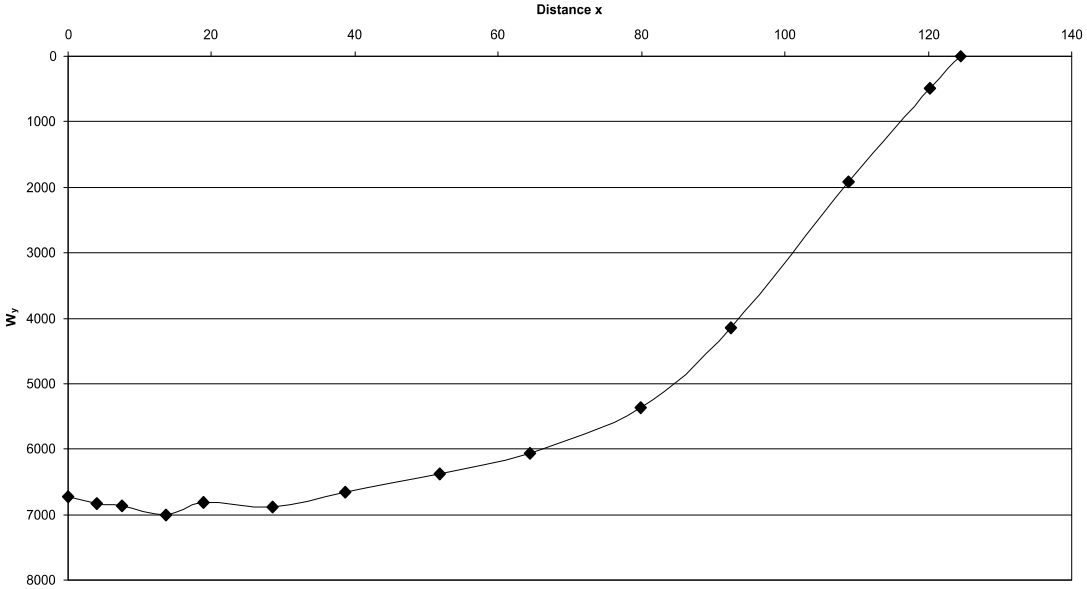

Fig. A.28: Section modulus in the Batrachognathus rostrum construction. See chapter 6.4 for legend.

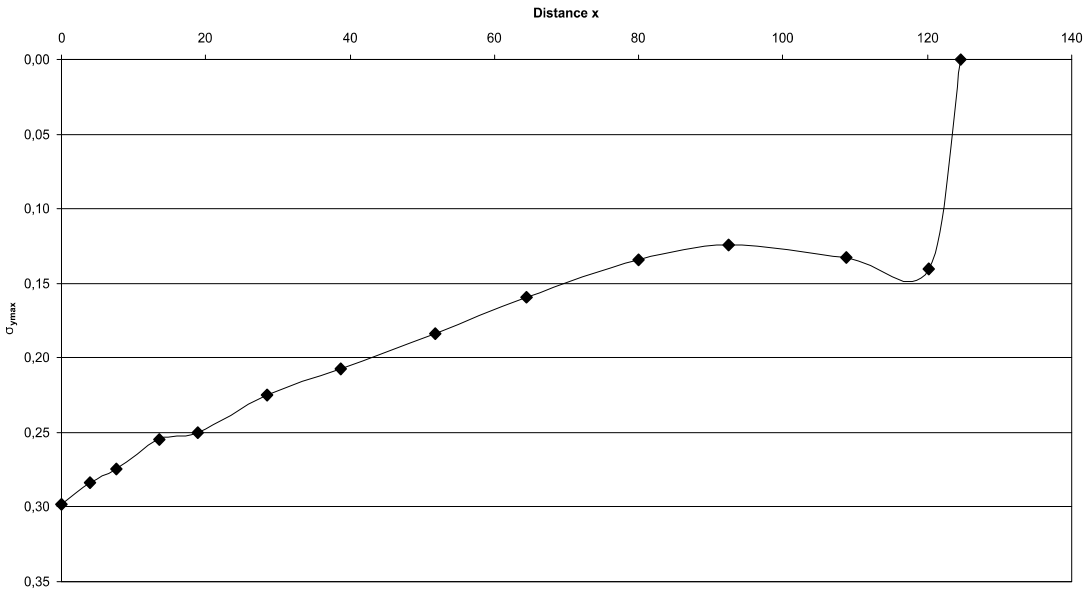

Fig. A.29: Maximum bending stress in the Batrachognathus rostrum construction. See chapter 6.4 for legend.

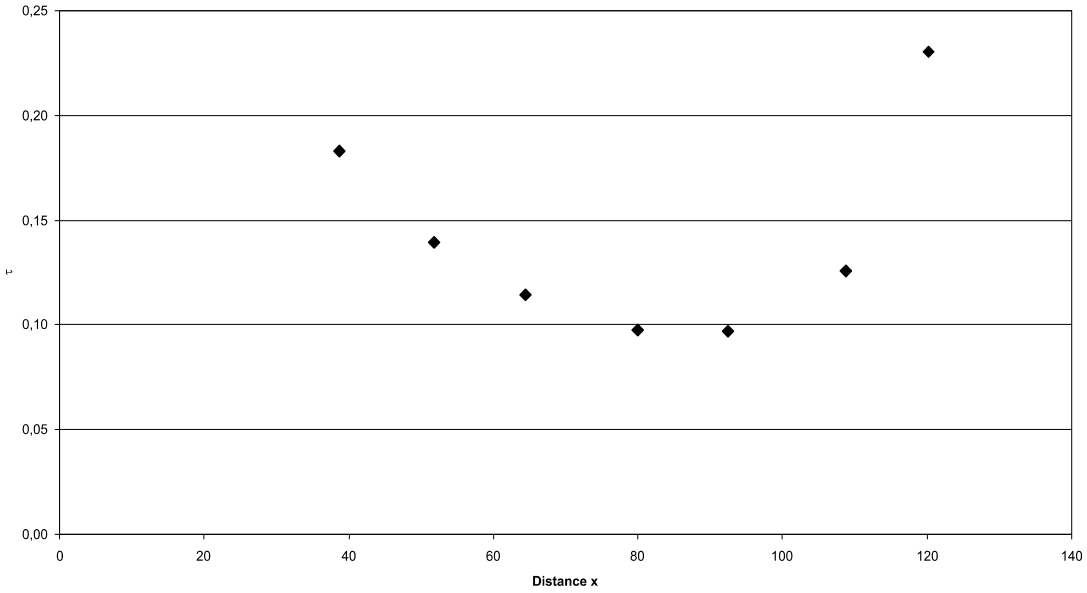

Fig. A.30: Shear stress in the Batrachognathus rostrum construction. See chapter 6.4 for legend.

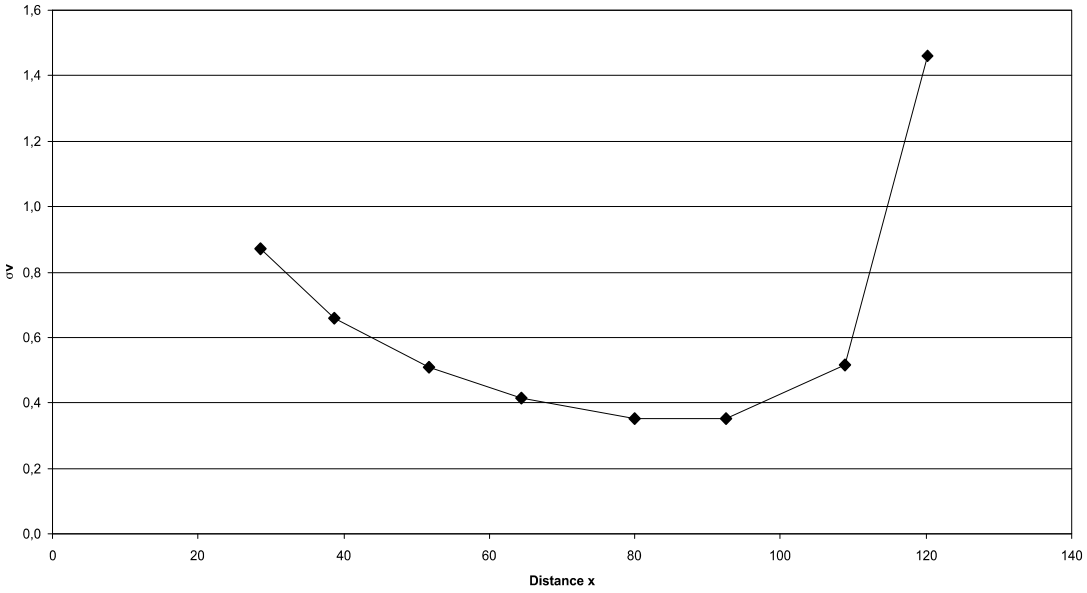

Fig. A.31: Comparison stress in the Batrachognathus rostrum construction. See chapter 6.4 for legend.

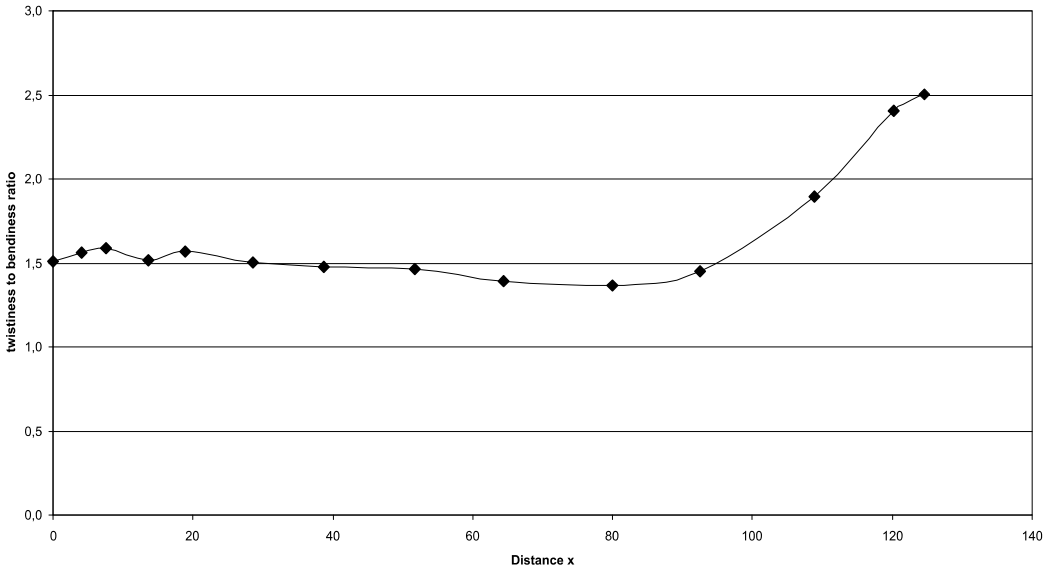

Fig. A.32: Twistiness to bendiness ratio in the Batrachognathus rostrum construction. See chapter 6.4 for legend.

A.5. Cacibupteryx skull construction (see also chapter 7.5)

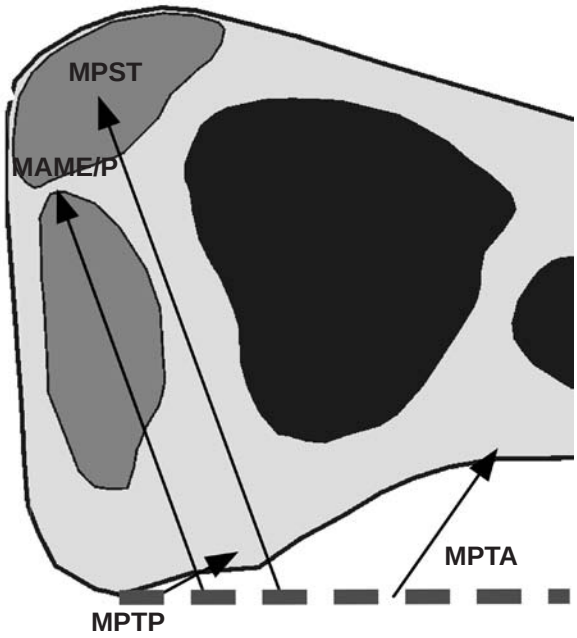

Fig. A.33: Reconstruction of the principal pulling direction of the main adductor muscles in the skull of *Cacibupteryx*. See chapter 6 for abbreviations.

Muscles	F_1	l_1	α_1	F_2	l_2	α_1
MAME/P	36	11.47	70	2.03	203.61	110
MPST	92	21.04	70	9.98	194.04	110
MPTA	14	34.18	55	2.65	180.89	125
MPTP	88	7.28	30	3.08	207.8	150

Tab. A.9: Reconstructed lever parameters for the scaled Cacibupteryx skull construction. See chapter 6.2 for abbreviations.

	F_B	F_J	α_J
1st tooth position	13.57	206.62	-51.71
1st to 4th tooth position	59.70	822.23	-51.48
last tooth position	50.52	179.09	-44.37
average	23.75	198.85	-49.81

Tab. A.10: Reconstructed bite and joint reaction forces and angle of joint reaction force in the scaled Cacibupteryx skull construction. Negative angle values mean anterodorsal direction of force. See chapter 6.2 for abbreviations.

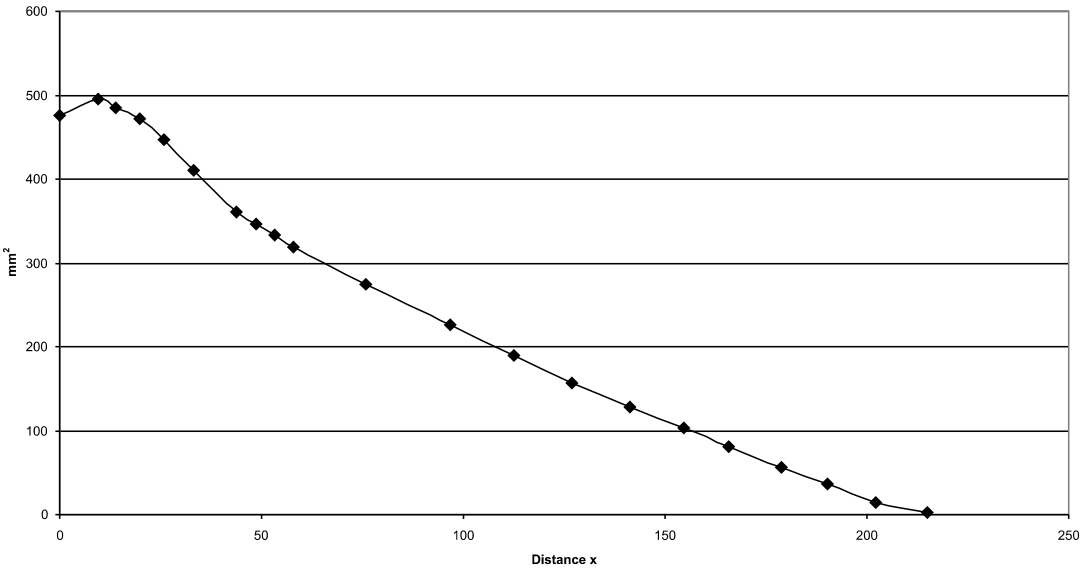

Fig A.34: Cross-sectional area of the Cacibupteryx rostrum construction. See chapter 6.4 for legend.

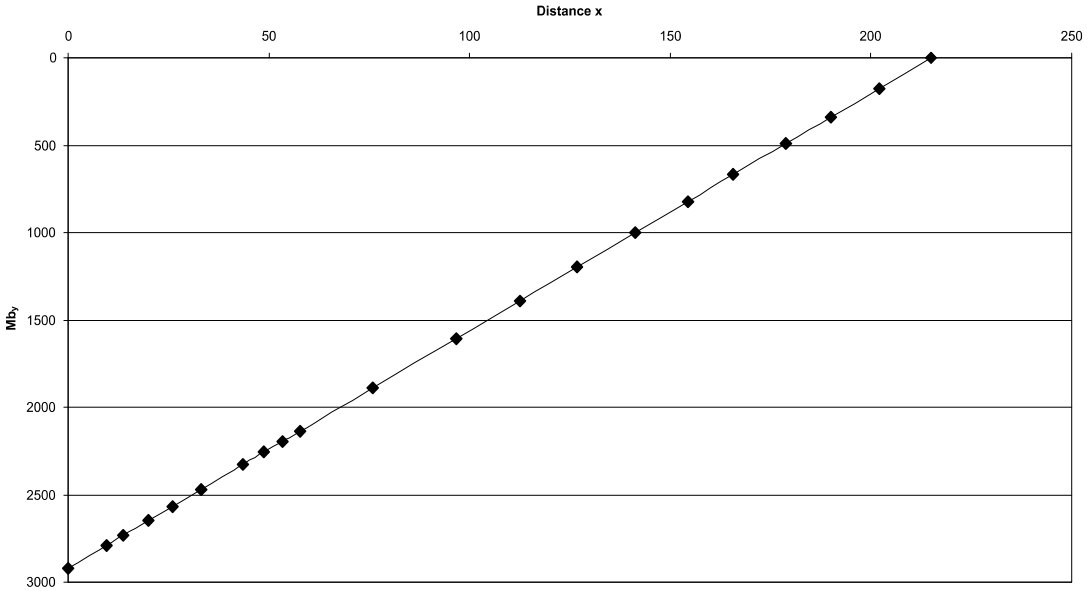

Fig A.35: Bending moments in the Cacibupteryx rostrum construction. See chapter 6.4 for legend.

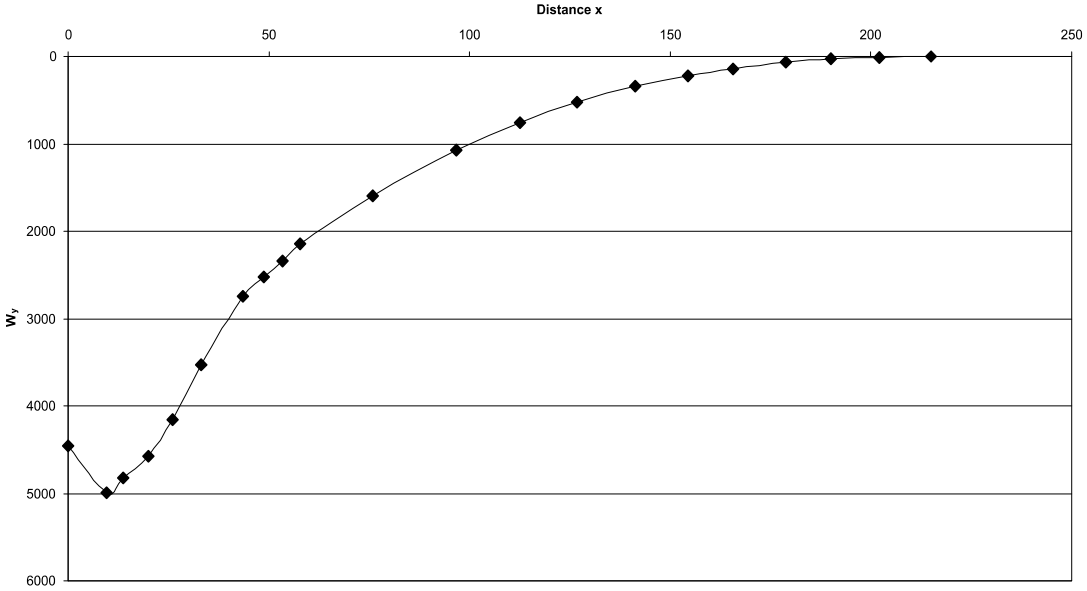

Fig A.36: Section modulus in the Cacibupteryx rostrum construction. See chapter 6.4 for legend.

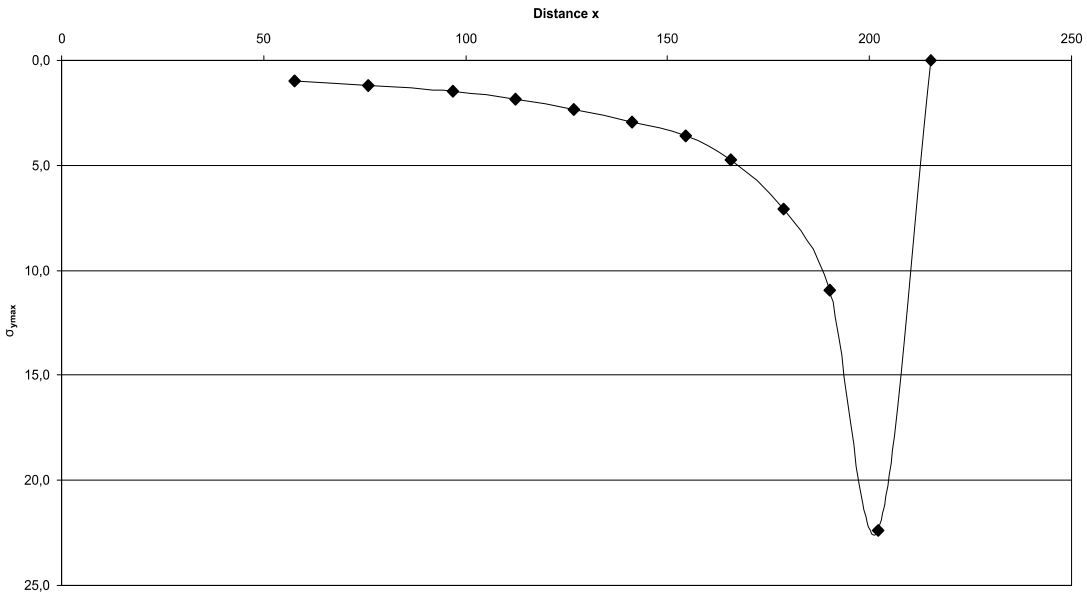

Fig A.37: Maximum bending stress in the Cacibupteryx rostrum construction. See chapter 6.4 for legend.

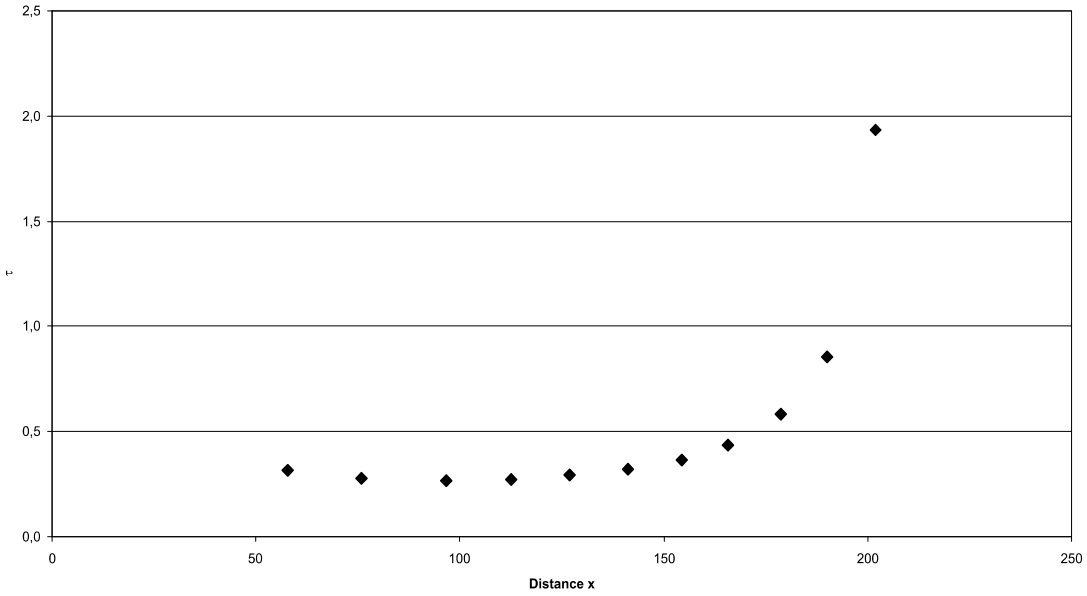

Fig. A.38: Shear stress in the Cacibupteryx rostrum construction. See chapter 6.4 for legend.

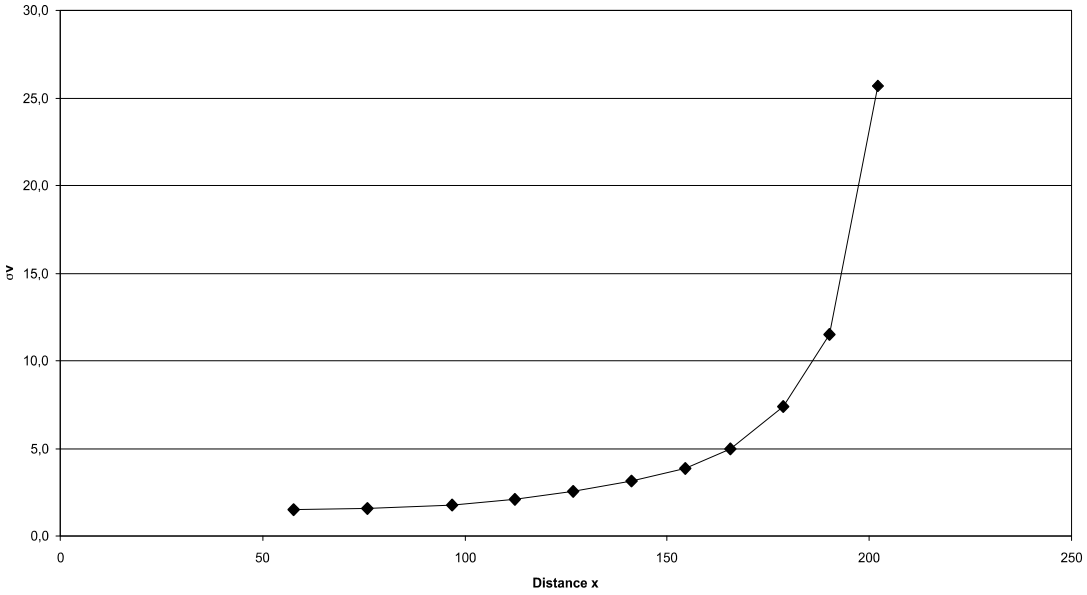

Fig. A.39: Comparison stress in the Cacibupteryx rostrum construction. See chapter 6.4 for legend.

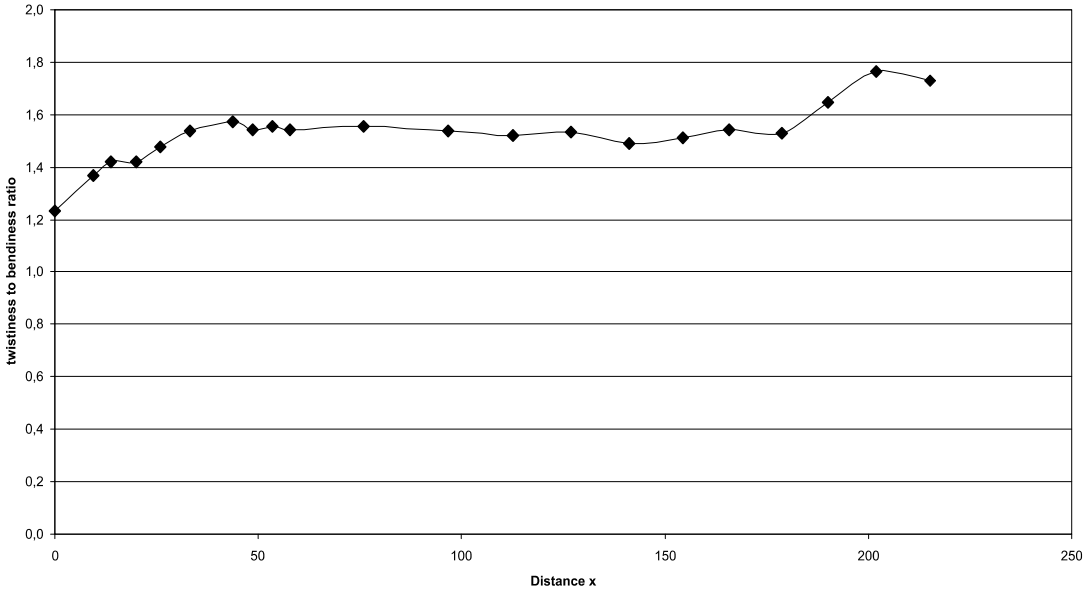

Fig. A.40: Twistiness to bendiness ratio in the Cacibupteryx rostrum construction. See chapter 6.4 for legend.

A.6. Campylognathoides skull construction (see also chapter 7.6)

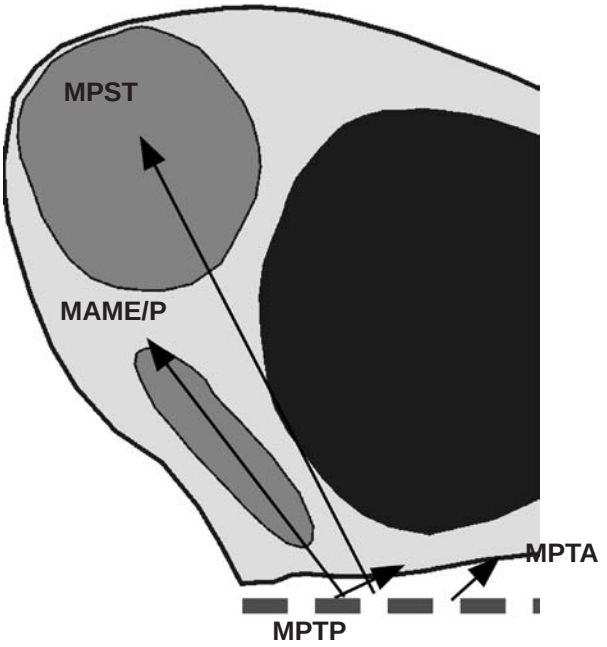

Fig A.41: Reconstruction of the principal pulling direction of the main adductor muscles in the skull of *Campylognathoides*. See chapter 6 for abbreviations.

Muscles	F_1	l_1	α_1	F_2	l_2	α_1
MAME/P	36	10.8	53	2.72	142.84	127
MPST	92	15.3	63	10.17	138.34	117
MPTA	14	24.36	25	2.41	141.43	138
MPTP	88	12.21	25	8.31	129.28	155

Tab. A.11: Reconstructed lever parameters for the scaled Campylognathoides skull construction. See chapter 6.2 for abbreviations.

	F_B	F_J	α_J
1st tooth position	14.63	209.62	-42.89
1st to 4th tooth position	63.48	835.11	-42.63
last tooth position	57.20	183.32	-33.09
average	30.00	199.76	-39.52

Tab. A.12: Reconstructed bite and joint reaction forces and angle of joint reaction force in the scaled Campylognathoides skull construction. Negative angle values mean anterodorsal direction of force. See chapter 6.2 for abbreviations.

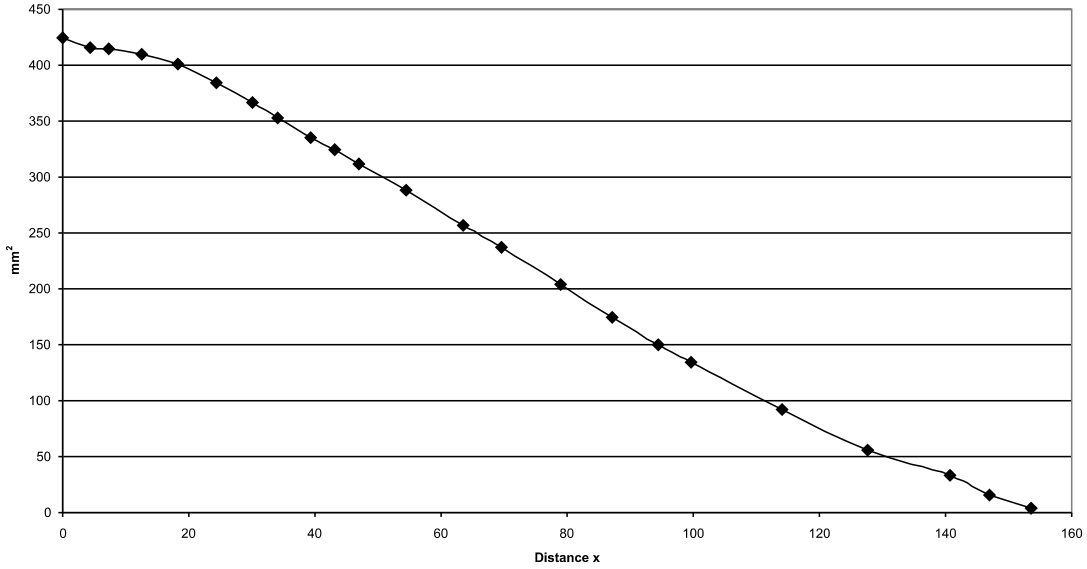

Fig A.42: Cross-sectional area of the Campylognathoides rostrum construction. See chapter 6.4 for legend.

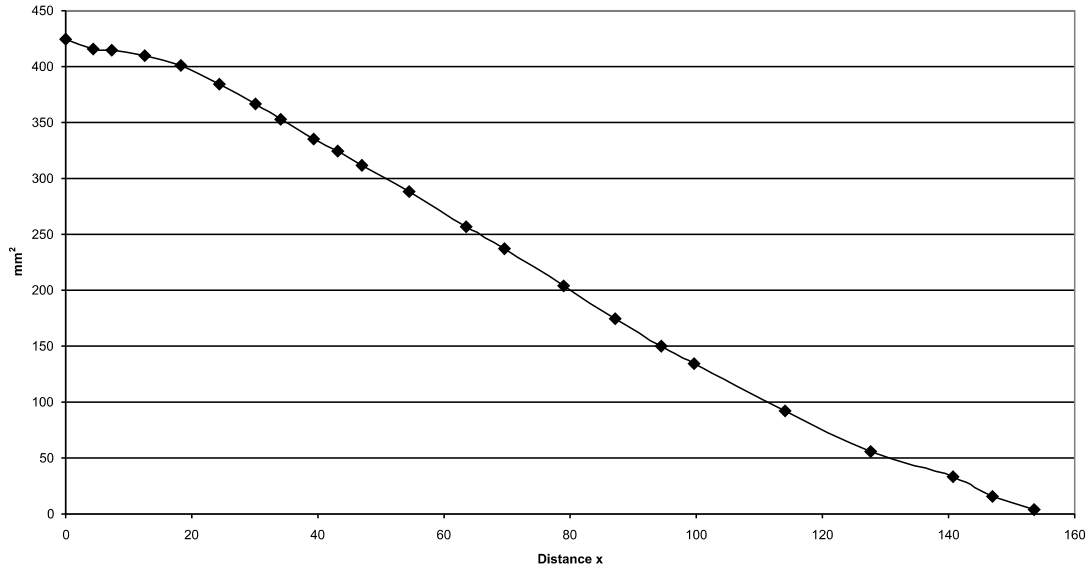

Fig A.43: Bending moments in the Campylognathoides rostrum construction. See chapter 6.4 for legend.

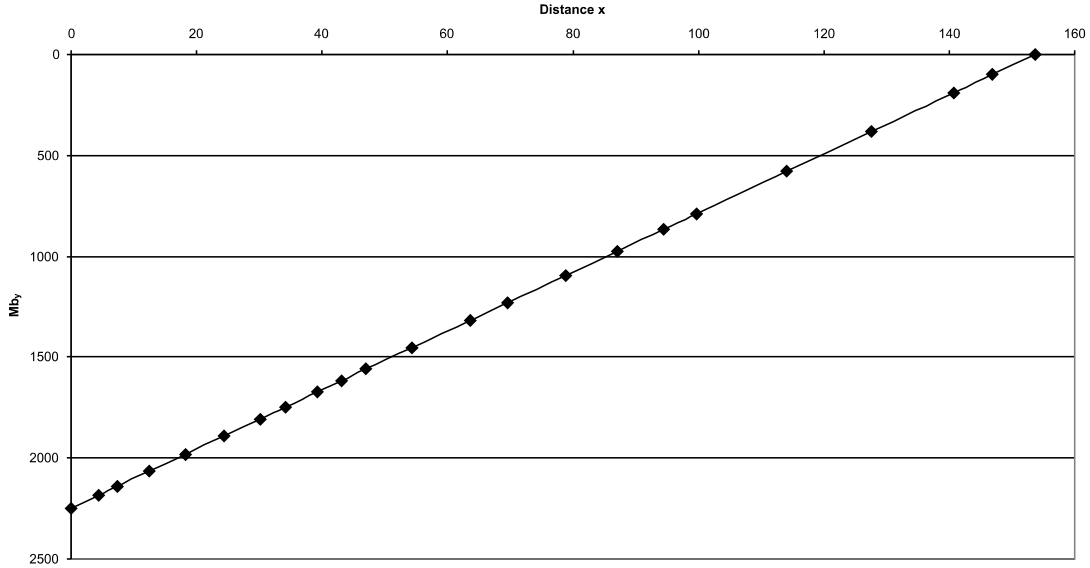

Fig A.44: Section modulus in the Campylognathoides rostrum construction. See chapter 6.4 for legend.

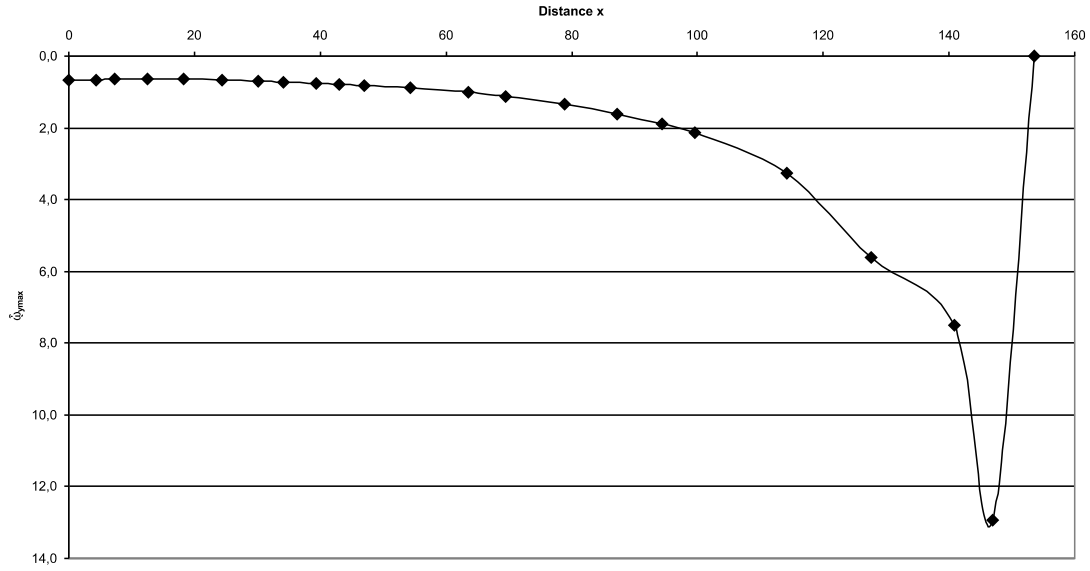

Fig A.45: Maximum bending stress in the Campylognathoides rostrum construction. See chapter 6.4 for legend.

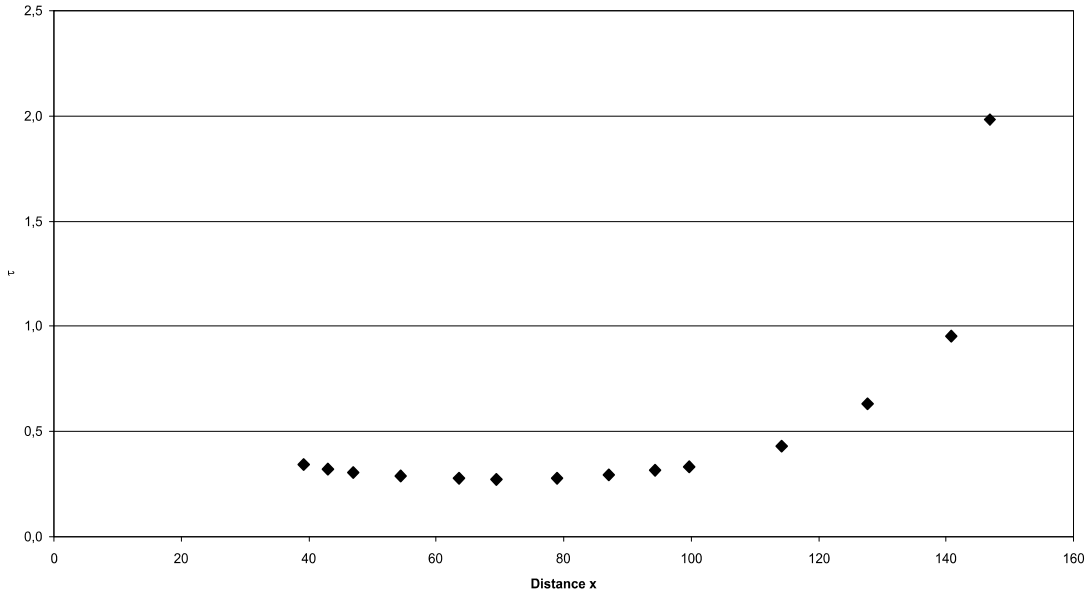

Fig. A.46: Shear stress in the Campylognathoides rostrum construction. See chapter 6.4 for legend.

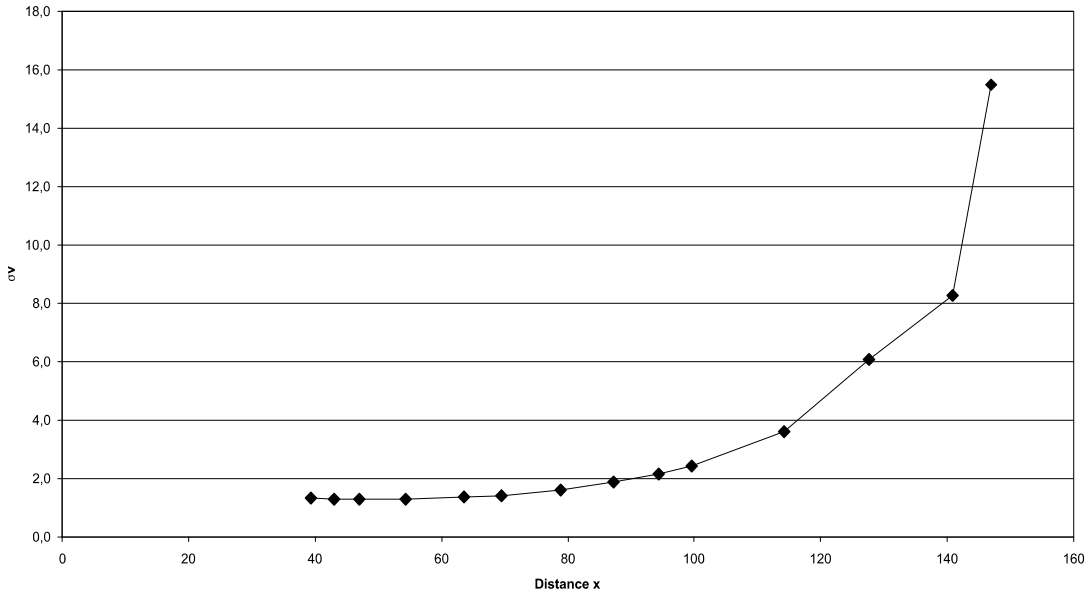

Fig. A.47: Comparison stress in the Campylognathoides rostrum construction. See chapter 6.4 for legend.

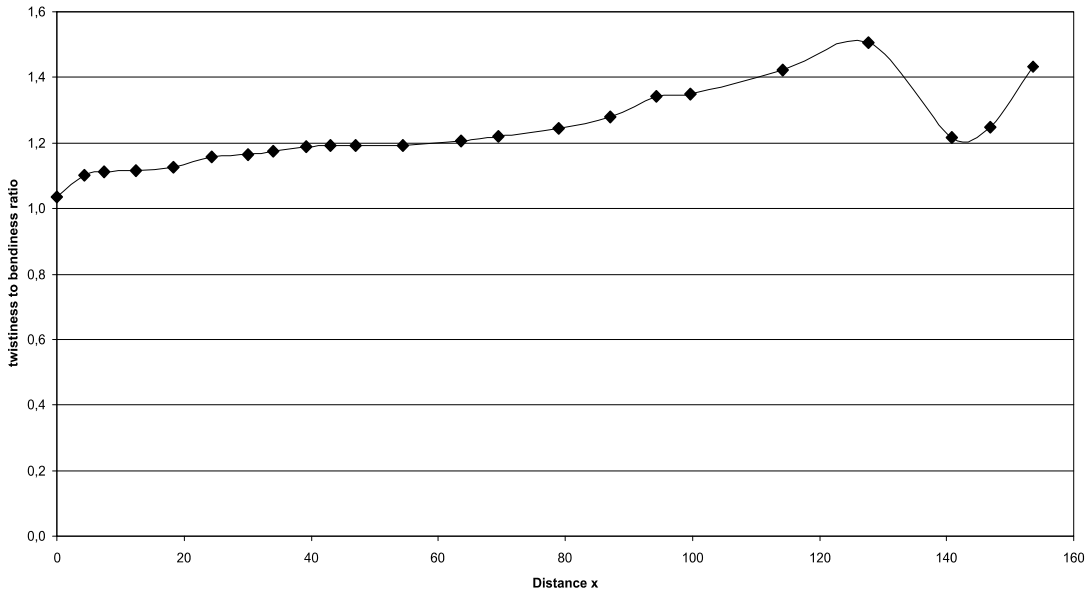

Fig. A.48: Twistiness to bendiness ratio in the Campylognathoides rostrum construction. See chapter 6.4 for legend.

A.7. Cearadactylus skull construction (see also chapter 7.7)

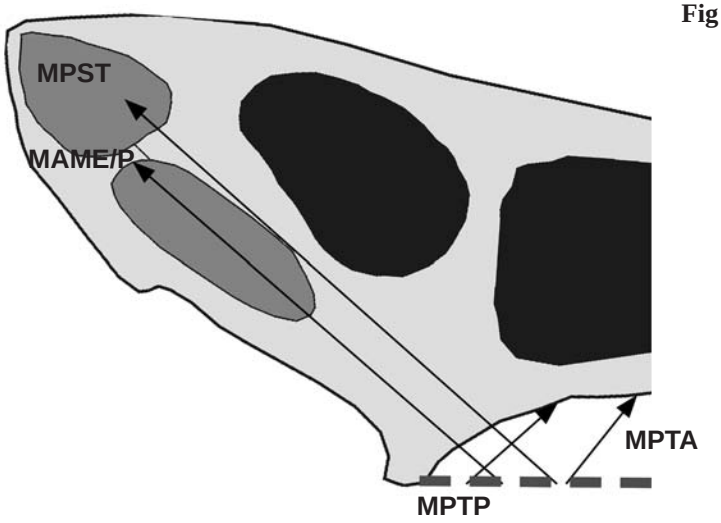

Fig A.49: Reconstruction of the principal pulling direction of the main adductor muscles in the skull of *Cearadactylus*. See chapter 6 for abbreviations.

Muscles	F_1	l_1	α_1	F_2	l_2	α_1
MAME/P	36	12.39	41	1.4	319.44	139
MPST	92	22.71	42	6.76	309.12	138
MPTA	14	24.09	51	1.10	307.75	129
MPTP	88	8.61	42	3.26	232.22	138

Tab. A.13: Reconstructed lever parameters for the scaled Cearadactylus skull construction. See chapter 6.2 for abbreviations.

	F_B	F_J	α_J
1st tooth position	7.41	224.90	-40.99
1st to 4th tooth position	31.42	898.43	-40.91
last tooth position	15.23	219.85	-39.46
average	10.24	223.06	-40.44

Tab. A.14: Reconstructed bite and joint reaction forces and angle of joint reaction force in the scaled Cearadactylus skull construction. Negative angle values mean anterodorsal direction of force. See chapter 6.2 for abbreviations.

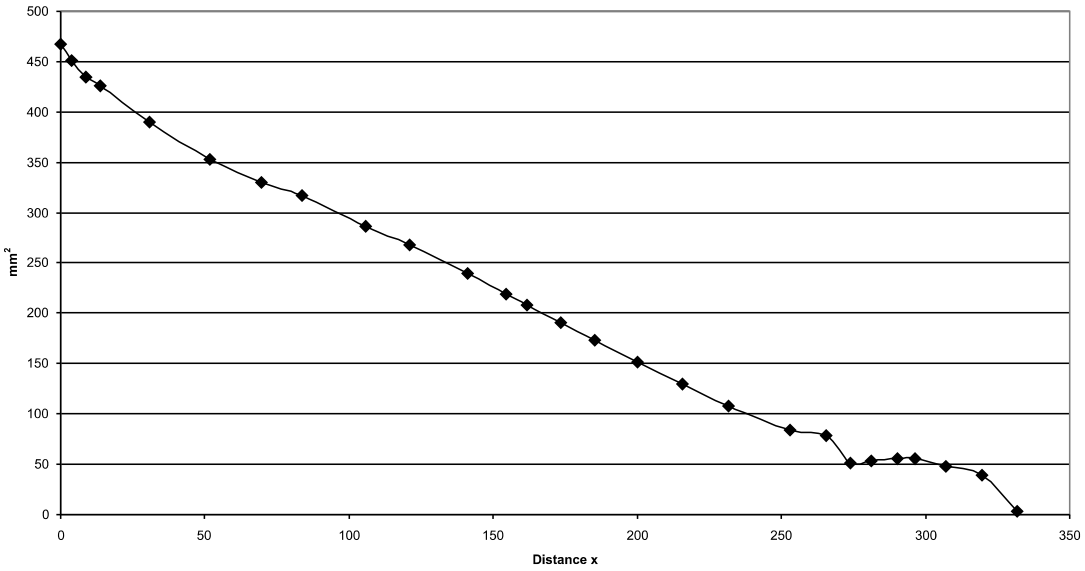

Fig A.50: Cross-sectional area of the Cearadactylus rostrum construction. See chapter 6.4 for legend.

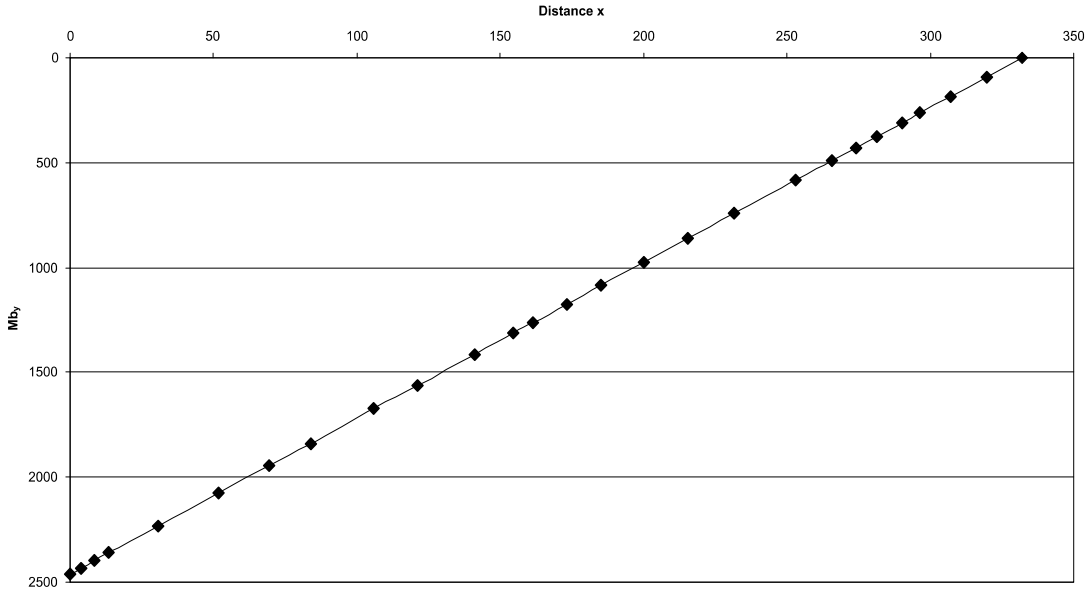

Fig A.51: Bending moments in the Cearadactylus rostrum construction. See chapter 6.4 for legend.

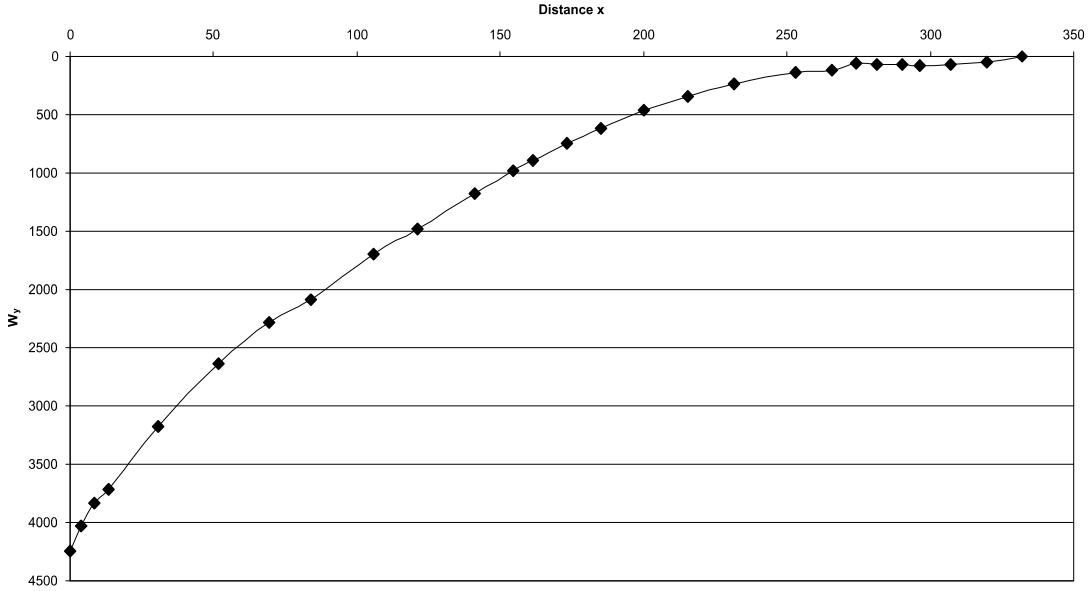

Fig A.52: Section modulus in the Cearadactylus rostrum construction. See chapter 6.4 for legend.

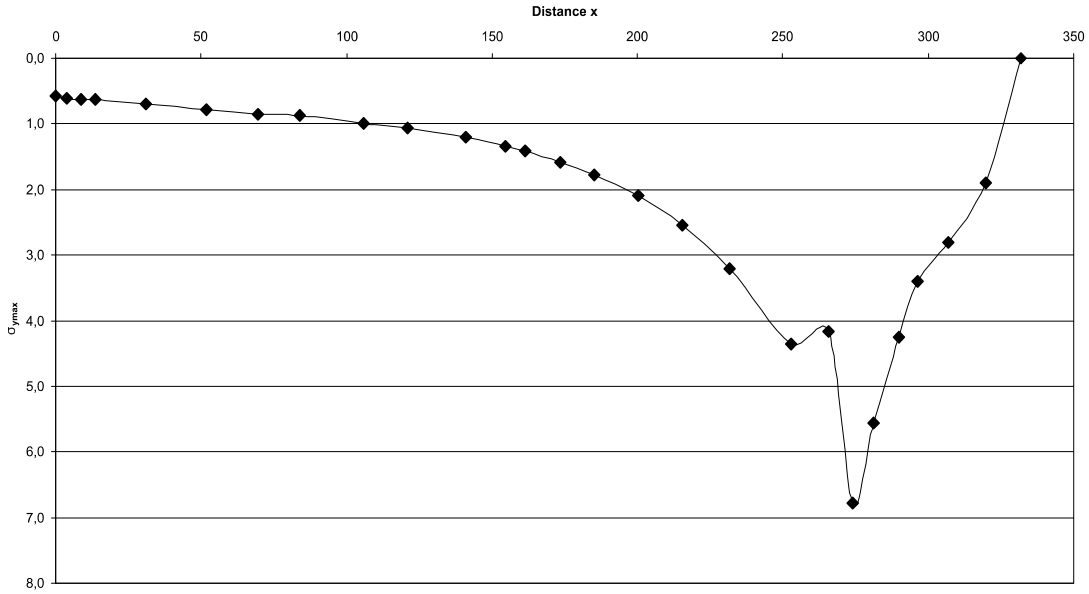

Fig A.53: Maximum bending stress in the Cearadactylus rostrum construction. See chapter 6.4 for legend.

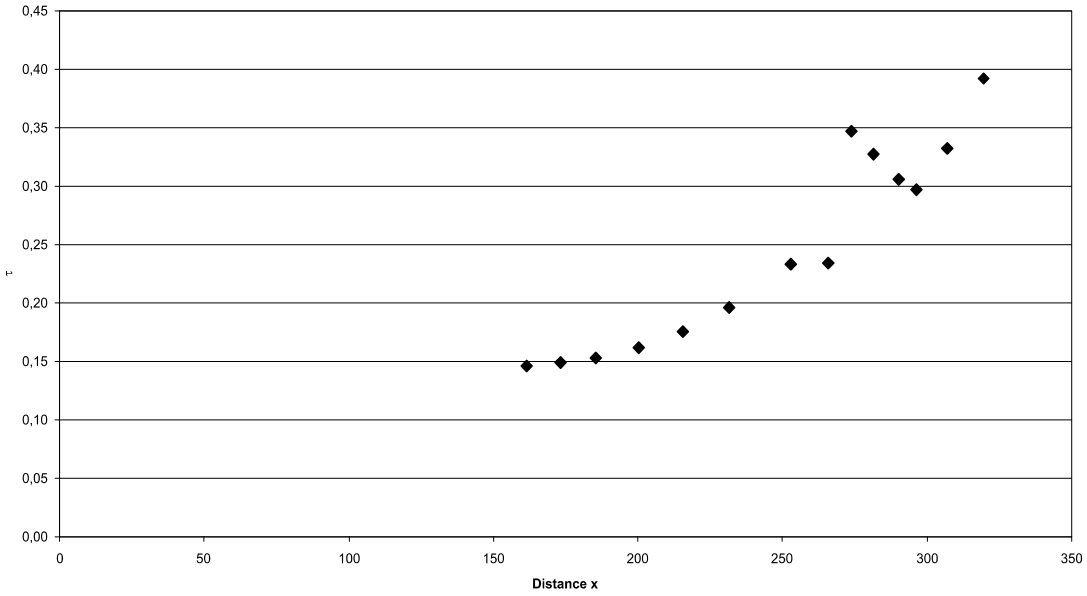

Fig. A.54: Shear stress in the Cearadactylus rostrum construction. See chapter 6.4 for legend.

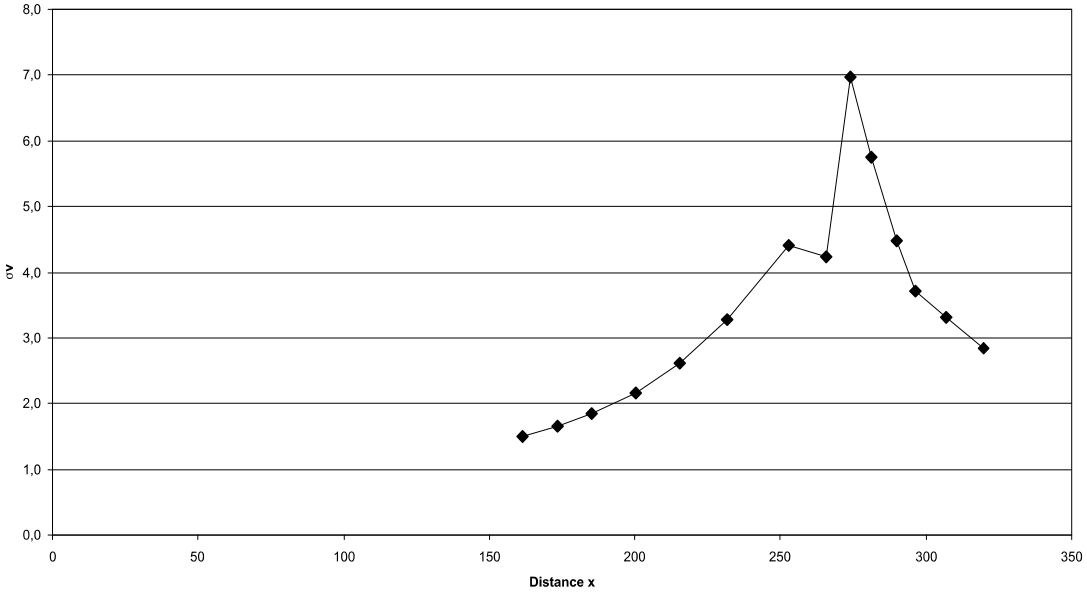

Fig. A.55: Comparison stress in the Cearadactylus rostrum construction. See chapter 6.4 for legend.

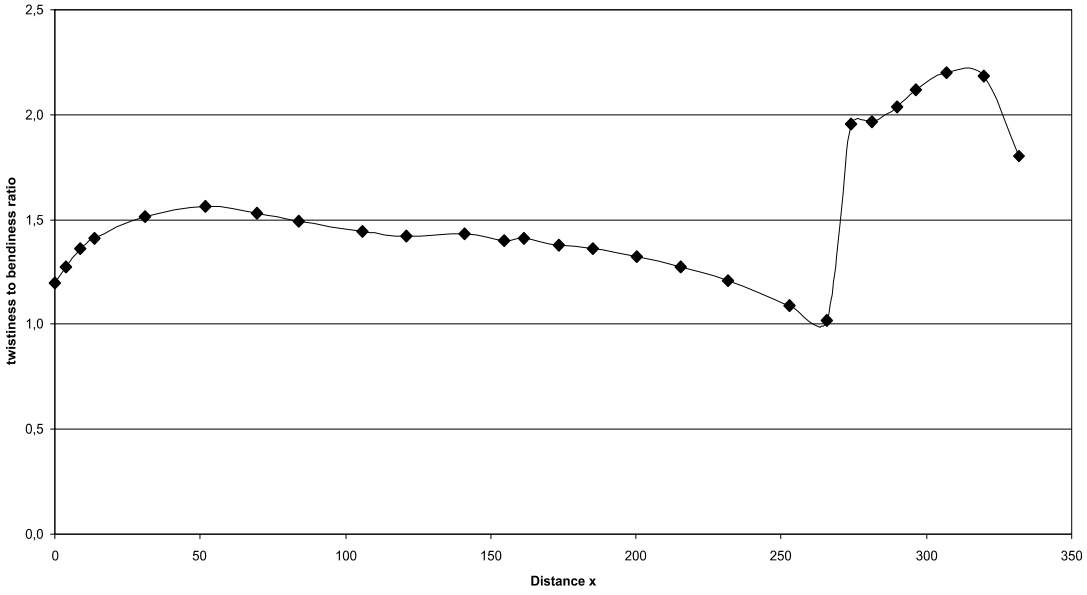

Fig. A.56: Twistiness to bendiness ratio in the Cearadactylus rostrum construction. See chapter 6.4 for legend.

A.8. Coloborhynchus skull construction (see also chapter 7.8)

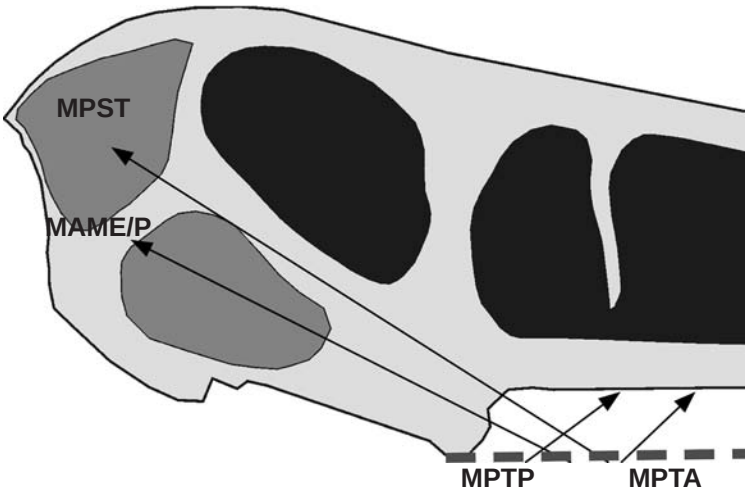

Fig A.57: Reconstruction of the principal pulling direction of the main adductor muscles in the skull of *Coloborhynchus*. See chapter 6 for abbreviations.

Muscles	F_1	l_1	α_1	F_2	l_2	α_1
MAME/P	36	15.04	32	1.90	284.78	148
MPST	92	22.76	27	7.56	277.07	153
MPTA	14	27.93	44	1.44	272.44	136
MPTP	88	10.93	37	3.33	288.90	136

Tab. A.15: Reconstructed lever parameters for the scaled Coloborhynchus skull construction. See chapter 6.2 for abbreviations.

	F_B	F_J	α_J
1st tooth position	6.96	225.34	-31.15
1st to 4th tooth position	29.10	900.73	-31.08
last tooth position	23.04	217.46	-27.52
average	11.94	222.85	-30.04

Tab. A.16: Reconstructed bite and joint reaction forces and angle of joint reaction force in the scaled Coloborhynchus skull construction. Negative angle values mean anterodorsal direction of force. See chapter 6.2 for abbreviations.

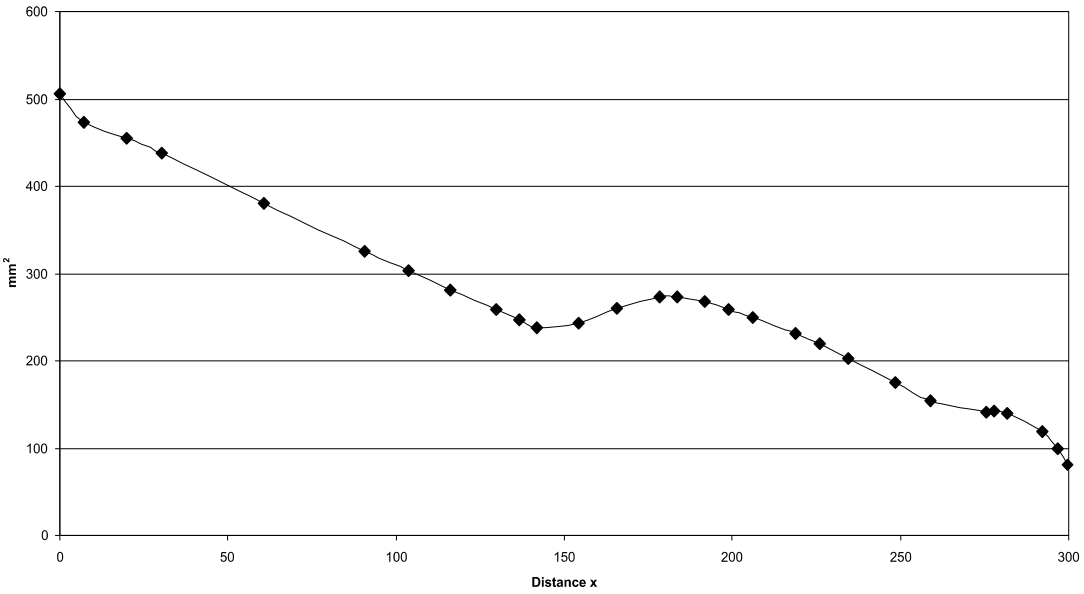

Fig A.58: Cross-sectional area of the Coloborhynchus rostrum construction. See chapter 6.4 for legend.

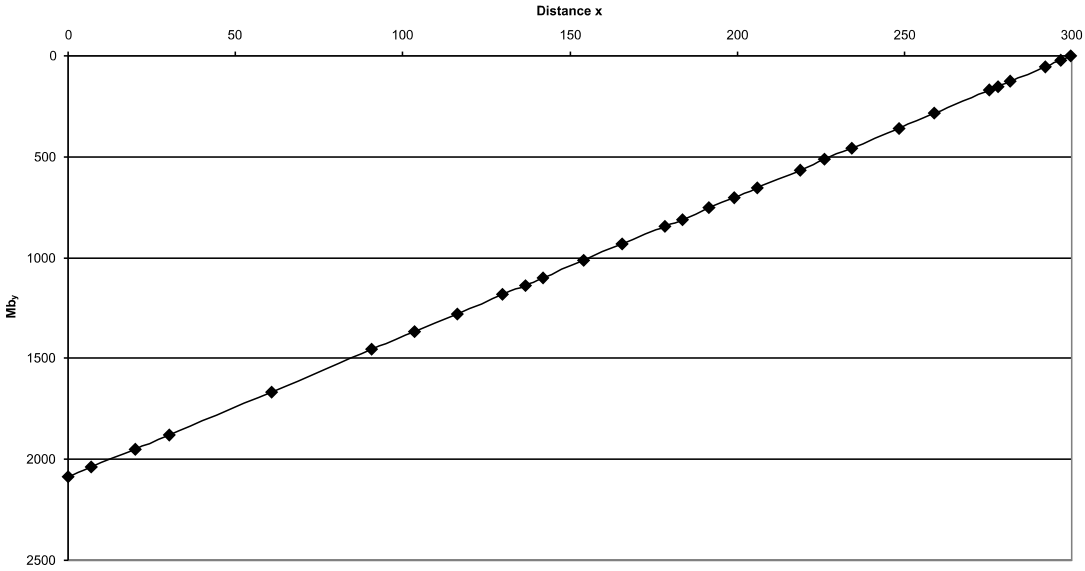

Fig A.59: Bending moments in the Coloborhynchus rostrum construction. See chapter 6.4 for legend.

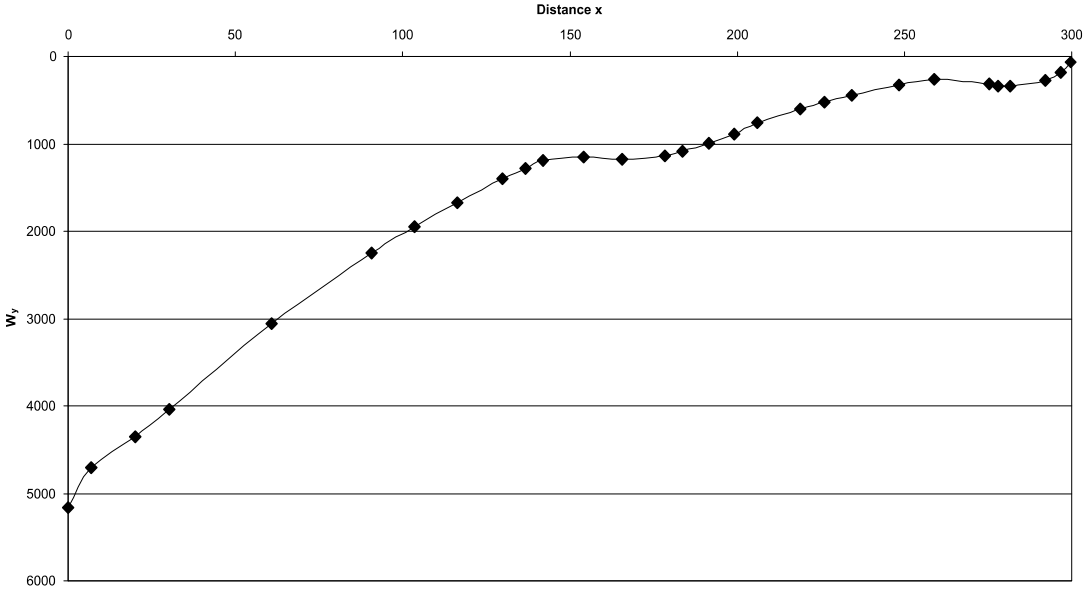

Fig A.60: Section modulus in the Coloborhynchus rostrum construction. See chapter 6.4 for legend.

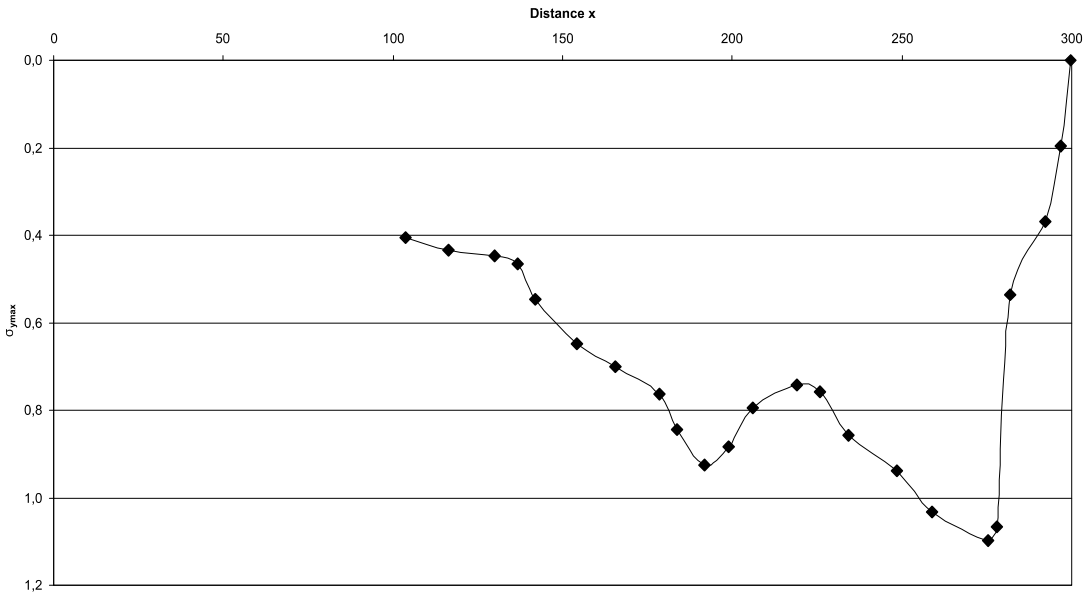

Fig A.61: Maximum bending stress in the Coloborhynchus rostrum construction. See chapter 6.4 for legend.

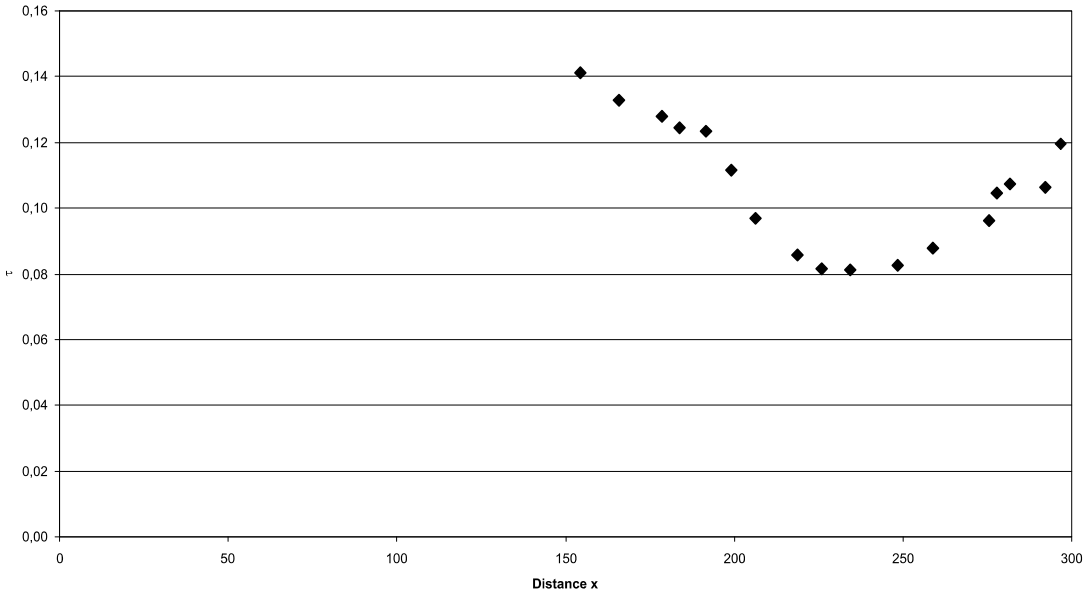

Fig. A.62: Shear stress in the Coloborhynchus rostrum construction. See chapter 6.4 for legend.

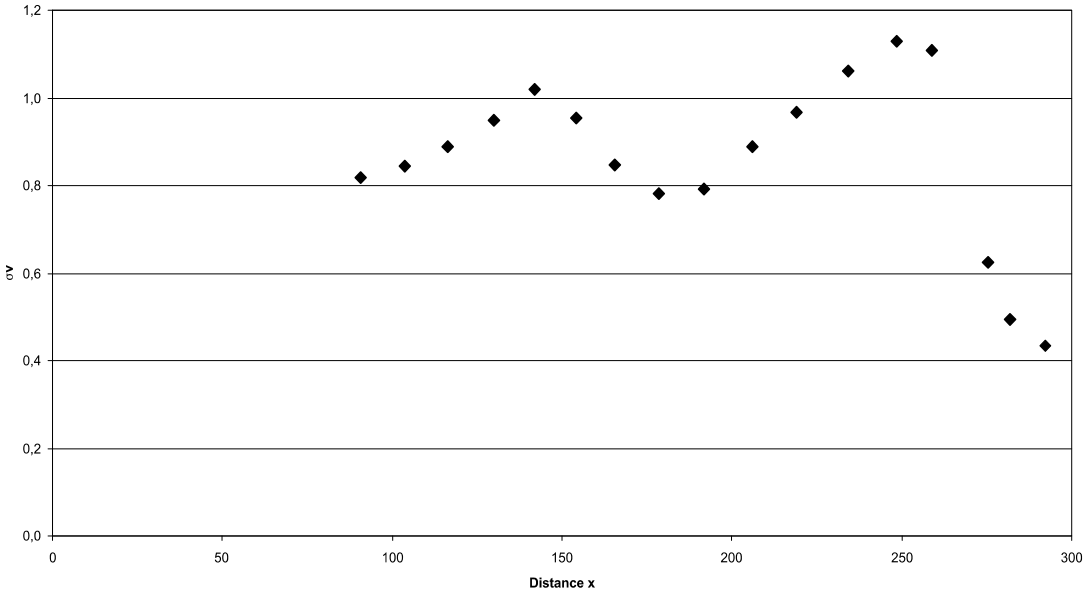

Fig. A.63: Comparison stress in the Coloborhynchus rostrum construction. See chapter 6.4 for legend.

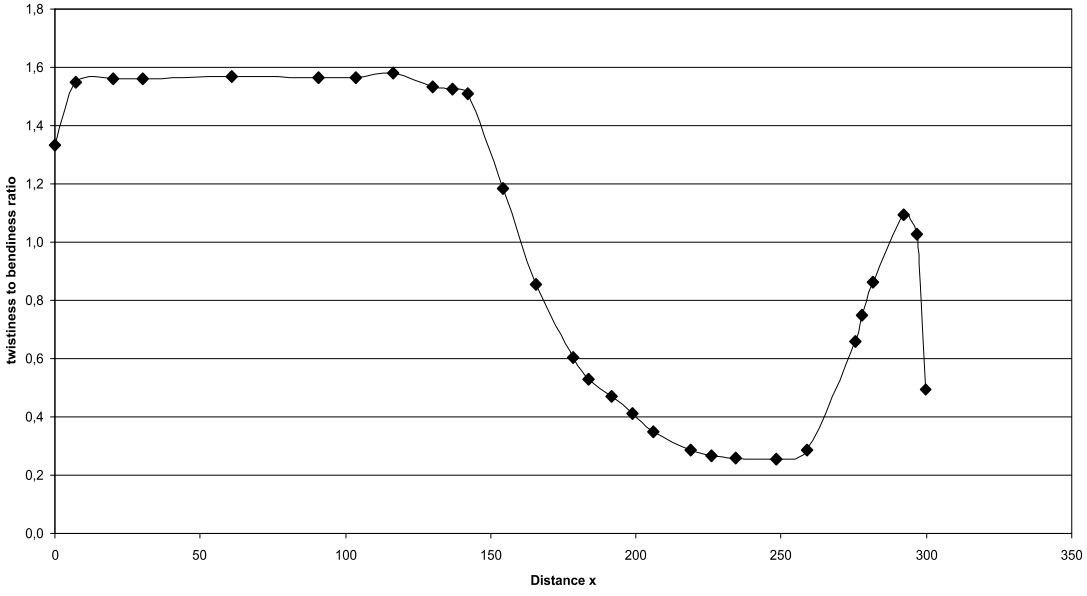

Fig. A.64: Twistiness to bendiness ratio in the Coloborhynchus rostrum construction. See chapter 6.4 for legend.

A.9. Criorhynchus skull construction (see also chapter 7.6)

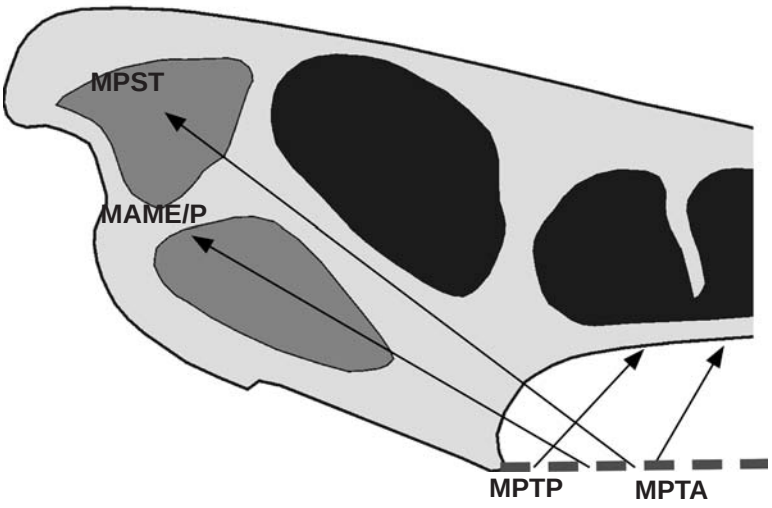

Fig A.65: Reconstruction of the principal pulling direction of the main adductor muscles in the skull of *Criorhynchus*. See chapter 6 for abbreviations.

Muscles	F_1	l_1	α_1	F_2	l_2	α_1
MAME/P	36	15.08	30	1.68	323.39	150
MPST	92	22.96	37	6.70	315.5	143
MPTA	14	27.38	60	1.23	311.08	120
MPTP	88	6.56	47	1.74	331.9	133

Tab. A.17: Reconstructed lever parameters for the scaled Criorhynchus skull construction. See chapter 6.2 for abbreviations.

	F_B	F_J	α_J
1st tooth position	6.79	223.47	-39.81
1st to 4th tooth position	28.24	893.16	-39.75
last tooth position	18.43	216.2	-37.44
average	10.05	221.41	-39.15

Tab. A.18: Reconstructed bite and joint reaction forces and angle of joint reaction force in the scaled Criorhynchus skull construction. Negative angle values mean anterodorsal direction of force. See chapter 6.2 for abbreviations.

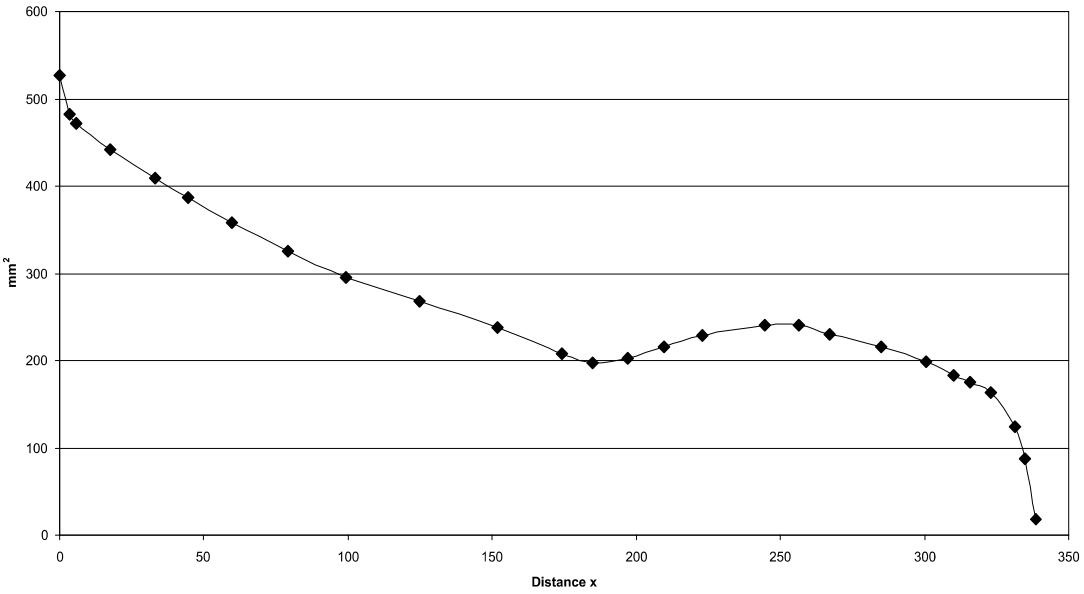

Fig A.66: Cross-sectional area of the Criorhynchus rostrum construction. See chapter 6.4 for legend.

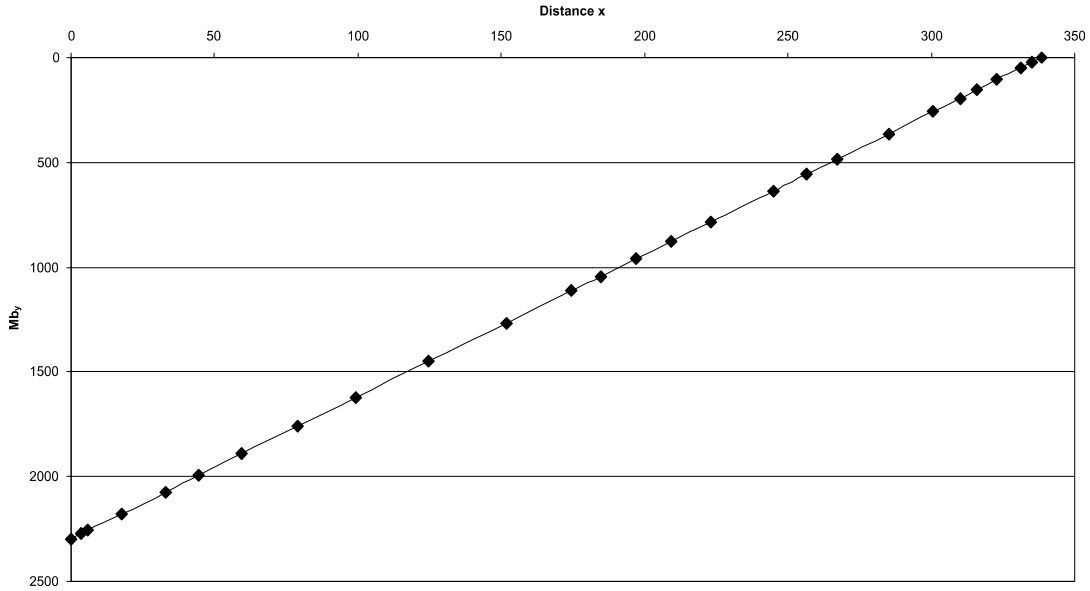

Fig A.67: Bending moments in the Criorhynchus rostrum construction. See chapter 6.4 for legend.

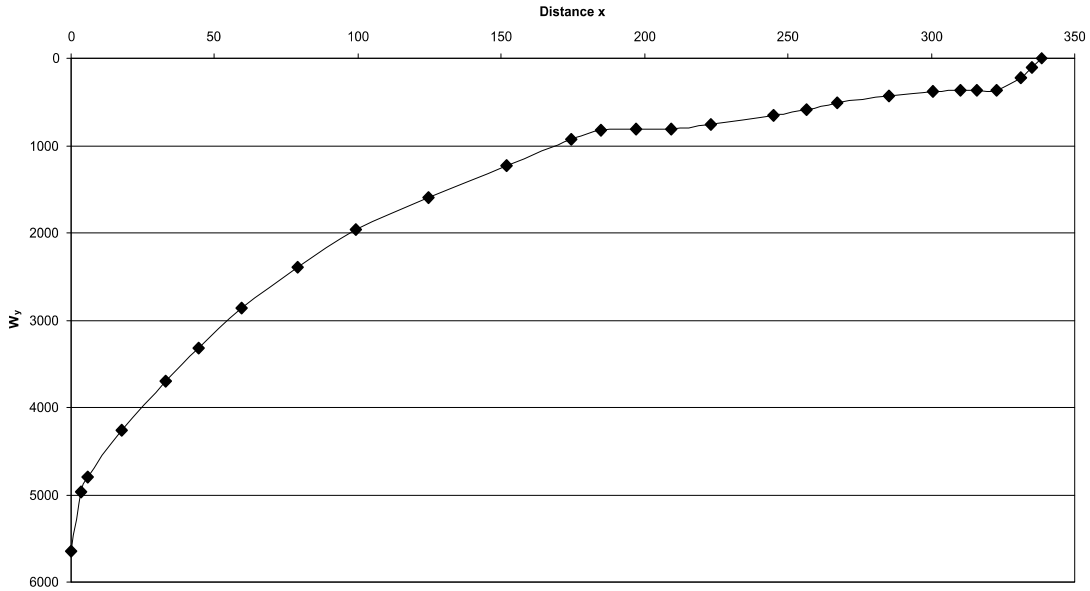

Fig A.68: Section modulus in the Criorhynchus rostrum construction. See chapter 6.4 for legend.

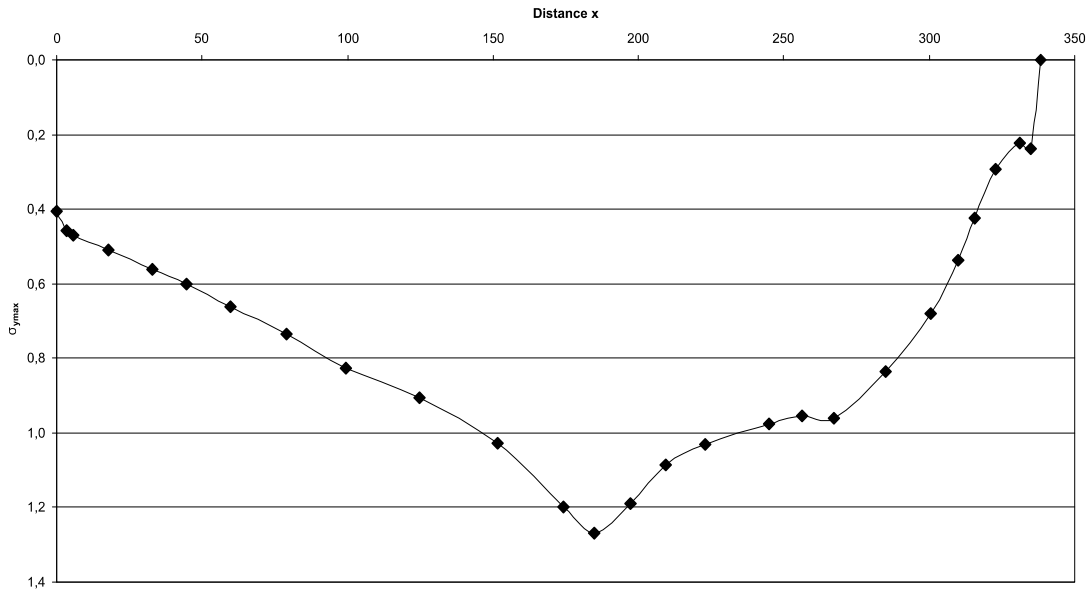

Fig A.69: Maximum bending stress in the Criorhynchus rostrum construction. See chapter 6.4 for legend.

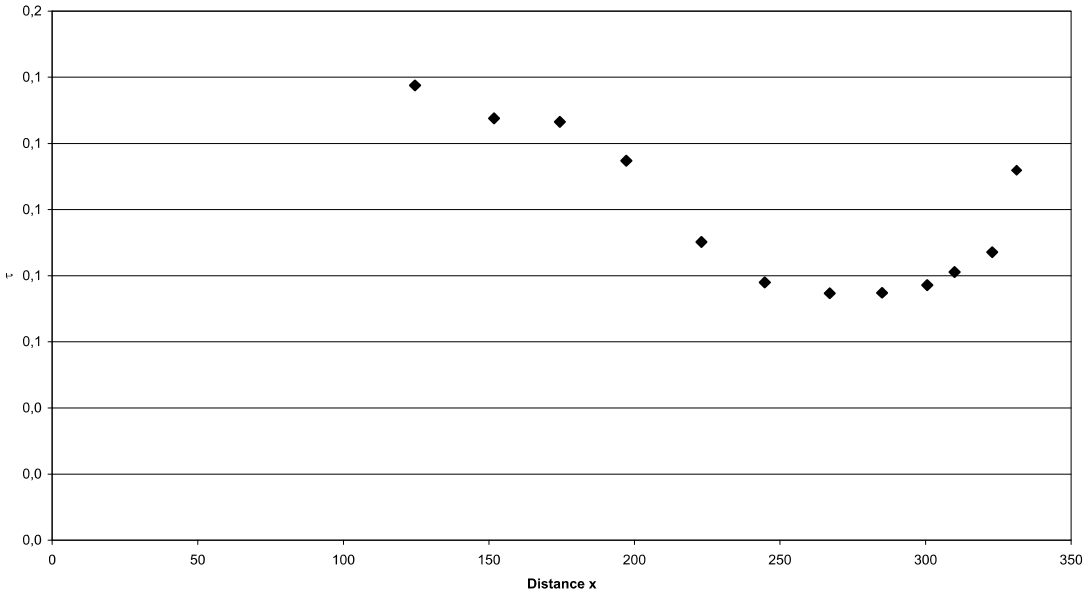

Fig. A.70: Shear stress in the Criorhynchus rostrum construction. See chapter 6.4 for legend.

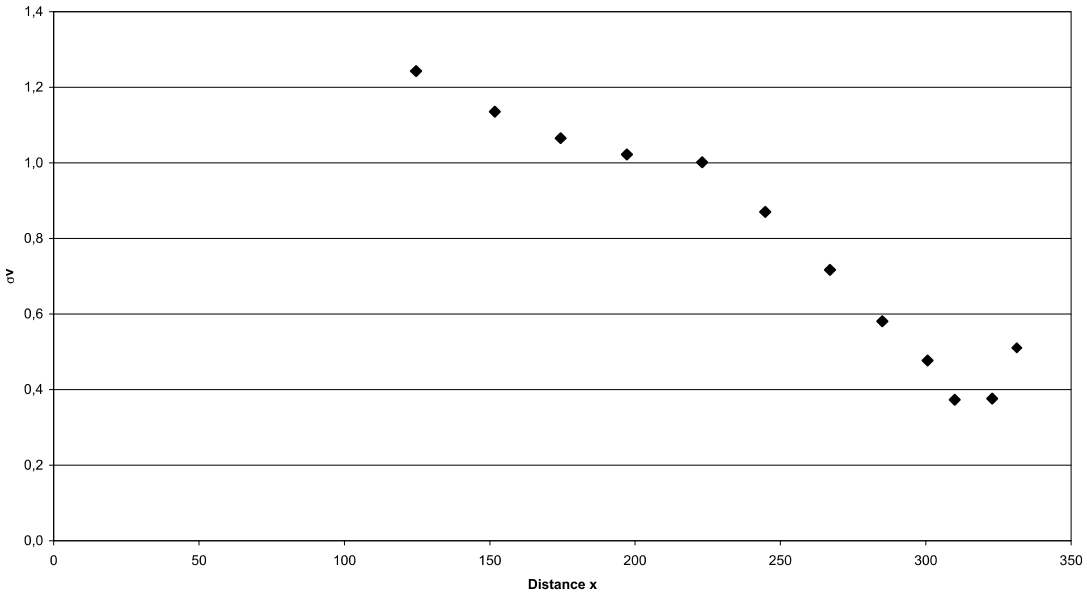

Fig. A.71: Comparison stress in the Criorhynchus rostrum construction. See chapter 6.4 for legend.

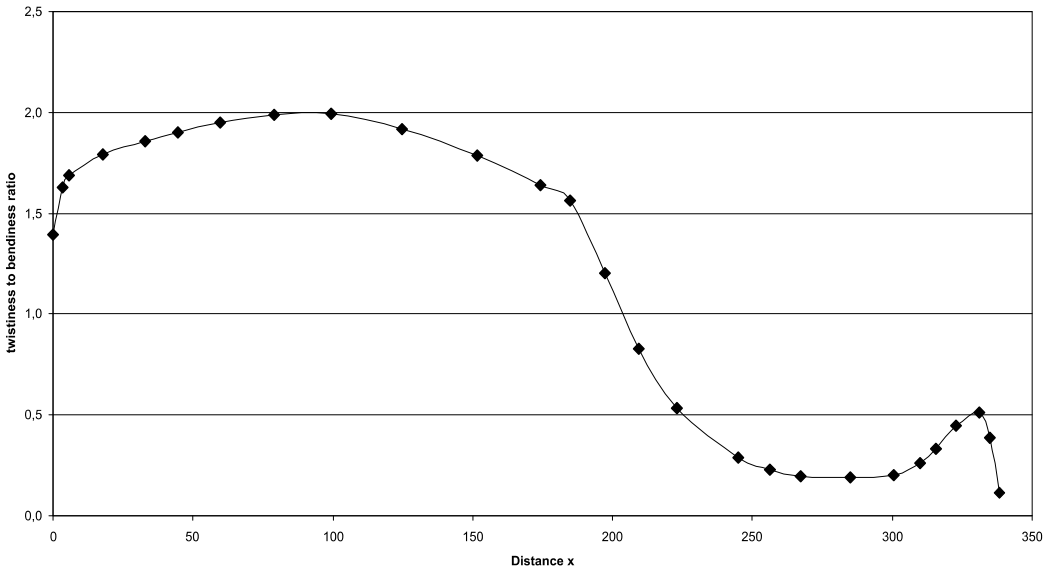

Fig. A.72: Twistiness to bendiness ratio in the Criorhynchus rostrum construction. See chapter 6.4 for legend.

A.10. Ctenochasma skull construction (see also chapter 7.10)

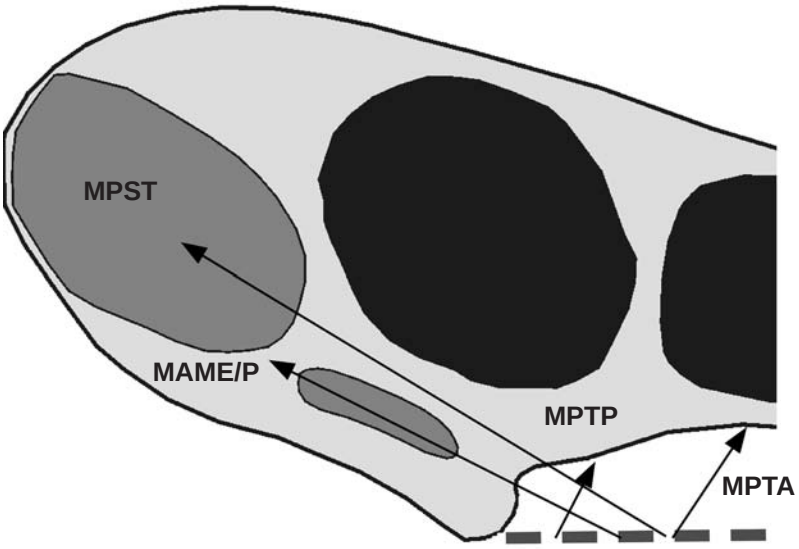

Fig A.73: Reconstruction of the principal pulling direction of the main adductor muscles in the skull of *Ctenochasma*. See chapter 6 for abbreviations.

Muscles	F_1	l_1	α_1	F_2	l_2	α_1
MAME/P	36	17.37	27	1.59	392.39	153
MPST	92	24.01	31	5.73	385.75	149
MPTA	14	25.1	56	0.91	384.65	124
MPTP	88	7.39	53	4.62	402.37	127

Tab. A.19: Reconstructed lever parameters for the scaled Ctenochasma skull construction. See chapter 6.2 for abbreviations.

	F_B	F_J	α_J
1st tooth position	5.45	221.67	-39.22
1st to 4th tooth position	22.37	886.30	-29.19
last tooth position	17.08	214.50	-36.81
average	7.75	218.10	-38.02

Tab. A.20: Reconstructed bite and joint reaction forces and angle of joint reaction force in the scaled Ctenochasma skull construction. Negative angle values mean anterodorsal direction of force. See chapter 6.2 for abbreviations.

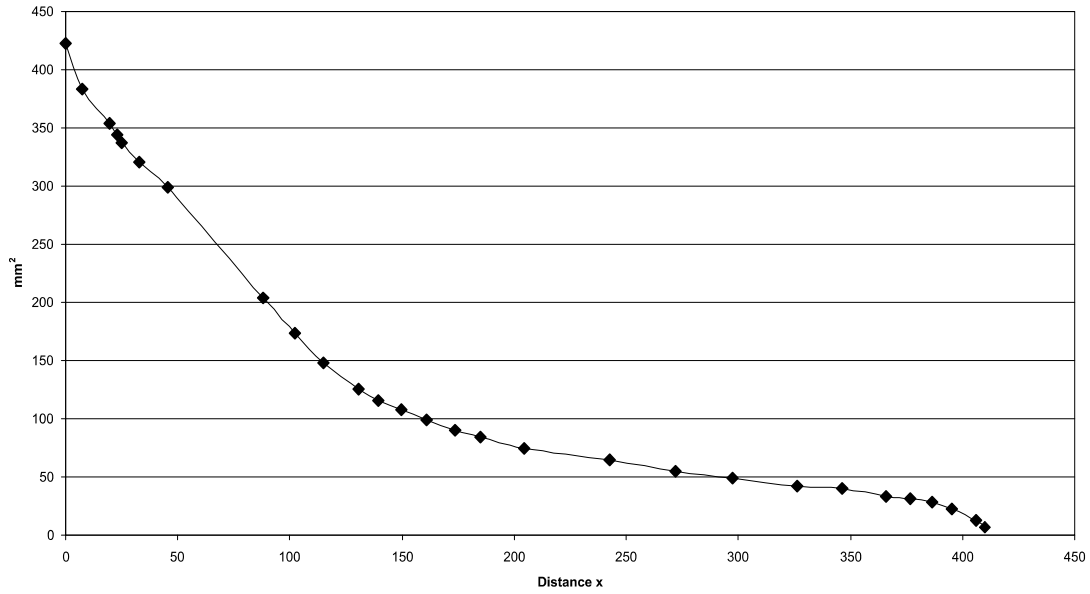

Fig A.74: Cross-sectional area of the Ctenochasma rostrum construction. See chapter 6.4 for legend.

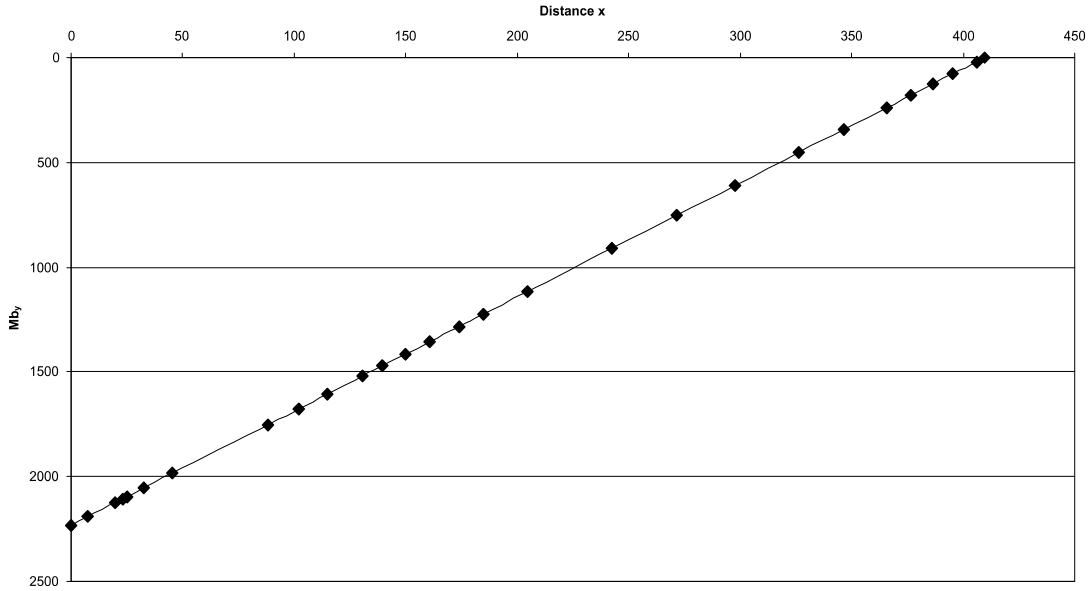

Fig A.75: Bending moments in the Ctenochasma rostrum construction. See chapter 6.4 for legend.

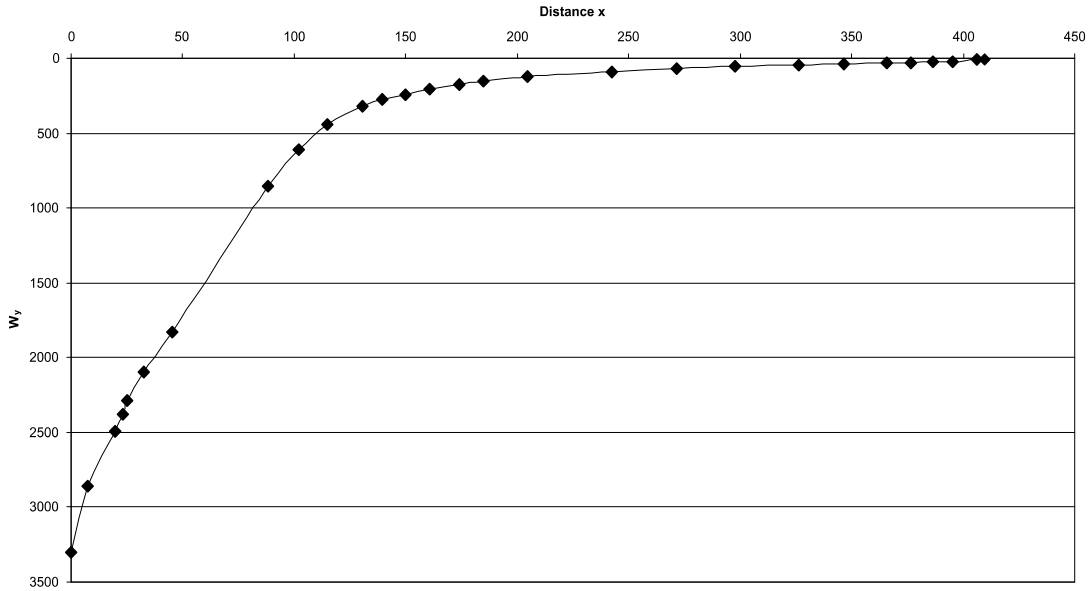

Fig A.76: Section modulus in the Ctenochasma rostrum construction. See chapter 6.4 for legend.

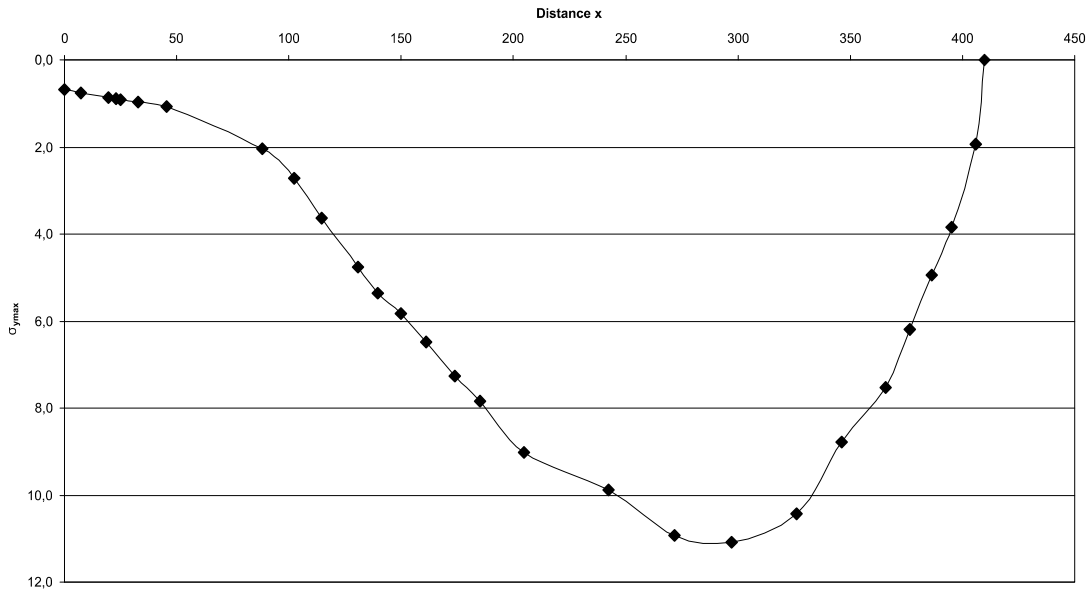

Fig A.77: Maximum bending stress in the Ctenochasma rostrum construction. See chapter 6.4 for legend.

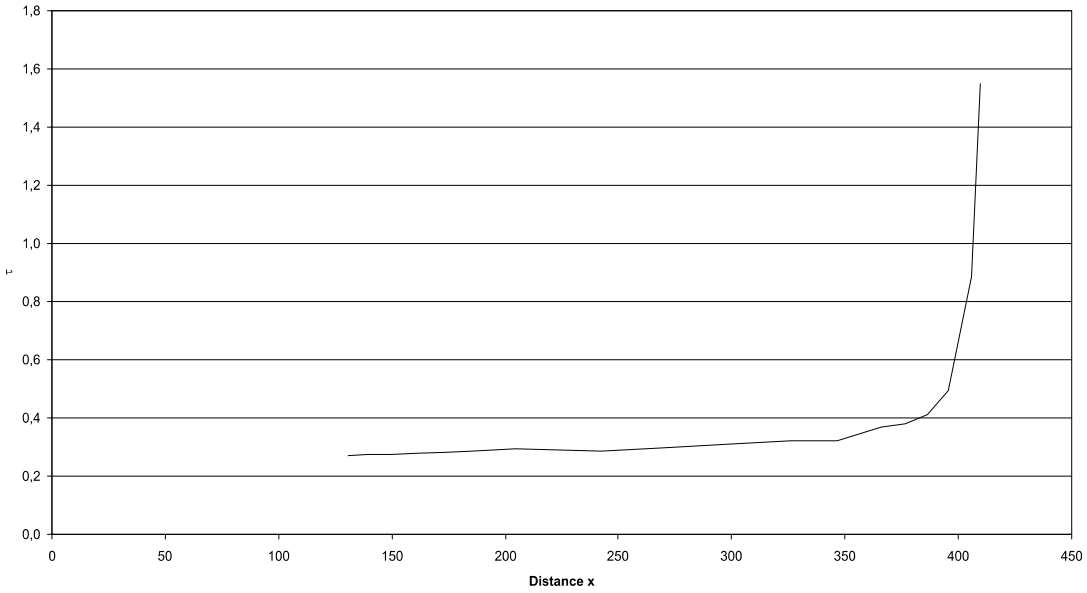

Fig. A.78: Shear stress in the Ctenochasma rostrum construction. See chapter 6.4 for legend.

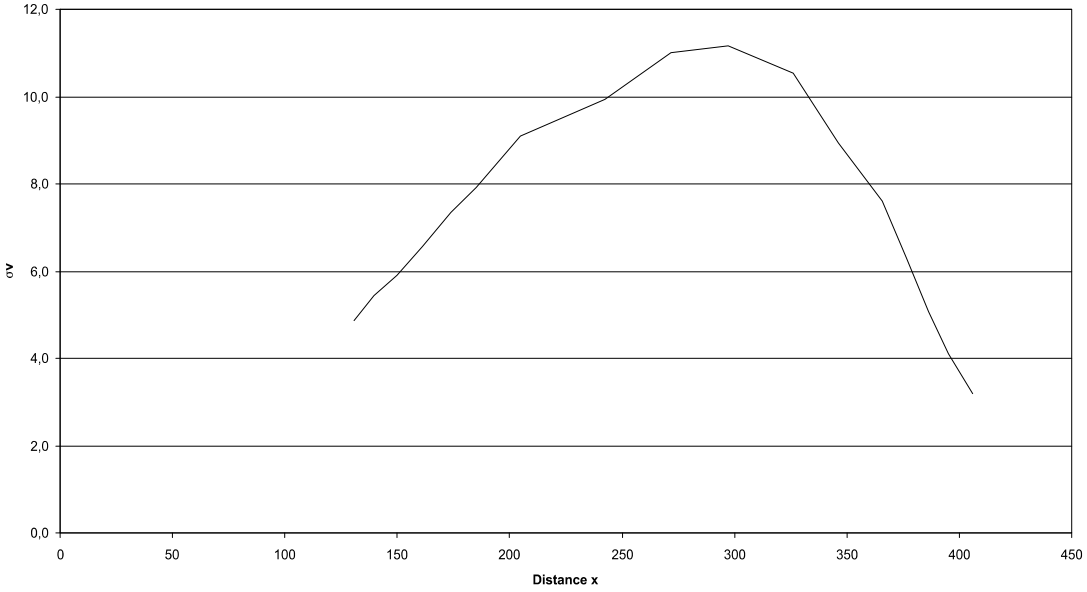

Fig. A.79: Comparison stress in the Ctenochasma rostrum construction. See chapter 6.4 for legend.

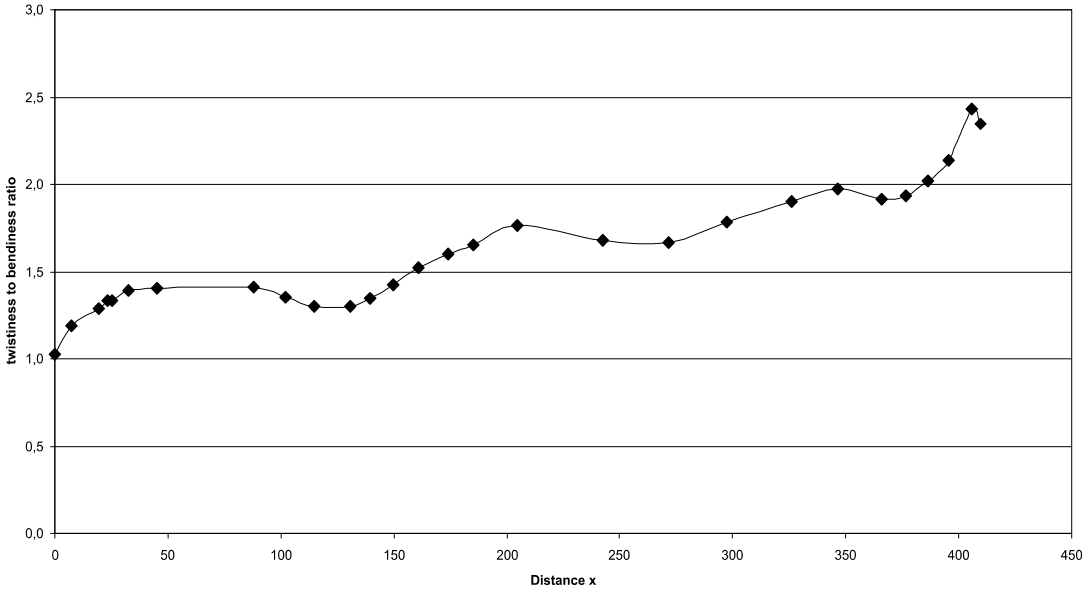

Fig. A.80: Twistiness to bendiness ratio in the Ctenochasma rostrum construction. See chapter 6.4 for legend.

A.11. Dimorphodon skull construction (see also chapter 7.11)

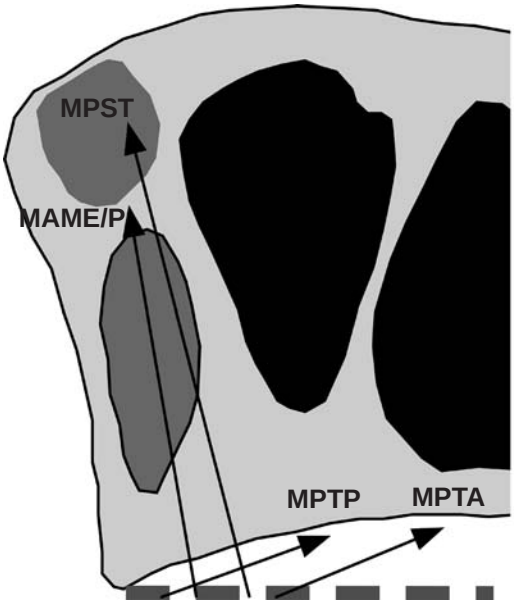

Fig A.81: Reconstruction of the principal pulling direction of the main adductor muscles in the skull of *Dimorphodon*. See chapter 6 for abbreviations.

Muscles	F_1	l_1	α_1	F_2	l_2	α_1
MAME/P	36	10.52	80	2.40	157.82	100
MPST	92	16.95	76	10.30	151.39	104
MPTA	14	20.03	23	1.89	148.31	157
MPTP	88	6.15	20	3.34	162.19	160

Tab. A.21: Reconstructed lever parameters for the scaled Dimorphodon skull construction. See chapter 6.2 for abbreviations.

	F_B	F_J	α_J
1st tooth position	12.95	192.63	-49.90
1st to 4th tooth position	57.04	766.53	-49.64
last tooth position	41.48	171.79	-43.75
average	27.45	181.90	-46.87

Tab. A.22: Reconstructed bite and joint reaction forces and angle of joint reaction force in the scaled Dimorphodon skull construction. Negative angle values mean anterodorsal direction of force. See chapter 6.2 for abbreviations.

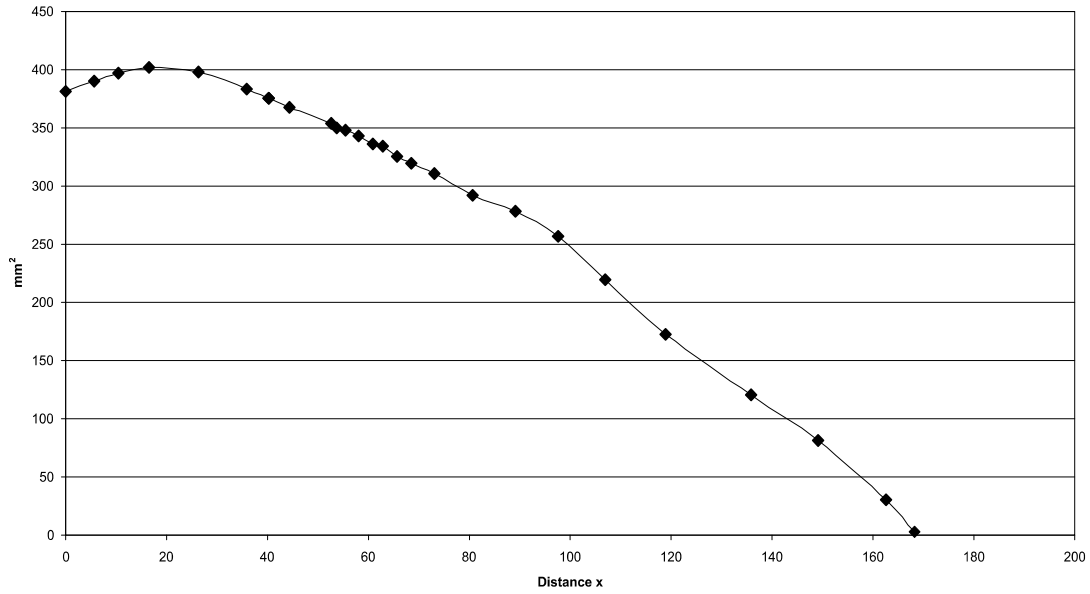

Fig A.82: Cross-sectional area of the Dimorphodon rostrum construction. See chapter 6.4 for legend.

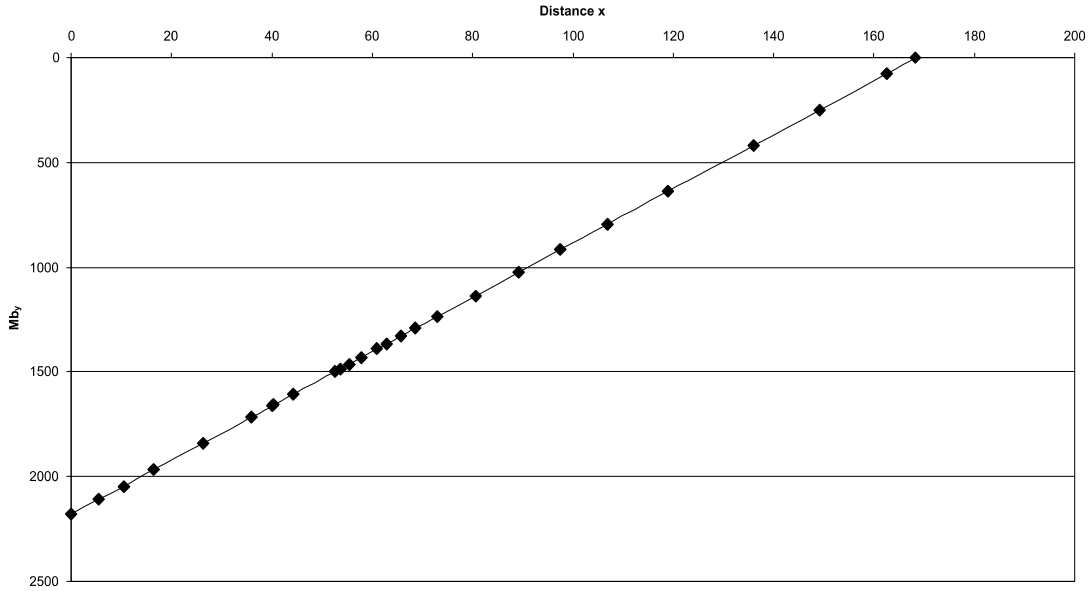

Fig A.83: Bending moments in the Dimorphodon rostrum construction. See chapter 6.4 for legend.

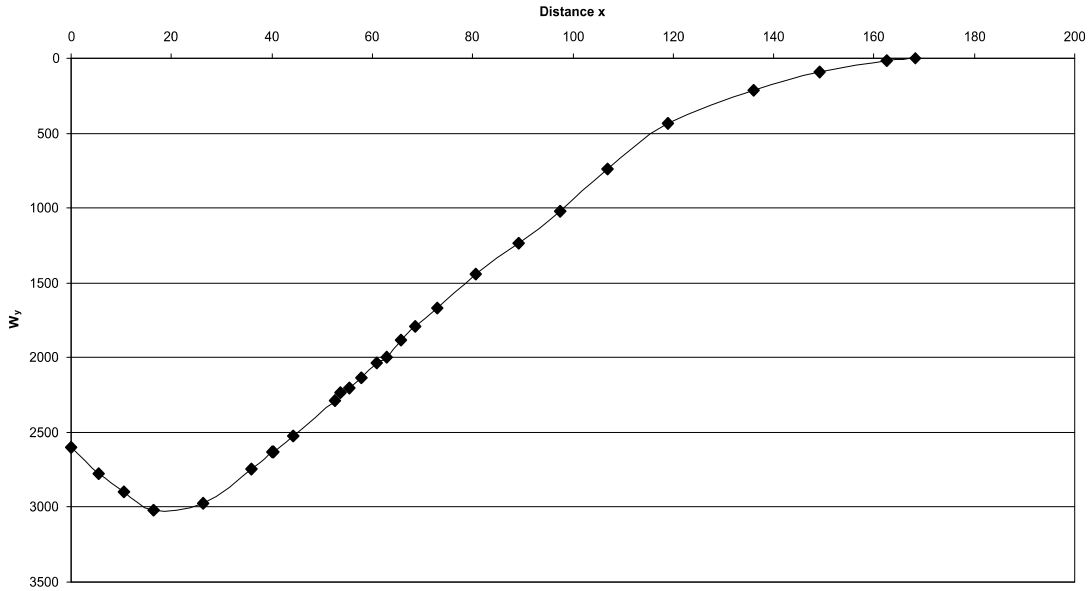

Fig A.84: Section modulus in the Dimorphodon rostrum construction. See chapter 6.4 for legend.

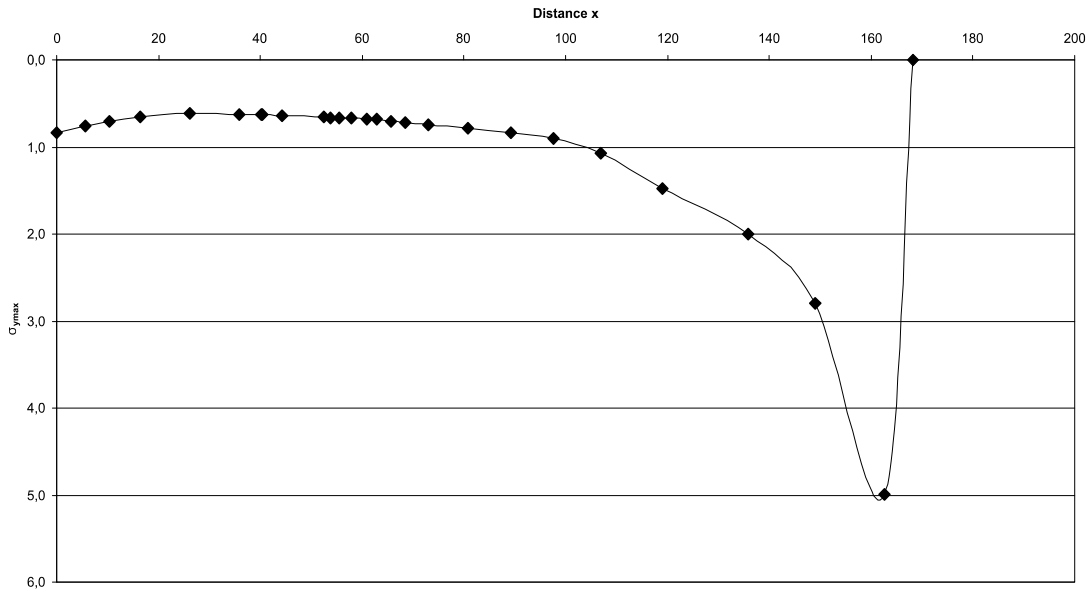

Fig A.85: Maximum bending stress in the Dimorphodon rostrum construction. See chapter 6.4 for legend.

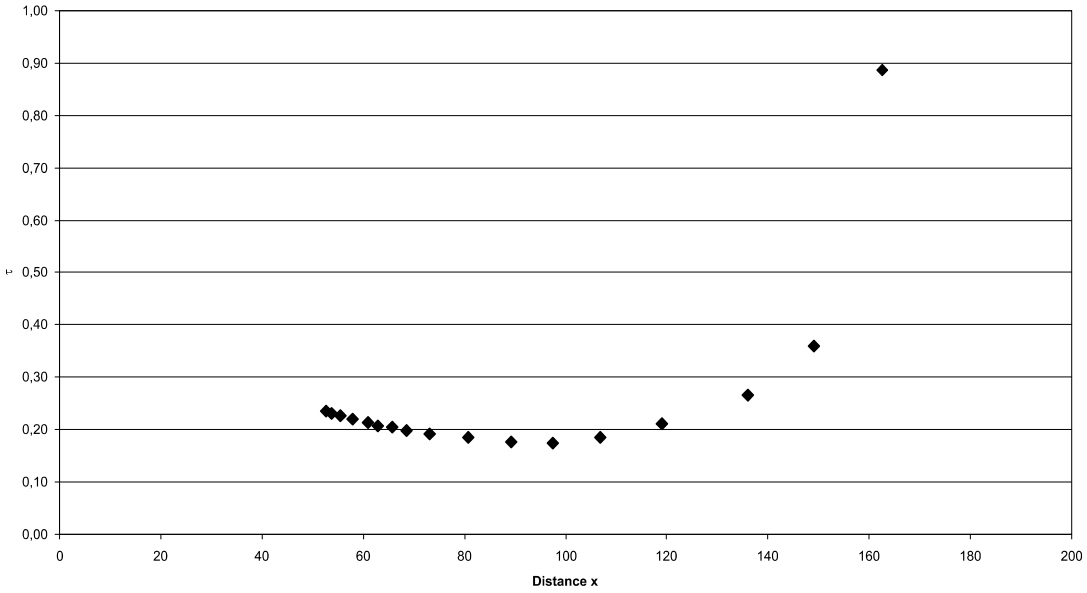

Fig. A.86: Shear stress in the Dimorphodon rostrum construction. See chapter 6.4 for legend.

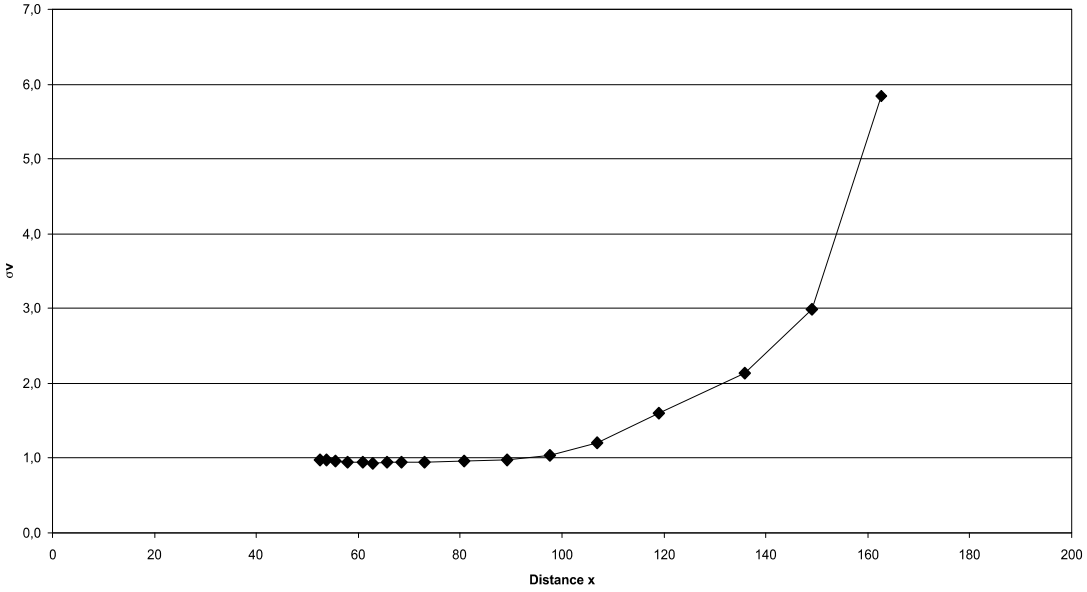

Fig. A.87: Comparison stress in the Dimorphodon rostrum construction. See chapter 6.4 for legend.

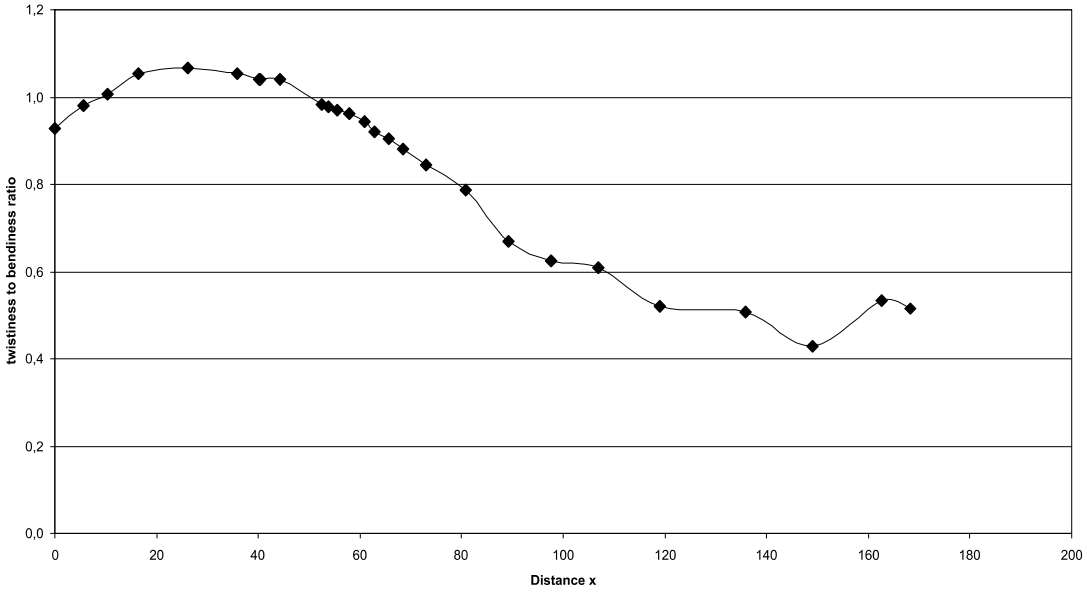

Fig. A.88: Twistiness to bendiness ratio in the Dimorphodon rostrum construction. See chapter 6.4 for legend.

A.12. Dorygnathus skull construction (see also chapter 7.12)

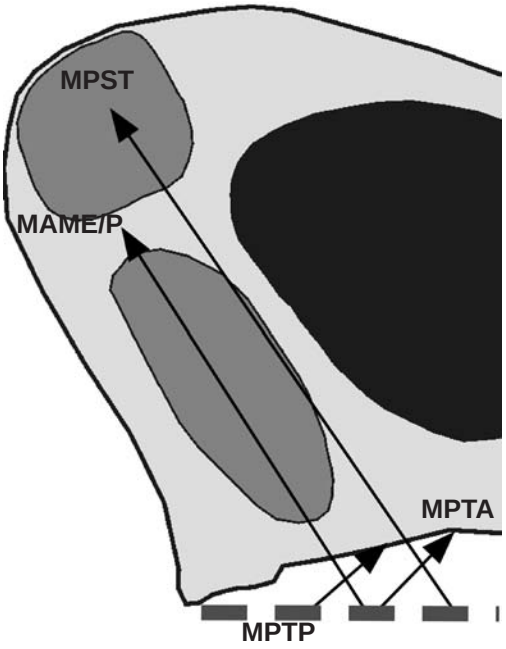

Fig A.89: Reconstruction of the principal pulling direction of the main adductor muscles in the skull of *Dorygnathus*. See chapter 6 for abbreviations.

Muscles	F_1	l_1	α_1	F_2	l_2	α_1
MAME/P	36	8.87	57	2.34	135.54	123
MPST	92	19.41	56	14.17	126	124
MPTA	14	11.44	46	1.20	133.97	134
MPTP	88	3.73	41	2.32	141.69	139

Tab. A.23: Reconstructed lever parameters for the scaled Dorygnathus skull construction. See chapter 6.2 for abbreviations.

	F_B	F_J	α_J
1st tooth position	14.30	217.39	-47.38
1st to 4th tooth position	66.47	862.75	-46.96
last tooth position	50.22	192.49	-40.12
average	28.12	207.56	-44.71

Tab. A.24: Reconstructed bite and joint reaction forces and angle of joint reaction force in the scaled Dorygnathus skull construction. Negative angle values mean anterodorsal direction of force. See chapter 6 .2for abbreviations.

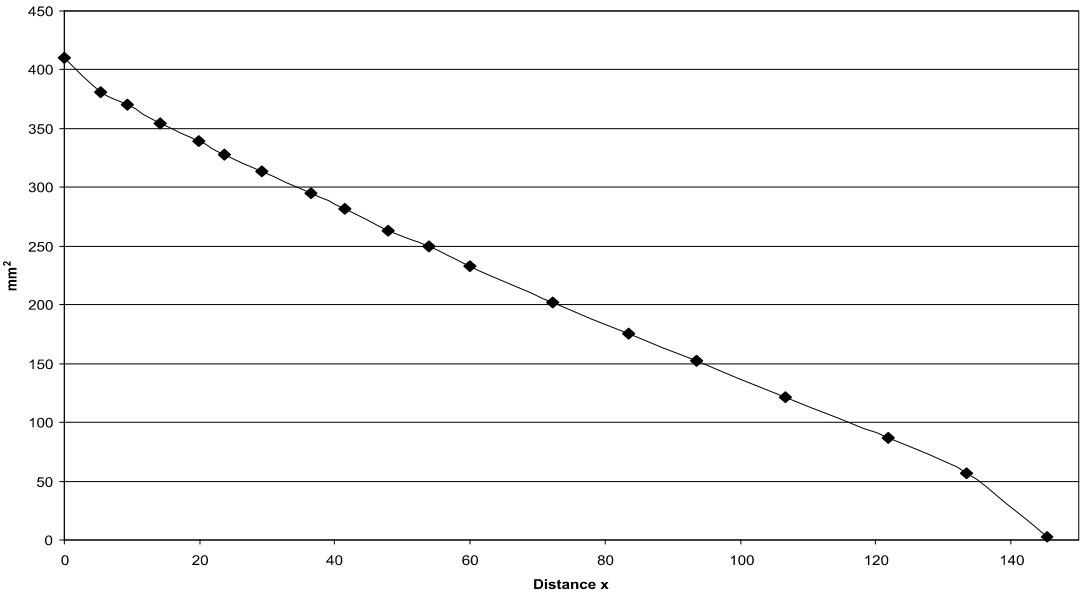

Fig A.90: Cross-sectional area of the Dorygnathus rostrum construction. See chapter 6.4 for legend.

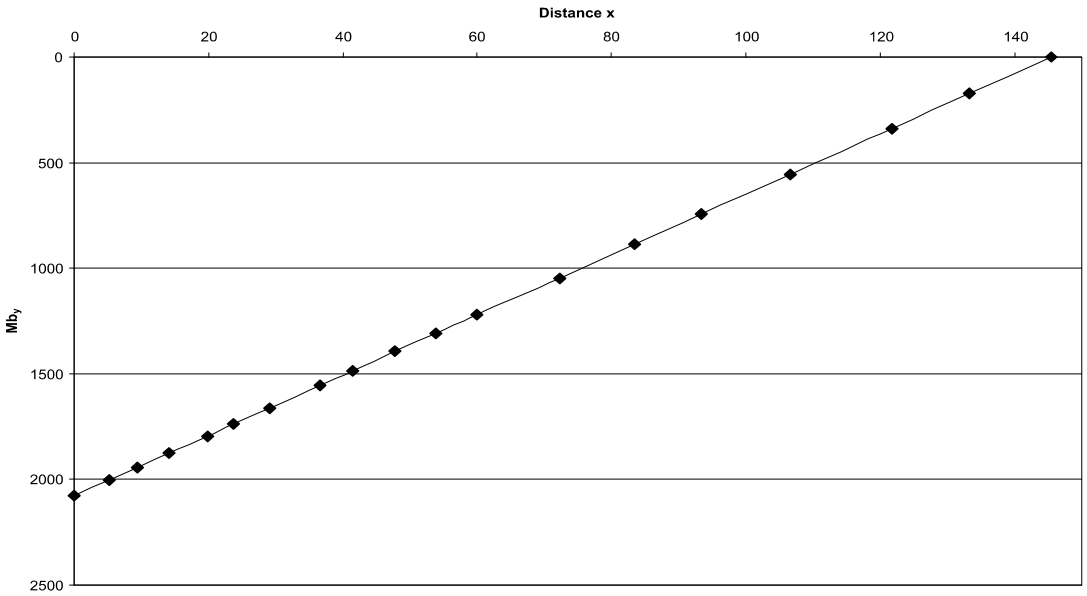

Fig A.91: Bending moments in the Dorygnathus rostrum construction. See chapter 6.4 for legend.

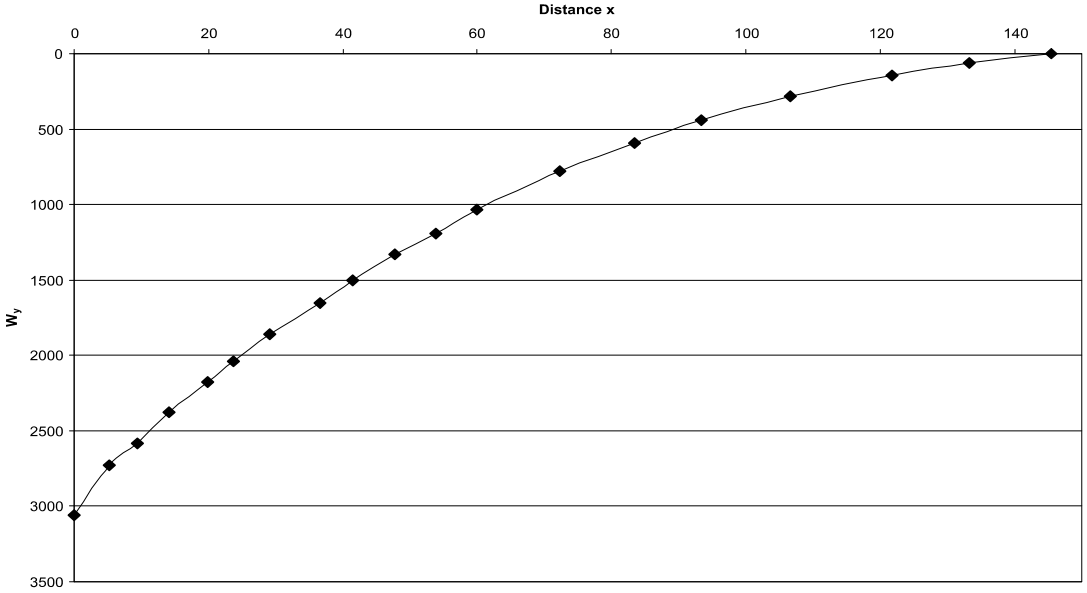

Fig A.92: Section modulus in the Dorygnathus rostrum construction. See chapter 6.4 for legend.

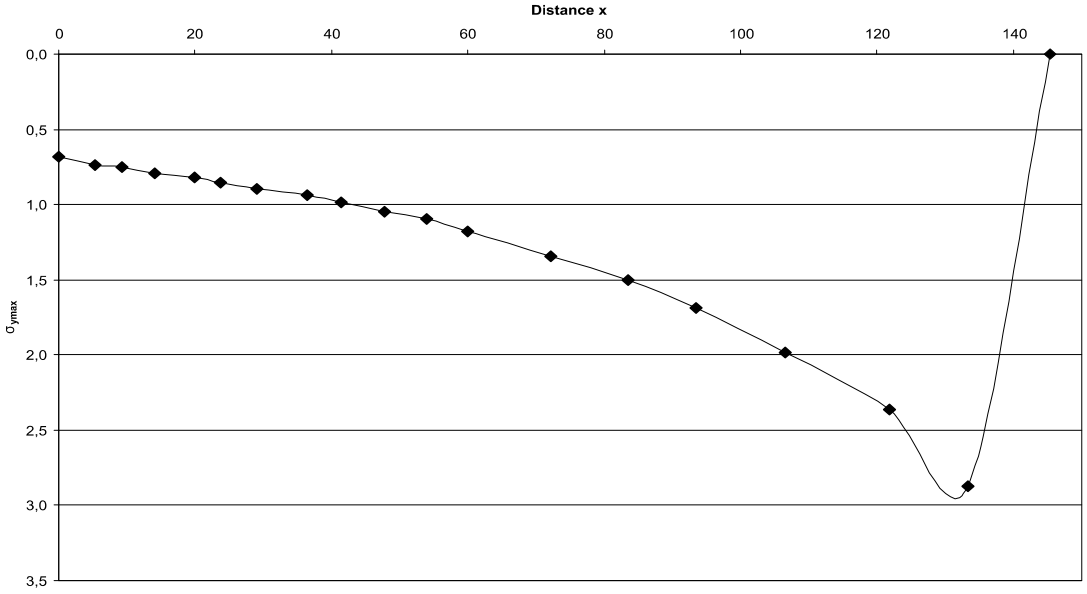

Fig A.93: Maximum bending stress in the Dorygnathus rostrum construction. See chapter 6.4 for legend.

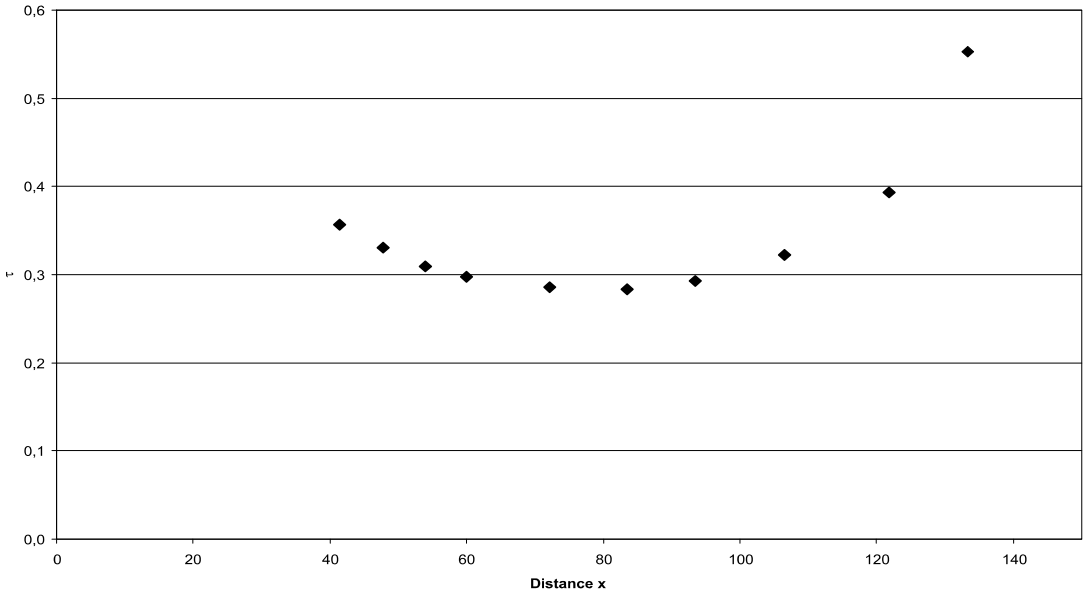

Fig. A.94: Shear stress in the Dorygnathus rostrum construction. See chapter 6.4 for legend.

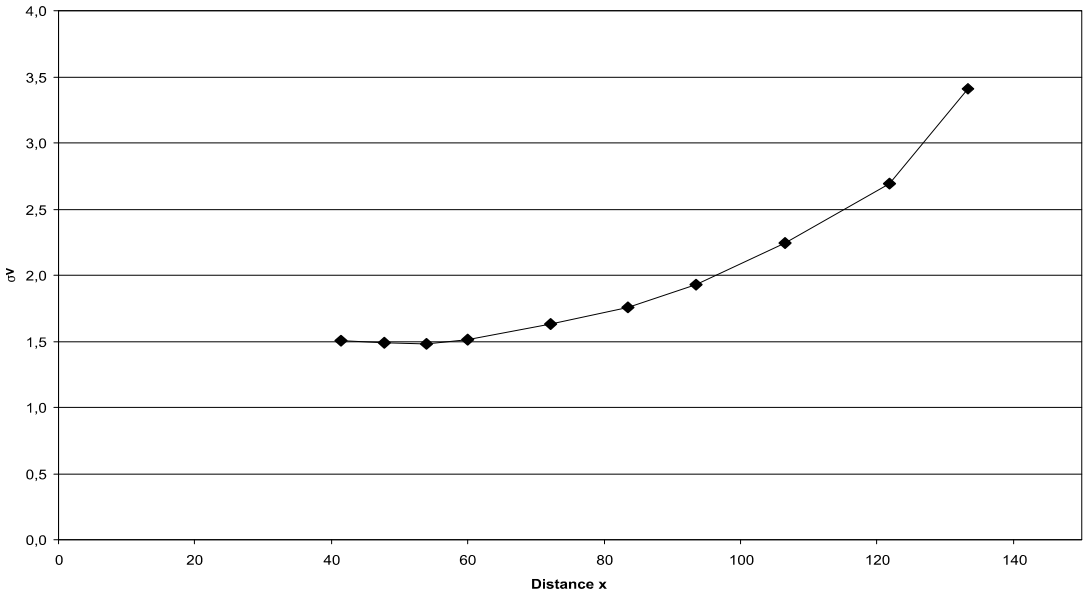

Fig. A.95: Comparison stress in the Dorygnathus rostrum construction. See chapter 6.4 for legend.

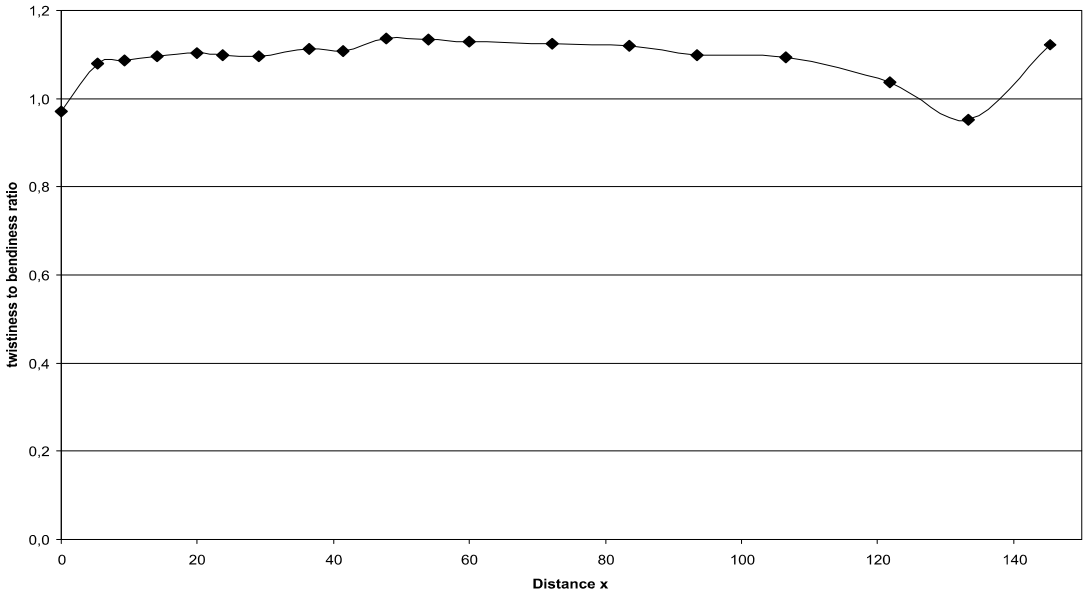

Fig. A.96: Twistiness to bendiness ratio in the Dorygnathus rostrum construction. See chapter 6.4 for legend.

A.13. Dsungaripterus skull construction (see also chapter 7.13)

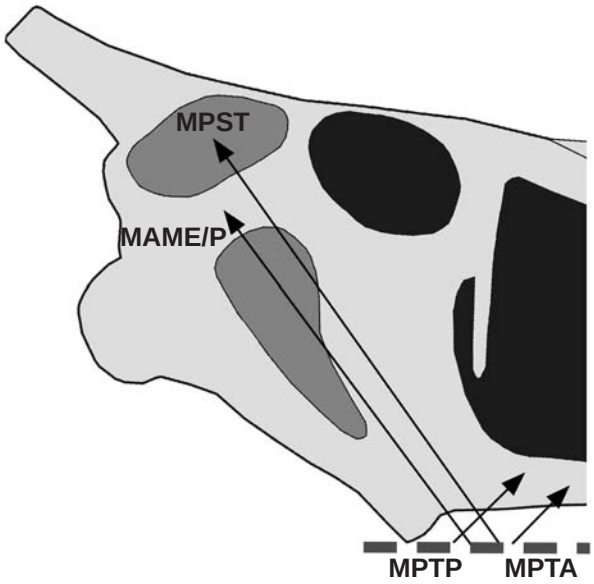

Fig A.97: Reconstruction of the principal pulling direction of the main adductor muscles in the skull of *Dsungaripterus*. See chapter 6 for abbreviations.

Muscles	F_1	l_1	α_1	F_2	l_2	α_1
MAME/P	36	9.99	53	1.73	207.81	127
MPST	92	14.3	55	6.47	203.49	125
MPTA	14	16.74	46	1.17	201.06	134
MPTP	88	7.37	44	2.77	233.96	136

Tab. A.25: Reconstructed lever parameters for the scaled Dsungaripterus skull construction. See chapter 6.2 for abbreviations.

	F_B	F_J	α_J
anterior end of rostrum	9.11	222.19	-48.42
1st tooth position	13.07	219.24	-47.73
1st to 4th tooth position	56.84	873.61	-47.53
last tooth position	26.92	209.20	-45.18
average	18.66	215.17	-46.71

Tab. A.26: Reconstructed bite and joint reaction forces and angle of joint reaction force in the scaled Dsungaripterus skull construction. Negative angle values mean anterodorsal direction of force. See chapter 6 for abbreviations.

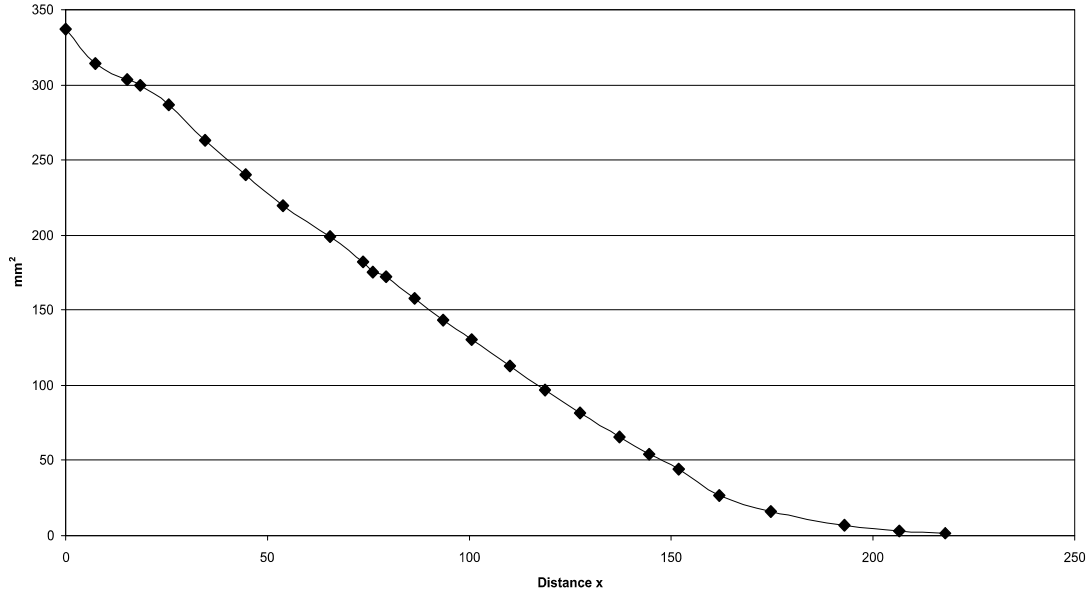

Fig A.98: Cross-sectional area of the Dsungaripterus rostrum construction. See chapter 6.4 for legend.

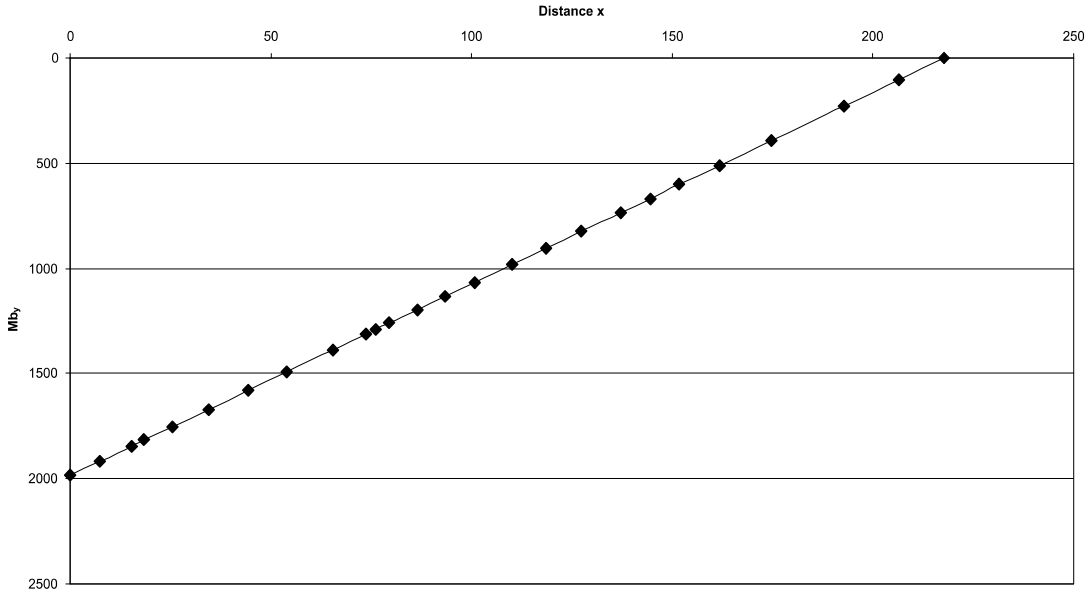

Fig A.99: Bending moments in the Dsungaripterus rostrum construction. See chapter 6.4 for legend.

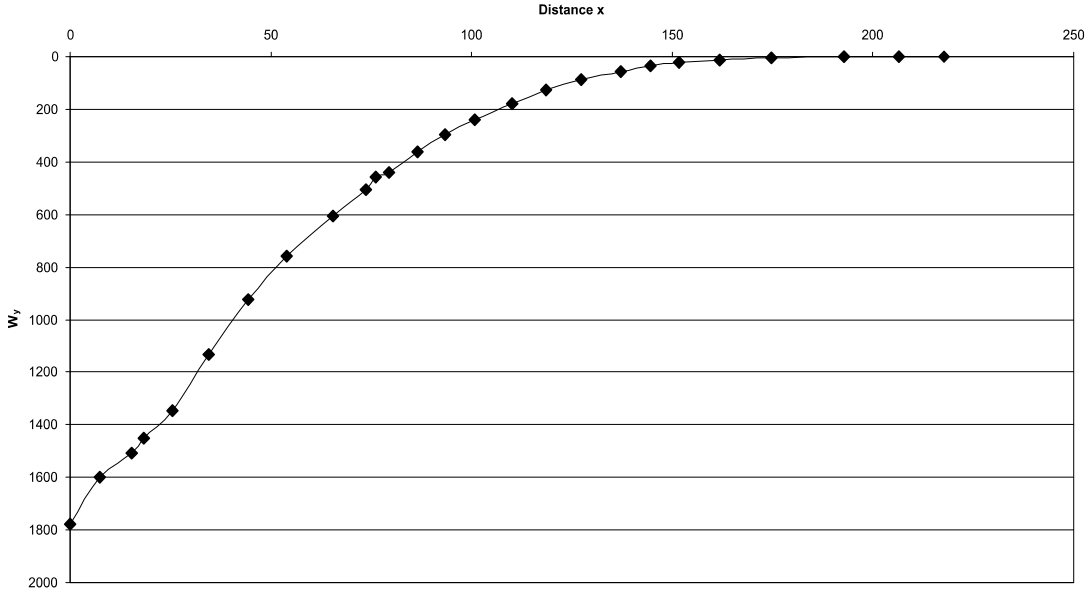

Fig A.100: Section modulus in the Dsungaripterus rostrum construction. See chapter 6.4 for legend.

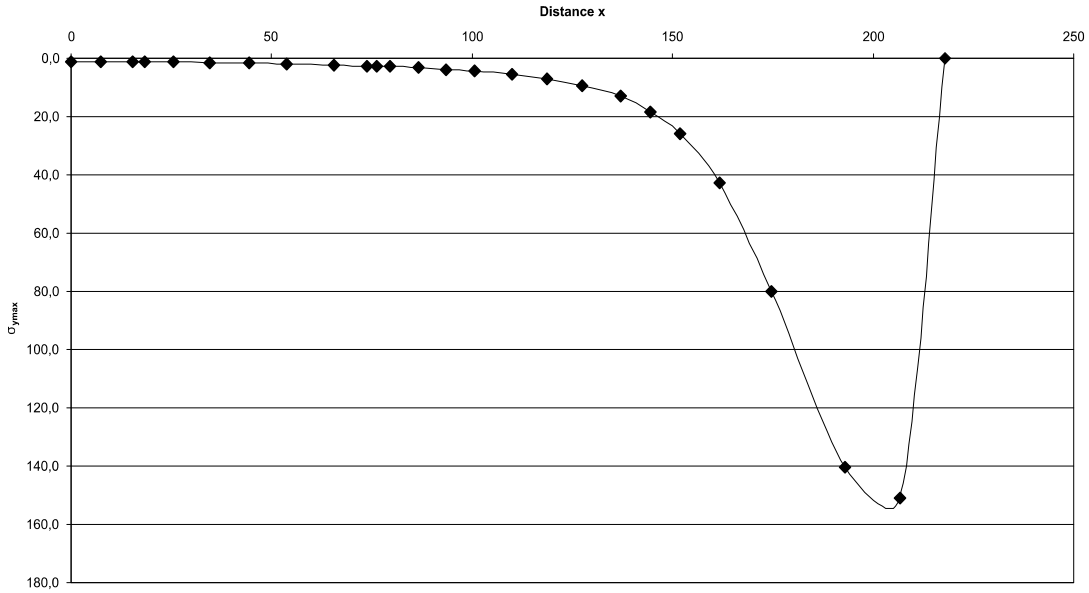

Fig A.101: Maximum bending stress in the Dsungaripterus rostrum construction. See chapter 6.4 for legend.

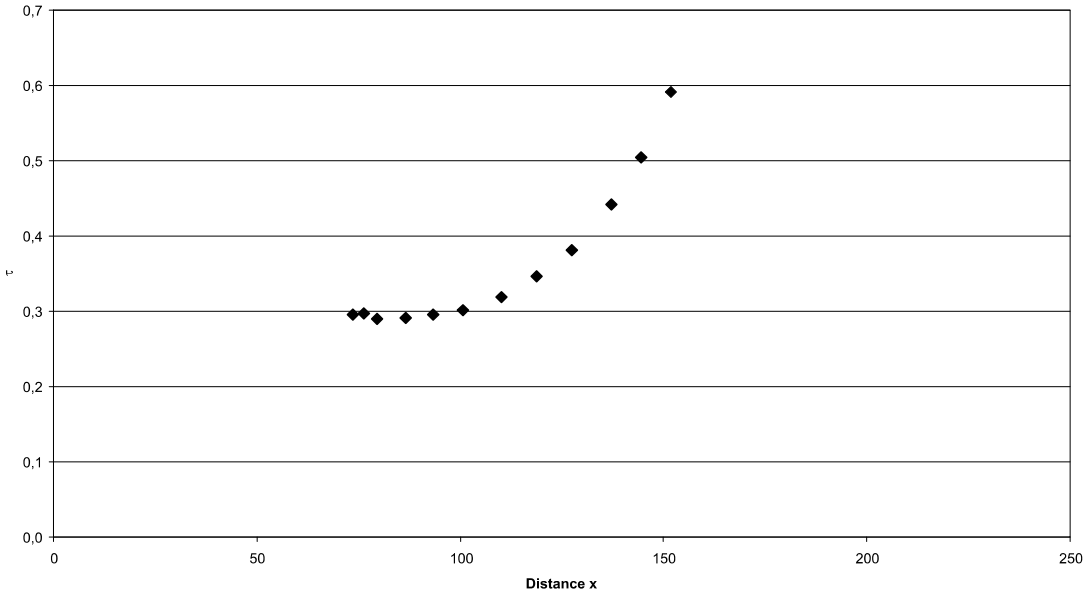

Fig. A.102: Shear stress in the Dsungaripterus rostrum construction. See chapter 6.4 for legend.

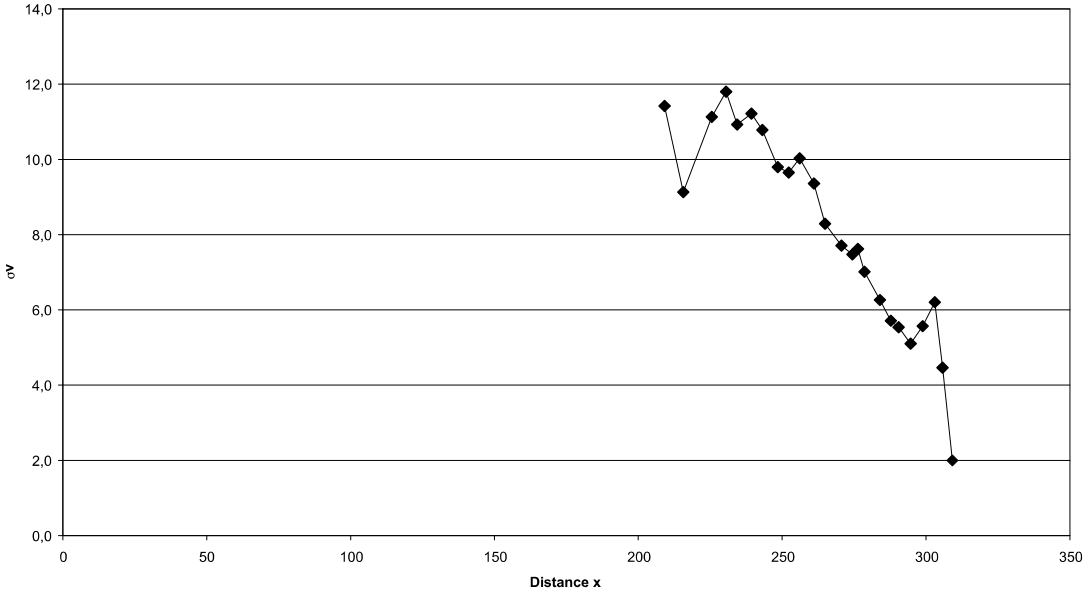

Fig. A.103: Comparison stress in the Dsungaripterus rostrum construction. See chapter 6.4 for legend.

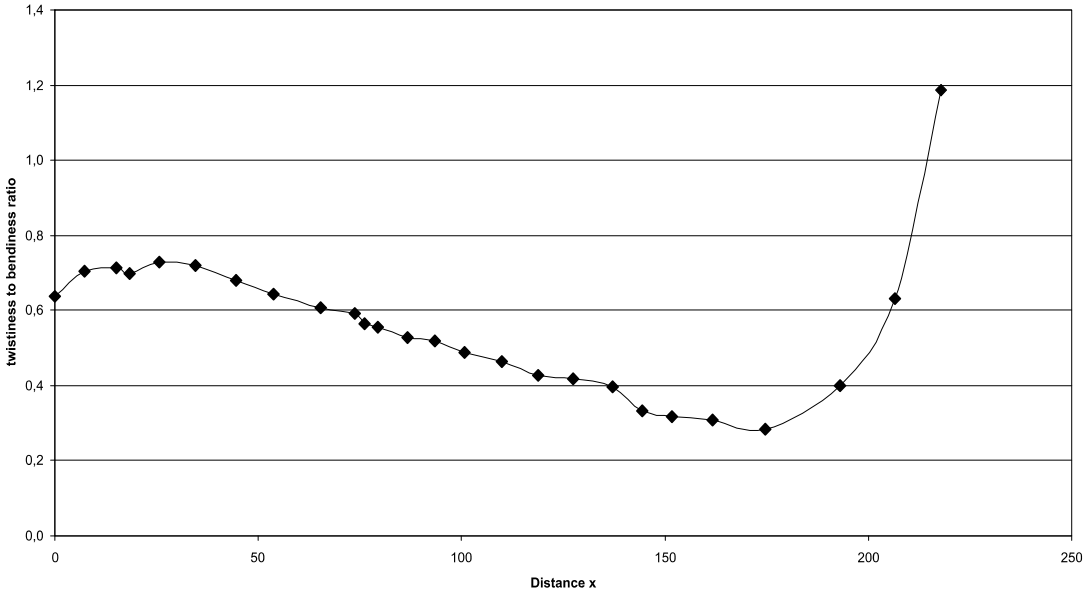

Fig. A.104: Twistiness to bendiness ratio in the Dsungaripterus rostrum construction. See chapter 6.4 for legend.

A.14. Eudimorphodon skull construction (see also chapter 7.14)

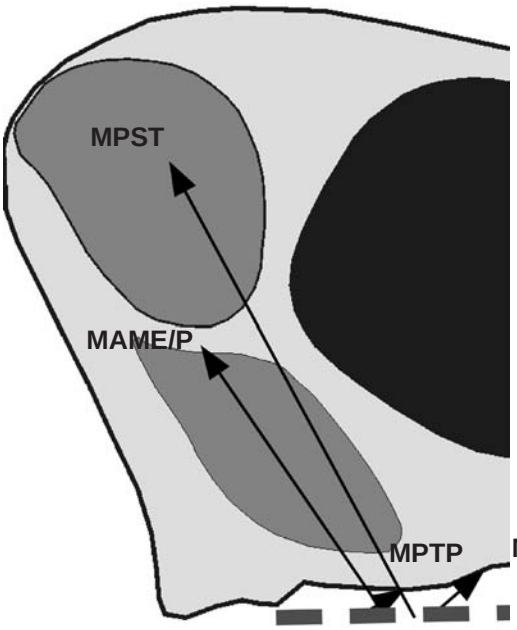

Fig A.105: Reconstruction of the principal pulling direction of the main adductor muscles in the skull of *Eudimorphodon*. See chapter 6 for abbreviations.

Muscles	F_1	l_1	α_1	F_2	l_2	α_1
MAME/P	36	11.83	56	2.83	150.62	124
MPST	92	15.69	62	9.84	146.76	118
MPTA	14	18.26	41	1.77	144.19	139
MPTP	88	9	31	5.16	153.45	149

Tab. A.27: Reconstructed lever parameters for the scaled Eudimorphodon skull construction. See chapter 6.2 for abbreviations.

	F_B	F_J	α_J
1st tooth position	13.65	213.09	-45.51
1st to 4th tooth position	61.45	847.25	-45.17
last tooth position	72.93	175.73	-31.82
average	31.11	108.07	-41.82

Tab. A.28: Reconstructed bite and joint reaction forces and angle of joint reaction force in the scaled Eudimorphodon skull construction. Negative angle values mean anterodorsal direction of force. See chapter 6.2 for abbreviations.

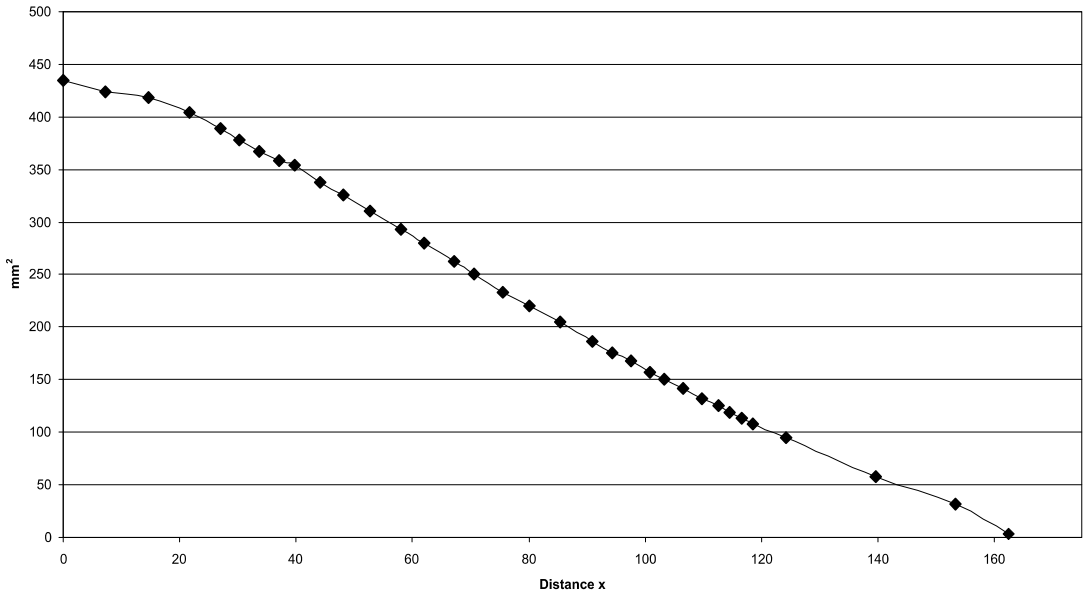

Fig A.106: Cross-sectional area of the Eudimorphodon rostrum construction. See chapter 6.4 for legend.

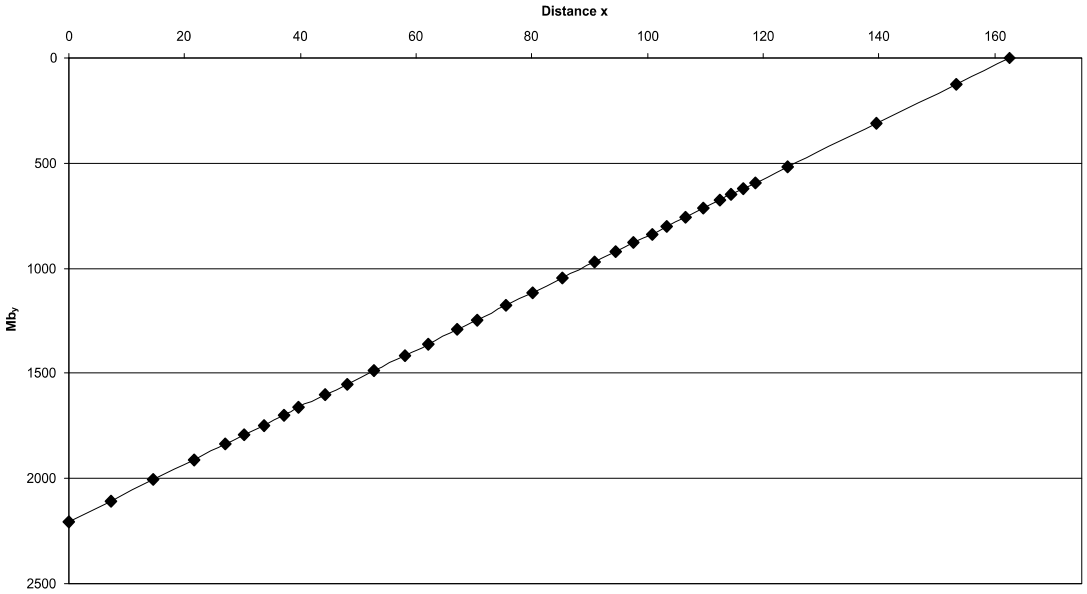

Fig A.107: Bending moments in the Eudimorphodon rostrum construction. See chapter 6.4 for legend.

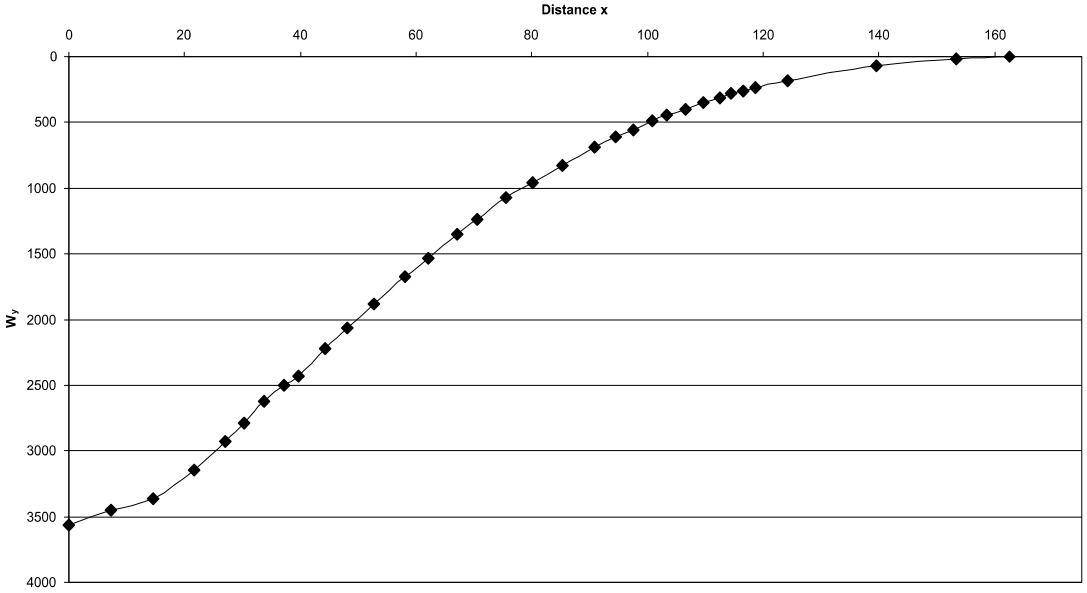

Fig A.108: Section modulus in the Eudimorphodon rostrum construction. See chapter 6.4 for legend.

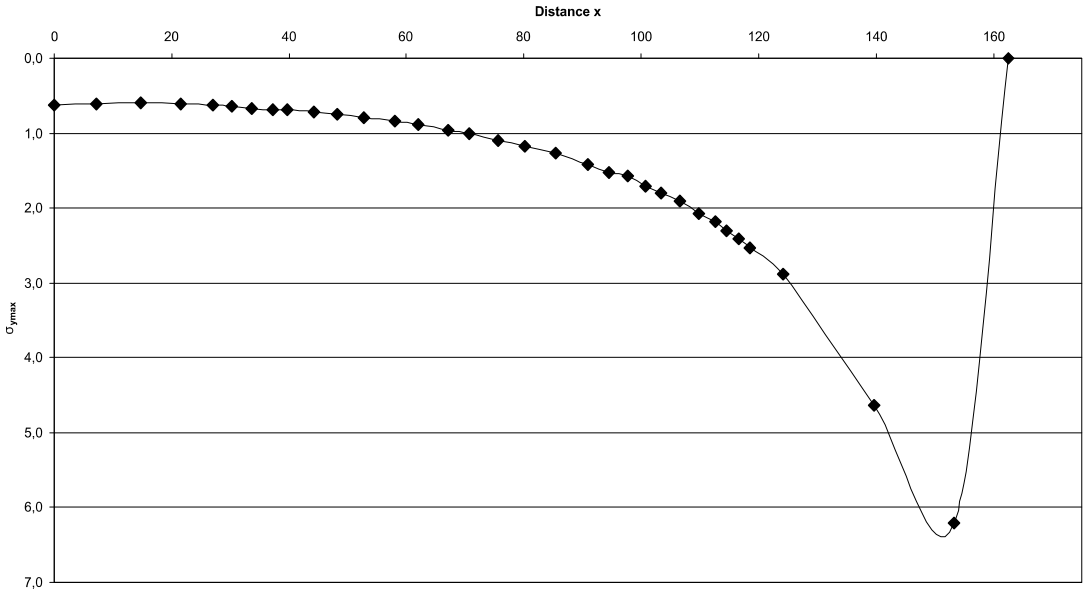

Fig A.109: Maximum bending stress in the Eudimorphodon rostrum construction. See chapter 6.4 for legend.

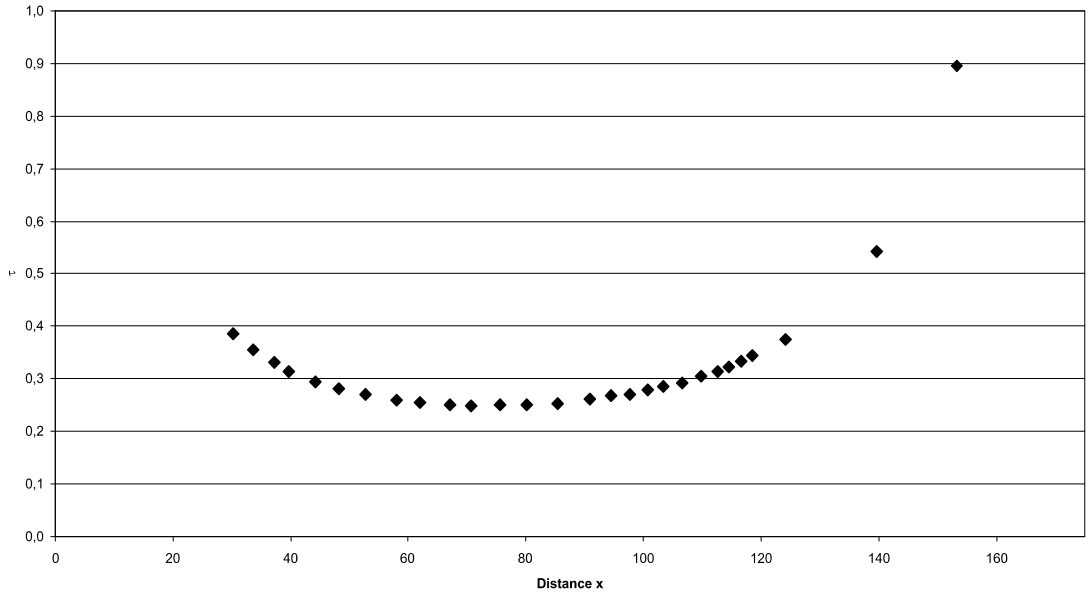

Fig. A.110: Shear stress in the Eudimorphodon rostrum construction. See chapter 6.4 for legend.

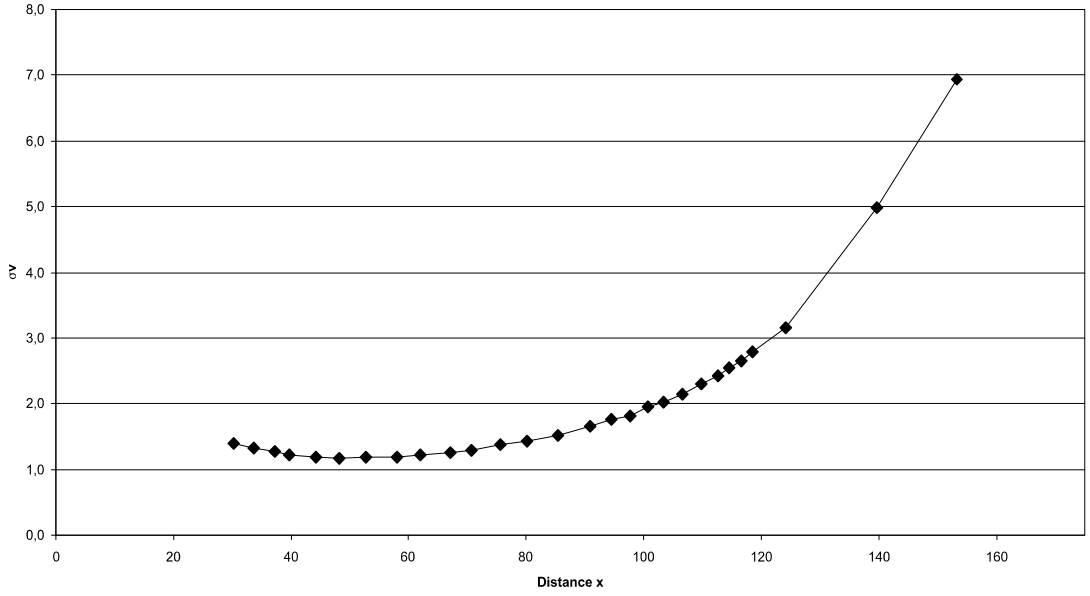

Fig. A.111: Comparison stress in the Eudimorphodon rostrum construction. See chapter 6.4 for legend.

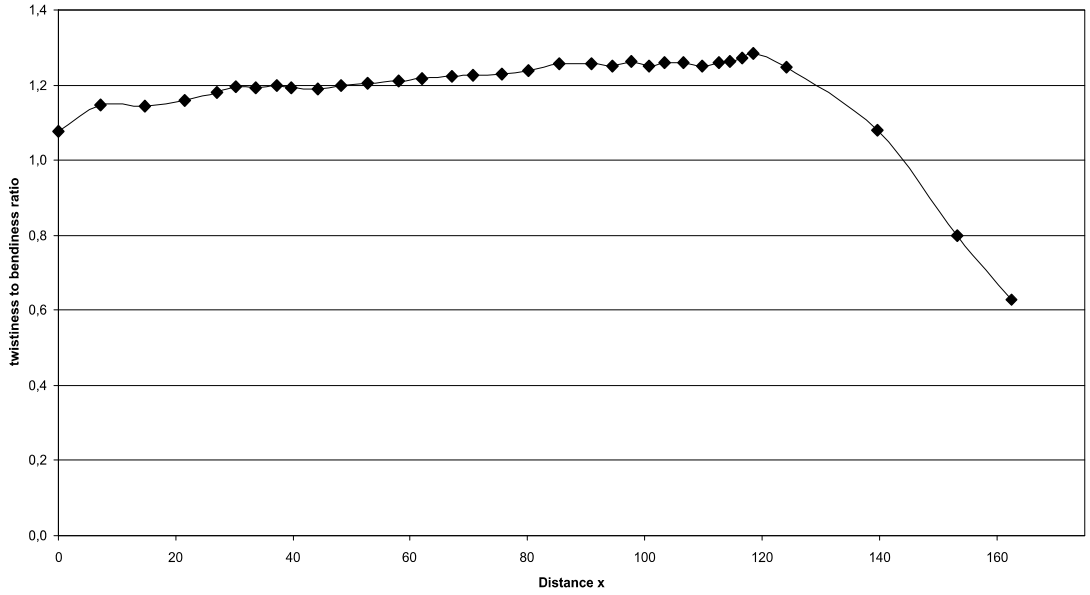

Fig. A.112: Twistiness to bendiness ratio in the Eudimorphodon rostrum construction. See chapter 6.4 for legend.

A.15. Gallodactylus skull construction (see also chapter 7.15)

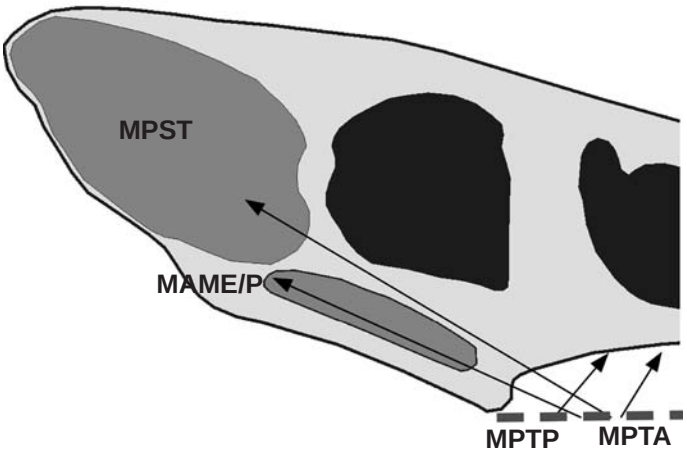

Fig A.113: Reconstruction of the principal pulling direction of the main adductor muscles in the skull of *Gallodactylus*. See chapter 6 for abbreviations.

Muscles	F_1	l_1	α_1	F_2	l_2	α_1
MAME/P	36	16.59	24	2.78	214.84	156
MPST	92	22.24	31	9.78	209.18	149
MPTA	14	24.3	58	1.64	207.13	122
MPTP	88	11.44	50	4.58	219.98	130

Tab. A.29: Reconstructed lever parameters for the scaled Gallodactylus skull construction. See chapter 6.2 for abbreviations.

	F_B	F_J	α_J
1st tooth position	10.18	219.26	-36.73
1st to 4th tooth position	42.18	876.18	-36.65
last tooth position	12.18	218.07	-36.31
average	11.11	218.71	-36.54

Tab. A.30: Reconstructed bite and joint reaction forces and angle of joint reaction force in the scaled Gallodactylus skull construction. Negative angle values mean anterodorsal direction of force. See chapter 6.2 for abbreviations.

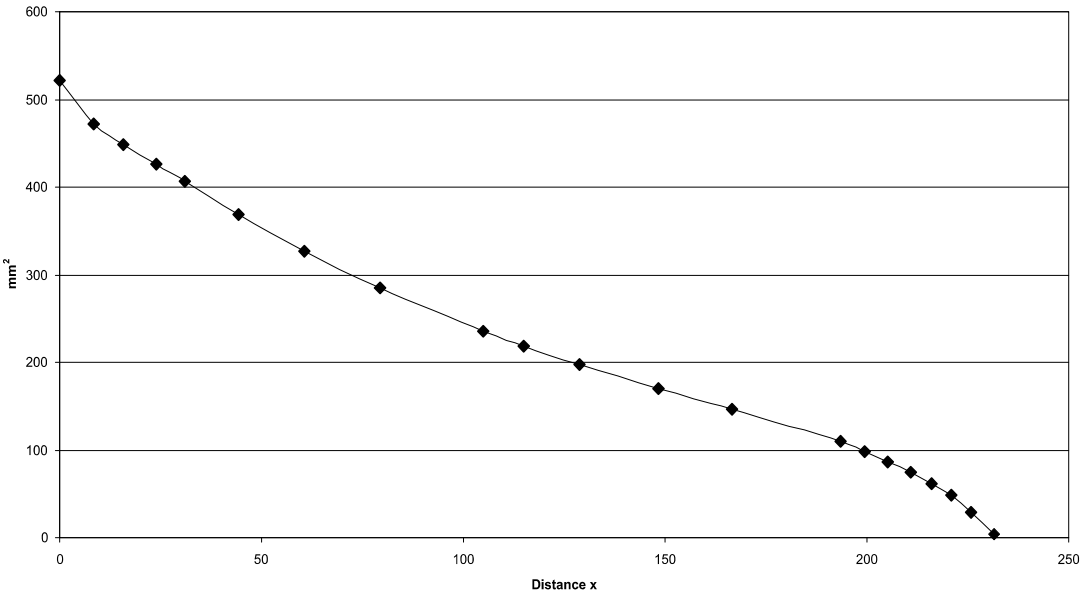

Fig A.114: Cross-sectional area of the Gallodactylus rostrum construction. See chapter 6.4 for legend.

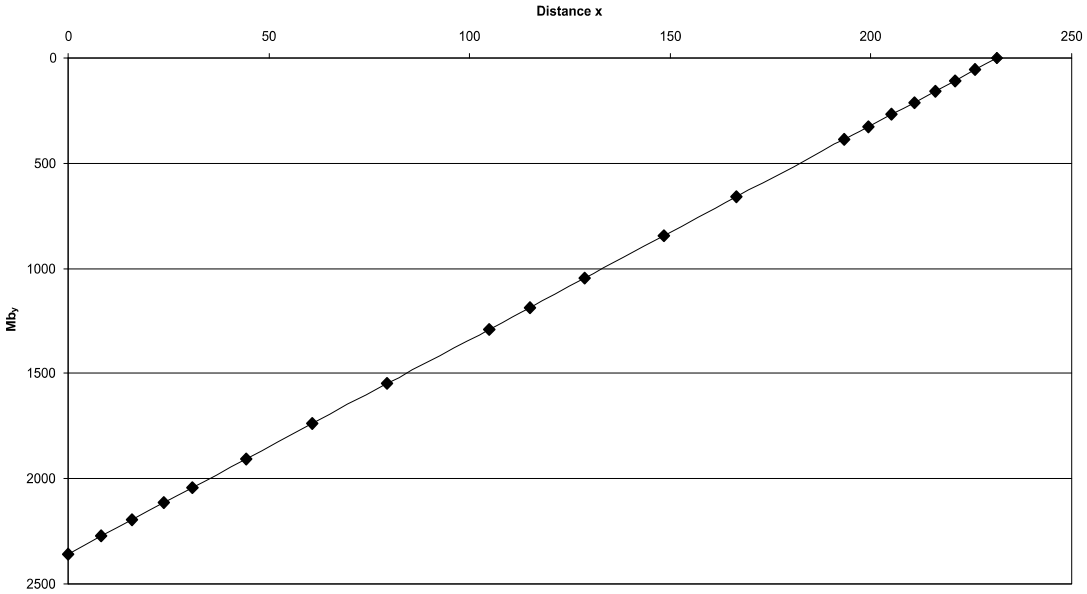

Fig A.115: Bending moments in the Gallodactylus rostrum construction. See chapter 6.4 for legend.

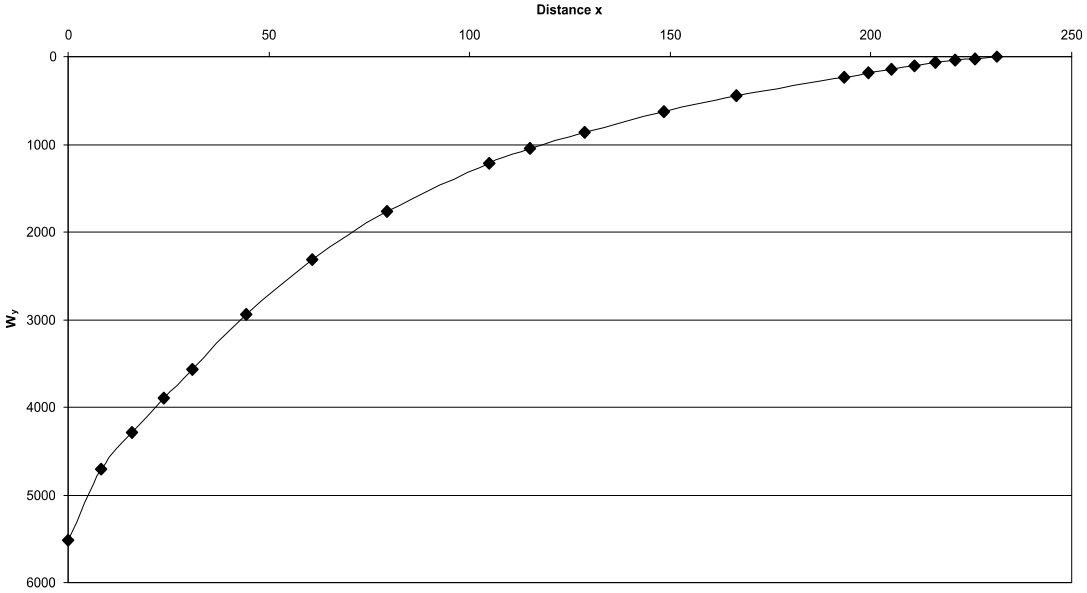

Fig A.116: Section modulus in the Gallodactylus rostrum construction. See chapter 6.4 for legend.

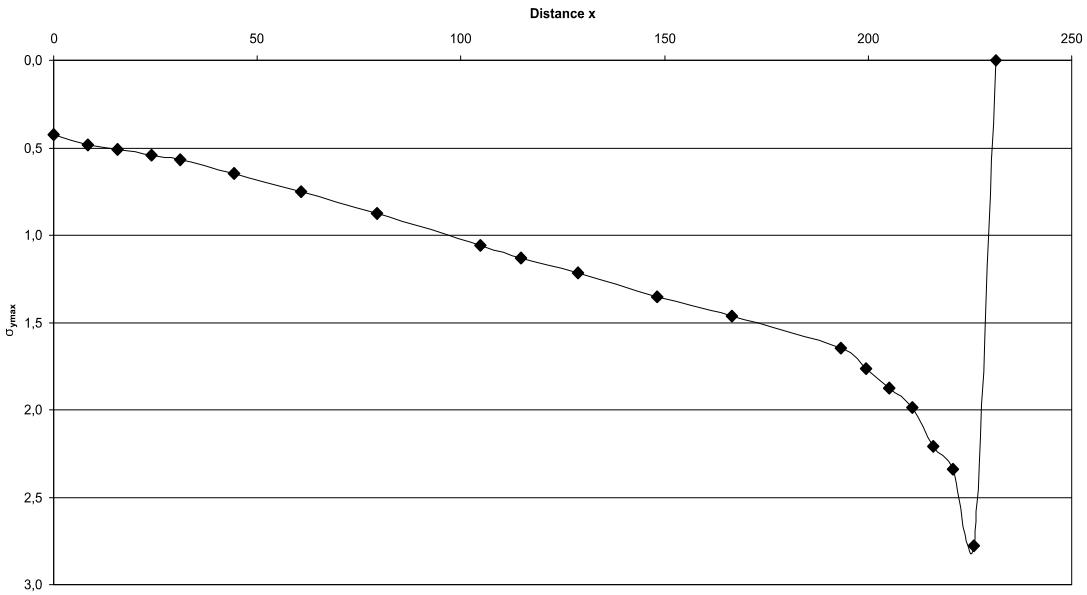

Fig A.117: Maximum bending stress in the Gallodactylus rostrum construction. See chapter 6.4 for legend.

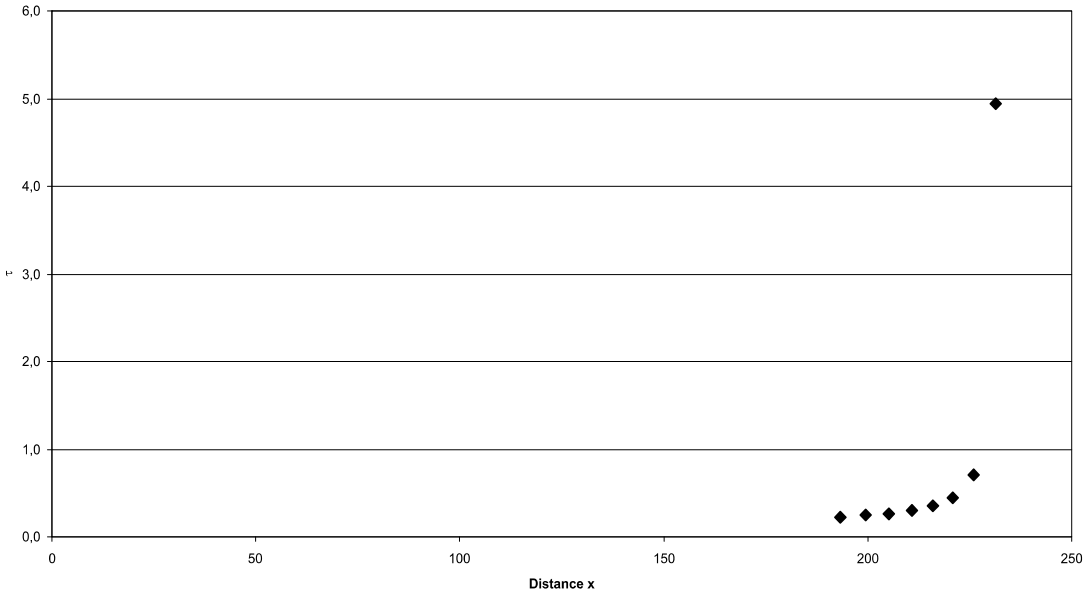

Fig. A.118: Shear stress in the Gallodactylus rostrum construction. See chapter 6.4 for legend.

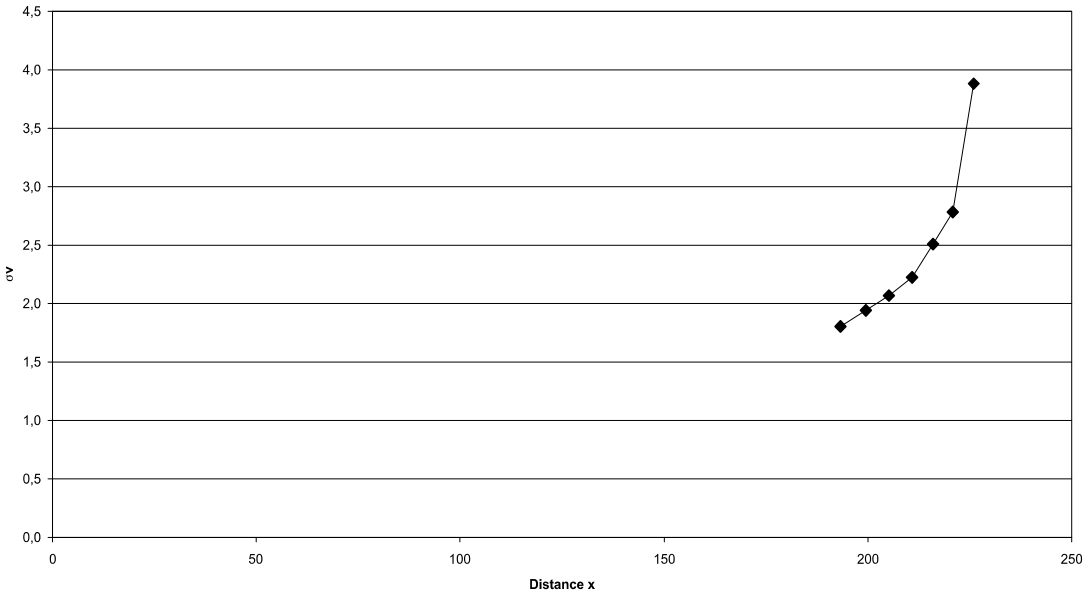

Fig. A.119: Comparison stress in the Gallodactylus rostrum construction. See chapter 6.4 for legend.

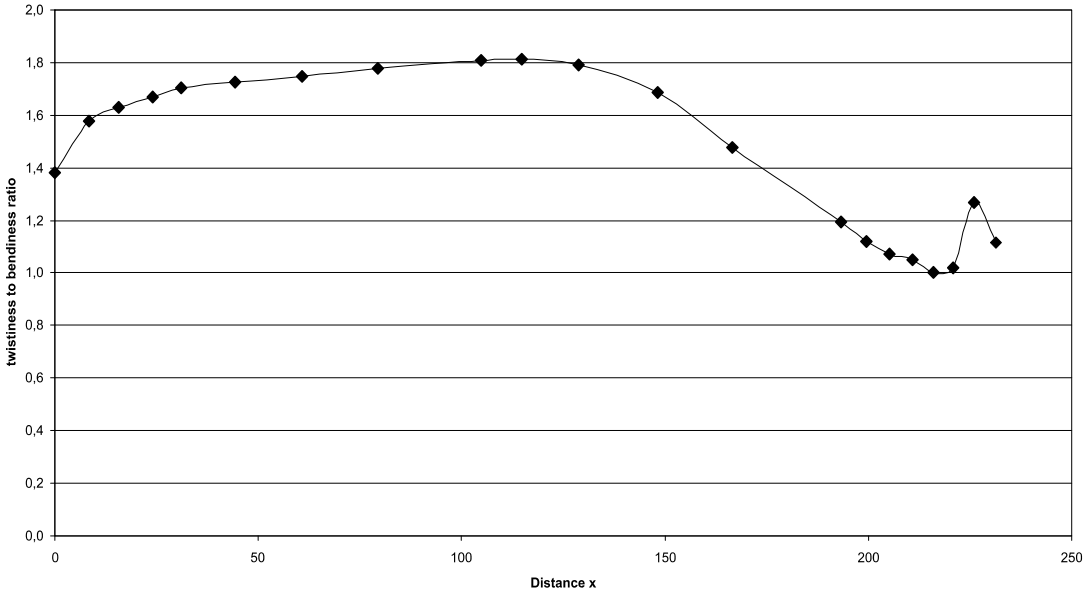

Fig. A.120: Twistiness to bendiness ratio in the Gallodactylus rostrum construction. See chapter 6.4 for legend.

A.16. Germanodactylus skull construction (see also chapter 7.16)

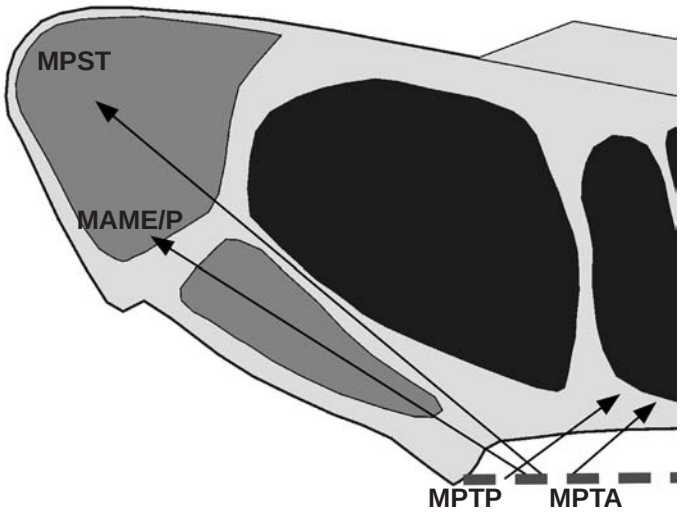

Fig A.121: Reconstruction of the principal pulling direction of the main adductor muscles in the skull of *Germanodactylus*. See chapter 6 for abbreviations.

Muscles	F_1	l_1	α_1	F_2	l_2	α_1
MAME/P	36	10.93	32	1.65	238.50	148
MPST	92	14.01	36	5.48	235.41	140
MPTA	14	19.16	41	1.16	230.27	139
MPTP	88	8.10	36	2.95	241.33	144

Tab. A.31: Reconstructed lever parameters for the scaled Germanodactylus skull construction. See chapter 6.2 for abbreviations.

	F_B	F_J	α_J
anterior end of rostrum	6.54	225.79	-35.96
1st tooth position	7.23	225.39	-35.82
1st to 4th tooth position	30.51	900.62	-35.73
last tooth position	20.18	219.00	-33.43
average	11.16	223.13	-34.99

Tab. A.32: Reconstructed bite and joint reaction forces and angle of joint reaction force in the scaled Germanodactylus skull construction. Negative angle values mean anterodorsal direction of force. See chapter 6.2 for abbreviations.

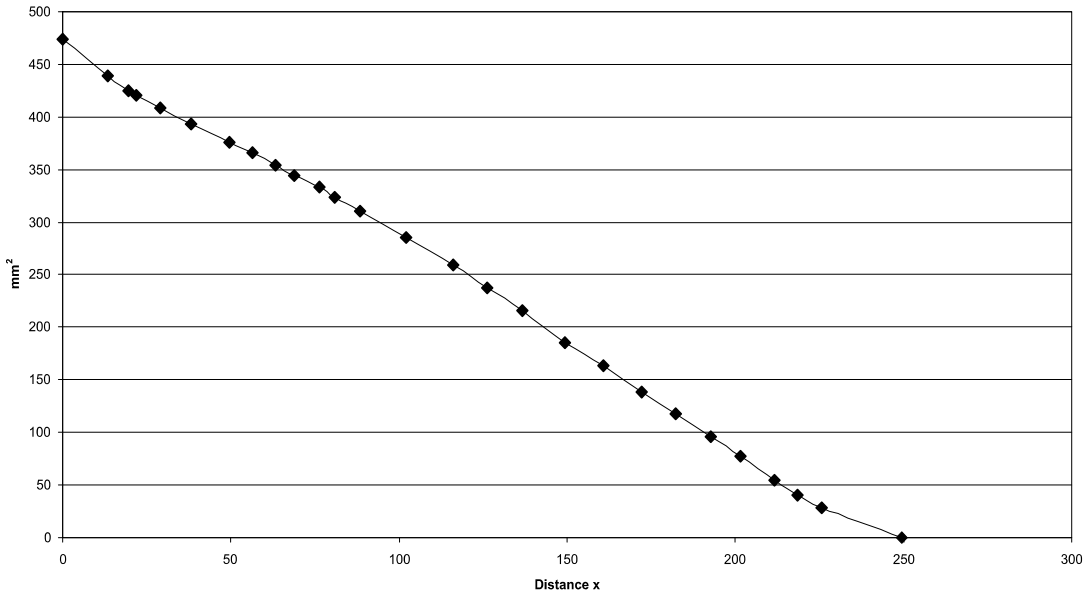

Fig A.122: Cross-sectional area of the Germanodactylus rostrum construction. See chapter 6.4 for legend.

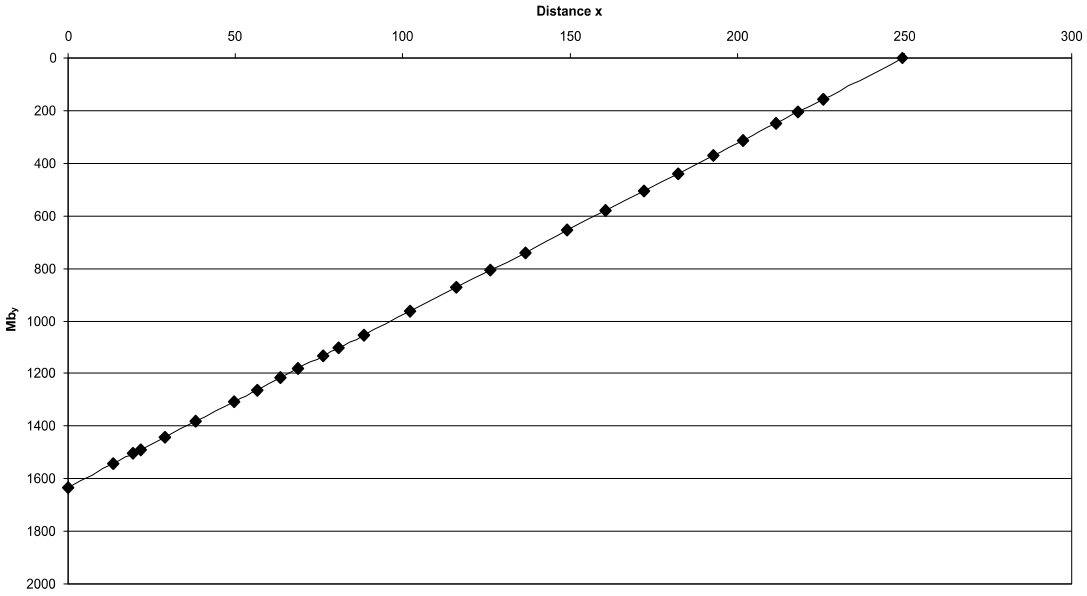

Fig A.123: Bending moments in the Germanodactylus rostrum construction. See chapter 6.4 for legend.

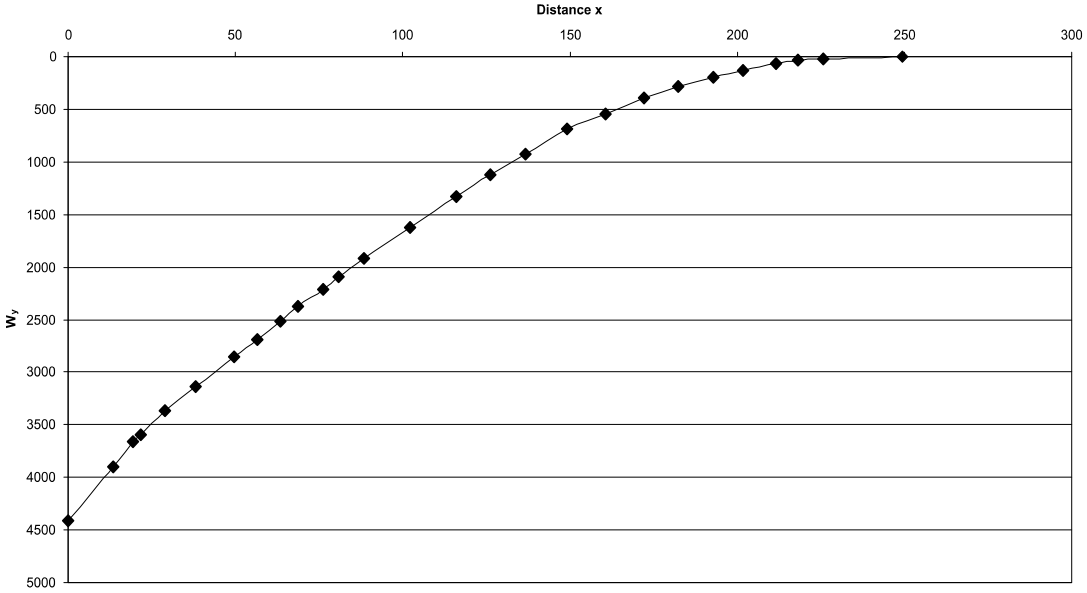

Fig A.124: Section modulus in the Germanodactylus rostrum construction. See chapter 6.4 for legend.

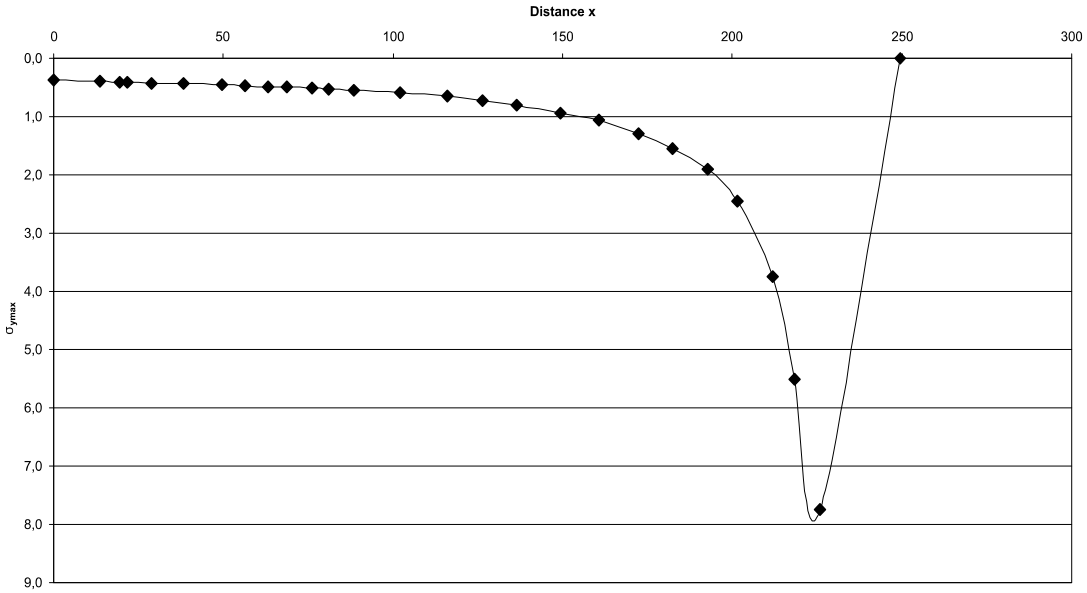

Fig A.125: Maximum bending stress in the Germanodactylus rostrum construction. See chapter 6.4 for legend.

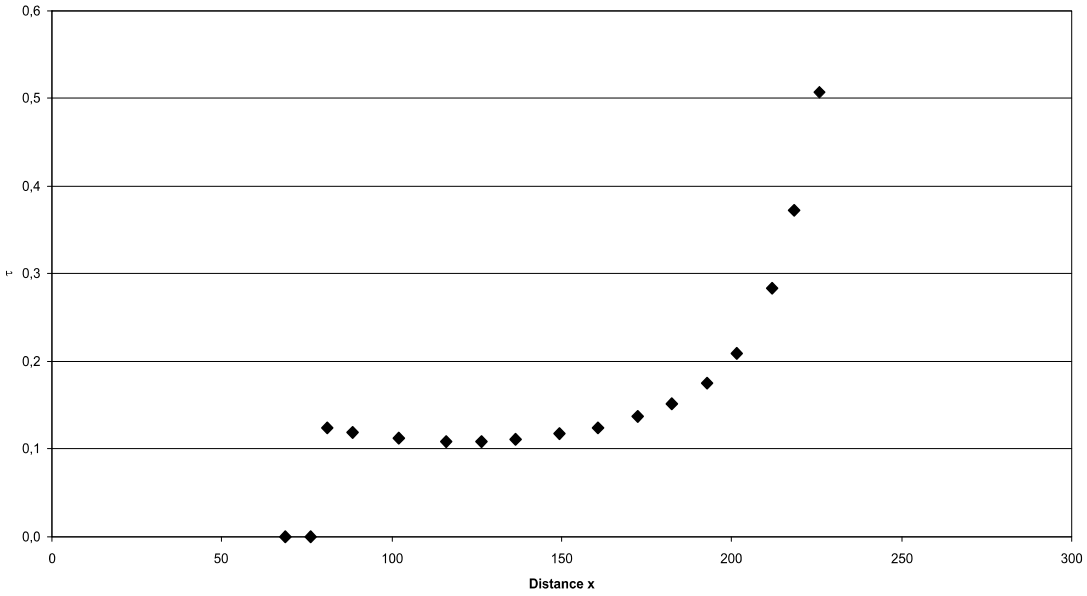

Fig. A.126: Shear stress in the Germanodactylus rostrum construction. See chapter 6.4 for legend.

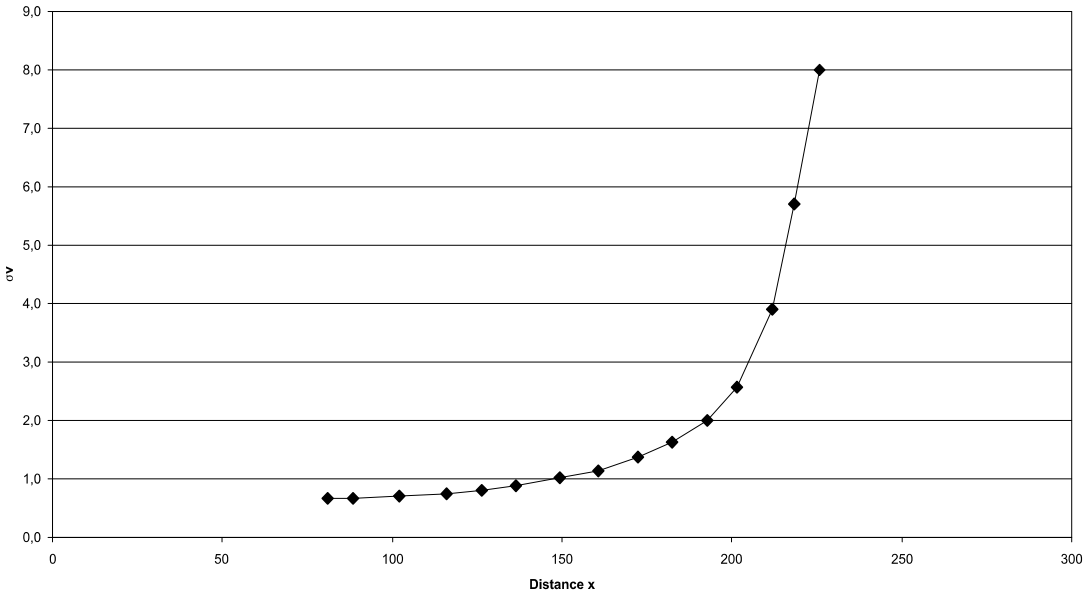

Fig. A.127: Comparison stress in the Germanodactylus rostrum construction. See chapter 6.4 for legend.

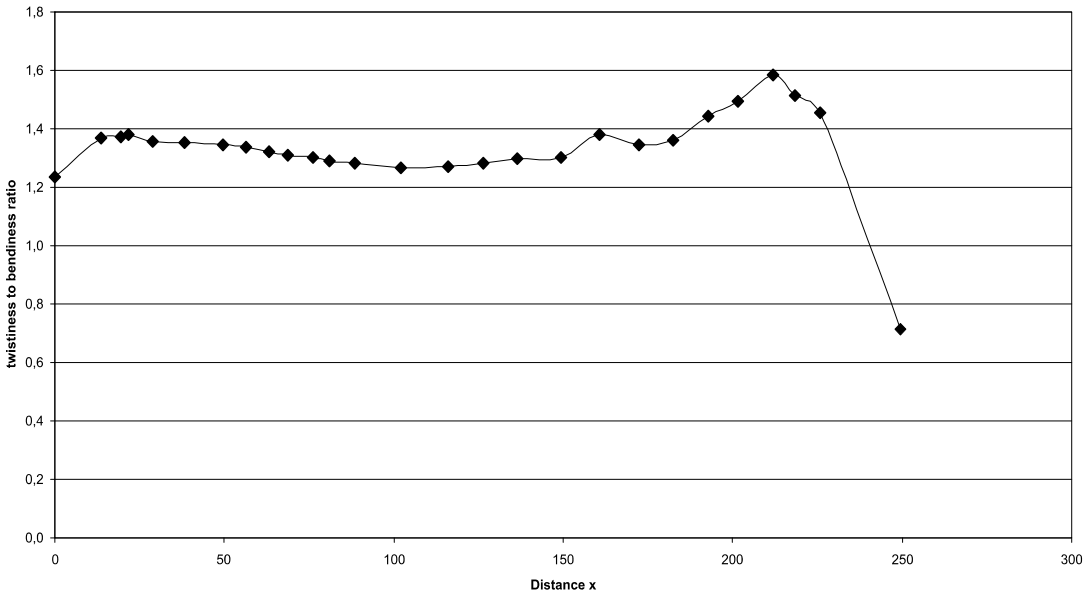

Fig. A.128: Twistiness to bendiness ratio in the Germanodactylus rostrum construction. See chapter 6.4 for legend.

A.17. Gnathosaurus skull construction (see also chapter 7.17)

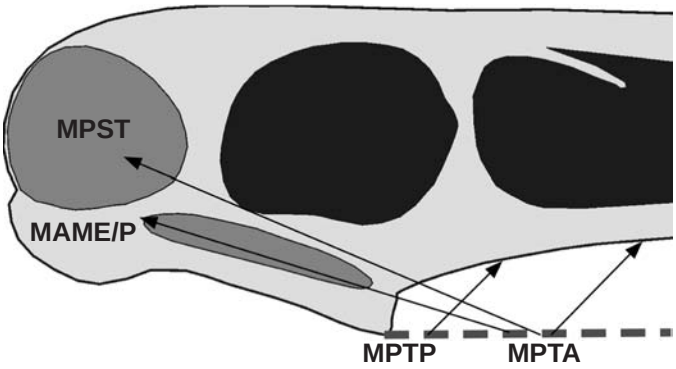

Fig A.129: Reconstruction of the principal pulling direction of the main adductor muscles in the skull of *Gnathosaurus*. See chapter 6 for abbreviations.

Muscles	F_1	l_1	α_1	F_2	l_2	α_1
MAME/P	36	26.86	17	2.67	362.63	163
MPST	92	33.36	23	8.62	356.13	157
MPTA	14	38.85	46	2.16	353.36	134
MPTP	88	9.33	45	2.16	380.36	135

Tab. A.33: Reconstructed lever parameters for the scaled Gnathosaurus skull construction. See chapter 6.2 for abbreviations.

	F_B	F_J	α_J
1st tooth position	6.22	221.75	-30.50
1st to 4th tooth position	25.24	886.82	-30.48
last tooth position	16.82	216.56	-28.08
average	9.62	220.06	-29.73

Tab. A.34: Reconstructed bite and joint reaction forces and angle of joint reaction force in the scaled Gnathosaurus skull construction. Negative angle values mean anterodorsal direction of force. See chapter 6.2 for abbreviations.

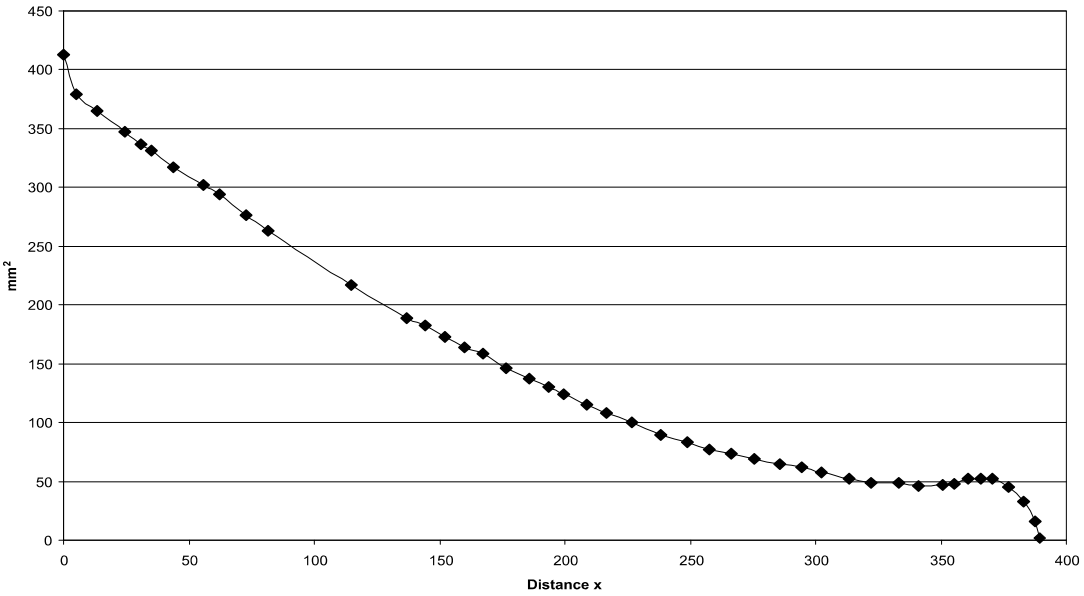

Fig A.130: Cross-sectional area of the Gnathosaurus rostrum construction. See chapter 6.4 for legend.

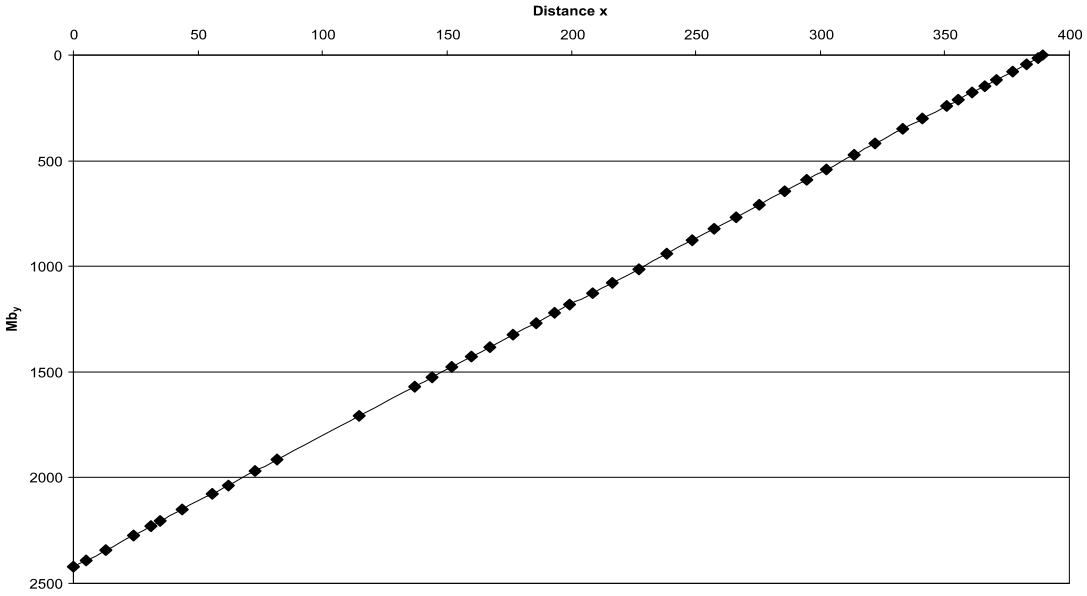

Fig A.131: Bending moments in the Gnathosaurus rostrum construction. See chapter 6.4 for legend.

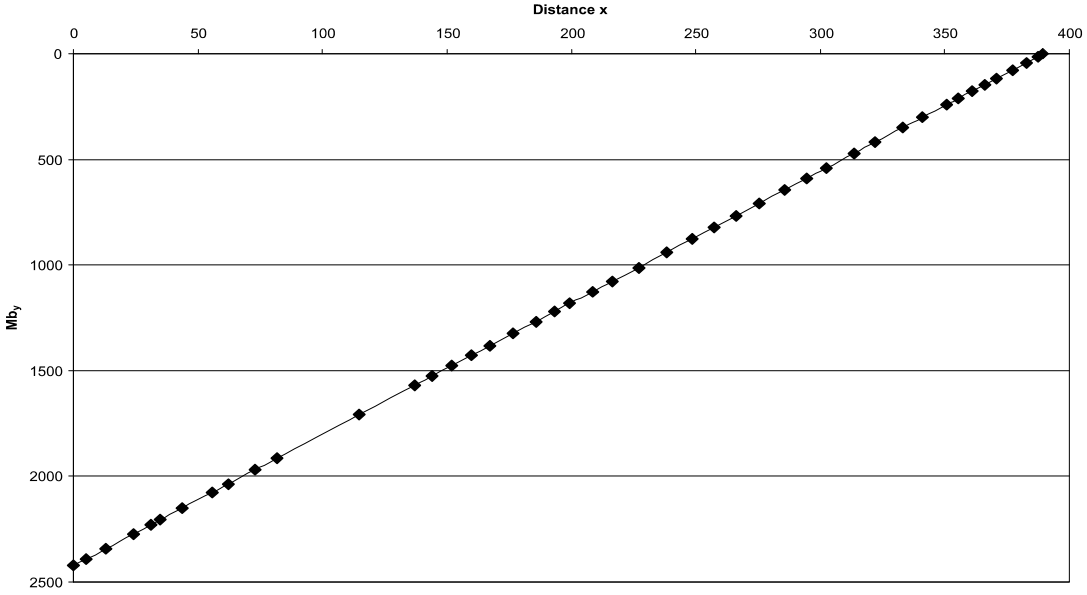

Fig A.132: Section modulus in the Gnathosaurus rostrum construction. See chapter 6.4 for legend.

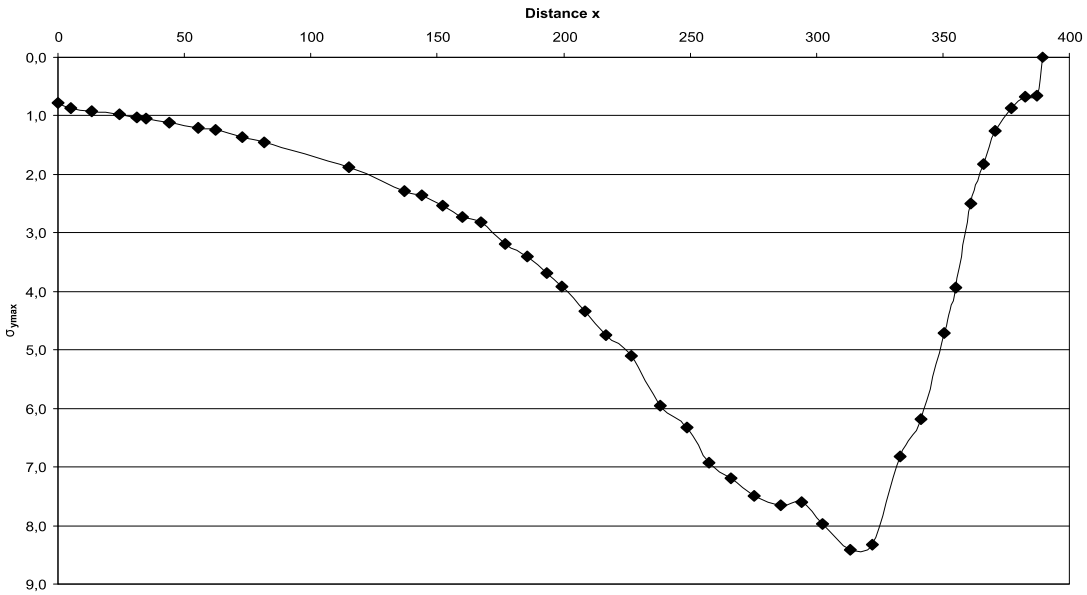

Fig A.133: Maximum bending stress in the Gnathosaurus rostrum construction. See chapter 6.4 for legend.

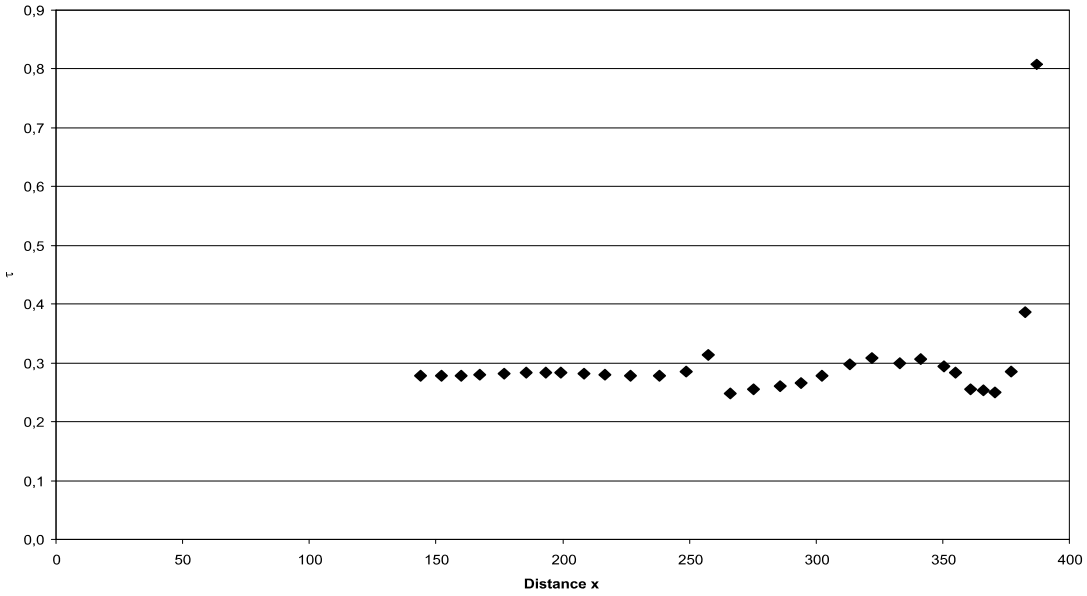

Fig. A.134: Shear stress in the Gnathosaurus rostrum construction. See chapter 6.4 for legend.

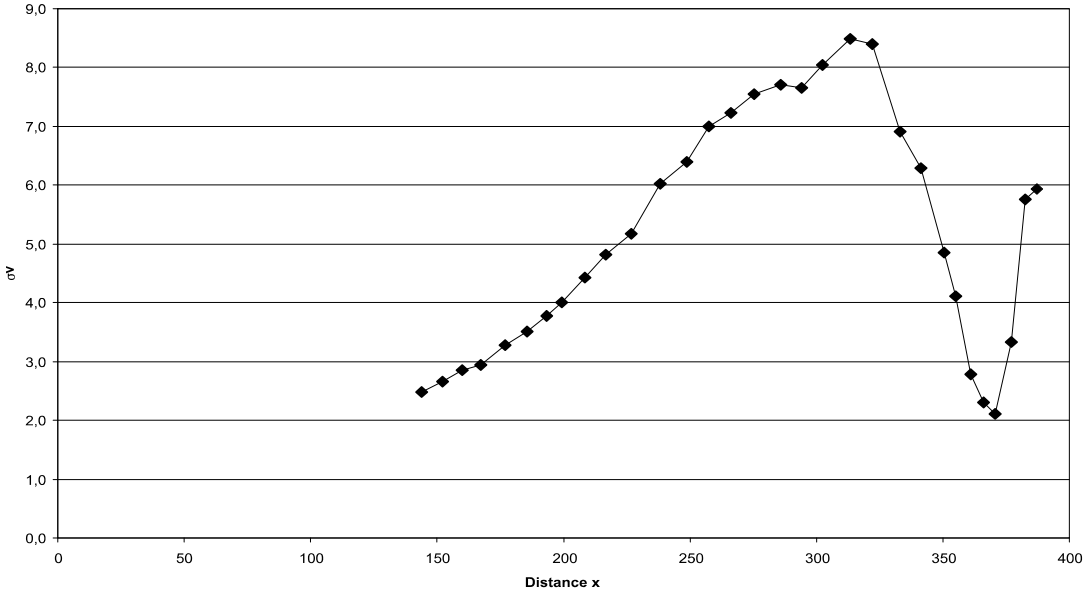

Fig. A.135: Comparison stress in the Gnathosaurus rostrum construction. See chapter 6.4 for legend.

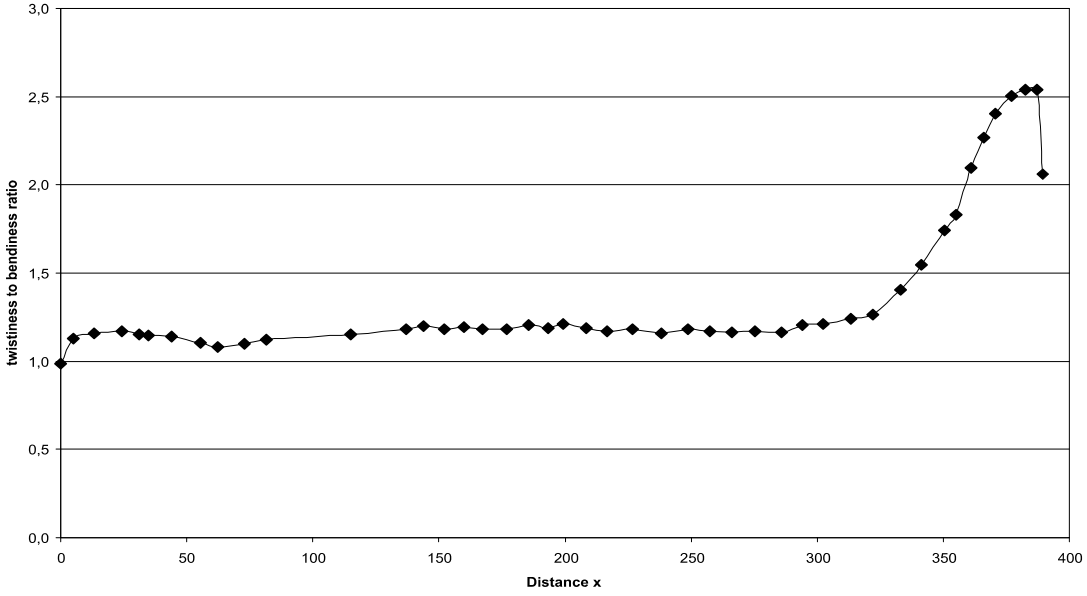

Fig. A.136: Twistiness to bendiness ratio in the Gnathosaurus rostrum construction. See chapter 6.4 for legend.

A.18. Huanhepterus skull construction (see also chapter 7.18)

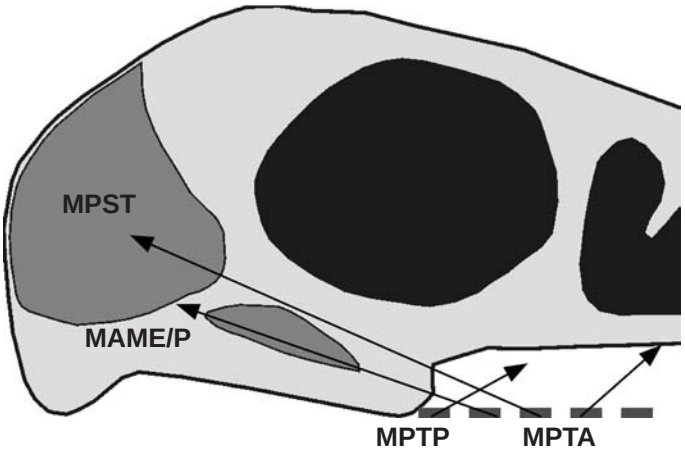

Fig A.137: Reconstruction of the principal pulling direction of the main adductor muscles in the skull of *Huanhepterus*. See chapter 6 for abbreviations.

Muscles	F_1	l_1	α_1	F_2	l_2	α_1
MAME/P	36	11.63	23	1.39	300.29	157
MPST	92	24.01	26	7.61	290.18	154
MPTA	14	23.95	35	1.19	282.21	145
MPTP	88	5.14	39	1.48	306.68	141

Tab. A.35: Reconstructed lever parameters for the scaled Huanhepterus skull construction. See chapter 6.2 for abbreviations.

	F_B	F_J	α_J
1st tooth position	5.16	225.79	-29.93
1st to 4th tooth position	20.93	903.02	-29.91
last tooth position	80.12	199.28	-10.9
average	14.10	231.16	-29.08

Tab. A.36: Reconstructed bite and joint reaction forces and angle of joint reaction force in the scaled Huanhepterus skull construction. Negative angle values mean anterodorsal direction of force. See chapter 6.2 for abbreviations.

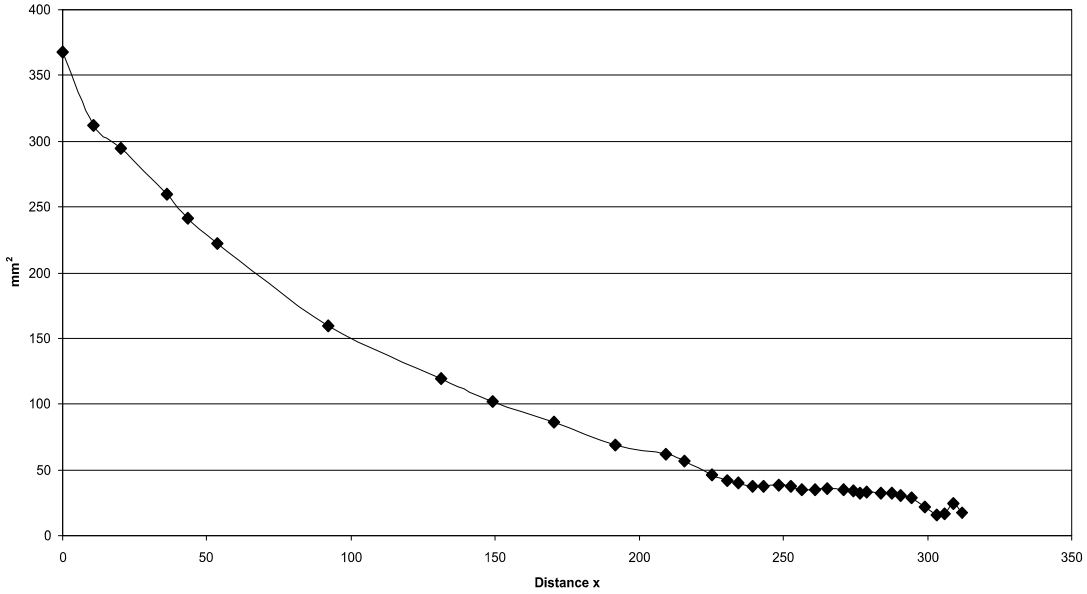

Fig A.138: Cross-sectional area of the Huanhepterus rostrum construction. See chapter 6.4 for legend.

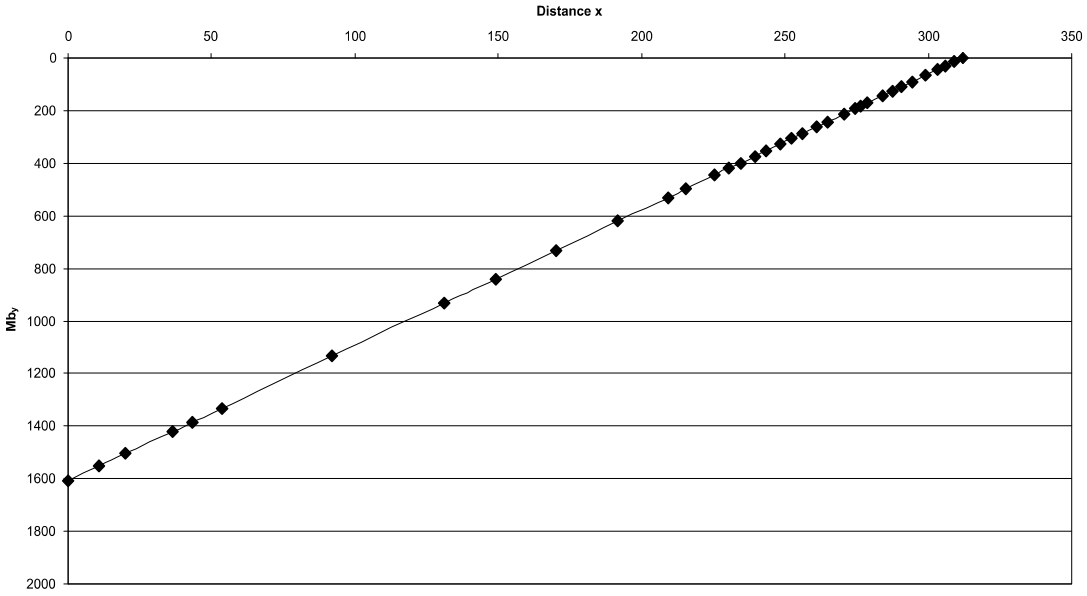

Fig A.139: Bending moments in the Huanhepterus rostrum construction. See chapter 6.4 for legend.

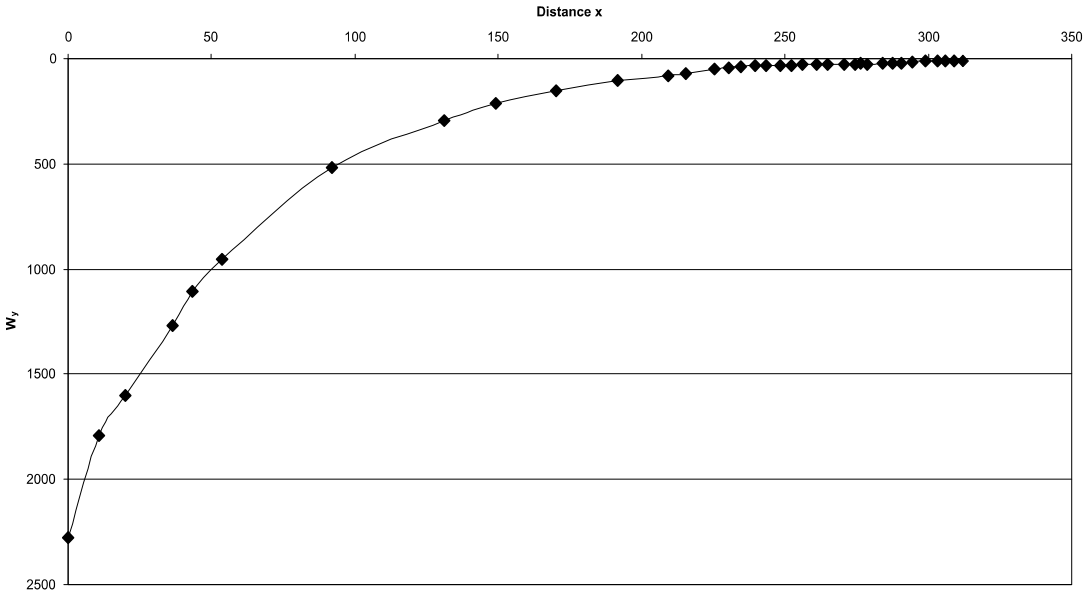

Fig A.140: Section modulus in the Huanhepterus rostrum construction. See chapter 6.4 for legend.

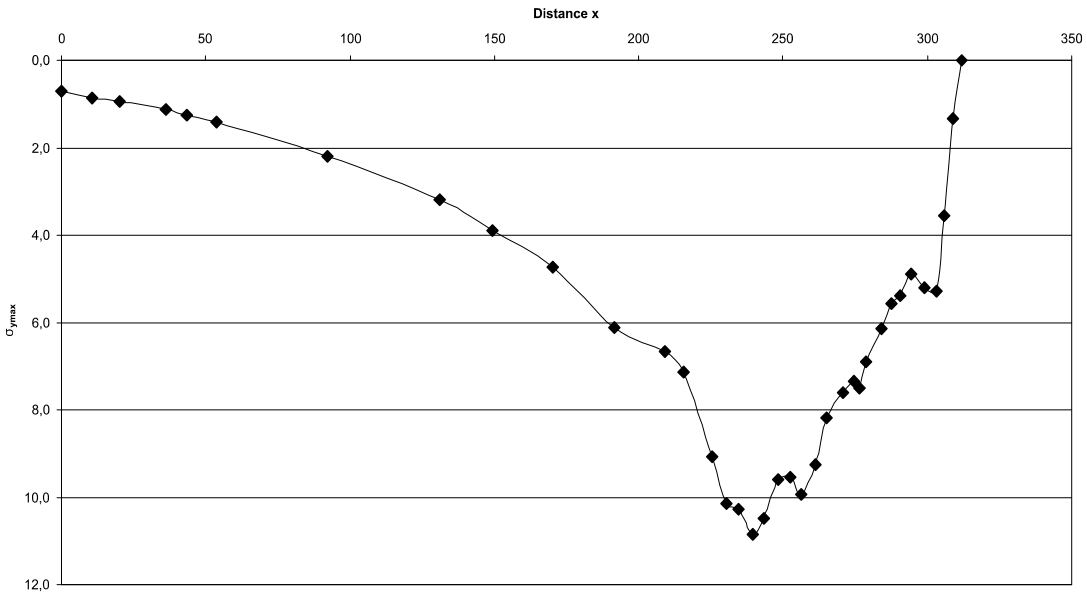

Fig A.141: Maximum bending stress in the Huanhepterus rostrum construction. See chapter 6.4 for legend.

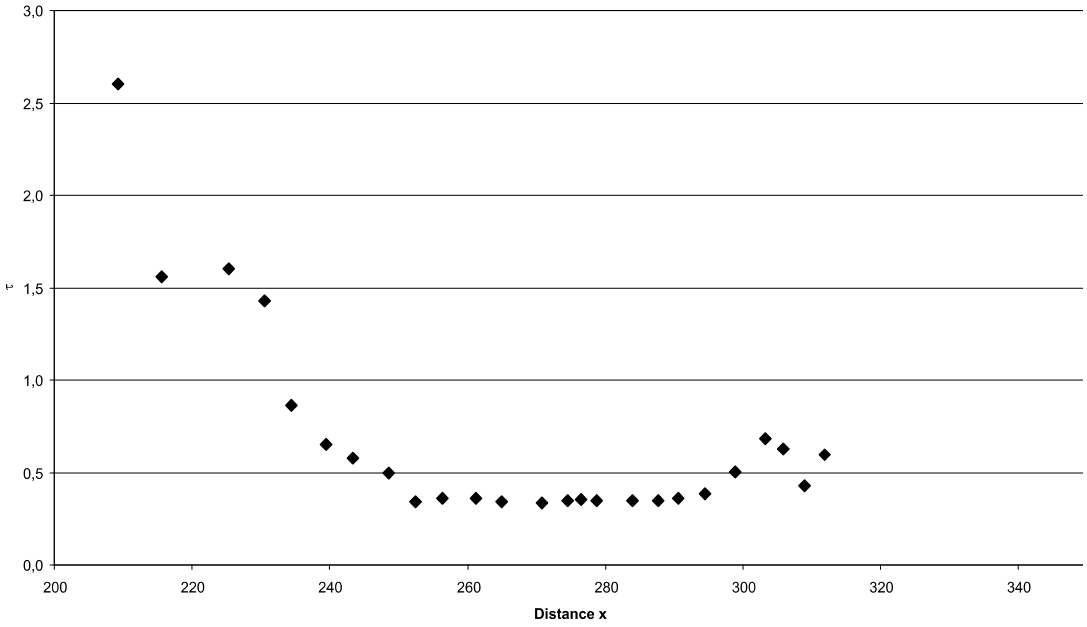

Fig. A.142: Shear stress in the Huanhepterus rostrum construction. See chapter 6.4 for legend.

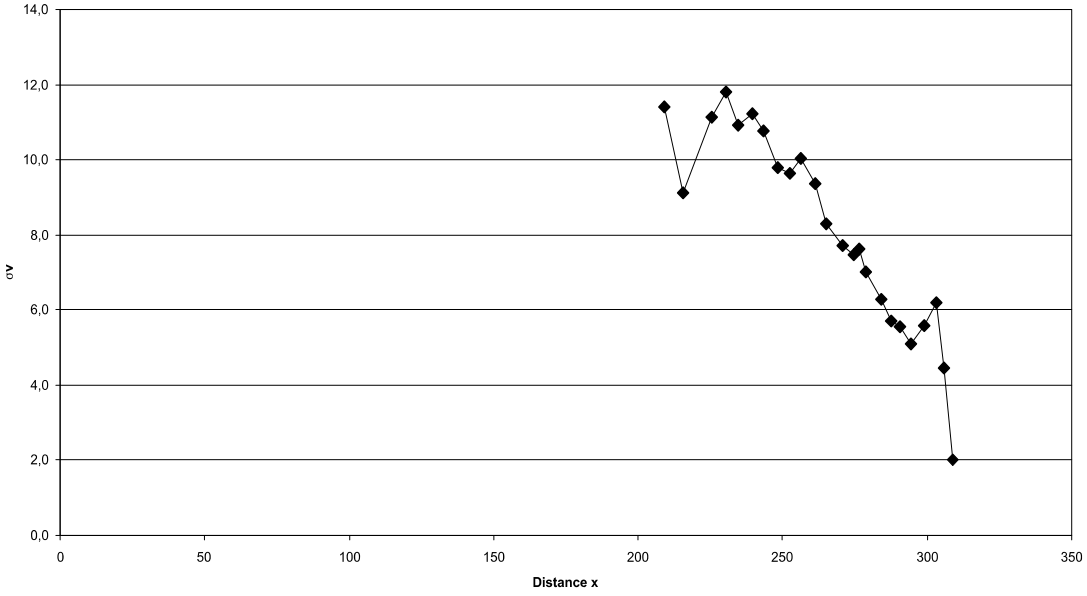

Fig. A.143: Comparison stress in the Huanhepterus rostrum construction. See chapter 6.4 for legend.

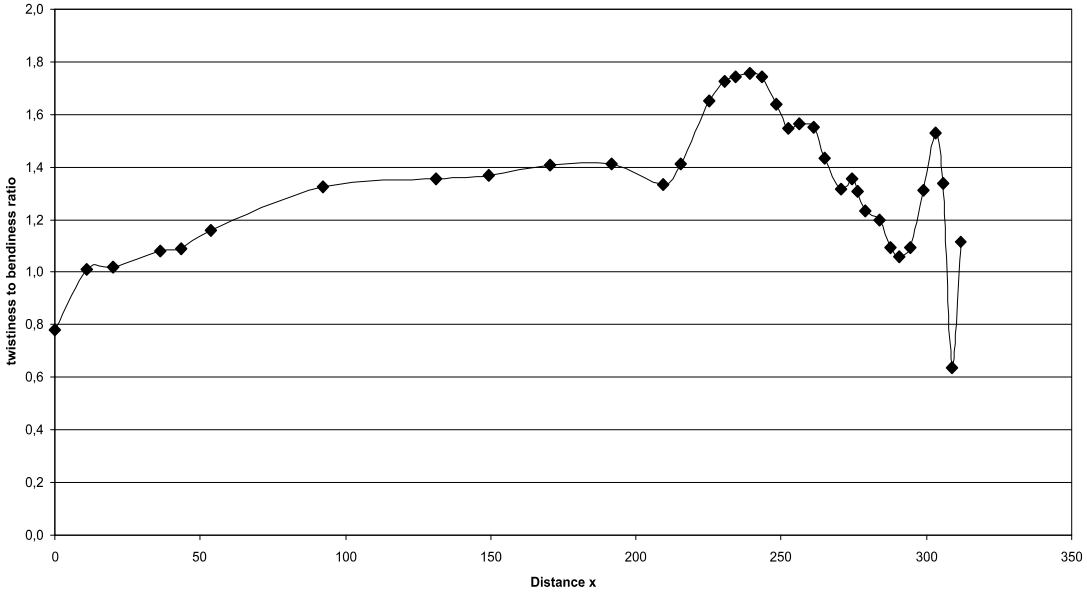

Fig. A.144: Twistiness to bendiness ratio in the Huanhepterus rostrum construction. See chapter 6.4 for legend.

A.19 Istiodactylus skull construction (see also chapter 7.19)

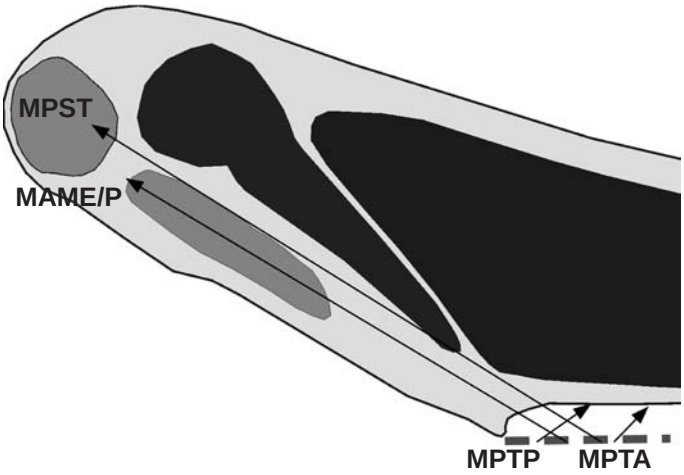

Fig A.145: Reconstruction of the principal pulling direction of the main adductor muscles in the skull of *Istiodactylus*. See chapter 6 for abbreviations.

Muscles	F_1	l_1	α_1	F_2	l_2	α_1
MAME/P	36	13.23	31	2.13	223.68	149
MPST	92	20.83	32	8.87	216.08	148
MPTA	14	23.68	46	1.55	213.22	134
MPTP	88	6.74	35	2.58	230.17	145

Tab. A.37: Reconstructed lever parameters for the scaled Istiodactylus skull construction. See chapter 6.2 for abbreviations.

	F_B	F_J	α_J
1st tooth position	7.76	225.34	-32.20
1st to 4th tooth position	31.60	901.09	-32.17
last tooth position	10.07	224.12	-31.70
average	8.60	224.90	-32.02

Tab. A.38: Reconstructed bite and joint reaction forces and angle of joint reaction force in the scaled Istiodactylus skull construction. Negative angle values mean anterodorsal direction of force. See chapter 6.2 for abbreviations.

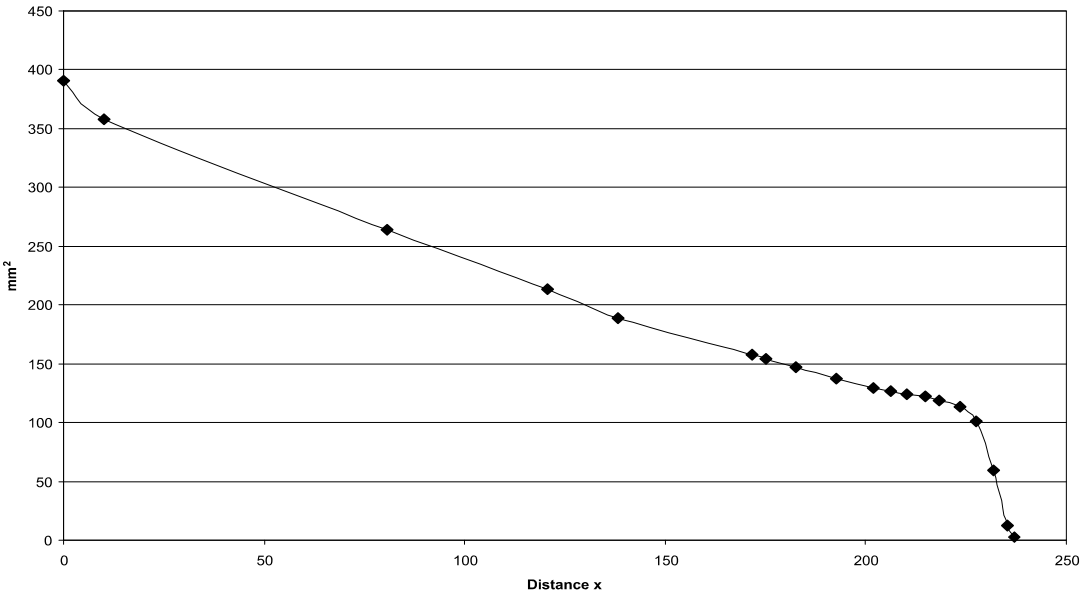

Fig A.146: Cross-sectional area of the Istiodactylus rostrum construction. See chapter 6.4 for legend.

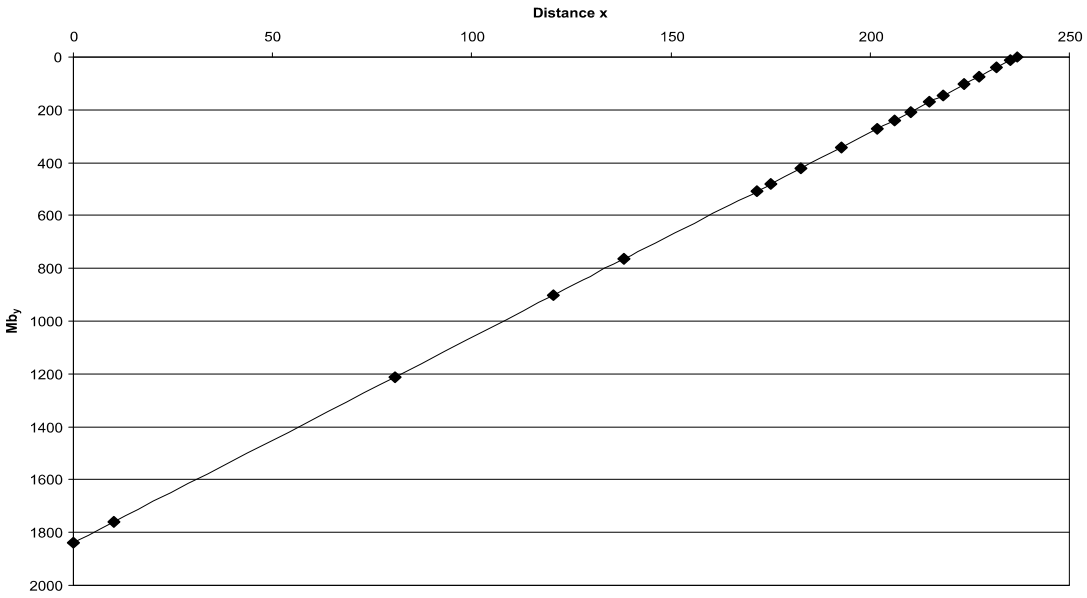

Fig A.147: Bending moments in the Istiodactylus rostrum construction. See chapter 6.4 for legend.

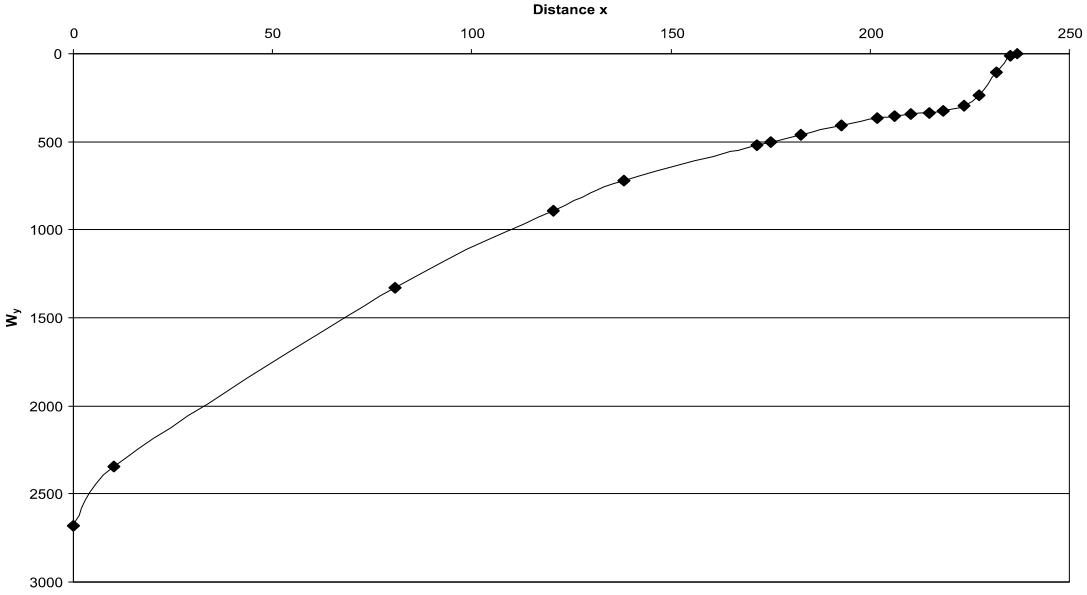

Fig A.148: Section modulus in the Istiodactylus rostrum construction. See chapter 6.4 for legend.

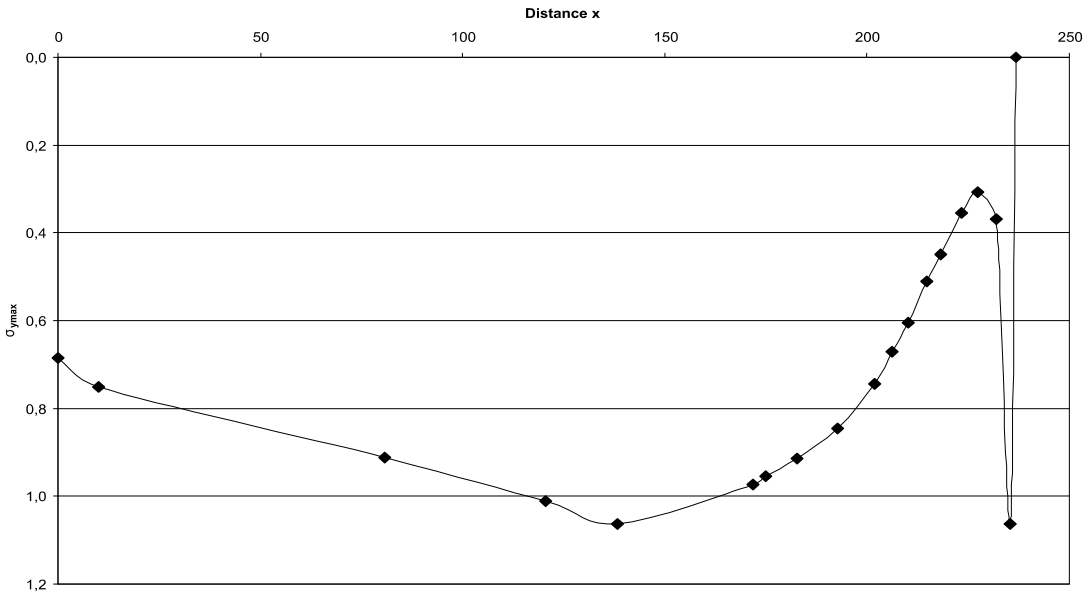

Fig A.149: Maximum bending stress in the Istiodactylus rostrum construction. See chapter 6.4 for legend.

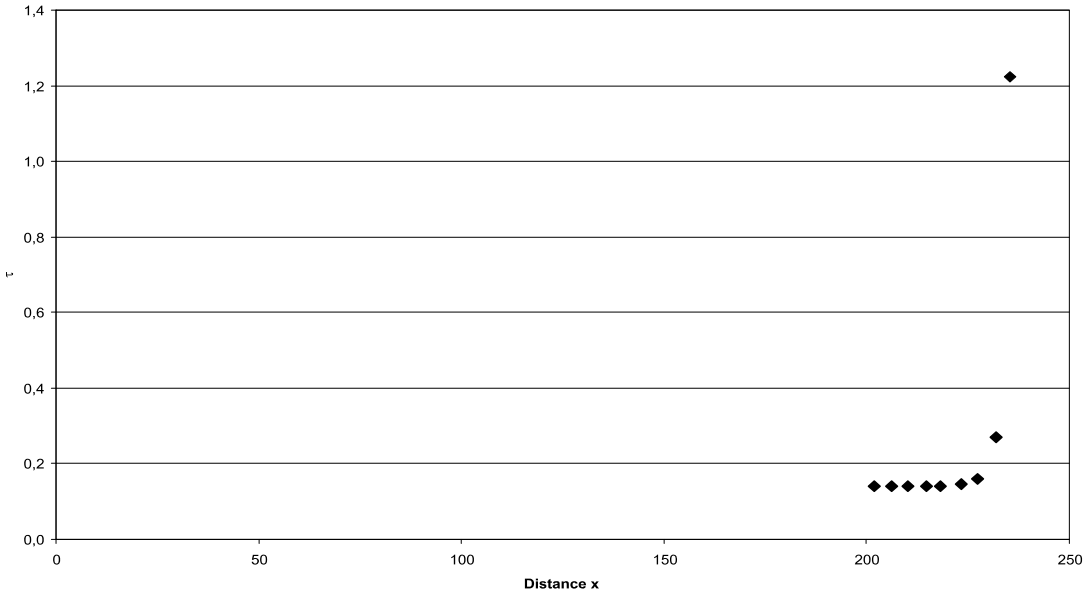

Fig. A.150: Shear stress in the Istiodactylus rostrum construction. See chapter 6.4 for legend.

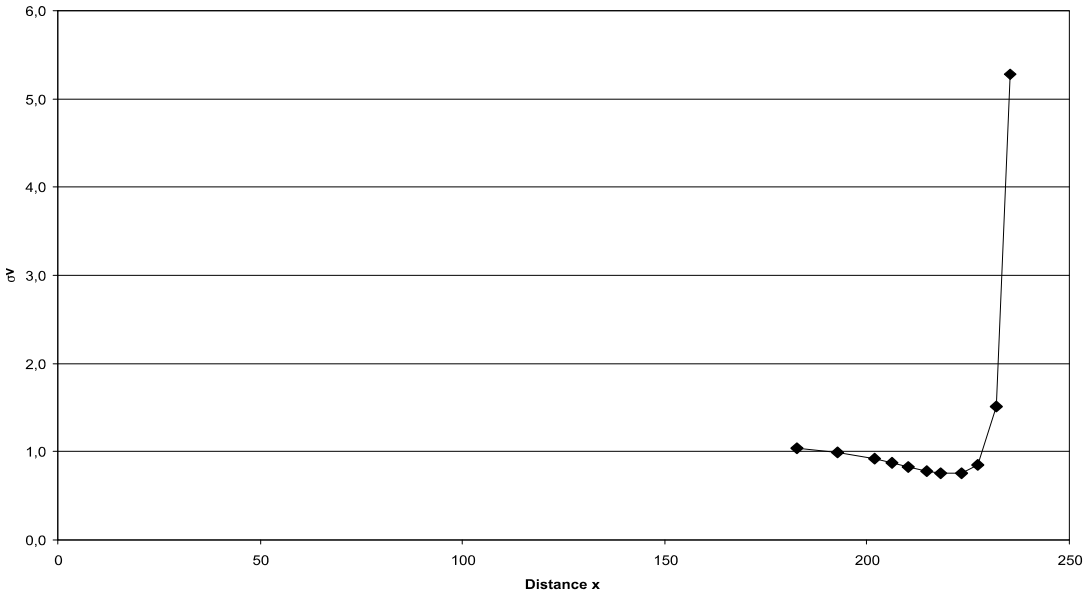

Fig. A.151: Comparison stress in the Istiodactylus rostrum construction. See chapter 6.4 for legend.

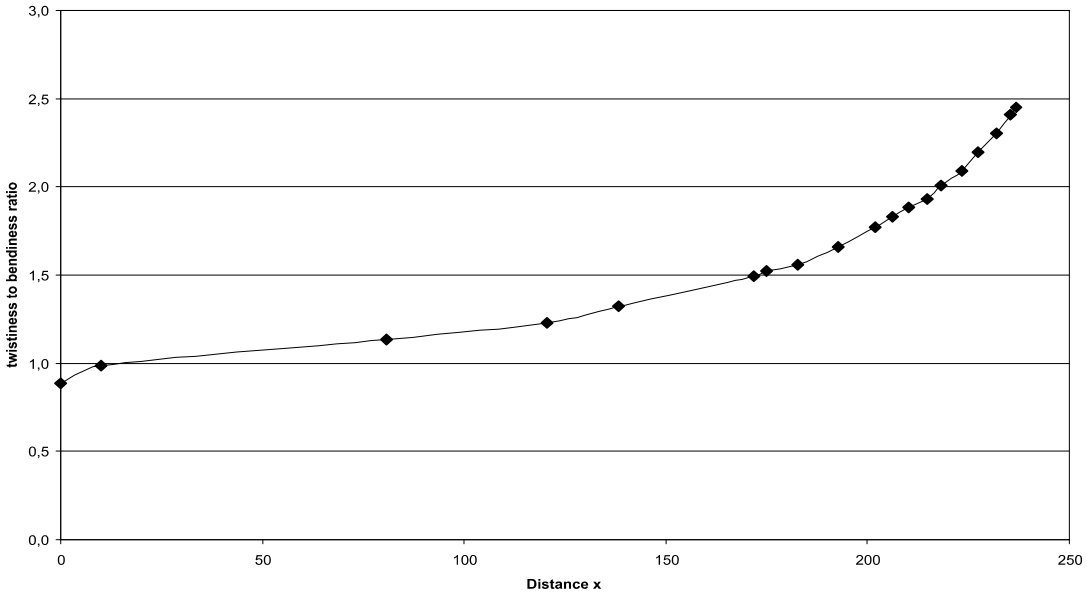

Fig. A.152: Twistiness to bendiness ratio in the Istiodactylus rostrum construction. See chapter 6.4 for legend.

A.20 Jeholopterus skull construction (see also chapter 7.20)

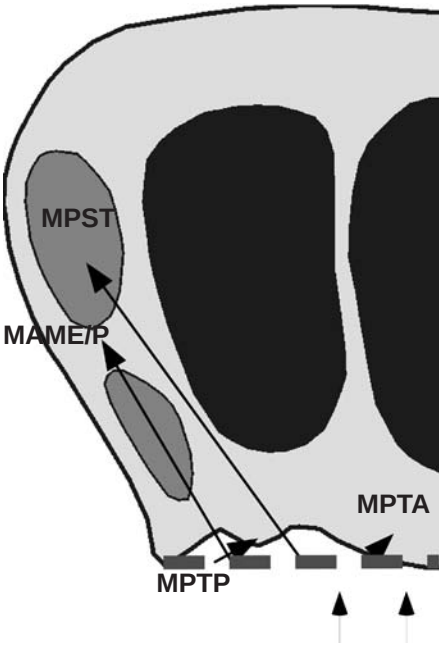

Fig A.153: Reconstruction of the principal pulling direction of the main adductor muscles in the skull of *Jeholopterus*. See chapter 6 for abbreviations.

Muscles	F_1	l_1	α_1	F_2	l_2	α_1
MAME/P	36	8.24	60	3.35	88.60	120
MPST	92	16.88	54	19.61	79.21	126
MPTA	14	24.97	43	4.86	71.87	137
MPTP	88	5.96	28	5.77	90.88	152

Tab. A.39: Reconstructed lever parameters for the scaled Jeholopterus skull construction. See chapter 6.2 for abbreviations.

	F_B	F_J	α_J
1st tooth position	20.63	209.90	-40.33
1st to 4th tooth position	93.18	832.77	-39.76
last tooth position	90.86	172.94	-22.30
average	41.24	198.10	-35.40

Tab. A.40: Reconstructed bite and joint reaction forces and angle of joint reaction force in the scaled Jeholopterus skull construction. Negative angle values mean anterodorsal direction of force. See chapter 6.2 for abbreviations.

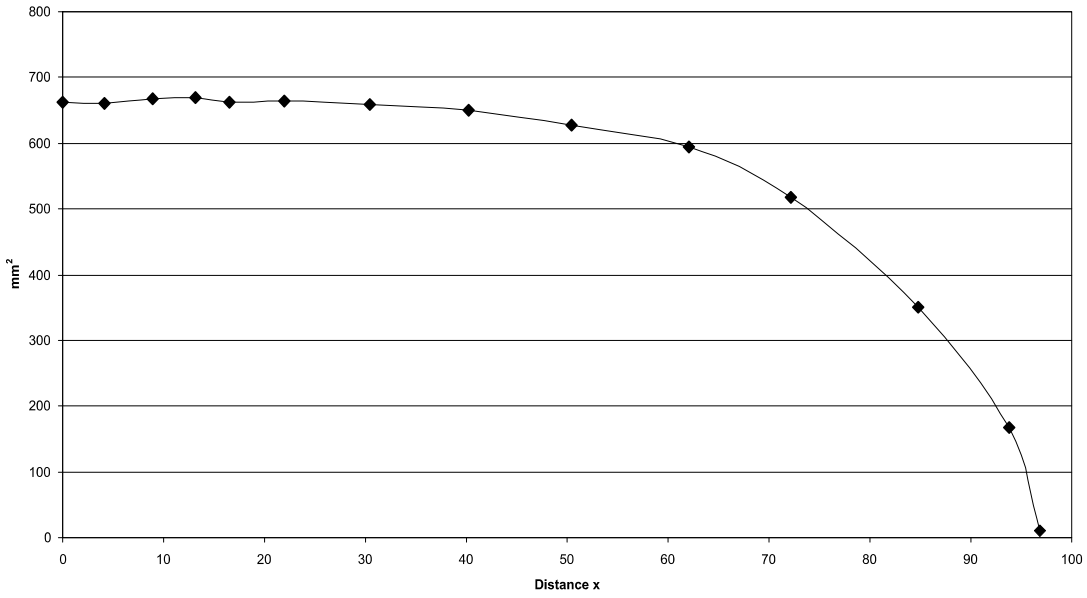

Fig A.154: Cross-sectional area of the Jeholopterus rostrum construction. See chapter 6.4 for legend.

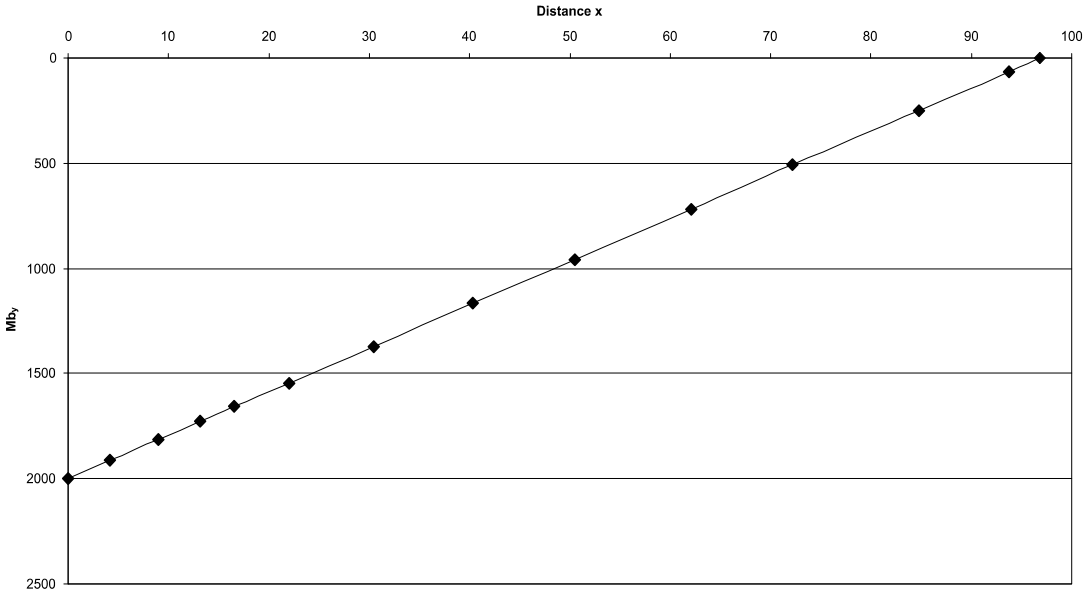

Fig A.155: Bending moments in the Jeholopterus rostrum construction. See chapter 6.4 for legend.

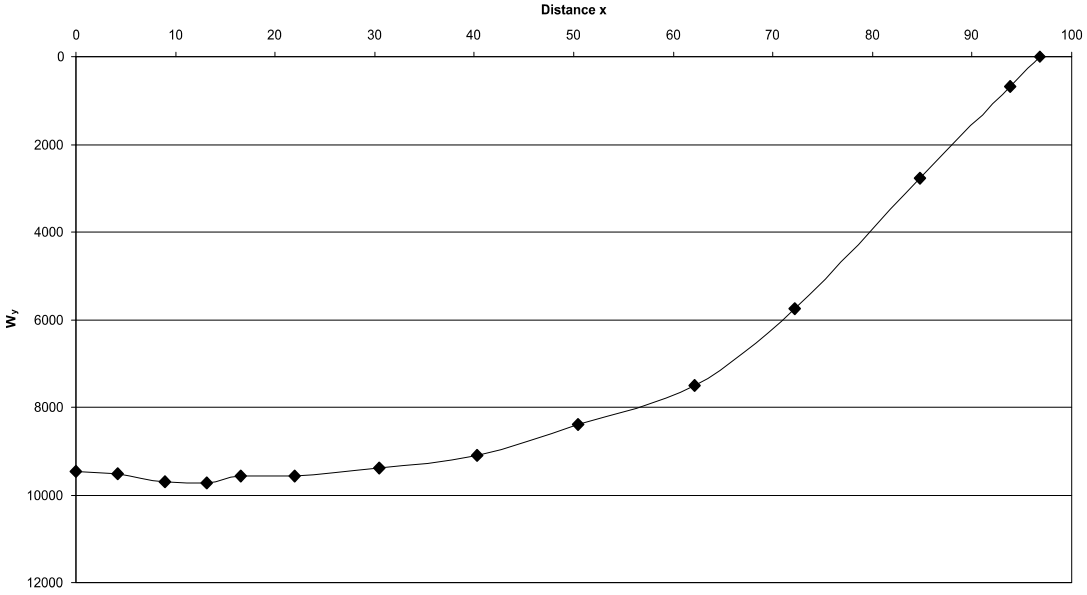

Fig A.156: Section modulus in the Jeholopterus rostrum construction. See chapter 6.4 for legend.

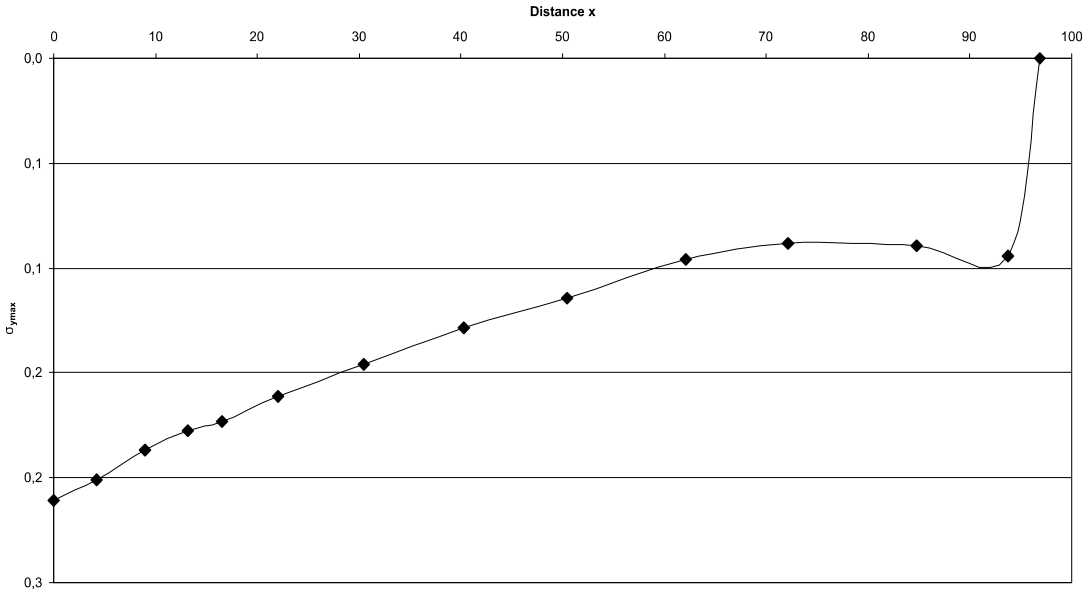

Fig A.157: Maximum bending stress in the Jeholopterus rostrum construction. See chapter 6.4 for legend.

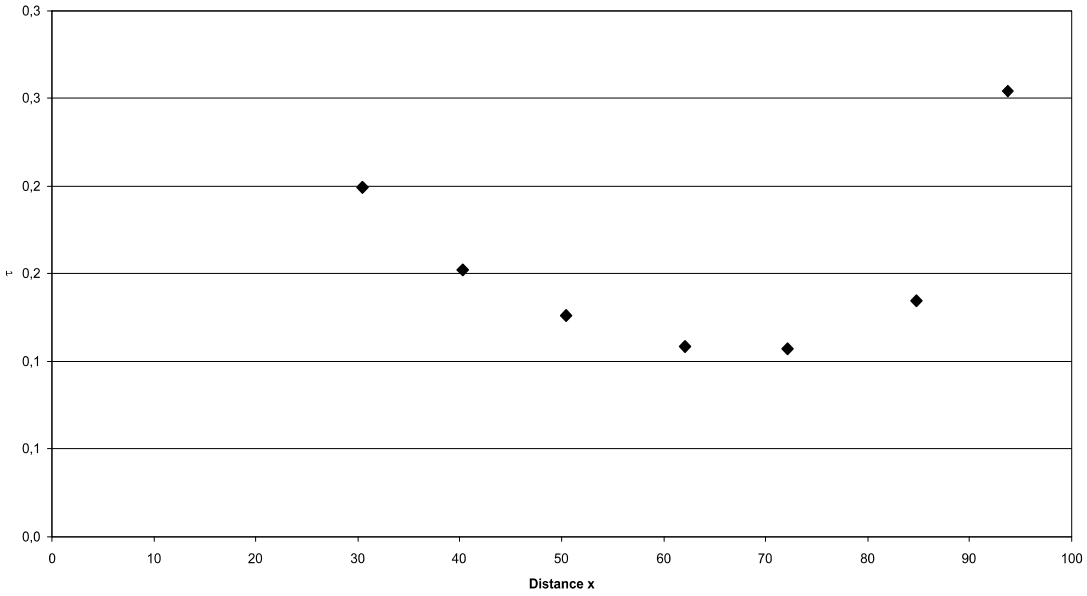

Fig. A.158: Shear stress in the Jeholopterus rostrum construction. See chapter 6.4 for legend.

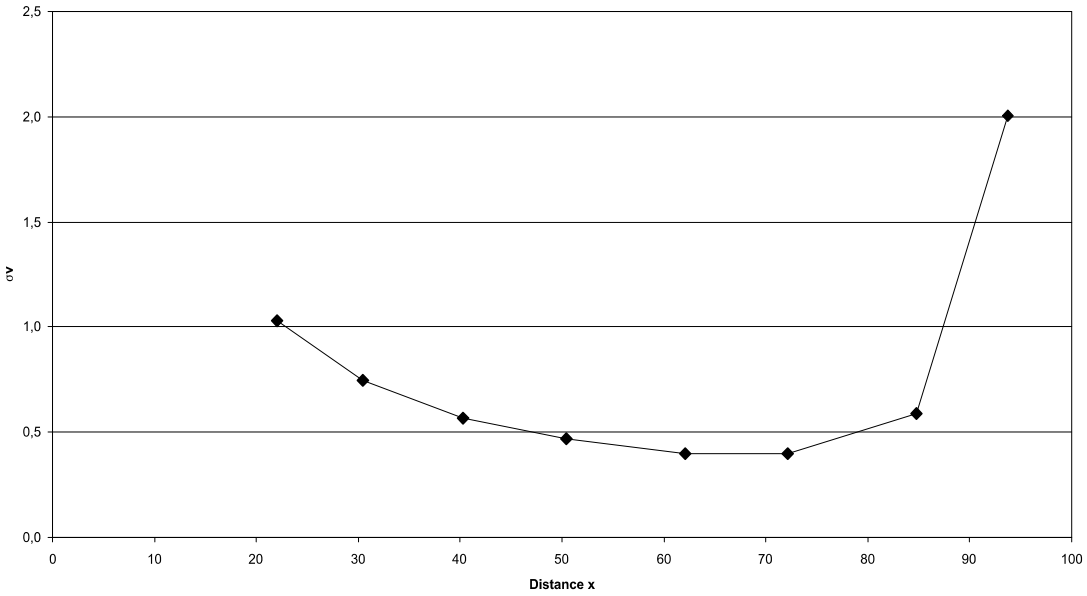

Fig. A.159: Comparison stress in the Jeholopterus rostrum construction. See chapter 6.4 for legend.

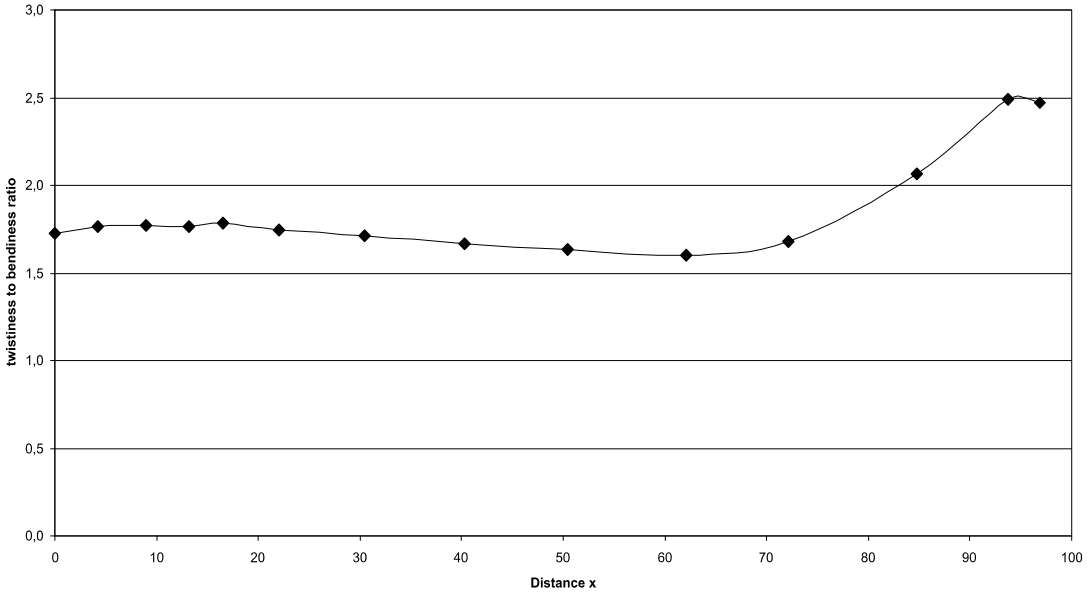

Fig. 7.160: Twistiness to bendiness ratio in the Jeholopterus rostrum construction. See chapter 6.4 for legend.

A.21 Ludodactylus skull construction (see also chapter 7.21)

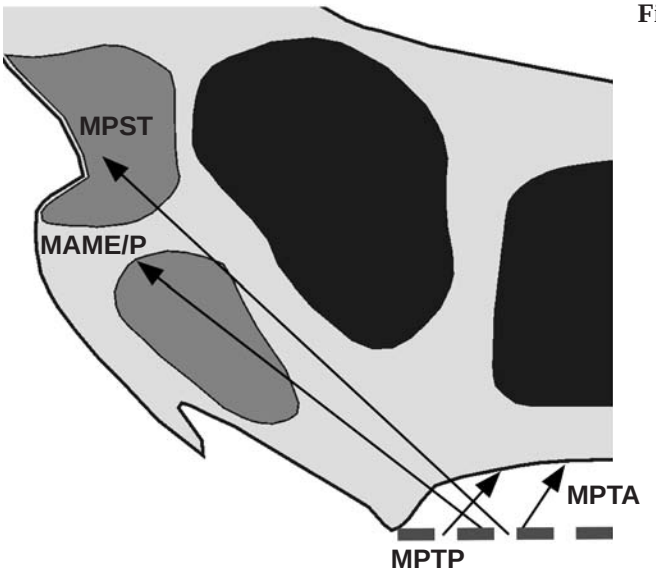

Fig A.161: Reconstruction of the principal pulling direction of the main adductor muscles in the skull of *Ludodactylus*. See chapter 6 for abbreviations.

Muscles	F_1	l_1	α_1	F_2	l_2	α_1
MAME/P	36	13.24	38	1.82	261.83	142
MPST	92	15.83	43	5.62	259.24	137
MPTA	14	17.18	56	0.09	268.71	124
MPTP	88	6.37	48	2.17	257.83	132

Tab. A.39: Reconstructed lever parameters for the scaled Ludodactylus skull construction. See chapter 6.2 for abbreviations.

	F_B	F_J	α_J
1st tooth position	6.92	224.47	-43.67
1st to 4th tooth position	28.10	897.57	-43.65
last tooth position	32.70	207.51	-38.51
average	13.70	219.91	-42.36

Tab. A.40: Reconstructed bite and joint reaction forces and angle of joint reaction force in the scaled Ludodactylus skull construction. Negative angle values mean anterodorsal direction of force. See chapter 6.2 for abbreviations.

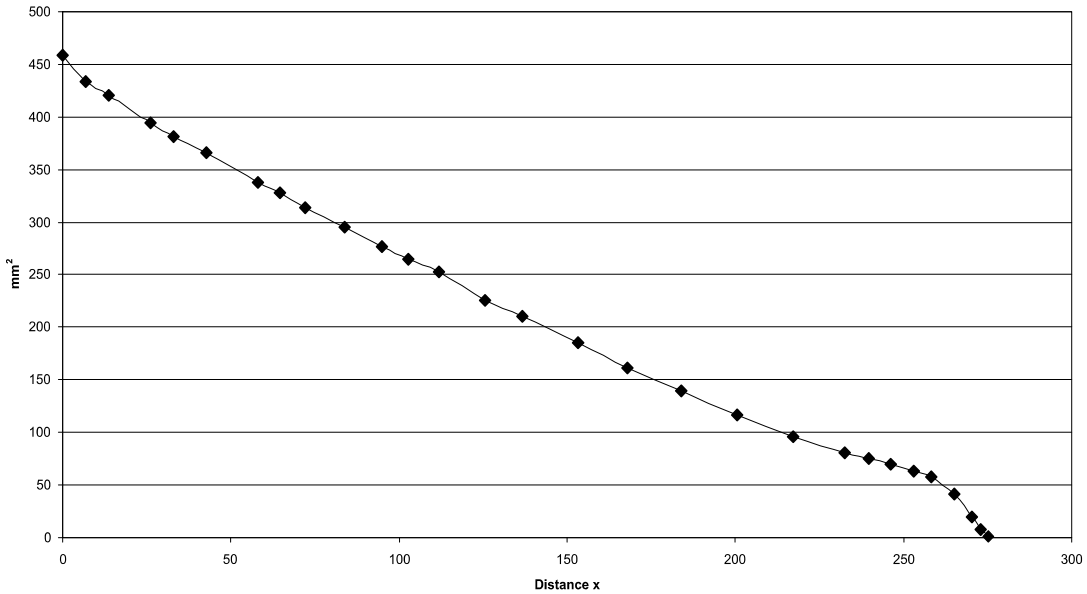

Fig A.162: Cross-sectional area of the Ludodactylus rostrum construction. See chapter 6.4 for legend.

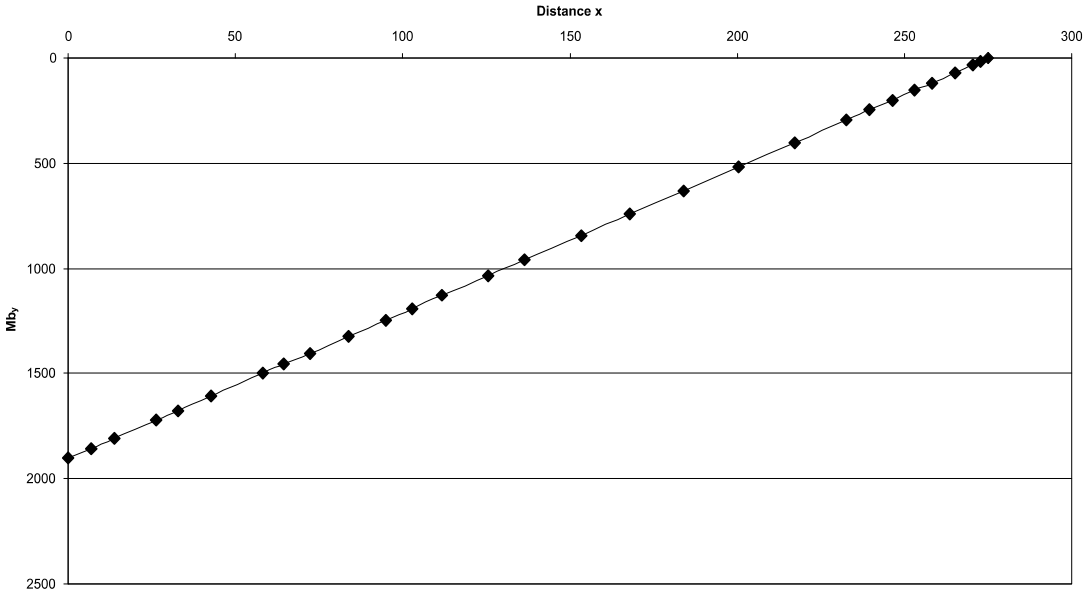

Fig A.163: Bending moments in the Ludodactylus rostrum construction. See chapter 6.4 for legend.

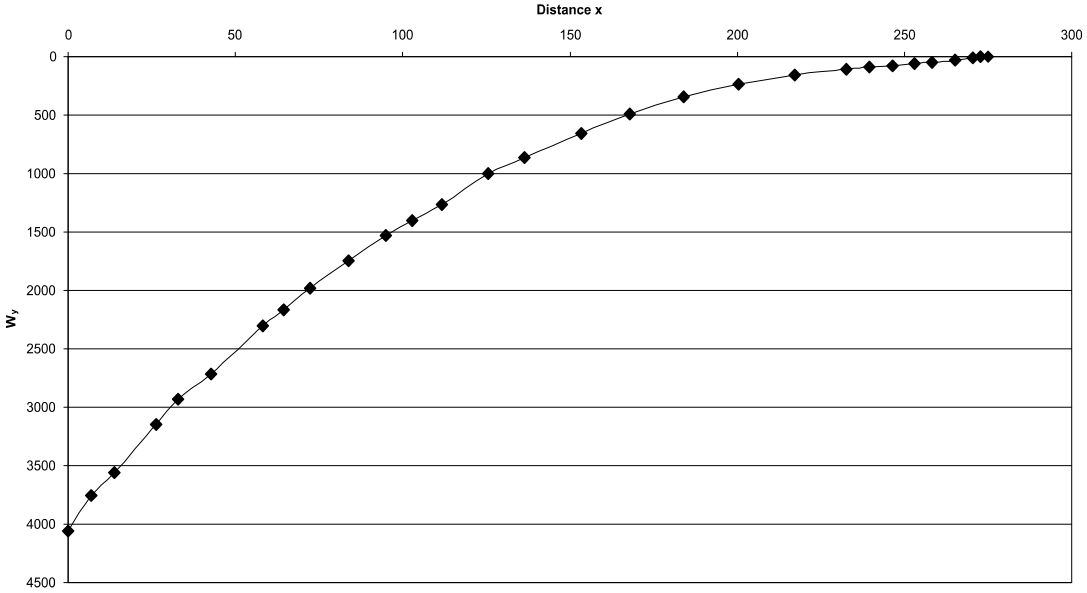

Fig A.164: Section modulus in the Ludodactylus rostrum construction. See chapter 6.4 for legend.

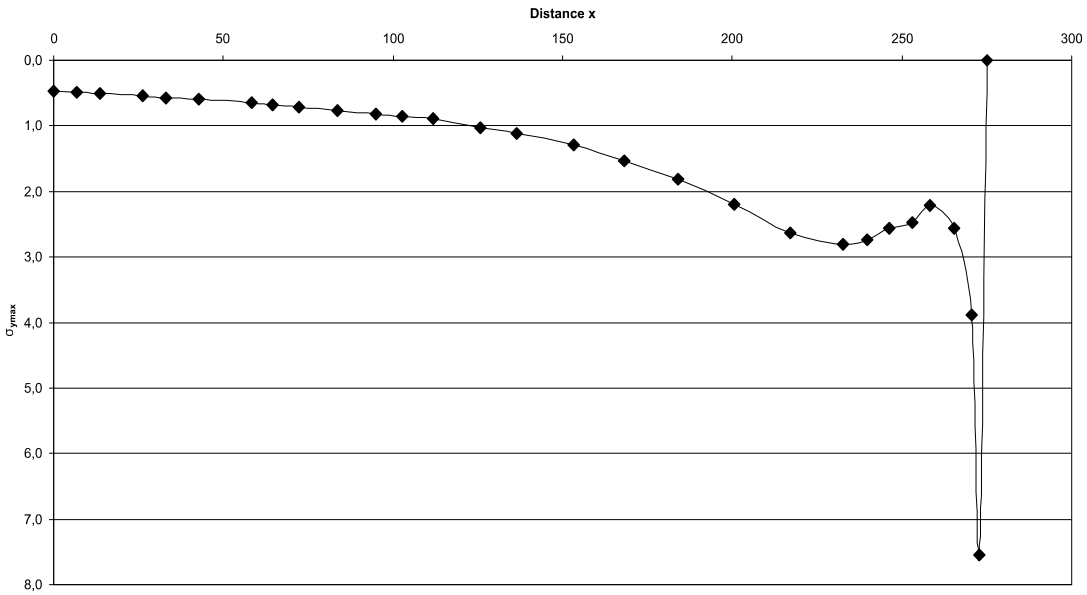

Fig A.165: Maximum bending stress in the Ludodactylus rostrum construction. See chapter 6.4 for legend.

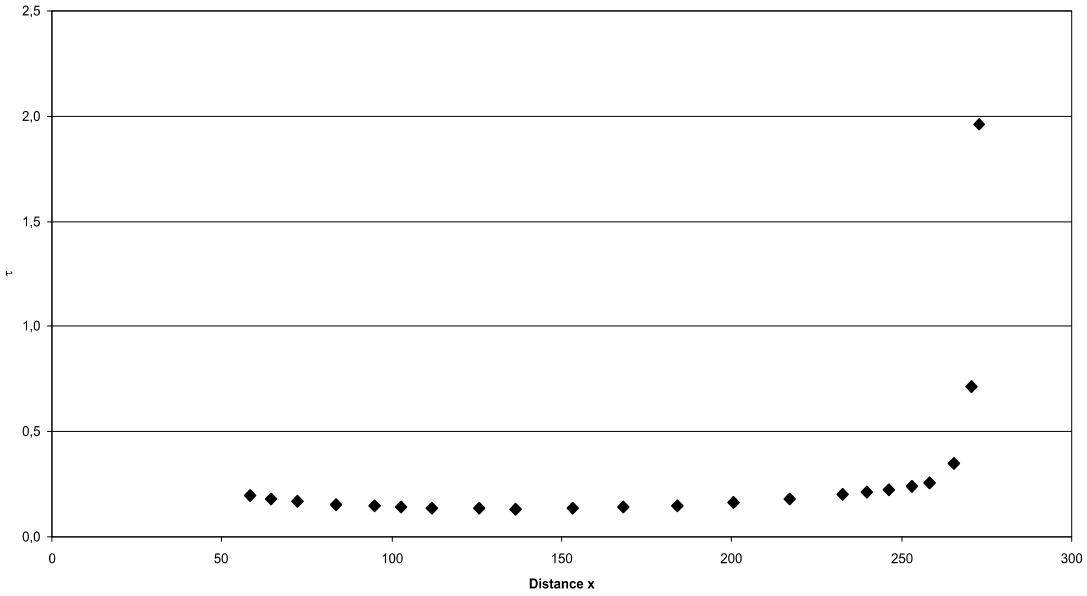

Fig. A.166: Shear stress in the Ludodactylus rostrum construction. See chapter 6.4 for legend.

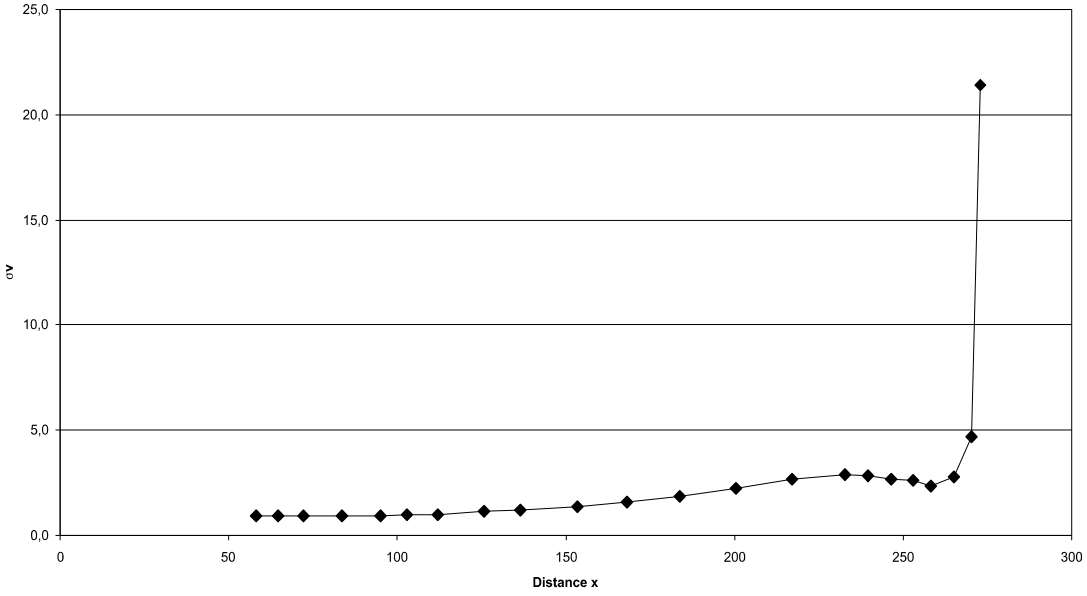

Fig. A.167: Comparison stress in the Ludodactylus rostrum construction. See chapter 6.4 for legend.

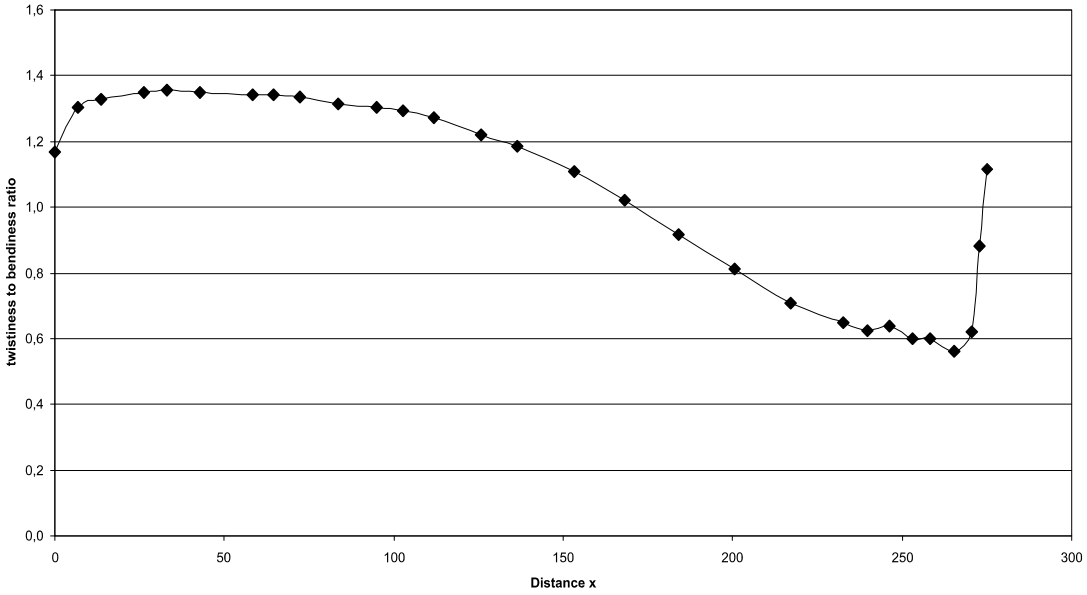

Fig. A.168: Twistiness to bendiness ratio in the Ludodactylus rostrum construction. See chapter 6.4 for legend.

A.22 Nyctosaurus skull construction (see also chapter 7.22)

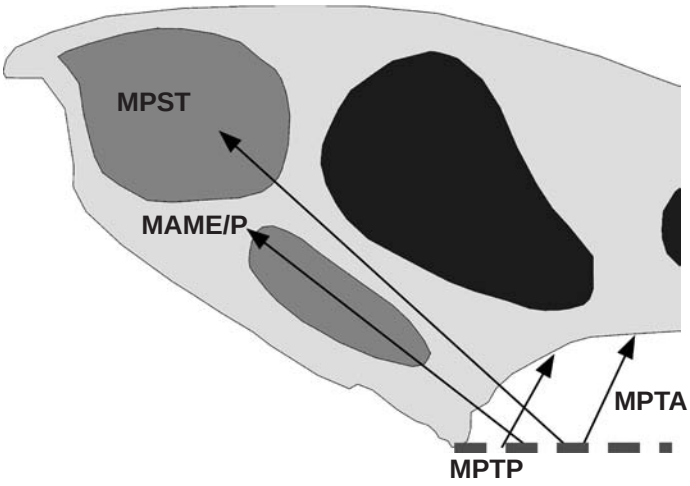

Fig A.169: Reconstruction of the principal pulling direction of the main adductor muscles in the skull of *Nyctosaurus*. See chapter 6 for abbreviations.

Muscles	F_1	l_1	α_1	F_2	l_2	α_1
MAME/P	36	9.06	38	0.93	350.74	142
MPST	92	15.79	42	4.22	343.92	138
MPTA	14	18.89	65	0.78	340.19	115
MPTP	88	5.66	61	4.41	354.14	119

Tab. A.41: Reconstructed lever parameters for the scaled Nyctosaurus skull construction. See chapter 6.2 for abbreviations.

	F_B	F_J	α_J
anterior tip of jaw	5.14	222.31	-49.18
anterior to nasoant. fen.	21.95	209.87	-46.18
average	13.55	216.09	-47.99

Tab. A.42: Reconstructed bite and joint reaction forces and angle of joint reaction force in the scaled Nyctosaurus skull construction. Negative angle values mean anterodorsal direction of force. See chapter 6.2 for abbreviations.

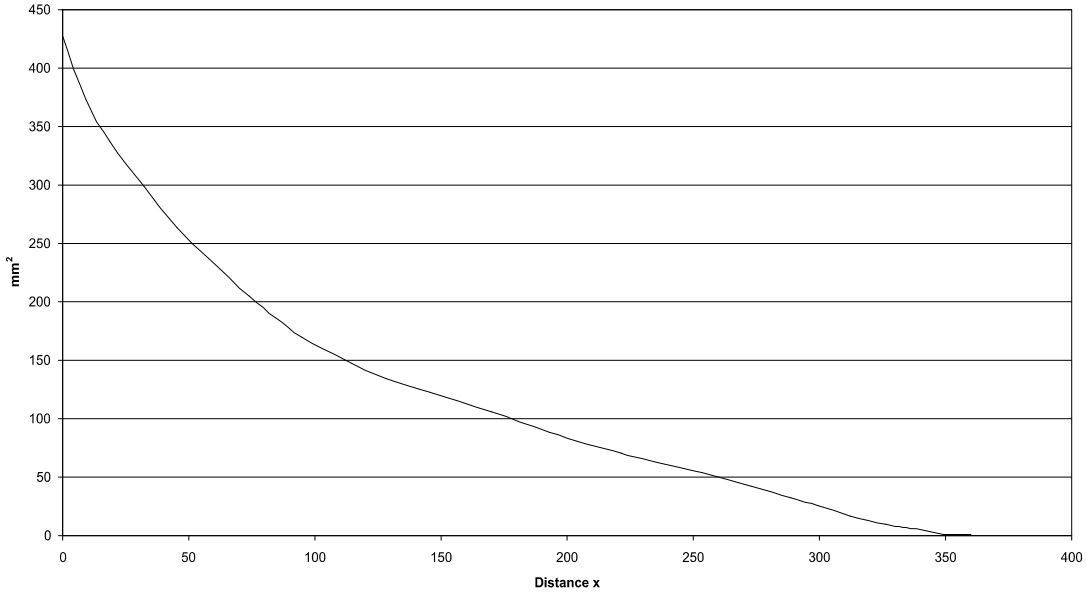

Fig A.170: Cross-sectional area of the Nyctosaurus rostrum construction. See chapter 6.4 for legend.

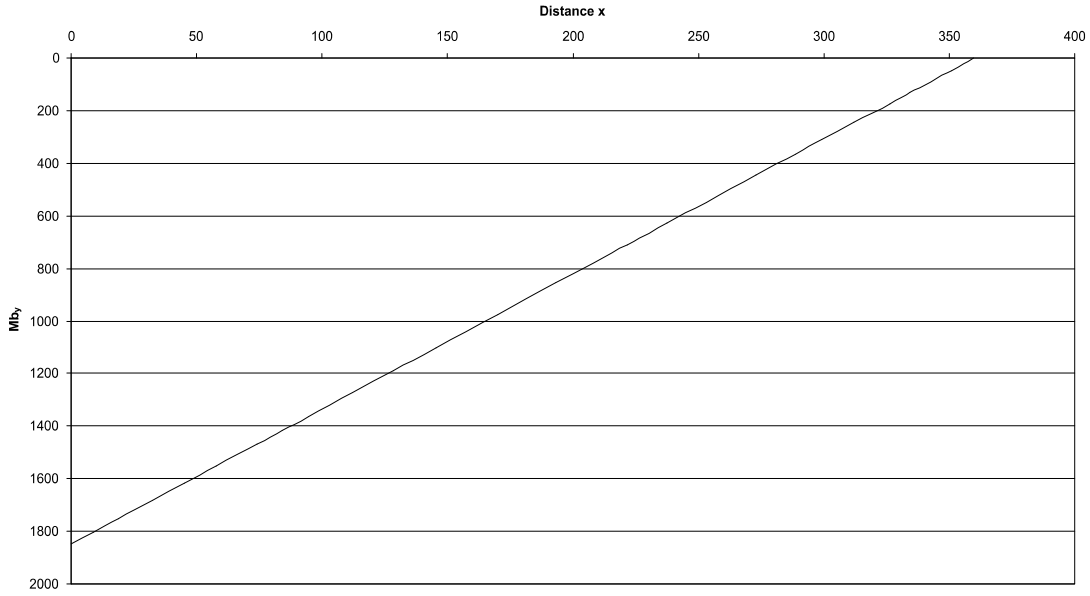

Fig A.171: Bending moments in the Nyctosaurus rostrum construction. See chapter 6.4 for legend.

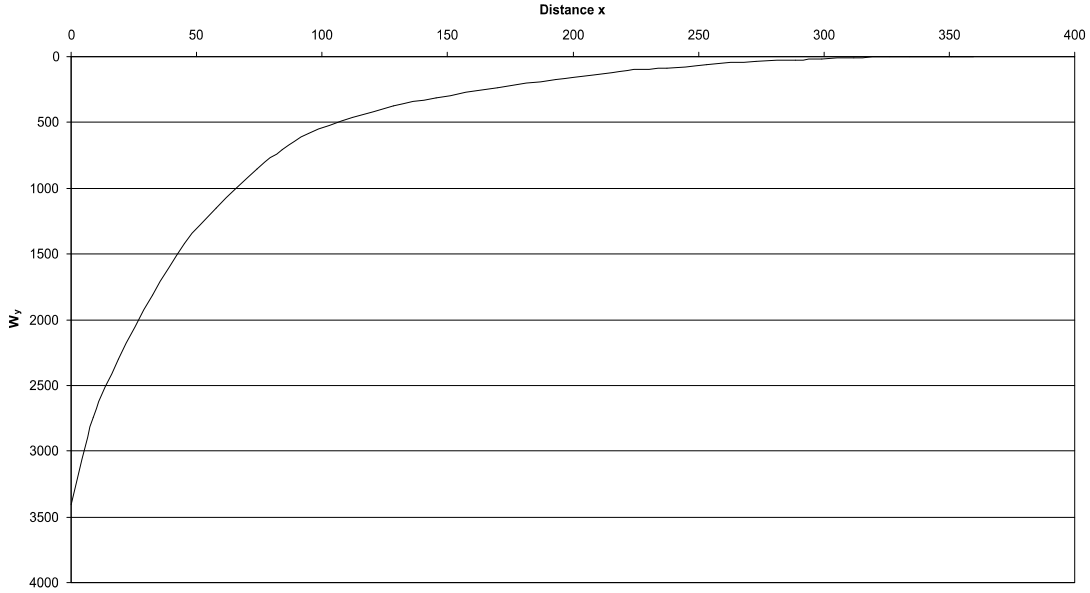

Fig A.172: Section modulus in the Nyctosaurus rostrum construction. See chapter 6.4 for legend.

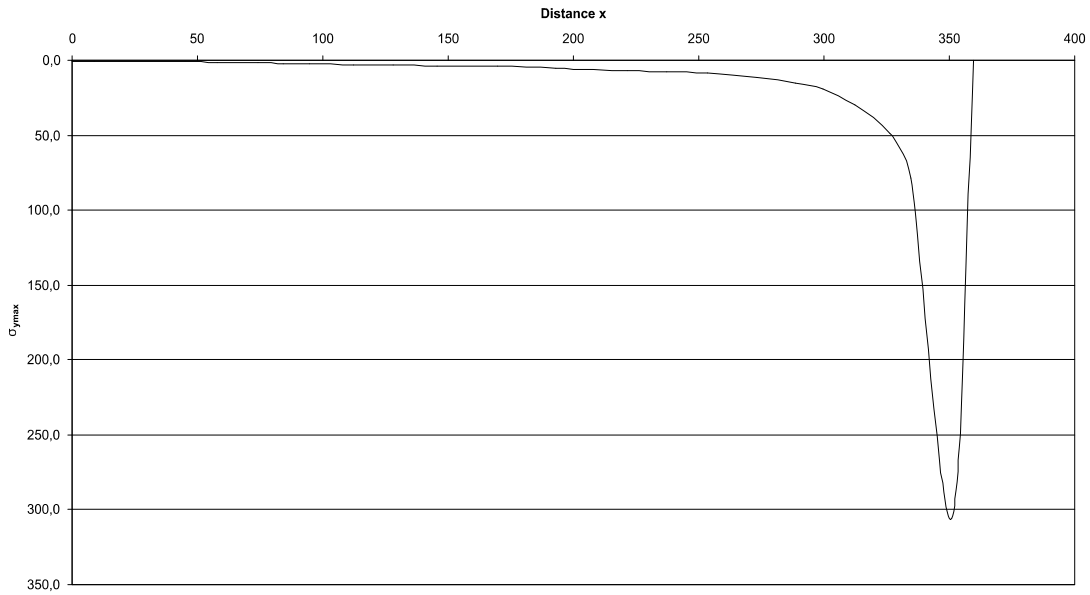

Fig A.173: Maximum bending stress in the Nyctosaurus rostrum construction. See chapter 6.4 for legend.

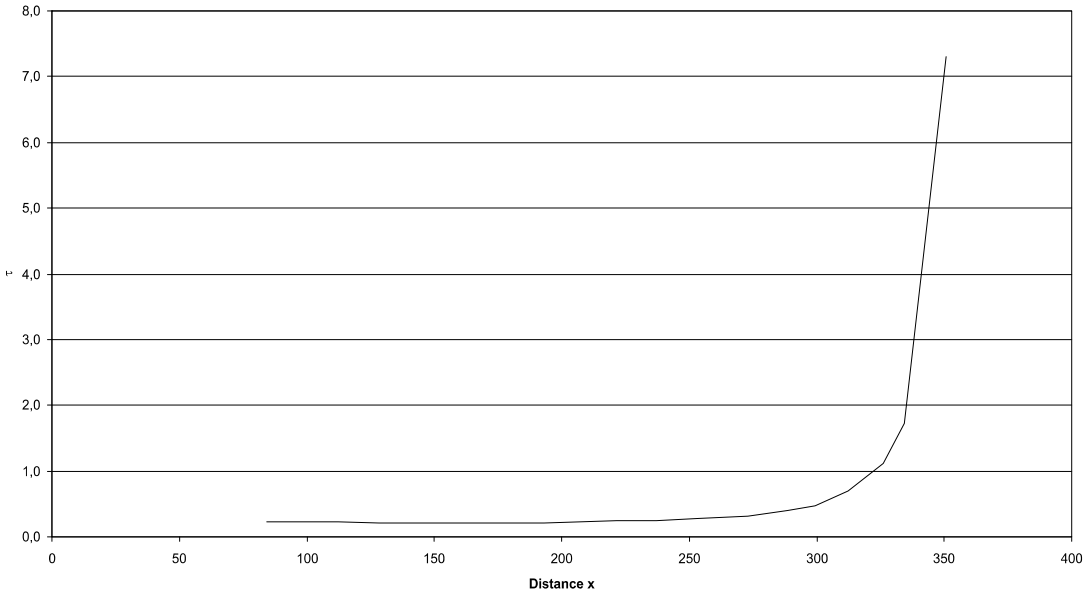

Fig. A.174: Shear stress in the Nyctosaurus rostrum construction. See chapter 6.4 for legend.

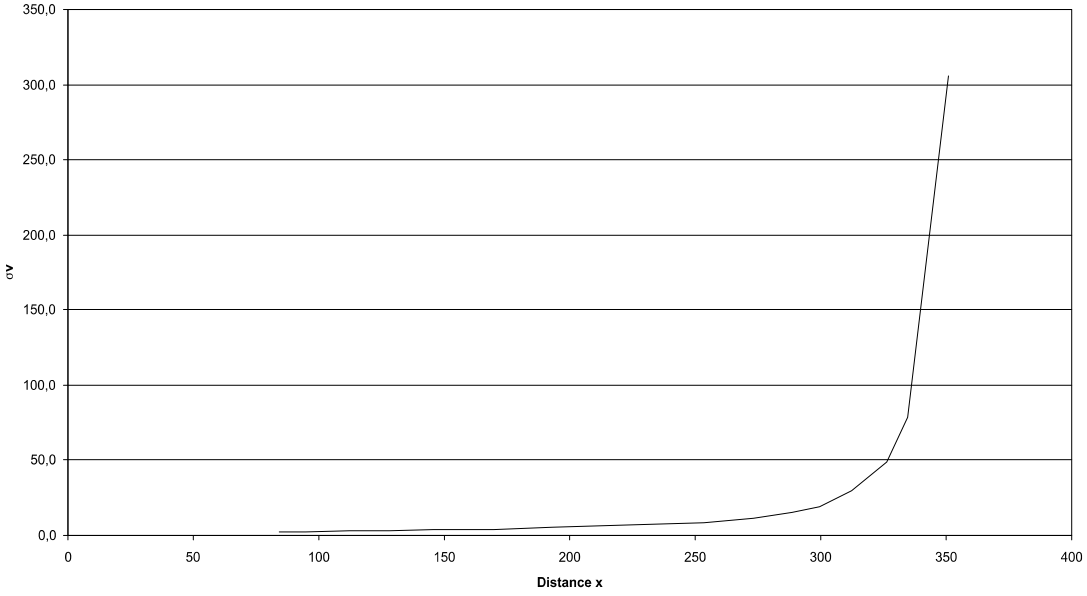

Fig. A.175: Comparison stress in the Nyctosaurus rostrum construction. See chapter 6.4 for legend.

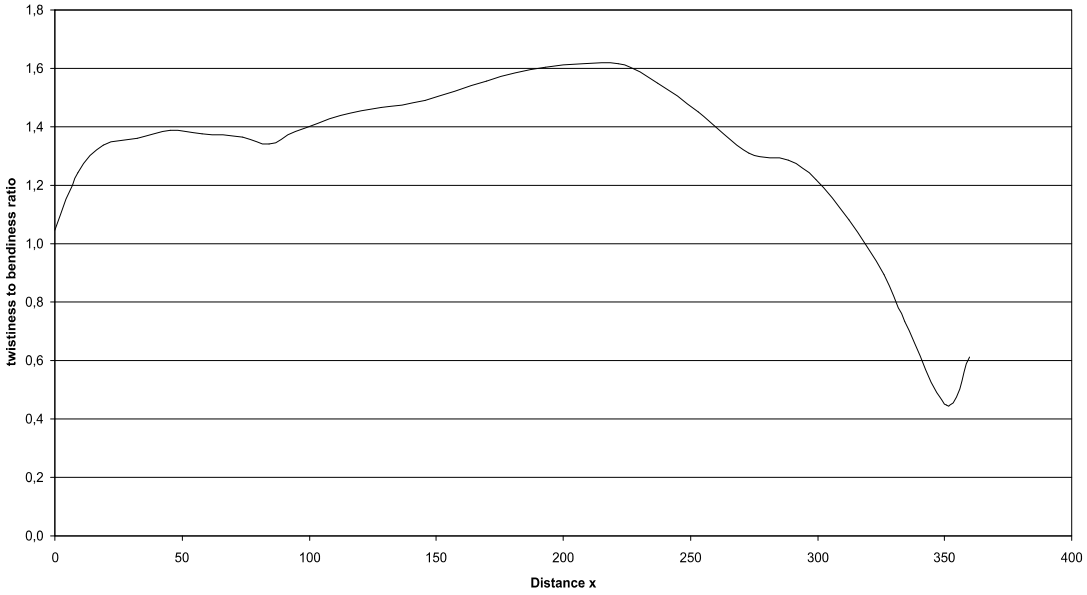

Fig. A.176: Twistiness to bendiness ratio in the Nyctosaurus rostrum construction. See chapter 6.4 for legend.

A.23 Parapsicephalus skull construction (see also chapter 7.23)

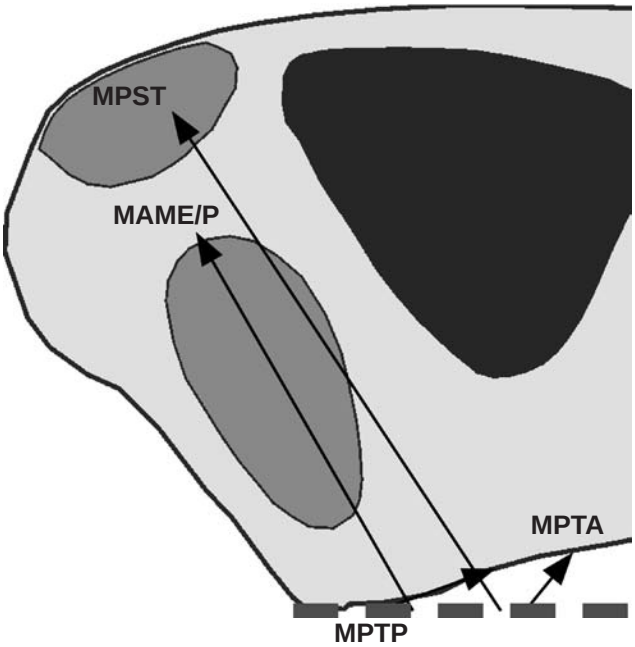

Fig A.177: Reconstruction of the principal pulling direction of the main adductor muscles in the skull of *Parapsicephalus*. See chapter 6 for abbreviations.

Muscles	F_1	l_1	α_1	F_2	l_2	α_1
MAME/P	36	9.00	60	1.32	244.93	120
MPST	92	19.29	57	7.56	234.64	123
MPTA	14	22.89	51	1.39	231.04	129
MPTP	88	6.17	20	2.19	247.76	160

Tab. A.43: Reconstructed lever parameters for the scaled Parapsicephalus skull construction. See chapter 6.2 for abbreviations.

	F_B	F_J	α_J
1st tooth position	8.68	212.73	-41.38
1st to 4th tooth position	36.71	849.60	-41.28
last tooth position	17.41	207.06	-39.57
average	12.00	210.56	-40.70

Tab. A.44: Reconstructed bite and joint reaction forces and angle of joint reaction force in the scaled Parapsicephalus skull construction. Negative angle values mean anterodorsal direction of force. See chapter 6.2 for abbreviations.

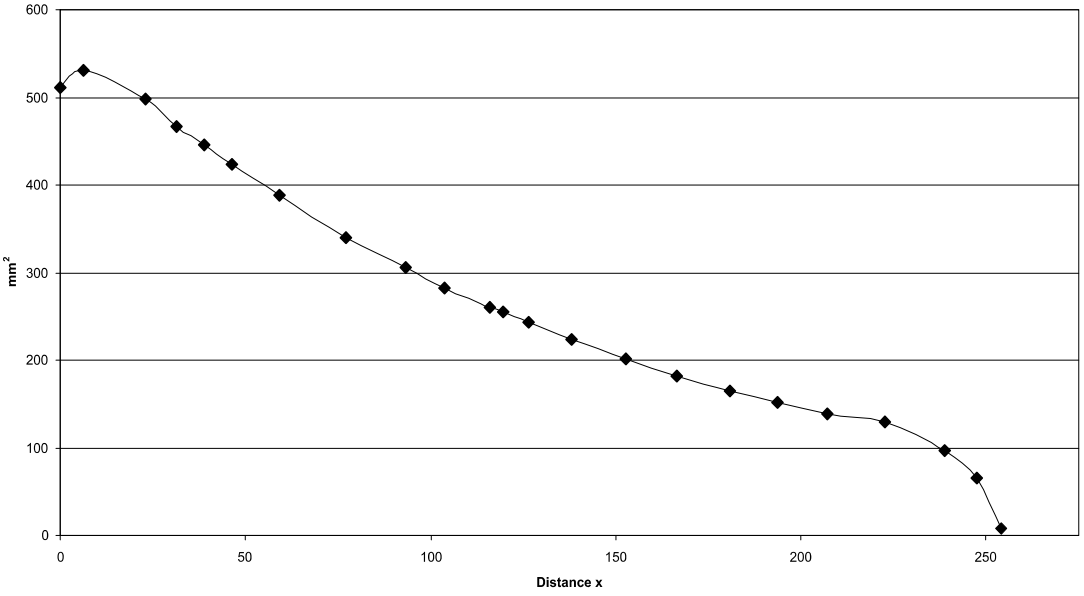

Fig A.178: Cross-sectional area of the Parapsicephalus rostrum construction. See chapter 6.4 for legend.

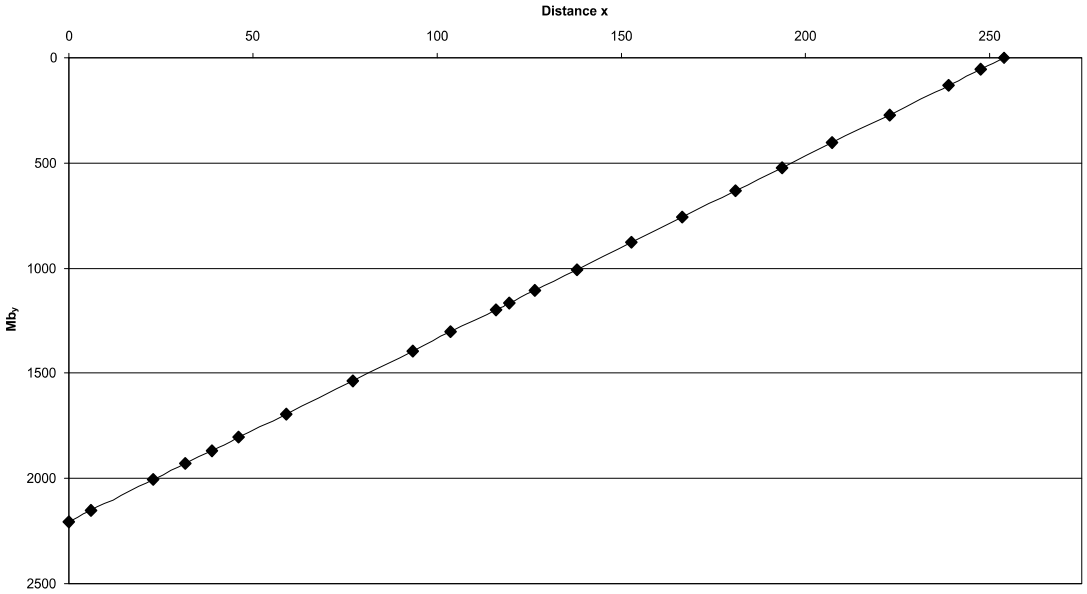

Fig A.179: Bending moments in the Parapsicephalus rostrum construction. See chapter 6.4 for legend.

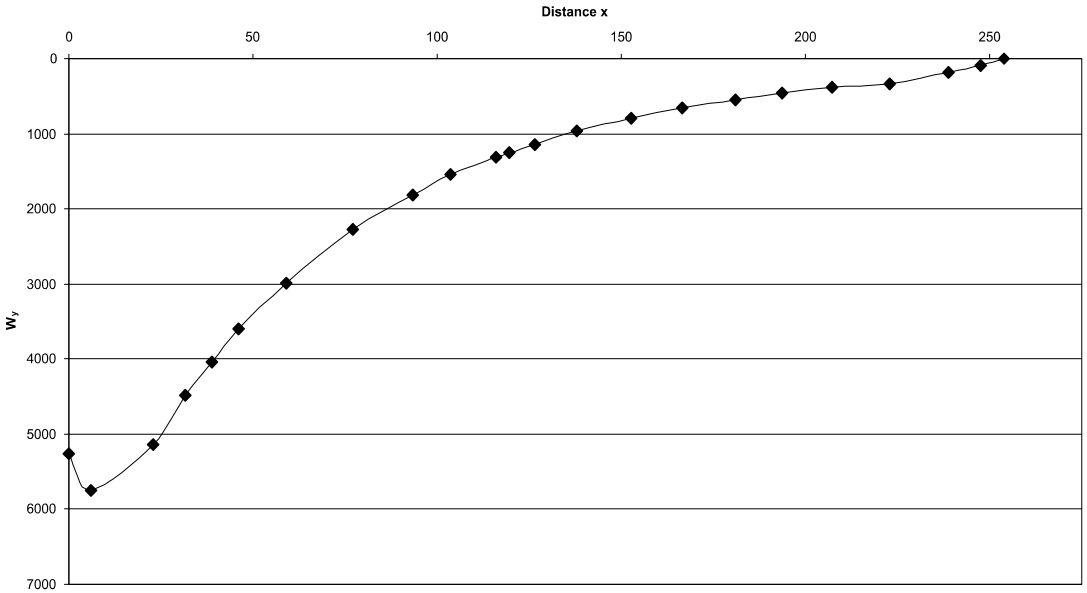

Fig A.180: Section modulus in the Parapsicephalus rostrum construction. See chapter 6.4 for legend.

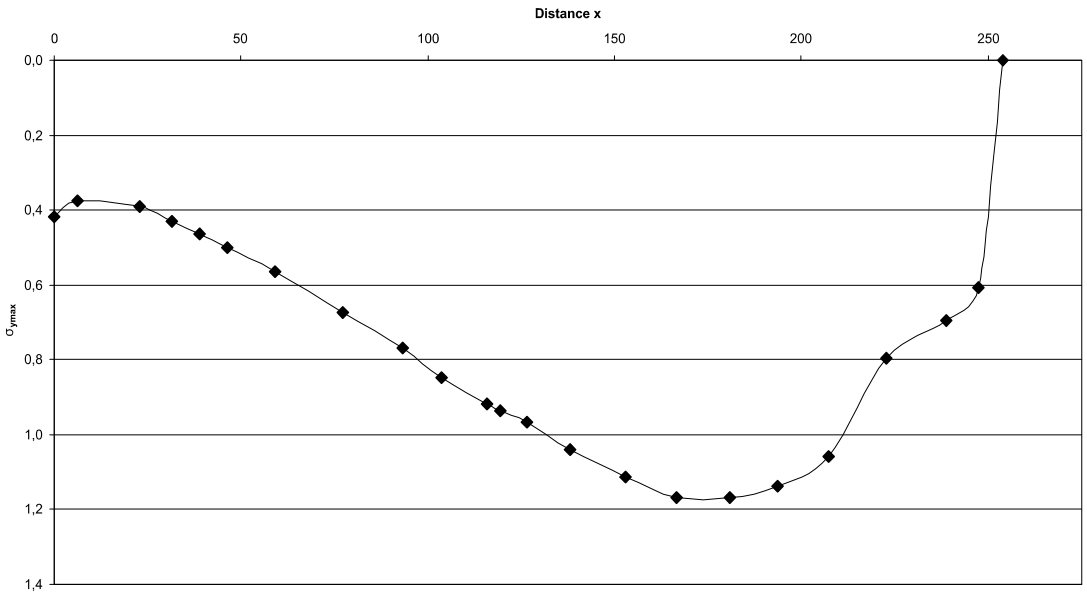

Fig A.181: Maximum bending stress in the Parapsicephalus rostrum construction. See chapter 6.4 for legend.

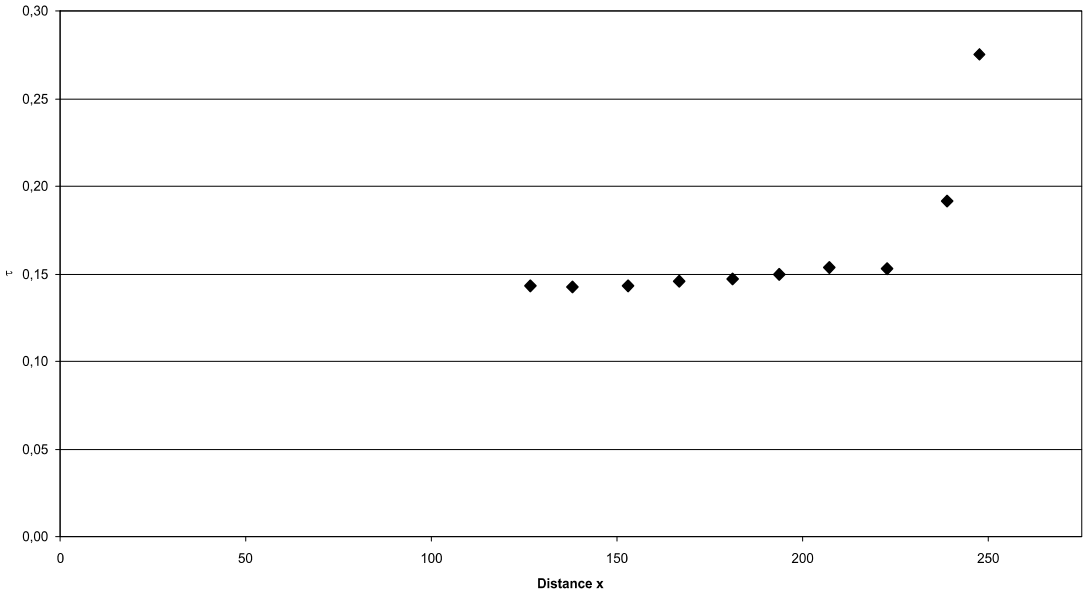

Fig. A.182: Shear stress in the Parapsicephalus rostrum construction. See chapter 6.4 for legend.

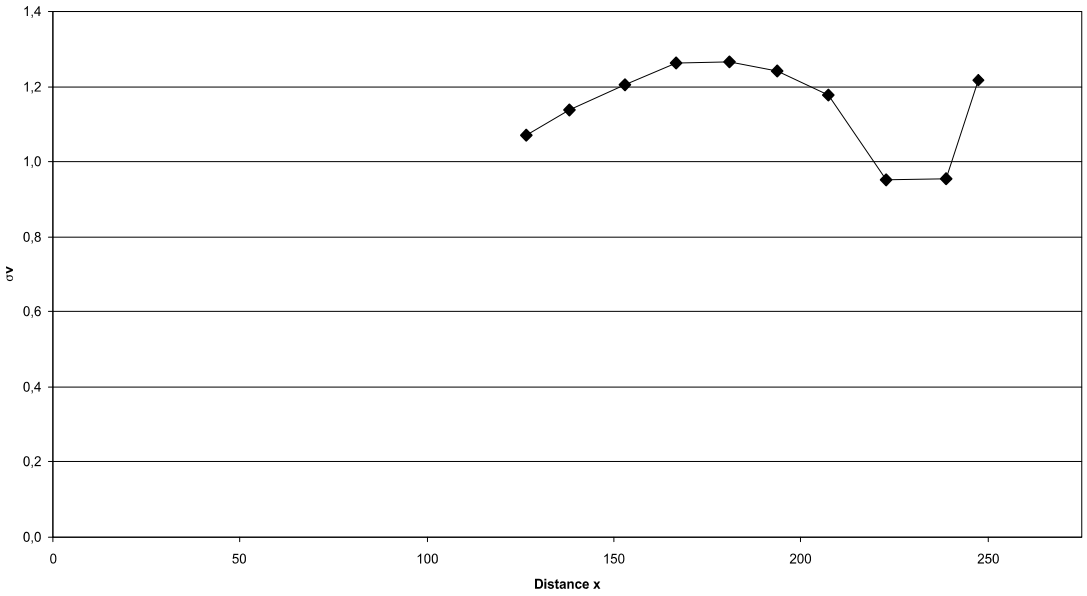

Fig. A.183: Comparison stress in the Parapsicephalus rostrum construction. See chapter 6.4 for legend.

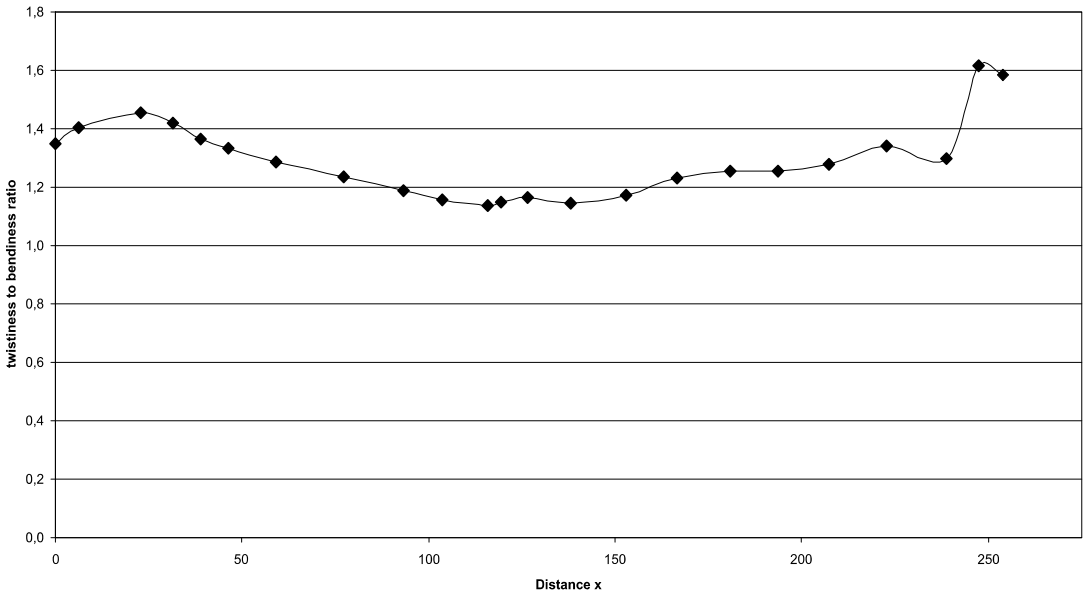

Fig. A.184: Twistiness to bendiness ratio in the Parapsicephalus rostrum construction. See chapter 6.4 for legend.

A.24 Peteinosaurus skull construction (see also chapter 7.24)

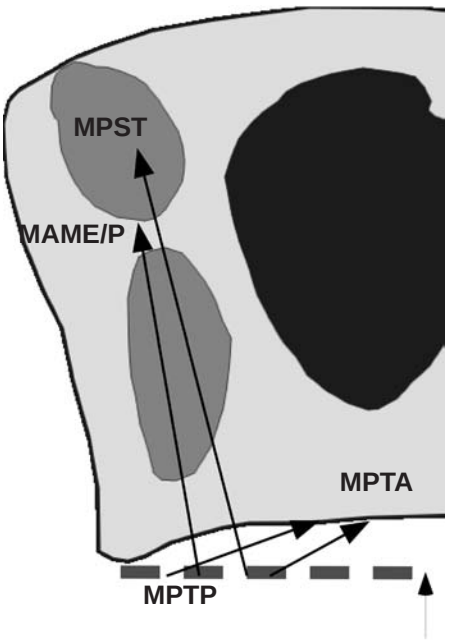

Fig A.185: Reconstruction of the principal pulling direction of the main adductor muscles in the skull of *Peteinosaurus*. See chapter 6 for abbreviations.

Muscles	F_1	l_1	α_1	F_2	l_2	α_1
MAME/P	36	10.52	80	2.35	161.4	100
MPST	92	16.95	76	10.06	154.97	104
MPTA	14	20.03	23	1.85	151.89	157
MPTP	88	6.15	20	3.26	165.77	160

Tab. A.45: Reconstructed lever parameters for the scaled Peteinosaurus skull construction. See chapter 6.2 for abbreviations.

	F_B	F_J	α_J
1st tooth position	12.62	192.83	-49.95
1st to 4th tooth position	54.29	768.62	-49.78
last tooth position	53.45	163.75	-40.73
average	24.75	183.90	-47.43

Tab. A.46: Reconstructed bite and joint reaction forces and angle of joint reaction force in the scaled Peteinosaurus skull construction. Negative angle values mean anterodorsal direction of force. See chapter 6.2 for abbreviations.

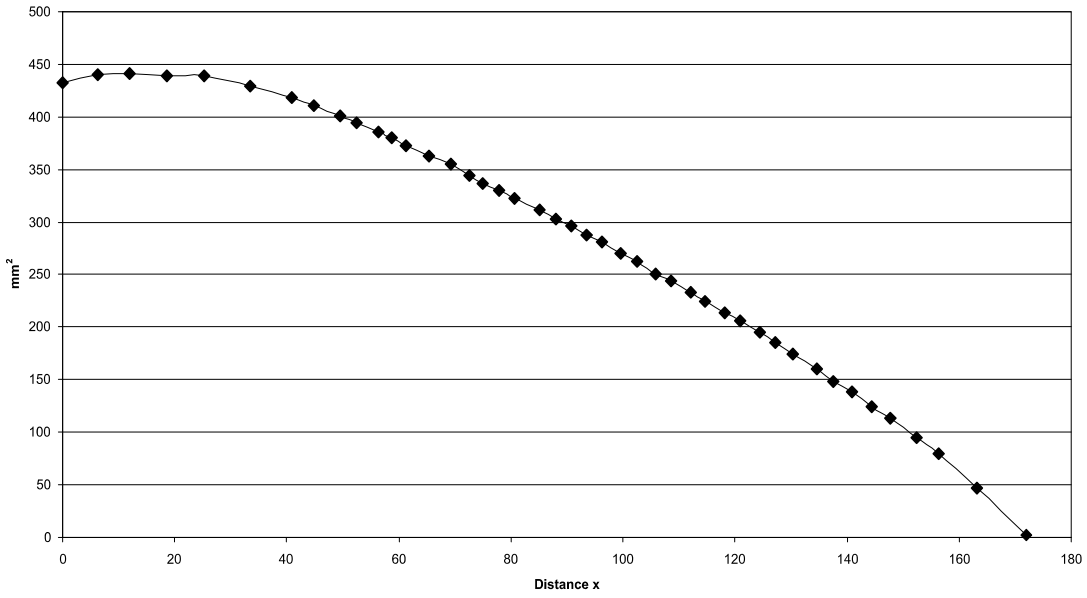

Fig A.186: Cross-sectional area of the Peteinosaurus rostrum construction. See chapter 6.4 for legend.

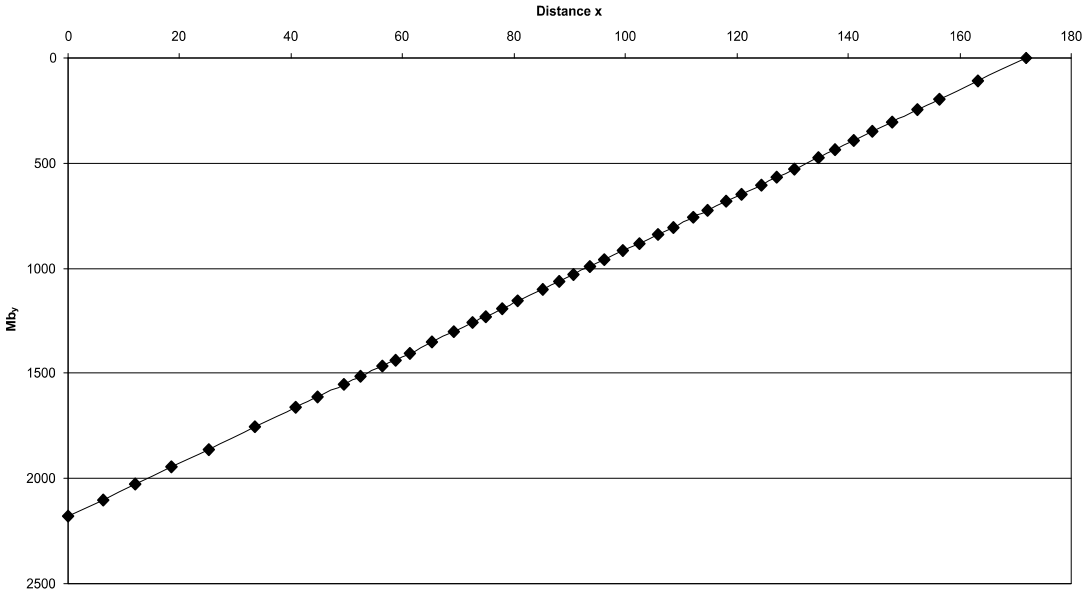

Fig A.187: Bending moments in the Peteinosaurus rostrum construction. See chapter 6.4 for legend.

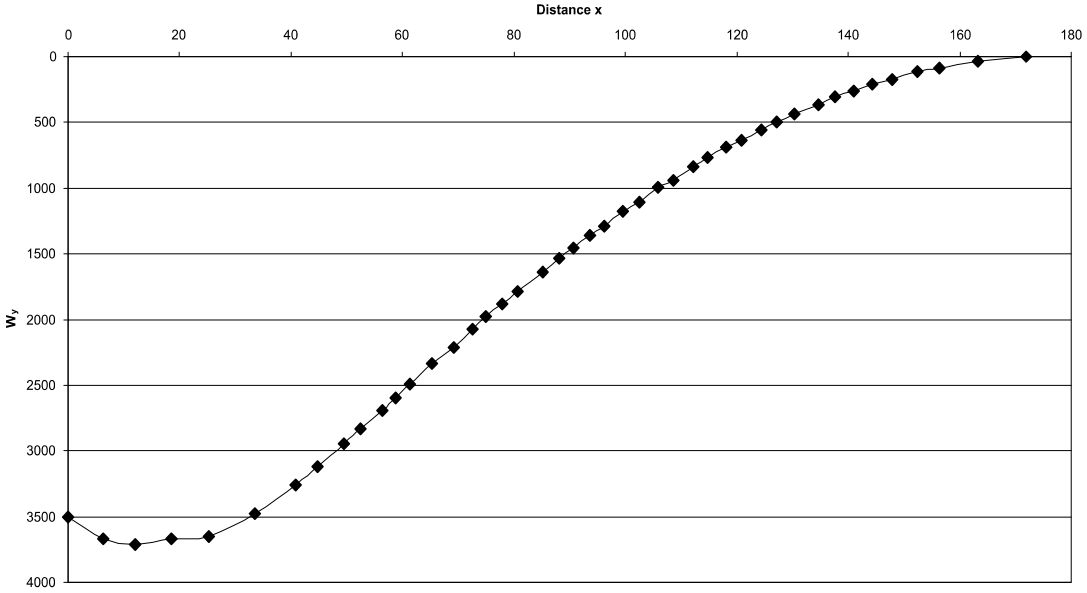

Fig A.188: Section modulus in the Peteinosaurus rostrum construction. See chapter 6.4 for legend.

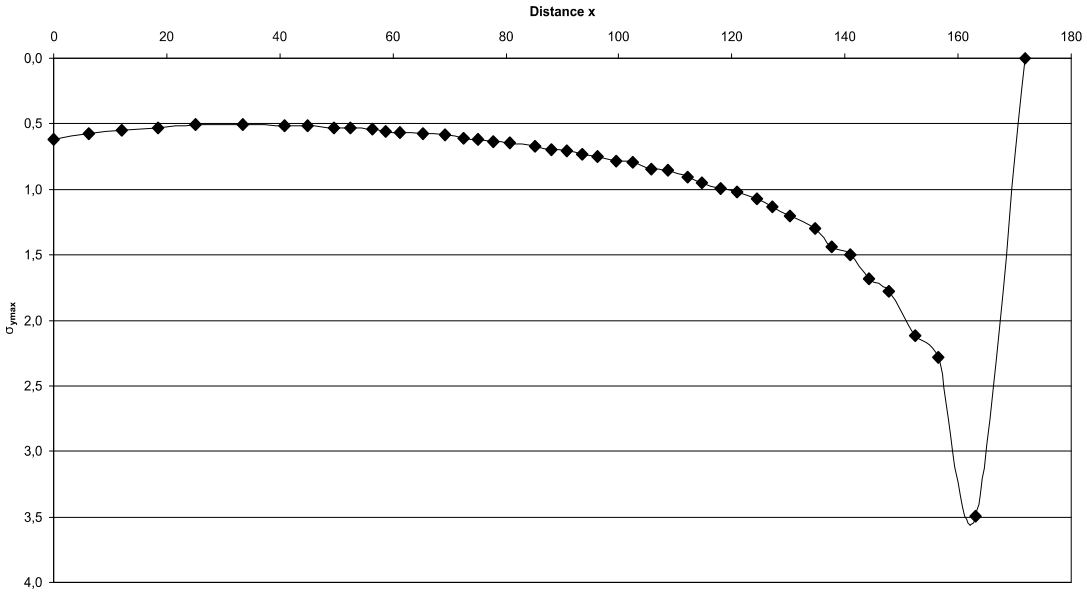

Fig A.189: Maximum bending stress in the Peteinosaurus rostrum construction. See chapter 6.4 for legend.

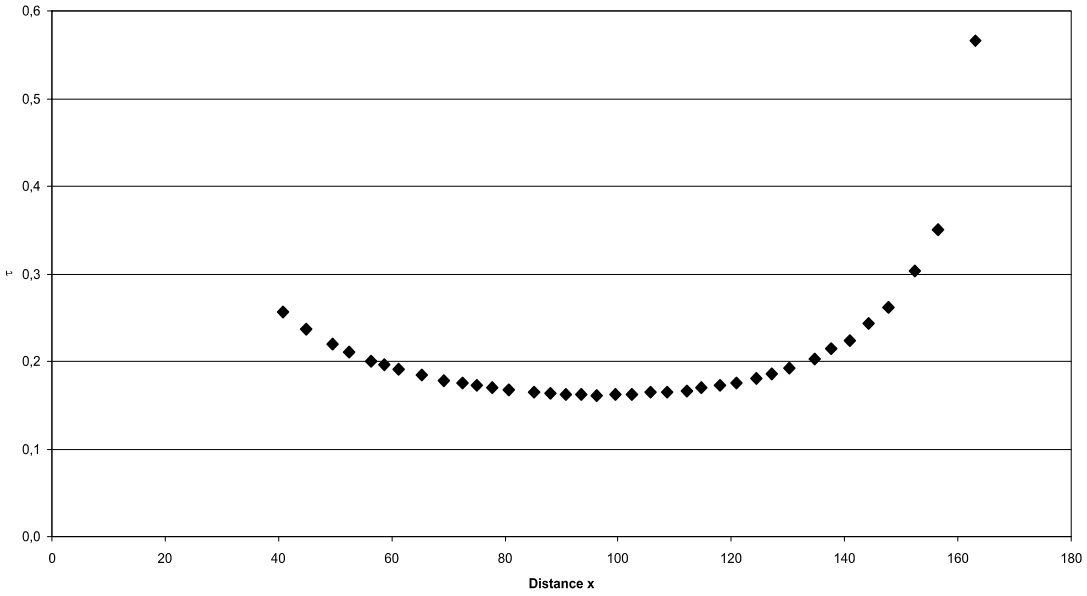

Fig. A.190: Shear stress in the Peteinosaurus rostrum construction. See chapter 6.4 for legend.

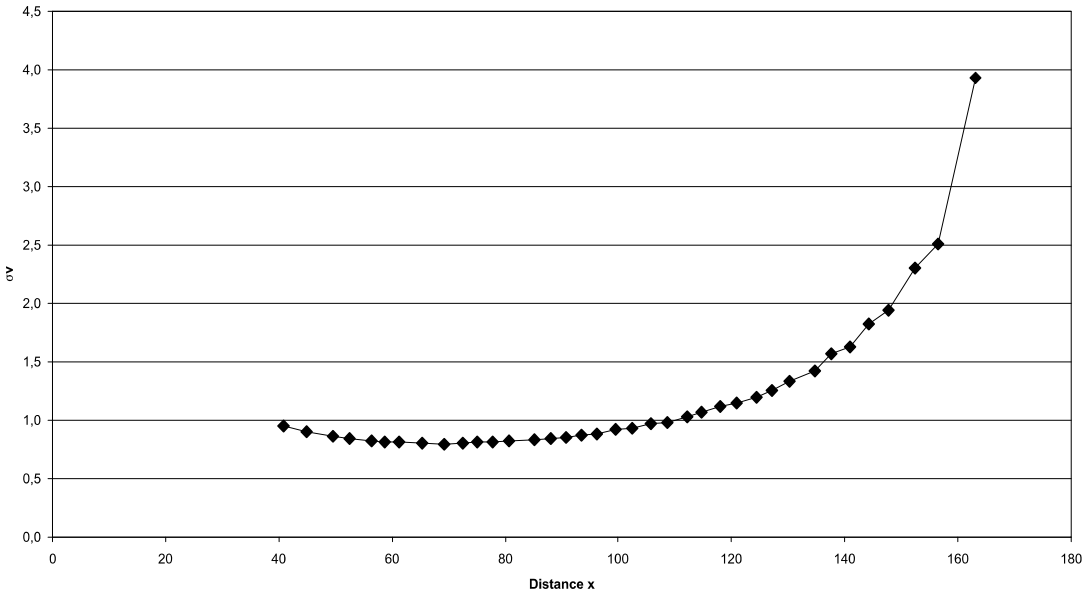

Fig. A.191: Comparison stress in the Peteinosaurus rostrum construction. See chapter 6.4 for legend.

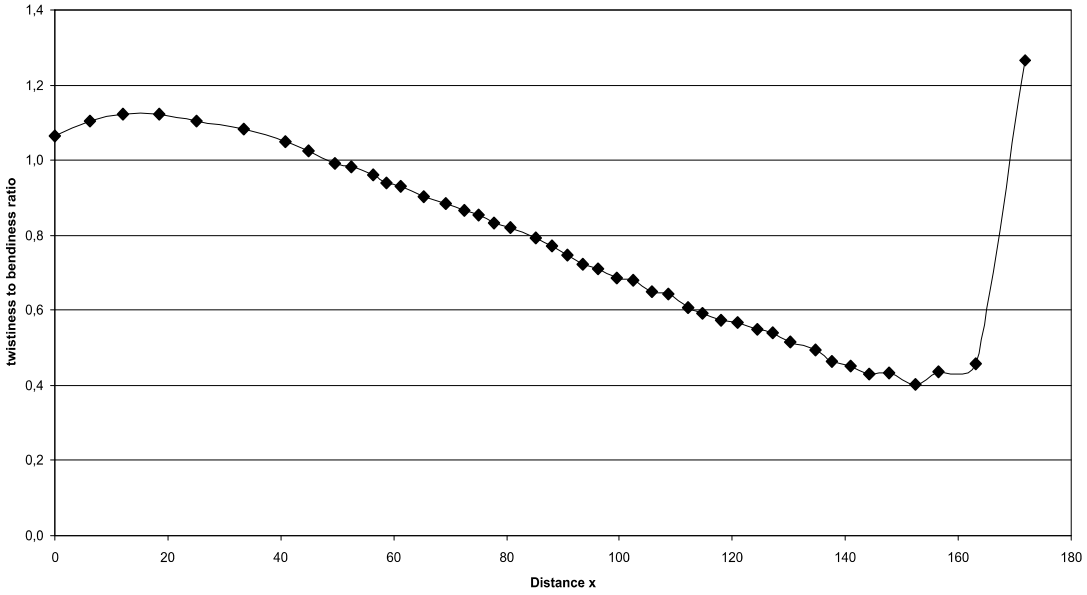

Fig. A.192: Twistiness to bendiness ratio in the Peteinosaurus rostrum construction. See chapter 6.4 for legend.

A.25 Phobetopter skull construction (see also chapter 7.25)

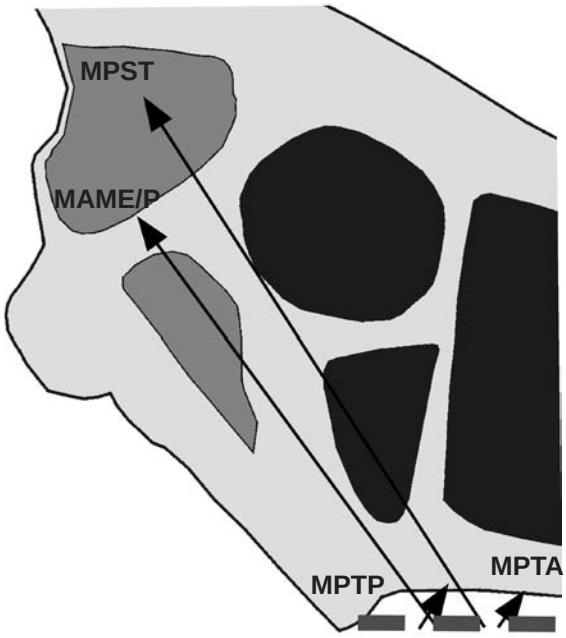

Fig A.193: Reconstruction of the principal pulling direction of the main adductor muscles in the skull of *Phobetopter*. See chapter 6 for abbreviations.

Muscles	F_1	l_1	α_1	F_2	l_2	α_1
MAME/P	36	10.52	54	2.08	182.01	126
MPST	92	15.47	57	8.00	177.95	123
MPTA	14	17.13	55	1.37	175.39	125
MPTP	88	8.1	57	3.87	184.42	123

Tab. A.47: Reconstructed lever parameters for the scaled Phobetopter skull construction. See chapter 6.2 for abbreviations.

	F_B	F_J	α_J
anterior end of rostrum	11.92	220.13	-54.69
1st tooth position	18.42	214.85	-53.69
1st to 4th tooth position	69.85	862.75	-53.85
last tooth position	44.52	194.43	-49.13
average	28.64	223.76	-52.29

Tab. A.48: Reconstructed bite and joint reaction forces and angle of joint reaction force in the scaled Phobetopter skull construction. Negative angle values mean anterodorsal direction of force. See chapter 6.2 for abbreviations.

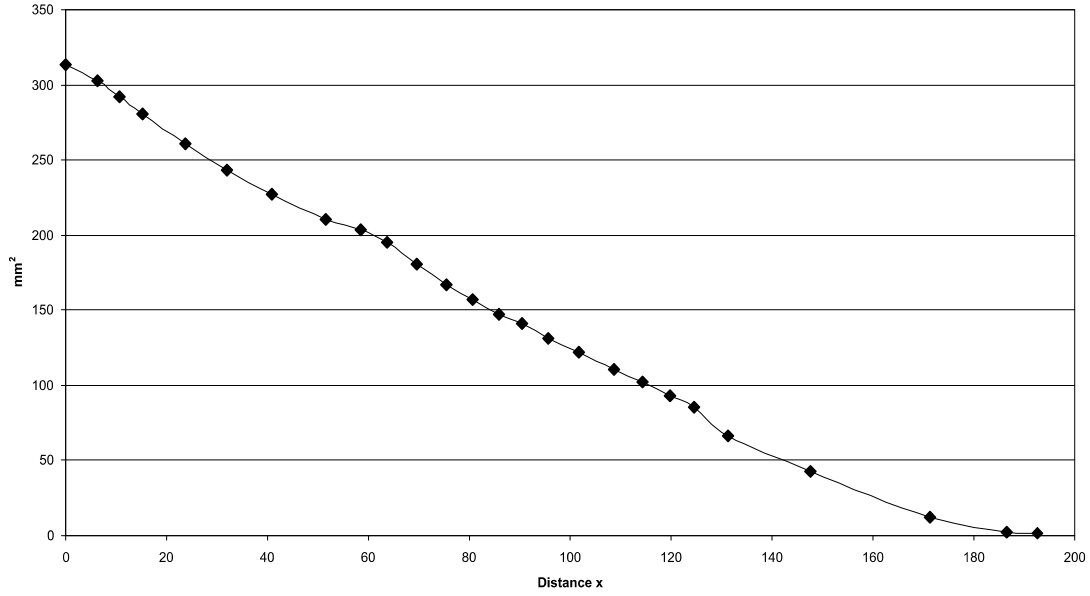

Fig A.194: Cross-sectional area of the Phobetopter rostrum construction. See chapter 6.4 for legend.

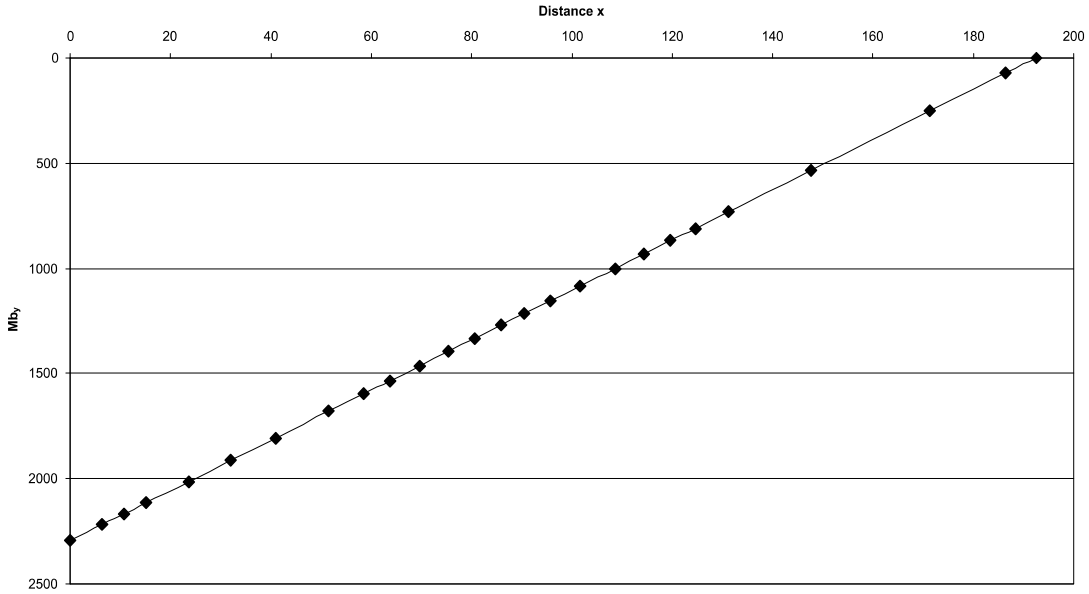

Fig A.195: Bending moments in the Phobetopter rostrum construction. See chapter 6.4 for legend.

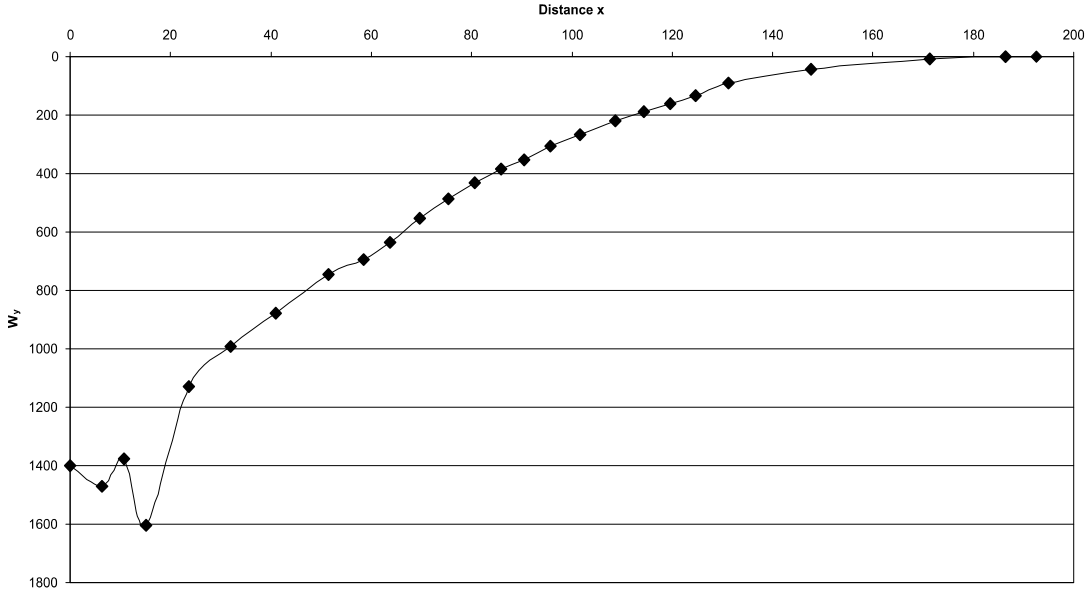

Fig A.196: Section modulus in the Phobetopter rostrum construction. See chapter 6.4 for legend.

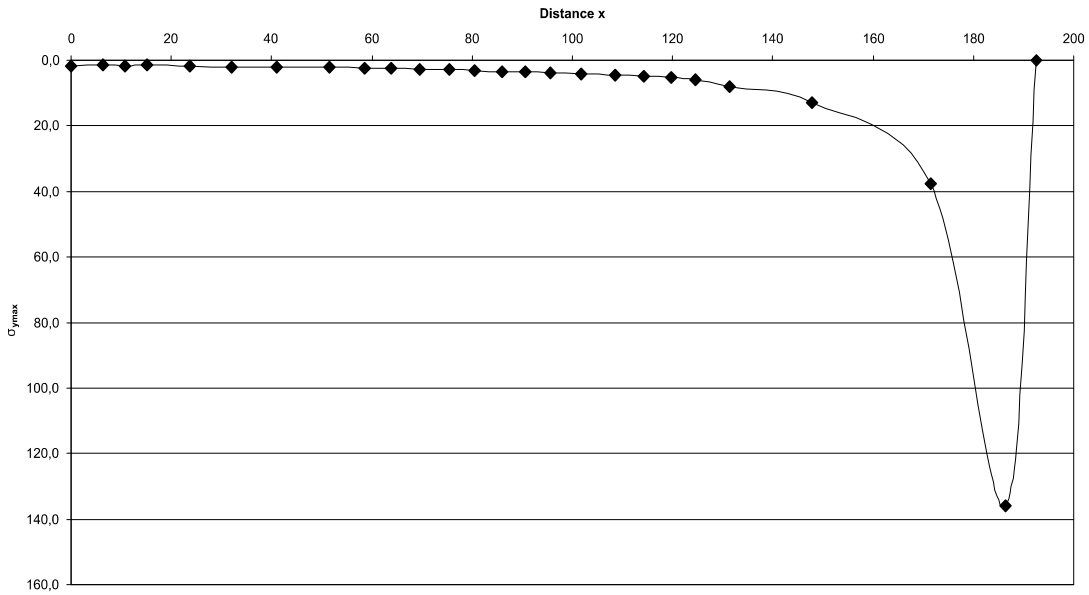

Fig A.197: Maximum bending stress in the Phobetopter rostrum construction. See chapter 6.4 for legend.

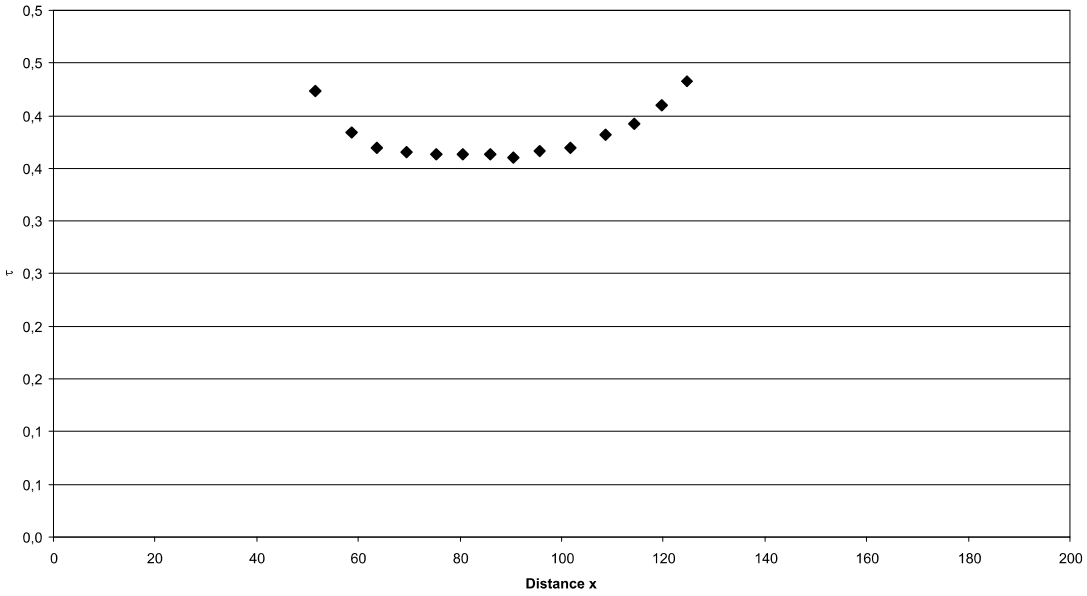

Fig. A.198: Shear stress in the Phobetopter rostrum construction. See chapter 6.4 for legend.

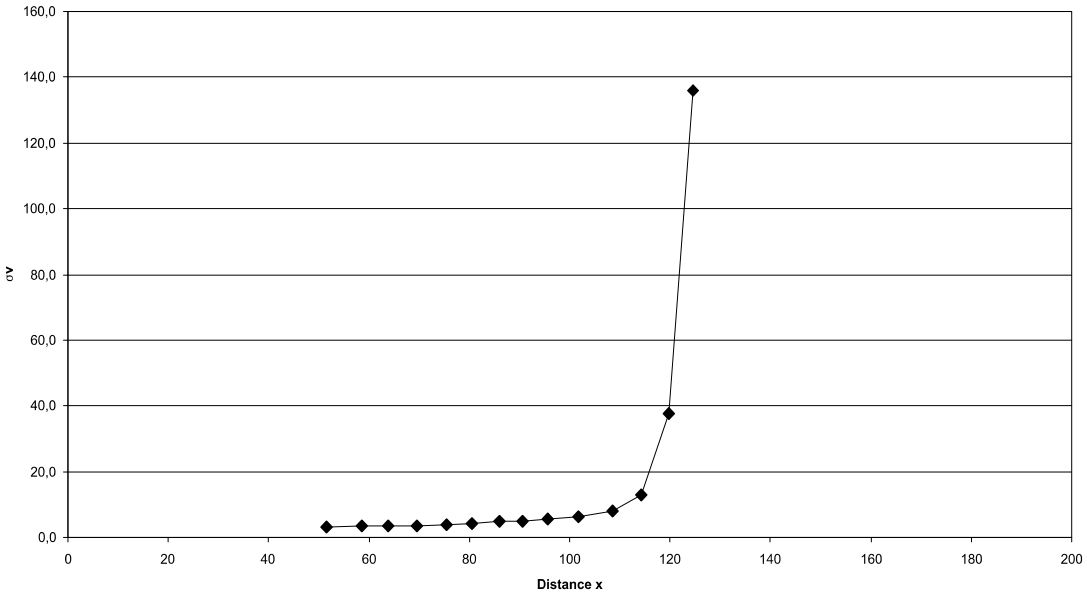

Fig. A.199: Comparison stress in the Phobetopter rostrum construction. See chapter 6.4 for legend.

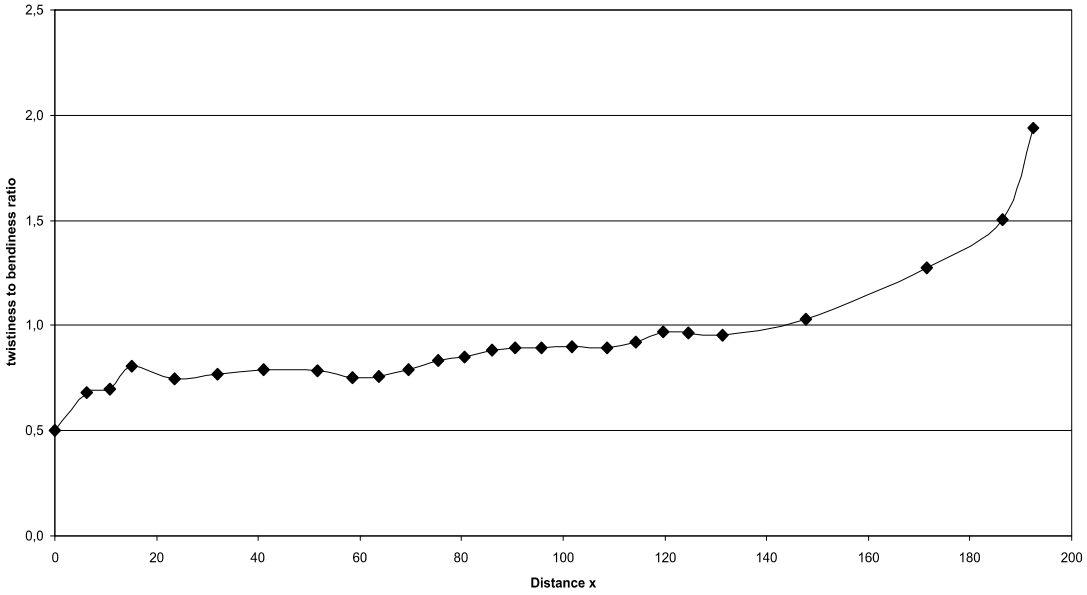

Fig. A.200: Twistiness to bendiness ratio in the Phobetopter rostrum construction. See chapter 6.4 for legend.

A.26 Plataleorhynchus skull construction (see also chapter 7.26)

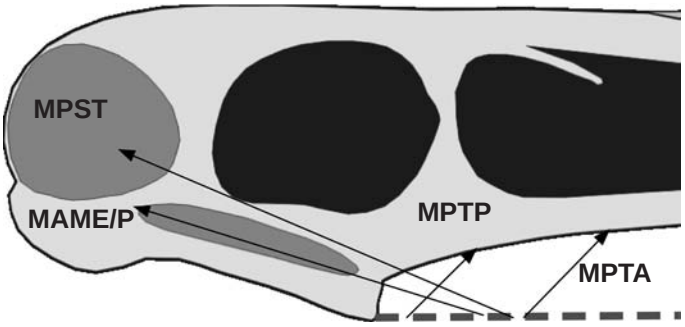

Fig A.201: Reconstruction of the principal pulling direction of the main adductor muscles in the skull of *Plataleorhynchus*. See chapter 6.2 for abbreviations.

Muscles	F_1	l_1	α_1	F_2	l_2	α_1
MAME/P	36	23.78	17	2.42	354.05	163
MPST	92	31.12	23	8.25	347.00	157
MPTA	14	33.79	46	1.37	244.42	134
MPTP	88	7.29	45	1.73	370.82	135

Tab. A.49: Reconstructed lever parameters for the scaled Plataleorhynchus skull construction. See chapter 6.2 for abbreviations.

	F_B	F_J	α_J
1st tooth position	5.72	222.00	-30.61
1st to 4th tooth position	23.05	887.93	-30.60
1st to 13th tooth position	79.15	2883.6	-30.53
last tooth position	15.10	217.38	-28.48
average	8.34	220.69	-30.02

Tab. A.50: Reconstructed bite and joint reaction forces and angle of joint reaction force in the scaled Plataleorhynchus skull construction. Negative angle values mean anterodorsal direction of force. See chapter 6.2 for abbreviations.

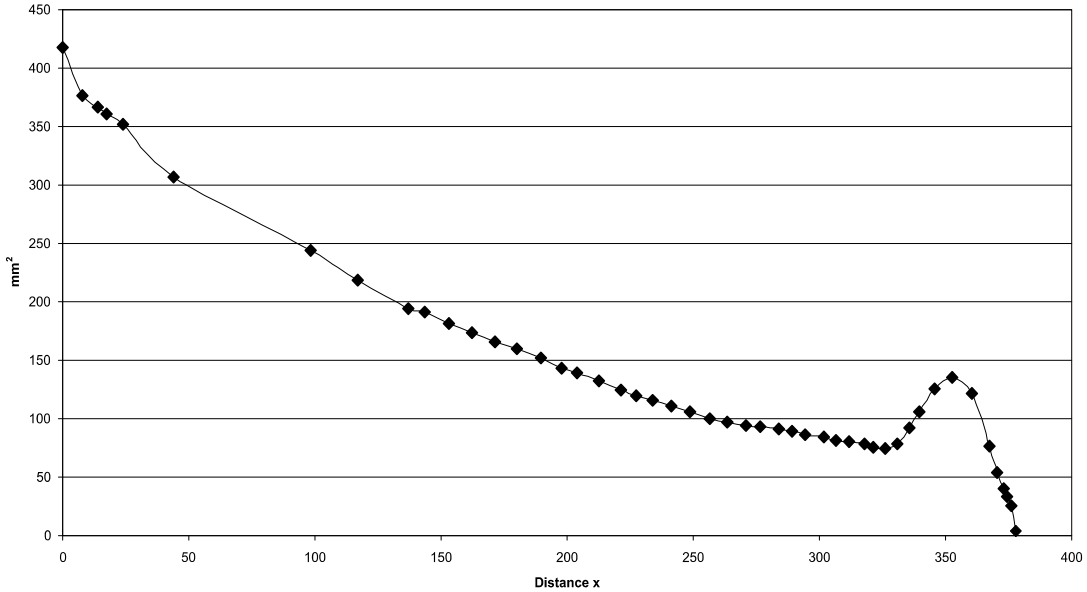

Fig A.202: Cross-sectional area of the Plataleorhynchus rostrum construction. See chapter 6.4 for legend.

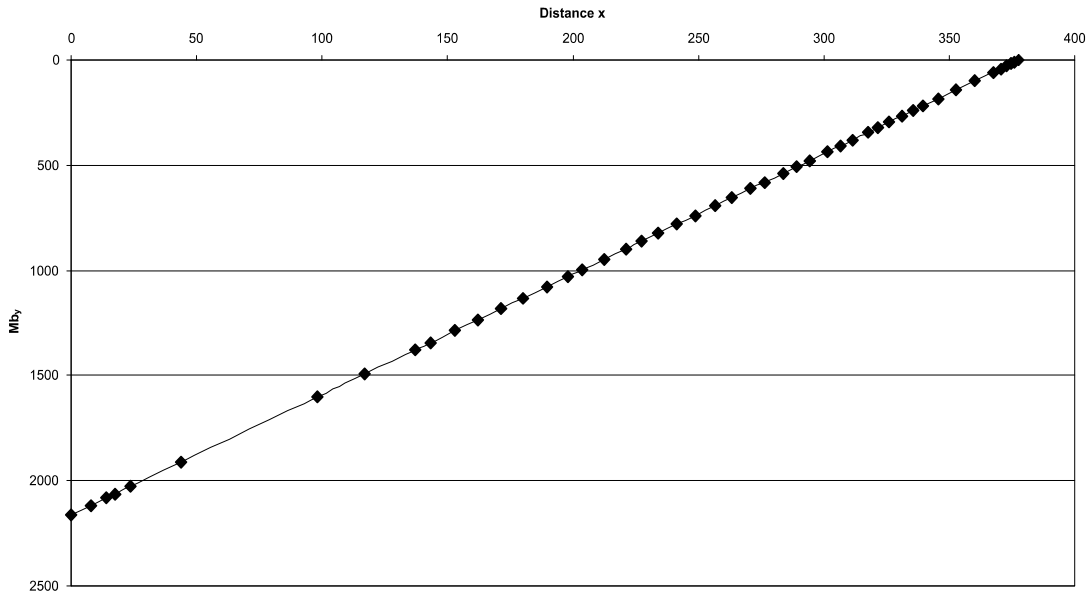

Fig A.203: Bending moments in the Plataleorhynchus rostrum construction. See chapter 6.4 for legend.

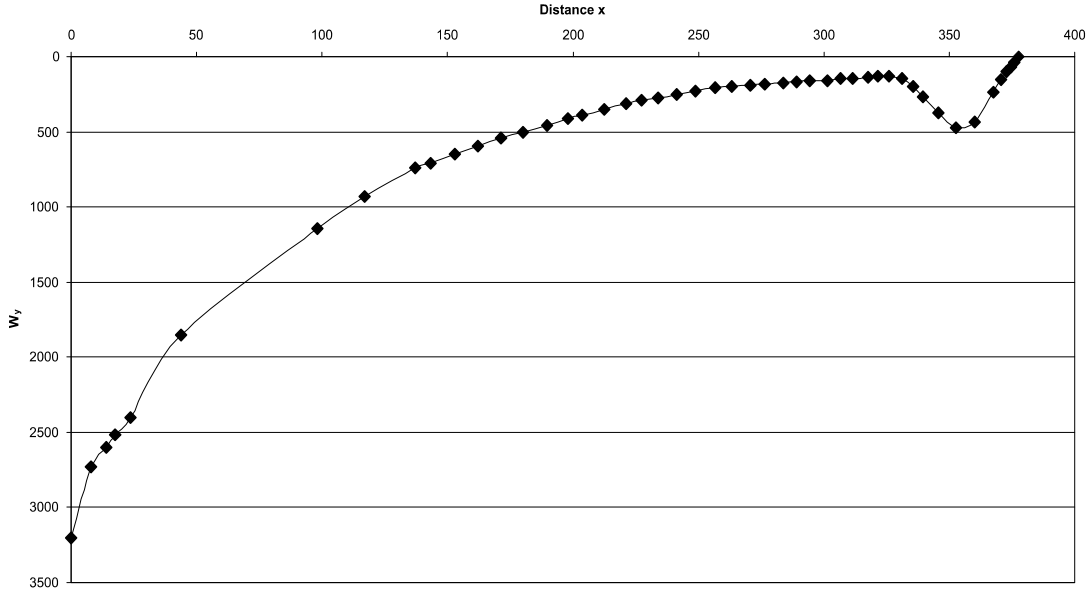

Fig A.204: Section modulus in the Plataleorhynchus rostrum construction. See chapter 6.4 for legend.

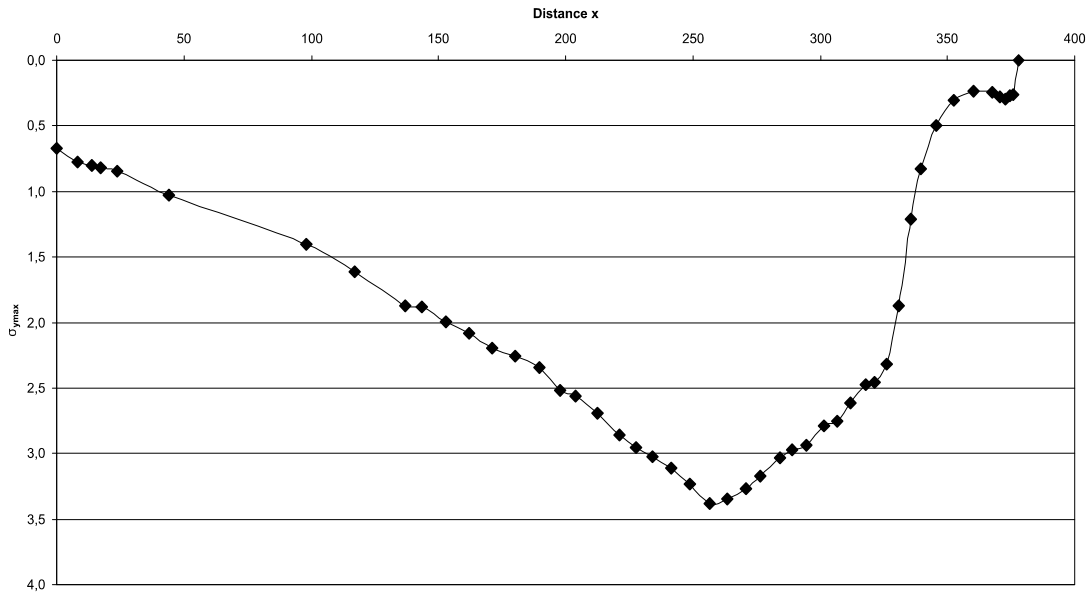

Fig A.205: Maximum bending stress in the Plataleorhynchus rostrum construction. See chapter 6.4 for legend.

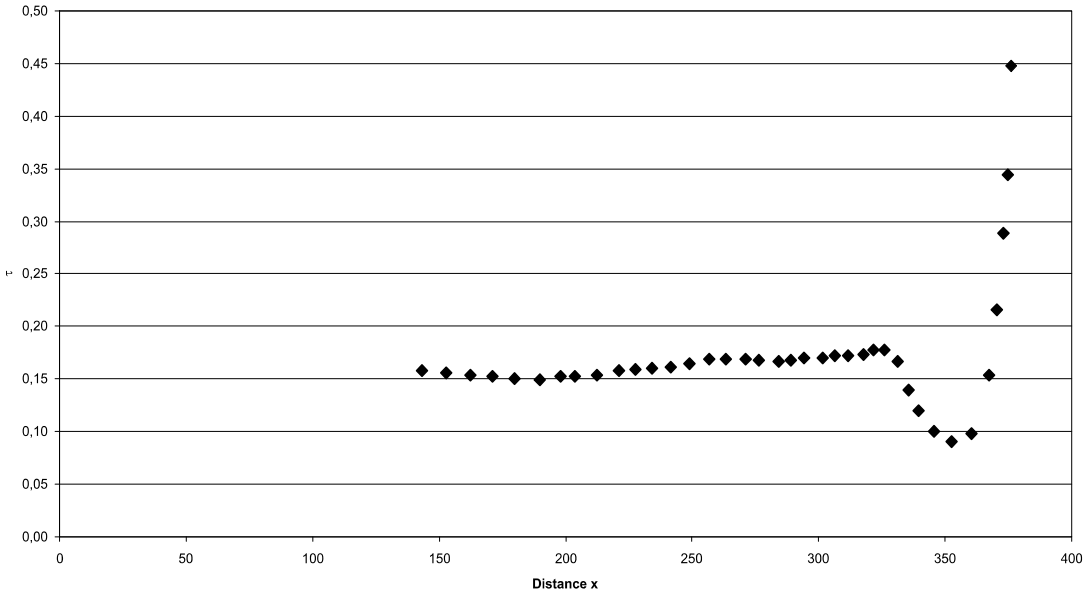

Fig. 7.206: Shear stress in the Plataleorhynchus rostrum construction. See chapter 6.4 for legend.

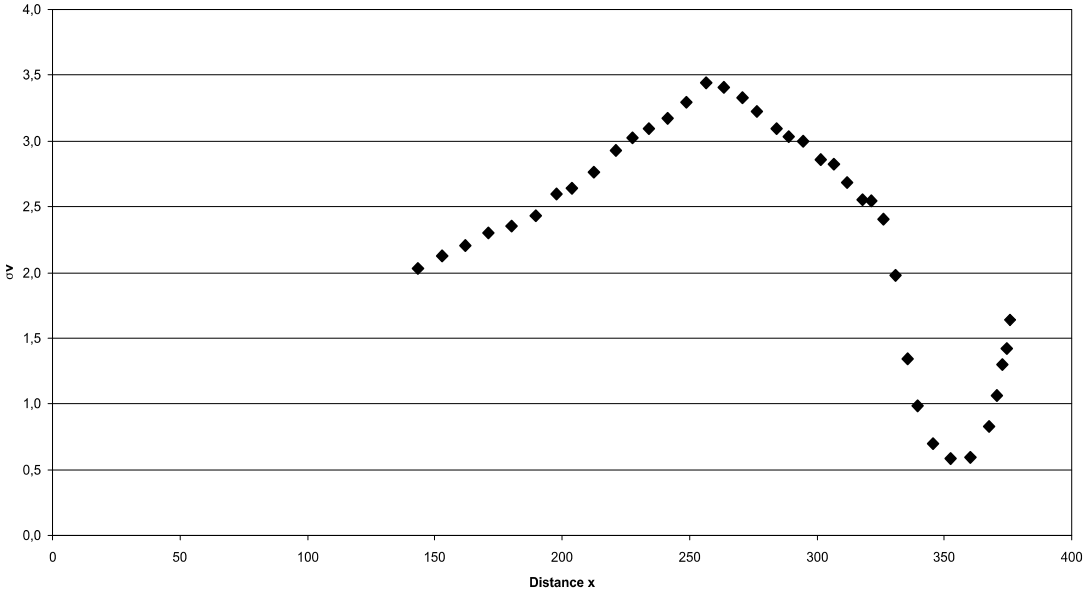

Fig. A.207: Comparison stress in the Plataleorhynchus rostrum construction. See chapter 6.4 for legend.

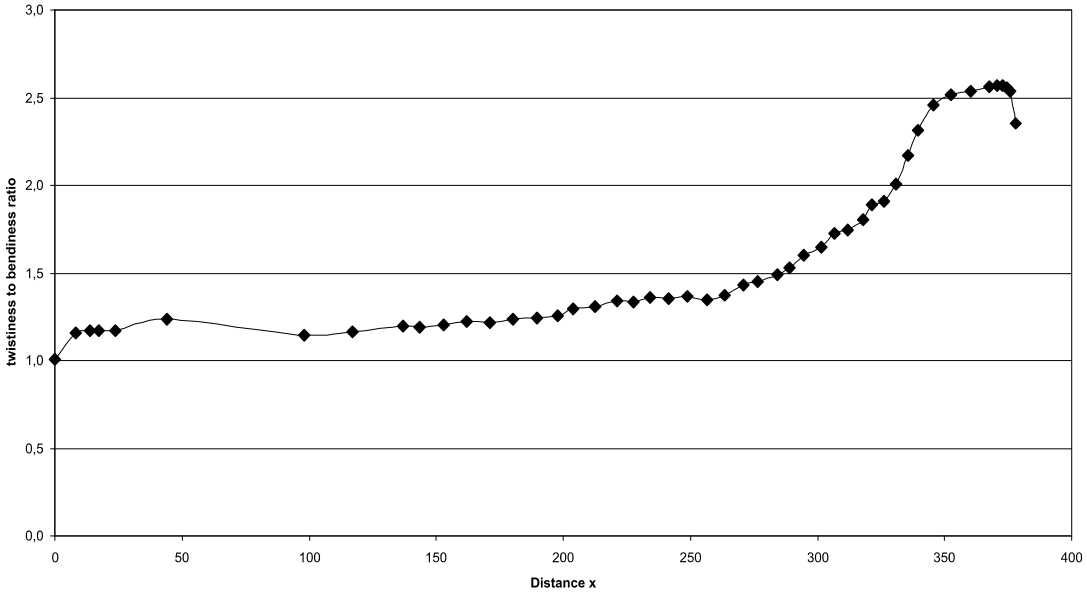

Fig. A.208: Twistiness to bendiness ratio in the Plataleorhynchus rostrum construction. See chapter 6.4 for legend.

A.27 Preondactylus skull construction (see also chapter 7.27)

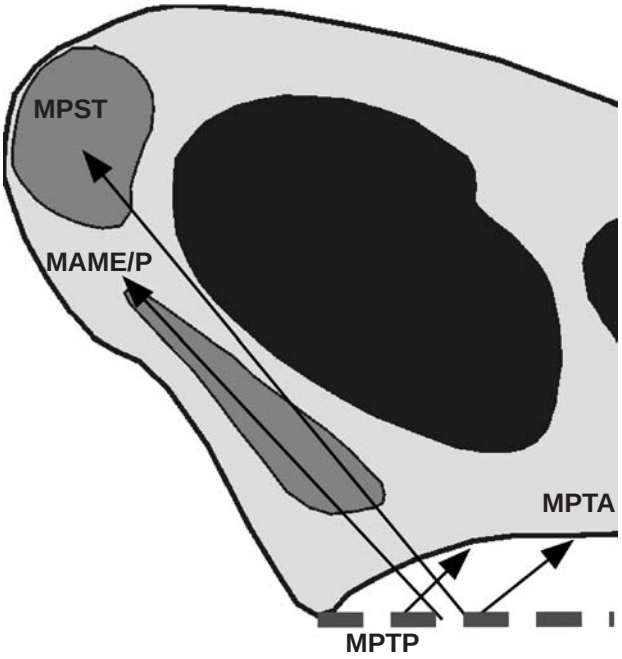

Fig A.209: Reconstruction of the principal pulling direction of the main adductor muscles in the skull of *Preondactylus*. See chapter 6 for abbreviations.

Muscles	F_1	l_1	α_1	F_2	l_2	α_1
MAME/P	36	14.15	47	3.31	154.06	133
MPST	92	16.94	51	10.30	151.27	129
MPTA	14	19.26	39	1.81	148.94	141
MPTP	88	9.96	45	5.54	158.25	135

Tab. A.51: Reconstructed lever parameters for the scaled Preondactylus skull construction. See chapter 6.2 for abbreviations.

	F_B	F_J	α_J
1st tooth position	14.11	219.42	-44.85
1st to 4th tooth position	59.92	875.24	-44.69
last tooth position	58.24	190.88	-35.42
average	29.18	209.29	-41.81

Tab. A.52: Reconstructed bite and joint reaction forces and angle of joint reaction force in the scaled Preondactylus skull construction. Negative angle values mean anterodorsal direction of force. See chapter 6.2 for abbreviations.

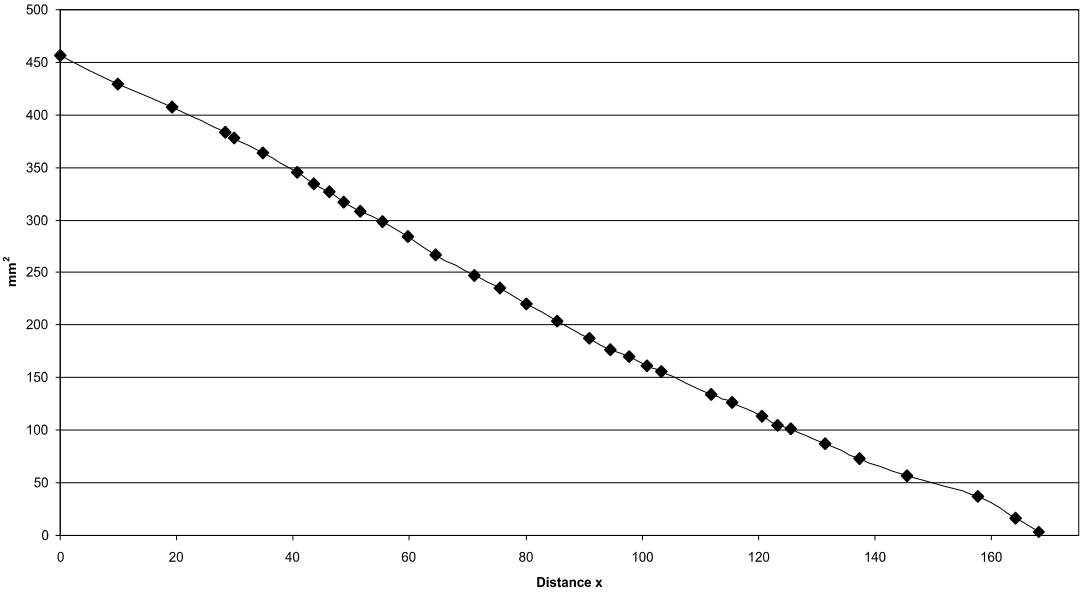

Fig A.210: Cross-sectional area of the Preondactylus rostrum construction. See chapter 6.4 for legend.

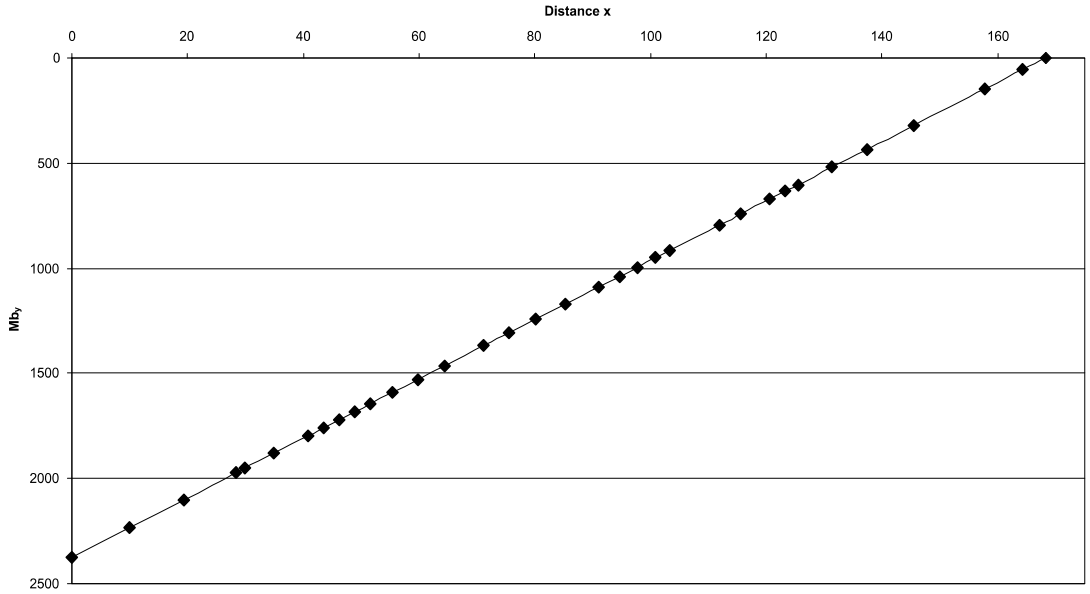

Fig A.211: Bending moments in the Preondactylus rostrum construction. See chapter 6.4 for legend.

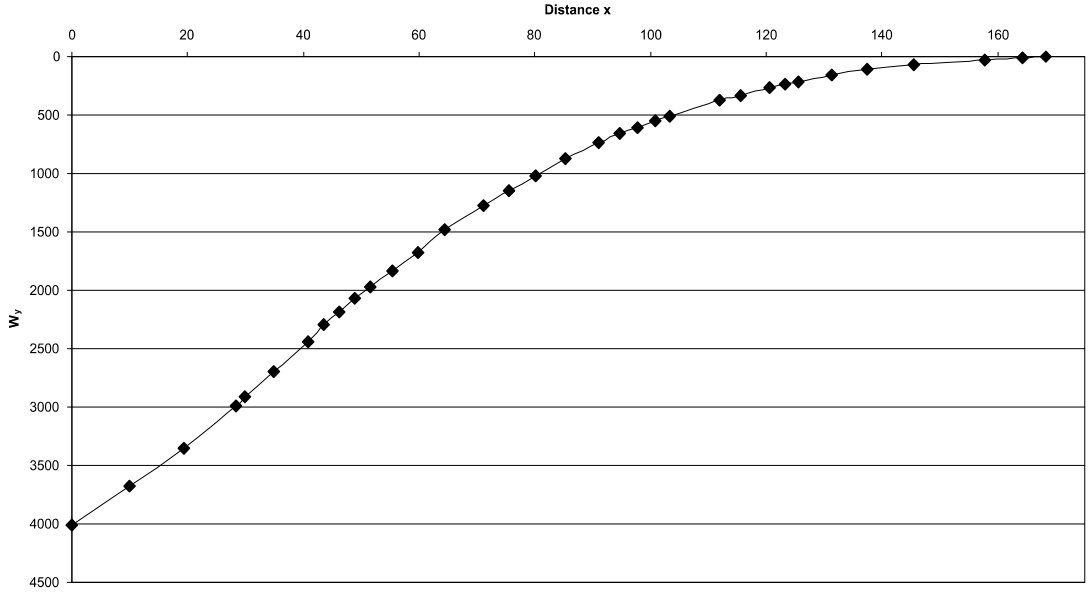

Fig A.212: Section modulus in the Preondactylus rostrum construction. See chapter 6.4 for legend.

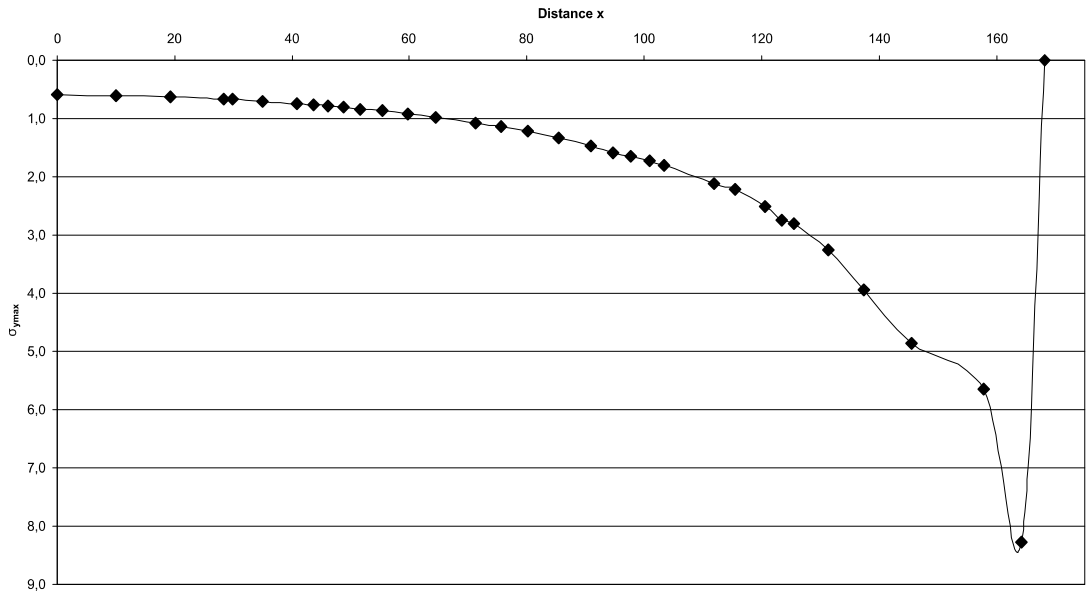

Fig A.213: Maximum bending stress in the Preondactylus rostrum construction. See chapter 6.4 for legend.

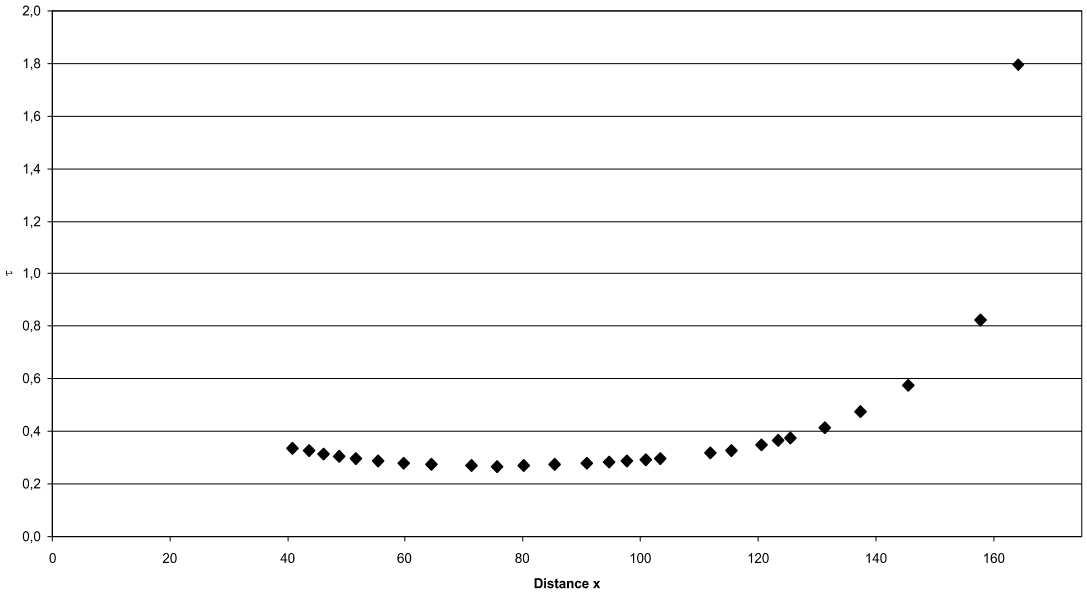

Fig. A.214: Shear stress in the Preondactylus rostrum construction. See chapter 6.4 for legend.

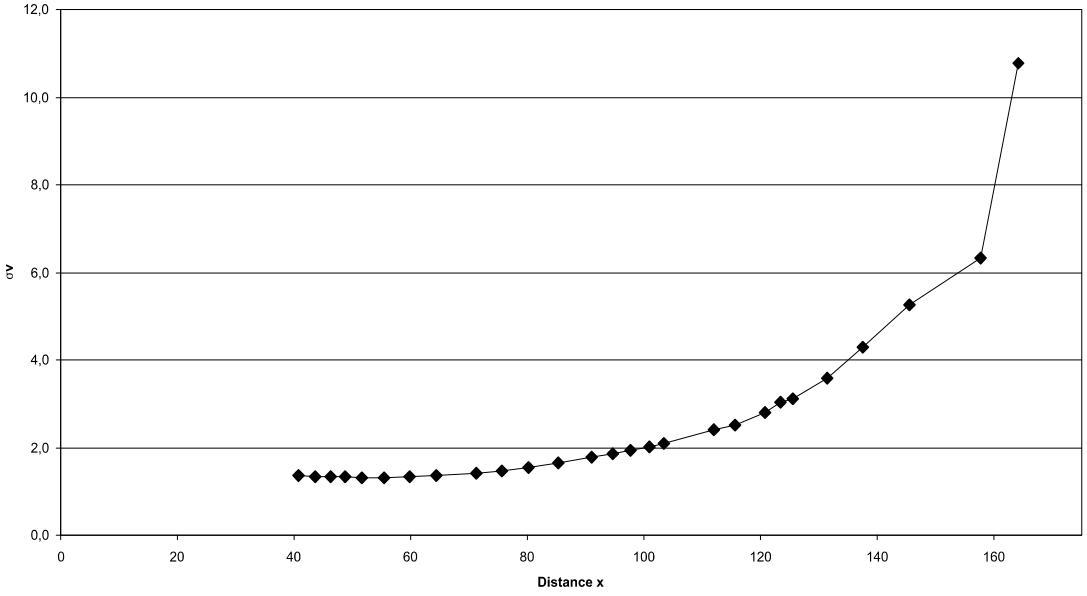

Fig. A.215: Comparison stress in the Preondactylus rostrum construction. See chapter 6.4 for legend.

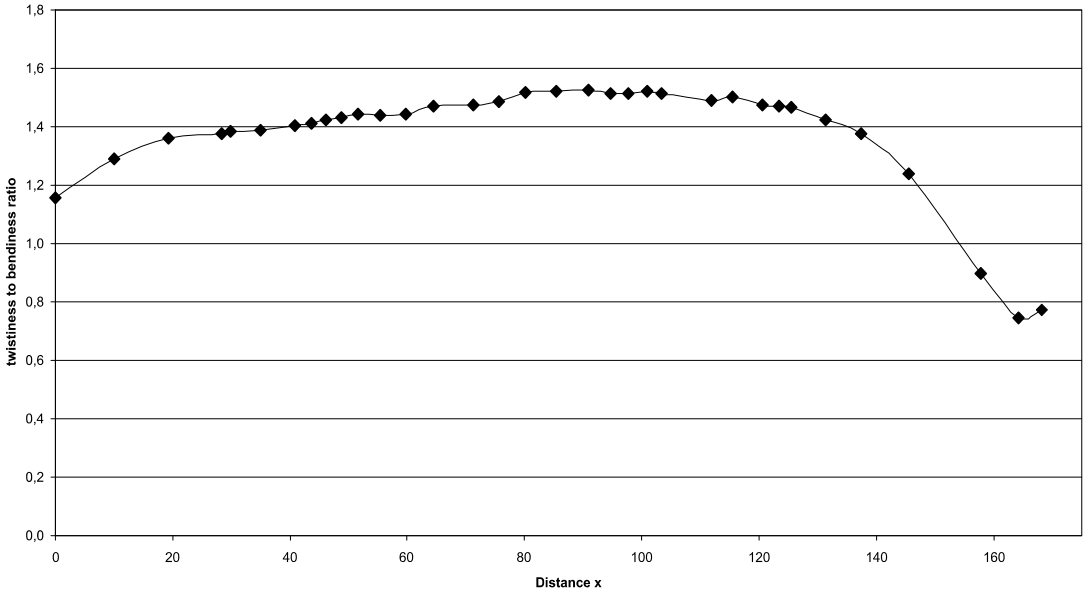

Fig. A.216: Twistiness to bendiness ratio in the Preondactylus rostrum construction. See chapter 6.4 for legend.

A.28 Pteranodon skull construction (see also chapter 7.28)

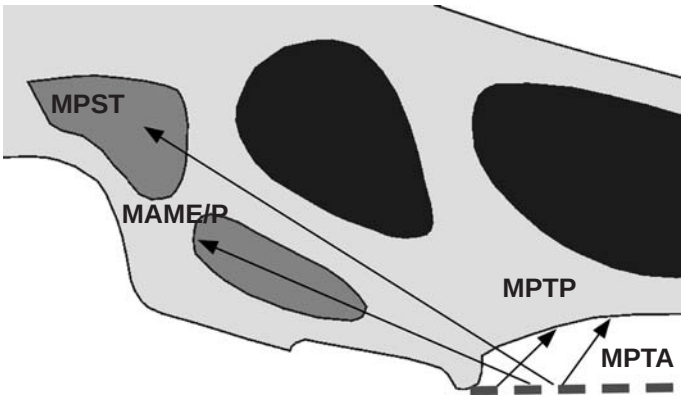

Fig A.217: Reconstruction of the principal pulling direction of the main adductor muscles in the skull of *Pteranodon*. See chapter 6 for abbreviations.

Muscles	F_1	l_1	α_1	F_2	l_2	α_1
MAME/P	36	9.06	24	0.92	355.43	156
MPST	92	13.56	32	3.55	350.93	148
MPTA	14	15.49	53	0.62	349.01	127
MPTP	88	2.76	44	0.67	361.73	136

Tab. A.53: Reconstructed lever parameters for the scaled Pteranodon skull construction. See chapter 6.2 for abbreviations.

	F_B	F_J	α_J
anterior tip of jaw	3.12	225.69	-35.98
anterior to nasoant. fen.	16.94	217.86	-33.04
average	10.03	221.78	-34.51

Tab. A.54: Reconstructed bite and joint reaction forces and angle of joint reaction force in the scaled Pteranodon skull construction. Negative angle values mean anterodorsal direction of force. See chapter 6.2 for abbreviations.

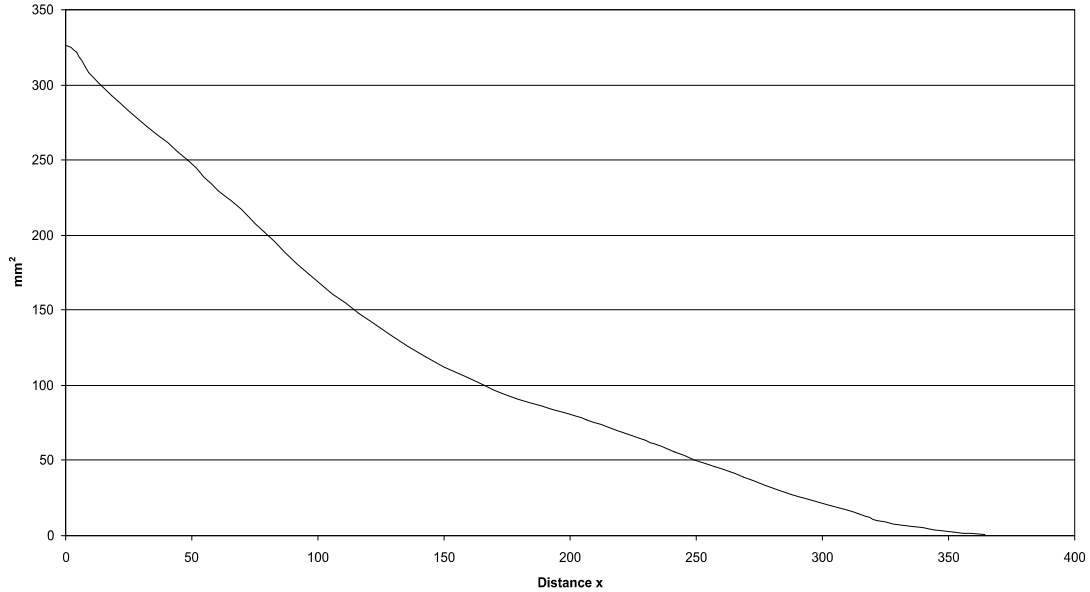

Fig A.218: Cross-sectional area of the Pteranodon rostrum construction. See chapter 6.4 for legend.

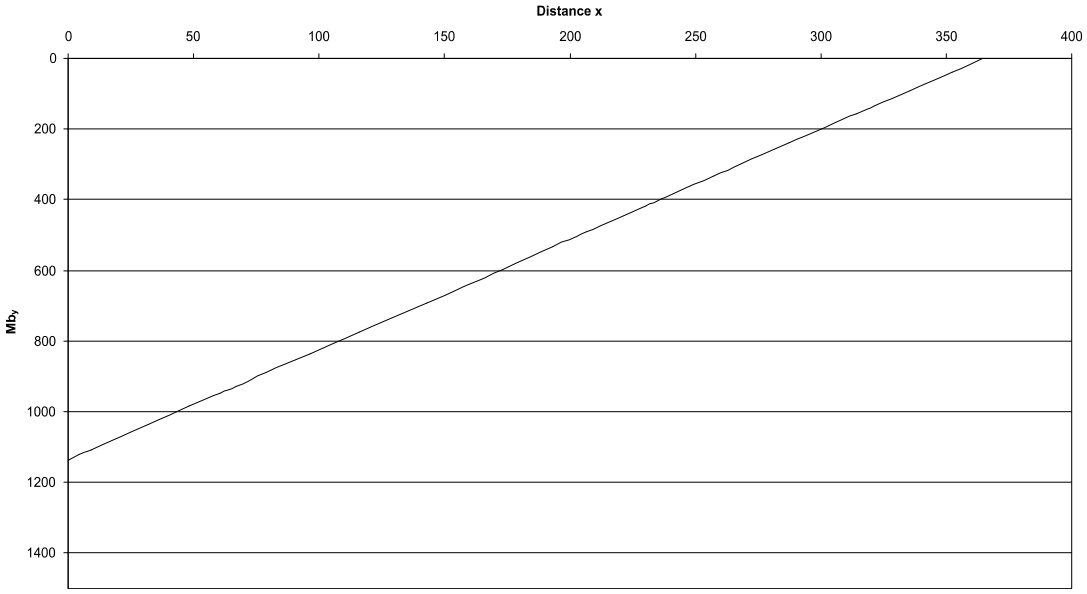

Fig A.219: Bending moments in the Pteranodon rostrum construction. See chapter 6.4 for legend.

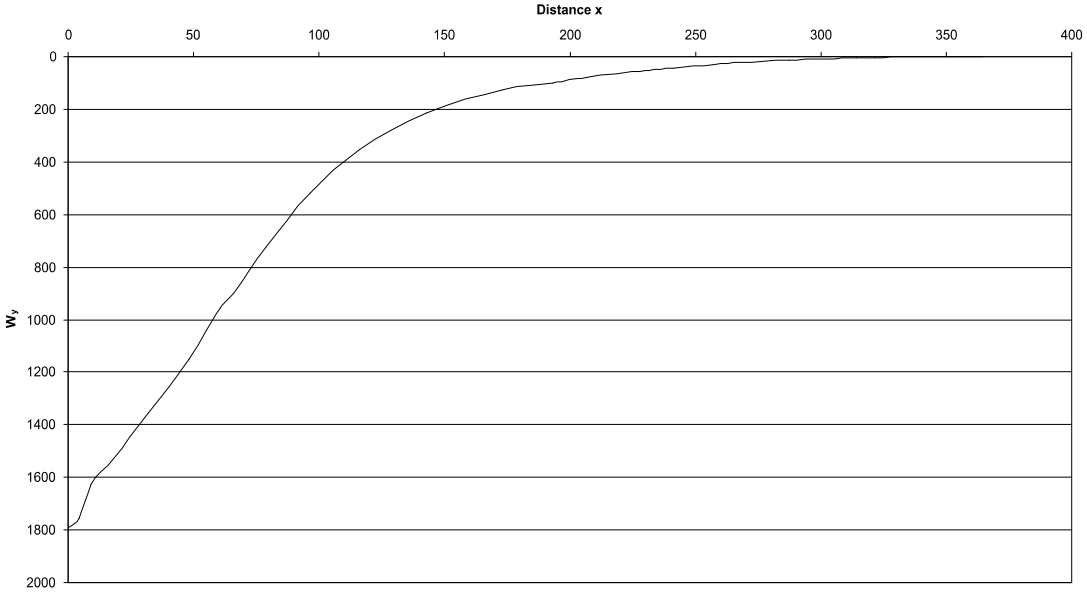

Fig A.220: Section modulus in the Pteranodon rostrum construction. See chapter 6.4 for legend.

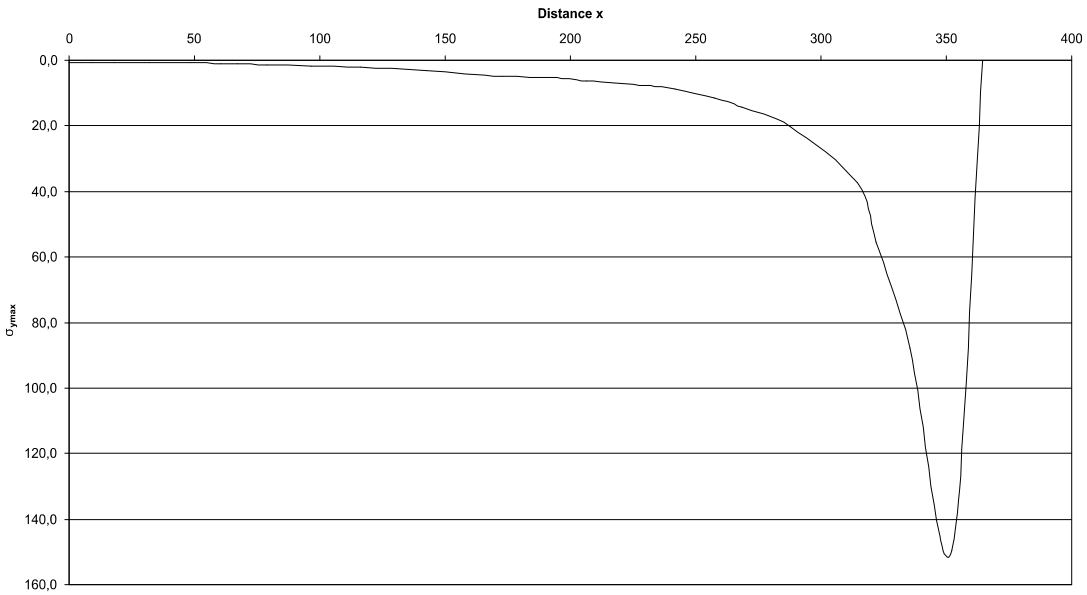

Fig A.221: Maximum bending stress in the Pteranodon rostrum construction. See chapter 6.4 for legend.

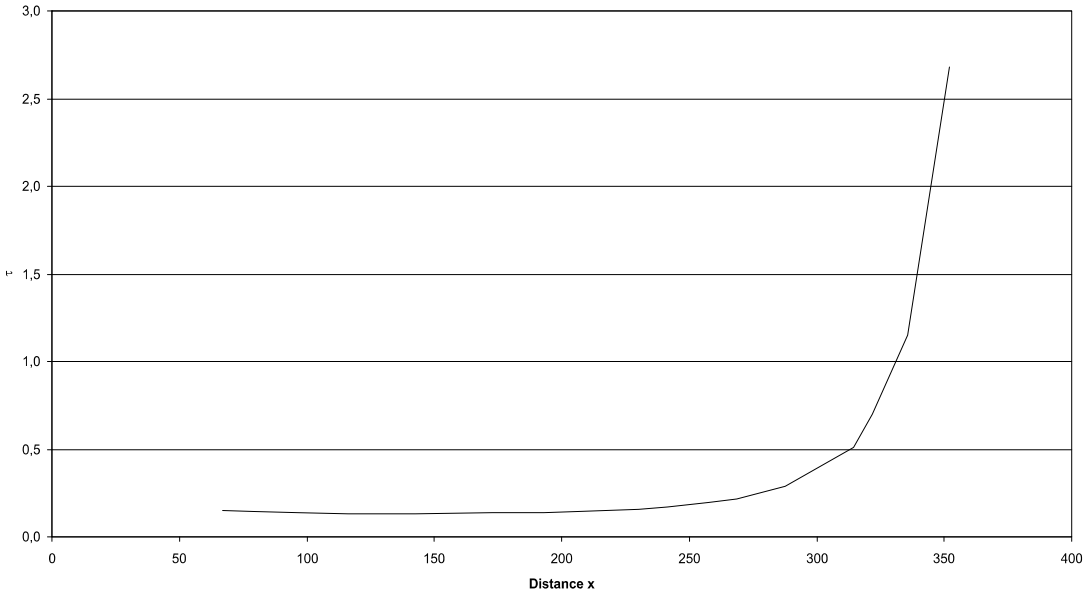

Fig. A.222: Shear stress in the Pteranodon rostrum construction. See chapter 6.4 for legend.

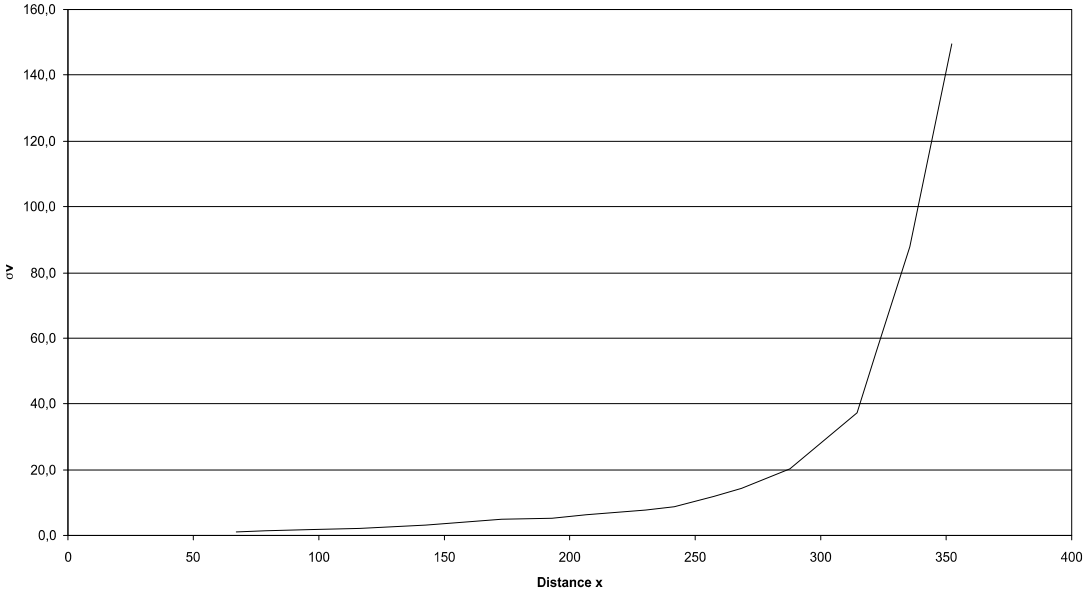

Fig. A.223: Comparison stress in the Pteranodon rostrum construction. See chapter 6.4 for legend.

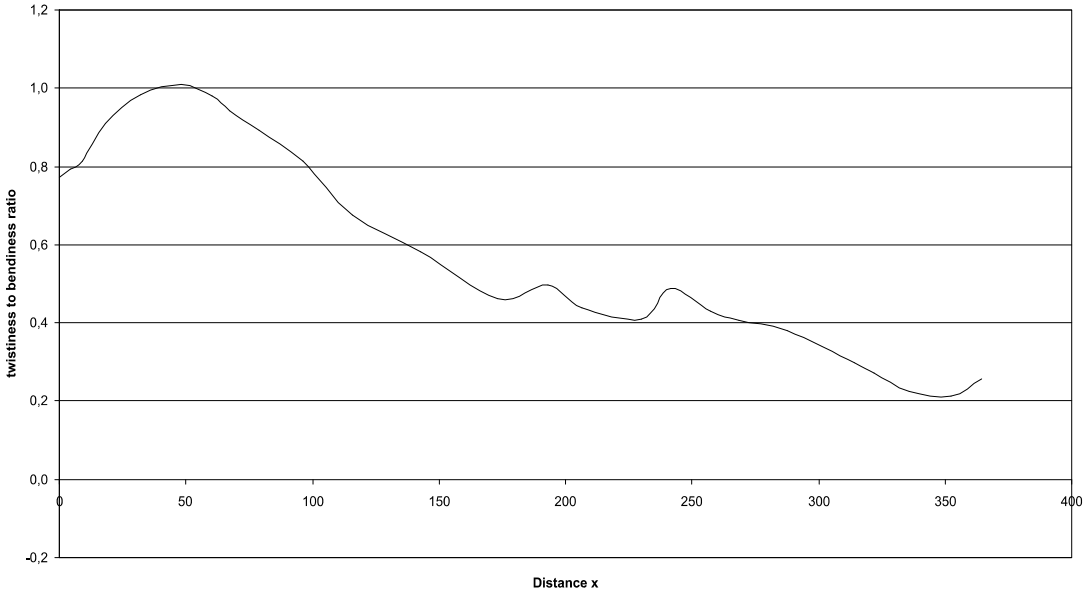

Fig. A.224: Twistiness to bendiness ratio in the Pteranodon rostrum construction. See chapter 6.4 for legend.

A.29 Pterodactylus antiquus skull construction (see also chapter 7.29)

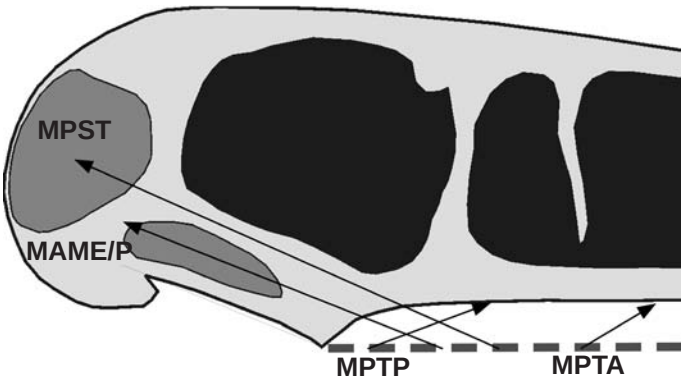

Fig A.225: Reconstruction of the principal pulling direction of the main adductor muscles in the skull of *Pterodactylus antiquus*. See chapter 6 for abbreviations.

Muscles	F_1	l_1	α_1	F_2	l_2	α_1
MAME/P	36	23.18	22	2.62	318.69	158
MPST	92	34.78	24	10.42	307.09	156
MPTA	14	53.4	31	2.59	288.47	149
MPTP	88	10.76	21	2.86	331.11	159

Tab. A.55: Reconstructed lever parameters for the scaled Pterodactylus antiquus skull construction. See chapter 6.2 for abbreviations.

	F_B	F_J	α_J
1st tooth position	6.86	227.30	-21.37
1st to 4th tooth position	28.46	908.44	-21.31
last tooth position	14.42	224.56	-19.58
average	9.73	226.19	-20.69

Tab. A.56: Reconstructed bite and joint reaction forces and angle of joint reaction force in the scaled Pterodactylus antiquus skull construction. Negative angle values mean anterodorsal direction of force. See chapter 6.2 for abbreviations.

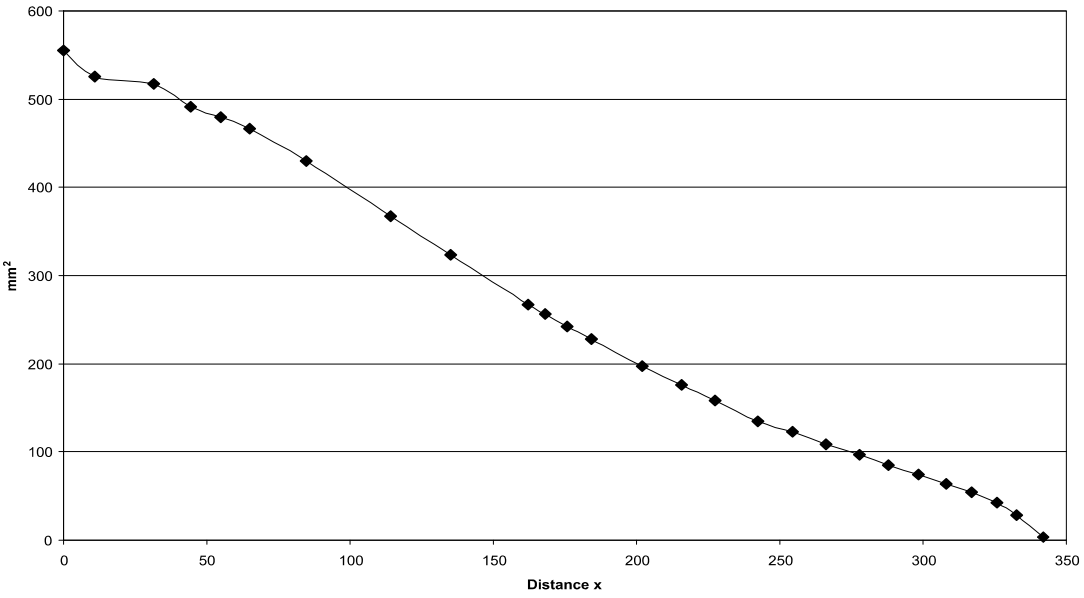

Fig A.226: Cross-sectional area of the Pterodactylus antiquus rostrum construction. See chapter 6.4 for legend.

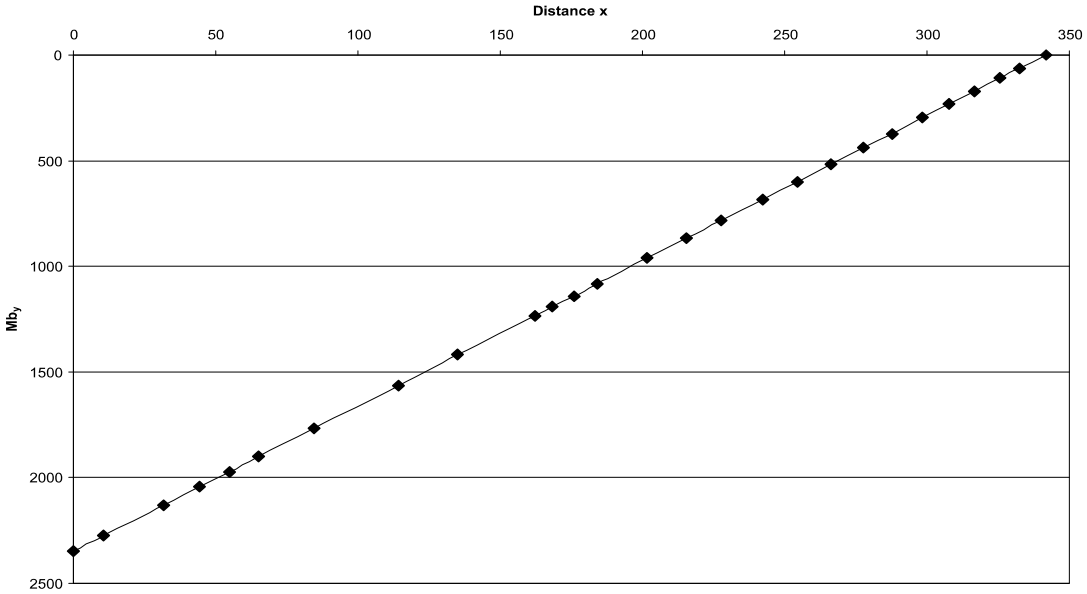

Fig A.227: Bending moments in the Pterodactylus antiquus rostrum construction. See chapter 6.4 for legend.

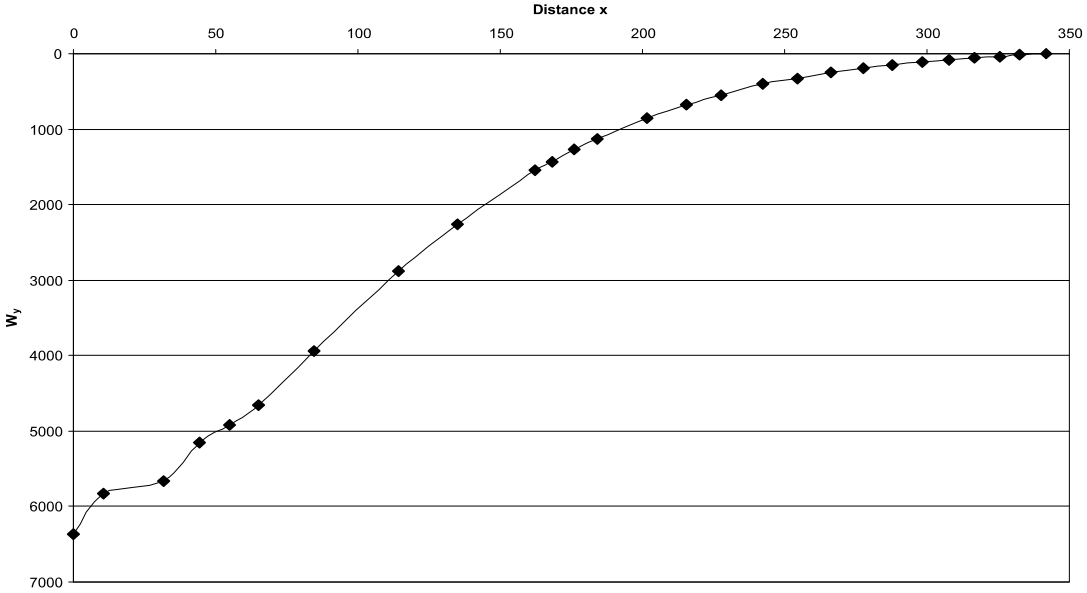

Fig A.228: Section modulus in the Pterodactylus antiquus rostrum construction. See chapter 6.4 for legend.

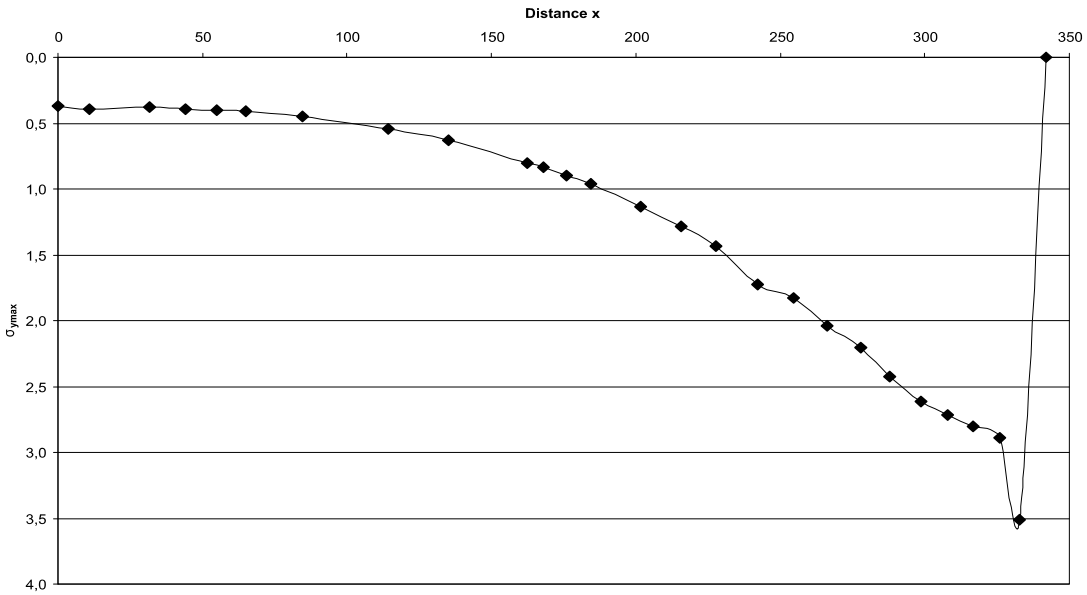

Fig A.229: Maximum bending stress in the Pterodactylus antiquus rostrum construction. See chapter 6.4 for legend.

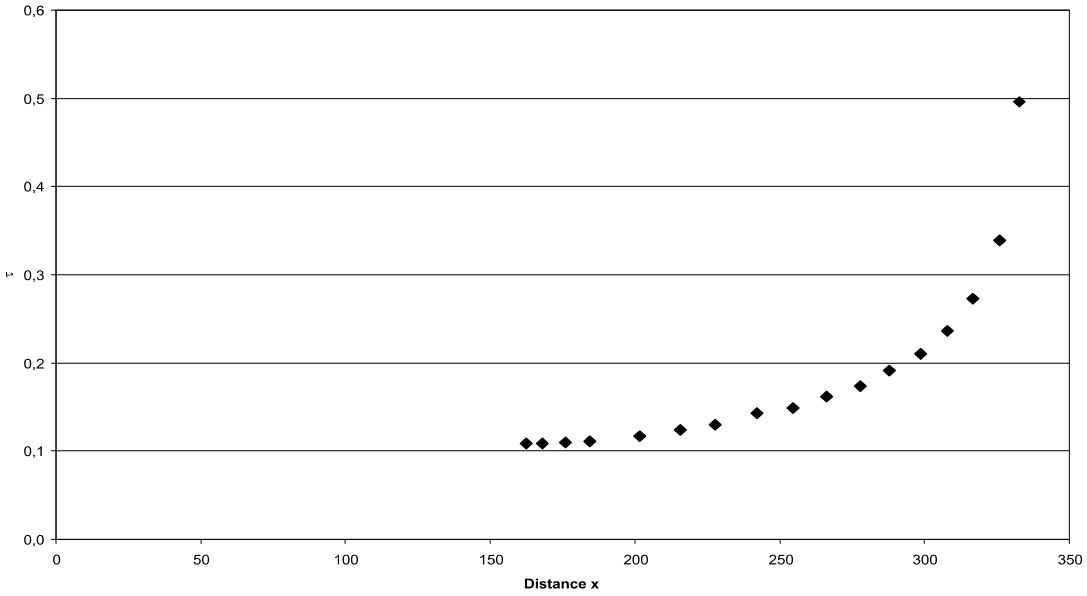

Fig. A.230: Shear stress in the Pterodactylus antiquus rostrum construction. See chapter 6.4 for legend.

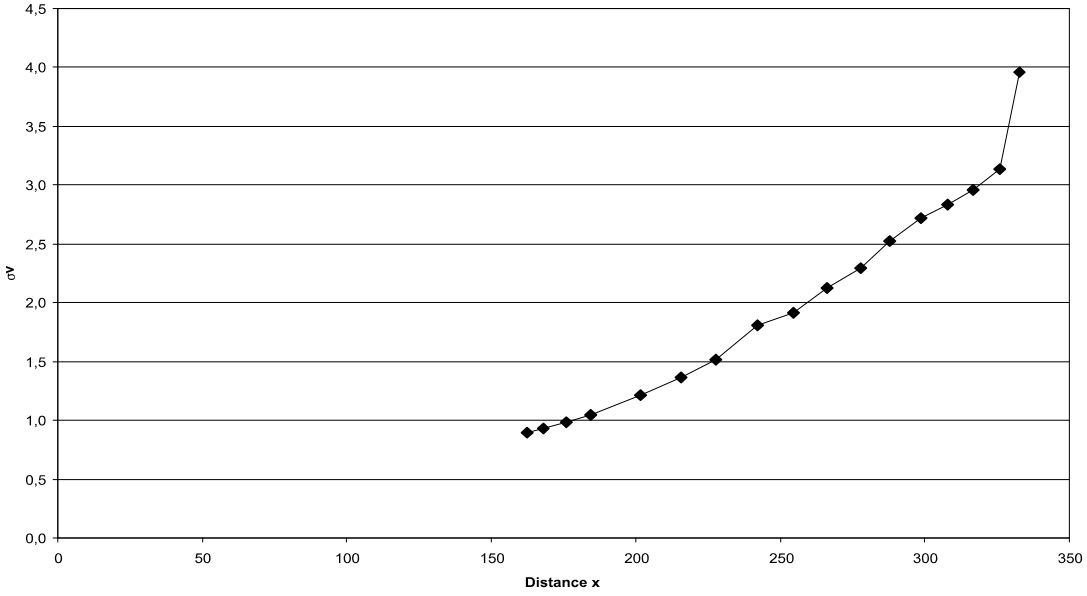

Fig. A.231: Comparison stress in the Pterodactylus antiquus rostrum construction. See chapter 6.4 for legend.

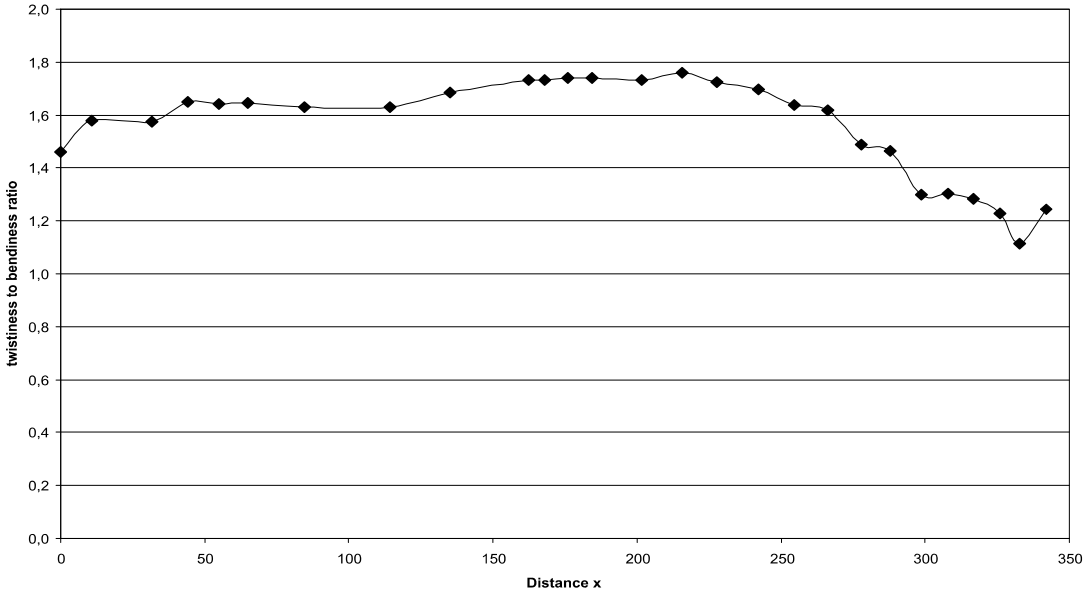

Fig. A.232: Twistiness to bendiness ratio in the Pterodactylus antiquus rostrum construction. See chapter 6.4 for legend.

A.30 Pterodactylus elegans skull construction (see also chapter 7.30)

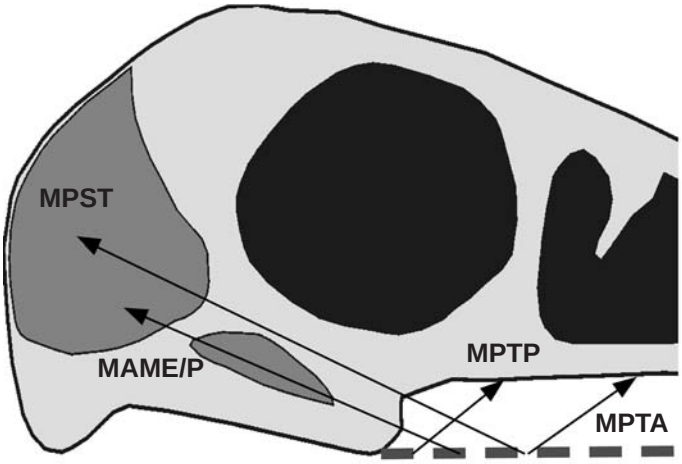

Fig A.233: Reconstruction of the principal pulling direction of the main adductor muscles in the skull of *Pterodactylus elegans*. See chapter 6 for abbreviations.

Muscles	F_1	l_1	α_1	F_2	l_2	α_1
MAME/P	36	11.63	23	1.96	213.3	157
MPST	92	24.01	26	11.00	200.88	154
MPTA	14	23.95	35	1.67	200.94	145
MPTP	88	5.14	39	2.06	219.72	141

Tab. A.57: Reconstructed lever parameters for the scaled Pterodactylus elegans skull construction. See chapter 6.2 for abbreviations.

	F_B	F_J	α_J
1st tooth position	7.15	224.80	-29.49
1st to 4th tooth position	29.40	898.83	-29.44
last tooth position	10.20	223.32	-28.81
average	8.55	224.12	-29.17

Tab. A.58: Reconstructed bite and joint reaction forces and angle of joint reaction force in the scaled Pterodactylus elegans skull construction. Negative angle values mean anterodorsal direction of force. See chapter 6.2 for abbreviations.

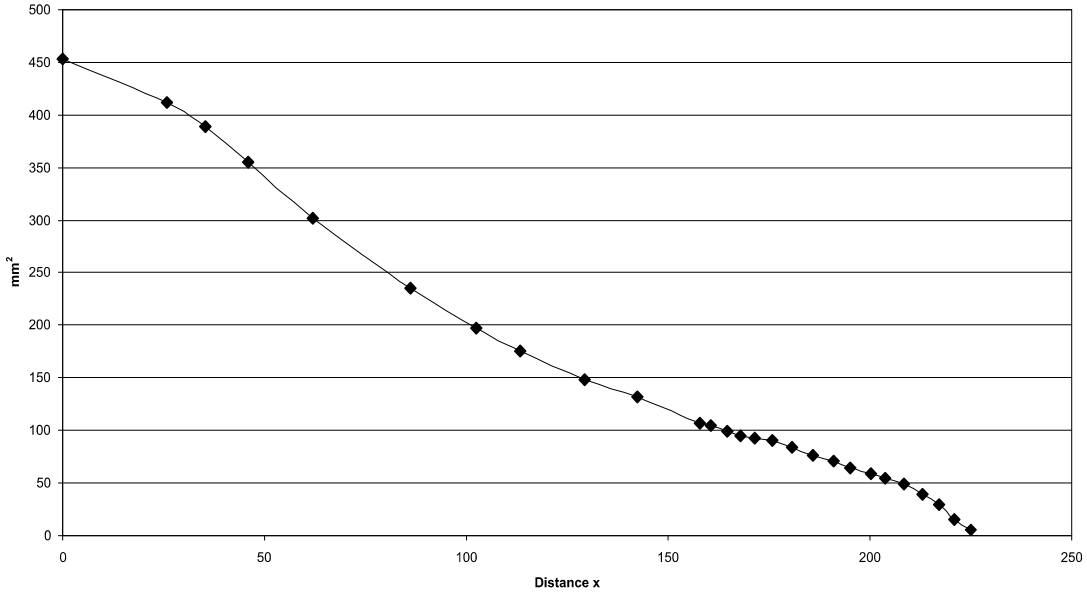

Fig A.234: Cross-sectional area of the Pterodactylus elegans rostrum construction. See chapter 6.4 for legend.

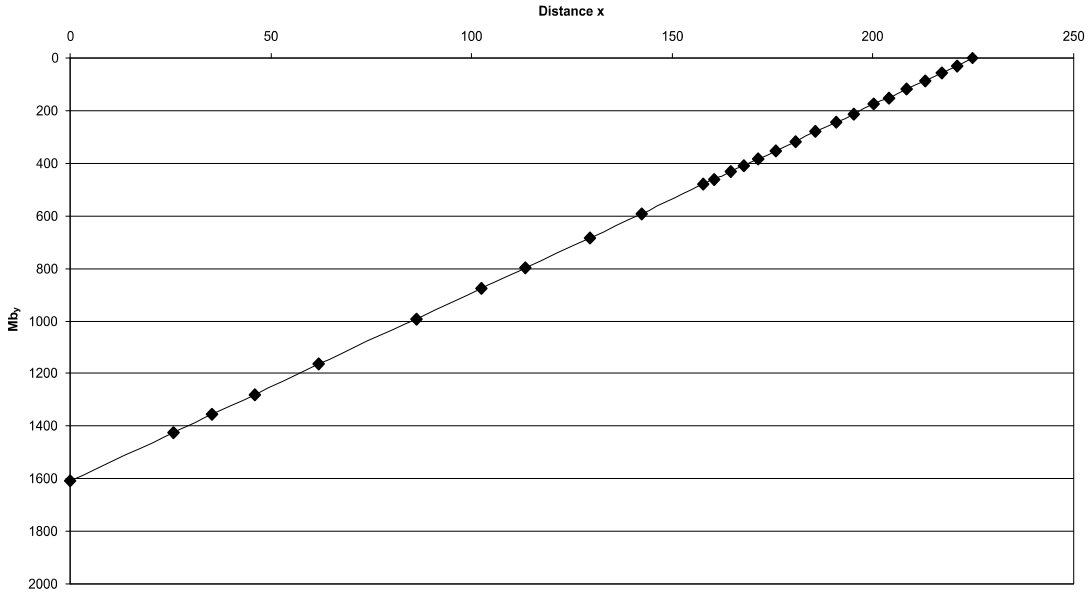

Fig A.235: Bending moments in the Pterodactylus elegans rostrum construction. See chapter 6.4 for legend.

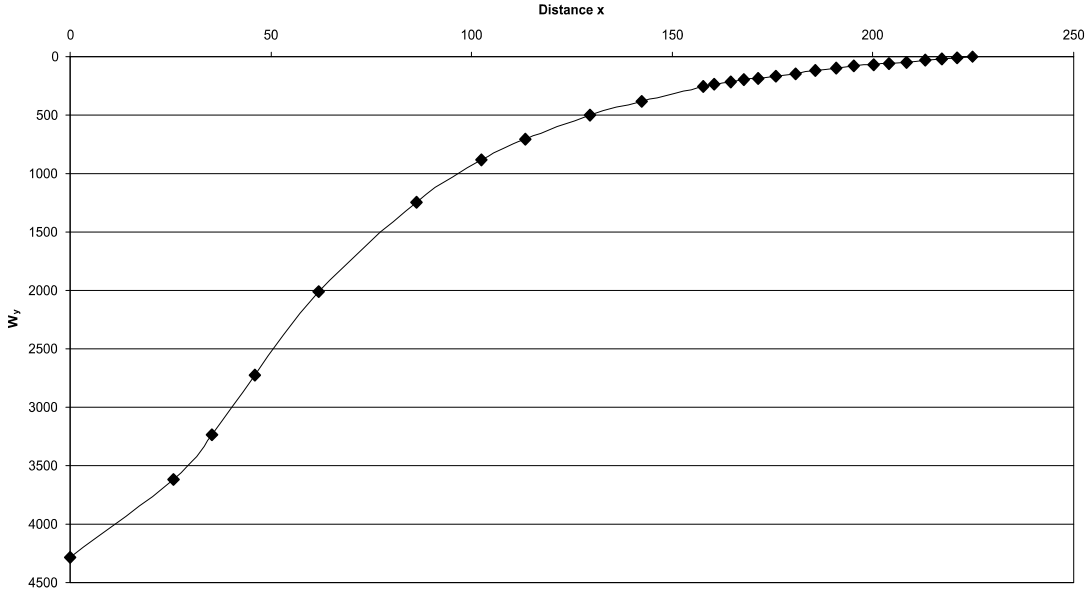

Fig A.236: Section modulus in the Pterodactylus elegans rostrum construction. See chapter 6.4 for legend.

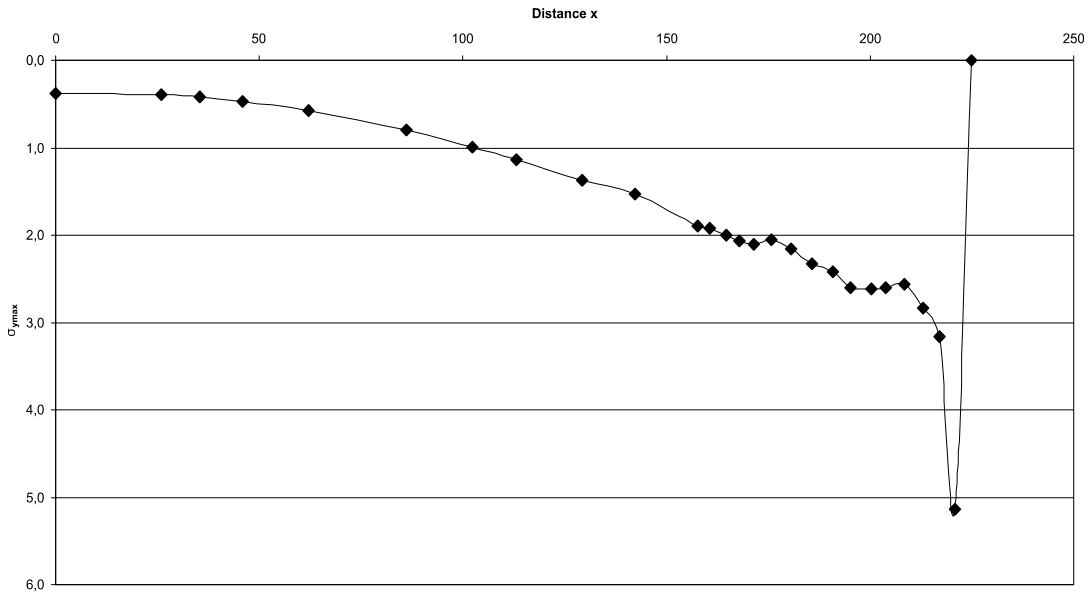

Fig A.237: Maximum bending stress in the Pterodactylus elegans rostrum construction. See chapter 6.4 for legend.

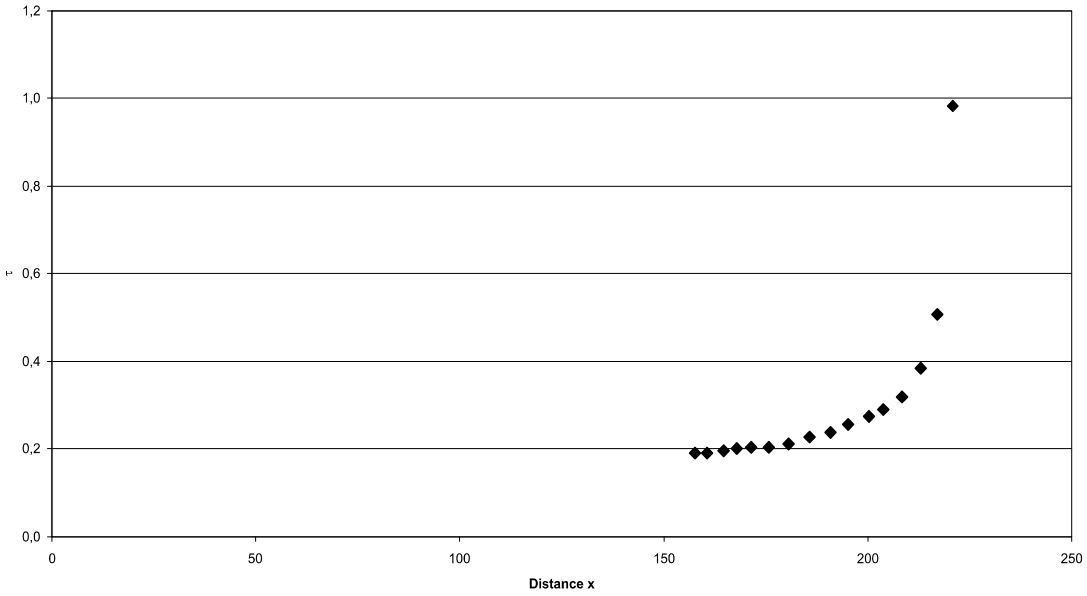

Fig. A.238: Shear stress in the Pterodactylus elegans rostrum construction. See chapter 6.4 for legend.

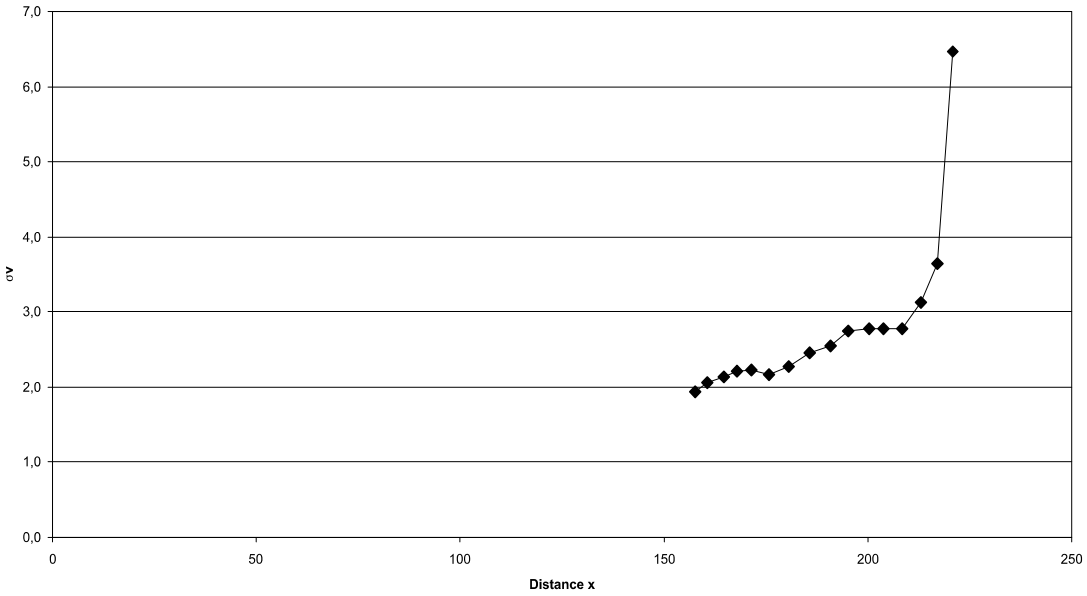

Fig. A.239: Comparison stress in the Pterodactylus elegans rostrum construction. See chapter 6.4 for legend.

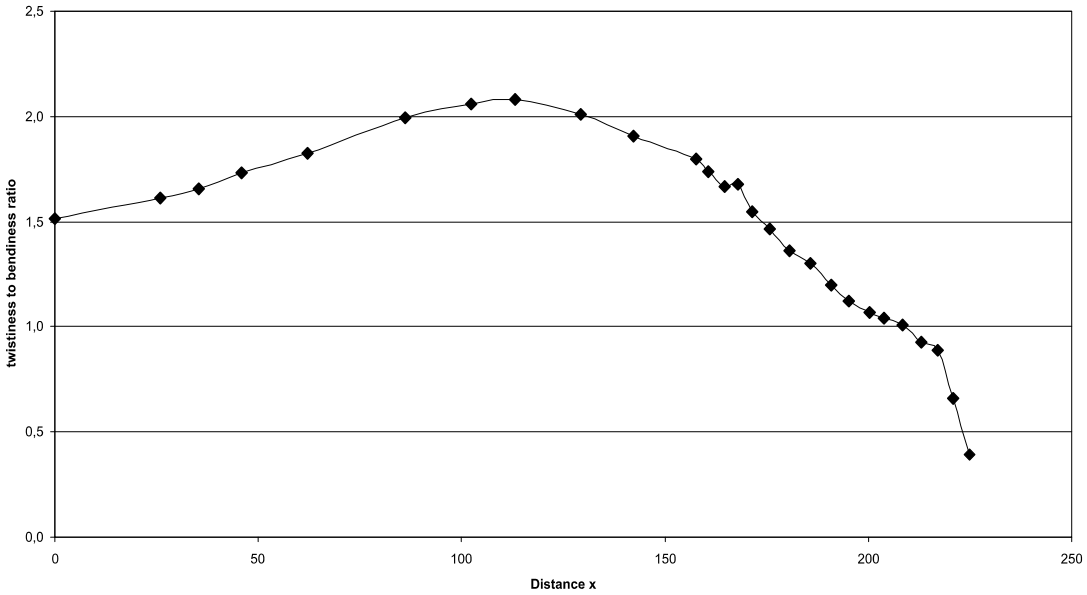

Fig. A.240: Twistiness to bendiness ratio in the Pterodactylus elegans rostrum construction. See chapter 6.4 for legend.

A.31 Pterodactylus kochi skull construction (see also chapter 7.31)

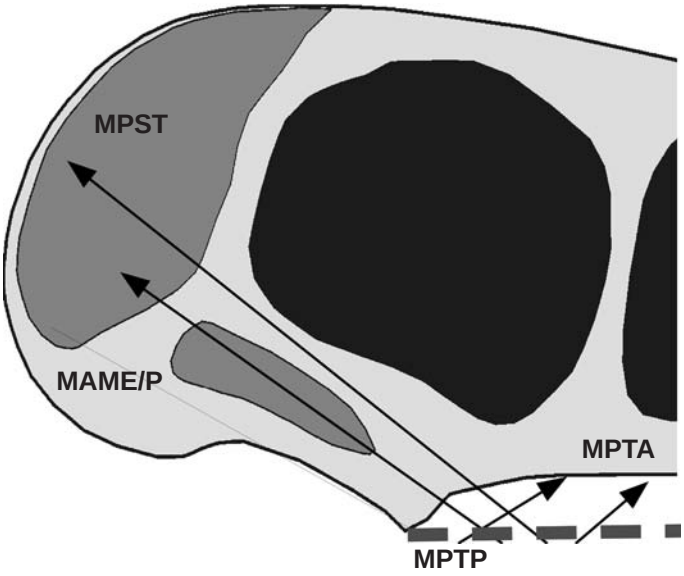

Fig A.241: Reconstruction of the principal pulling direction of the main adductor muscles in the skull of *Pterodactylus kochi*. See chapter 6 for abbreviations.

Muscles	F_1	l_1	α_1	F_2	l_2	α_1
MAME/P	36	12.34	35	1.57	283.34	145
MPST	92	18.00	39	5.96	277.68	141
MPTA	14	22.37	40	1.15	273.31	140
MPTP	88	6.69	32	2.04	289.00	148

Tab. A.59: Reconstructed lever parameters for the scaled Pterodactylus kochi skull construction. See chapter 6.2 for abbreviations.

	F_B	F_J	α_J
1st tooth position	6.12	226.10	-34.50
1st to 4th tooth position	25.28	903.95	-34.46
last tooth position	12.81	222.38	-33.08
average	8.63	224.70	-33.97

Tab. A.60: Reconstructed bite and joint reaction forces and angle of joint reaction force in the scaled Pterodactylus kochi skull construction. Negative angle values mean anterodorsal direction of force. See chapter 6.2 for abbreviations.

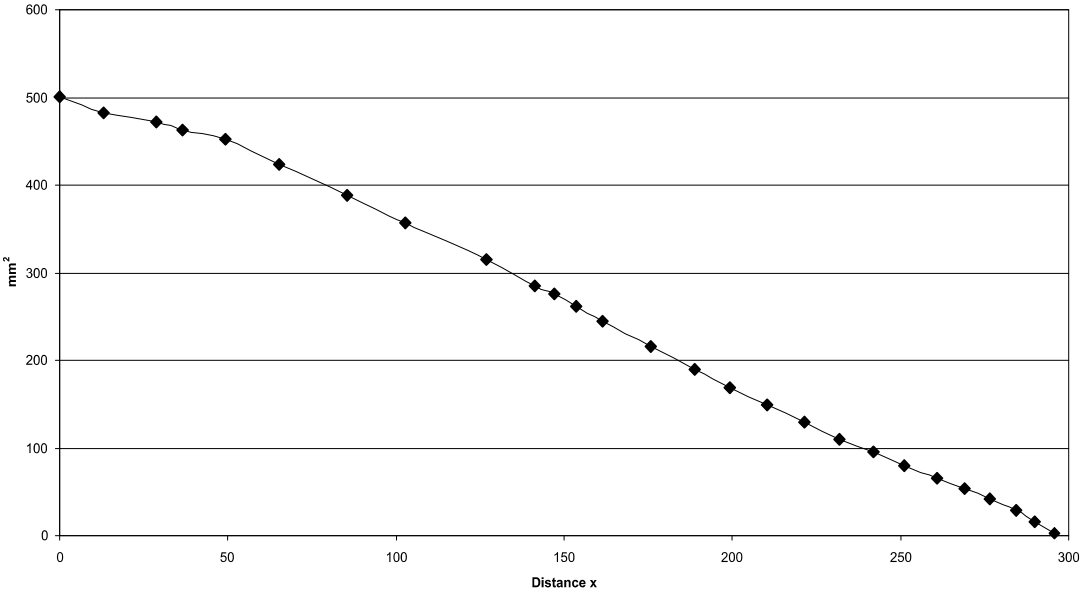

Fig A.242: Cross-sectional area of the Pterodactylus kochi rostrum construction. See chapter 6.4 for legend.

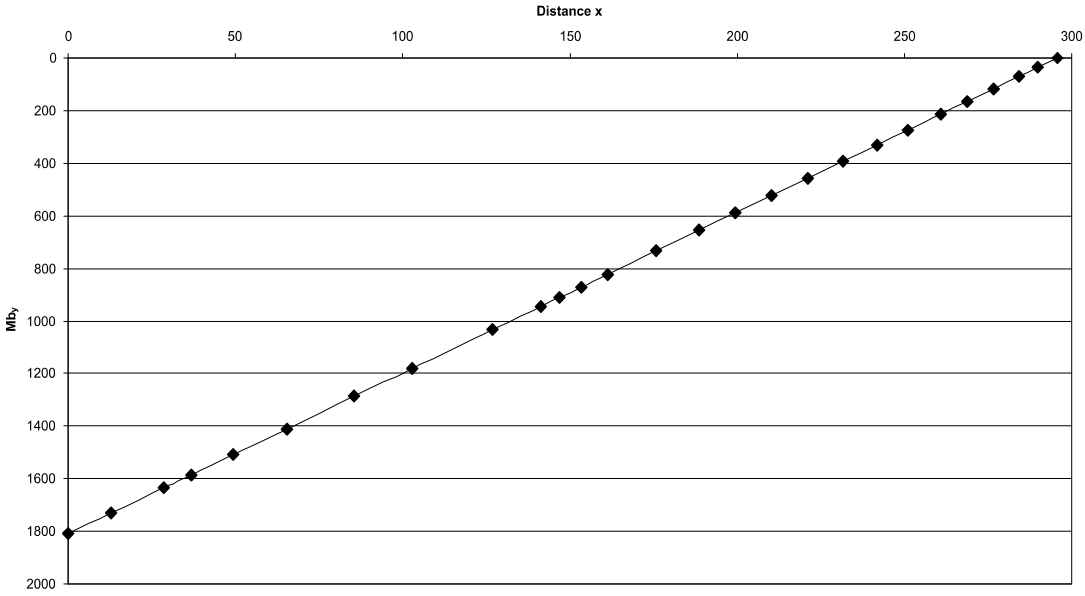

Fig A.243: Bending moments in the Pterodactylus kochi rostrum construction. See chapter 6.4 for legend.

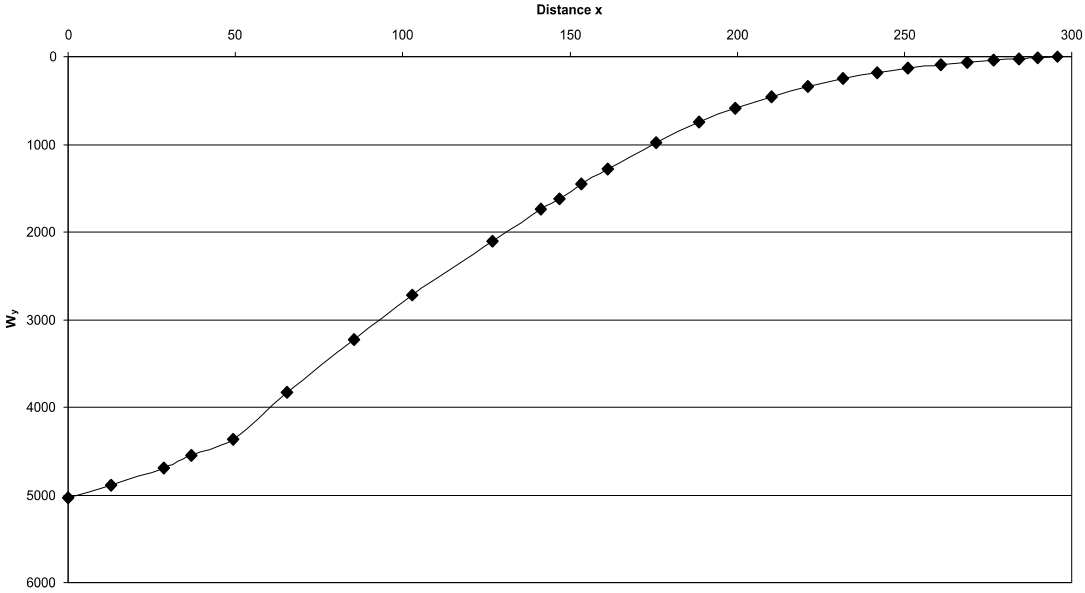

Fig A.244: Section modulus in the Pterodactylus kochi rostrum construction. See chapter 6.4 for legend.

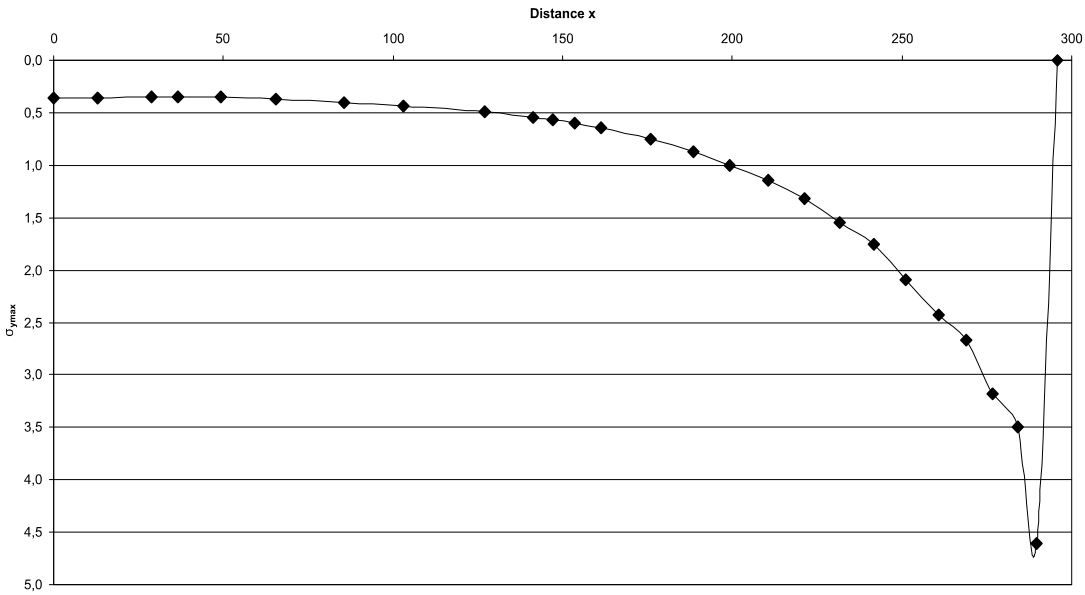

Fig A.245: Maximum bending stress in the Pterodactylus kochi rostrum construction. See chapter 6.4 for legend.

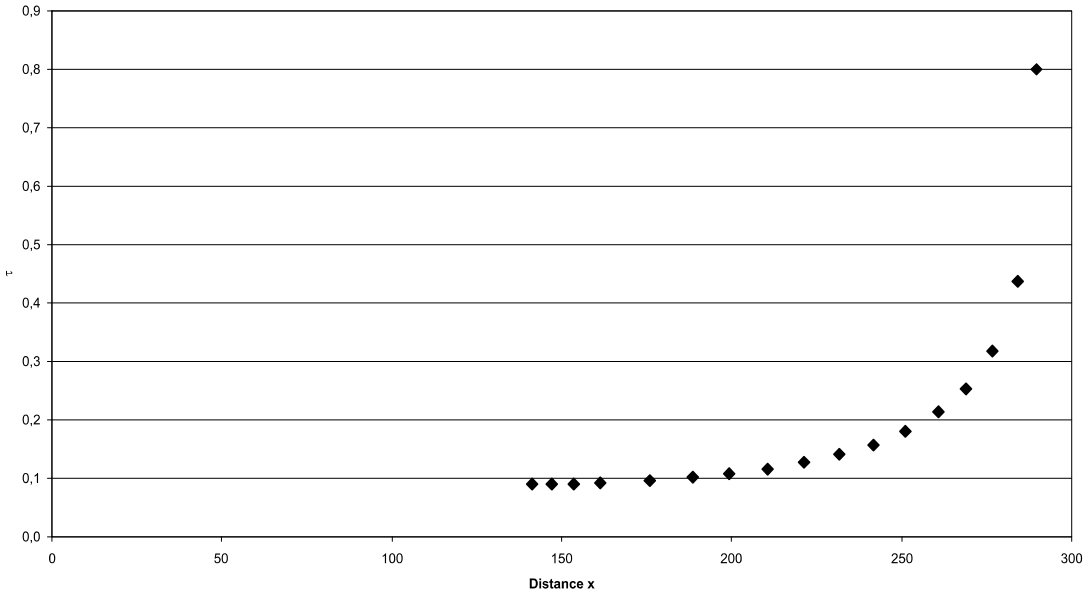

Fig. A.246: Shear stress in the Pterodactylus kochi rostrum construction. See chapter 6.4 for legend.

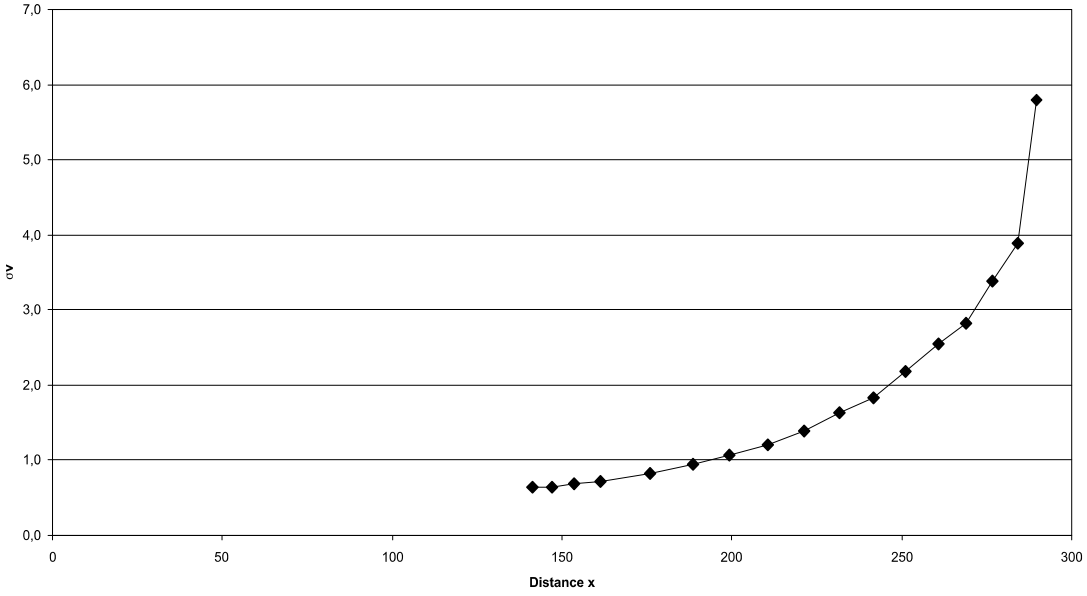

Fig. A.247: Comparison stress in the Pterodactylus kochi rostrum construction. See chapter 6.4 for legend.

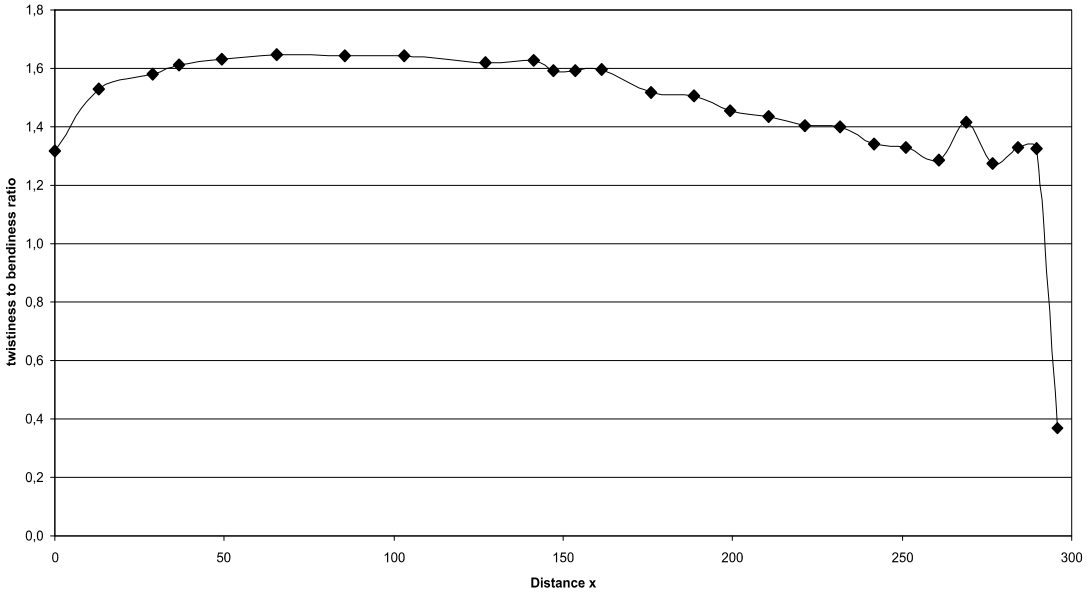

Fig. A.248: Twistiness to bendiness ratio in the Pterodactylus kochi rostrum construction. See chapter 6.4 for legend.

A.32 Pterodactylus micronyx skull construction (see also chapter 7.32)

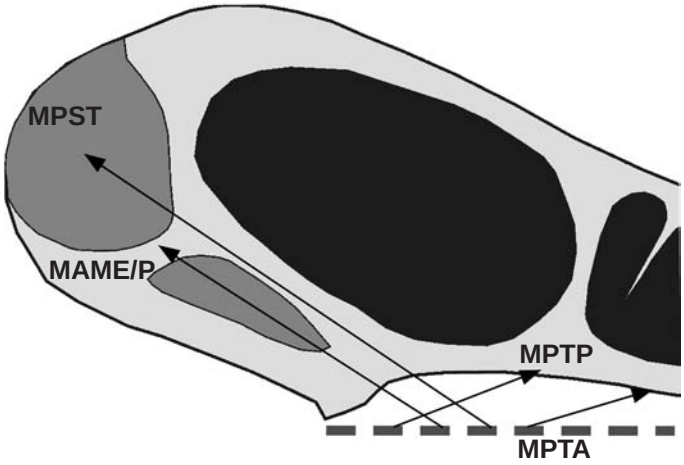

Fig A.249: Reconstruction of the principal pulling direction of the main adductor muscles in the skull of *Pterodactylus micronyx*. See chapter 6 for abbreviations.

Muscles	F_1	l_1	α_1	F_2	l_2	α_1
MAME/P	36	20.57	33	2.82	262.86	147
MPST	92	29.7	34	10.77	253.73	146
MPTA	14	36.39	17	2.06	247.05	163
MPTP	88	12.34	21	4.01	247.05	163

Tab. A.61: Reconstructed lever parameters for the scaled Pterodactylus micronyx skull construction. See chapter 6.2 for abbreviations.

	F_B	F_J	α_J
1st tooth position	8.71	224.51	-25.87
1st to 4th tooth position	35.59	897.72	-25.83
last tooth position	14.70	221.96	-24.48
average	10.73	223.64	-25.41

Tab. A.62: Reconstructed bite and joint reaction forces and angle of joint reaction force in the scaled Pterodactylus micronyx skull construction. Negative angle values mean anterodorsal direction of force. See chapter 6.2 for abbreviations.

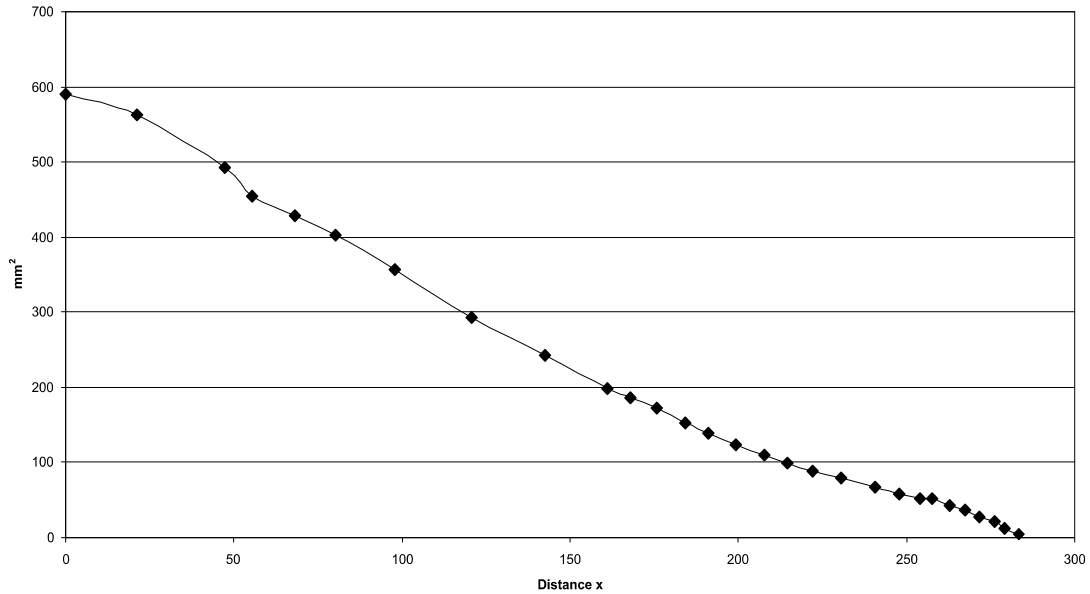

Fig A.250: Cross-sectional area of the Pterodactylus micronyx rostrum construction. See chapter 6.4 for legend.

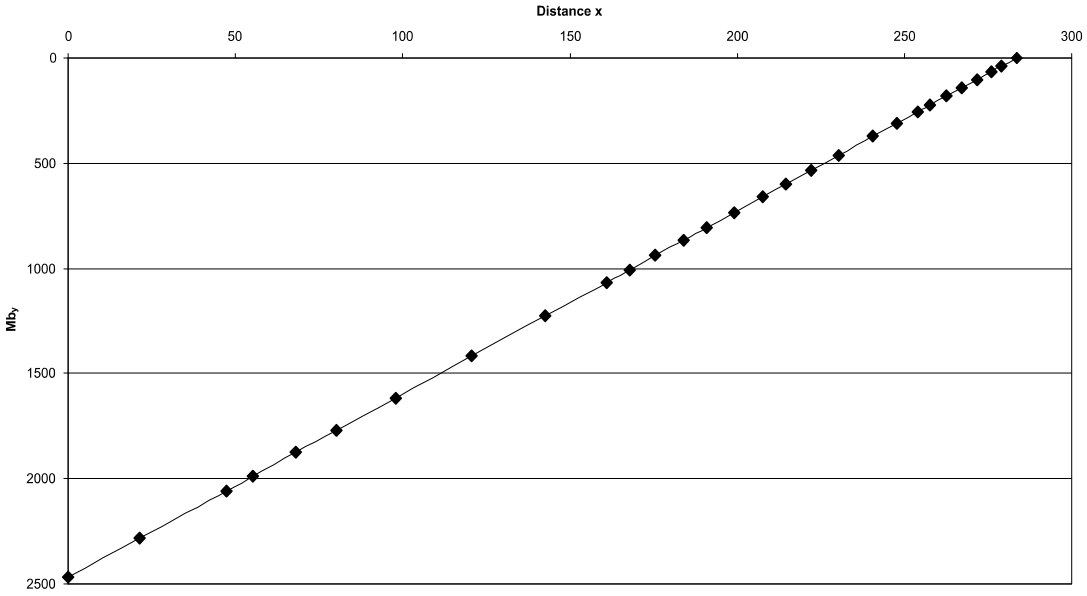

Fig A.251: Bending moments in the Pterodactylus micronyx rostrum construction. See chapter 6.4 for legend.

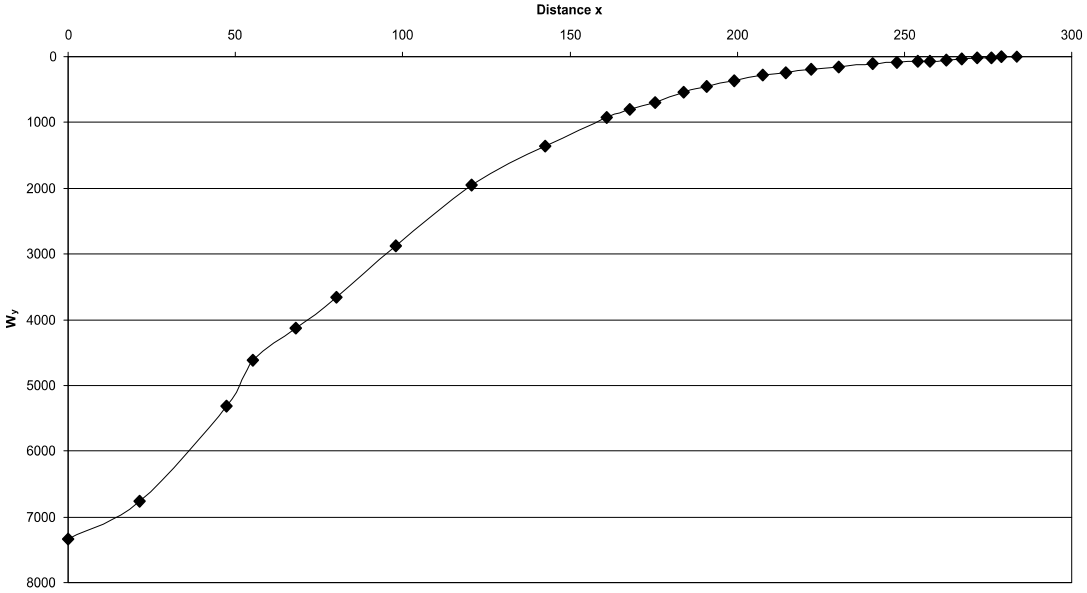

Fig A.252: Section modulus in the Pterodactylus micronyx rostrum construction. See chapter 6.4 for legend.

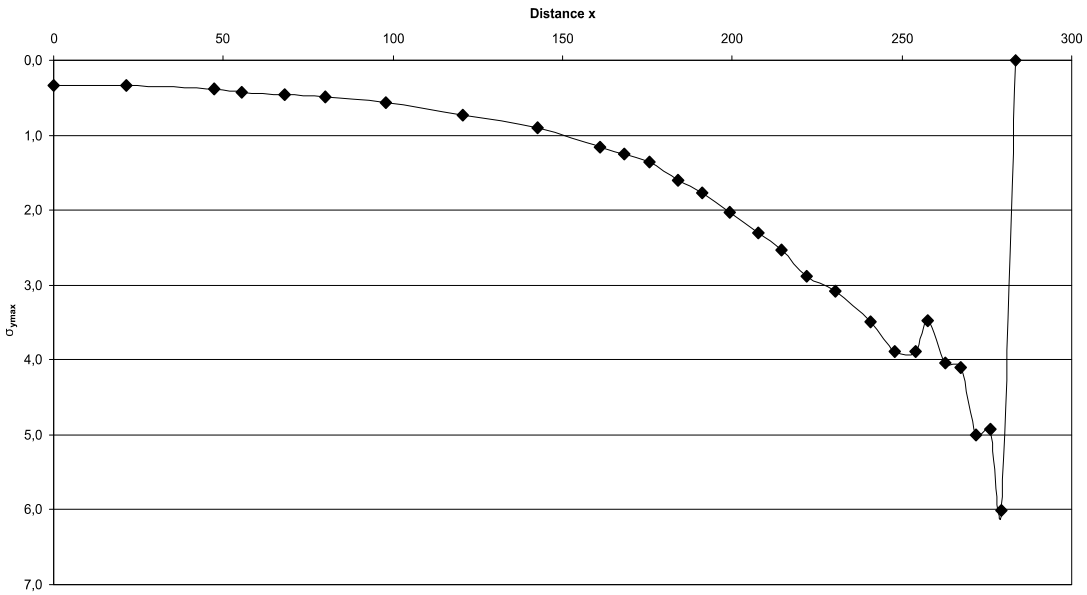

Fig A.253: Maximum bending stress in the Pterodactylus micronyx rostrum construction. See chapter 6.4 for legend.

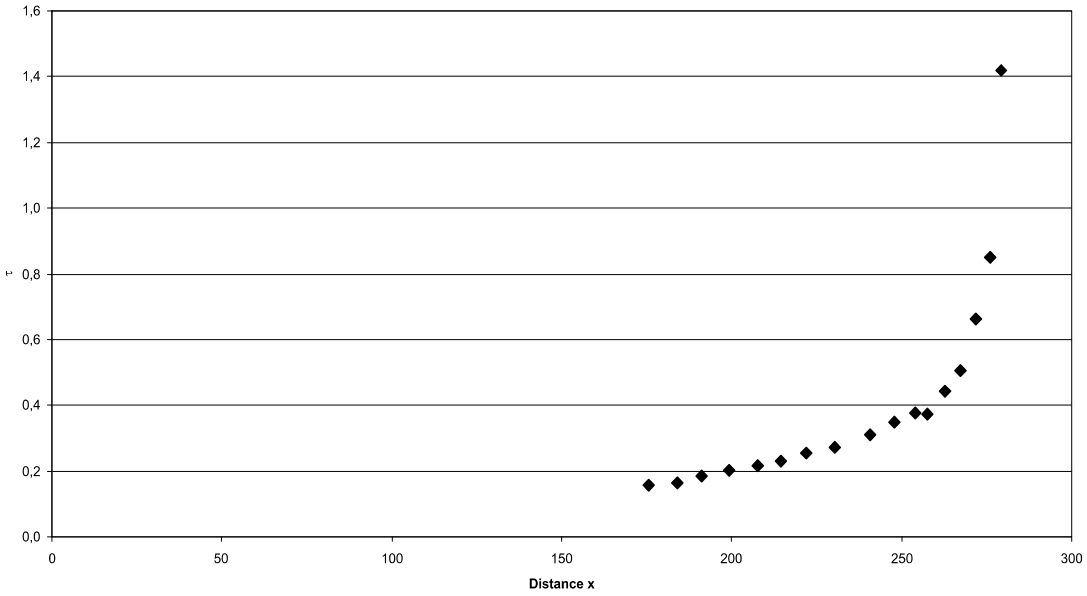

Fig. A.254: Shear stress in the Pterodactylus micronyx rostrum construction. See chapter 6.4 for legend.

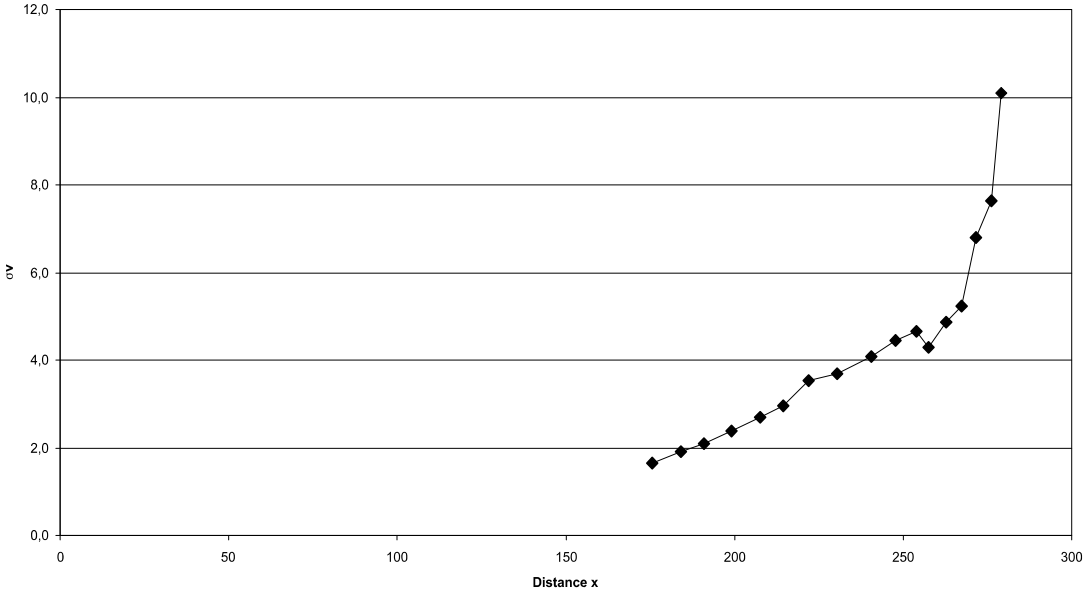

Fig. A.255: Comparison stress in the Pterodactylus micronyx rostrum construction. See chapter 6.4 for legend.

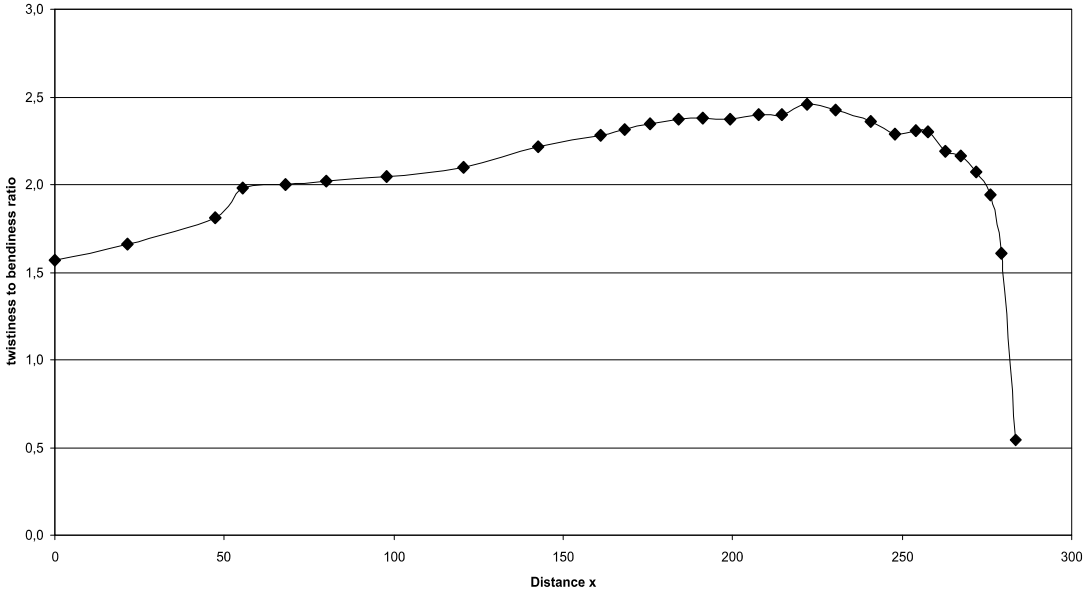

Fig. A.256: Twistiness to bendiness ratio in the Pterodactylus micronyx rostrum construction. See chapter 6.4 for legend.

A.33 Pterodaustro skull construction (see also chapter 7.33)

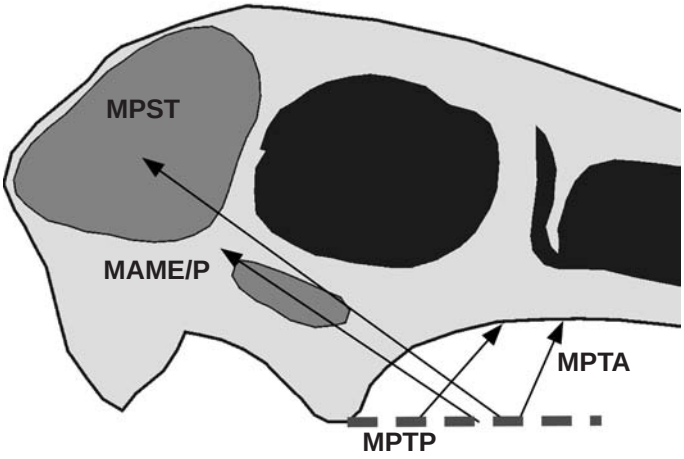

Fig A.257: Reconstruction of the principal pulling direction of the main adductor muscles in the skull of *Pterodaustro*. See chapter 6 for abbreviations.

Muscles	F_1	l_1	α_1	F_2	l_2	α_1
MAME/P	36	22.71	34	1.31	623.62	146
MPST	92	26.88	36	3.99	619.45	144
MPTA	14	30.22	66	0.69	616.11	114
MPTP	88	13.12	49	1.82	633.21	131

Tab. A.63: Reconstructed lever parameters for the scaled Pterodaustro skull construction. See chapter 6.2 for abbreviations.

	F_B	F_J	α_J
anterior end of rostrum	4.90	224.01	-41.53
1st tooth position	5.00	223.94	-41.51
last tooth position	45.59	199.37	-32.74
average	25.30	211.66	-37.12

Tab. A.64: Reconstructed bite and joint reaction forces and angle of joint reaction force in the scaled Pterodaustro skull construction. Negative angle values mean anterodorsal direction of force. See chapter 6.2 for abbreviations.

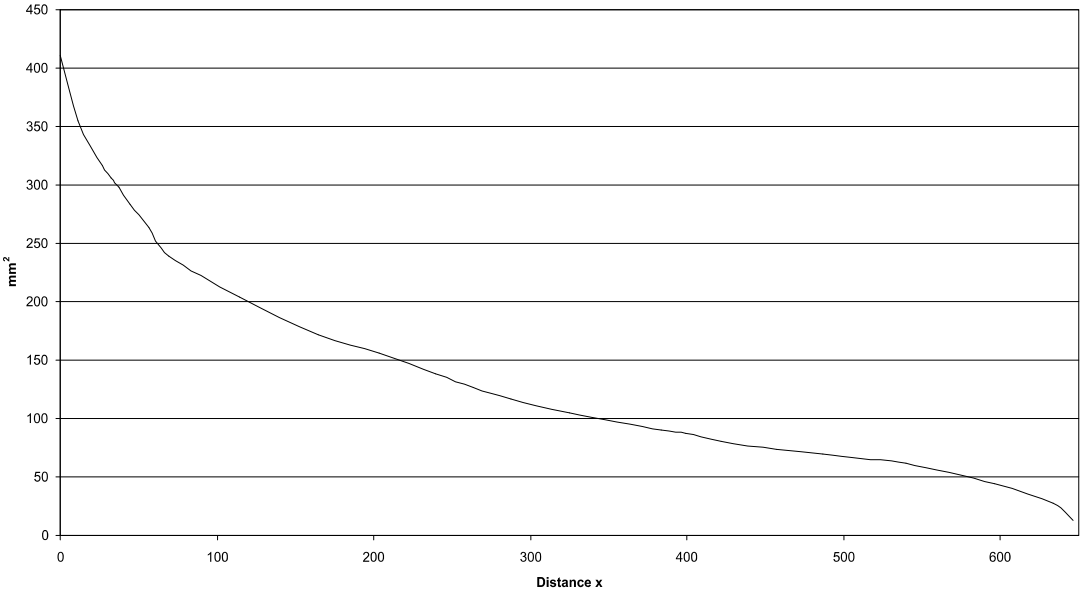

Fig A.258: Cross-sectional area of the Pterodaustro rostrum construction. See chapter 6.4 for legend.

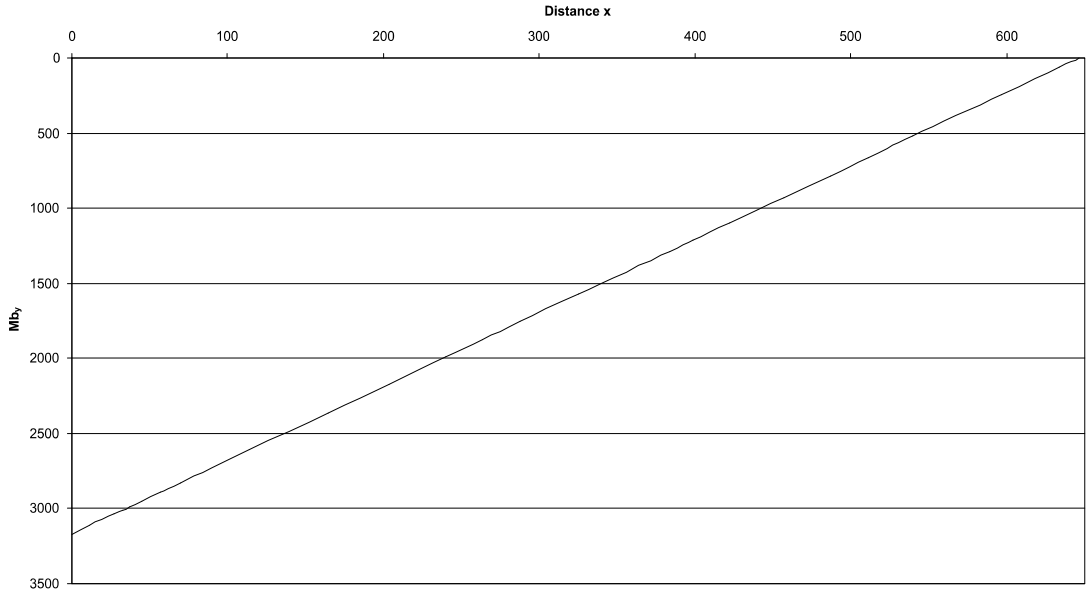

Fig A.259: Bending moments in the Pterodaustro rostrum construction. See chapter 6.4 for legend.

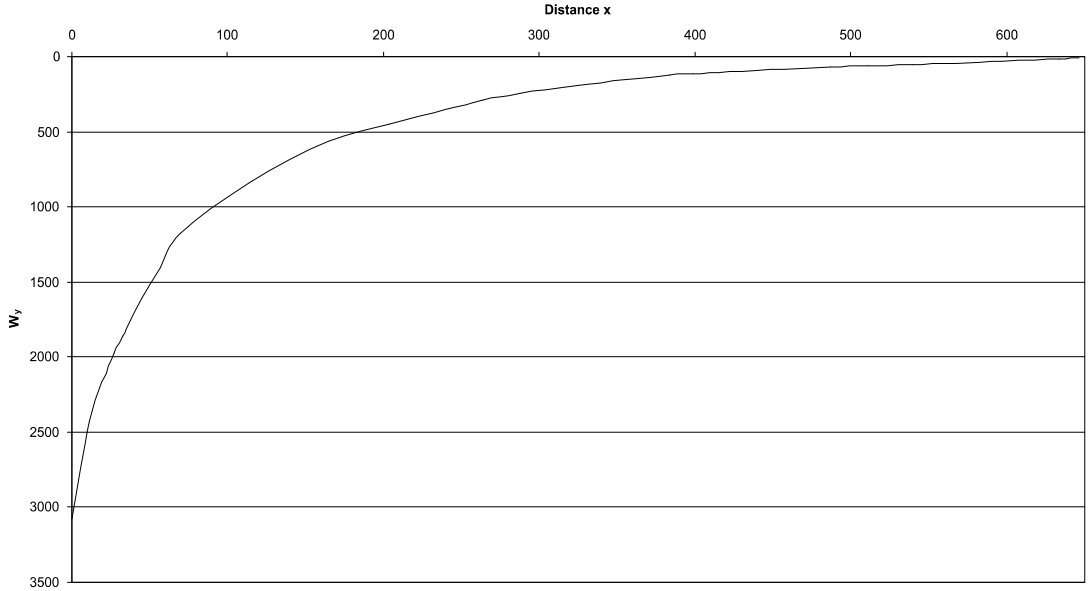

Fig A.260: Section modulus in the Pterodaustro rostrum construction. See chapter 6.4 for legend.

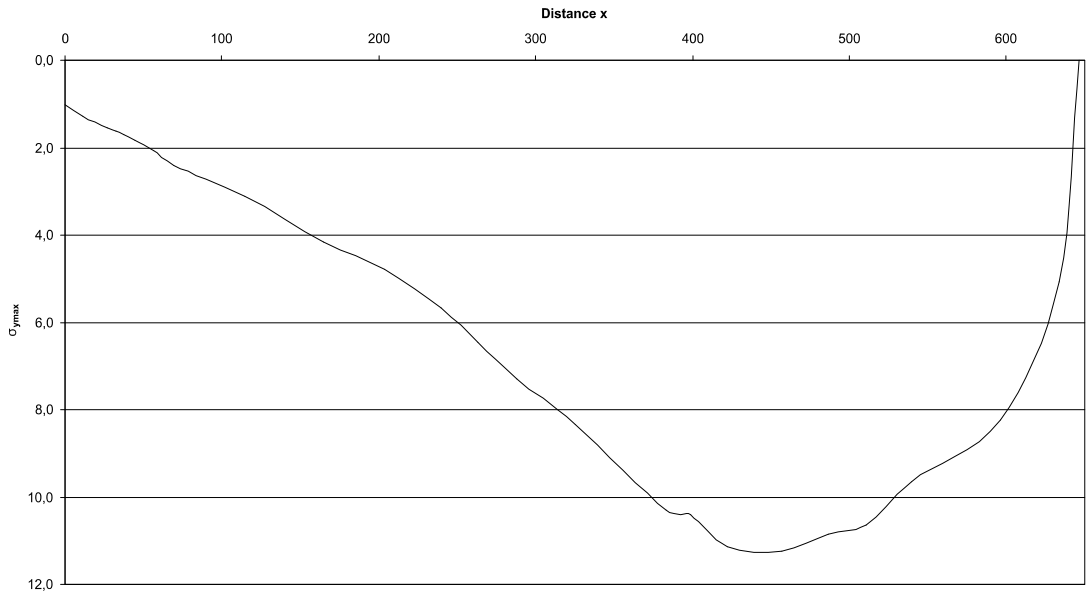

Fig A.261: Maximum bending stress in the Pterodaustro rostrum construction. See chapter 6.4 for legend.

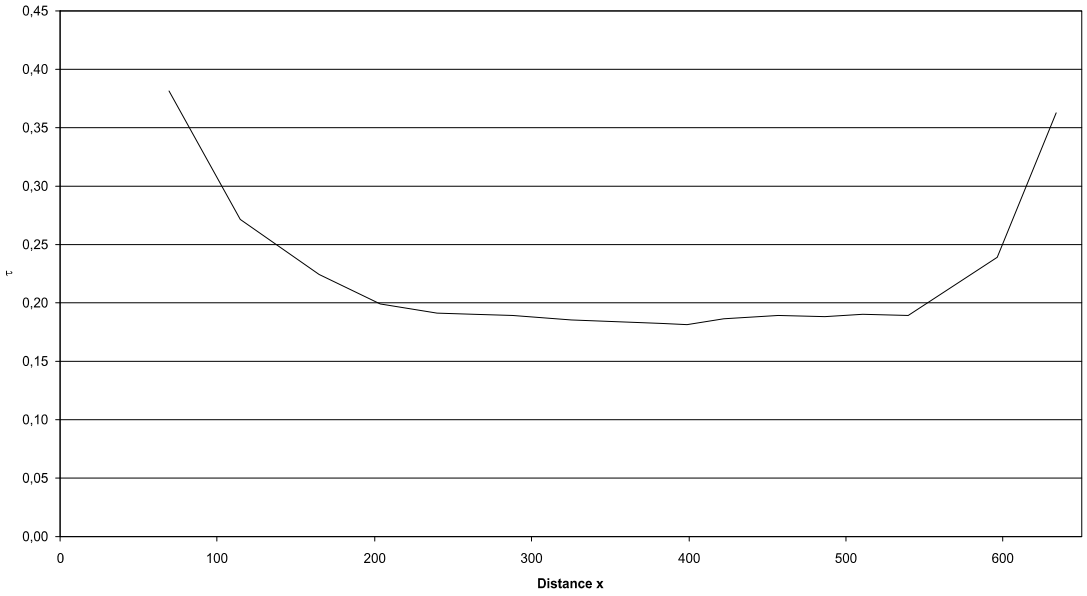

Fig. A.262: Shear stress in the Pterodaustro rostrum construction. See chapter 6.4 for legend.

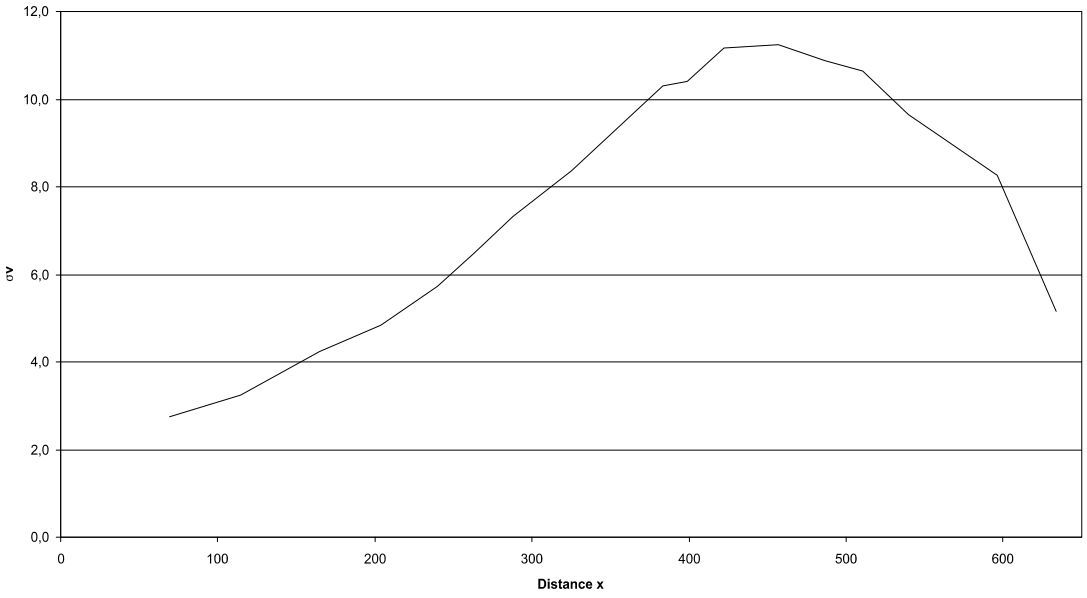

Fig. A.263: Comparison stress in the Pterodaustro rostrum construction. See chapter 6.4 for legend.

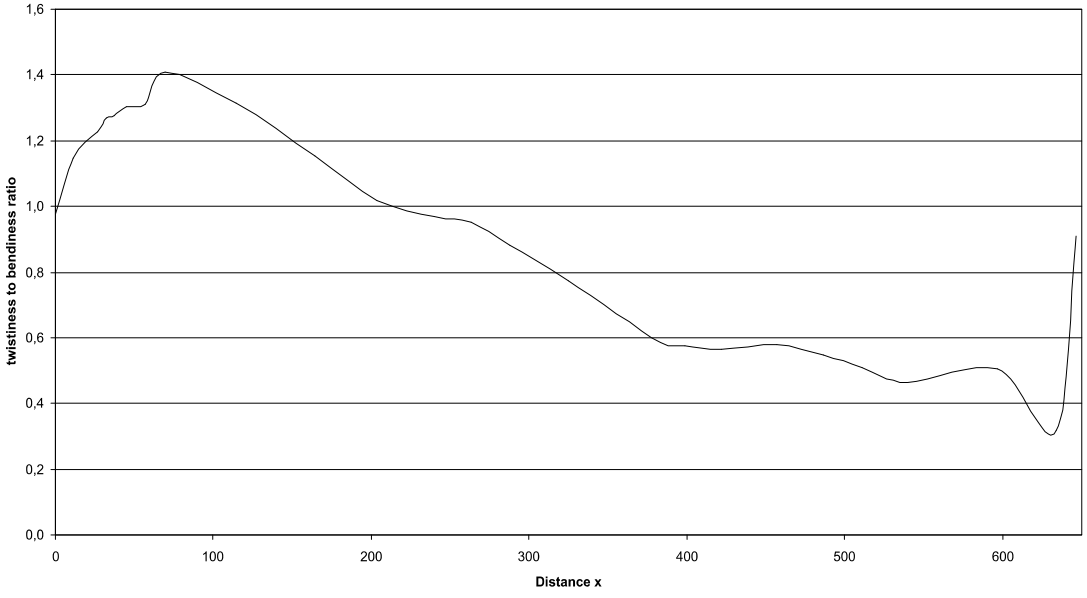

Fig. A.264: Twistiness to bendiness ratio in the Pterodaustro rostrum construction. See chapter 6.4 for legend.

A.34 Quetzalcoatlus skull construction (see also chapter 7.34)

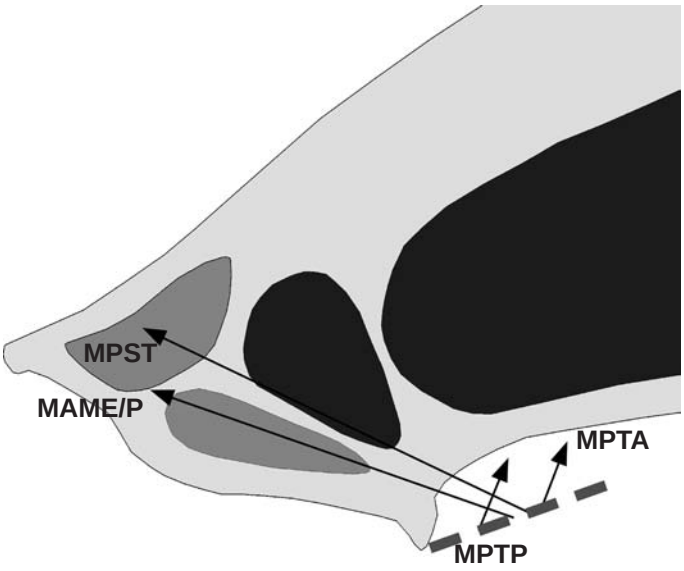

Fig A.265: Reconstruction of the principal pulling direction of the main adductor muscles in the skull of *Quetzalcoatlus*. See chapter 6 for abbreviations.

Muscles	F_1	l_1	α_1	F_2	l_2	α_1
MAME/P	36	14.14	39	1.32	385.95	141
MPST	92	17.2	46	4.13	382.89	134
MPTA	14	19.88	49	0.71	391.09	131
MPTP	88	9.01	48	2.09	380.22	132

Tab. A.65: Reconstructed lever parameters for the scaled Quetzalcoatlus skull construction. See chapter 6.2 for abbreviations.

	F_B	F_J	α_J
anterior end of rostrum	5.64	225.64	-44.86
anterior to half of the length of nasoant. fen.	26.17	211.67	-40.91
average	15.91	218.66	-42.89

Tab. A.66: Reconstructed bite and joint reaction forces and angle of joint reaction force in the scaled Quetzalcoatlus skull construction. Negative angle values mean anterodorsal direction of force. See chapter 6.4 for legend.

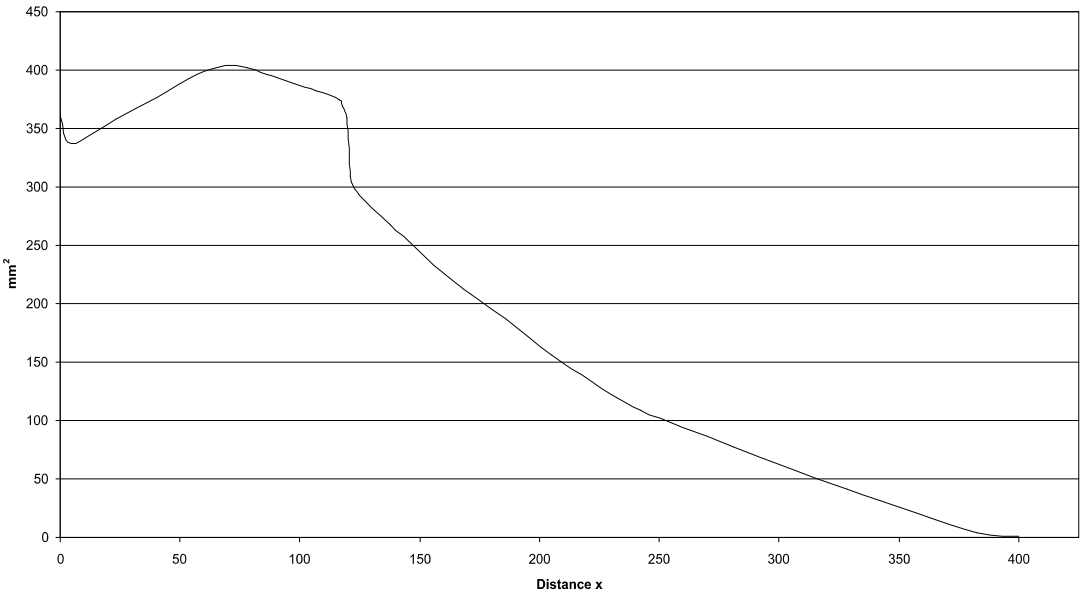

Fig A.266: Cross-sectional area of the Quetzalcoatlus rostrum construction. See chapter 6.4 for legend.

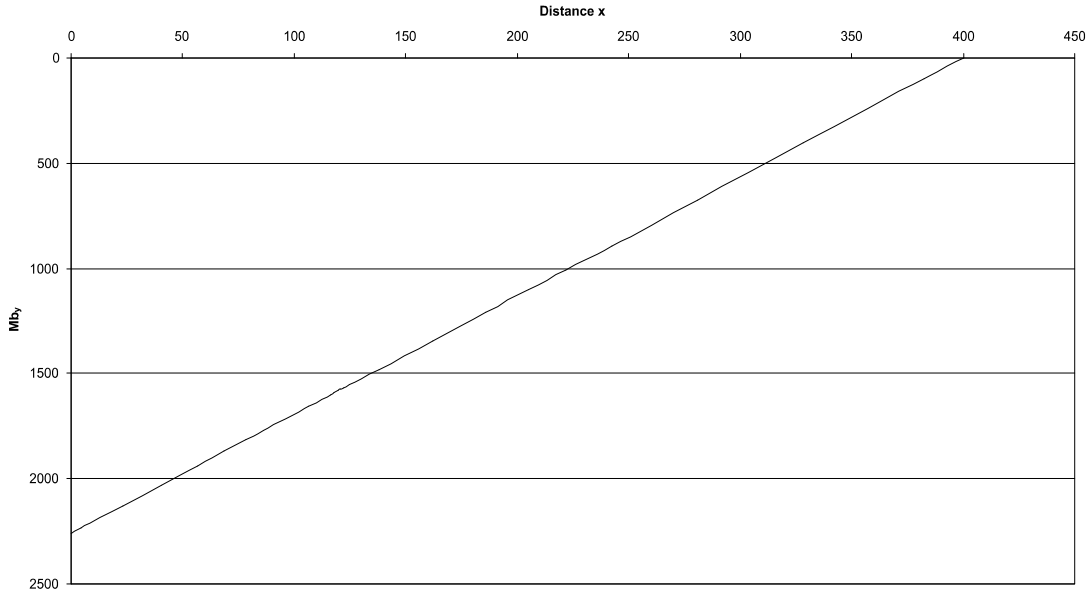

Fig A.267: Bending moments in the Quetzalcoatlus rostrum construction. See chapter 6.4 for legend.

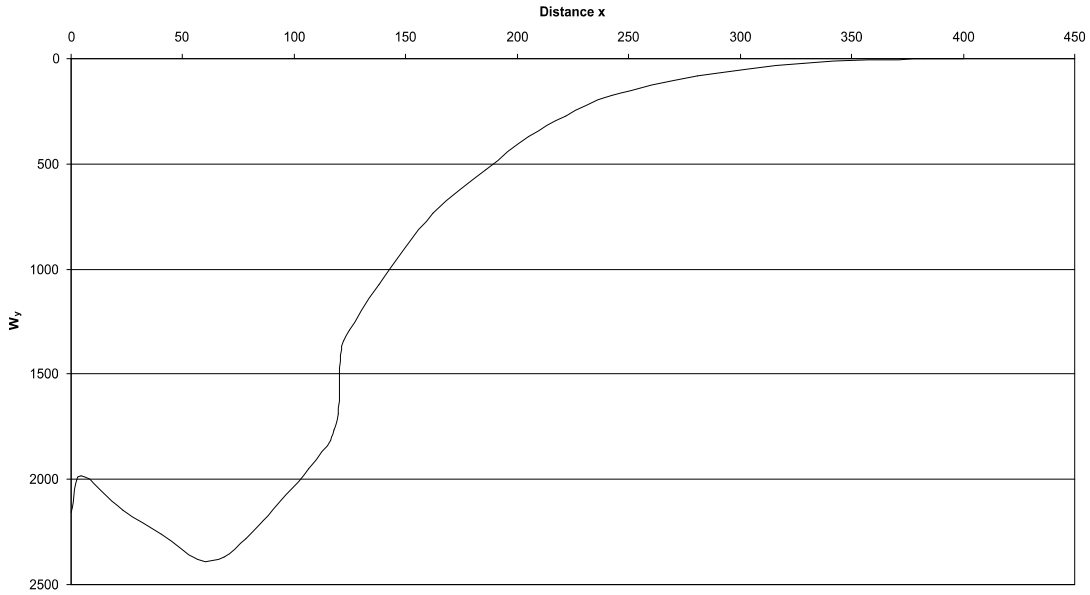

Fig A.268: Section modulus in the Quetzalcoatlus rostrum construction. See chapter 6.4 for legend.

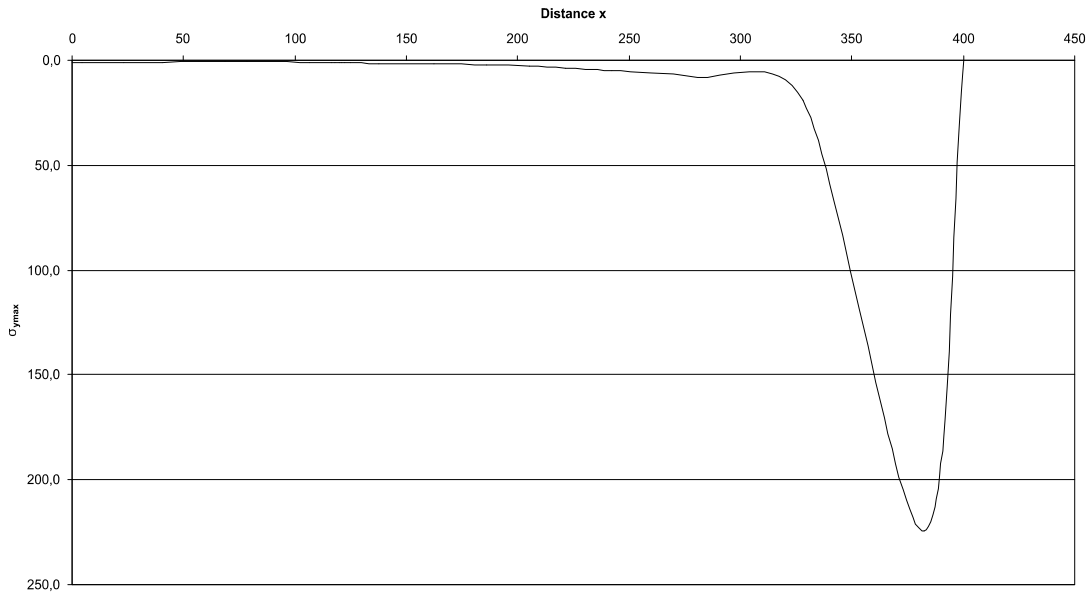

Fig A.269: Maximum bending stress in the Quetzalcoatlus rostrum construction. See chapter 6.4 for legend.

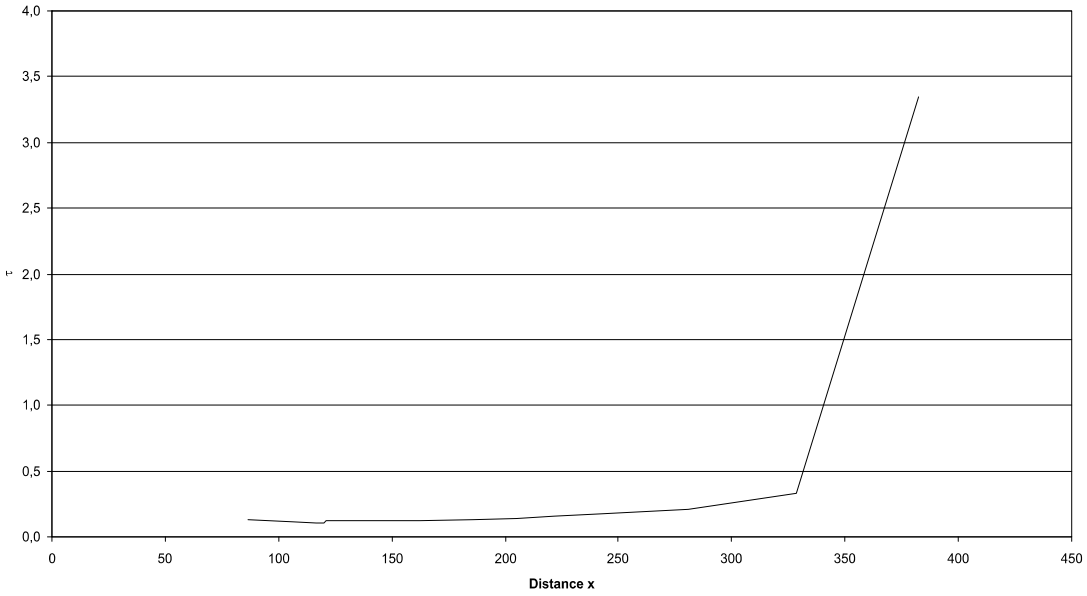

Fig. A.270: Shear stress in the Quetzalcoatlus rostrum construction. See chapter 6.4 for legend.

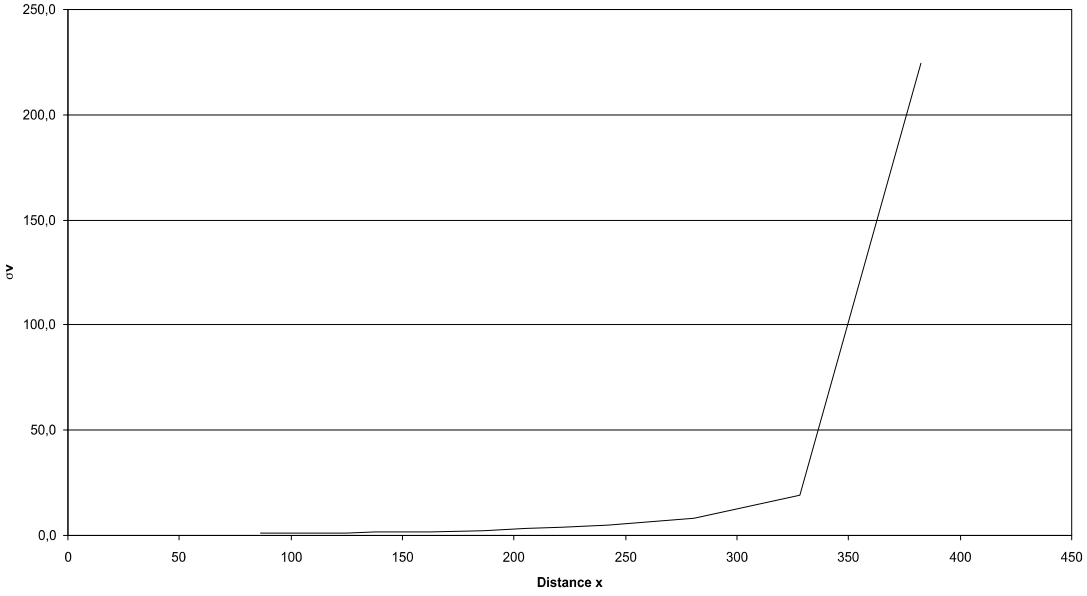

Fig. A.271: Comparison stress in the Quetzalcoatlus rostrum construction. See chapter 6.4 for legend.

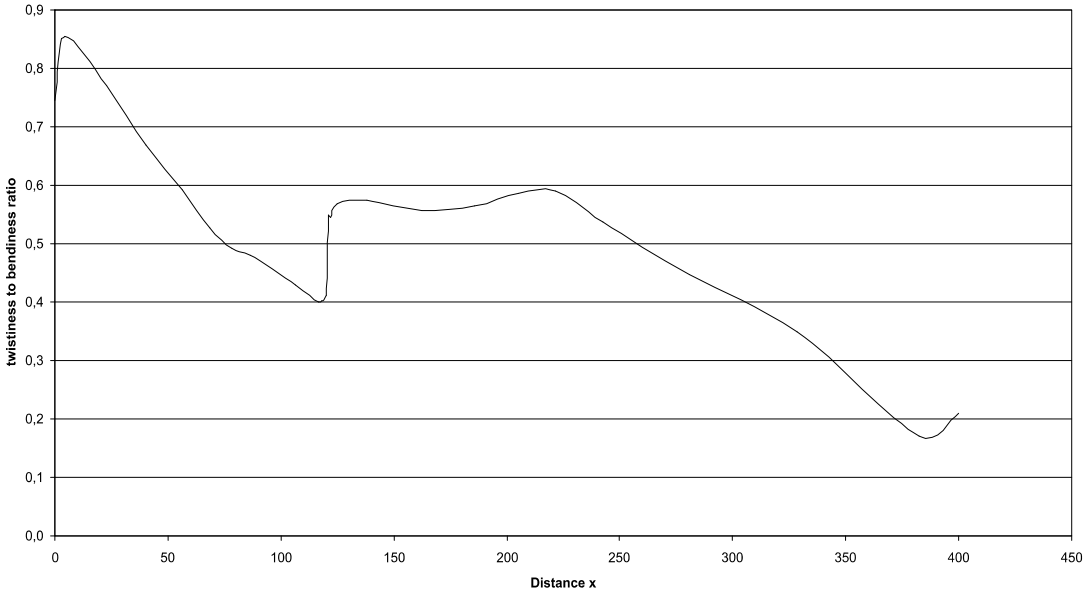

Fig. A.272: Twistiness to bendiness ratio in the Quetzalcoatlus rostrum construction. See chapter 6.4 for legend.

A.35 Rhamphorhynchus skull construction (see also chapter 7.34)

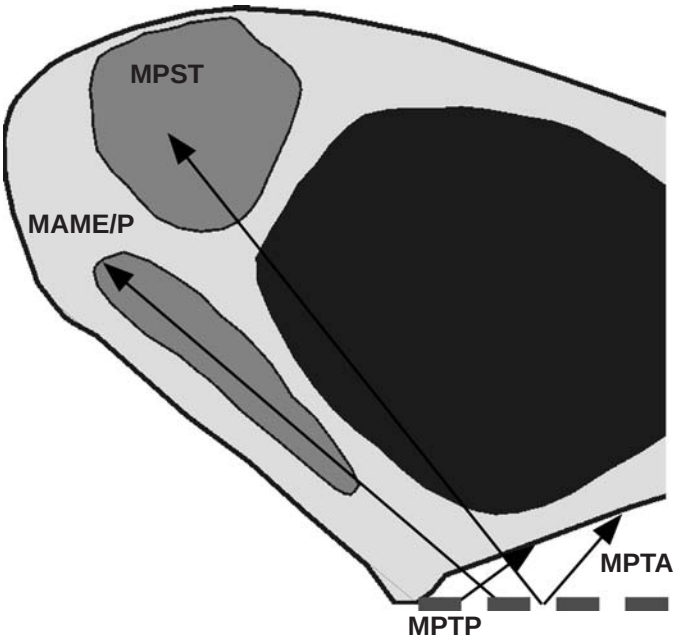

Fig A.273: Reconstruction of the principal pulling direction of the main adductor muscles in the skull of *Rhamphorhynchus*. See chapter 6 for abbreviations.

Muscles	F_1	l_1	α_1	F_2	l_2	α_1
MAME/P	36	8.74	41	1.53	206.10	139
MPST	92	14.91	52	6.86	199.93	128
MPTA	14	15.69	50	1.10	199.16	130
MPTP	88	4.89	37	2.05	209.96	143

Tab. A.67: Reconstructed lever parameters for the scaled Rhamphorhynchus skull construction. See chapter 6.2 for abbreviations.

	F_B	F_J	α_J
anteriormost rostrum	7.98	222.82	-42.95
1st tooth position	9.65	221.68	-42.64
1st to 4th tooth position	44.49	882.76	-42.35
last tooth position	38.69	203.14	-36.60
average	17.85	237.96	-40.98

Tab. A.68: Reconstructed bite and joint reaction forces and angle of joint reaction force in the scaled Rhamphorhynchus skull construction. Negative angle values mean anterodorsal direction of force. See chapter 6.2 for abbreviations.

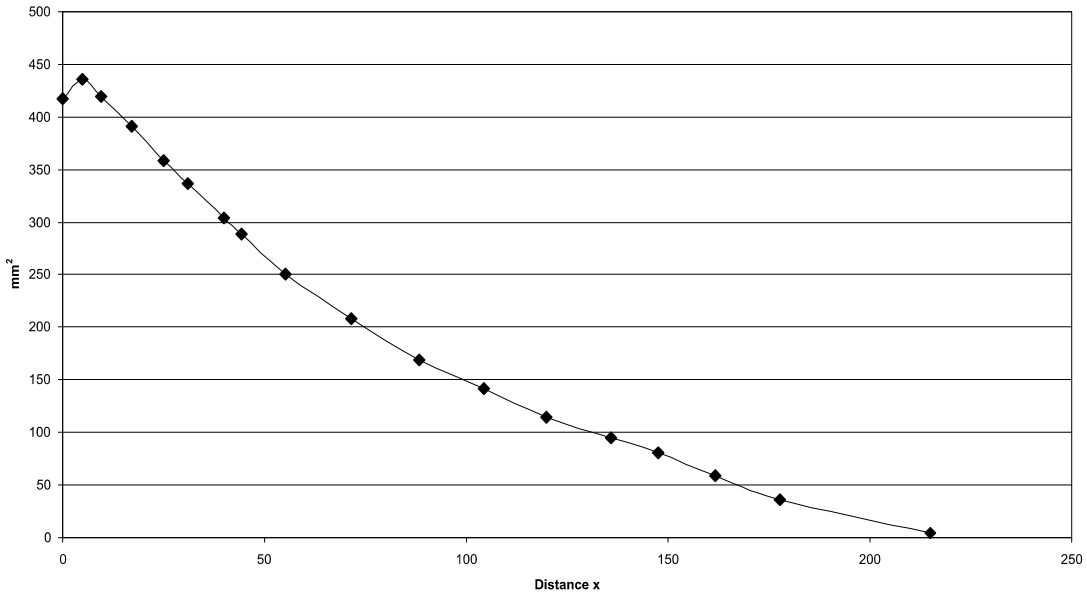

Fig A.274: Cross-sectional area of the Rhamphorhynchus rostrum construction. See chapter 6.4 for legend.

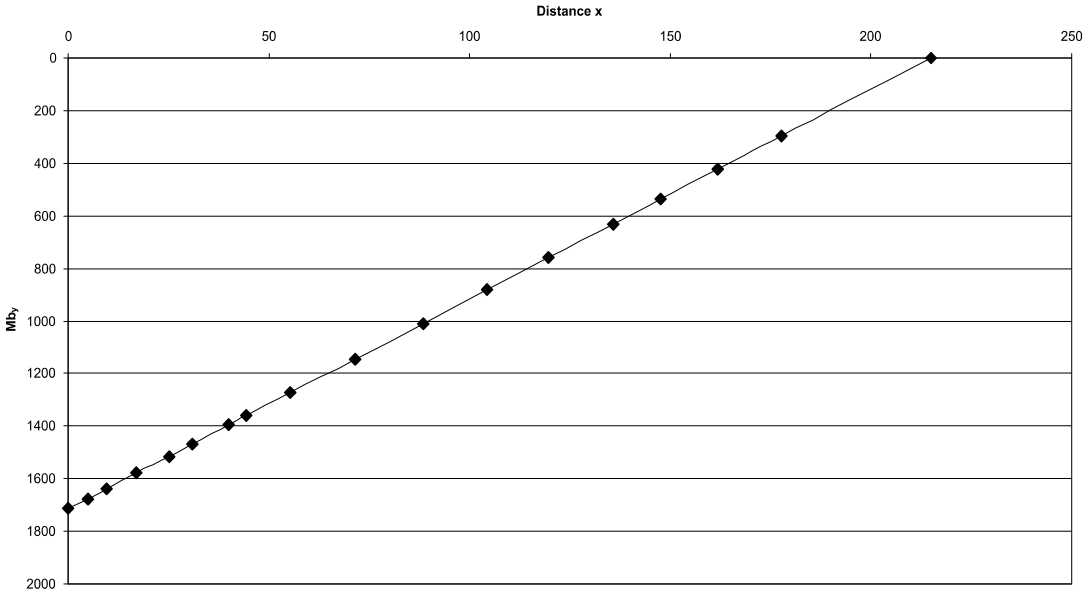

Fig A.275: Bending moments in the Rhamphorhynchus rostrum construction. See chapter 6.4 for legend.

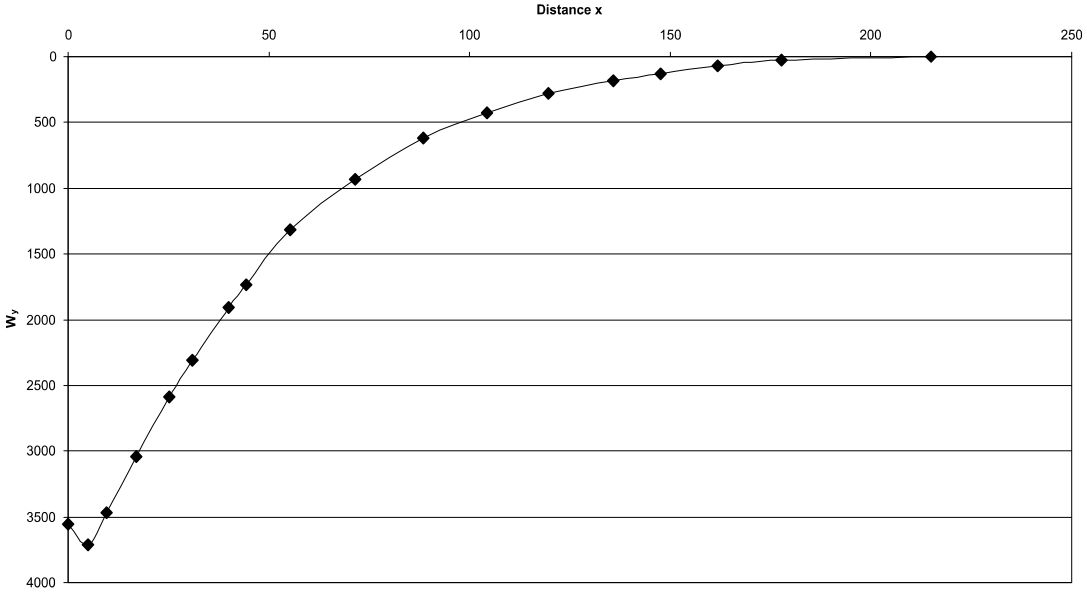

Fig A.276: Section modulus in the Rhamphorhynchus rostrum construction. See chapter 6.4 for legend.

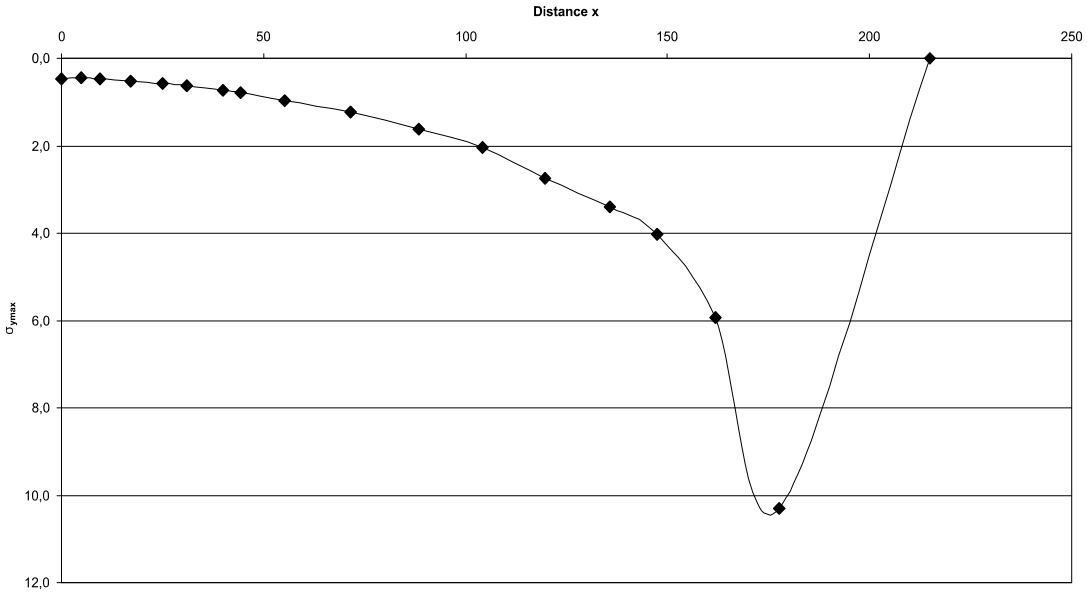

Fig A.277: Maximum bending stress in the Rhamphorhynchus rostrum construction. See chapter 6.4 for legend.

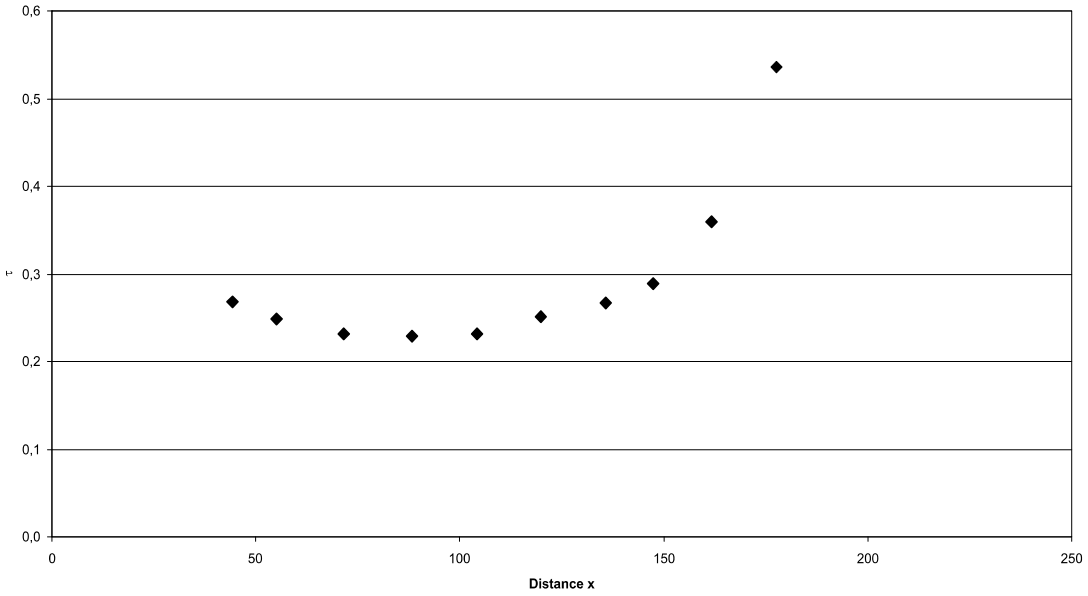

Fig. A.278: Shear stress in the Rhamphorhynchus rostrum construction. See chapter 6.4 for legend.

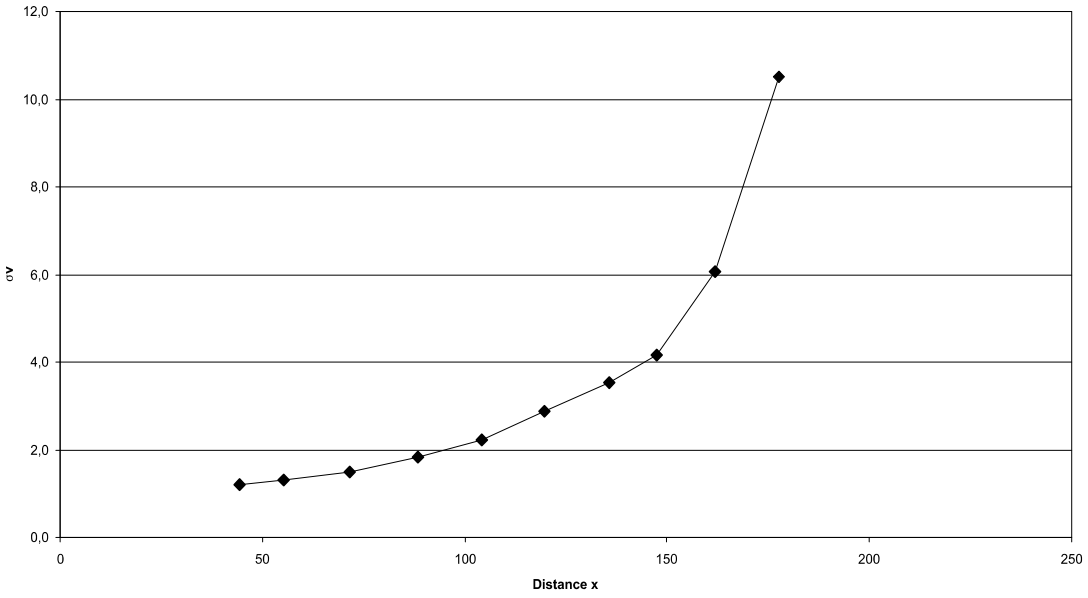

Fig. A.279: Comparison stress in the Rhamphorhynchus rostrum construction. See chapter 6.4 for legend.

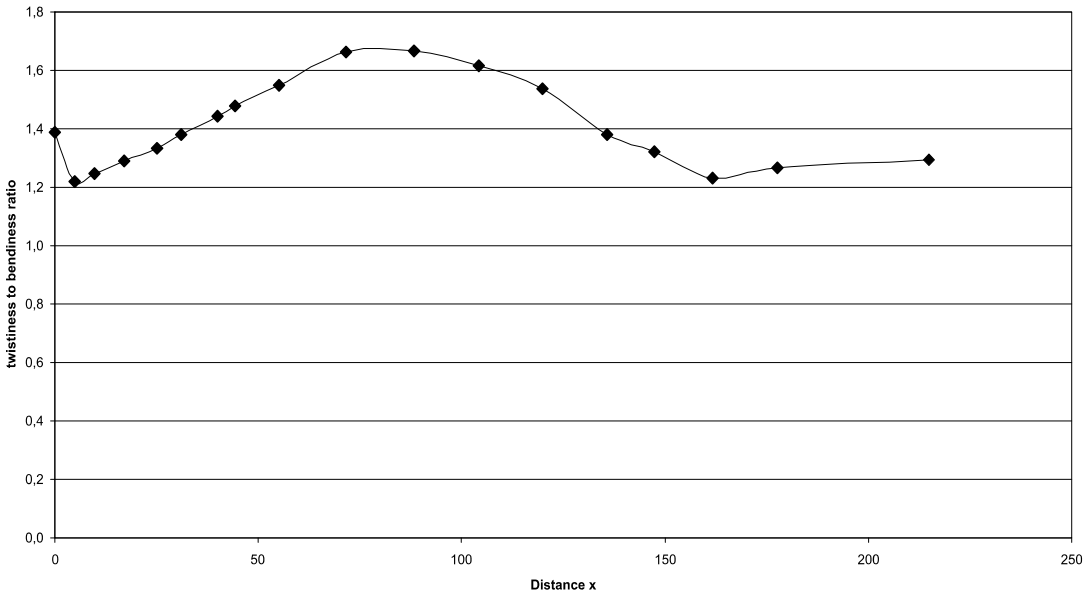

Fig. A.280: Twistiness to bendiness ratio in the Rhamphorhynchus rostrum construction. See chapter 6.4 for legend.

A.36 Santanadactylus skull construction (see also chapter 7.36)

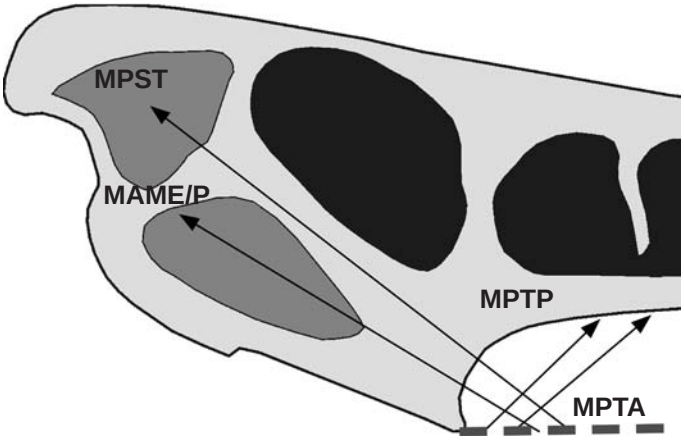

Fig A.281: Reconstruction of the principal pulling direction of the main adductor muscles in the skull of *Santanadactylus*. See chapter 6 for abbreviations.

Muscles	F_1	l_1	α_1	F_2	l_2	α_1
MAME/P	36	15.08	30	1.67	324.28	150
MPST	92	22.96	37	6.68	316.40	143
MPTA	14	27.38	60	1.23	311.98	120
MPTP	88	6.56	47	1.73	332.80	133

Tab. A.69: Reconstructed lever parameters for the scaled Santanadactylus skull construction. See chapter 6.2 for abbreviations.

	F_B	F_J	α_J
1st tooth position	6.77	223.48	-39.81
1st to 4th tooth position	28.24	893.16	-39.75
last tooth position	45.75	200.76	-31.23
average	15.99	217.87	-37.87

Tab. A.68: Reconstructed bite and joint reaction forces and angle of joint reaction force in the scaled Santanadactylus skull construction. Negative angle values mean anterodorsal direction of force. See chapter 6.2 for abbreviations.

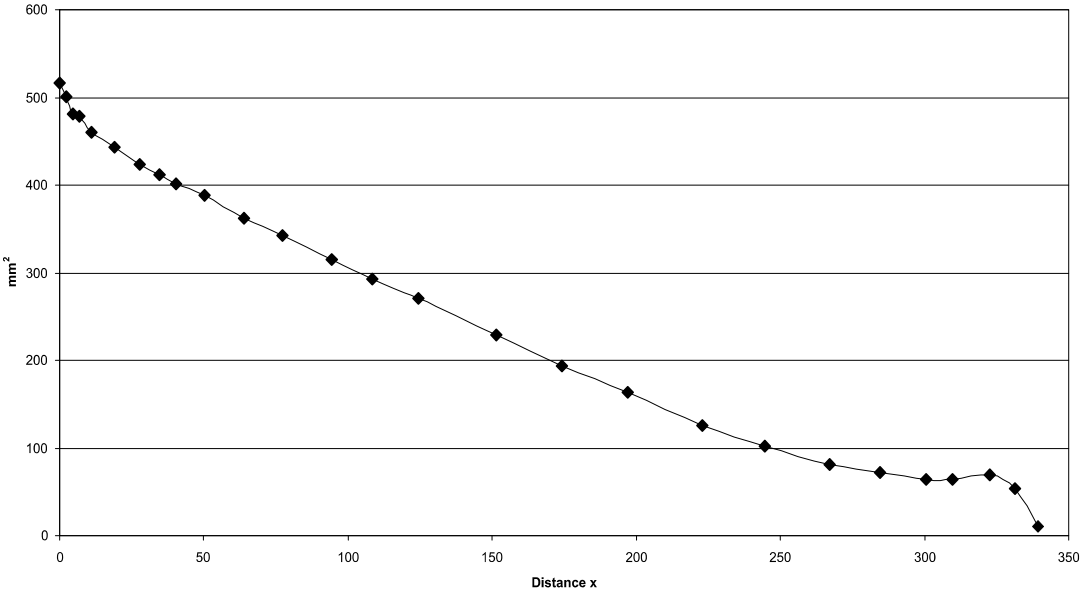

Fig A.282: Cross-sectional area of the Santanadactylus rostrum construction. See chapter 6.4 for legend.

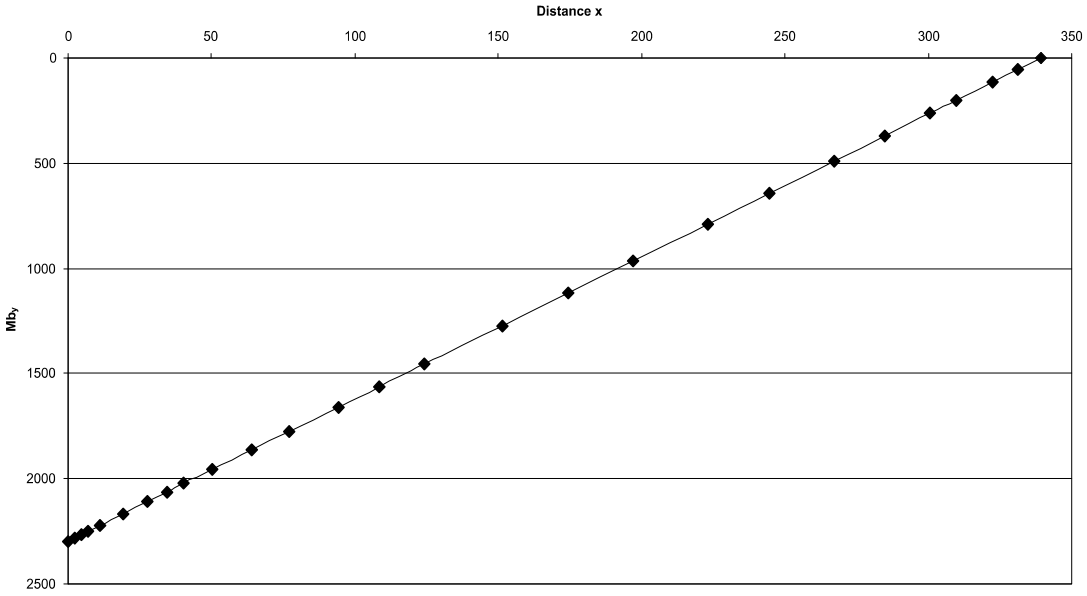

Fig A.283: Bending moments in the Santanadactylus rostrum construction. See chapter 6.4 for legend.

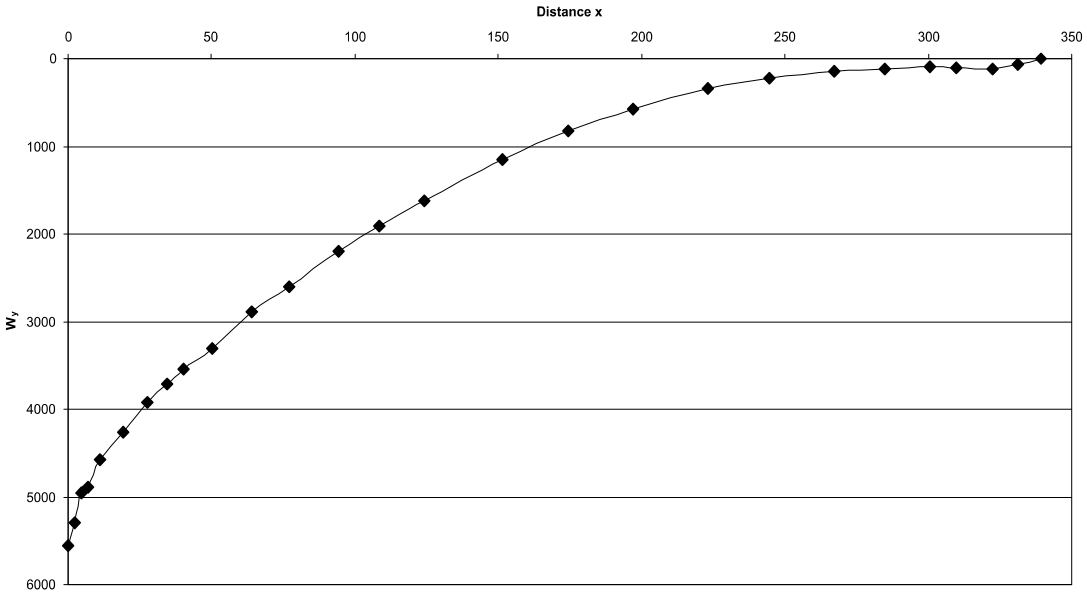

Fig A.284: Section modulus in the Santanadactylus rostrum construction. See chapter 6.4 for legend.

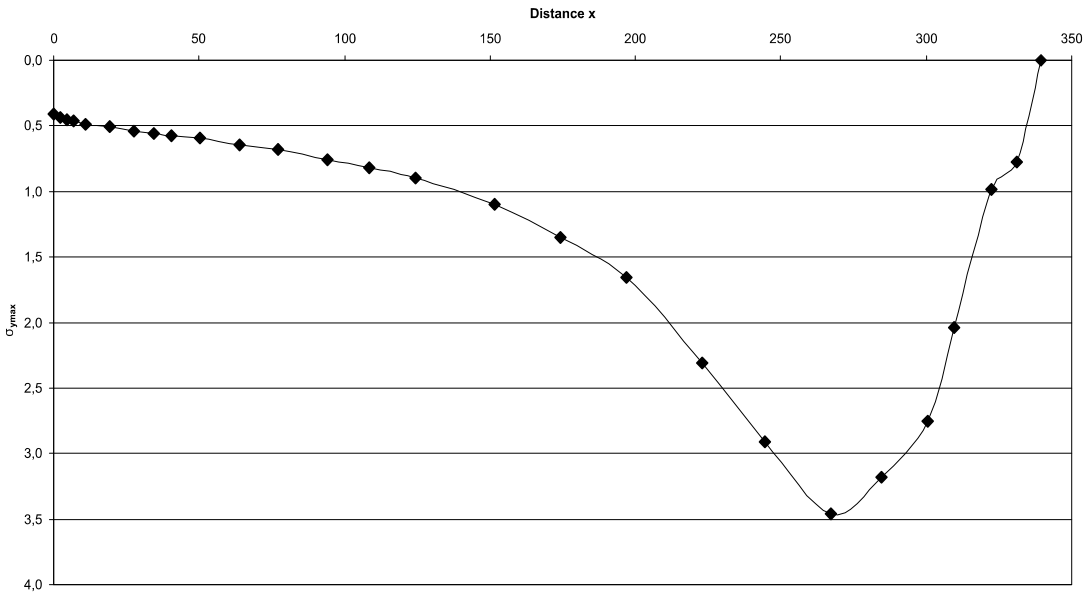

Fig A.285: Maximum bending stress in the Santanadactylus rostrum construction. See chapter 6.4 for legend.

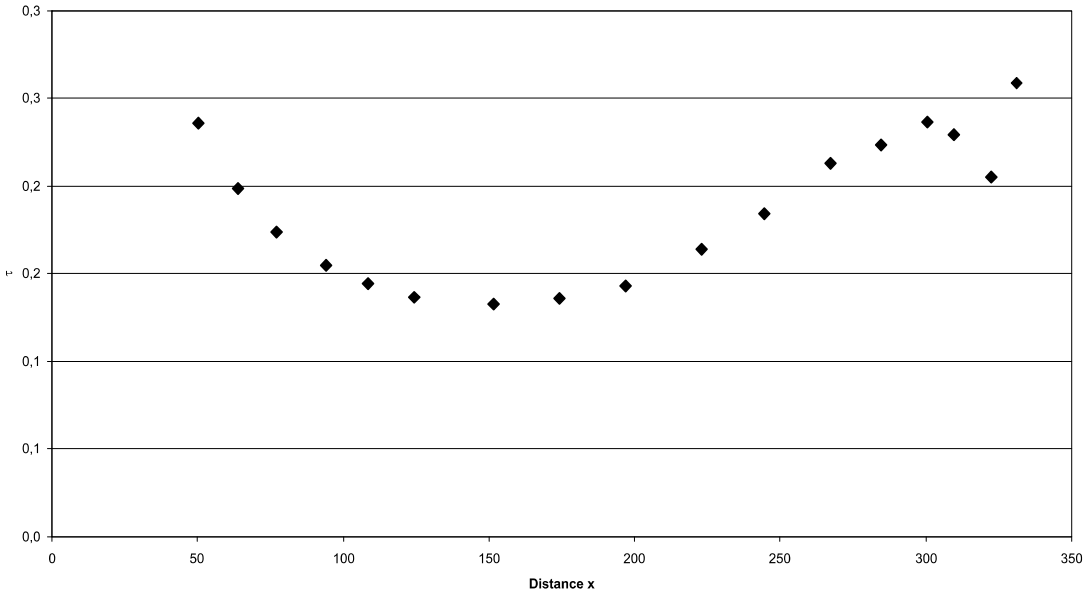

Fig. A.286: Shear stress in the Santanadactylus rostrum construction. See chapter 6.4 for legend.

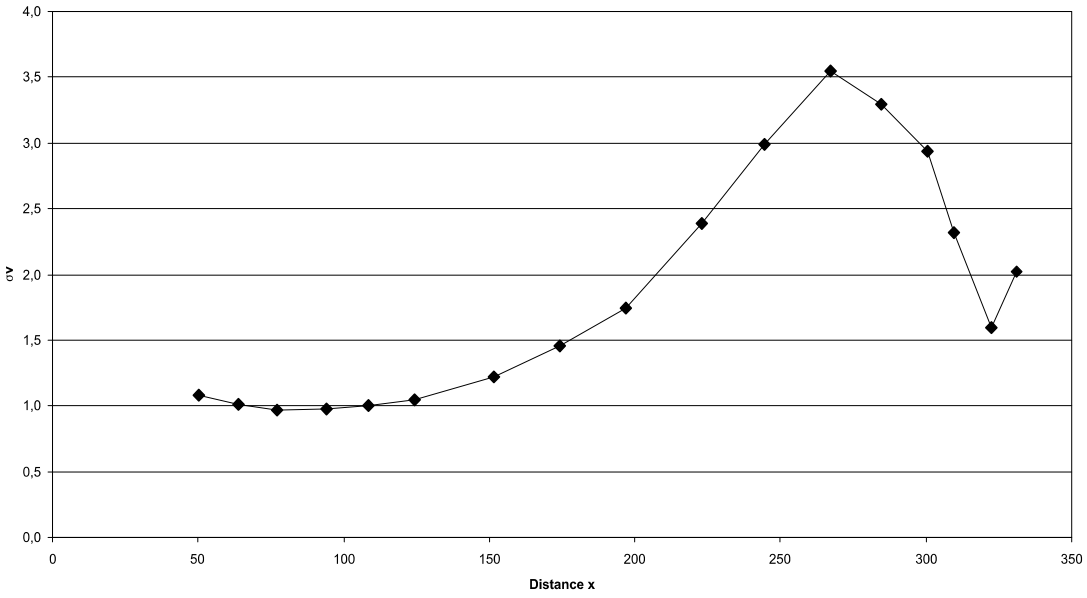

Fig. A.287: Comparison stress in the Santanadactylus rostrum construction. See chapter 6.4 for legend.

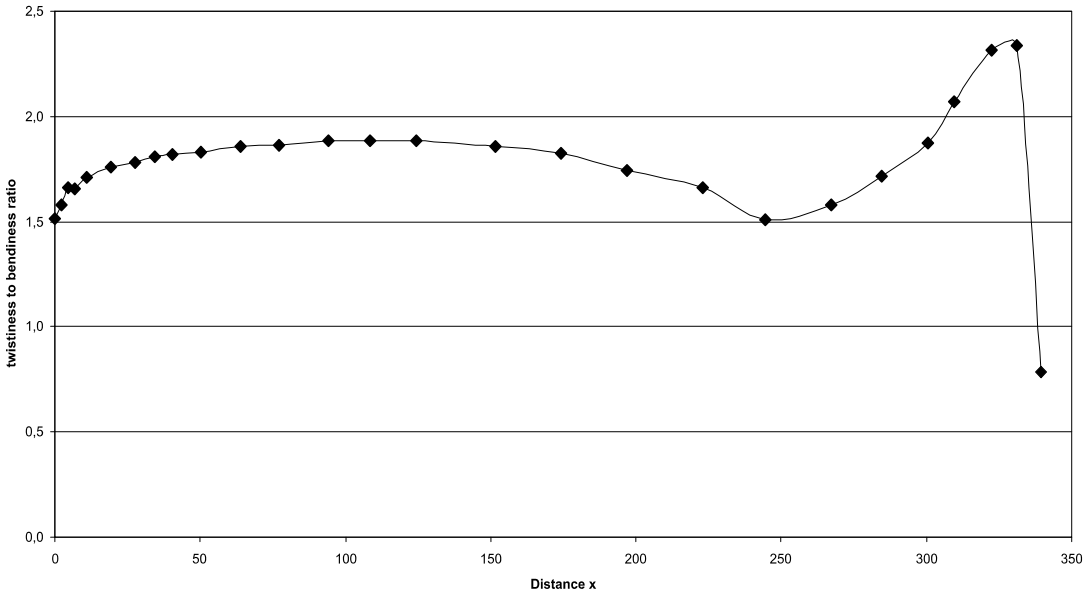

Fig. A.288: Twistiness to bendiness ratio in the Santanadactylus rostrum construction. See chapter 6.4 for legend.

A.37 Scaphognathus skull construction (see also chapter 7.37)

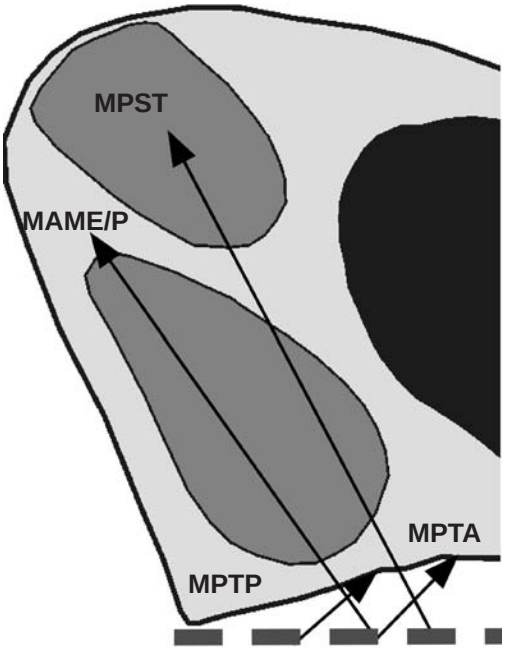

Fig A.289: Reconstruction of the principal pulling direction of the main adductor muscles in the skull of *Scaphognathus*. See chapter 6 for abbreviations.

Muscles	F_1	l_1	α_1	F_2	l_2	α_1
MAME/P	36	11.85	55	2.73	156.19	125
MPST	92	18.28	62	11.23	149.76	118
MPTA	14	13.14	46	1.19	154.91	134
MPTP	88	4.39	41	2.36	163.55	139

Tab. A.71: Reconstructed lever parameters for the scaled Scaphognathus skull construction. See chapter 6.2 for abbreviations.

	F_B	F_J	α_J
anteriormost rostrum	13.21	216.62	-49.74
1st tooth position	13.40	216.47	-49.74
1st to 4th tooth position	56.53	863.66	-49.59
last tooth position	41.00	196.23	-44.49
average	20.90	210.90	-48.34

Tab. A.72: Reconstructed bite and joint reaction forces and angle of joint reaction force in the scaled Scaphognathus skull construction. Negative angle values mean anterodorsal direction of force. See chapter 6.2 for abbreviations.

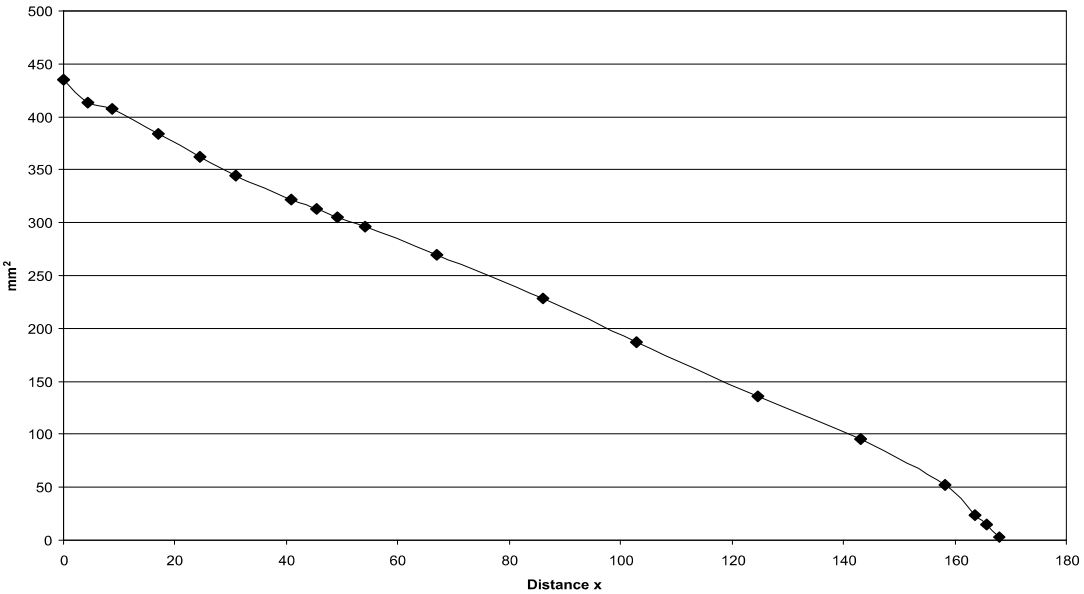

Fig A.290: Cross-sectional area of the Scaphognathus rostrum construction. See chapter 6.4 for legend.

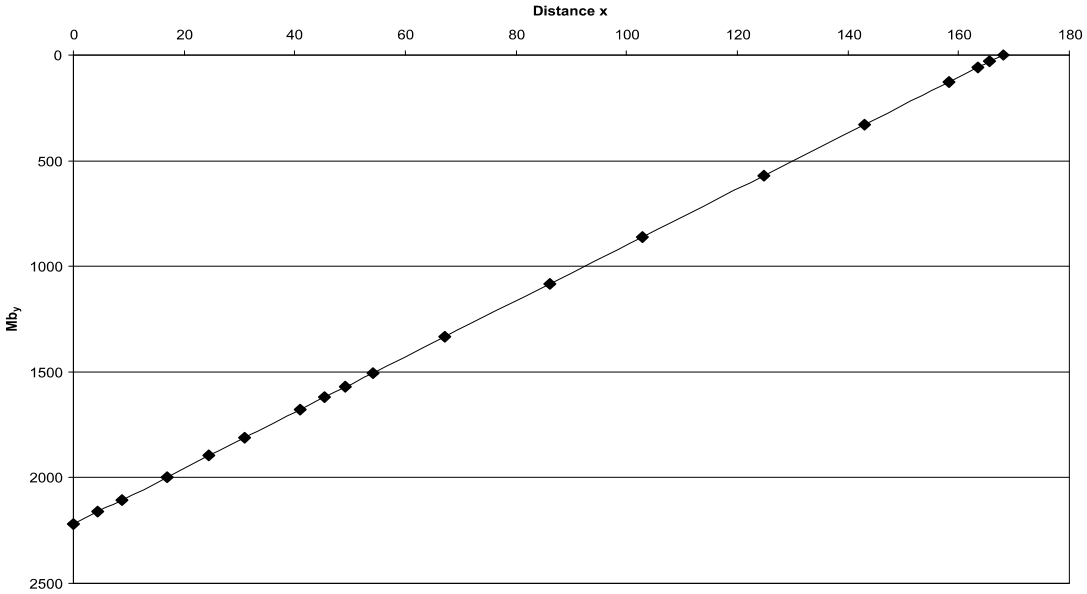

Fig A.291: Bending moments in the Scaphognathus rostrum construction. See chapter 6.4 for legend.

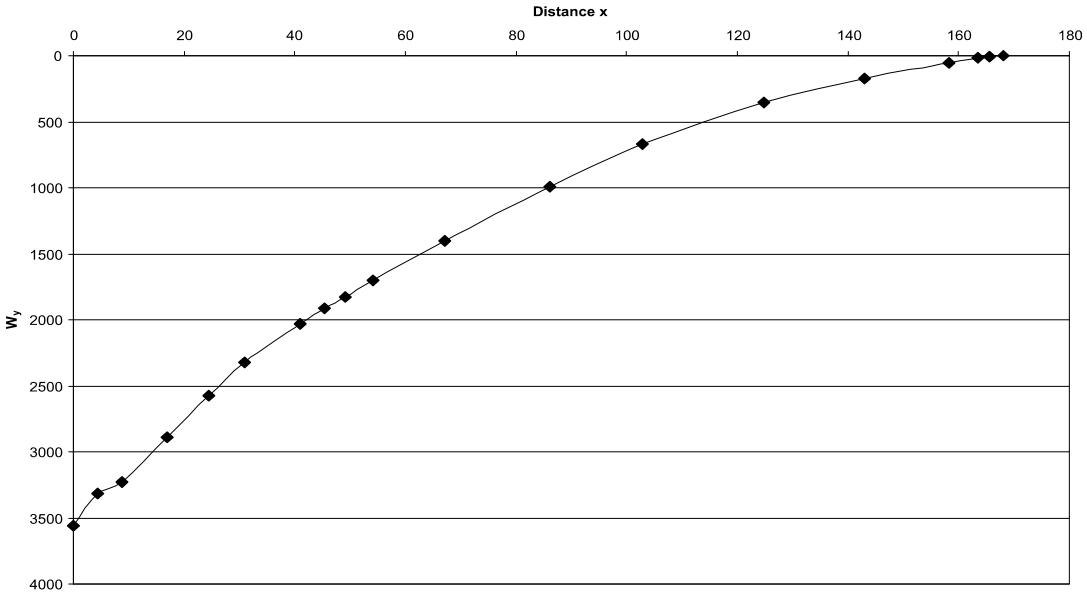

Fig A.292: Section modulus in the Scaphognathus rostrum construction. See chapter 6.4 for legend.

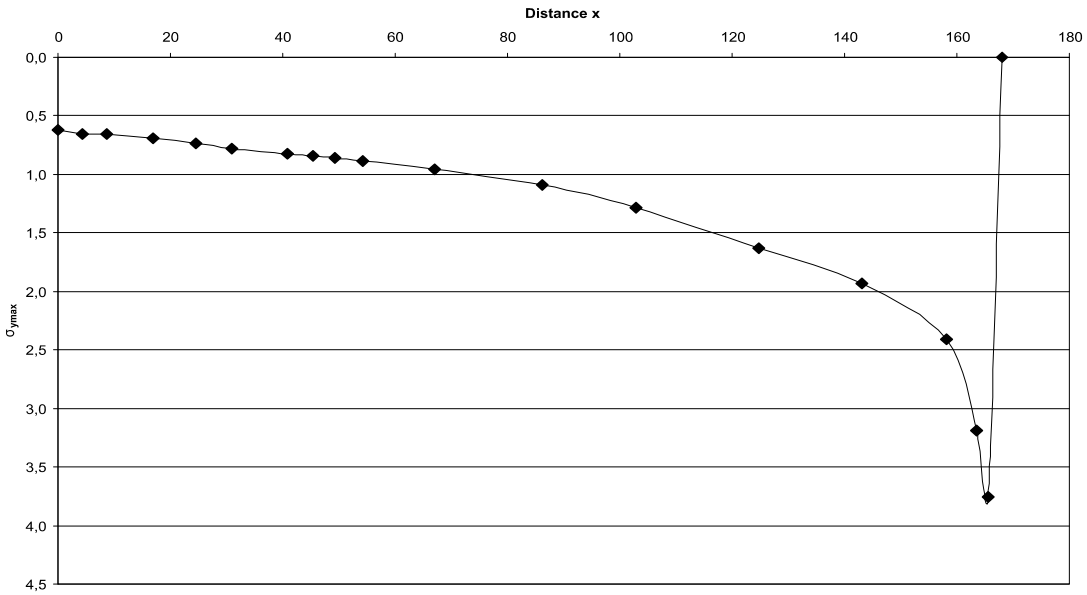

Fig A.293: Maximum bending stress in the Scaphognathus rostrum construction. See chapter 6.4 for legend.

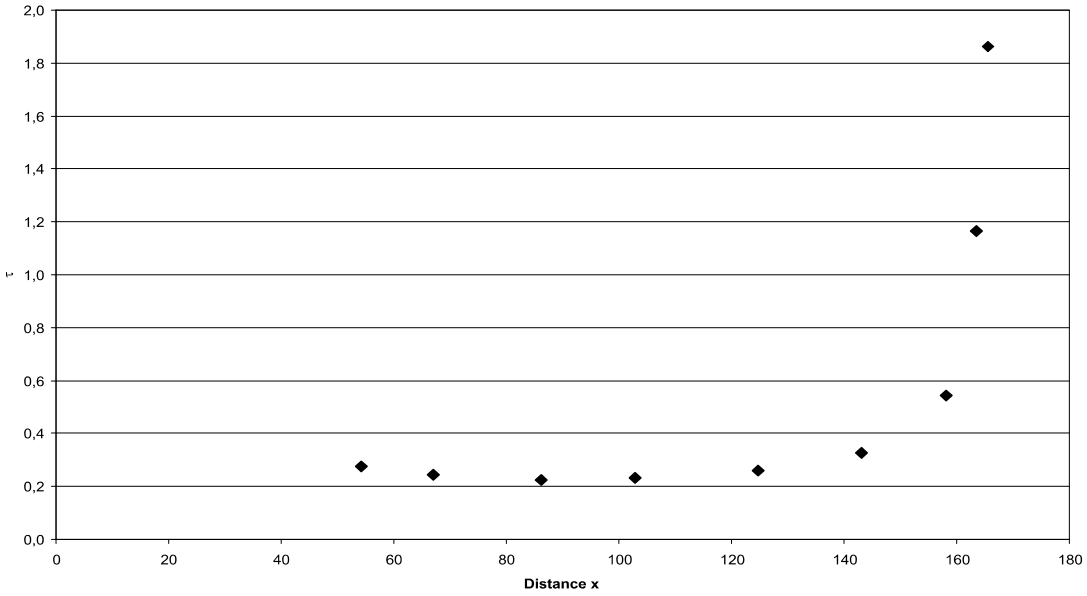

Fig. A.294: Shear stress in the Scaphognathus rostrum construction. See chapter 6.4 for legend.

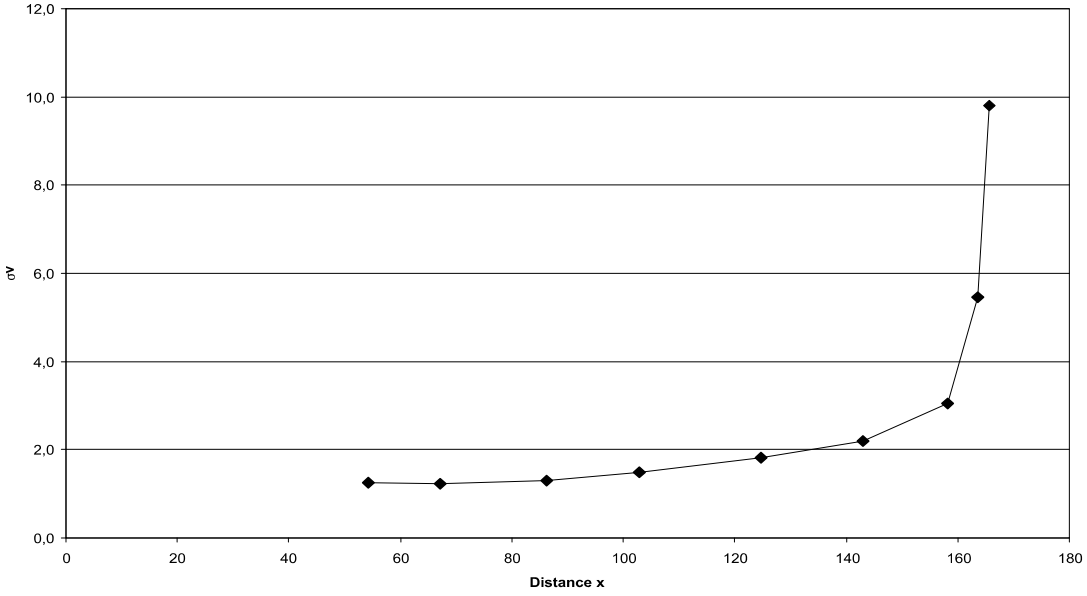

Fig. A.295: Comparison stress in the Scaphognathus rostrum construction. See chapter 6.4 for legend.

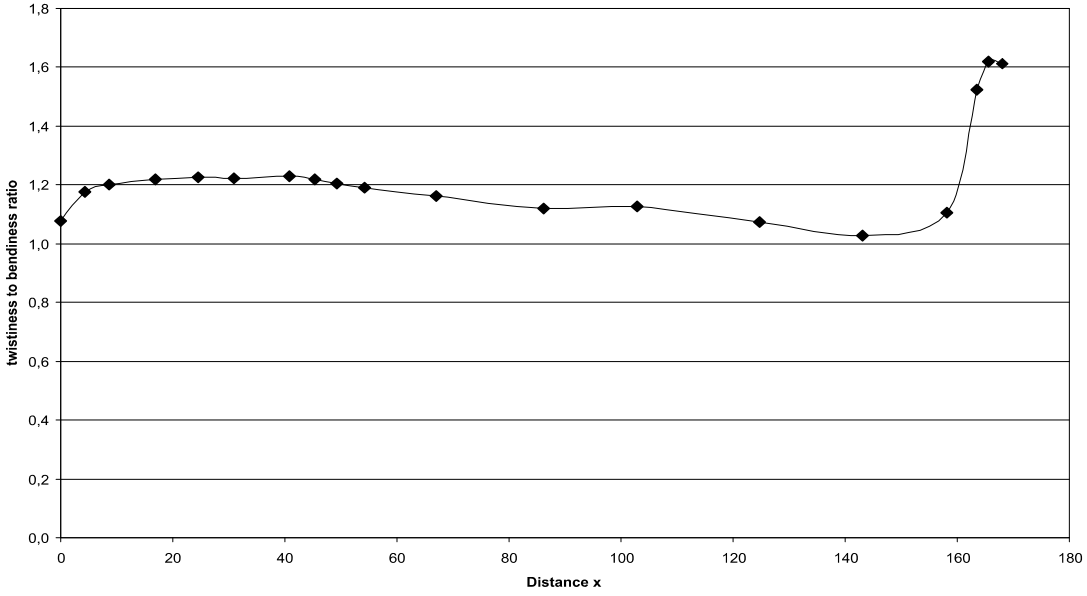

Fig. A.296: Twistiness to bendiness ratio in the Scaphognathus rostrum construction. See chapter 6.4 for legend.

A.38 Sinopterus skull construction (see also chapter 7.38)

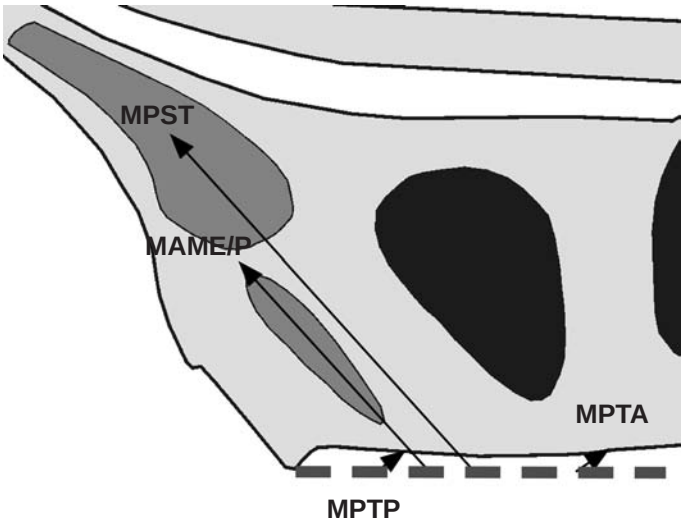

Fig A.297: Reconstruction of the principal pulling direction of the main adductor muscles in the skull of *Sinopterus*. See chapter 6 for abbreviations.

Muscles	F_1	l_1	α_1	F_2	l_2	α_1
MAME/P	36	21.91	47	3.50	225.58	133
MPST	92	27.94	48	11.71	219.55	132
MPTA	14	42.46	38	2.90	205.03	142
MPTP	88	12.30	36	4.60	235.19	144

Tab. A.73: Reconstructed lever parameters for the scaled Sinopterus skull construction. See chapter 6.2 for abbreviations.

	F_B	F_J	α_J
anteriormost rostrum	14.10	219.55	-39.94
level of half of the length of nasoant. fen.	25.34	212.51	-37.61
average	19.72	216.03	-38.78

Tab. A.74: Reconstructed bite and joint reaction forces and angle of joint reaction force in the scaled Sinopterus skull construction. Negative angle values mean anterodorsal direction of force. See chapter 6.2 for abbreviations.

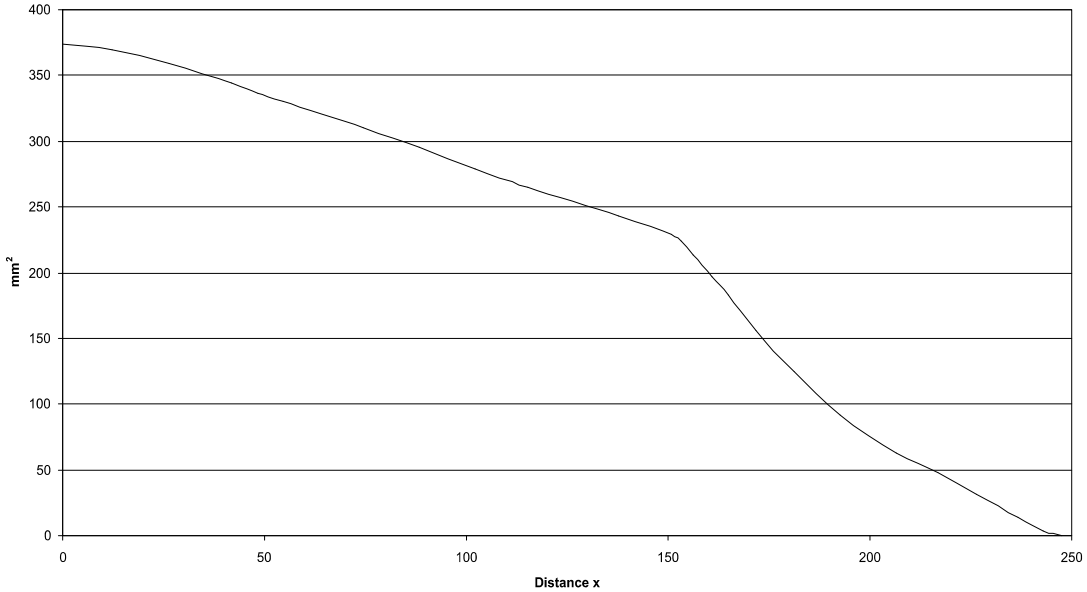

Fig A.298: Cross-sectional area of the Sinopterus rostrum construction. See chapter 6.4 for legend.

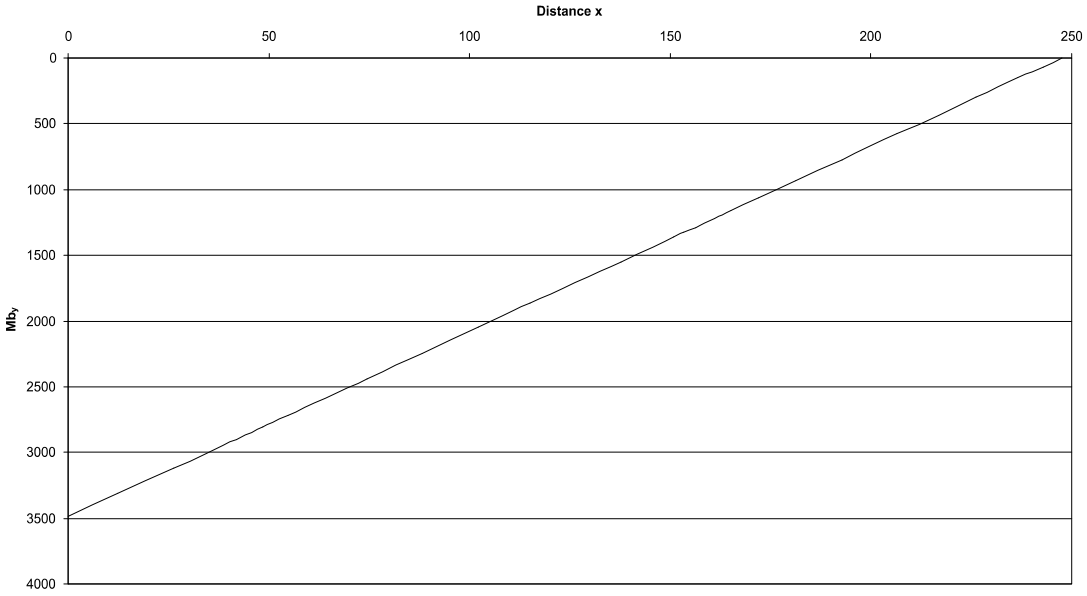

Fig A.299: Bending moments in the Sinopterus rostrum construction. See chapter 6.4 for legend.

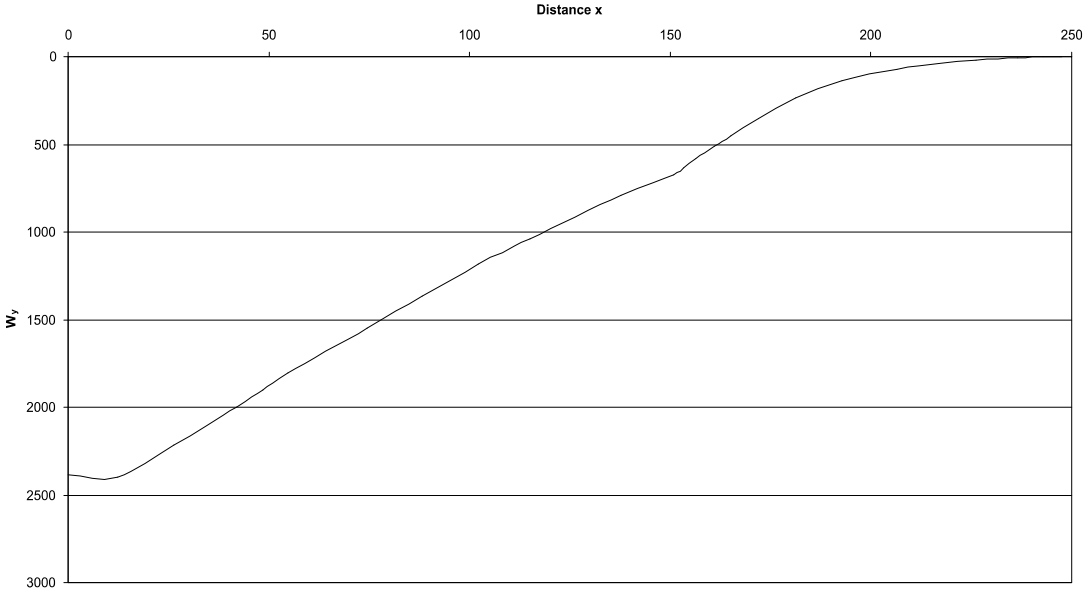

Fig A.300: Section modulus in the Sinopterus rostrum construction. See chapter 6.4 for legend.

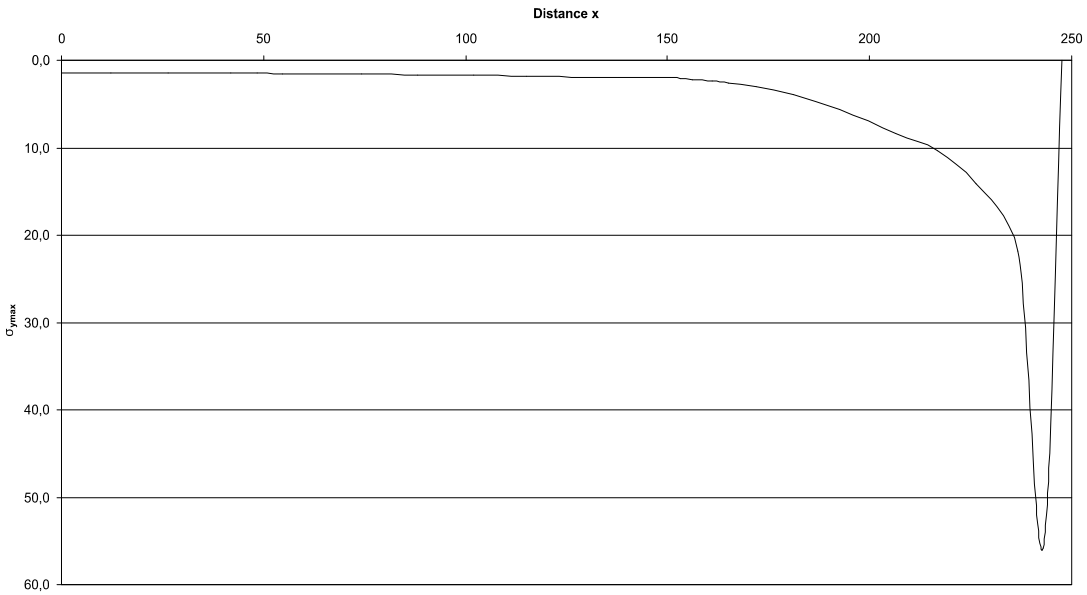

Fig A.301: Maximum bending stress in the Sinopterus rostrum construction. See chapter 6.4 for legend.

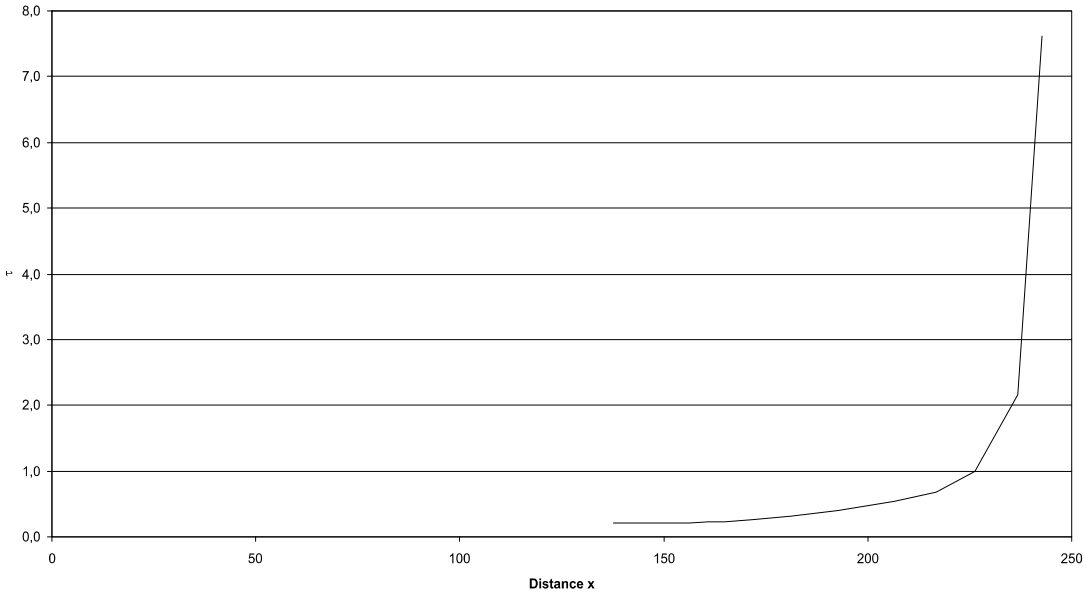

Fig. A.302: Shear stress in the Sinopterus rostrum construction. See chapter 6.4 for legend.

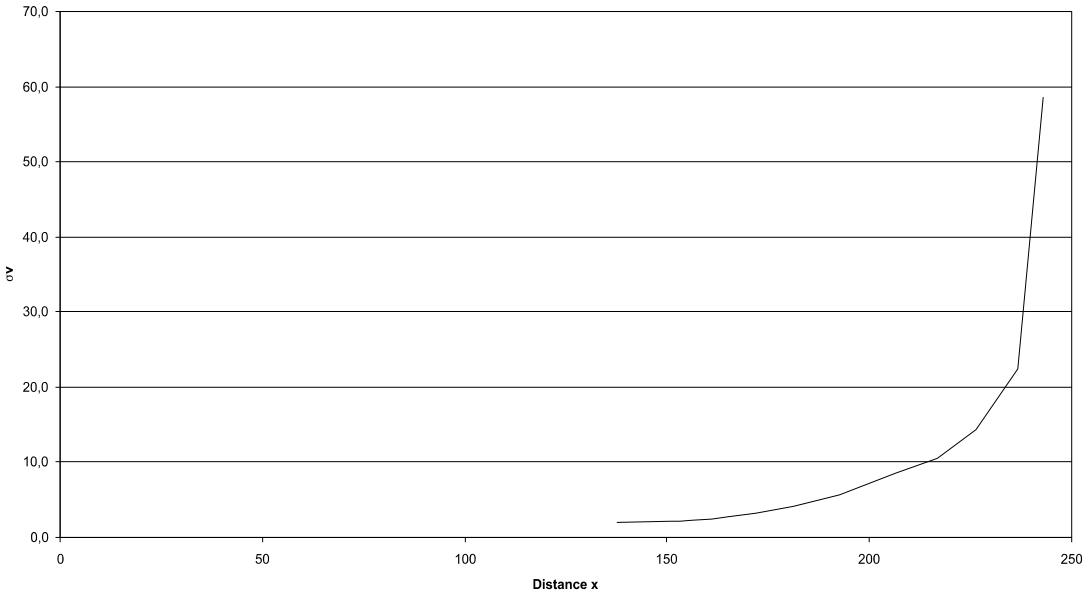

Fig. A.303: Comparison stress in the Sinopterus rostrum construction. See chapter 6.4 for legend.

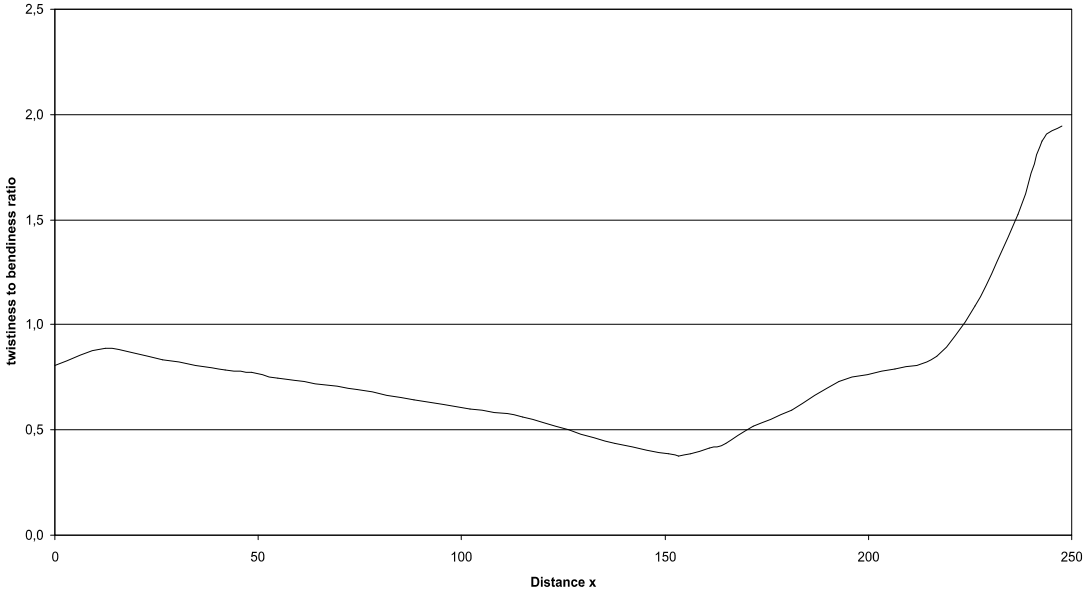

Fig. A.304: Twistiness to bendiness ratio in the Sinopterus rostrum construction. See chapter 6.4 for legend.

A.39 Sordes skull construction (see also chapter 7.39)

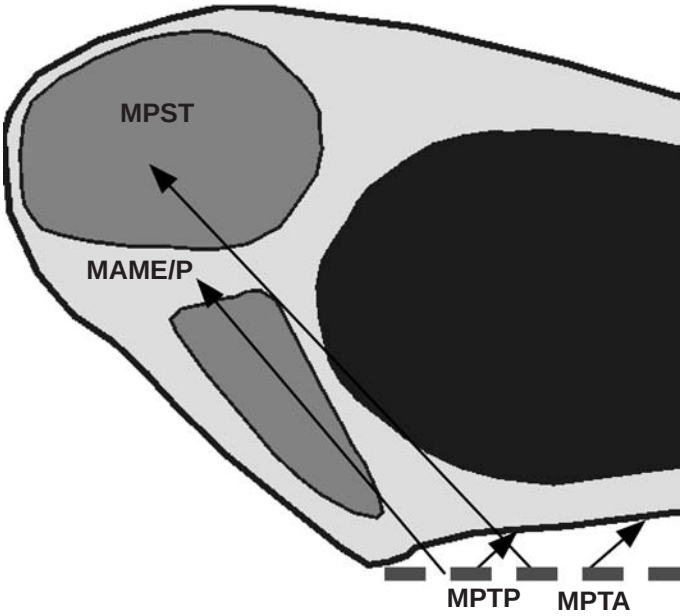

Fig A.305: Reconstruction of the principal pulling direction of the main adductor muscles in the skull of *Sordes*. See chapter 6 for abbreviations.

Muscles	F_1	l_1	α_1	F_2	l_2	α_1
MAME/P	36	7.52	50	1.36	198.58	130
MPST	92	18.32	56	8.98	187.78	124
MPTA	14	26.81	41	2.09	179.29	139
MPTP	88	11.12	43	5.02	198.98	137

Tab. A.75: Reconstructed lever parameters for the scaled Sordes skull construction. See chapter 6.2 for abbreviations.

	F_B	F_J	α_J
1st tooth position	12.22	219.59	-47.09
1st to 4th tooth position	57.11	872.36	-46.72
last tooth position	34.61	203.77	-42.80
average	19.62	214.28	-45.71

Tab. A.76: Reconstructed bite and joint reaction forces and angle of joint reaction force in the scaled Sordes skull construction. Negative angle values mean anterodorsal direction of force. See chapter 6.2 for abbreviations.

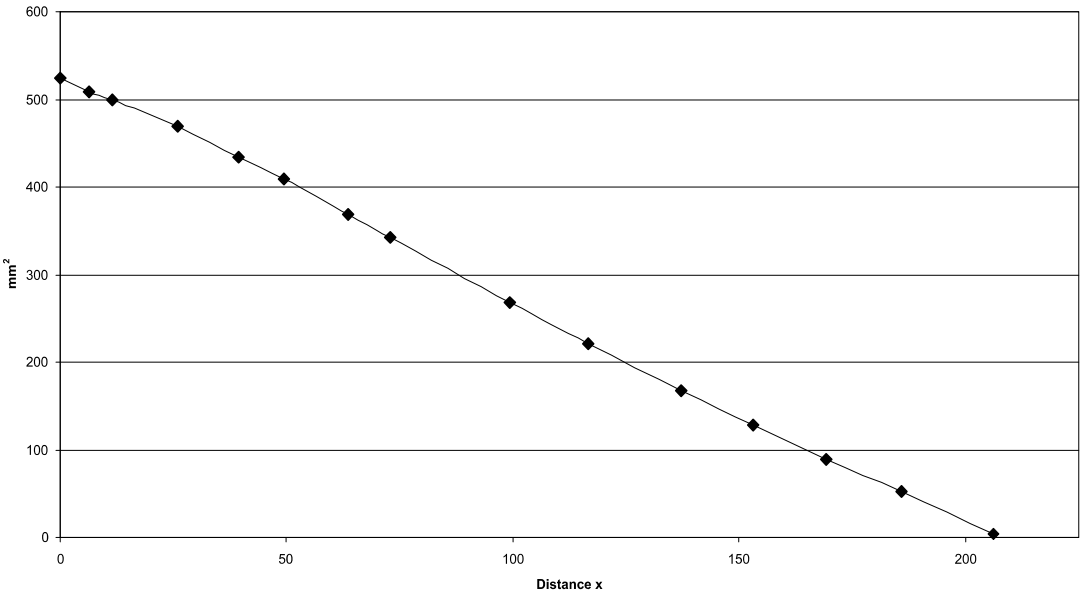

Fig A.306: Cross-sectional area of the Sordes rostrum construction. See chapter 6.4 for legend.

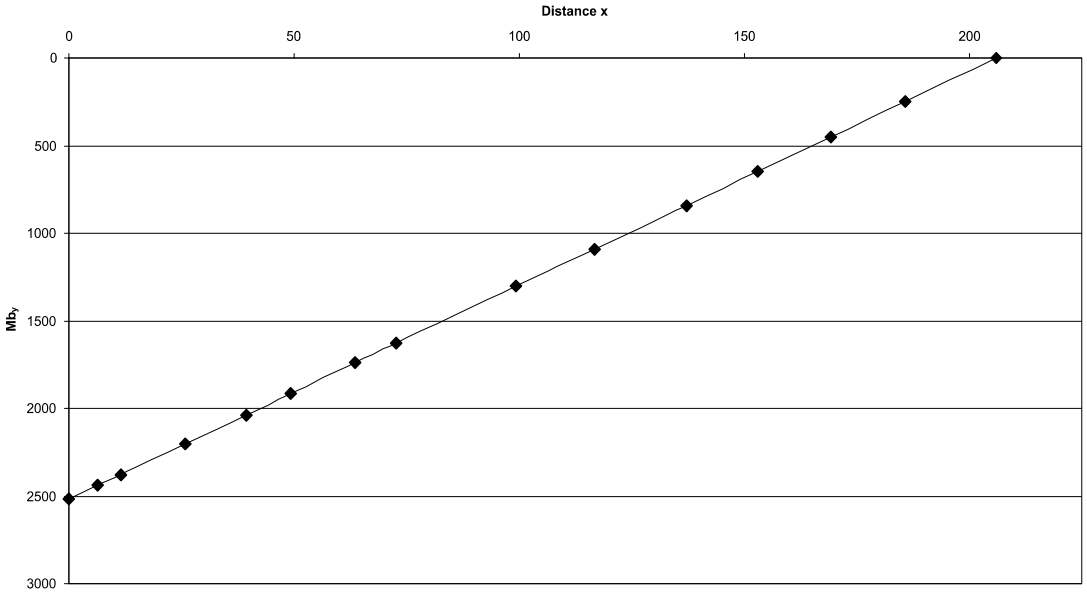

Fig A.307: Bending moments in the Sordes rostrum construction. See chapter 6.4 for legend.

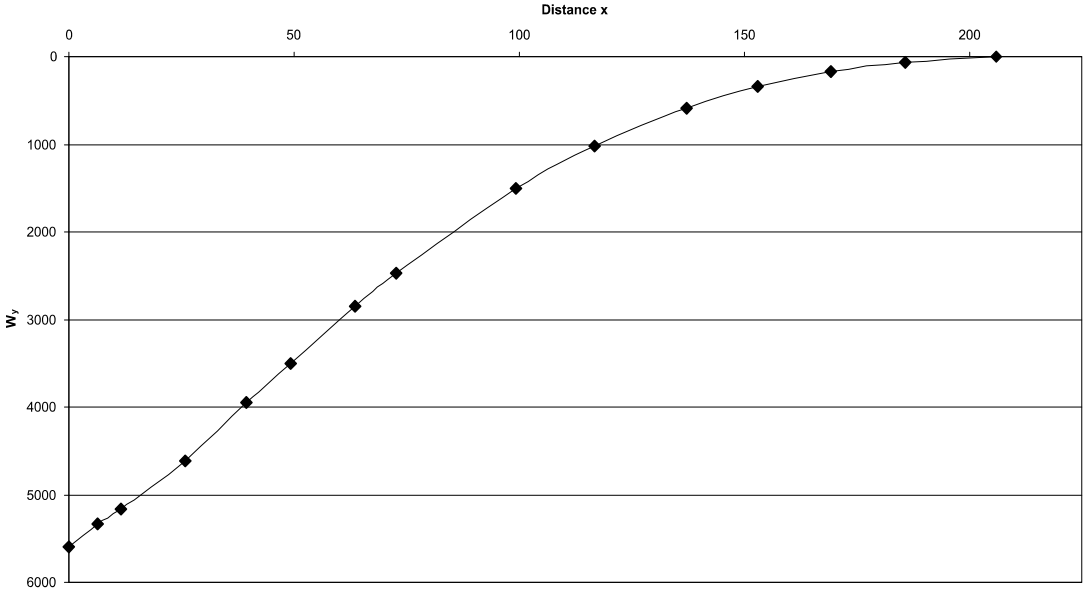

Fig A.308: Section modulus in the Sordes rostrum construction. See chapter 6.4 for legend.

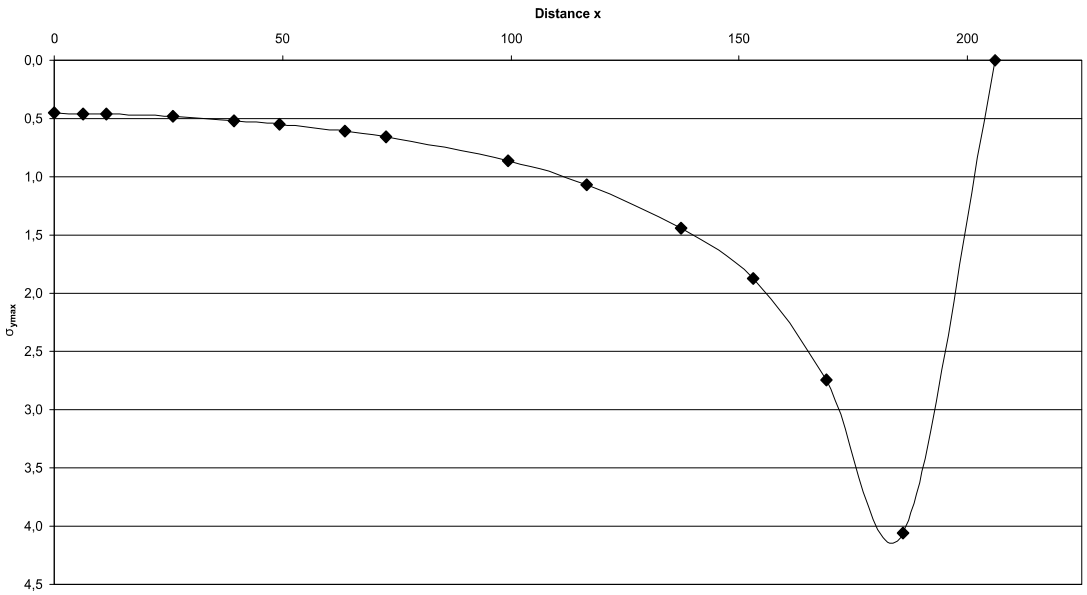

Fig A.309: Maximum bending stress in the Sordes rostrum construction. See chapter 6.4 for legend.

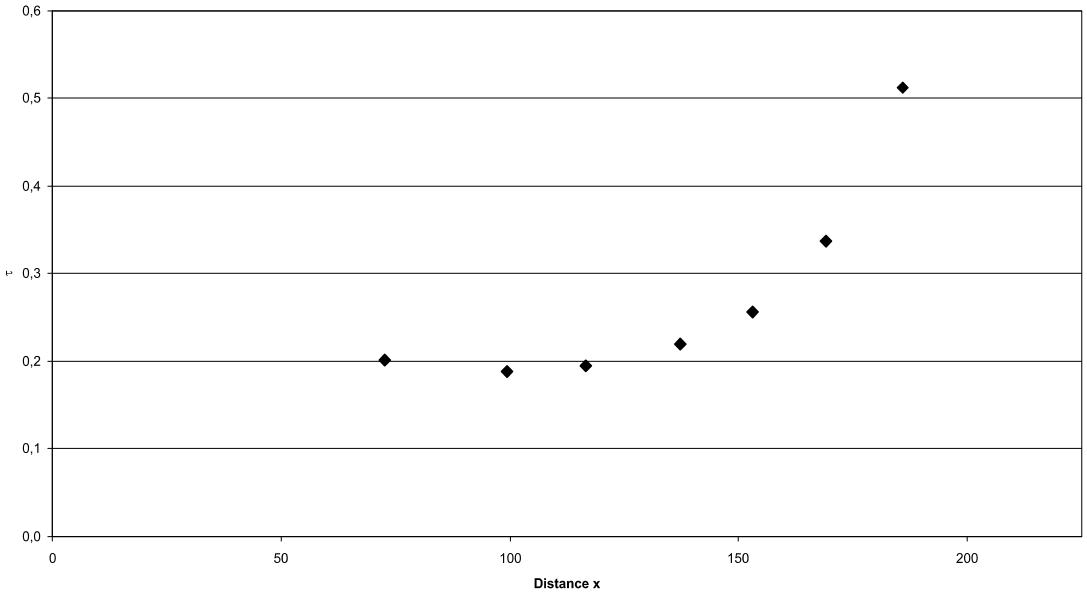

Fig. A.310: Shear stress in the Sordes rostrum construction. See chapter 6.4 for legend.

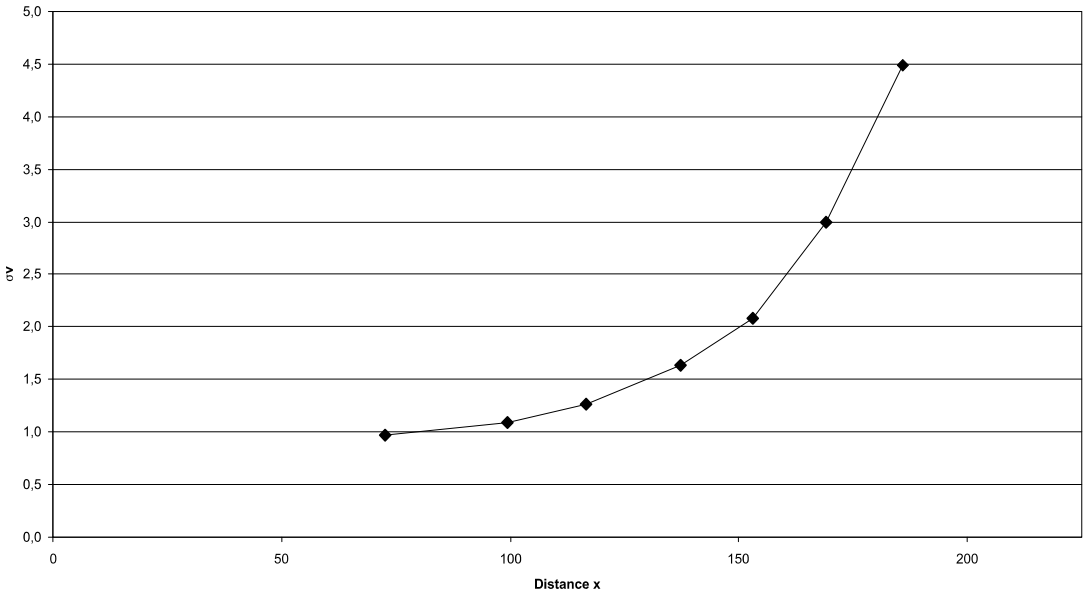

Fig. A.311: Comparison stress in the Sordes rostrum construction. See chapter 6.4 for legend.

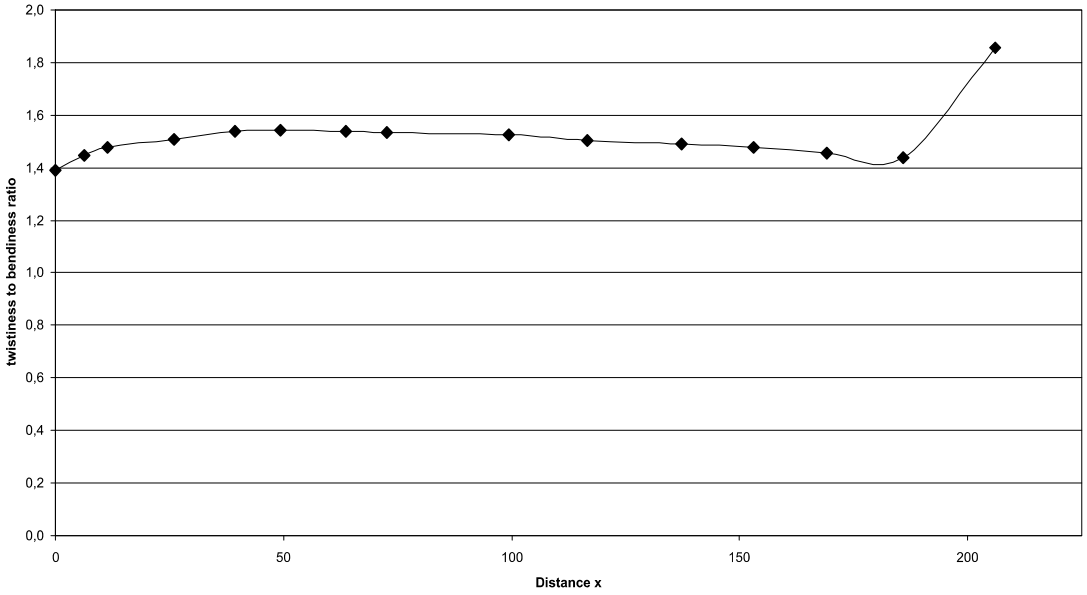

Fig. A.312: Twistiness to bendiness ratio in the Sordes rostrum construction. See chapter 6.4 for legend.

A.40 Tapejara skull construction (see also chapter 7.40)

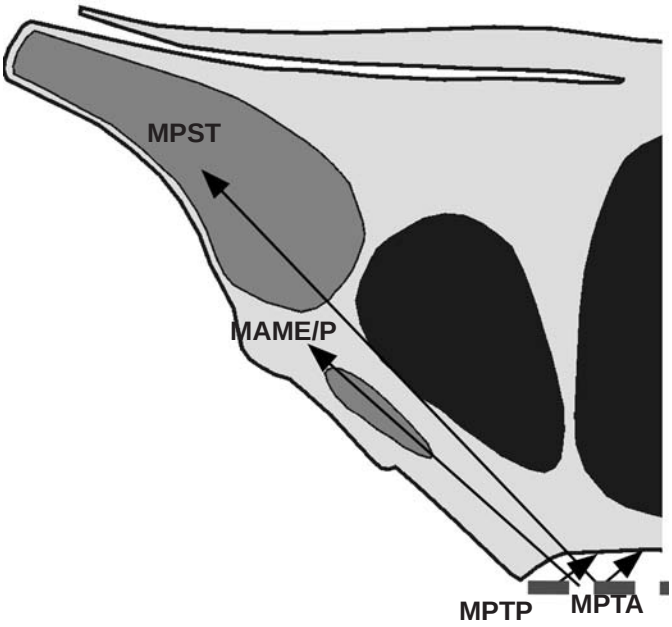

Fig A.313: Reconstruction of the principal pulling direction of the main adductor muscles in the skull of *Tapejara*. See chapter 6 for abbreviations..

Muscles	F_1	l_1	α_1	F_2	l_2	α_1
MAME/P	36	6.30	42	2.05	110.77	138
MPST	92	8.74	46	7.42	108.33	134
MPTA	14	10.03	41	1.31	107.04	139
MPTP	88	3.99	36	3.11	113.08	144

Tab. A.77: Reconstructed lever parameters for the scaled Tapejara skull construction. See chapter 6.2 for abbreviations.

	F_B	F_J	α_J
anteriormost rostrum	8.79	223.62	-39.55
level of half of the length of nasoant. fen.	39.98	205.17	-32.82
average	24.39	214.40	-35.88

Tab. A.78: Reconstructed bite and joint reaction forces and angle of joint reaction force in the scaled Tapejara skull construction. Negative angle values mean anterodorsal direction of force. See chapter 6.2 for abbreviations.

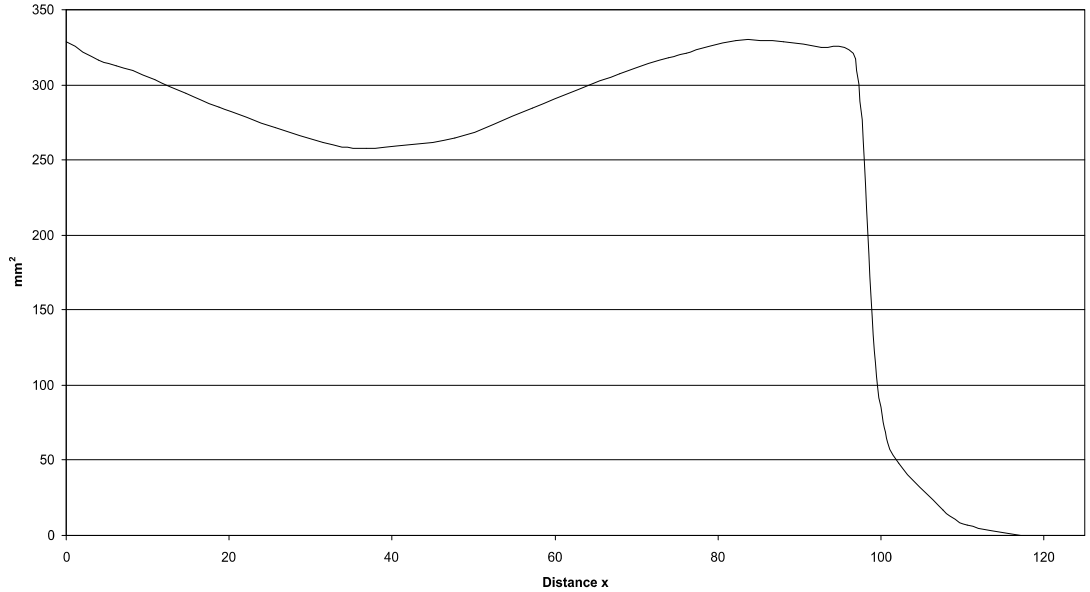

Fig A.314: Cross-sectional area of the Tapejara rostrum construction. See chapter 6.4 for legend.

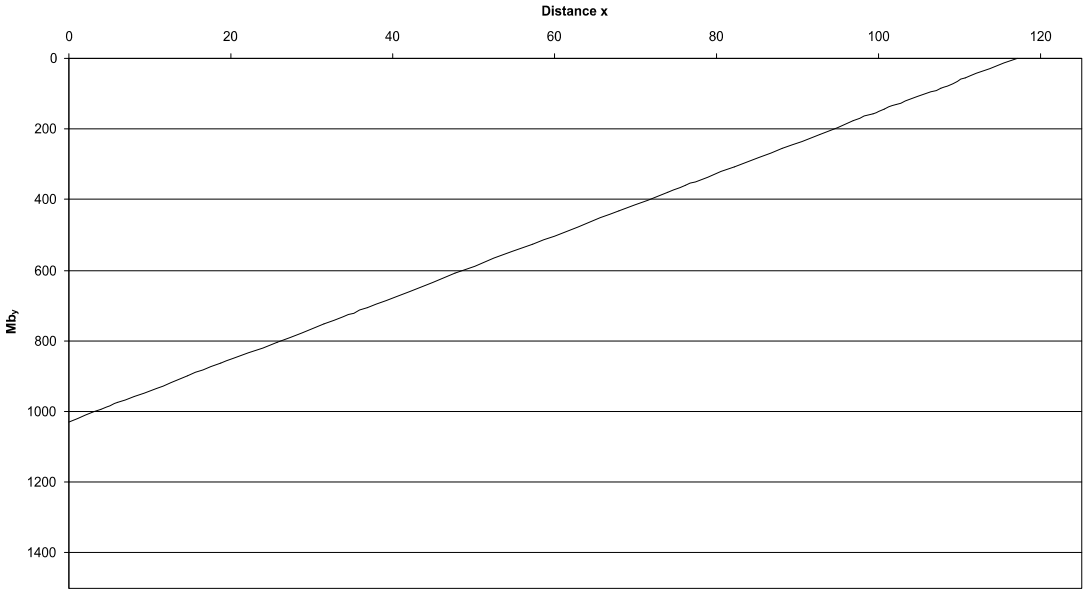

Fig A.315: Bending moments in the Tapejara rostrum construction. See chapter 6.4 for legend.

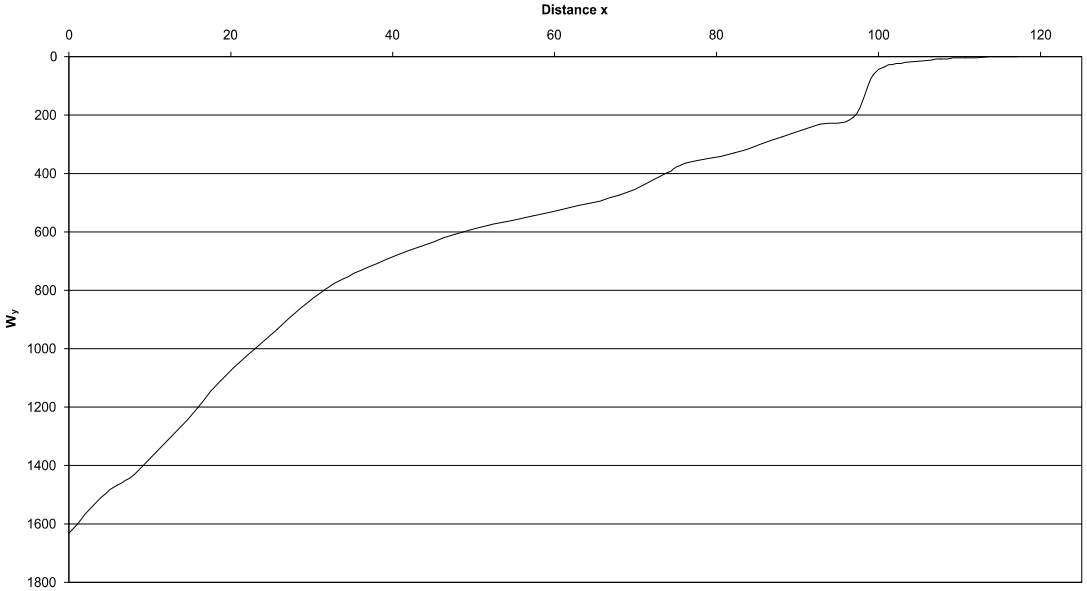

Fig A.316: Section modulus in the Tapejara rostrum construction. See chapter 6.4 for legend.

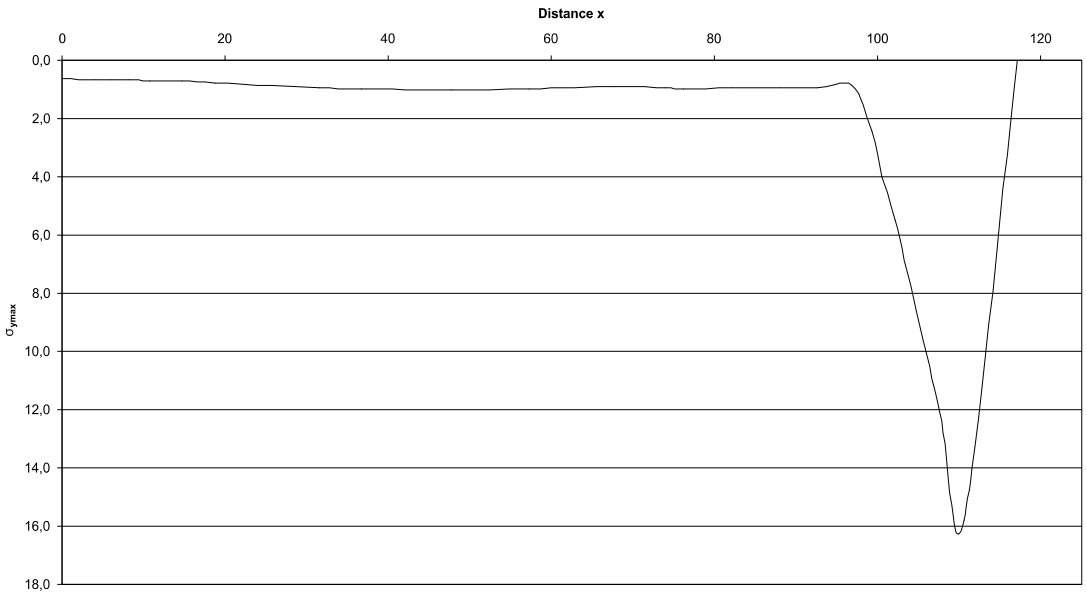

Fig A.317: Maximum bending stress in the Tapejara rostrum construction. See chapter 6.4 for legend.

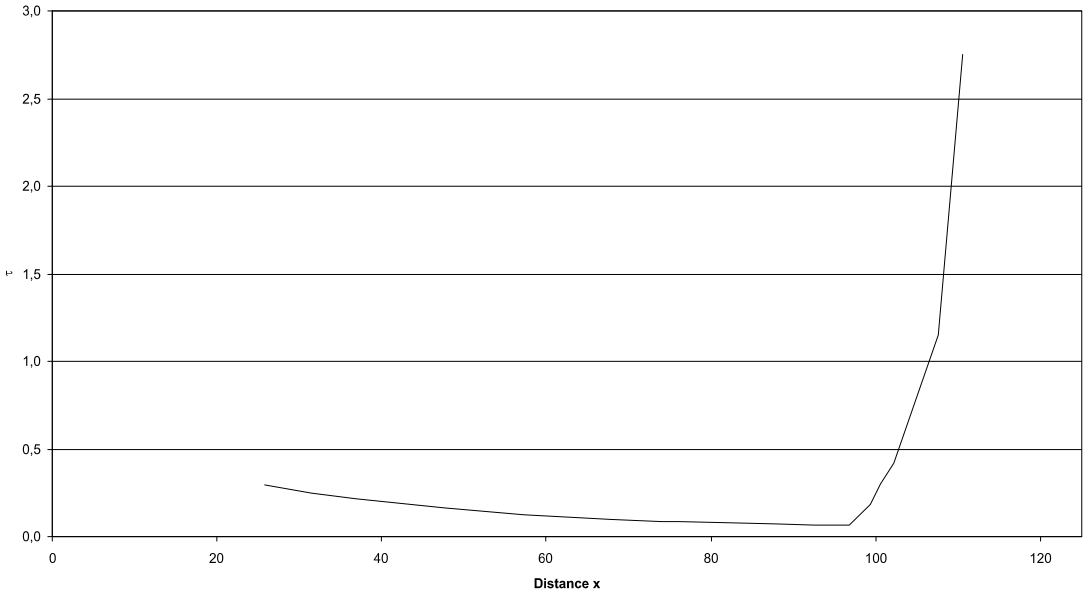

Fig. A.318: Shear stress in the Tapejara rostrum construction. See chapter 6.4 for legend.

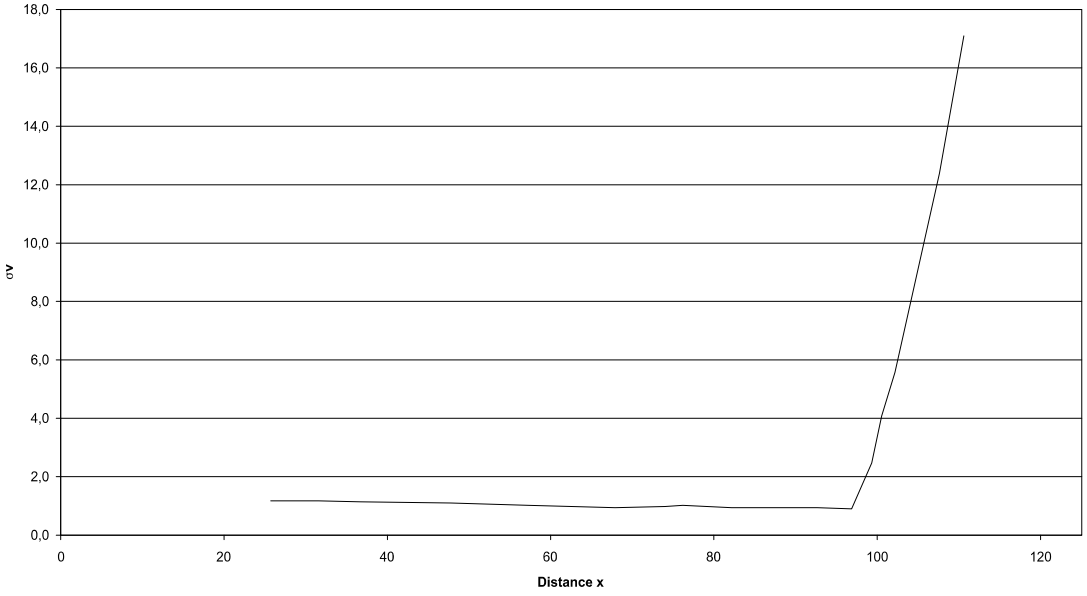

Fig. A.319: Comparison stress in the Tapejara rostrum construction. See chapter 6.4 for legend.

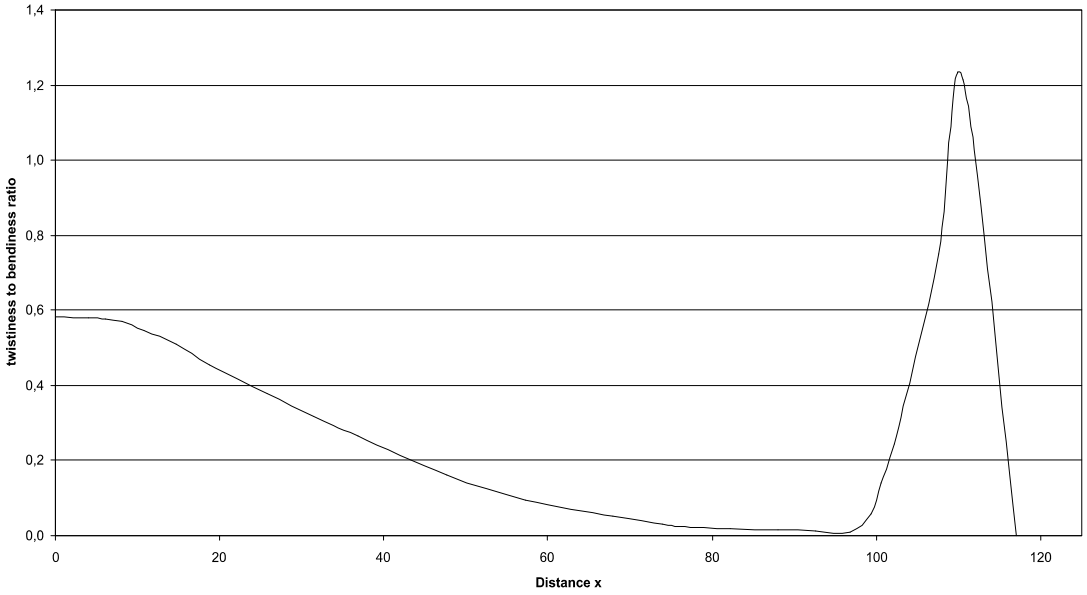

Fig. A.320: Twistiness to bendiness ratio in the Tapejara rostrum construction. See chapter 6.4 for legend.

A.41 Thalassodromeus skull construction (see also chapter 7.41)

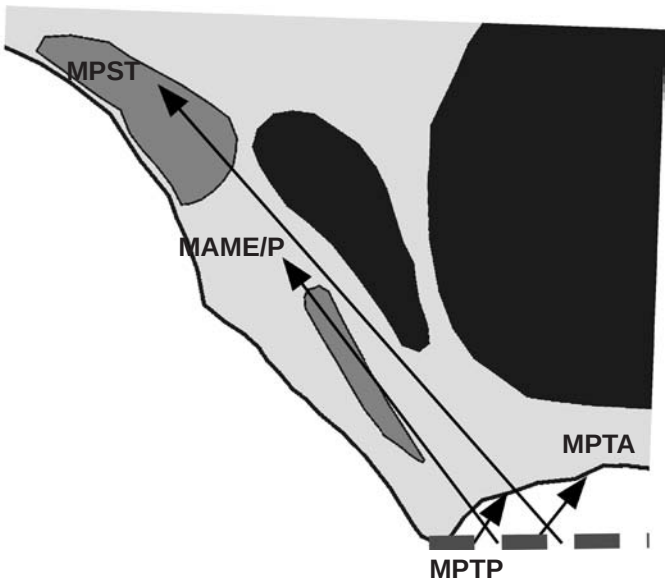

Fig A.321: Reconstruction of the principal pulling direction of the main adductor muscles in the skull of *Thalassodromeus*. See chapter 6 for abbreviations.

Muscles	F_1	l_1	α_1	F_2	l_2	α_1
MAME/P	36	7.83	53	1.53	184.20	127
MPST	92	15.14	49	7.87	176.88	131
MPTA	14	12.09	51	0.94	179.93	129
MPTP	88	5.72	57	2.70	186.75	123

Tab. A.79: Reconstructed lever parameters for the scaled Thalassodromeus skull construction. See chapter 6.2 for abbreviations.

	F_B	F_J	α_J
anteriormost rostrum	9.53	222.04	-51.32
level of half of the length of nasoant. fen.	33.21	204.09	-47.16
average	21.37	231.07	-49.24

Tab. A.80: Reconstructed bite and joint reaction forces and angle of joint reaction force in the scaled Thalassodromeus skull construction. Negative angle values mean anterodorsal direction of force. See chapter 6.2 for abbreviations.

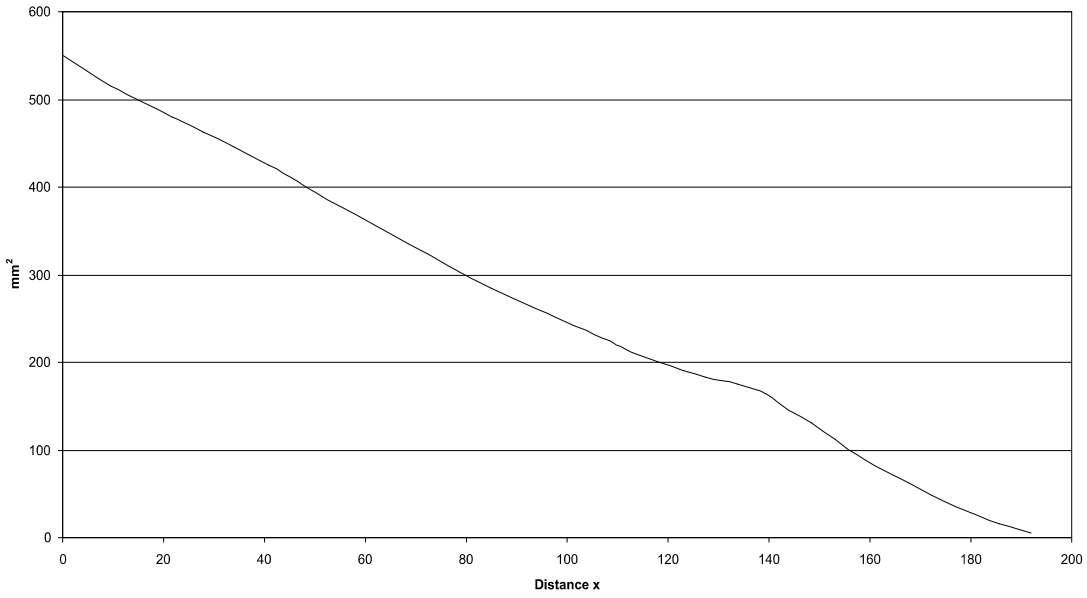

Fig A.322: Cross-sectional area of the Thalassodromeus rostrum construction. See chapter 6.4 for legend.

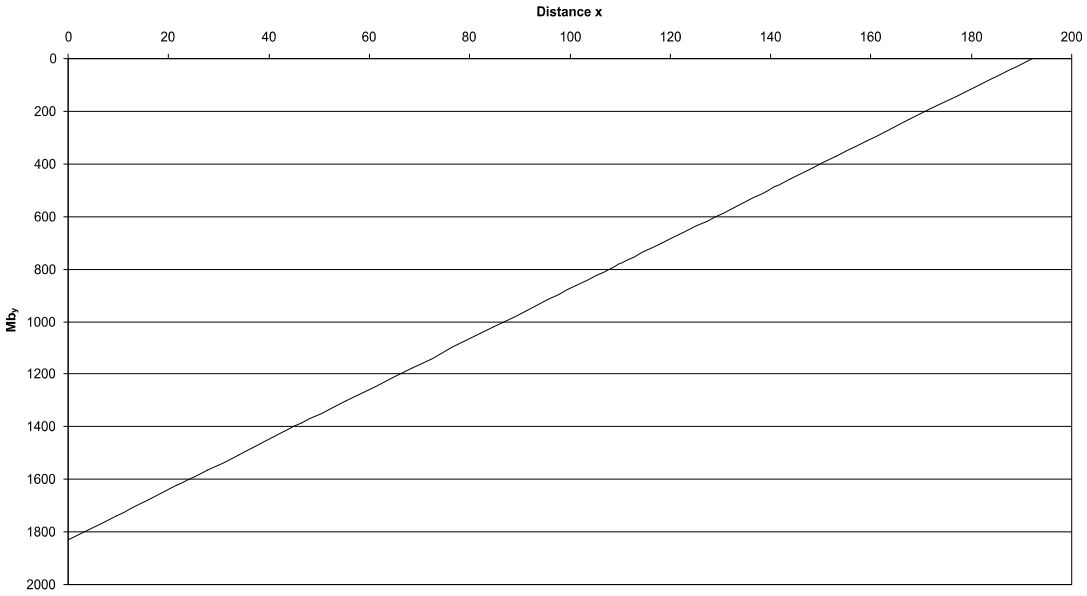

Fig A.323: Bending moments in the Thalassodromeus rostrum construction. See chapter 6.4 for legend.

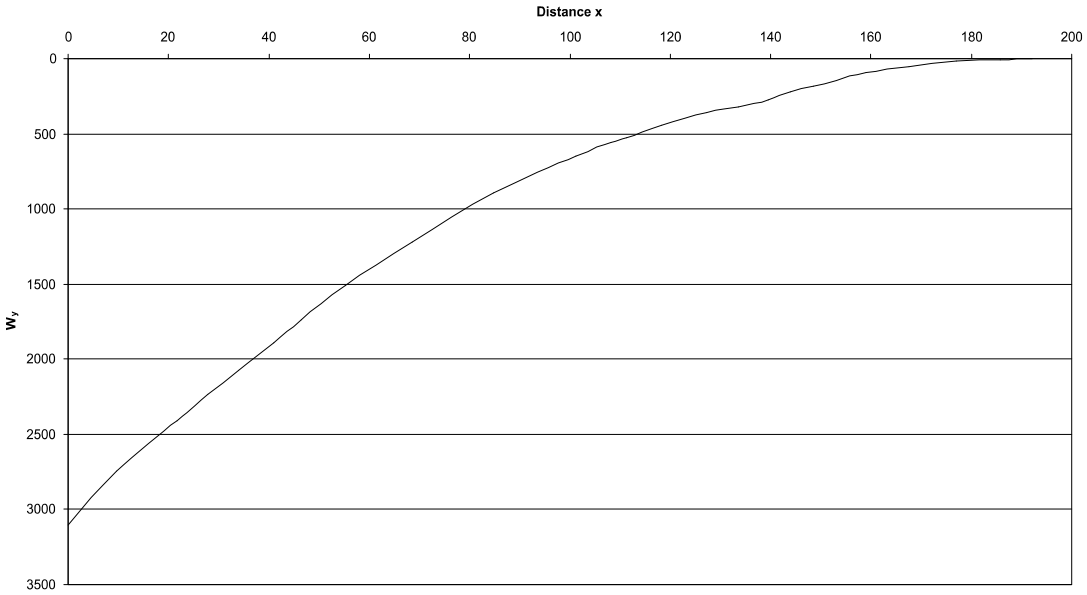

Fig A.324: Section modulus in the Thalassodromeus rostrum construction. See chapter 6.4 for legend.

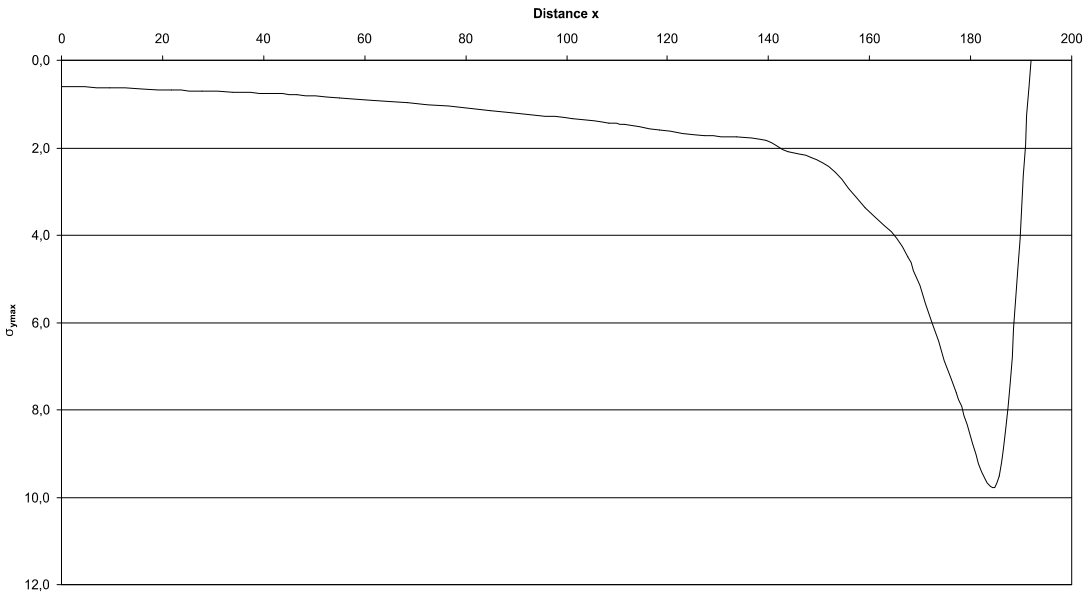

Fig A.325: Maximum bending stress in the Thalassodromeus rostrum construction. See chapter 6.4 for legend.

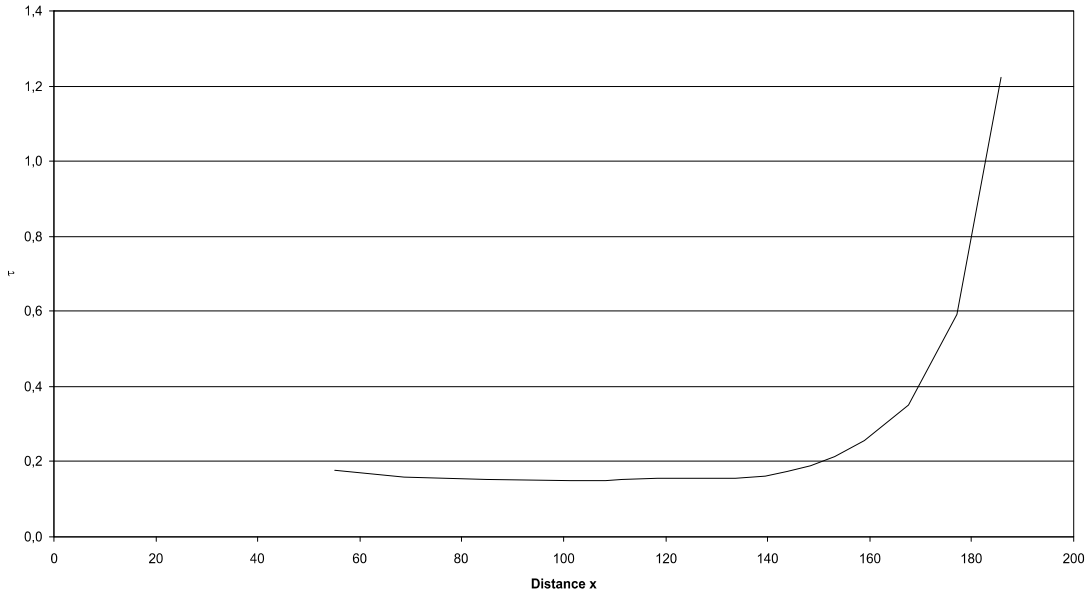

Fig. A.326: Shear stress in the Thalassodromeus rostrum construction. See chapter 6.4 for legend.

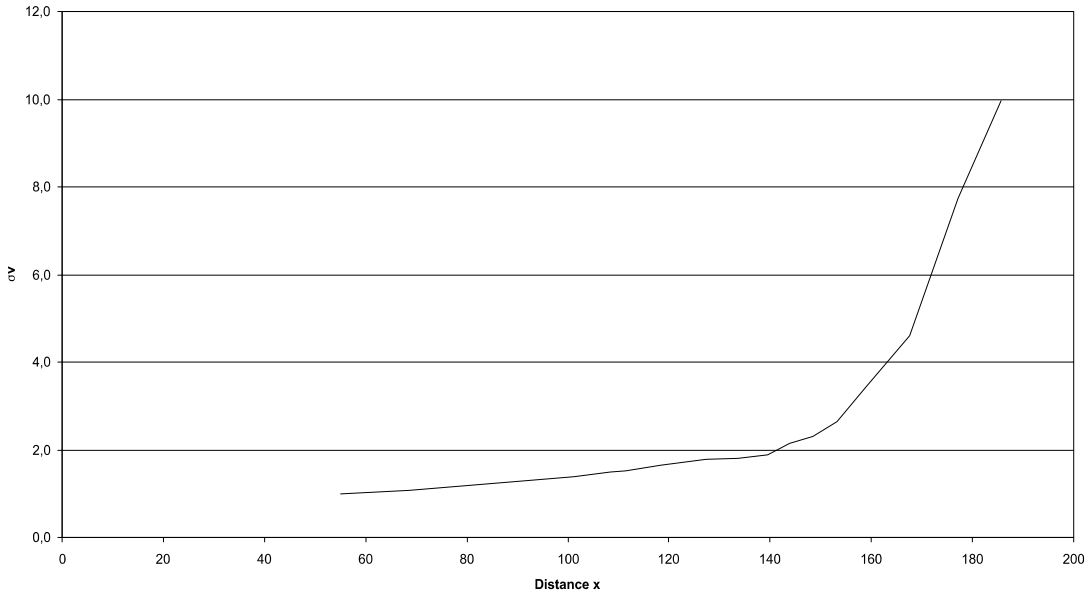

Fig. A.327: Comparison stress in the Thalassodromeus rostrum construction. See chapter 6.4 for legend.

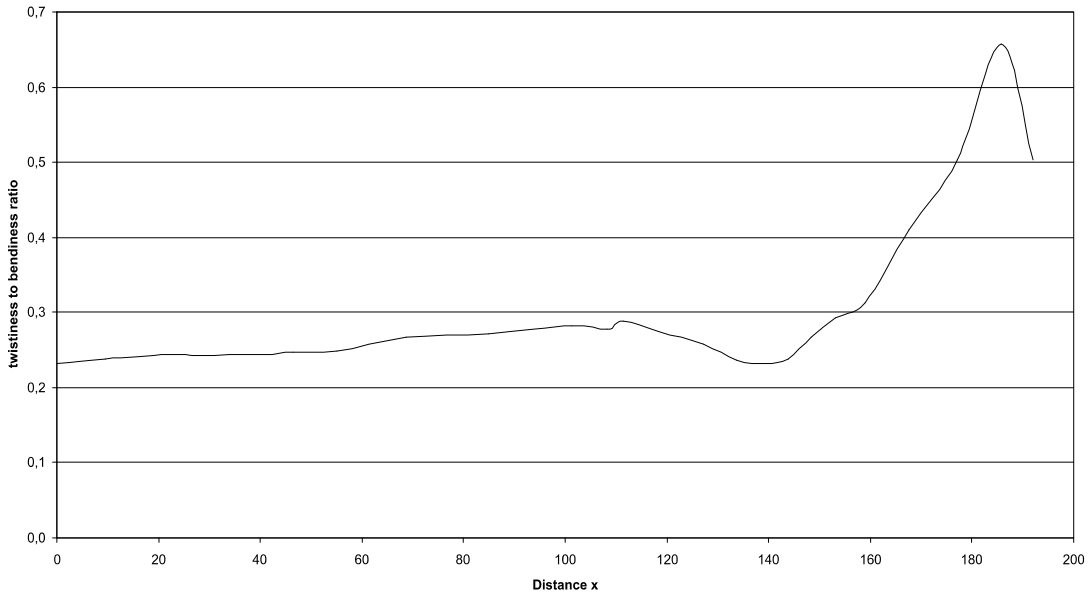

Fig. A.328: Twistiness to bendiness ratio in the Thalassodromeus rostrum construction. See chapter 6.4 for legend.

A.42 Tupuxuara skull construction (see also chapter 7.42)

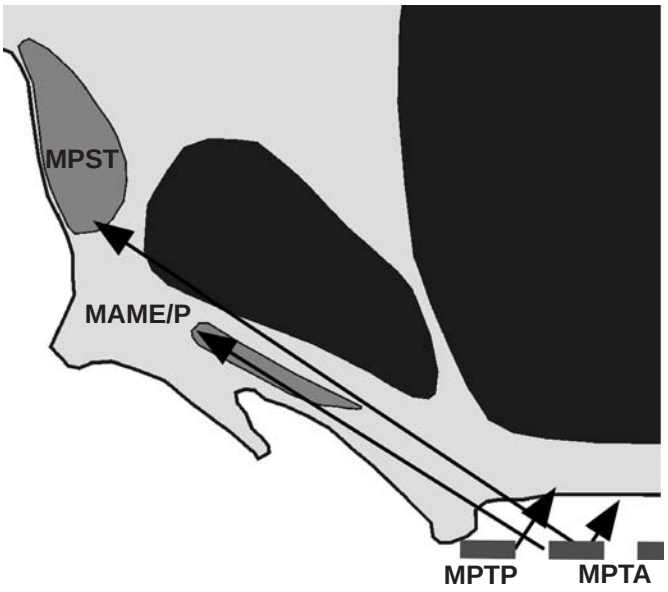

Fig A.329: Reconstruction of the principal pulling direction of the main adductor muscles in the skull of *Tupuxuara*. See chapter 6 for abbreviations.

Muscles	F_1	l_1	α_1	F_2	l_2	α_1
MAME/P	36	7.71	32	1.51	184.20	148
MPST	92	10.62	34	5.39	181.40	146
MPTA	14	12.36	57	0.96	179.66	123
MPTP	88	5.27	57	2.48	186.75	123

Tab. A.81: Reconstructed lever parameters for the scaled Tupuxuara skull construction. See chapter 6.2 for abbreviations.

	F_B	F_J	α_J
anteriormost rostrum	6.40	220.82	-42.67
level of half of the length of nasoant. fen.	31.41	204.69	-37.52
average	18.91	212.76	-40.10

Tab. A.82: Reconstructed bite and joint reaction forces and angle of joint reaction force in the scaled Tupuxuara skull construction. Negative angle values mean anterodorsal direction of force. See chapter 6.2 for abbreviations.

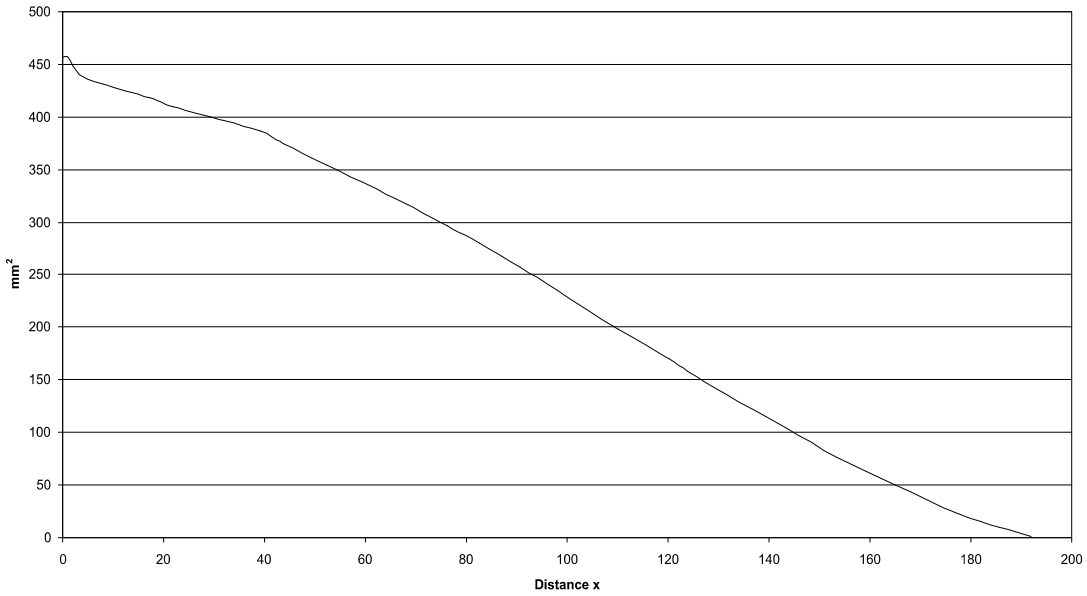

Fig A.330: Cross-sectional area of the Tupuxuara rostrum construction. See chapter 6.4 for legend.

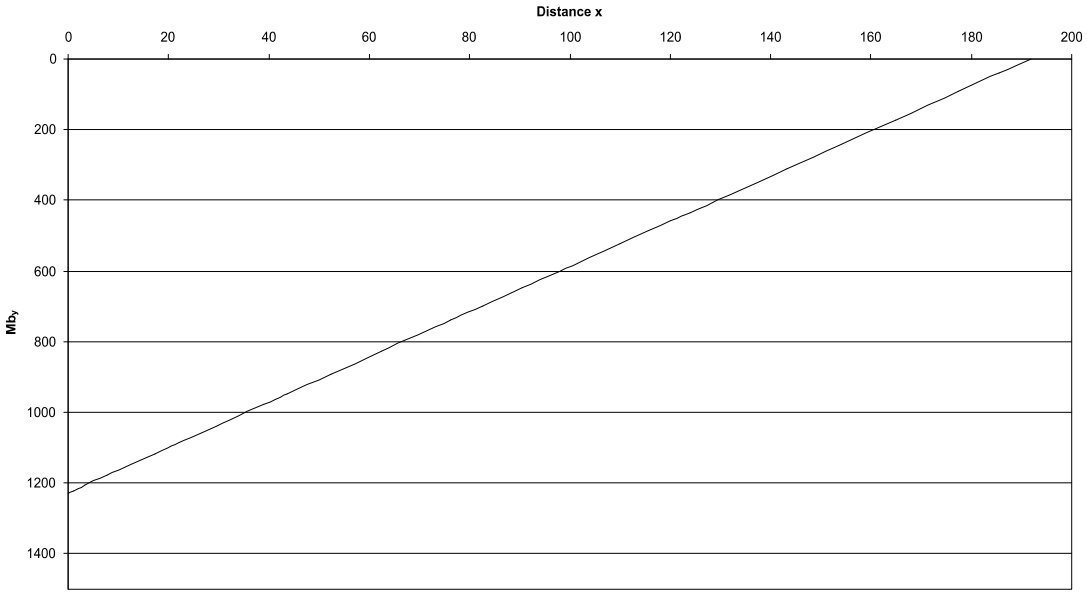

Fig A.331: Bending moments in the Tupuxuara rostrum construction. See chapter 6.4 for legend.

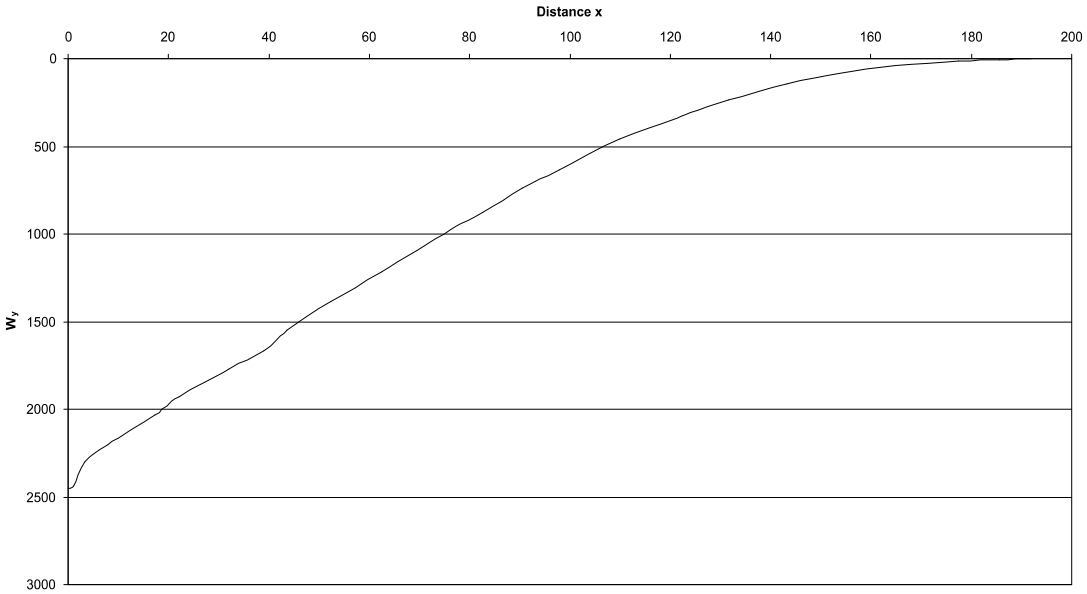

Fig A.332: Section modulus in the Tupuxuara rostrum construction. See chapter 6.4 for legend.

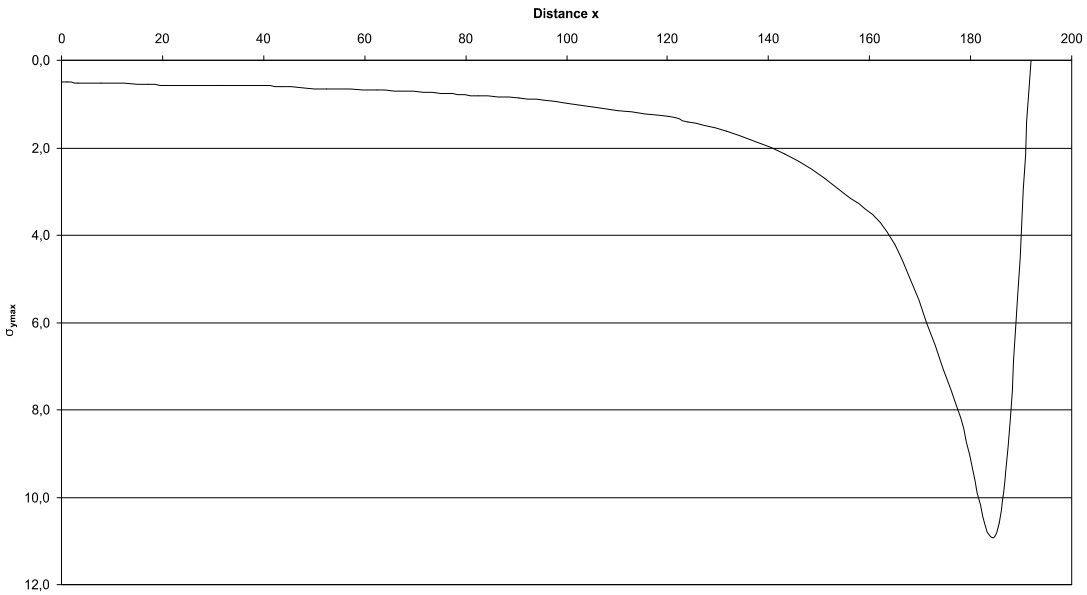

Fig A.333: Maximum bending stress in the Tupuxuara rostrum construction. See chapter 6.4 for legend.

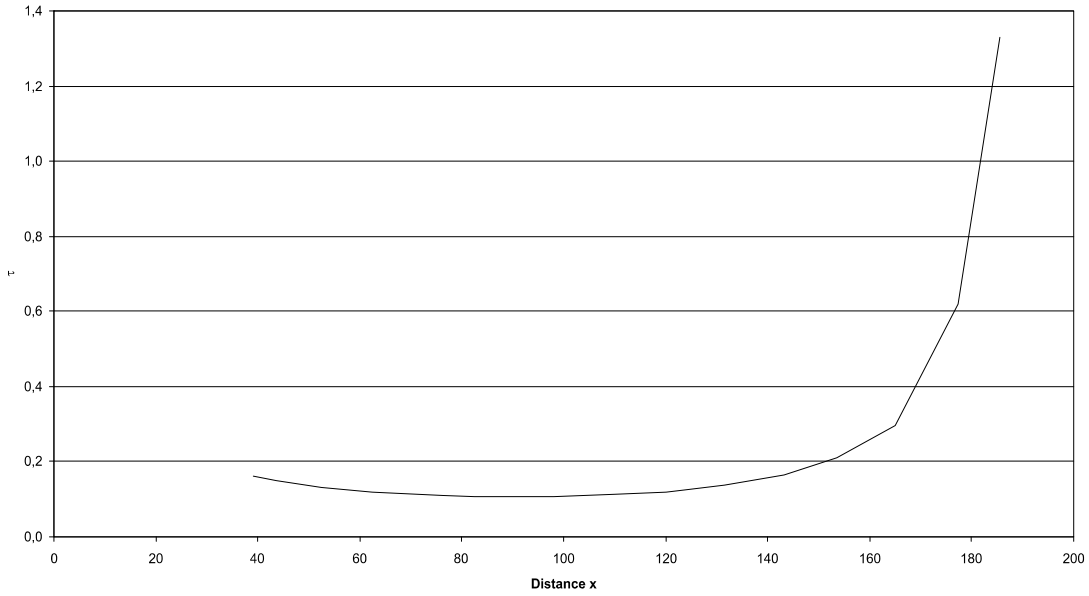

Fig. A.334: Shear stress in the Tupuxuara rostrum construction. See chapter 6.4 for legend.

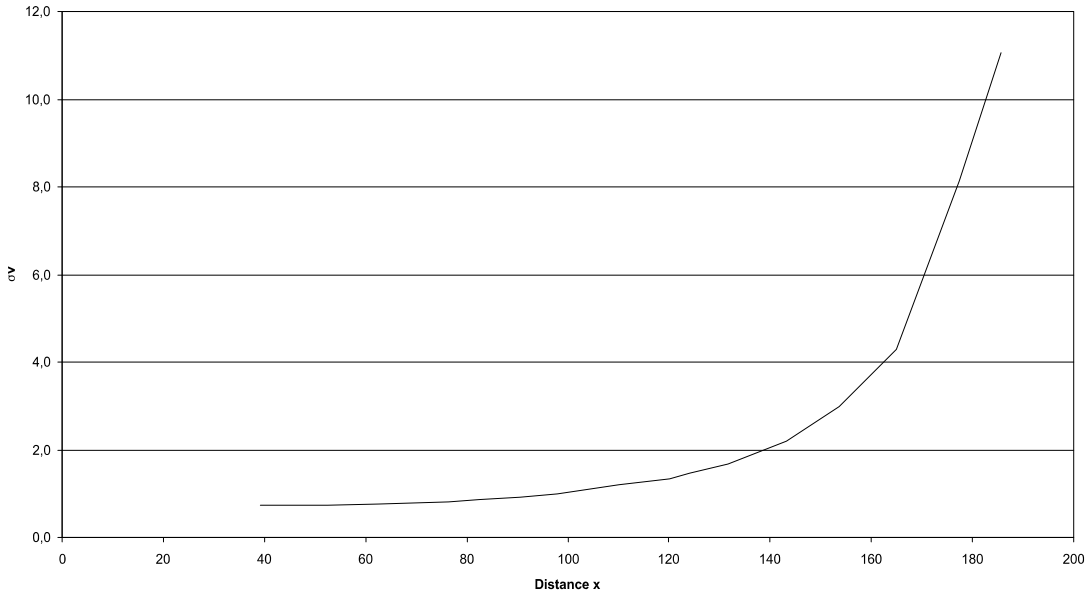

Fig. A.335: Comparison stress in the Tupuxuara rostrum construction. See chapter 6.4 for legend.

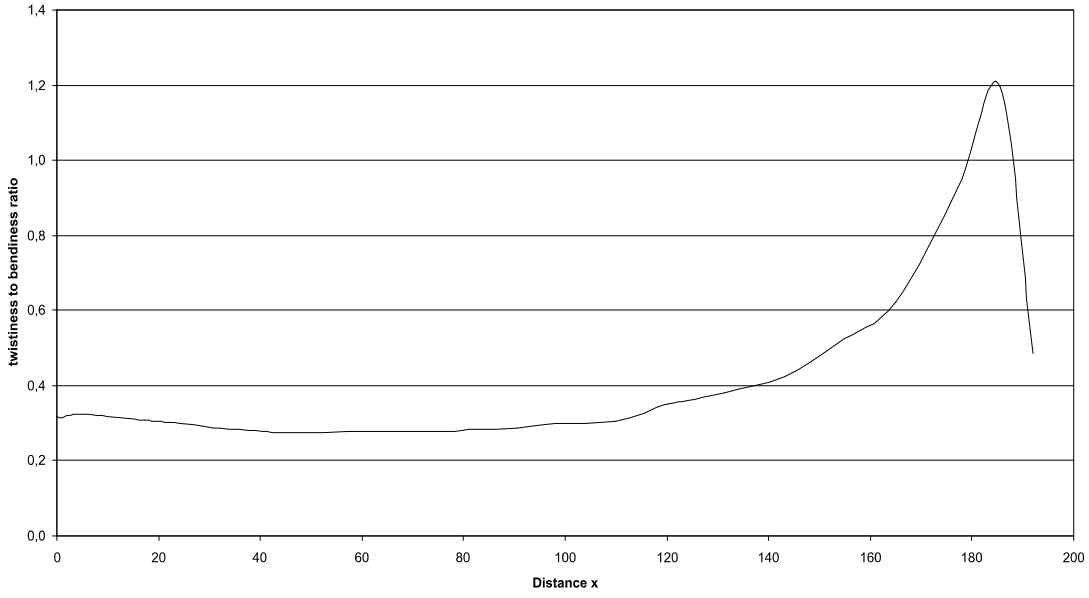

Fig. A.336: Twistiness to bendiness ratio in the Tupuxuara rostrum construction. See chapter 6.4 for legend.

A.43 Zhejiangopterus skull construction (see also chapter 7.43)

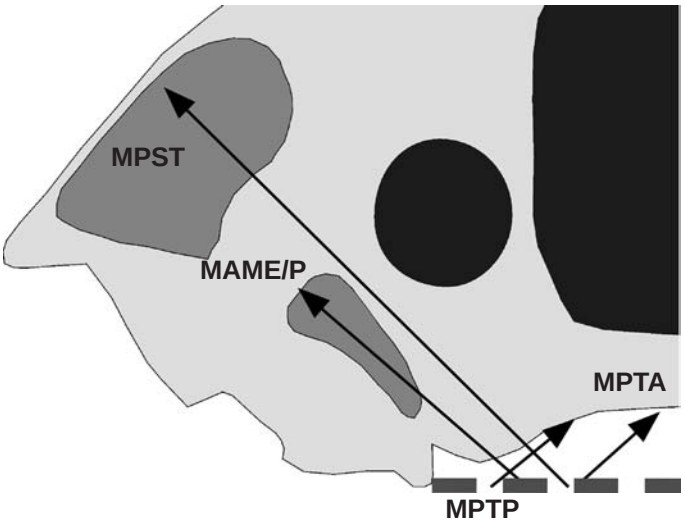

Fig A.337: Reconstruction of the principal pulling direction of the main adductor muscles in the skull of *Zhejiangopterus*. See chapter 6 for abbreviations.

Muscles	F_1	l_1	α_1	F_2	l_2	α_1
MAME/P	36	10.90	41	1.13	347.83	139
MPST	92	16.76	45	4.51	341.97	135
MPTA	14	18.23	42	0.75	340.50	138
MPTP	88	7.80	39	1.96	350.92	141

Tab. A.83: Reconstructed lever parameters for the scaled Zhejiangopterus skull construction. See chapter 6.2 for abbreviations.

	F_B	F_J	α_J
anteriormost rostrum	5.44	226.15	-40.87
level of half of the length of nasoant. fen.	41.53	204.37	-33.20
average	23.32	215.26	-37.04

Tab. A.84: Reconstructed bite and joint reaction forces and angle of joint reaction force in the scaled Zhejiangopterus skull construction. Negative angle values mean anterodorsal direction of force. See chapter 6.2 for abbreviations.

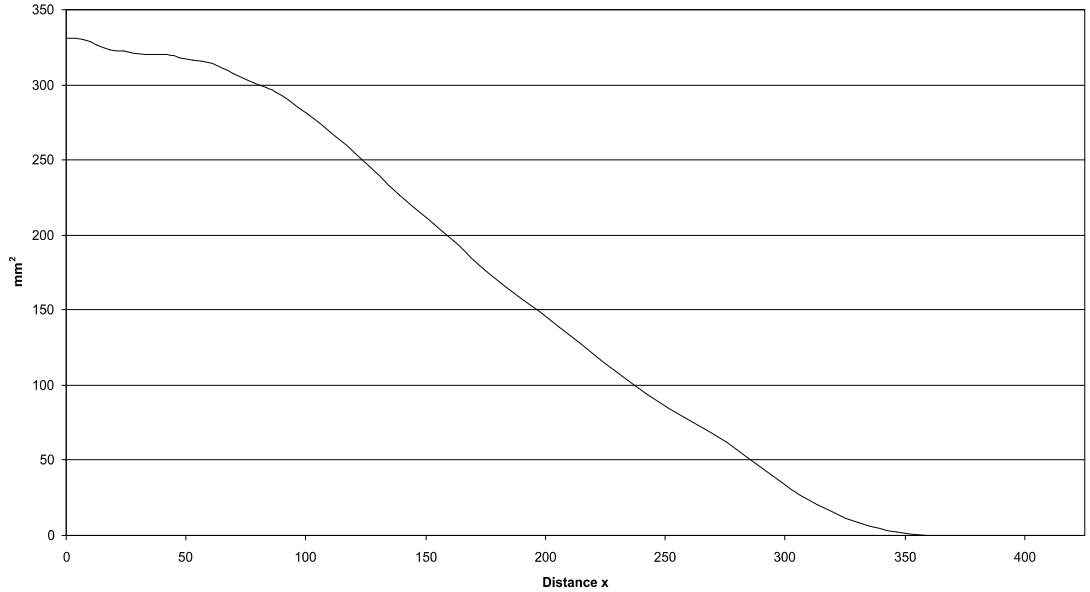

Fig A.338: Cross-sectional area of the Zhejiangopterus rostrum construction. See chapter 6.4 for legend.

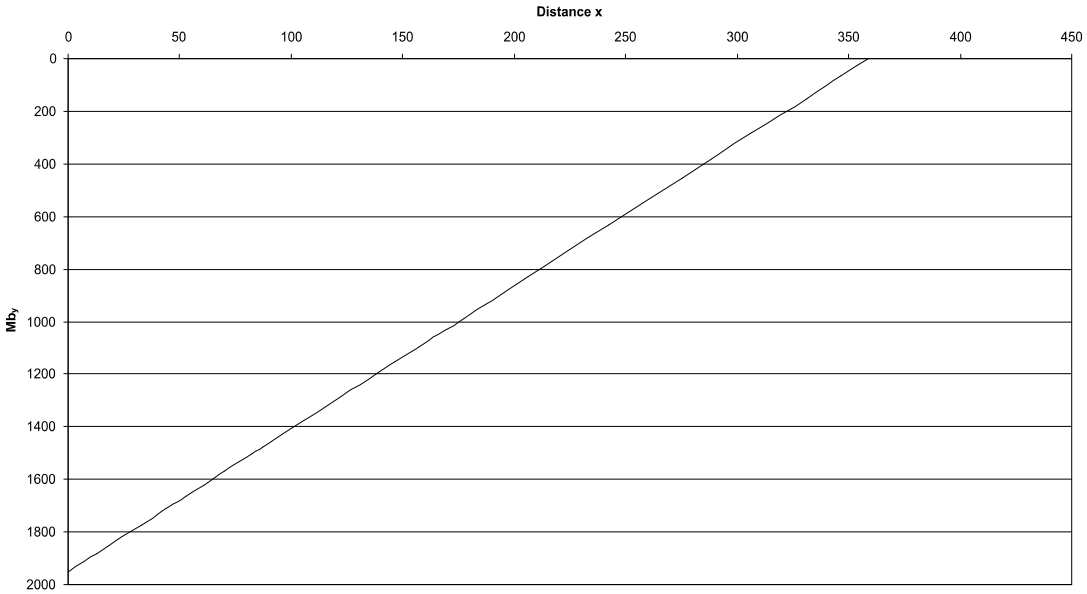

Fig A.339: Bending moments in the Zhejiangopterus rostrum construction. See chapter 6.4 for legend.

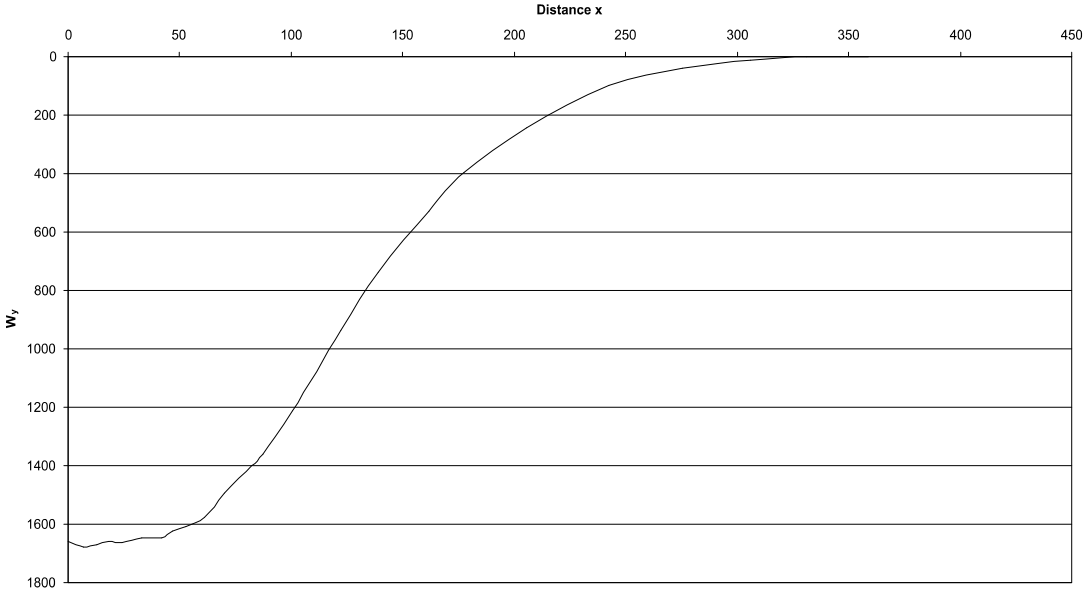

Fig A.340: Section modulus in the Zhejiangopterus rostrum construction. See chapter 6.4 for legend.

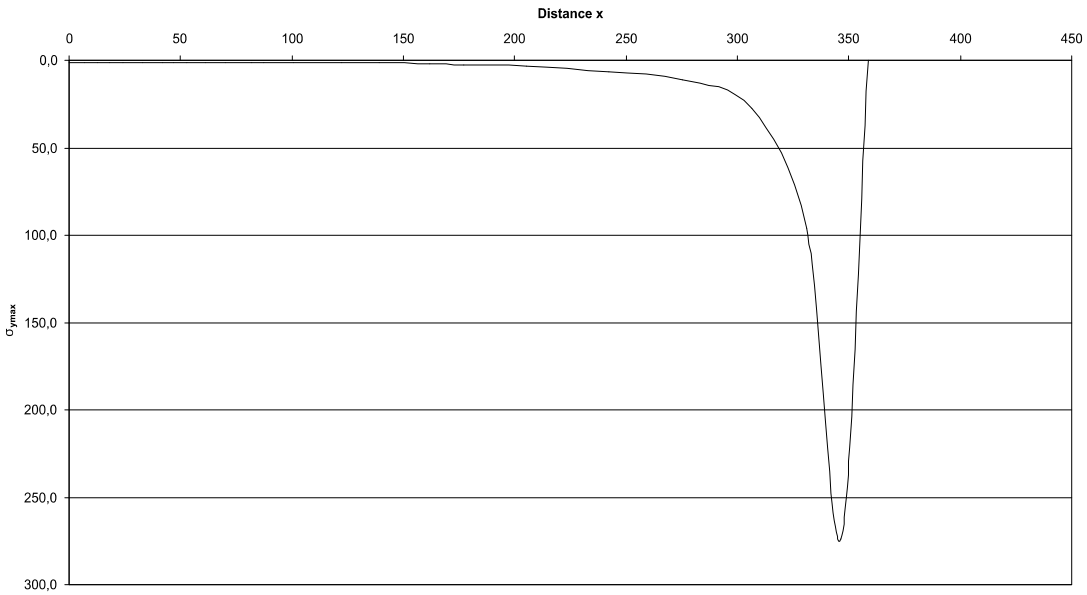

Fig A.341: Maximum bending stress in the Zhejiangopterus rostrum construction. See chapter 6.4 for legend.

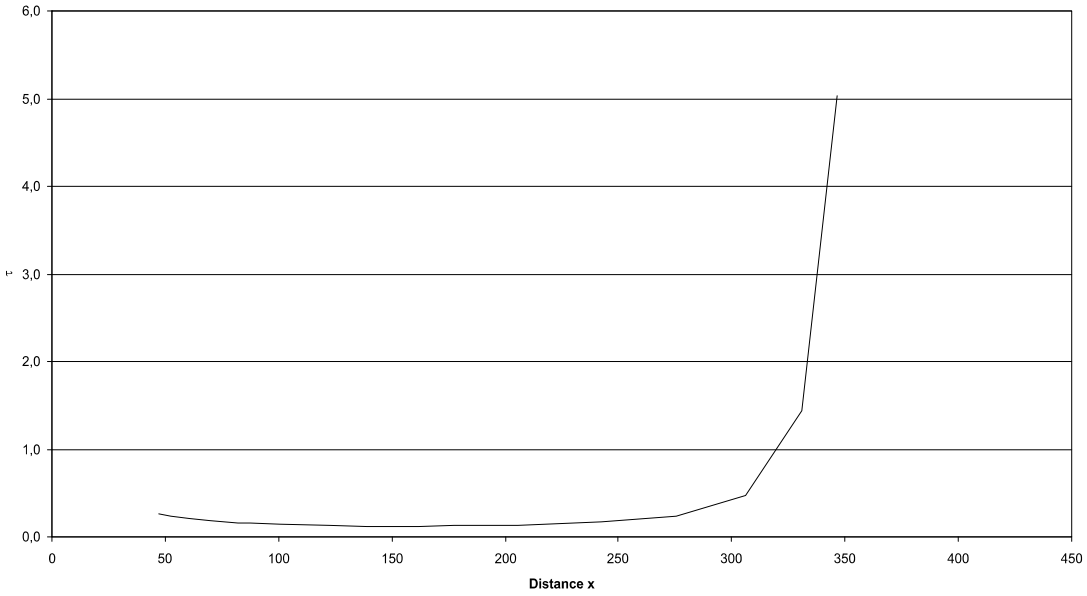

Fig. A.342: Shear stress in the Zhejiangopterus rostrum construction. See chapter 6.4 for legend.

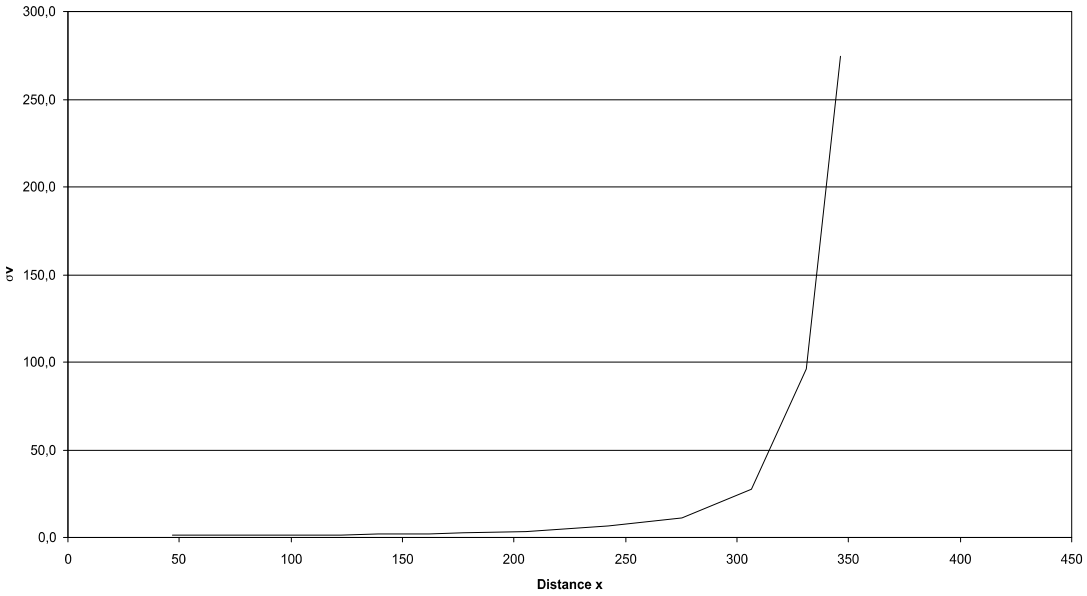

Fig. A.343: Comparison stress in the Zhejiangopterus rostrum construction. See chapter 6.4 for legend.

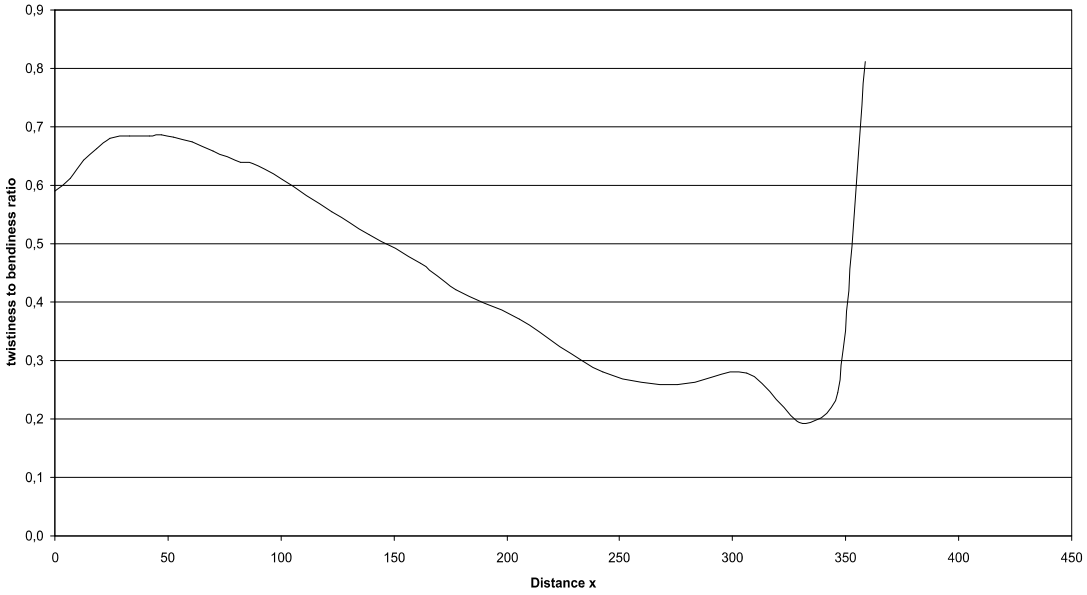

Fig. A.344: Twistiness to bendiness ratio in the Zhejiangopterus rostrum construction. See chapter 6.4 for legend.

APPENDIX B:
COMPARISON OF CHARACTERISTICS AND BIOMECHANICAL PARAMETER OF SKULL CONSTRUCTIONS

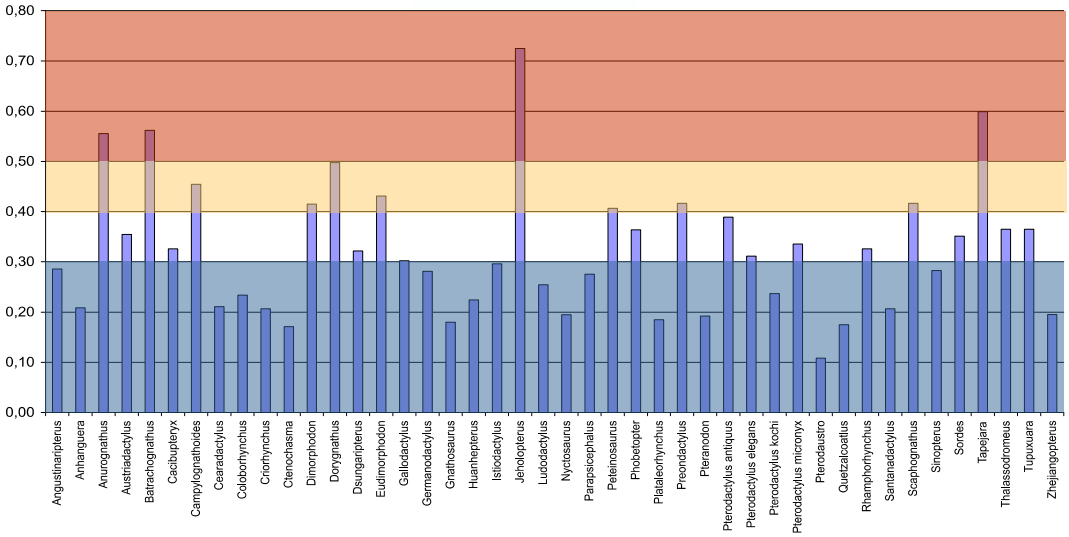

Fig. A.345: Comparison of height to length-ratio. Purple = very low, blue = low, white = medium, orange = high, red = very high.

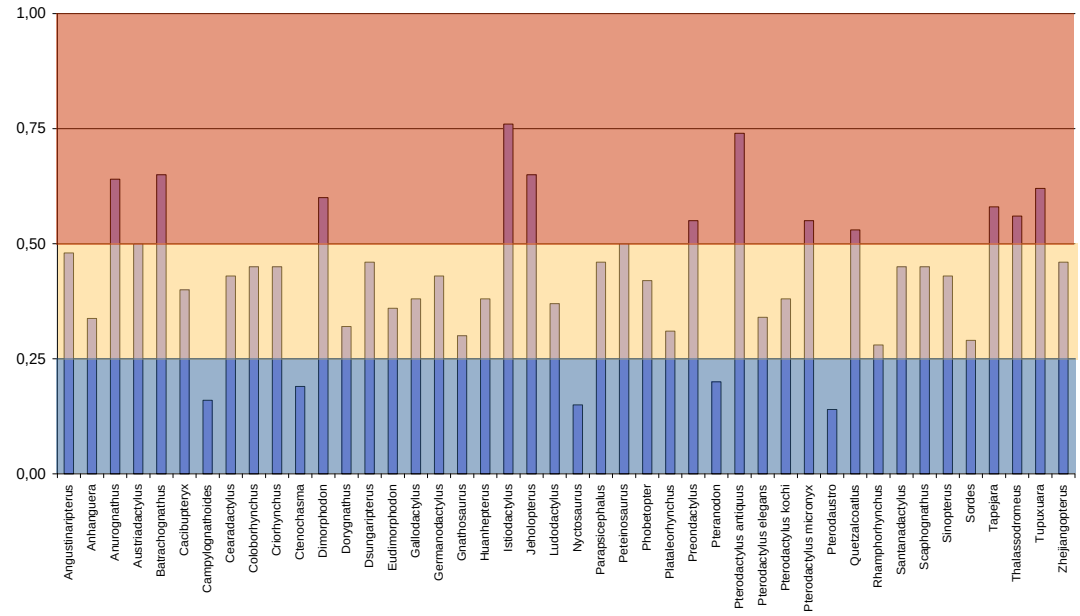

Fig. A.346: Comparison of length of antorbital fenestra + naris, resp. nasoantorbital-fenestra (length of rostrum = 1,00). Blue = small, orange = medium, red = large.

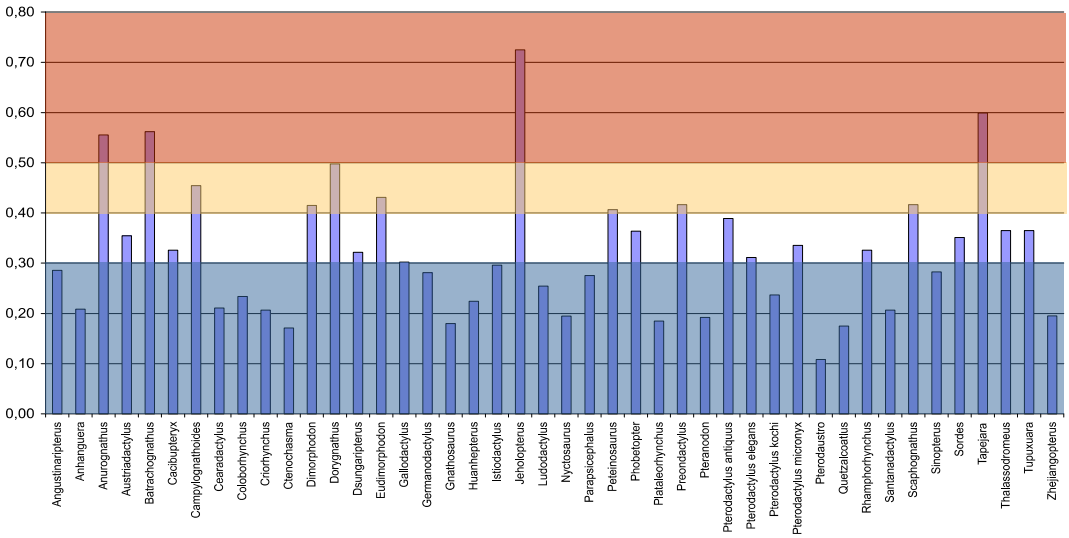

Fig. A.347: Comparison of basal height to basal width-ratio. See Fig. A.346 for legend.

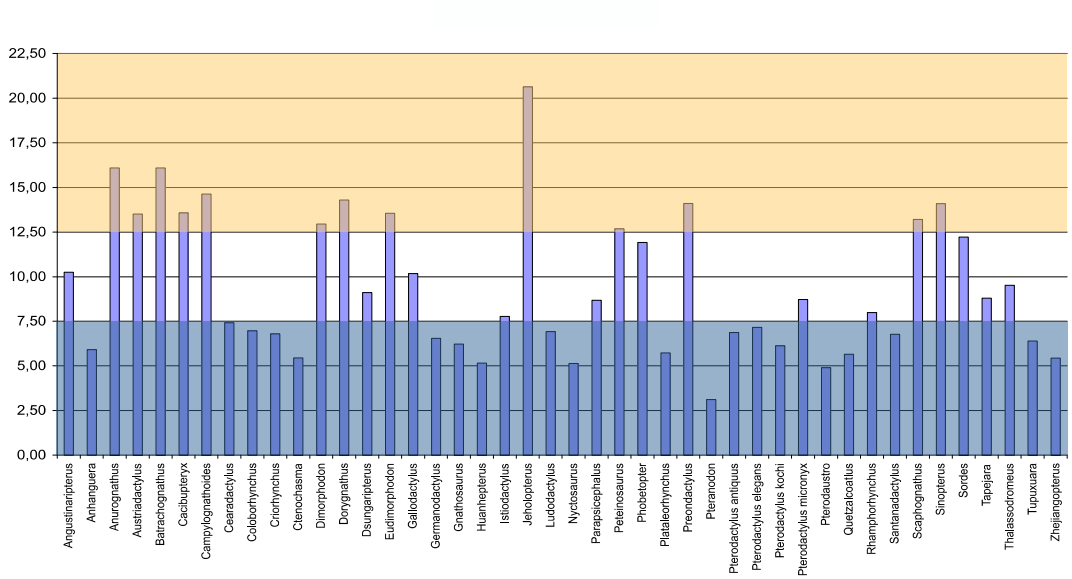

Fig. A.348: Comparison of bite force F_B. F_B in N. See Fig. A.346 for legend.

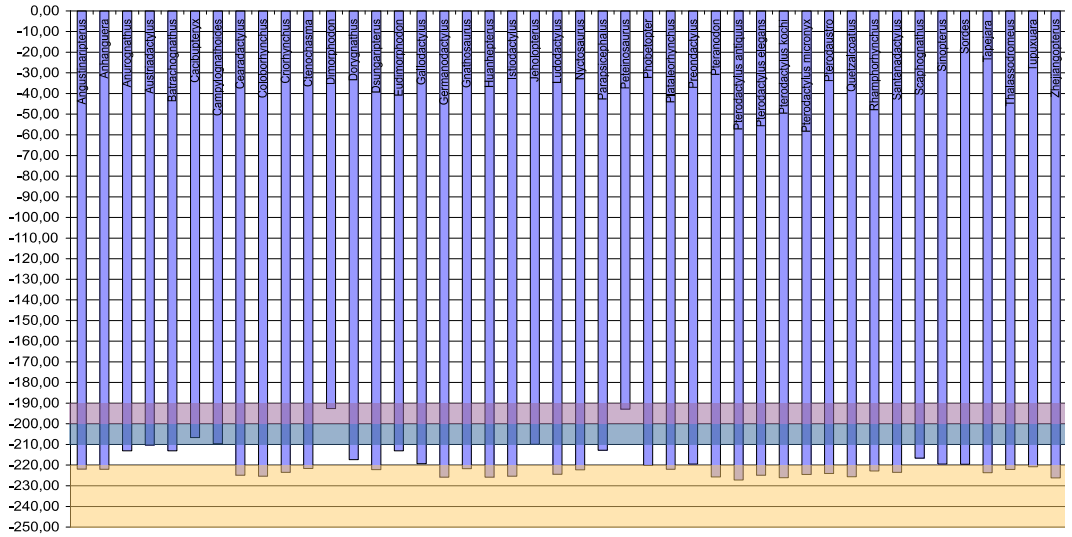

Fig. A.349: Comparison of joint reaction force F_J. F_J in N. See Fig. A.346 for legend.

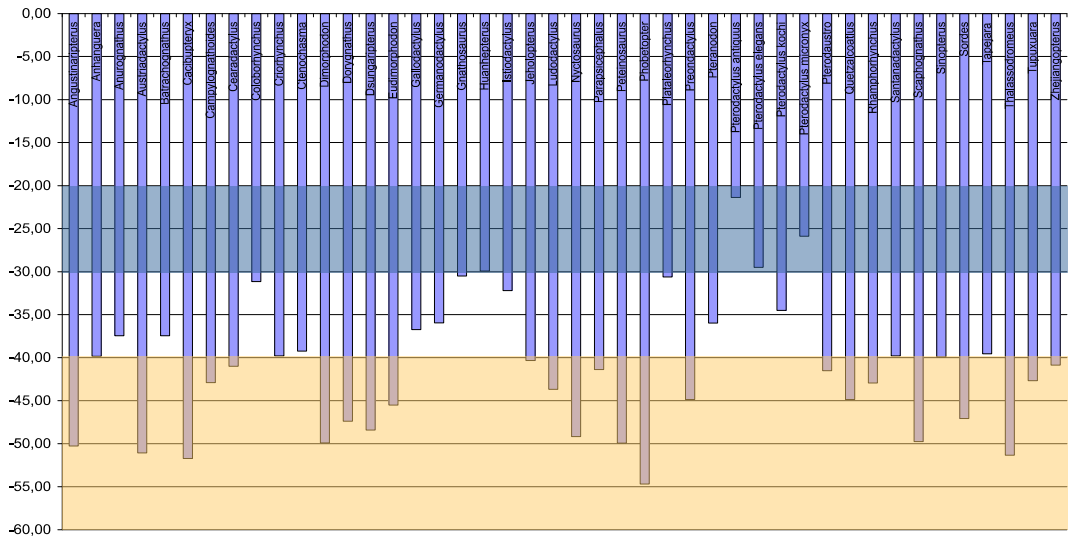

Fig. A.350: Comparison of the angle α_J of the joint reaction force F_J. Angle in degree. See Fig. A.346 for legend.

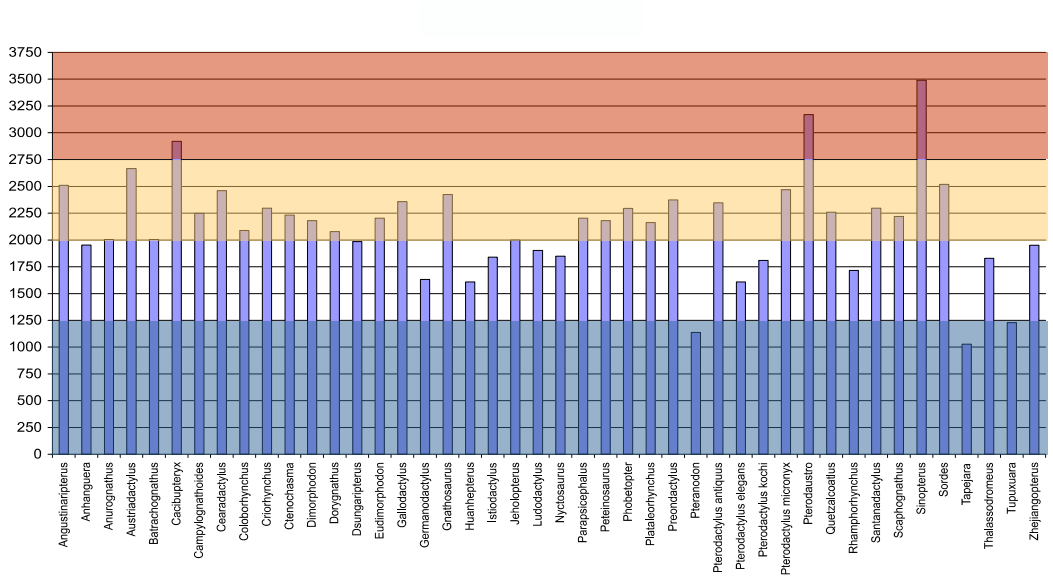

Fig. A.351: Comparison of the maximum bending moment Mb_{ymax}. See Fig. A.346 for legend.

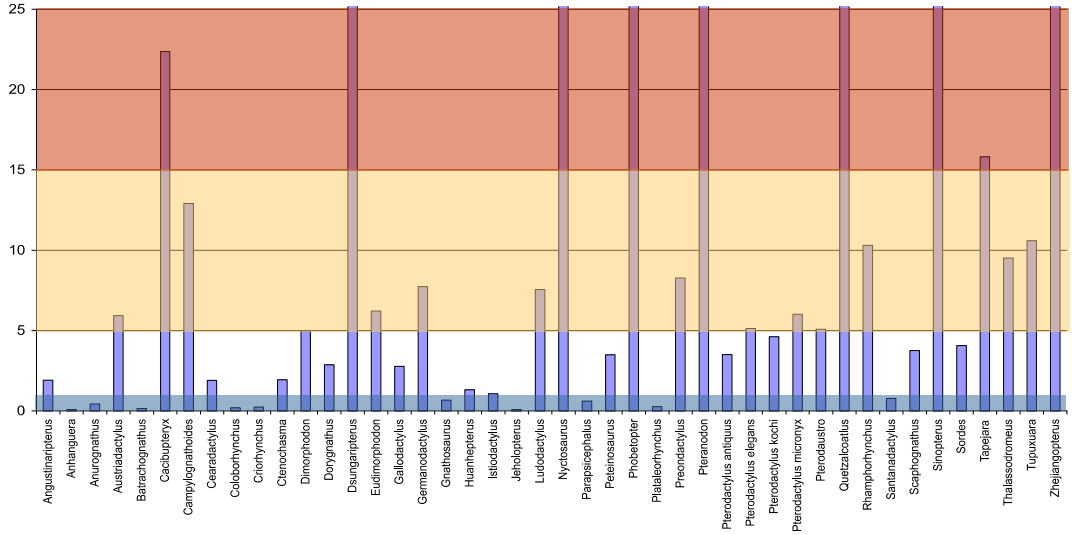

Fig. A.352: Comparison of the maximum anterior bending stress σ_{ymax}. σ_{ymax} in N/m^{-2}. See Fig. A.346 for legend.

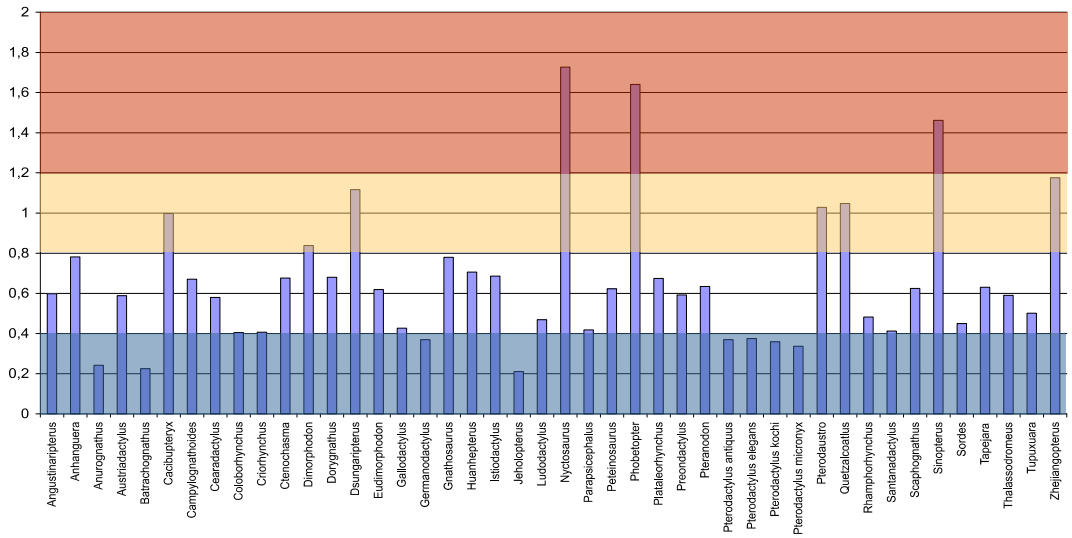

Fig. A.353: Comparison of the maximum posterior bending stress σ_{ymax}. σ_{ymax} in N/m^{-2}. See Fig. A.346 for legend.

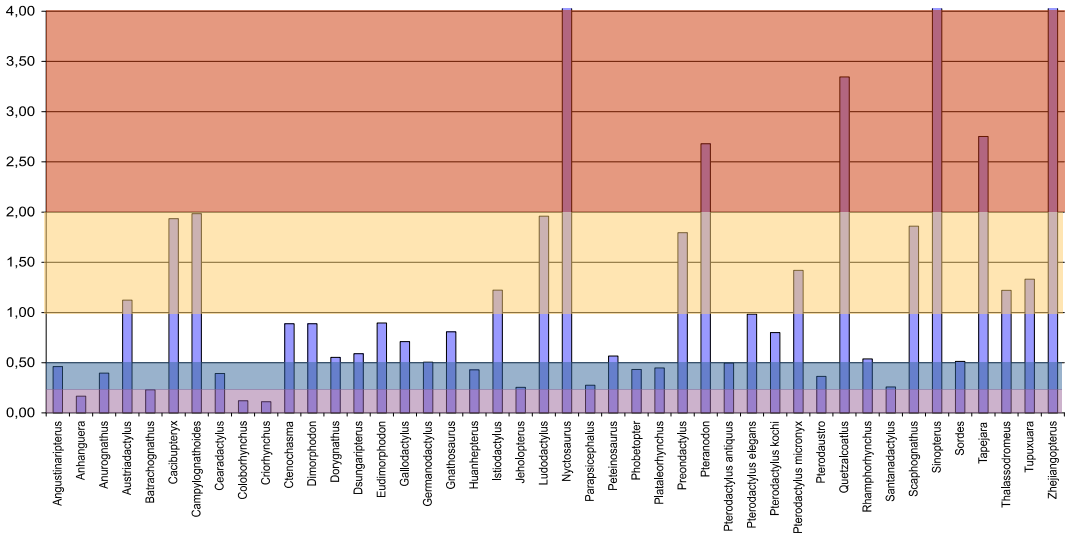

Fig. A.354: Comparison of the maximum anterior shear stress τ. τ in N/m^{-2}. See Fig. A.346 for legend.

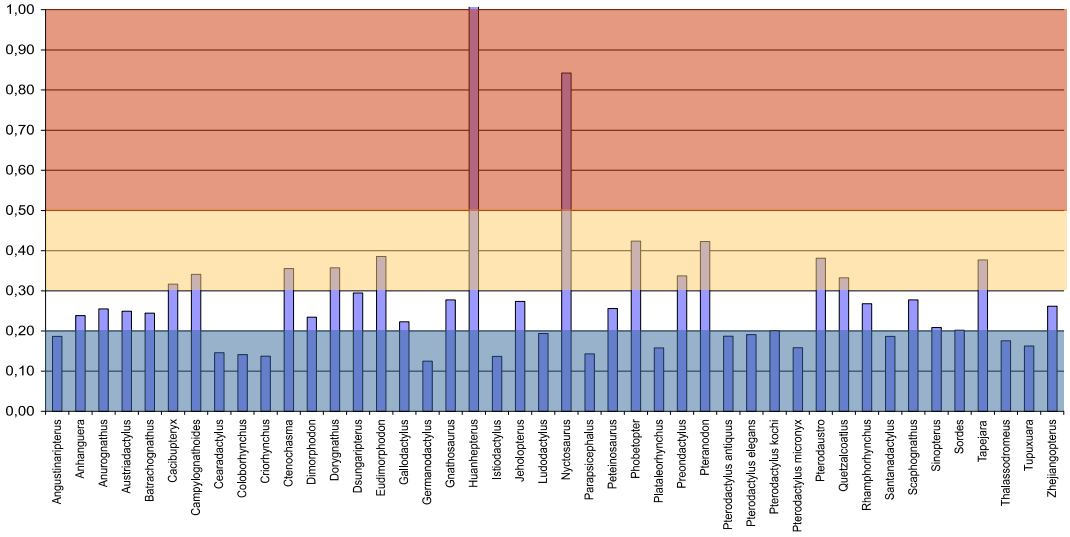

Fig. A.355: Comparison of the maximum posterior shear stress τ. τ in N/m^{-2}. See Fig. A.346 for legend.

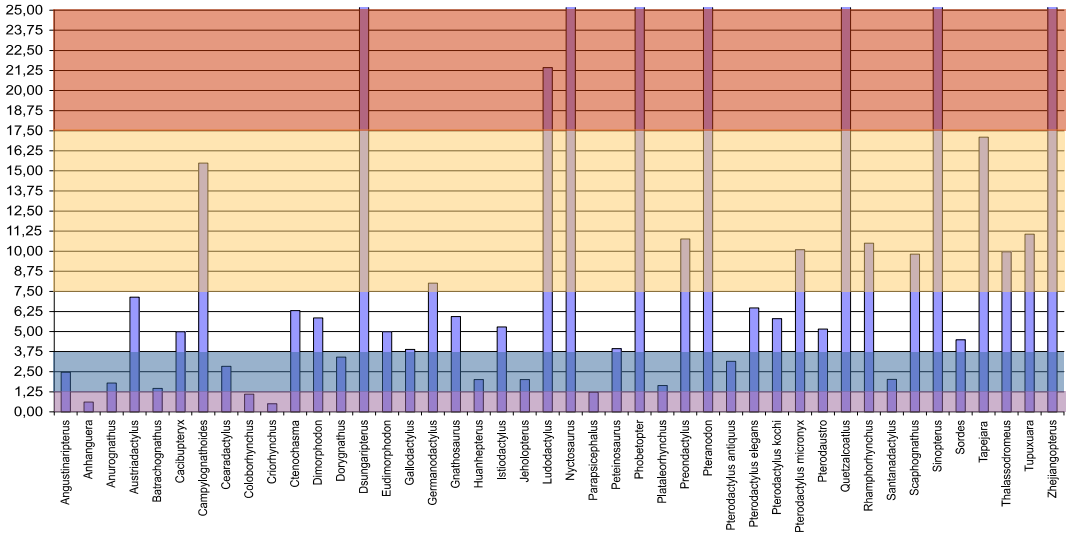

Fig. A.356: Comparison of the maximum anterior comparison stress σ_v. σ_v in N/m^{-2}. See Fig. A.346 for legend.

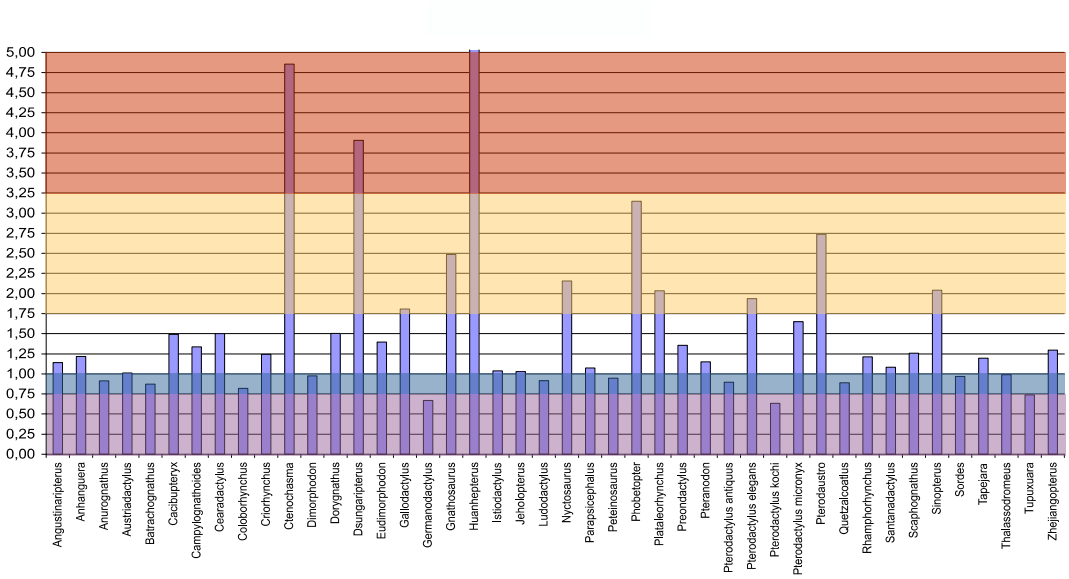

Fig. A.357: Comparison of the maximum posterior comparison stress σ_v. σ_v in N/m^{-2}. See Fig. A.346 for legend.

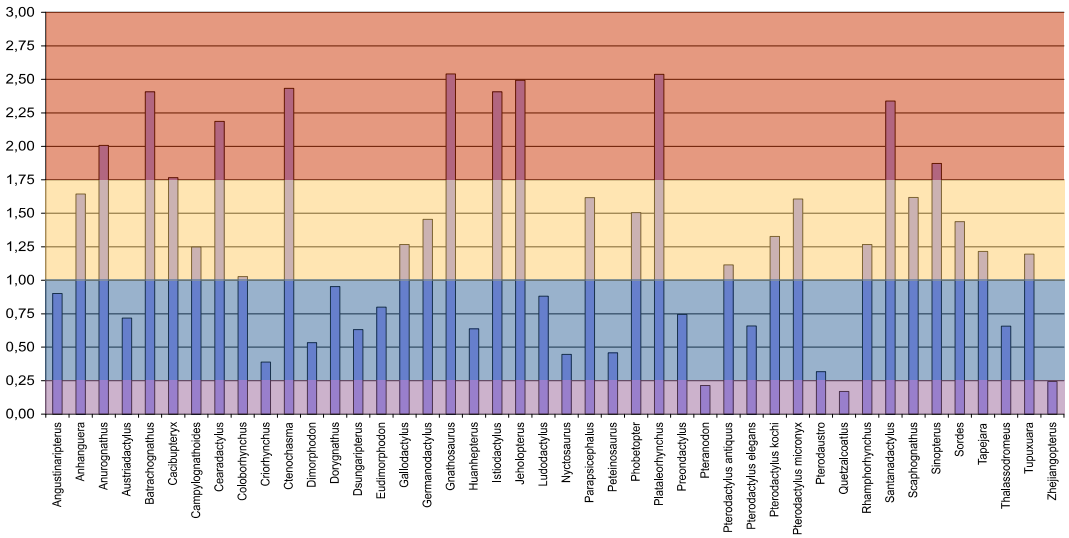

Fig. A.358: Comparison of the anterior twistiness to bendiness-ratio. See Fig. A.346 for legend.

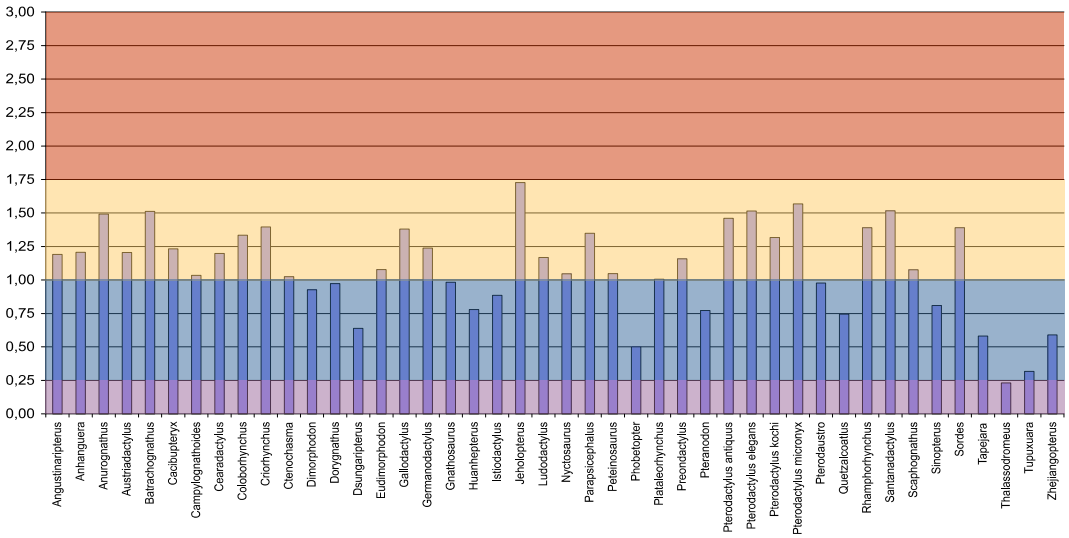

Fig. A.359: Comparison of the posterior twistiness to bendiness-ratio. See Fig. A.346 for legend.

skull construction type	AngusCT	AnuroCT	AzhdarchCT	CaciCT	CampCT	CearaCT	CtenoCT
nasoantorbital fenestra	large	large	large	small	large	large	small
bar between nares and antorbital fenestra	slightly oblique	vertically	-	oblique	oblique	-	-
crest	not present	not present	medial, optional	not present	not present	not present	not present
orientation of occipital region	~55°	~55°	~25°-35°	~85°	~55°	~20°	~25°
tooth construction	Rhamphorhynchus	Pterodactylus	edentulous	unknown	Pterodactylus	Ornithocheirus high and low	Ctenochasma
length of tooth row	anterior third of antorbital fenestra	fully developed	-	fully developed	fully developed	anterior border of nasoantorbital fenestra	anterior to nasoantorbital fenestra
length of rostrum	long	very short	long, straight to bent in ventral direction	medium	short	long, festooned	very long
basal width	medium	high	low	medium	medium	medium	medium
F_B	medium	high	low	high	high	medium	low
F_J	high	medium	high	low	low	high	high
orientation of F_J	-50°	-37°- -40°	-40° - -45°	-52°	-4°	-40°	-40°
max. bend moment	high	high	medium to high	very high	high	high	high
bending stress	medium	low	very high	very high	high	high	high
shear stress	low	very low	very high	high	high	low	medium
comparison stress	low	very low	very high	medium	high	low	medium
twistiness to bendiness ratio	low	very high	very low to low	very high	high	high	very high

Tab. A.85: Comparison of the main characteristics of the skull constructional levels. See chapter 5 for abbreviations and Figs. A.345-A.359 for relative criteria.

skull construction type	DimoCT	DsungCT	EudiCT	GalloCT	GnathoCT	HuanCT	IstioCT
nasoantorbital fenestra	large	large	large	large	small	small	very large
bar between nares and antorbital fenestra	vertically	-	steeply oblique	-	-	-	-
crest	not present	medial and orbito-temporal	not present	not present	medial	medial	not present
orientation of occipital region	75°-77°	35°-45°	~70°	~40°	~20°	~10°	~30°
tooth construction	Pterodactylus	Dsungaripterus	Eudimorphodon tooth constructions	Ornithocheirus low and high	Gnathosaurus	Rhamphorhynchus	Ornithocheirus low
length of tooth row	fully developed	anterior rostrum edentulous	fully developed	anterior fifth part of rostrum	anterior border of nasoant. fen.	anterior third of rostrum	anterior quarter of rostrum
length of rostrum	short	medium	short	long	very long, anteriorly expanded spatulate	very long	long
basal width	medium	low	medium	medium	medium	medium	medium
F_B	high	medium	high	medium	low	low	medium
F_J	very low	high	medium	medium	high	high	high
orientation of F_J	-50°	–55° - -48°	-45°	-37°	-30°	-40°	-32°
max. bend moments	high	medium to high	high	high	high	very high	medium
bending stress	medium	very high	high	medium	low	high	low
shear stress	medium	low to medium	medium	medium	low to medium	low	high
comparison stress	medium	very high	medium	medium	medium	medium	medium
twistiness to bendiness ratio	low	very high	very low to low	very high	high	high	very high

Tab. A.85 (continued)

skull construction type	OrnithoCT	ParaCT	PreonCT	PteranoCT	PteroCT	PterodauCT	RhamCT
nasoantorbital fenestra	large	large	large	small	large	small	small
bar between nares and antorbital fenestra	-	oblique	steeply oblique	-	-	-	slightly oblique
crest	medial	not present	medial soft-tissue	orbitotemporal optional	medial (Germandodactylus), soft-tissue	not present	not present
orientation of occipital region	~20°-33°	~50°	55°-58°	~12°-32°	~12°-30°	~30°	~40°
tooth construction	Ornithocheirus high and low	unknown	Preondactylus and Eudimorphodon monocuspid	edentulous	Pterodactylus	Pterodaustro low	Rhamphorhynchus
length of tooth row	half of the length of the nasoantorbital fenestra	anterior end of antorbital fenestra	fully developed	-	fully developed to restricted to anterior third of rostrum	anteriormost rostrum edentulous, teeth reaching to posterior two thirds of rostrum	full developed, anteriormost rostrum edentulous and covered with rhamphotheca
length of rostrum	long	long	short to medium	long	medium to long	very long, bent in dorsal direction	medium
basal width	low to medium	medium	medium	low	medium to high	medium	medium
F_B	low	medium	high	low	low to medium	low	medium
F_J	high	medium	medium	high	high	high	high
orientation of F_J	–30°-40°	-41°	-45°- -50°	-35° - -50°	-20° - -35°	-40°	-43°
max. bend moments	medium to high	high	high	low to medium	medium to high	high	medium
bending stress	low	low	high	very high	medium to high	low	high
shear stress	very low	low	high	very high	medium to high	low to medium	medium
comparison stress	very low	low	medium to high	very high	medium to high	medium	high
twistiness to bendiness ratio	low to high	high	high	low to high	high	very high	high

Tab. A.85 (continued)

skull construction type	ScaphoCT	SordCT	TapeCT	TupCT
nasoantorbital fenestra	large	large	large	small
bar between nares and antorbital fenestra	oblique	oblique	-	-
crest	not present	not present	anterior and orbitotemporal bony crest, soft-tissue crest	anterior to orbitotemporal crest
orientation of occipital region	~60°-65°	~40°	~45°-50°	~40°-50°
tooth construction	Rhamphorhynchus	Pterodactylus	edentulous	edentulous
length of tooth row	fully developed	fully developed	-	-
length of rostrum	short	medium	short	medium
basal width	medium	high	low	low
F_B	high	medium	medium to high	medium
F_J	medium	low	high	high
orientation of F_J	-47° - -49°	-47°	~40°	-42° - -51°
max. bend mom.	high	high	low to very high	low to medium
bending stress	medium	medium	high	high
shear stress	medium to high	medium	high	high
comparison stress	low to high	medium	high	high
twistiness to bendiness ratio	high	high	very low to low	low

Tab. A.85 (continued)

APPENDIX C:
CD-ROM WITH CT SCANS OF *ANHANGUERA SP.*, SMNK 3895 PAL

(MAY NOT BE USED FOR PUBLICATION WITHOUT PERMISSION OF AUTHOR)